

**DOCTOR OF PHILOSOPHY**

**A Case Study of the Effectiveness of Tree Planting as a Method of Natural Flood Management (NFM) to Increase Infiltration and Reduce River Flows**

Revell, Nathaniel

*Award date:*  
2022

*Awarding institution:*  
Coventry University

[Link to publication](#)

**General rights**

Copyright and moral rights for the publications made accessible in the public portal are retained by the authors and/or other copyright owners and it is a condition of accessing publications that users recognise and abide by the legal requirements associated with these rights.

- Users may download and print one copy of this thesis for personal non-commercial research or study
- This thesis cannot be reproduced or quoted extensively from without first obtaining permission from the copyright holder(s)
- You may not further distribute the material or use it for any profit-making activity or commercial gain
- You may freely distribute the URL identifying the publication in the public portal

**Take down policy**

If you believe that this document breaches copyright please contact us providing details, and we will remove access to the work immediately and investigate your claim.

**A Case Study of the Effectiveness of Tree Planting  
as a Method of Natural Flood Management (NFM)  
to Increase Infiltration and Reduce River Flows**



By

**Nathaniel Revell**

**PhD**

**July 2022**

**A Case Study of the Effectiveness of Tree Planting  
as a Method of Natural Flood Management (NFM)  
to Increase Infiltration and Reduce River Flows**

**Nathaniel Revell**

**July 2022**

*This thesis is submitted in partial fulfilment of the University's requirements for the Degree  
of Doctor of Philosophy*



## ABSTRACT

Urbanisation and the consequent loss of permeable surfaces, is influencing the likelihood and severity of flood events. This, coupled with recent climate change predictions which suggest that sea levels will rise and that extreme weather events will become more frequent, has pushed the issue of flooding up the public agenda, encouraging the relevant authorities to more robustly target the challenges of increased flood risk.

Tree planting is gaining momentum as a potential method of natural flood management (NFM) due to its capacity to break up soil and increase infiltration and water storage. Consequently, the aims of this study were to simulate the influences of woodland planting on infiltration and area hydrology through use of empirical observations and hydrological modelling, and extrapolate data to predict the likely hydrological changes across the area in the future, considering climate change. The infiltration characteristics throughout defined Heart of England (HofE) Forest owned areas of Warwickshire (England), planted with woodland between 2006 and 2020, were sampled using a Mini Disk infiltrometer (MDI). In total, 1686 measurements were taken at both proximities between November 2019 and August 2021. Two individual hydrological models were built, calibrated and validated using the US Hydrologic Engineering Centre's Hydrological Modelling System (HEC-HMS). In total 448 HEC-HMS simulations were undertaken.

Infiltration was found to be 75.87% higher at 10 cm proximity compared with the 200 cm proximity in winter, and 25.19% higher in summer. The mean 10 cm infiltration was 192% higher in summer compared with winter, and mean 200 cm infiltration is 310% higher in summer compared with winter. Regarding the hydrological simulations, woodland planting reduced peak flow intensity compared to impermeable land cover by an average of 6%, 2%, and 1% for 6-, 24-, and 96-hour winter storms respectively, and 48%, 18%, and 3% for 6-, 24-, and 96-hour summer storms respectively. Grassland simulations show the greatest reduction in peak flows, being 32%, 21%, and 10%, lower than woodland for 6-, 24-, and 96-hour winter storms respectively, and 6%, 3%, and 0.5% lower than woodland for 6-, 24-, and 96-hour summer storms respectively. Model projections show that woodland planting is unlikely to mitigate future projected peak flow and total discharge from the HofE site throughout the winter, however it is more likely to have an impact throughout summer. This is primarily due to soil texture characteristics across the site, the influence of hydrological model parameters, and the inclusion of interception throughout the summer.

Overall, tree planting does influence infiltration on a case-by-case basis, however ‘present-day’ hydrological simulations show grassland to reduce peak and total discharge from the site to a greater extent than woodland. Projections show that this will likely change as woodland matures, however further research will have to be conducted to further solidify this finding. It is concluded that woodland is beneficial as a method of NFM, however should not be relied upon to mitigate against larger storm events.

The outcomes of this study are contextualised, and recommendations posed, with regards to the construction and forestry industry, and current and future water policy; namely, the Department of Food and Rural Affairs (DEFRA) policies, the Agricultural Act, the 25-year plan, the England trees action plan, and additional international policy. The overarching conclusions are that tree planting is featuring more prominently in recent and upcoming policy, however the main motivation being the ability of woodland to sequester carbon. It is recommended that more emphasis be targeted towards the hydrological benefits of trees, to further justify the planting of large-scale woodland, and encourage researchers to investigate the hydrological benefits of woodland planting, as has been done throughout this study. This, in turn, would aid in the current knowledge gap regarding woodland planting as a method of NFM.

## TABLE OF CONTENTS

<b>Chapter 1 Introduction .....</b>	<b>1-1</b>
1.1 The UK and Flood Risk Management .....	1-2
1.2 Flood Modelling.....	1-4
1.3 Aims & Objectives.....	1-4
1.4 Structure of Thesis .....	1-8
<b>Chapter 2 Literature Review .....</b>	<b>2-1</b>
2.1 Conventional Flood Management.....	2-1
2.2 Natural Flood Management .....	2-4
2.2.1 Scale .....	2-13
2.2.2 NFM and Climate Change .....	2-16
2.2.3 Current Barriers of Natural Flood Management.....	2-23
2.3 Tree Planting .....	2-24
2.3.1 Tree Root Growth and Infiltration .....	2-26
2.3.2 Biological activity .....	2-27
2.3.3 Interception .....	2-28
2.3.4 Tree Planting and Surface Roughness .....	2-29
2.4 Tree Planting as a Method of NFM .....	2-30
2.4.1 Long-Term Tree Planting and Infiltration Case Studies.....	2-32
2.5 Infiltration, Soil Texture, Soil Structure and Compaction.....	2-33
2.6 Chapter Summary .....	2-37
<b>Chapter 3 Review of Previous Studies, Methods, and Tools .....</b>	<b>3-1</b>
3.1 Infiltration Measurement .....	3-1
3.1.1 Single and Double Ring Infiltrimeters .....	3-2
3.1.2 Minidisk Infiltrimeter (MDI) .....	3-5
3.1.3 Chosen Method for Study .....	3-9
3.2 Flood Modelling.....	3-10
3.2.1 Hydraulic Modelling .....	3-11
3.2.2 Hydrological (Rainfall-Runoff) Modelling.....	3-14
3.2.3 Chosen Flood Model for Study .....	3-19
3.3 Flood Model Calibration and Validation .....	3-20
3.3.1 Nash and Sutcliffe Efficiency (NSE).....	3-21
3.4 Limitations and Uncertainties of Flood Modelling.....	3-22
3.5 Chapter Summary .....	3-23
<b>Chapter 4 Study Site.....</b>	<b>4-1</b>
4.1 Characterising the Study Site.....	4-1
4.1.1 The Heart of England Forest and Planted Tree Species .....	4-2
4.2 Sernal Study Site.....	4-6

4.2.1 Watershed Delineation .....	4-8
4.2.2 Study Area: Topography .....	4-11
4.2.3 Study Area: Hydrology .....	4-13
4.2.4 Study Area: Geology .....	4-14
4.3 Chapter Summary .....	4-16
<b>Chapter 5 Research Design and Methodology .....</b>	<b>5-1</b>
5.1 Research Philosophy and Hypotheses .....	5-7
5.2 Field Sample Plots, Sampling Methods, Data Collection and Data Recording .....	5-10
5.2.1 Infiltration Sampling Sites (Spernal) .....	5-11
5.2.2 Field Sampling Methods and Data Collection .....	5-19
5.3 Hydrometric Data and HEC-HMS modelling.....	5-28
5.3.1 Collected Hydrometric Data for Modelling .....	5-31
5.3.2 Model GIS Preparation and Cross Section Design .....	5-33
5.3.3 Selected Model Parameters .....	5-39
5.4 Model Calibration .....	5-44
5.4.1 Winter Calibration Events.....	5-50
5.4.2 Summer Calibration Events .....	5-52
5.5 Model Validation .....	5-55
5.5.1 Winter Validation Events.....	5-58
5.5.2 Summer Validation Events .....	5-60
5.6 Post-Validation Model Parameters and Simulations .....	5-63
5.6.1 Simulation Durations and Intensities .....	5-63
5.6.2 Rainfall Data, Design Storms, and Interception .....	5-64
5.6.3 Simulating Infiltration.....	5-66
5.6.4 Baseflow and Antecedent River Conditions .....	5-67
5.7 Precipitation, Infiltration and Baseflow Projections .....	5-69
5.7.1 Projected Variations in Precipitation due to Climate Change .....	5-69
5.7.2 Projected Variation to Infiltration Values due to Climate Change .....	5-70
5.7.3 Projected Variation to Baseflow due to Climate Change .....	5-73
5.8 Summary of Simulations and Data Used .....	5-75
5.9 Chapter Summary .....	5-77
<b>Chapter 6 Pilot Results and Reflection for Infiltration Tests .....</b>	<b>6-1</b>
6.1 Mini Disk Infiltrimeter Testing and Validation .....	6-1
6.2 Chapter Summary .....	6-4
<b>Chapter 7 Results and Analysis.....</b>	<b>7-1</b>
7.1 Tree Proximity, Infiltration and Maturity .....	7-1
7.1.1 Summary of Collected Field Data.....	7-11
7.2 Modelled Results .....	7-13

7.2.1 6-hour storm Duration.....	7-13
7.2.2 24-hour storm Duration.....	7-16
7.2.3 96-hour storm Duration.....	7-19
7.2.4 Summary of Model Results .....	7-21
7.3 Seasonal Model Projections .....	7-23
7.3.1 Winter Modelled Projections .....	7-23
7.3.2 Summer Modelled Projections.....	7-35
7.3.3 Summary of Modelled Projections .....	7-47
<b>Chapter 8 Discussion .....</b>	<b>8-1</b>
8.1 Aim 1: Determine to what extent tree planting by the Heart of England Forest has influenced infiltration, with reference to tree proximity and tree maturity. ....	8-1
8.1.1 Summary of Aim 1 Findings.....	8-5
8.2 Aim 3: Simulate current and future hydrology from the study site and determine to what extent HofE woodland planting has influenced runoff and flood risk. ....	8-6
8.2.1 Present Day (current) Hydrological Simulations .....	8-7
8.2.2 Modelled Future Impacts of Woodland Planting.....	8-12
8.2.3 Woodland Planting as a Method of NFM .....	8-14
8.2.4 Summary of Aim 3 Findings.....	8-22
<b>Chapter 9 Implications and Recommendations for Stakeholders.....</b>	<b>9-1</b>
9.1 Aim 4: The Implications, Applications and Recommendations of Study Findings ....	9-1
9.1.1 The Heart of England Forest.....	9-1
9.1.2 Woodland and Construction .....	9-2
9.1.3 Woodland Management Practice: Planting, Felling and Woodland Structure .....	9-5
9.1.4 Department for Environment, Food and Rural Affairs (DEFRA) and the Environment Agency .....	9-7
9.1.5 International and Domestic Flood Risk Management Policy and NFM.....	9-12
9.1.6 Summary of Aim 4 Findings.....	9-13
<b>Chapter 10 Conclusion .....</b>	<b>10-1</b>
10.1 Review of Aims and Objectives .....	10-1
10.1.1 Aim 1	10-1
10.1.2 Aim 2	10-2
10.1.3 Aim 3	10-3
10.1.4 Aim 4	10-5
10.2 Contributions to Knowledge .....	10-6
10.3 Limitations and Sources of Uncertainty .....	10-8
10.3.1 Data and Data Collection .....	10-8
10.3.2 Methods and Modelling .....	10-9
10.4 Further Work and Recommendations .....	10-10
<b>Chapter 11 References.....</b>	<b>11-1</b>

**Chapter 12 Appendices .....i**

## LIST OF FIGURES

<u>Figure</u>	<u>Page</u>
Figure 2.1. Channelisation of the River Ravensbourne at Cornmill Gardens, Lewisham, London (European Centre for River Restoration, 2022). .....	2-2
Figure 2.2. Flood walls installed along the River Don, Sheffield (BBC News, 2019).....	2-3
Figure 2.3. River Medlock, Manchester, flowing into a culverted section of watercourse (Geograph, 2015). .....	2-3
Figure 2.4. Leaky/debris dam installed in the Cairn Beck River (Eden Rivers Trust, 2021).	2-7
Figure 2.5. Example vegetation planting (saplings in the this example) (Suffolk Wildlife Trust, 2020) .....	2-7
Figure 2.6. The re-meandering 200 m section of the Cairn Beck River (Eden Rivers Trust, 2021). .....	2-8
Figure 2.7. Example hydrograph representing pre and post NFM discharge (Adapted from Güçlü and Şen 2016).....	2-11
Figure 2.8. Example hydrograph demonstrating the cumulative effects of hydrograph synchronicity on a receiving watercourse (Adapted from Singer and Dunne 2004, Dixon et al. 2016, Rachelle Ngai et al. 2017).....	2-12
Figure 2.9. The effect of hydrograph peak de-synchronisation. Peak time of inflowing watercourses is staggered and overall flow of the receiving watercourse is lower, however over a longer duration (Adapted from Singer and Dunne 2004, Dixon et al. 2016, Rachelle Ngai et al. 2017). .....	2-13
Figure 2.10. NFM methods and their varying locations throughout the upper, middle and lower reaches of a river (Burgess-Gamble et al., 2018).....	2-14
Figure 2.11. Hills to levels area map outlining the permeability and storage of soil throughout the catchment (Peukert et al., 2017).....	2-15
Figure 2.12. Projected impact of conventional fluvial flood risk mitigation measures (left) and NFM methods (right) in response to climate change after installation (Lacob et al., 2014). ..	2-17
Figure 2.13. Changes in winter mean temperature for 2080 for RCP 2.6 (upper row) and RCP 8.5 (lower row) across 10% (column 1), 50% (column2) and 90% (column 3) percentiles (adapted from Lowe et al., 2019).....	2-19
Figure 2.14. Changes in summer mean temperature for 2080 for RCP 2.6 (upper row) and RCP 8.5 (lower row) across 10% (column 1), 50% (column2) and 90% (column 3) percentiles (adapted from Lowe et al., 2019).....	2-20

Figure 2.15. Changes in winter mean precipitation for 2080 for RCP 2.6 (upper row) and RCP 8.5 (lower row) across 10% (column 1), 50% (column2) and 90% (column 3) percentiles (adapted from Lowe et al., 2019).....	2-21
Figure 2.16. Changes in summer mean precipitation for 2080 for RCP 2.6 (upper row) and RCP 8.5 (lower row) across 10% (column 1), 50% (column2) and 90% (column 3) percentiles (adapted from Lowe et al., 2019).....	2-22
Figure 2.17. Schematic diagram of the interaction between trees and hydrological processes (Adapted from Fazio 2012).....	2-26
Figure 2.18. UK Soil Texture Triangle and tabulated soil texture classifications. Note ‘loam’ refers to the matrix comprising of equal parts of each specified separate (adapted from Avery, 1973 and LandIS, 2020).....	2-35
Figure 2.19. Exaggerated a) highly permeable soil comprising of frequent, large, interconnected pore spaces, b) a compressed soil with low permeability comprising of infrequent, smaller, disconnected pores (Adapted from Hornberger et al., 2014).....	2-36
Figure 3.1. The infiltration processes of both a) SRI’s and b) DRI’s.....	3-3
Figure 3.2. The Mini disk infiltrometer with parts labelled (Decagon Devices, 2006; Robichaud et al., 2008) .....	3-6
Figure 4.1. The catchment area of the Arrow and Alne rivers, shown in reference to the UK (Data from Ordnance Survey, 2021, 2022).....	4-3
Figure 4.2. Newly planted area of HofE woodland showing planting populations and walkways. ....	4-4
Figure 4.3. HofE owned grassland area .....	4-5
Figure 4.4. HofE Sernal site, tributary and river Arrow (aerial photography courtesy of Ordnance Survey, 2020). ....	4-6
Figure 4.5. Output catchment following watershed delineation. The study site area is 220 Ha (2.2 km <sup>2</sup> ) (aerial photography courtesy of Ordnance Survey, 2020).....	4-9
Figure 4.6. The Arrow-Alne catchment area, with Sernal study site highlighted (in red), in proximity to Alcester and Redditch (Data from Ordnance Survey, 2021, 2022). ....	4-10
Figure 4.7. Extent of LiDAR data collected by the drone (Boundary data from Ordnance Survey, 2021, 2022).....	4-11
Figure 4.8. Elevation model of the study catchment as a result of merging drone and prior topographical (2 m) data (Data from Environment Agency et al., 2020; Ordnance Survey, 2021, 2022). ....	4-12
Figure 4.9. Process of creating the study site flow direction analysis vector overlay .....	4-13

Figure 4.10. The resultant output of the flow direction analysis described (aerial photography courtesy of Ordnance Survey, 2020). .....	4-14
Figure 4.11. Bedrock and superficial geology of the study area (Geology data from British Geological Survey, 2019). .....	4-15
Figure 5.1. Conceptual methods framework outlining how previous chapters, and the upcoming methodology interlink with the aims and objectives of study. This Figure describes Aim 1 of this stud. Green boxes indicate aims/objectives, and red boxes indicate key processes.....	5-3
Figure 5.2. Conceptual methods framework outlining how previous chapters, and the upcoming methodology interlink with the aims and objectives of study. This Figure describes Aim 2 of this study. Green boxes indicate aims/objectives, and red boxes indicate key processes.....	5-4
Figure 5.3. Conceptual methods framework outlining how previous chapters, and the upcoming methodology interlink with the aims and objectives of study. This Figure describes Aim 3 of this study. Green boxes indicate aims/objectives, and red boxes indicate key processes.....	5-5
Figure 5.4. Conceptual methods framework outlining how previous chapters, and the upcoming methodology interlink with the aims and objectives of study. This Figure describes Aim 4 of this study. Green boxes indicate aims/objectives, and red boxes indicate key processes.....	5-6
Figure 5.5. The research onion model by (Saunders et al., 2019) outlining the layered approach to study design and data collection. ....	5-8
Figure 5.6. Study area showing the tributary, owned HofE woodland and the year areas were planted (plot data was provided by the HofE Forest Charity, aerial photography courtesy of Ordnance Survey, 2020). ....	5-12
Figure 5.7. Species group of wooded areas across the study area (aerial photography courtesy of Ordnance Survey, 2020). ....	5-13
Figure 5.8. Woodland areas, year planted and sample points for sampling (aerial photography courtesy of Ordnance Survey, 2020). ....	5-15
Figure 5.9. Additional 2014 and 2020 sample areas. 2014 is to the southeast of Studley, 2.5 km north of the Spernal site; and 2020 is to the south of Newnham, 6 km southeast of the Spernal (aerial photography courtesy of Ordnance Survey, 2020). ....	5-16
Figure 5.10. MDI measurements in proximity to the sample tree. Black/red crosses indicate measurement location. ....	5-22
Figure 5.11. Overview of MDI sampling locations at 10 and 200 cm proximities. ....	5-24
Figure 5.12. Infiltration sampling method for the control and 2020 sample areas. ....	5-25
Figure 5.13. a) and b) saturation of the 2006 sample site, c) and d) cracking of the 2006 and 2008 sample sites. ....	5-26

Figure 5.14. The methods and processes undertaken to build the hydrological models, leading on from the spatial data collected throughout aforementioned sections. The primary processes are outlined in red, processes relating to aims and objectives are outlined in green. \*indicates accordance with Environment Agency (2008) guidance. .... 5-29

Figure 5.15. Locations of the downstream flow gauge and the rain gauge located at the NextGen (2020) waste treatment plant to the north of the study site (Data from Ordnance Survey, 2020, 2021). .... 5-32

Figure 5.16. 2010\_2 plot before woodland and grassland area calculation (left), and after woodland (10 and 200 cm) and grassland area calculation (right). Tables below indicate the difference in land cover area calculation. .... 5-35

Figure 5.17. The study catchment area after land cover digitisation. Grey = impermeable surface, dark green = woodland, light green = grassland, and blue = water..... 5-36

Figure 5.18. (top) upstream and (bottom) downstream river profile cross-sections in HEC-HMS..... 5-37

Figure 5.19. Final HEC-HMS hydrological model. The brown areas indicate woodland plots, the green areas indicate grassland only plots, the grey areas indicate impermeable surfaces, and the cross-hatched areas represent infiltration sample areas.  denotes a node (subbasin node),  denotes a reach (watercourse reach), and  denotes a junction. .... 5-39

Figure 5.20. Average monthly rainfall and temperature, used to define the sample periods for winter and summer..... 5-46

Figure 5.21. Observed and simulated flow the 24-hour winter calibration event..... 5-50

Figure 5.22. Observed and simulated flow the 72-hour winter calibration event..... 5-51

Figure 5.23. Observed and simulated flow the 96-hour winter calibration event..... 5-51

Figure 5.24. Observed and simulated flow the 120-hour winter calibration event..... 5-52

Figure 5.25. Observed and simulated flow the 24-hour summer calibration event..... 5-53

Figure 5.26. Observed and simulated flow the 72-hour summer calibration event..... 5-54

Figure 5.27. Observed and simulated flow the 96-hour summer calibration event..... 5-54

Figure 5.28. Observed and simulated flow the 120-hour summer calibration event..... 5-55

Figure 5.29. Observed and simulated flow the 24-hour winter validation event..... 5-58

Figure 5.30. Observed and simulated flow the 72-hour winter validation event..... 5-58

Figure 5.31. Observed and simulated flow the 96-hour winter validation event..... 5-59

Figure 5.32. Observed and simulated flow the 120-hour winter validation event..... 5-59

Figure 5.33. Observed and simulated flow the 24-hour summer validation event ..... 5-60

Figure 5.34. Observed and simulated flow the 72-hour summer validation event ..... 5-61

Figure 5.35. Observed and simulated flow the 96-hour summer validation event.....	5-61
Figure 5.36. Observed and simulated flow the 120-hour summer validation event.....	5-62
Figure 5.37. Collected telemetry data for a) summer and b) winter, red line indicates mean flow (taken as baseflow for hydrological modelling) .....	5-68
Figure 6.1. Graphical display of infiltration / duration results from the MDI validation. ....	6-2
Figure 7.1 Comparison of mean infiltration data from 10 and 200 cm proximity throughout summer and winter in a) 2019/2020 and b) 2020/2021. ....	7-2
Figure 7.2. Peak flow and total discharge values for winter and summer 6-hour 50%, 10%, 2% and 1% AEP events over each landcover type.....	7-13
Figure 7.3. Peak flow and total discharge values for winter and summer 24-hour 50%, 10%, 2% and 1% AEP events over each landcover type .....	7-16
Figure 7.4. Peak flow and total discharge values for winter and summer 96-hour 50%, 10%, 2% and 1% AEP events over each landcover type .....	7-19
Figure 7.5. 50% AEP 6-hour peak flow and total discharge ranges winter. Please note the variable y-axis values.....	7-24
Figure 7.6. 10% AEP 6-hour peak flow and total discharge ranges winter. Please note the variable y-axis values.....	7-24
Figure 7.7. 2% AEP 6-hour peak flow and total discharge ranges winter. Please note the variable y-axis values.....	7-25
Figure 7.8. 1% AEP 6-hour peak flow and total discharge ranges winter. Please note the variable y-axis values.....	7-25
Figure 7.9. 50% AEP 24-hour peak flow and total discharge ranges winter. Please note the variable y-axis values.....	7-28
Figure 7.10. 10% AEP 24-hour peak flow and total discharge ranges winter. Please note the variable y-axis values.....	7-28
Figure 7.11. 2% AEP 24-hour peak flow and total discharge ranges winter. Please note the variable y-axis values.....	7-29
Figure 7.12. 1% AEP 24-hour peak flow and total discharge ranges winter. Please note the variable y-axis values.....	7-29
Figure 7.13. 50% AEP 96-hour peak flow and total discharge ranges winter. Please note the variable y-axis values.....	7-32
Figure 7.14. 10% AEP 96-hour peak flow and total discharge ranges winter. Please note the variable y-axis values.....	7-32
Figure 7.15. 2% AEP 96-hour peak flow and total discharge ranges winter. Please note the variable y-axis values.....	7-33

Figure 7.16. 1% AEP 96-hour peak flow and total discharge ranges winter. Please note the variable y-axis values.....	7-33
Figure 7.17. 50% AEP 6-hour peak flow and total discharge ranges summer. Please note the variable y-axis values.....	7-36
Figure 7.18. 10% AEP 6-hour peak flow and total discharge ranges summer. Please note the variable y-axis values.....	7-36
Figure 7.19. 2% AEP 6-hour peak flow and total discharge ranges summer. Please note the variable y-axis values.....	7-37
Figure 7.20. 1% AEP 6-hour peak flow and total discharge ranges summer. Please note the variable y-axis values.....	7-37
Figure 7.21. 50% AEP 24-hour peak flow and total discharge ranges summer. Please note the variable y-axis values.....	7-40
Figure 7.22. 10% AEP 24-hour peak flow and total discharge ranges summer. Please note the variable y-axis values.....	7-40
Figure 7.23. 2% AEP 24-hour peak flow and total discharge ranges summer. Please note the variable y-axis values.....	7-41
Figure 7.24. 1% AEP 24-hour peak flow and total discharge ranges summer. Please note the variable y-axis values.....	7-41
Figure 7.25. 50% AEP 96-hour peak flow and total discharge ranges summer. Please note the variable y-axis values.....	7-43
Figure 7.26. 10% AEP 96-hour peak flow and total discharge ranges summer. Please note the variable y-axis values.....	7-43
Figure 7.27. 2% AEP 96-hour peak flow and total discharge ranges summer. Please note the variable y-axis values.....	7-44
Figure 7.28. 1% AEP 96-hour peak flow and total discharge ranges summer. Please note the variable y-axis values.....	7-44
Figure 8.1. Surface pooling of clay-textured sites. a) 2020, b) 2014, c) 2006 and d) 2012 ..	8-3
Figure 8.2. Saturation of the (a) 2006 and (b)2008 sample sites during winter data collection, (c) cracking of the 2006 and (d) 2008 sample sites in the summer .....	8-10
Figure 8.3. 1:625k superficial geology map of the UK with the Arrow-Alne River catchment highlighted by red circle (British Geological Survey, 2021).....	8-18

## LIST OF TABLES

<u>Table</u>	<u>Page</u>
Table 2.1. Common and alternative acronyms for NFM. ....	2-5
Table 2.2. Definitions and examples of NFM methods implemented across a catchment (adapted from Dadson et al., (2017)). ....	2-9
Table 3.1. Studies utilising single and double ring infiltrometers with application and size noted. ....	3-4
Table 3.2. Mini Disk Infiltrator application, objective, and selected suction. ....	3-8
Table 3.3. Literature uses of HEC-HMS with selected loss (L), transform (T), baseflow (B) and routing (R) models specified. ....	3-17
Table 5.1. Sections in which the primary requirements of the aims and objectives are met.	5-1
Table 5.2. Categories of the research onion with regard to the philosophy, hypothesis and methodology of this study. ....	5-9
Table 5.3. Separate percentiles and UK soil classification of sample site soil textures. ....	5-17
Table 5.4. Sample tree species and sample area for all plots. ....	5-18
Table 5.5. Calibration event timeframes and rainfall volumes for winter and summer storms	5-49
Table 5.6. Validation event timeframes and rainfall volumes for winter and summer storms	5-57
Table 5.7. Mean interception loss from grassland and broadleaf trees. ....	5-65
Table 5.8. Total FEH values before (for winter) and after (for summer) interception loss.	5-66
Table 5.9. Percentage increase for total event rainfall for given timescales. ....	5-69
Table 5.10. Species of sampled woodland. ....	5-71
Table 5.11. Percentage increase for baseflow for specified future year range ....	5-74
Table 5.12. Baseflow values after applying EA uplifts ....	5-75
Table 5.13. Simulations and data used for each. Each simulation was computed for both winter and summer. ....	5-76
Table 6.1. Tabulated results of the MDI validation showing time to infiltrate, infiltration volume and reasons for measurement conclusion. ....	6-2
Table 6.2. 10-minute MDI measurement (columns B) compared to the data displayed in Table 6.1 (columns A). ....	6-3
Table 7.1. Mean infiltration for 10 and 200 cm proximities throughout both winter and summer sample periods. The control site infiltration values are shown here for reference. S.D. refers to the standard deviation of infiltration values, and n indicates the values included in measurement. ....	7-3

Table 7.2. Percent variation in infiltration measurement at 10 cm and 200 cm proximity varying by measurement period .....	7-4
Table 7.3. Overall mean percent difference in infiltration measurements at 10 cm and 200 cm proximity.....	7-4
Table 7.4. Mann-Whitney U test results from comparing equivalent infiltration proximity data from winter and summer .....	7-6
Table 7.5. Sample sites ordered in ascending order based on mean infiltration (ml) in winter and summer at both 10 and 200 cm proximity. n indicates the number of values used to calculate the mean. ....	7-7
Table 7.6. Test criteria, P values and significance levels of Mann-Whitney U testing. Green indicates a significant difference; red indicates a significance level higher than 0.05. ....	7-9
Table 7.7. Sample sites sorted in ascending order of the relationship between infiltration change at 10 cm and 200 cm for winter and summer.....	7-10
Table 7.8. Peak flow, time to peak and total discharge for winter and summer 6-hour 50%, 10%, 2% and 1% AEP events over HofE, impermeable and grassland land cover.....	7-14
Table 7.9. Peak flow, time to peak and total discharge for winter and summer 24-hour 50%, 10%, 2% and 1% AEP events over HofE, impermeable and grassland land cover.....	7-17
Table 7.10. Peak flow, time to peak and total discharge for winter and summer 50%, 10%, 2% and 1% AEP events over HofE, impermeable and grassland land cover. ....	7-20

## LIST OF ABBREVIATIONS

<b>AEP</b>	Annual Exceedance Probability
<b>BGS</b>	British Geological Survey
<b>DEFRA</b>	Department of Environment Food and Rural Affairs
<b>DEM</b>	Digital Elevation Model
<b>DRI</b>	Double Ring Infiltrometer
<b>DTM</b>	Digital Terrain Model
<b>EA</b>	Environment Agency
<b>ELMS</b>	Environmental Land Management Scheme
<b>FEH</b>	Flood Estimation Handbook
<b>FRM</b>	Flood Risk Management
<b>GIS</b>	Geographic Information Systems
<b>GPR</b>	Ground Penetrating Radar
<b>GPS</b>	Global Positioning System
<b>HEC-HMS</b>	Hydraulic Engineering Centre's Hydrological Modelling System
<b>HofE</b>	Heart of England
<b>LiDAR</b>	Light Detection and Ranging
<b>MDI</b>	Mini Disk Infiltrometer
<b>MDPI</b>	Multidisciplinary Digital Publishing Institute
<b>NFM</b>	Natural Flood Management
<b>NPPF</b>	National Planning Policy Framework (2021)
<b>NSE</b>	Nash and Sutcliffe Efficiency
<b>NVC</b>	National Vegetation Classification
<b>OS</b>	Ordnance Survey
<b>RMSE</b>	Root Mean Square Error
<b>SRI</b>	Single Ring Infiltrometer
<b>SuDS</b>	Sustainable Drainage Systems
<b>UK</b>	United Kingdom
<b>UKCP18</b>	United Kingdom Climate Projections (2018)

## ACKNOWLEDGEMENTS

First and foremost, I would like to thank Dr Craig Lashford for his involvement and encouragement in me undertaking postgraduate research and for his efforts in securing funding and his mentorship throughout this study. Additionally, thanks to Dr Matteo Rubinato and Dr Matthew Blackett for their positions on my supervisory team, and the rounded support and encouragement they provided throughout the course of study. Particular thanks are extended to Matteo for his extensive assistance and expertise in successfully publishing elements of this study in two peer-reviewed academic journals.

I would like to thank Dr Frank Warwick for his continued interest, support and guidance throughout both my undergraduate and postgraduate studies.

I would like to extend thanks to the Heart of England Forest, in particular Stephen Coffey, for his interest, experience and early support in allowing the use of Heart of England owned land for this study.

Thanks are extended to all persons and organisations who supplied data for this project. All are listed in the Appendix of this study (Table B.16). I apologise for any organisations or names omitted from this list.

---

*I would especially like to thank my mum and dad, Angela and Adrian Revell, for their continuous support and belief in me throughout the entirety of both my undergraduate and postgraduate education. Without their encouragement and support (and copious volumes of beer, whisky and summer BBQ's), I truly do not believe that I would be where I am today.*

*For that I am forever grateful.*

xxxxx

---

*I would like to thank my little brother, Hayden Revell, for cramming-in as many snooker sessions as possible with me, within the confines of us both being at home at the same time and COVID not ruining the fun (not to mention the pub crawls).*

*Cheers mate!!*

xxxxx

---

*Lastly, but never least, I would like to thank my beautiful fiancé, Hannah Gregory. You have been my rock throughout the entirety of my PhD, anchored me to reality, and accompanied me through my spontaneous 'sympathy' take-aways and pub trips!! Through three lockdowns and a house-move, you have remained continually supportive, always encouraging me to follow my passion and be the best I can be. I will never forget all you have done for me*

*Hannah.*

*All my love, always and forever. Nathaniel*

xxxxxxx

## Chapter 1 Introduction

Flooding is the most frequently occurring natural hazard resulting in the loss of life, damages to public infrastructure, and personal property (Bosseler *et al.*, 2021; The World Health Organisation, 2021). Urbanisation and the replacement of permeable and vegetated surfaces to impermeable surfaces, such as asphalt and concrete, is reducing lag times to and increasing peak flows in receiving watercourses, influencing the likelihood and severity of high-flow or flooding events (Ferguson and Fenner, 2020a; Ellis *et al.*, 2021). In the UK, flooding frequently draws public attention, more-so in recent years due to increased public interest and understanding regarding the influences of climate change, and the likely changes in the frequency and severity of heavy rainfall and flooding (Taylor *et al.*, 2014; Lamond *et al.*, 2015; Beddoes *et al.*, 2018; Whitmarsh and Capstick, 2018; Hasan and Kumar, 2019; Lowe *et al.*, 2019).

The global climate is predicted to change in ways unseen in recorded history (Lowe *et al.*, 2019). In the UK, sea levels will rise, extreme weather events will become more frequent, winters will become warmer and wetter and summers will become hotter and drier (Lowe *et al.*, 2019; Murphy *et al.*, 2021). The effects of a changing climate are increasingly observed across the world. Studies show that in the US, an average of 6520 floods have occurred per year from 1996–2016, totalling mean economic losses of 3986 million US dollars (Zhou *et al.*, 2018b; Bosseler *et al.*, 2021). Furthermore, widespread flooding occurred in Western Germany throughout the summer of 2021 as a result of heavy rainfall, causing loss of life and affecting the livelihoods of 40,000 people (Bosseler *et al.*, 2021). In the UK, areas of London experienced severe flooding throughout July 2021. On the 12<sup>th</sup>, close to 76 mm of rain fell in 90 minutes in Kensington and Chelsea and Kew (south-west London) received nearly 48 mm in one hour (the average monthly rainfall is 44.5mm) (JBA Risk Management, 2021). On the 17<sup>th</sup>, Portobello Road received 76 mm of rainfall in 90 minutes, and on the 25<sup>th</sup> July, southern

areas of England were severely affected by rainfall; where 48.5 mm of rain fell on areas of Kent in one hour, and the Isle of Wight, received around 38.5 mm (JBA Risk Management, 2021). The London floods were heavily publicised in comparison to previous UK floods, bringing both climate change and flooding to the forefront of the public agenda; prompting both the Mayor of London and the UK Government to target the challenges of increased flood risk (Mayor of London, 2021).

### **1.1 The UK and Flood Risk Management**

The 2007 UK summer floods, which killed 13 people, caused an estimated £3.2 billion in damages and flooded 55,000 properties, prompted the drafting of the Pitt Review (Pitt, 2008; Chatterton *et al.*, 2010). The review investigated the shortfalls of flood response at the time, and made 92 recommendations to be implemented over a 25-year period focusing on improving the way flood risk is mitigated and managed (HM Government, 2009; Warwick, 2017). Recommendation 27 and sections 7.101 – 7.127 of the review suggested that responsible authorities should seek to work with nature wherever possible, emphasising the benefits that this can have considering climate change and in comparison with conventional methods (section 2.1) (Pitt, 2008). The review acknowledged that flood risk cannot be managed by simply building ever bigger concrete defences, and softer approaches, such as flood storage and land management, can offer more sustainable ways of mitigating flood risk (Defra, 2010; McLean *et al.*, 2013). Consequently, the UK pledged to increased investment in alternative, more sustainable methods of mitigating and managing flood risk (Metcalf *et al.*, 2018; Shuttleworth *et al.*, 2019; Ferguson and Fenner, 2020a); commonly referred to as Natural Flood Management, or NFM methods (Burgess-Gamble *et al.*, 2018).

At present (2022), the UK is 14 years into the 25-year implementation time of Pitt Review recommendations. Granted, more recent ‘NFM relevant’ documentation has been published by the EA and UK Government, such as the ‘Working with Natural Processes: Evidence Directory

and Literature review (Ngai *et al.*, 2017; Burgess-Gamble *et al.*, 2018) (see section 2.2); however, NFM uptake and implementation has generally been slow (Waylen *et al.*, 2018; Wells *et al.*, 2020) (see section 2.4). One method of NFM that is often considered beneficial is tree planting - trees can enhance soil macro-porosity, connect flow pathways, reduce compaction and improve soil structure which increases infiltration and water storage capacity (see section 2.3) (Chandler *et al.*, 2018; Leung *et al.*, 2018; Malik *et al.*, 2019; Zhang *et al.*, 2019a; Xie *et al.*, 2020; Guo *et al.*, 2021). There has been a recent policy push towards increasing UK woodland cover – the '25-year Environmental Plan' was introduced in 2018, recommending the increase in woodland planting; and the 'England Trees Action Plan 2021 – 2024' was introduced in 2021 to increase woodland cover for the benefit of CO<sub>2</sub> sequestration, flood risk and biodiversity (HM Government, 2018; UK Government, 2021a). These policies interlink with the scope and outcomes of the most recent (2021) Conference of the Parties (COP26) meeting and are discussed in greater detail throughout section 2.4.

However, regardless of the general push towards woodland planting, particularly for the benefit of CO<sub>2</sub> sequestration and biodiversity, little research has been undertaken to quantify the benefits of tree planting and their influence on infiltration dependent on tree proximity and maturity (Waylen *et al.*, 2018; Kay *et al.*, 2019; Cooper *et al.*, 2021; Murphy *et al.*, 2021; Xiao *et al.*, 2021). Developing an understanding of the influences of tree planting on infiltration and applying such findings in the context of the wider implementation of NFM and existing policy, would aid in the justification and subsequent uptake of NFM methods (McLean *et al.*, 2013; Burgess-Gamble *et al.*, 2018). This would allow for enhanced flood risk reduction both at present, and in the future, considering the predicted impacts of climate change and continued urbanisation.

## **1.2 Flood Modelling**

Advancements in computing have allowed for the development and refinement of flood modelling software, and such software is commonly utilised by practitioners and academics alike to simulate the likely response of an area to varying input data (Barthélémy *et al.*, 2018; Li *et al.*, 2020). Flood models can be hydraulic, where flow is simulated in 1 dimension (1-D), 2 dimensions (2-D), or both (1-D/2-D); or hydrological, where the portrayal of many other ‘process models’ can be applied to a whole catchment, accounting for hydrological losses (section 3.2) (Barthélémy *et al.*, 2018; Patil *et al.*, 2019).

It is identified in section 1.1 that tree planting and the influence of infiltration depending on proximity and maturity is scarcely investigated, as is the case with NFM in general (Wells *et al.*, 2020). Both hydraulic and hydrological models have been used to simulate the impacts of NFM instillations (Ferguson and Fenner, 2020a; Cooper *et al.*, 2021; Lo *et al.*, 2021), however, no studies have attempted to simulate the influence of tree planting on infiltration using a hydrological model, based on empirical infiltration data (Revell *et al.*, 2021). This gap in literature (discussed in greater detail throughout section 2.4), combined with the pressures of climate change and continued urbanisation, form the aims and objectives of this study outlined below.

## **1.3 Aims & Objectives**

Following the (above) discussed changes in flood frequency and flood severity, the lack of empirical hydrological modelling studies, the push towards woodland planting, and the current lack of supporting literature regarding NFM implementation, the aims and objectives of this work are:

***Aim 1: Through field investigation, determine to what extent tree planting by the Heart of England Forest has influenced infiltration, with reference to tree proximity and tree maturity.***

Whilst it is understood that tree planting can increase soil porosity, increasing infiltration and water storage capacity (sections 2.3 and 2.4); few long-term studies have been undertaken to record the influence of tree planting on infiltration dependent on tree proximity and maturity. UK tree planting studies exist (section 2.4), however the influence of infiltration is inferred through other means (telemetry, rainfall/runoff analysis). This aim intends to target this literature gap and contribute to what is understood about tree planting and infiltration and maturity using the Heart of England Forest (HofE) Spernal site.

*Objective 1a: Define suitable sampling locations and methods for infiltration data collection and gather data.*

The objective intended to use spatial data to define a suitable sample site wherein infiltration data could be collected continually for the duration of the study.

*Objective 1b: Using data collected in objective 1a, derive any relationships between infiltration and tree proximity and maturity.*

Upon the definition of infiltration sample locations (objective 1a), the collected data was statistically analysed to determine any relationships between infiltration relative to tree proximity and tree maturity.

***Aim 2: Using HEC-HMS, build, calibrate, and validate two-separate hydrological models using spatial and hydrometric data collected from the study site.***

Following infiltration data collection (objective 1b), a hydrological model was built, calibrated, and validated to simulate the hydrological response from the study site. The goal of the model was to identify the impact of tree planting, when compared to simulating an impermeable study or grassland area. This aim allowed the application of the collected long-term infiltration data, allowing for a better interpretation of the benefits of tree planting.

*Objective 2a: Build, calibrate and validate two hydrological models in HEC-HMS.*

Two hydrological models were built, one to represent summer infiltration and one to represent winter infiltration; this was due to the collected data showing large fluctuations between the seasons. Representing these changes in one model would inaccurately portray the hydrology of the site. Both models were individually calibrated and validated using the Nash and Sutcliffe Efficiency (NSE) indicator.

*Aim 3: Using the HEC-HMS model, simulate outflow hydrology from the study site dependent on changing storm intensity, duration, land cover, tree maturity and climate change; and determine to what extent HofE woodland planting has influenced infiltration, runoff and river flows.*

Aim 3 required the combination of both aim 1 and aim 2 to produce hydrological outputs from the site as a result of varying storm scenarios, tree maturity and climate change. The aim intended to conclude the overall applicability of woodland planting as a method of natural flood management (NFM) and determine the longevity of impact considering recent climate change predictions.

*Objective 3a: Using both field data collected in aim 1a, and the HEC-HMS model, simulate the hydrological responses of the HofE study site to varying land cover, tree maturity, storm duration and intensity.*

This objective combined the collected infiltration data and the two hydrological models to simulate the hydrological response from the study site at present. Infiltration data was used to simulate the hydrological response from the HofE site: with the current level of woodland cover, if the site was comprised of only grassland, and if the site was developed into impermeable surfaces.

*Objective 3b: Use recent Environment Agency climate change allowances, in conjunction with the HEC-HMS model, to predict the likely future changes to site hydrology considering developing tree maturity and climate change.*

This objective used published literature regarding root spread and sample tree species growth trends to extrapolate the collected infiltration data into the future. The hydrological models were then used to simulate precipitation and baseflow changes as a result of climate change, and the hydrological output of the site was analysed.

*Objective 3c: Using the empirical and simulated results of this study, evaluate the hydrological effects of tree planting as a method of NFM.*

This objective combined objectives 1b, 3a and 3b to contextualise their findings, and draw conclusions regarding the wider applicability of woodland planting as a method of NFM, both at present and into the future.

*Aim 4: Assess the implications of study findings, and provide recommendations and suggestions for relevant stakeholders and future policy.*

This aim combines the findings of both aim 1 and aim 3 to assess the implications of study results with regards to flood risk management policy, both past and future. The aim also intends to make suggestions to stakeholders, and suggest potential areas of exploration for NFM in the future, regarding climate change.

*Objective 4a: Using the findings of both aim 1 and aim 3, provide recommendations and suggestions for relevant stakeholders and future policy.*

This objective uses the findings derived throughout the field data collection stages and hydrological simulation stages of this study to assess their implications, and provide any recommendations for relevant stakeholders regarding future flood risk management policy.

#### ***1.4 Structure of Thesis***

The thesis is organised as follows:

**Chapter one**, introduction, introduces the subject area, along with the key overarching background, themes, and motivations for this work. The aims and objectives are defined in the is section.

**Chapter two**, literature review, reviews the current level of understanding regarding conventional flood risk management, natural flood management, tree planting, tree planting as a method of natural flood management, and the influences of varying soil characteristics on infiltration.

**Chapter three**, review of previous studies methods and tools, discusses commonly used methods of infiltration data collection and hydraulic and hydrological modelling software; model calibration and validation are discussed, and modelling limitations are outlined.

**Chapter four**, Study Site, discusses the rationale for study site selection, highlights the desired requirements, and explains the reasoning for choosing the selected site. further study site investigation is undertaken including watershed delineation, topographical analysis, hydrological analysis and geological analysis.

**Chapter five**, research design and methodology, introduces and evaluates the study methodology. Research philosophy is introduced as are the study hypotheses, in addition to the sampling methodology and the processes used in sample site design, the processes involved in hydrological model build, and the processes and results of model calibration, validation and simulation.

**Chapter six**, pilot results and reflection for infiltration tests, describes the process of adjusting the MDI user manual's suggestion of 30-40 ml of infiltrated water per measurement. Also discussed here is how this pilot was upscaled to the whole catchment.

**Chapter seven**, results and analysis, presents and interprets the results of the study. Filed infiltration results are statistically analysed with regard to proximity and maturity, and results

from both the present-day and projected hydrological models and interpreted for both summer and winter.

**Chapter eight**, discussion, contextualises the results presented throughout chapter seven considering the wider literature and the aims of this project, emphasising the findings and applications of this work.

**Chapter nine**, implications and recommendations for stakeholders, discusses the implications of the study results with regards to the HofE forest, the forestry industry, the construction industry, and DEFRA policy.

**Chapter ten**, conclusion, summarises the main research findings and reviews how and where the aims and objectives (section 1.3) were met. The contributions to knowledge are identified, as are any sources of error and opportunities for future work.

**Chapter eleven**, references, presents the reference list of citations referred to throughout the main body.

**Chapter twelve**, appendices, contains additional explanations, technical information, figures, and graphs in support/addition to the work included throughout the main body.

## Chapter 2 Literature Review

This section reviews the current level of understanding regarding conventional flood risk management (section 2.1), natural flood management (section 2.2), tree planting (section 2.3), tree planting as a method of natural flood management (section 2.4) and the influences of varying soil characteristics on infiltration (section 2.5).

### **2.1 Conventional Flood Management**

As outlined in section 1.1, changes to flood frequency severity, in conjunction with the uptake of Pitt Review (2008) recommendations, are changing the way flood risk is managed in the UK (Putro *et al.*, 2016; Miller and Hess, 2017). Natural and more sustainable methods of fluvial flood risk management (FRM) should now be considered by responsible authorities for implementation whenever possible, to encourage a movement away from conventional methods due to their decreasing sustainability (Environment Agency, 2007; Ngai *et al.*, 2017; Warwick, 2017).

Historically, the priority of conventional FRM methods has been to convey excess water downstream and away from urban areas as quickly as possible to prevent flooding (Cooper *et al.*, 2021). However, methods of this focus are problematic and are becoming increasingly unfeasible considering climate change - rainfall events are becoming more frequent and more severe, pushing conventional FRM methods beyond their designed capabilities (Lowe *et al.*, 2019; Murphy *et al.*, 2021). Conventional methods of FRM are designed to mitigate flood risk based on designed storm scenarios, meaning they become less effective over time (Lacob *et al.*, 2014). Therefore, infrastructure that was designed to mitigate (e.g.) 2% AEP (annual exceedance probability) storms (such as dams, levees and flood walls) are seeing more frequent strain than accounted for when designed (Lacob *et al.*, 2014; Ferguson and Fenner, 2020a). Common examples of conventional FRM include straightening river channels (channelisation)

(Figure 2.1), constructing higher levees and flood walls (Figure 2.2), and culverting long reaches of a watercourse (Figure 2.3).

This item has been removed due to 3rd Party Copyright. The unabridged version of the thesis can be found in the Lanchester Library, Coventry University.

*Figure 2.1. Channelisation of the River Ravensbourne at Cornmill Gardens, Lewisham, London (European Centre for River Restoration, 2022).*

This item has been removed due to 3rd Party Copyright. The unabridged version of the thesis can be found in the Lanchester Library, Coventry University.

*Figure 2.2. Flood walls installed along the River Don, Sheffield (BBC News, 2019).*

This item has been removed due to 3rd Party Copyright. The unabridged version of the thesis can be found in the Lanchester Library, Coventry University.

*Figure 2.3. River Medlock, Manchester, flowing into a culverted section of watercourse (Geograph, 2015).*

All of the aforementioned methods increase the velocity of contained water, increase erosion, and culverts reduce the capacity of a watercourse resulting in backflow during flood events (Butler and Davies, 2011; Hohensinner *et al.*, 2018; Cooper *et al.*, 2021). Additionally, they

are expensive to install and maintain, and are only implemented at a few targeted locations throughout a catchment (i.e. around urban areas or high-value assets), meaning flood protection varies from location to location based on asset value and local priorities (Merz *et al.*, 2010; Bracken *et al.*, 2016; Ngai *et al.*, 2017).

## **2.2 Natural Flood Management**

Increasing flood frequency and a general increase in public awareness has prompted a literature-wide shift towards alternative methods of managing and mitigating flood risk (Chapter 1)(Lavers and Charlesworth, 2016, 2018). The emerging method of alternative flood risk management in the UK is most commonly referred to as NFM, however several acronyms are used interchangeably within the literature (Forbes *et al.*, 2016; Lavers and Charlesworth, 2016, 2018; Environment Agency, 2017; West Cumbria Rivers Trust, 2018). See Table 2.1.

Table 2.1. Common and alternative acronyms for NFM.

Acronym	Definition	References
CaBA	Catchment Based Approach	(Dadson <i>et al.</i> , 2017; CaBA, 2022)
GI	Green Infrastructure	(European Commission, 2022; Lashford <i>et al.</i> , 2022)
NNBF	Natural and Nature Based Features	(Bridges <i>et al.</i> , 2021)
NFM	Natural Flood Management	(Forbes <i>et al.</i> , 2016; CBEC and Environment Agency, 2017)
NFRM	Natural Flood Risk Management	(Lavers and Charlesworth, 2016)
NWRM	Natural Water Retention Measures	(European Commission, 2014; Collentine and Futter, 2018)
NBS	Nature Based Solutions	(Short <i>et al.</i> , 2019; Bark <i>et al.</i> , 2021; Norbury <i>et al.</i> , 2021)
RSuDS	Rural Sustainable Drainage Systems	(Avery, 2012)
WwNP	Working with Natural Processes	(Ngai <i>et al.</i> , 2017; Burgess-Gamble <i>et al.</i> , 2018; Hankin <i>et al.</i> , 2018)

NFM methods aim to alter specific hydrological processes (e.g. interception, infiltration, evaporation, evapotranspiration and surface roughness) to store precipitation throughout the catchment, reducing the speed and intensity at which runoff can enter the receiving watercourse (Lavers and Charlesworth, 2018; Shuttleworth *et al.*, 2019; Ferguson and Fenner, 2020b; Ellis *et al.*, 2021). In addition to the ‘catchment’ methods discussed, in-channel methods of NFM aid in slowing watercourse flow. Debris (leaky) dams consist of wood and other vegetation placed adjacent to the flow direction of a watercourse to naturally impede flow, store water and restore rivers (Burgess-Gamble *et al.*, 2018; Hankin *et al.*, 2018; Ellis *et al.*, 2021) (Figure 2.4). Watercourse channels and floodplains can also be ‘roughened’ to slow the flow of flood waters to downstream areas during flood events (Shuttleworth *et al.*, 2019). Roughening involves planting trees, grasses, shrubs and hedgerows in floodplain areas to increase friction (Manning’s *n*) and create more turbulent flow throughout flood waters, leading to a slowing of the flow downstream (Kim *et al.*, 2012; Shuttleworth *et al.*, 2019) (Figure 2.5). Furthermore, river flow path length can be slowly reinstated naturally, through placing obstructions in defined locations of the flow path to develop meanders (re-meandering), which has additional benefits regarding wildlife (Burgess-Gamble *et al.*, 2018; Dittrich *et al.*, 2019). Whilst this method could be seen as human-induced, the processes that influence the lengthening process are natural and representative of the river geomorphology before human influence (Brookes, 1987; Glińska-Lewczuk and Burandt, 2011) (Figure 2.6).

This item has been removed due to 3rd Party Copyright. The unabridged version of the thesis can be found in the Lanchester Library, Coventry University.

*Figure 2.4. Leaky/debris dam installed in the Cairn Beck River (Eden Rivers Trust, 2021).*

This item has been removed due to 3rd Party Copyright. The unabridged version of the thesis can be found in the Lanchester Library, Coventry University.

*Figure 2.5. Example vegetation planting (saplings in the this example) (Suffolk Wildlife Trust, 2020)*

*Figure 2.6. The re-meandering 200 m section of the Cairn Beck River (Eden Rivers Trust, 2021).*

The design and operation of any NFM feature is based primarily on emulating the natural environment. Methods focus on slowing water using sustainable catchment wide interventions and in-channel obstructions, to reproduce the watercourses natural hydrology as it was prior to human interaction (Environment Agency, 2010; Hankin *et al.*, 2017; Ferguson, 2020). Table 2.2 (adapted from Dadson *et al.*, (2017)) outlines further methods of NFM commonly implemented across a catchment.

Table 2.2. Definitions and examples of NFM methods implemented across a catchment  
(adapted from Dadson et al., (2017)).

Flood Risk Management Theme	Specific Method	Examples
Catchment water retention through infiltration and overland flow management	Land-use changes	Arable to grassland conversion, afforestation, restrictions on hillslope cropping, peatland restoration
	Arable land-use practices	Spring cropping Vs. winter cropping, cover crops, extensification, set aside
	Livestock land practices	Lower stocking rates, grazing restrictions
	Tillage practices	Conservation tillage, contour/cross-slope ploughing
	Field drainage	Deep cultivations to reduce permeability
	Buffer zones	Contour grass planting, hedges, shelterbelts
	Machinery management	Low ground pressure, avoid wet conditions,
	Urban land use	Reduce impermeable land-cover and increase storage
Catchment water retention through managing connectivity and conveyance	Management of hillslope connectivity	Blockage of farm ditches and grips
	Buffer strips	Contour grass strips, hedges, shelterbelts, bunds, field margins, riparian buffer strips
	Channel maintenance	Modifications to maintenance of farm ditches
	Drainage and pumping operation	Modifications to drainage and pumping regimes
	Field and farm structures	Modifications to gates, yards, tracks and culverts
	On-farm retention	Retention ponds and ditches

	River restoration	Restoration of river profile and cross sections, channel realignment and changes to planform pattern
	Upland water retention	Farm ponds, ditches, wetlands
Making space for water through floodplain conveyance and storage	Water storage areas	On or off-line storage, washlands, polders, impoundment reservoir
	Wetlands	Wetland creation, engineered storage scrapes, controlled water levels
	River restoration / retraining	River re-profiling, channel works, riparian works
	River and watercourse management	Vegetation clearance, channel maintenance and riparian works
	Floodplain restoration	Setback of embankments, reconnection rivers and floodplains

The hydrological influence of NFM methods compared with FRM methods on a catchments hydrologic response is clearly demonstrated through use of a unit hydrograph. The shape of a hydrograph is influenced by the physical characteristics of the catchment- its size, topography, geology, land cover type, and features linked to the climate (Butler and Davies, 2011; Hornberger *et al.*, 2014). A hydrograph representing a catchment that was inclusive of the conventional FRM methods discussed would exhibit steep rising and falling limbs, a short lag time and a quick return to baseflow (Shaw, 1988; Hornberger *et al.*, 2014), representing that precipitation is falling on the area but quickly being conveyed to the watercourse. Conversely, the introduction of NFM methods across a catchment gradually reinstates the ‘pre-urbanised’ hydrology of the catchment, modifying the discharge hydrograph (Wingfield *et al.*, 2019; Stamataki and Kjeldsen, 2021). A hydrograph representing an area inclusive of NFM would exhibit a lower peak flow and shallower rising and falling limbs, showing that precipitation slowly moves through the catchment, contrary to that of conventional methods (Thomas and Nisbet, 2016; Janes *et al.*, 2017). See Figure 2.7.

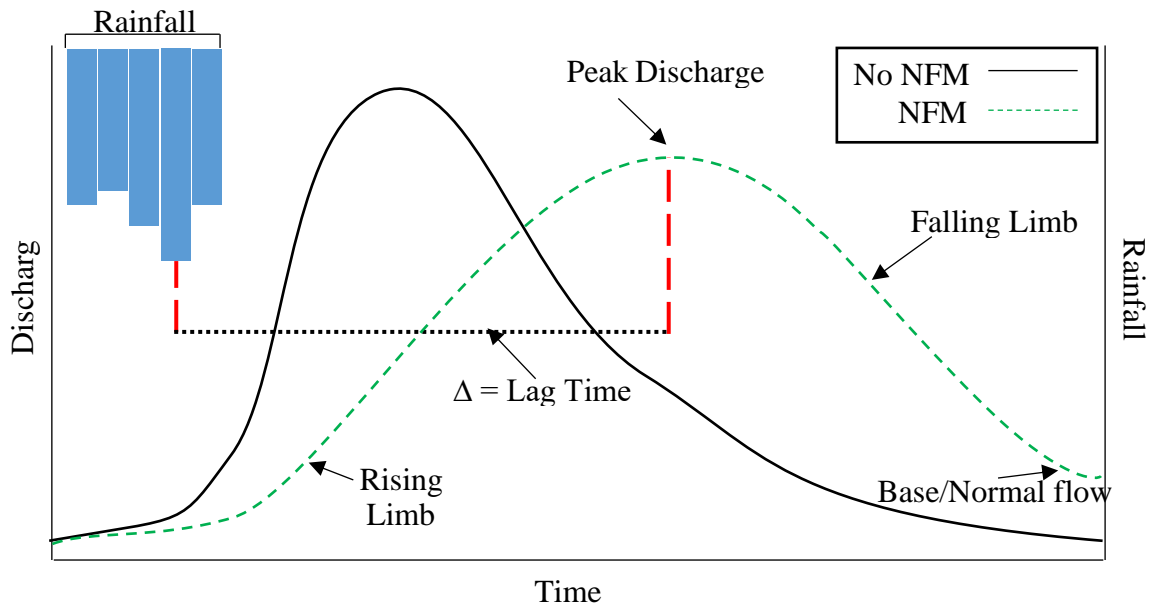


Figure 2.7. Example hydrograph representing pre and post NFM discharge (Adapted from Güçlü and Şen 2016).

Whilst NFM instillations can positively influence catchment hydrology through increasing catchment storage, infiltration, interception and evapotranspiration; there is reference in the literature to the potential for hydrograph synchronisation (Dixon *et al.*, 2016; Forbes *et al.*, 2016; Metcalfe *et al.*, 2017a; Hankin *et al.*, 2019; Shuttleworth *et al.*, 2019). Synchronisation refers to slowing catchment flow such that the post-intervention lag time matches that of the receiving watercourse, subsequently adding to the leading to the passing flood wave. See Figure 2.8

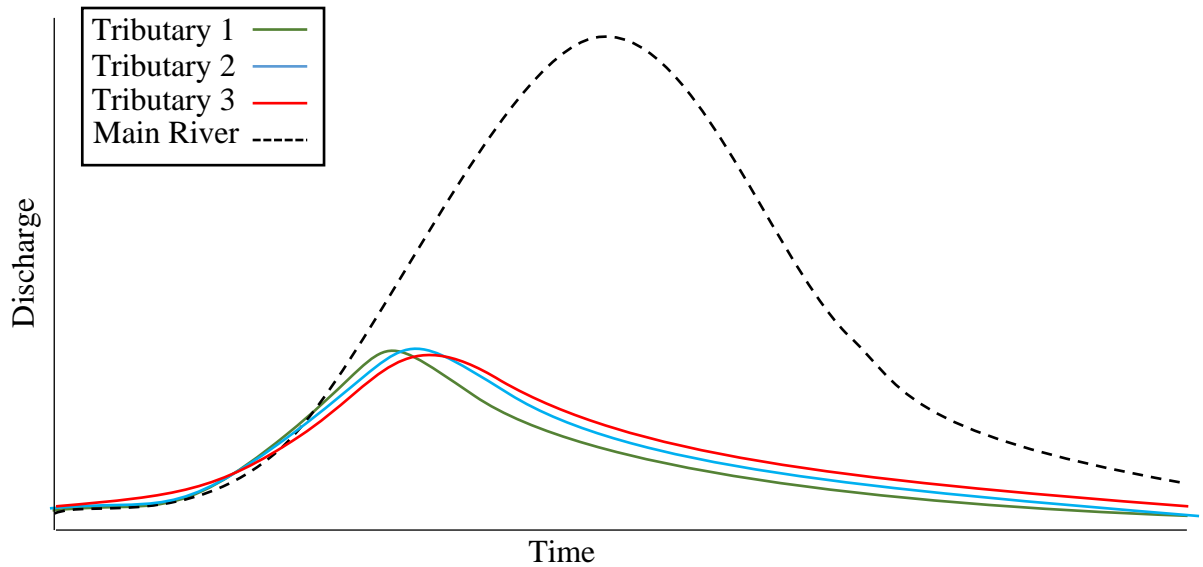
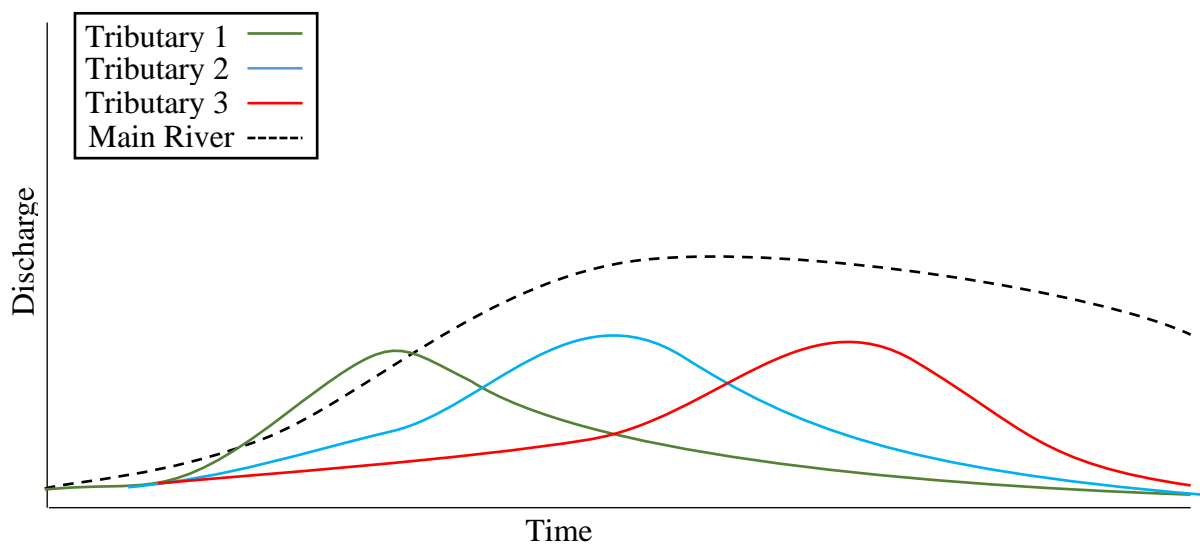


Figure 2.8. Example hydrograph demonstrating the cumulative effects of hydrograph synchronicity on a receiving watercourse (Adapted from Singer and Dunne 2004, Dixon *et al.* 2016, Rachelle Ngai *et al.* 2017)

Whilst there is a general acknowledgement to the process of synchronisation, the process is not well understood (Dixon *et al.*, 2016), nor are there any existing empirical studies to prove that NFM interventions cause synchronisation, rather it is cited as something to be aware of (Metcalf *et al.*, 2017a, 2018; Ferguson and Fenner, 2020b). Conversely, it is also suggested that NFM implementation could lead to hydrograph de-synchronisation, where existing synchronised flood waves are actually reduced through the staggered timing of flood waves.

See Figure 2.9



*Figure 2.9. The effect of hydrograph peak de-synchronisation. Peak time of inflowing watercourses is staggered and overall flow of the receiving watercourse is lower, however over a longer duration (Adapted from Singer and Dunne 2004, Dixon et al. 2016, Rachelle Ngai et al. 2017).*

Dixon et al. (2016) suggests that peak discharge could be reduced by as much as 19% over 25 years by afforestation in the Lymington catchment, Hampshire. Shuttleworth *et al.*, (2019) found that peatland re-vegetation (as a method of NFM) could reduce peak flows by 27% and increase lag times by 106%; and Nutt and Perfect (2011) explained that moorland restoration could lead to hydrograph de-synchronisation downstream over time.

Whilst synchronicity can impede the effectiveness of NFM, there is very little empirical literature proving that this phenomena can happen in real-world instances (Odoni and Lane, 2010; Lacob *et al.*, 2014; Burgess-Gamble *et al.*, 2018). Forbes *et al.*, (2016) makes reference to large scale woodland requiring careful planning before implementation; but Shuttleworth *et al.*, (2019) suggests that extreme upper-reach NFM instillations (peat moorland restoration) is not likely to influence synchronicity downstream. It is concluded that synchronicity varies on a case-by-case basis, and NFM implementation requires field work and modelling to assess all potential outcomes for both the short and long term (Pattison *et al.*, 2014; Forbes *et al.*, 2016; Hankin *et al.*, 2018; Shuttleworth *et al.*, 2019).

### 2.2.1 Scale

NFM methods differ from conventional fluvial flood risk methods, not only by the methods employed, but also in scale and location (Hankin *et al.*, 2017; West Cumbria Rivers Trust, 2018; Ferguson and Fenner, 2020a). Dissimilar to conventional methods, which are often implemented in and around urban areas, NFM measures are found to have the most positive impact on downstream flood risk when installed at different locations and scales throughout a catchment (Lacob *et al.*, 2014, 2017; West Cumbria Rivers Trust, 2018). See Figure 2.10.

*Figure 2.10. NFM methods and their varying locations throughout the upper, middle and lower reaches of a river (Burgess-Gamble et al., 2018)*

As initially presented in Table 2.2 and further demonstrated (with regard to their scale) in Figure 2.10, NFM methods in the upland reaches can include: cross-slope tree planting, grip blocking a peat restoration, woodland creation and management, in-channel leaky barriers and runoff pathways. In the middle reaches, can include: short rotation crops, soil and crop management, ponds and swales, river restoration and reprofiling, flow-path lengthening, floodplain woodland and riparian buffers. And in the lower reaches/estuaries, can include: salt marsh creation, beach management, managed realignment and controlled retreat (Forbes *et al.*, 2016; Dadson *et al.*, 2017; Ngai *et al.*, 2017; Burgess-Gamble *et al.*, 2018; West Cumbria Rivers Trust, 2018). The scale and location of NFM methods vary dependent on the availability

and suitability of land, particularly throughout the upland reaches (Figure 2.10) where soil texture, climate and topography have more of an influence (Ngai *et al.*, 2017; Burgess-Gamble *et al.*, 2018). The soil texture and structure, existing vegetation, infiltration rate, infiltration capacity and land-take play an important role in determining which NFM method is best suited (Archer *et al.*, 2013; Forbes *et al.*, 2016).

One example of where NFM has been specifically tailored to local hydrological characteristics is the Hills to Levels project, Somerset (Peukert *et al.*, 2017; Farming and Wildlife Advisory Group, 2020). The catchments geology had very low permeability, meaning precipitation entered nearby watercourses rapidly during rainfall events (discussed in section 2.3). See

Figure 2.11.

This item has been removed due to 3rd Party Copyright. The unabridged version of the thesis can be found in the Lanchester Library, Coventry University.

*Figure 2.11. Hills to levels area map outlining the permeability and storage of soil throughout the catchment (Peukert et al., 2017).*

Freely draining soils cover 30% of the catchment, and it was determined that improving soil structure across the catchment could significantly improve infiltration, adding 150–300 mm of precipitation storage (over a 24-hour period) (Peukert *et al.*, 2017). The methods employed

across the catchment involved: advising farmers on crop rotation to improve soil water storage; installing filter socks, filter fences, soil bunds, swales, banked hedges, silt traps; floodplain storage, leaky ponds; and implementing in-channel methods such as leaky woody dams, brash dams and leaky barriers (Peukert *et al.*, 2017). To date, attenuation features have created almost 15,000 m<sup>3</sup> of floodwater storage alone, and 130 NFM structures have been constructed, with another 105 under construction and a further 85 proposed (Peukert *et al.*, 2017; Farming and Wildlife Advisory Group, 2020).

### 2.2.2 Natural Flood Management and Climate Change

The anthropogenic drivers of climate change are increased carbon dioxide (CO<sub>2</sub>) and other greenhouse gasses; the predicted impacts of climate change are increased precipitation, storm frequency and storm severity (Dittrich *et al.*, 2019; Kay *et al.*, 2019; Lowe *et al.*, 2019; Cooper *et al.*, 2021; Murphy *et al.*, 2021). NFM methods can reduce CO<sub>2</sub> emissions through sequestration, and methods involving vegetation planting can not only store CO<sub>2</sub>, but convert some of it to oxygen (O<sub>2</sub>) in the process (Hankin *et al.*, 2017; Limpert *et al.*, 2020). For example, regarding the influence of trees on CO<sub>2</sub> reduction, Field *et al.*, (2020) estimate that 0.08 Gt of CO<sub>2</sub> is currently stored in UK woodland, and Hale *et al.*, (2019) discuss that older woodland areas contain double the CO<sub>2</sub> of younger trees (~60% stored in biomass). Coniferous woodlands can sequester between 14 and 24 tonnes of CO<sub>2</sub> per Ha/yr. and oak woodlands can sequester between 7 and 15 tonnes of CO<sub>2</sub> per Ha/yr. (Burgess-Gamble *et al.*, 2018). The hydrological implications of woodland are discussed in greater detail throughout section 2.3.

In addition to the aforementioned CO<sub>2</sub> reductions, NFM methods are advantageous as they also act to mitigate flood risk; however, an advantage of conventional FRM methods is that that flood risk reduction begins as soon as installation is complete (Lacob *et al.*, 2014). Whilst some methods of NFM can be mitigating flood risk from the day of installation (e.g. leaky dams and marshlands), methods that involve vegetation planting and land management are often not

immediately effective (Forbes *et al.*, 2016; Ngai *et al.*, 2017). Figure 2.12 demonstrates the differing hydrological impact of conventional FRM methods compared with NFM methods over time.

This item has been removed due to 3rd Party Copyright. The unabridged version of the thesis can be found in the Lanchester Library, Coventry University.

*Figure 2.12. Projected impact of conventional fluvial flood risk mitigation measures (left) and NFM methods (right) in response to climate change after installation (Lacob et al., 2014).*

Conventional FRM methods can reduce flood risk from the day of installation, whereas NFM methods cannot. However, whilst there is a lag before the impacts of NFM methods can be observed; once established, they offer a greater range of potential to mitigate the adversities faced due to climate change (Figure 2.12) (Cooper *et al.*, 2021; Murphy *et al.*, 2021). Quantifying the exact abilities of NFM methods to counter the projected adverse effects of climate change is an ongoing challenge, primarily due to there being a general lack of long-term empirically monitored data and hydrological modelling studies (see section 2.2.3) (Lacob *et al.*, 2014; Lavers and Charlesworth, 2016; Connelly *et al.*, 2020; Murphy *et al.*, 2021). This lack of data is further complicated by future UK climate projections showing precipitation and temperature to be heterogeneous (Lowe *et al.*, 2019).

The United Kingdom Climate Predictions 2018 (UKCP18) are a set of tools used for assessing how the climate is likely to change in the UK, both in-land and the surrounding waters (Lowe

*et al.*, 2019; Kay *et al.*, 2020). Figure 2.13 and Figure 2.14 show the projected changes to mean temperature, and Figure 2.15 and Figure 2.16 show the projected changes to mean precipitation in the 2080's under different representative concentration pathways (RCPs). RCPs (in W m<sup>-2</sup>) are based on the concentrations of greenhouse gases that would result in radiative forcing increasing by 2.6 W (+1.6°C), 4.5 W (+2.4°C), 6.0 W (+2.8°C) and 8.5 W (+4.3°C) by 2100, relative to pre-industrial levels (UK Met Office, 2018; Lowe *et al.*, 2019; The Met Office, 2019). Here, the 10<sup>th</sup>, 50<sup>th</sup> and 90<sup>th</sup> percentile outputs for RCP 2.6 and RCP 8.5 simulations are presented to demonstrate the heterogeneity of climate projections (Lowe *et al.*, 2019; The Met Office, 2019; Kay *et al.*, 2020).

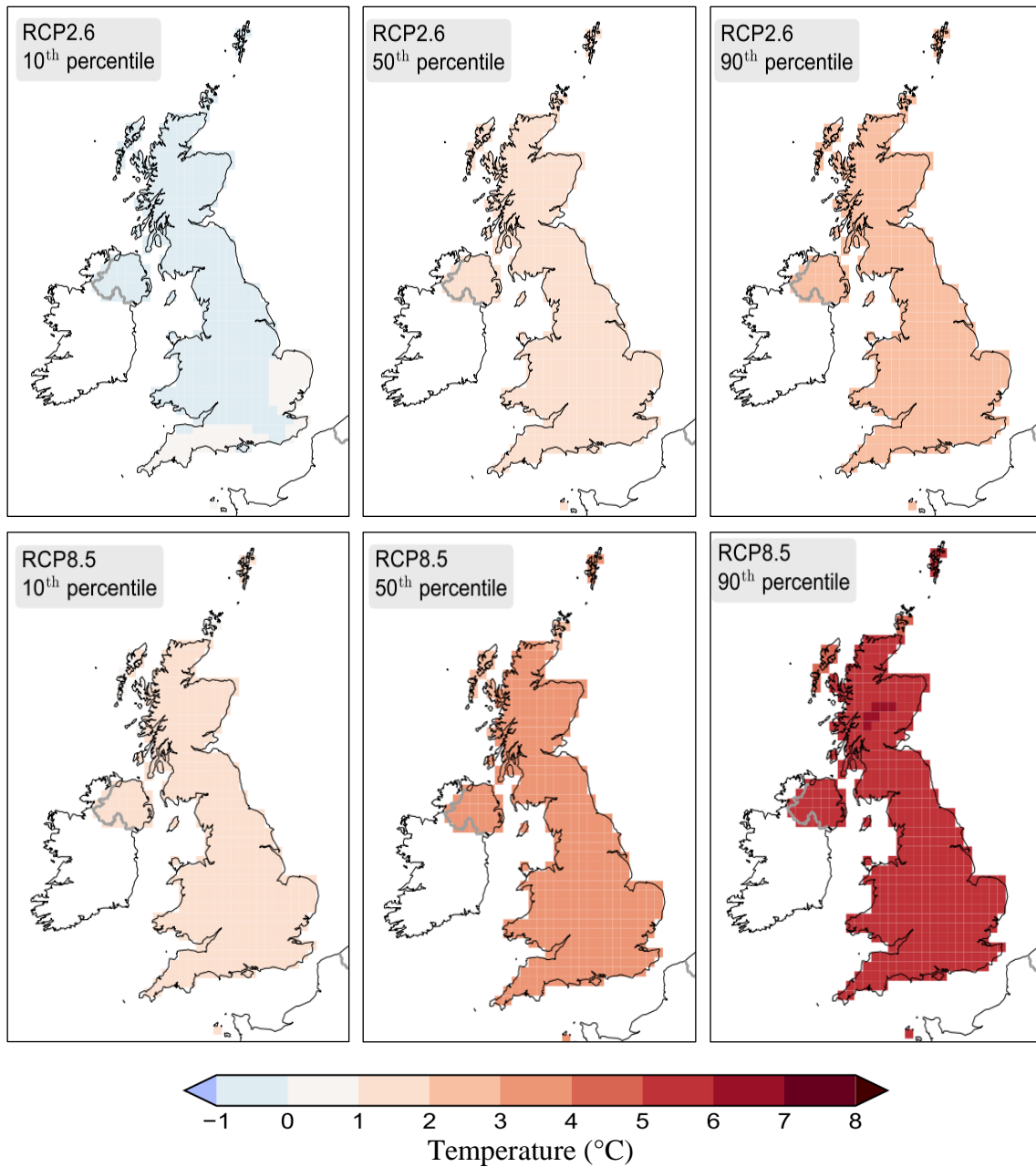


Figure 2.13. Changes in winter mean temperature for 2080 for RCP 2.6 (upper row) and RCP 8.5 (lower row) across 10% (column 1), 50% (column 2) and 90% (column 3) percentiles (adapted from Lowe et al., 2019).

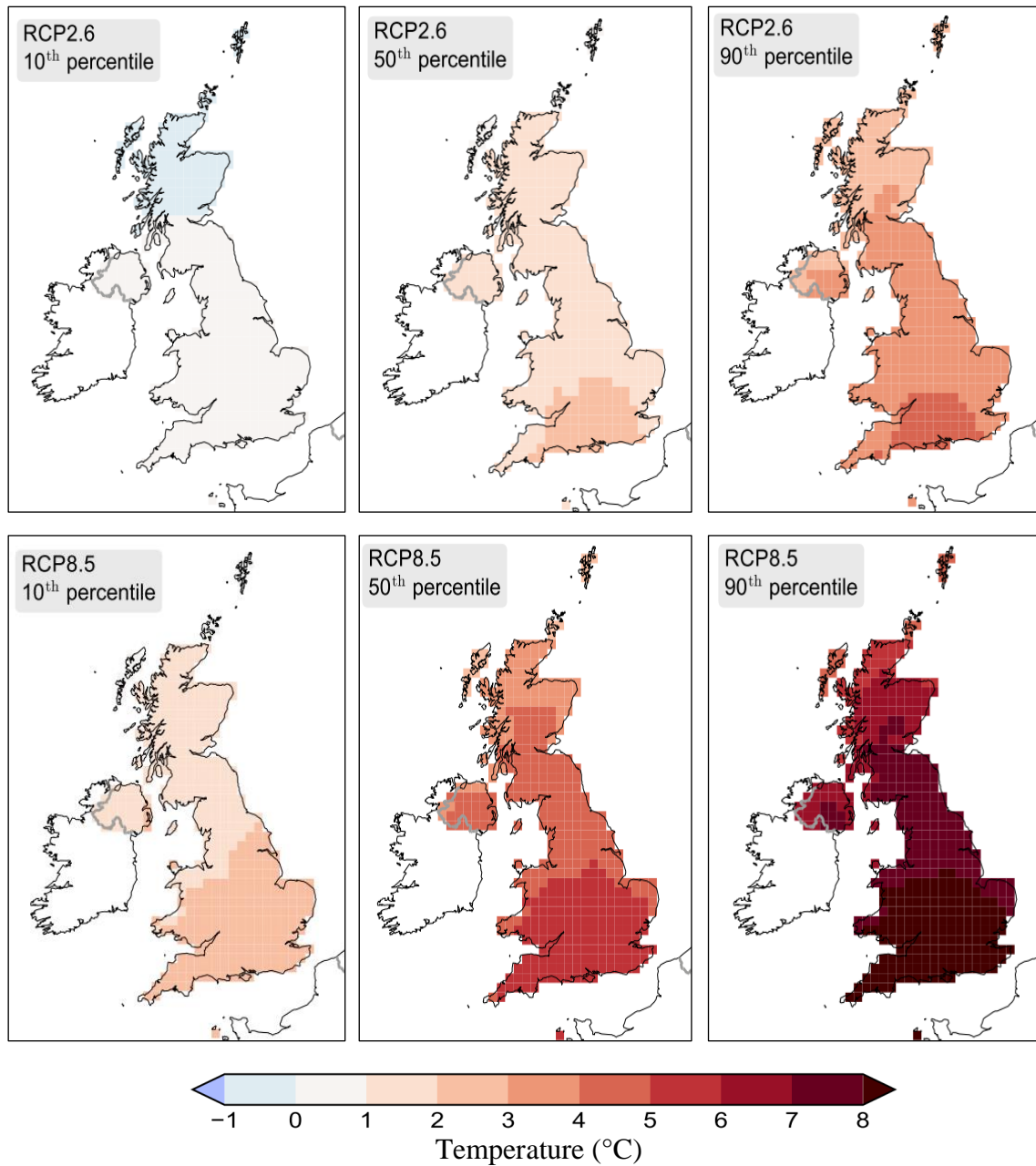
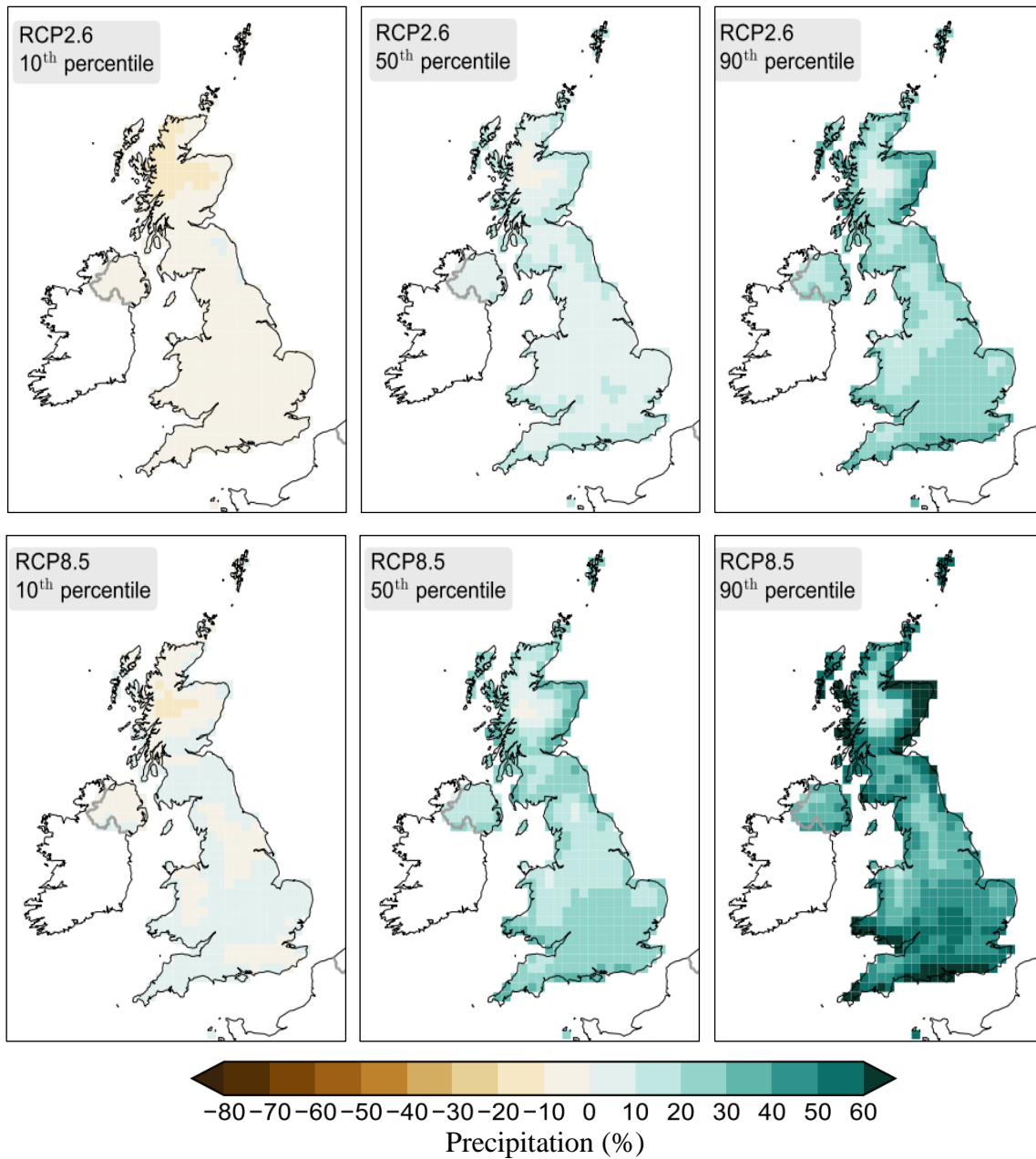
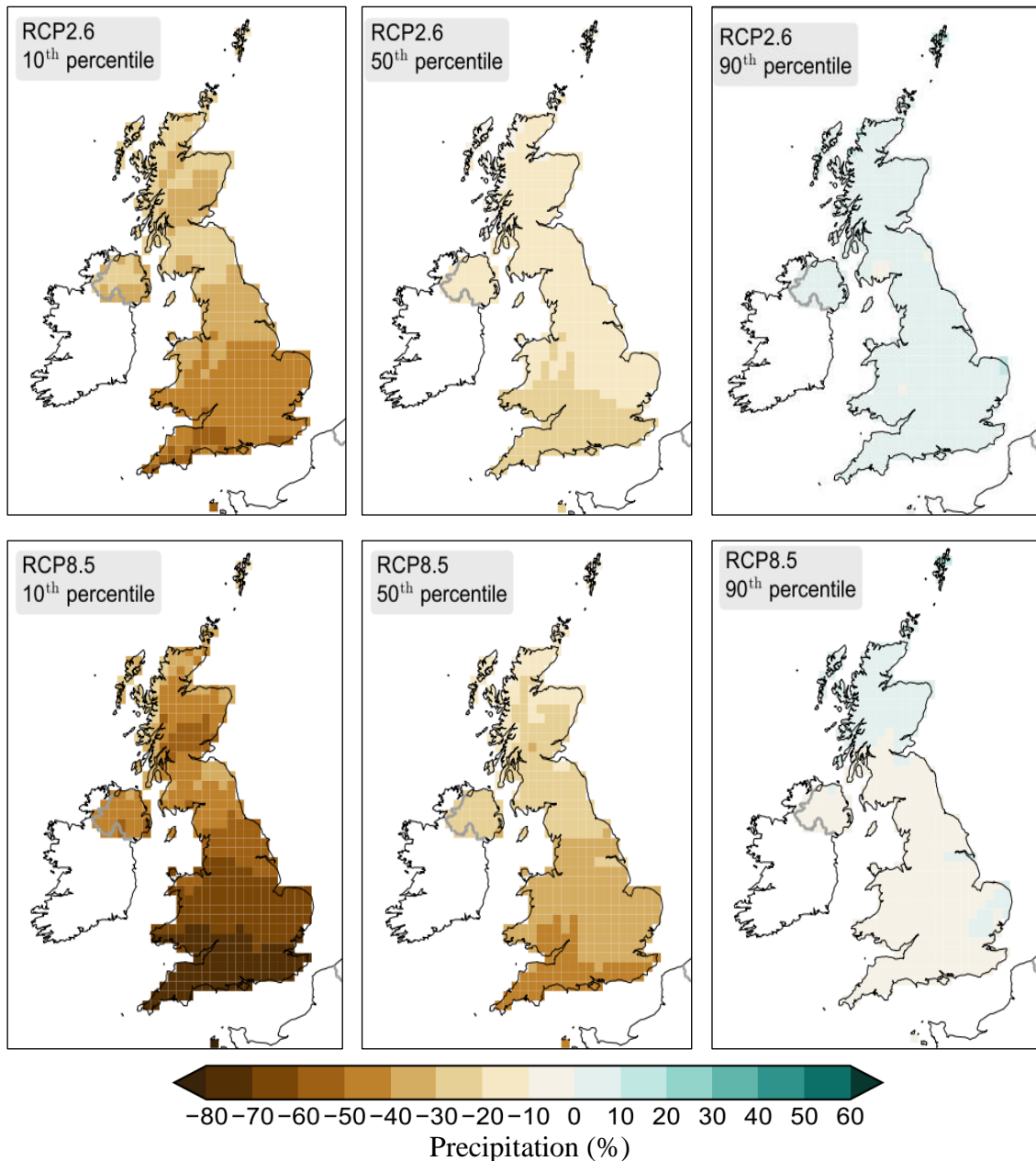


Figure 2.14. Changes in summer mean temperature for 2080 for RCP 2.6 (upper row) and RCP 8.5 (lower row) across 10% (column 1), 50% (column 2) and 90% (column 3) percentiles (adapted from Lowe et al., 2019).



*Figure 2.15. Changes in winter mean precipitation for 2080 for RCP 2.6 (upper row) and RCP 8.5 (lower row) across 10% (column 1), 50% (column 2) and 90% (column 3) percentiles (adapted from Lowe et al., 2019).*



*Figure 2.16. Changes in summer mean precipitation for 2080 for RCP 2.6 (upper row) and RCP 8.5 (lower row) across 10% (column 1), 50% (column 2) and 90% (column 3) percentiles (adapted from Lowe et al., 2019).*

Figure 2.13 to Figure 2.16 are chosen to demonstrate the heterogeneity of precipitation and temperature changes due to climate change. For further information regarding regional, National, European and global UKCP18 projections, see UK Met Office, (2018); Lowe *et al.*, (2019); The Met Office, (2019) and Kay *et al.*, (2020, 2021).

It is shown (Figure 2.13 to Figure 2.16) that across all presented scenarios, the extent and severity of seasonal temperature and precipitation will vary across the UK. Referring back to Figure 2.12, it can be seen that NFM (due to the observed ‘range’ of mitigative capabilities) is likely able to cope with the projected changes to a better extent than conventional methods (Lacob *et al.*, 2014, 2017; Dittrich *et al.*, 2019). This is due to the ability of NFM to be addressed on a case-by-case basis, and differing types can be installed across differing areas of the catchment to better counteract the adversities of climate change (Dittrich *et al.*, 2019; Kay *et al.*, 2019; Connelly *et al.*, 2020). Recent FRM policies supporting the implementation of NFM methods (Defra 25-Year Environment Plan, England Tree Action Plan 2021 – 2024 (see Chapter 9)) are primarily driven by the ability of NFM to potentially mitigate the turbidity of future climate projections. However, further research is needed to quantify and investigate (both empirically and through modelling) the potential for NFM methods to mitigate precipitation and temperature changes in future (Wells *et al.*, 2020; Bark *et al.*, 2021).

### 2.2.3 Current Barriers of Natural Flood Management

Current methods of FRM are rapidly becoming unsuitable in light of a changing climate (see sections 2.1 and 2.2.2), which has enabled a literature ‘push’ towards increased investigation into the useability and applicability of NFM methods (Wingfield *et al.*, 2019). However, there are still limitations regarding NFM and the impact of such methods. The first fundamental limitation is the lack of supporting literature and long-term empirically monitored field data regarding the applicability of NFM compared with conventional methods (Kay *et al.*, 2019; Wells *et al.*, 2020; Ellis *et al.*, 2021). The design and operation of conventional FRM methods are well documented, and they are designed to withstand pre-determined water volumes based on the maximum expected flow and AEP. However it is suggested by Waylen *et al.*, (2018) that the current methods of assessing conventional FRM have influenced the way that NFM is judged, i.e., NFM is always assessed in comparison to conventional FRM, whereas their

premise of operation is often different (Kay *et al.*, 2019; Wilkinson *et al.*, 2019; Xiao *et al.*, 2021). Moreover, public perception of NFM compared with conventional FRM can be a disadvantage (Lavers and Charlesworth, 2018). Conventional FRM methods are often more visible to the public and methods such as flood wall, weir and dam construction can be blatantly observed, which validates the public perception that the methods are working (because they are visible) (Lacob *et al.*, 2014; Waylen *et al.*, 2018). However, as discussed throughout section 2.2.2, NFM methods often involve tree planting and other vegetation across the entire catchment/floodplain; and in-channel methods of NFM are often installed in the upper/middle reaches of catchment, sometimes on riparian or private land, often designed to ‘blend in’ (Ngai *et al.*, 2017; Burgess-Gamble *et al.*, 2018; Ferguson and Fenner, 2020a). This removes the obviousness of the FRM method implementation, which fails to validate public perception to the extent of conventional methods (Environment Agency *et al.*, 2017; Ngai *et al.*, 2017). Furthermore, available funding for NFM projects is limited, and NFM implementation often struggles with justifying the benefits to stakeholders compared with other land uses over NFM (Waylen *et al.*, 2018). For example, a farm located in the rural upper reaches of a catchment is more profitable and desirable to a landowner compared with selling the land to establish an area of woodland (Wells *et al.*, 2020; Ellis *et al.*, 2021). Additionally, quantifying an exact cost/benefit value of any NFM scheme is difficult; partially due to the variety of factors at play when dealing with NFM, and partially due to the lack of literature focussing solely on this issue (Dittrich *et al.*, 2019; Short *et al.*, 2019; Seddon *et al.*, 2020).

### **2.3 Tree Planting**

It is already understood that woodlands are beneficial to the oxygen cycle, store carbon, are amenable and create new habitat for fauna and flora (Lacob *et al.*, 2014; Ellison *et al.*, 2017; Forestry Commission, 2018). However, the UK is one of the least densely wooded countries in Europe, with coverage being 3.21 million hectares (13%) (Forest Research, 2020), 22% less

than the 35% European average (Food and Agriculture Organisation of the United Nations (FAO), 2020). Discussed in section 2.2, NFM methods that involve vegetation planting can increase interception, evapotranspiration, infiltration, soil storage capacity and surface roughness (Burgess-Gamble *et al.*, 2018; Hankin *et al.*, 2018; Ellis *et al.*, 2021). Tree planting is known to influence surrounding hydrology (Lacob *et al.*, 2014; Dittrich *et al.*, 2019; Murphy *et al.*, 2021); however there is a lack of evidence based long-term projects and/or research surrounding the use of trees as a source control measure, and the hydrological implications of tree planting remain largely unquantified (Forbes *et al.*, 2016; Rahman and Ennos, 2016; Dadson *et al.*, 2017). The schematic in Figure 2.17 demonstrates the key processes and methods in which trees can influence the surrounding hydrological processes.

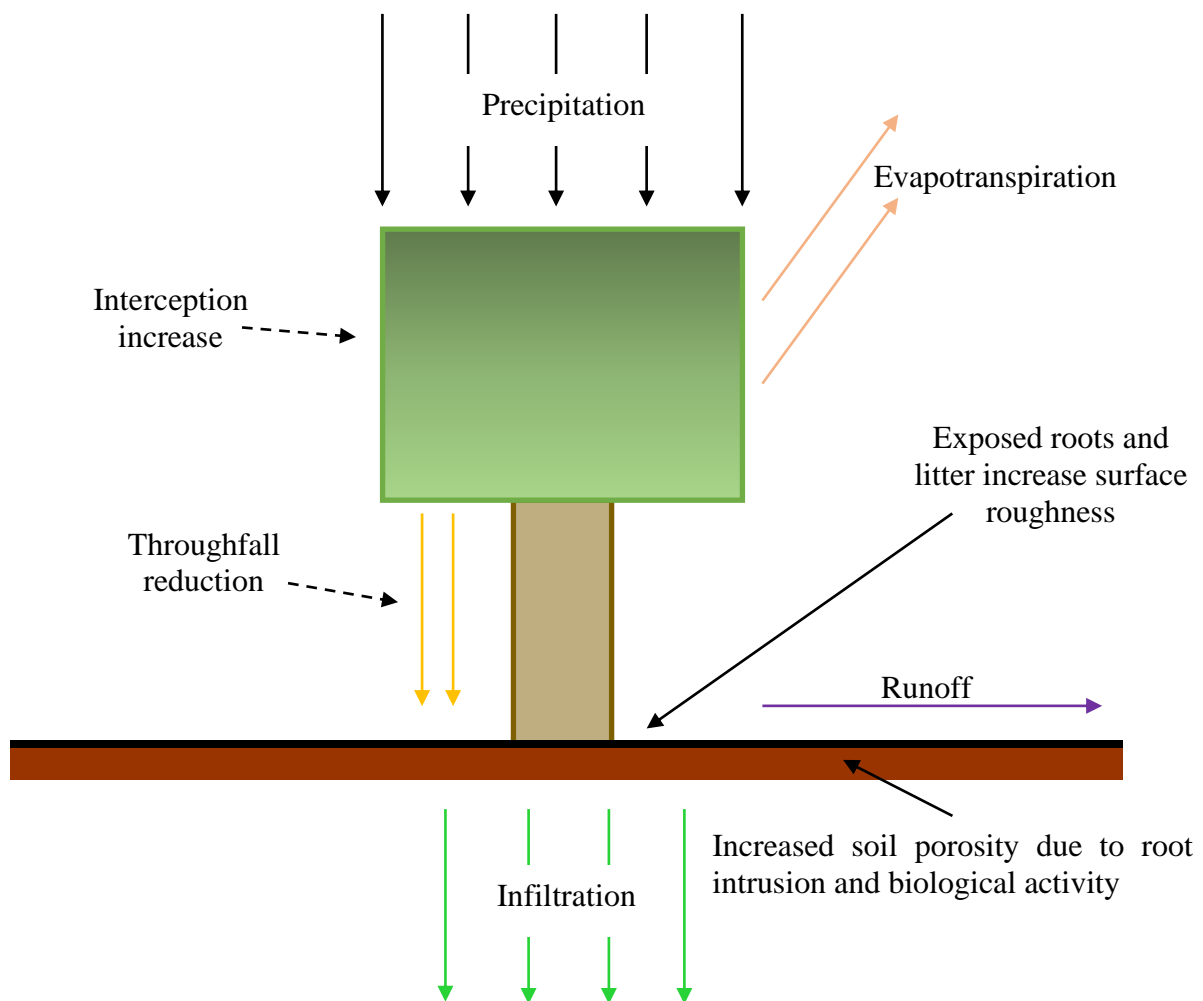


*Figure 2.17. Schematic diagram of the interaction between trees and hydrological processes  
(Adapted from Fazio 2012)*

When outlining the natural impacts that trees can have on their surrounding hydrology, and considering the effectiveness of tree planting as a potential method of NFM: tree roots break up the surrounding soil, increasing porosity and subsequent water storage and infiltration (Chandler *et al.*, 2018; Zhang *et al.*, 2019a, 2020) (see section 2.3.1). Tree litter improves soil health, encouraging biological activity in the soil which further enhances macro-porosity and soil structure (worm tunnels and animal burrows) (Dollinger *et al.*, 2019; Lozano-Baez *et al.*, 2019) (see section 2.3.2). Precipitation is intercepted by the canopy of the tree before reaching the soil surface, prolonging the time that the soil takes to reach saturation and/or runoff (Klamerus-Iwan, 2014; Lunka and Patil, 2016; Cooper *et al.*, 2021) (see section 2.3.3); and tree roots and litter can increase the surface roughness of an area, slowing and resisting overland flow (Ngai *et al.*, 2017; Zhu *et al.*, 2020a, 2020b) (see section 2.3.4). These features are discussed in further detail throughout the following sections, the current understanding of each is outlined and assessed, and a summary of the potential use of trees as a method of NFM will be outlined in section 2.4.

### 2.3.1 Tree Root Growth and Infiltration

Tree roots influence the porosity and soil structure of an area, increasing permeability and subsequent infiltration and storage; tree roots break up soils, increasing macro-porosity and connect flow pathways, reduce compaction and improve soil structure, which increases infiltration and water storage capacity (Jarvis, 2007; Zhang *et al.*, 2017b, 2019a; Chandler *et al.*, 2018; Leung *et al.*, 2018; Malik *et al.*, 2019; Xie *et al.*, 2020; Guo *et al.*, 2021). Additionally, precipitation is seen to follow tree roots, using them as conduits to infiltrate to deeper soil depths (Graham and Lin, 2012); and infiltrating water can travel via the ‘root

tunnels' left after a tree dies, indicating that the impacts of tree establishment on infiltration can outlive the tree (Zhang *et al.*, 2020; Cui *et al.*, 2021; Wu *et al.*, 2021).

The extent to which tree roots can influence infiltration is dependent on numerous external factors, such as soil moisture, pH, structure and organic matter (Dobson, 1995; Crow, 2005). This complicates that predictability of the impact of root spread on infiltration, which may result in some woodland areas influencing infiltration more than others (Jarvis, 2007; Guo *et al.*, 2021) – this in addition to the influences of soil texture, discussed throughout section 2.5. Regarding native British broadleaf woodland species, Perry (1982) discusses that mature Oak (*Quercus*) roots can spread up to 65 m in any given direction, however highlights that roots paths in general are hard to predict due to their opportunistic nature and local variations in topography and soil conditions. A study into 180 root systems and trunks of 15 and 20 year old Birch trees by Mauer and Palátová (2003) found that the average root spread was 6 m radially, which is supported by literature suggesting methods of deriving root growth through trunk size (Dobson, 1995; Crow, 2005). Regarding Aspen, Hepner *et al.*, (2020) suggest that lateral root spread is on average 15 m but can be up to 49 m, however it should be noted that this is only under hybrid-sucker conditions (where roots and trunks can encourage the growth of new tree-stands due to re-establishment (Landhäusser *et al.*, 2019)). Tree roots are difficult to survey in situ, particularly for projects investigating infiltration, as their locations are hard to detect without the use of expensive ground penetrating radar (GPR) methods (Alani and Lantini, 2020; Zou *et al.*, 2020; Aboudourib *et al.*, 2021). Example long-term woodland planting and infiltration case studies to date are introduced in section 2.4.

### 2.3.2 Biological activity

The introduction of trees to an area brings more opportunity for biological activity – flora and fauna on both the macro and micro scales (Dollinger *et al.*, 2019; Lozano-Baez *et al.*, 2019). When (deciduous) trees lose their leaves throughout autumn, micro-biota and other wildlife are

attracted to the surrounds of the tree to forage for food. This process is also combined with the microscopic breaking down of tree leaves, converting them into nutrients, that are incorporated into the soil (Li *et al.*, 2018). The increase in soil biological health attracts more biological activity from smaller animals (worms) that both enrich the soil and increase porosity at the same time (Anderson *et al.*, 2020). The presence of small-scale biological activity attracts larger scale animals, that begin to burrow (rabbits, badgers, and rodents), further increasing the porosity and subsequent infiltration of the surrounding soil. These biological processes, combined with the increased porosity as a result of root spread (section 2.3.1), initiates a cycle wherein porosity is continually improved, as is infiltration (Burgess-Gamble *et al.*, 2018; Jačka *et al.*, 2021). It is noted that soil biological activity is dependent on the soil texture (section 2.5), and sandier soils often see less biological activity due to their low organic matter content (Lozano-Baez *et al.*, 2019). However, sandier soils inherit more pore space so infiltration is already increased over less permeable geology types (Folorunso and Aribisala, 2018) (further discussed in section 2.5).

### 2.3.3 Interception

Labelled in Figure 2.17, interception refers to the process of precipitation accumulating on above-surface vegetation before reaching the soil surface (Lunka and Patil, 2016; Ngai *et al.*, 2017). Regarding tree species, precipitation is intercepted by the canopy before reaching the soil surface, where it will either infiltrate, pool in an area of low micro-topography, or runoff (Rahman and Ennos, 2016; Rahman *et al.*, 2019). Interception is dependent on several factors: the size and shape of the leaves, the density of leaves in the canopy (this is variable with seasonality if a deciduous tree), the antecedent conditions of the canopy and wind speed (Dohnal *et al.*, 2014; Klamerus-Iwan, 2014).

Quantifying the exact amount of precipitation stored as interception is challenging due to the need for specialised equipment or continuous monitoring, and few studies have focussed solely

on this parameter (Komatsu *et al.*, 2011; Klamerus-Iwan, 2014; Rahman and Ennos, 2016). Referring to native UK broadleaf species (see section 5.2.1.1), interception loss as a percentage of total precipitation is estimated to be between 10–34% (mean 24.25 %) (Calder, 2003; Lunka and Patil, 2016). As a comparison, interception loss for grassland is negligible, being <1% (Nisbet, 2005; Ngai *et al.*, 2017). The values presented differ for coniferous trees, as they retain their leaves throughout the winter seasons (Komatsu *et al.*, 2011; Klamerus-Iwan, 2015). It should be noted that interception allows for the process of evapotranspiration (the combination of evaporation and vegetation transpiration (Huntington *et al.*, 2018; Rahman *et al.*, 2019)). A detailed knowledge of evapotranspiration can aid in the understanding of ‘big-picture’ area hydrology (i.e., atmospheric water-cycle analysis); but from a hydrological modelling perspective (such as this study), a knowledge of interception is of greater value (Ficchi *et al.*, 2019; Iida *et al.*, 2020). Interception can be quantified as a loss throughout hydrological modelling, enabling a more accurate representation of rainfall-runoff processes (discussed in greater detail in section 5.6.2) (Ficchi *et al.*, 2019; Iida *et al.*, 2020; Cooper *et al.*, 2021).

#### 2.3.4 Tree Planting and Surface Roughness

It is acknowledged that tree butts, surface roots, deadwood and leaf litter associated with trees can increase the surrounding surface roughness through creating areas of micro-topography and slowing the speed of overland flow (Marshall, 2016; Ngai *et al.*, 2017; Rossi *et al.*, 2018; Tzioutzios and Kastridis, 2020). However, this is difficult to quantify due to limited evidence-based and the complexity of involved parameters (Zhu *et al.*, 2020b). Few studies quantify the exact impacts of surface roughness on overland flow, meaning an actual numerical value (i.e., a Manning’s *n* value) is difficult to quantify (e.g., for use in hydrological modelling) (Hessel *et al.*, 2003; Sarkar *et al.*, 2008; Zhou *et al.*, 2018a; Annis *et al.*, 2020). Whilst the value of surface roughness has not been accurately quantified, it is seen as a method in which trees can

slow runoff and act as FRM, and ‘shelterbelts’ are a method of NFM that takes advantage of this known phenomena (Burgess-Gamble *et al.*, 2018; Li *et al.*, 2018). The following section will apply what has been reviewed throughout this section and evaluate the uses of tree planting as a method of NFM.

#### **2.4 Tree Planting as a Method of NFM**

Discussed in section 2.2, NFM methods commonly revolve around improving soil porosity and health, with the intention of improving soil infiltration and water storage potential (Ferguson and Fenner, 2020b). Section 2.3 discusses how tree planting can improve porosity, interception and surface roughness, which are all common goals of NFM, indicating that tree planting has potential as a method of NFM (Xiao *et al.*, 2021).

As outlined in section 1.1, the value of tree planting has been acknowledged, and is now being actively encouraged, by the UK Government. The ‘25-year Environment Plan’, which suggests increased woodland planting as a method of working towards a greener environment was introduced in 2018 (HM Government, 2018). Additionally, in 2021, the UK Government also announced the ‘England Trees Action Plan 2021 – 2024’, which aims to increase woodland cover for the benefits of CO<sub>2</sub> sequestration, flood risk and biodiversity (UK Government, 2021a). Further to this, the UK Government have allocated £4 million to organizations aiming to increase UK woodland coverage; and £1.4 million to the Environment Agency (England) for the same purpose (GOV.UK, 2020). Government grants have been introduced to encourage farmers to convert arable land to woodland via the ‘Woodland for Water’ scheme, run in coalition with the Environment Agency and the Forestry Commission (GOV.UK *et al.*, 2019). Furthermore, the UK Government have pledged to plant 30,000 ha of trees per year until 2024 (the end of the current Government (UK Government, 2021a). There were also additional protections warranted to trees in the Environment Act (UK Government, 2021b), stating that the unnecessary or illegal felling of trees could result in prosecution or fines. All the above

policy indicates that the appropriate authorities are aware of the potential benefits of tree planting.

Murphy *et al.*, (2021) examined the impact of tree planting on infiltration, porosity and compaction in Dartmoor National Park, SW England; finding that trees doubled the saturated hydraulic conductivity (infiltration capacity), and improved soil health and porosity. Xiao *et al.*, (2021) removed varying quantities of coniferous woodland from three experimental catchments in the UK and compared the results against an adjoining control catchment. Results of the study showed an 8% - 41% change in baseflow and demonstrated an elevation in small event peak flows – indicating afforestation could suppress such changes. The study concluded that whilst afforestation may reduce baseflow and peak flow, woodlands should not be assumed to protect against larger flood events. Cooper *et al.*, (2021) undertook a review of the ability of catchment, cross-slope, floodplain, and riparian woodland to determine the effectiveness of each in mitigating flood risk. The study found that planned and managed woodland can mitigate flood risk, however the literature base for this subject is sparse, and more research is needed to improve the current state of knowledge regarding tree planting as a method of mitigating flood risk (Hankin *et al.*, 2018; Kay *et al.*, 2019; Ellis *et al.*, 2021). Spatial identification studies have also been undertaken; for example Tzioutzios and Kastridis, (2020) devised a method of combining GIS techniques with true/false statements to identify suitable areas for tree planting across Scotland.

In addition to the purely hydrological benefits of tree planting, trees and woodlands are of value when considering public amenity, biodiversity, habitat creation, and CO<sub>2</sub> entrapment and conversion (section 2.3). Therefore, increasing investigations into tree planting as a method of NFM would be beneficial for both reducing fluvial flood risk, and increasing national woodland coverage for the benefit of the discussed (Hankin *et al.*, 2018; Kay *et al.*, 2019; Ellis *et al.*, 2021). However, regardless of funding allocations and the increased investment in tree planting, the uptake of NFM in general is slow (Xiao *et al.*, 2021). Whilst some studies have

attempted to investigate the link between tree planting and soil infiltration characteristics (Chandler *et al.*, 2018; Murphy, 2021; Murphy *et al.*, 2021), overall, there is a current lack of evidence based long-term research surrounding the use of tree planting as a source control measure, and the hydrological benefits of tree planting remain largely unquantified (Forbes *et al.*, 2016; Dadson *et al.*, 2017; Cooper *et al.*, 2021; Murphy *et al.*, 2021).

#### 2.4.1 Long-Term Tree Planting and Infiltration Case Studies

Two long-term continuous studies in the UK have attempted to monitor and quantify the effect of woodland planting on infiltration; Pontbren and the Cefn Brwyn and Plynlimon catchments. The Pontbren (Powys, south Wales) study was established in 1997, and afforestation, shelterbelt planting and the improvement of existing woodlands and hedges began in 2001 (Woodland Trust *et al.*, 2013; Marshall *et al.*, 2014). Results from the catchment show that infiltration in woodland areas were 67 times higher than that of grazed pasture, and runoff-volumes from these areas were reduced by 78% compared with grassland (Marshall *et al.*, 2014; Ngai *et al.*, 2017). Additionally, the hydraulic conductivity woodland areas were 2.4 times that of grazed pasture, indicating that tree planting had increased and reconnected pore space (Solloway, 2012; Ngai *et al.*, 2017). These results were deemed a combined result of increased interception and evapotranspiration from the canopies of trees, and increased porosity and subsequent infiltration as a result of root spread (Marshall *et al.*, 2014).

Monitoring began at the Cefn Brwyn (10.55 km<sup>2</sup>, grassland) and Plynlimon (8.70 km<sup>2</sup>, 70% wooded) catchments (west Wales) in 1967 to investigate the impacts of conifer planting and clear-felling on surrounding hydrological processes (Kirby *et al.*, 1991; Centre for Ecology and Hydrology, 2014). The ages of trees ranged from 40 – 60 years. Results from the study show that the woodland catchment reduced runoff in comparison to the grassland catchment, and extrapolations have indicated that a completely wooded catchment could reduce runoff by 15% compared to a similarly sized grassland catchment (Kirby *et al.*, 1991). However, it must be

acknowledged that during both extreme low and extreme high-flow events, there was very little variation in runoff between the two catchments (Robinson and Newson, 1986; Kirby *et al.*, 1991), and this was attributed to the woodland catchment consisting of only a small amount of canopy storage, and generally drier soils beneath woodland stands compared with grassland. (Dadson *et al.*, 2017).

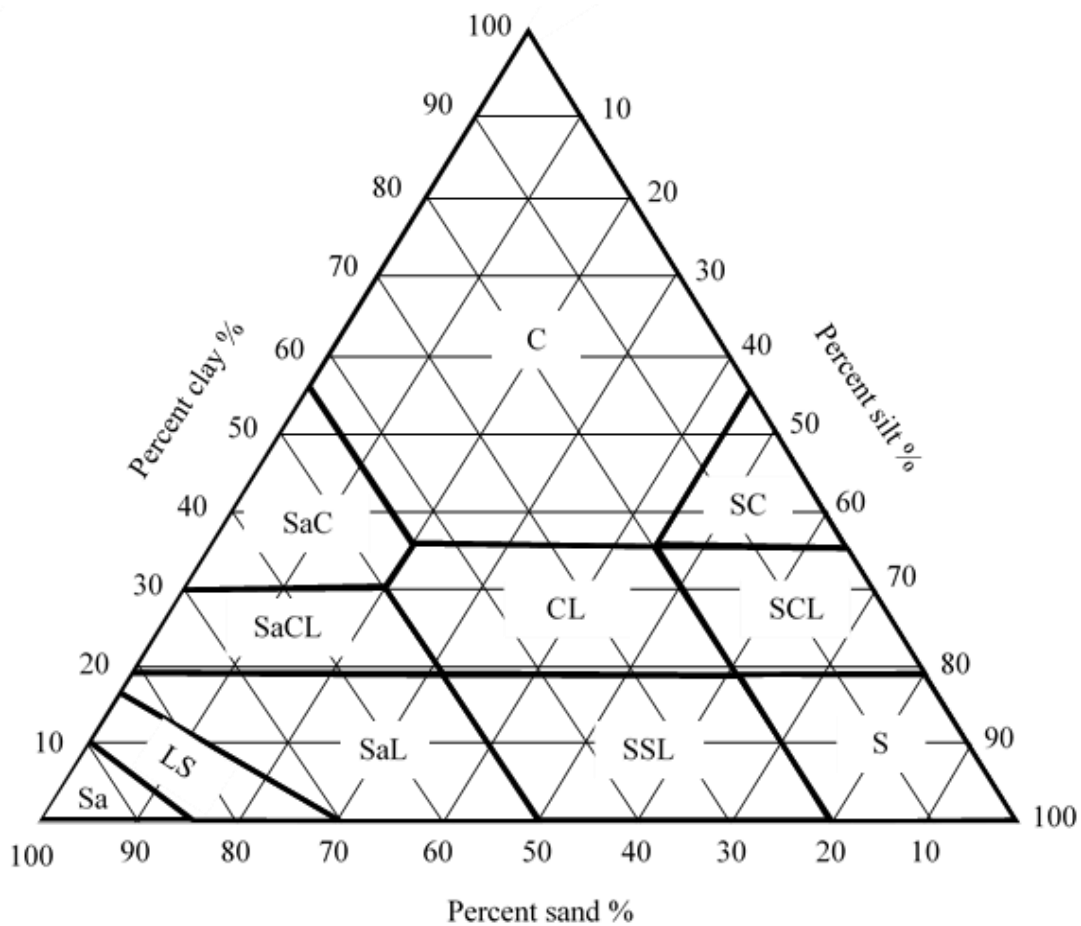
Both studies contribute to what is otherwise a sparse literature base, regarding the changes in infiltration over a longer time period, which is advantageous over most recent studies conducted over a shorter duration (Chandler *et al.*, 2018; Rahman *et al.*, 2019; Zhang *et al.*, 2020; Murphy *et al.*, 2021). However, whilst these studies focus on the impact of changing infiltration due to tree planting, neither has continually measured infiltration, nor analyse infiltration variation dependent on tree proximity and maturity. Instead, information regarding infiltration change is estimated based on input/output measurements of the catchment. This is a common limitation of similar studies due to the amount of time and resources required in continual infiltration data collection (Archer *et al.*, 2016; Lunka and Patil, 2016; Vergani and Graf, 2016; Guo *et al.*, 2021; Murphy *et al.*, 2021).

## **2.5 Infiltration, Soil Texture, Soil Structure and Compaction**

Discussed throughout sections 2.2, 2.3 and 2.4 is the common reliability of NFM methods on soil infiltration; however, infiltration is governed primarily by soil characteristics, which are outlined throughout this section. The permeability of a soil influences infiltration rate (speed, in mm/hr) and capacity (total volume, in mm), and is governed by the soil texture (the percentiles of sand, silt and clay), the soil structure (the distribution of sediments, pore and pore size) and the hydraulic conductivity (the connectivity of pore space) (Rabot *et al.*, 2018; Sun *et al.*, 2018; Silber, 2019; Bátková *et al.*, 2020; Ren *et al.*, 2020). From initial saturation, infiltration continues at a constant rate until reaching the soils capacity and overland flow

(surface runoff) will occur if saturation continues beyond this point (Lili *et al.*, 2008; Hornberger *et al.*, 2014).

Soils comprise of varying quantities of sand (0.06 mm – 2.0 mm), silt (0.002 mm – 0.06 mm) and clay (<0.002mm), referred to as separates, and the infiltration characteristics (permeability) of a soil can vary depending on the quantity and distribution of each (Folorunso and Aribisala, 2018). In the UK, 11 subcategories are used to define and classify soil texture dependent on the percentile of each separate in a sample, and the soil texture triangle (Figure 2.18) can be used to identify each after the sand/silt/clay percentiles of the sample soil has been identified. See Figure 2.18.



C	SaC	SC	CL	SaCL	SCL	Sa	LS	SaL	SSL	S
Clay	Sandy clay	Silty clay	Clay loam	Sandy clay loam	Silt clay loam	Sand	Loamy sand	Sandy loam	Silty loam	Silt

*Figure 2.18. UK Soil Texture Triangle and tabulated soil texture classifications. Note 'loam' refers to the matrix comprising of equal parts of each specified separate (adapted from Avery, 1973 and LandIS, 2020).*

In addition to soil texture, soil structure – referring to the distribution of particles, particle sizes, pores, and pore sizes within a soil matrix – also influences infiltration (Archer *et al.*, 2013). If particles throughout a soil matrix are well sorted (all particles are a similar size and distribution) and are larger in size, such as sand, they do not fit tightly together which increases the size and frequency of pore space within the matrix (Chesworth *et al.*, 2008; Archer *et al.*, 2013; Gee and Or, 2018). This pore space allows for the greater connectivity of hydraulic pathways meaning that as water infiltrates, it can transmit more quickly through the soil. In a poorly sorted soil such as a sandy-clay (Figure 2.18), the small clay particles will fill the pores between the sand particles, decreasing permeability and reducing infiltration rate and capacity (Chesworth *et al.*, 2008; Archer *et al.*, 2013). It is also worth noting that infiltration through a well-sorted clay soil is slow due to the clay particles fitting tightly together, representing the characteristics of an impermeable surface (Revell *et al.*, 2021).

Compaction can influence soil structure and infiltration characteristics (Marcotullio *et al.*, 2008; Yang and Zhang, 2011). Internally, a soil can become compacted due to a lack of organic matter, a breakdown of structure and pore space and a lack of water content in the soil (Franzluebbers, 2002; Sun *et al.*, 2018). Externally, soil can be compacted through wildlife grazing and trampling, heavy machinery, and repetitive vehicle and foot traffic (Al-Dousari *et al.*, 2019; Jordon, 2021). Figure 2.19 shows the impact of compaction on a soil column.

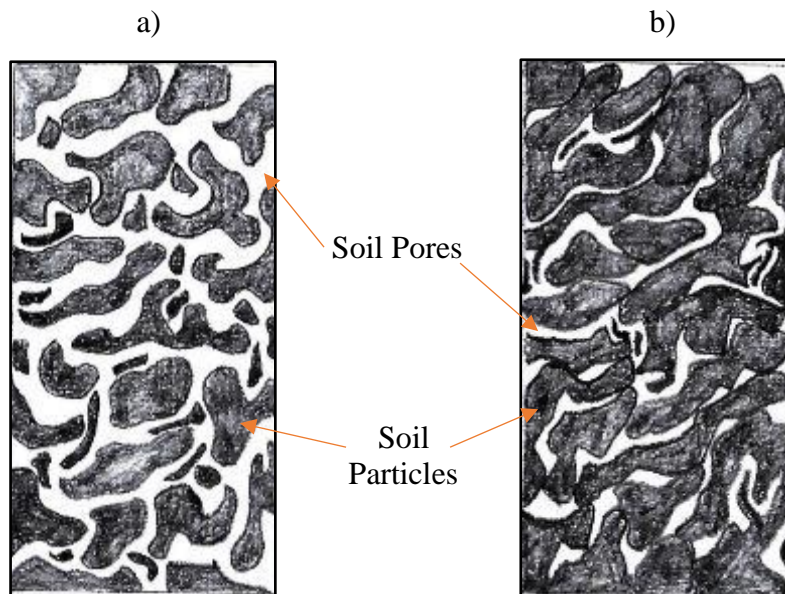


Figure 2.19. Exaggerated a) highly permeable soil comprising of frequent, large, interconnected pore spaces, b) a compressed soil with low permeability comprising of infrequent, smaller, disconnected pores (Adapted from Hornberger *et al.*, 2014).

Although permeability and pore storage can be reduced through compaction, the opposite is seen in areas that are biologically active; in areas that are inhabited by wildlife and other micro-biota, pore space can be increased and soil structure made more pervious (Graham and Lin, 2012). Biological activity such as worm holes, root channels (which can act as conduits for infiltrating water (see section 2.3.1), or animal burrows can increase the frequency of macropores and increase pore connectivity increasing permeability (Blok *et al.*, 2008; Osman, 2013; Kirkham, 2014a).

Regarding NFM, soil texture and structure can significantly influence the methods used. It is outlined in section 2.2 that NFM methods are not as consistent (in terms of flood risk reduction potential) as conventional methods (Lavers and Charlesworth, 2018; Wilkinson *et al.*, 2019; Wingfield *et al.*, 2019), and their effectiveness varies from catchment to catchment. Some NFM methods (vegetation and tree planting) rely on increasing porosity and infiltration to reduce overland flow and overall flood risk, so consideration must be given to the effectiveness of the NFM method used from area to area (Ngai *et al.*, 2017; Burgess-Gamble *et al.*, 2018; Xiao *et al.*, 2021).

## **2.6 Chapter Summary**

This section has discussed the current understanding of areas of relevance to this study using academic theories and up-to-date research, and highlighted several areas where research is sparse, inconsistent, or outdated. The first observation is that there is a lack of evidence regarding tree planting as a method to address high river flows, and more specifically, there is a lack of long-term studies focussing solely on the influence of tree planting on infiltration change due to proximity, root spread, and tree maturity. Additionally, it is understood that tree planting is of benefit to surrounding hydrology (roots breaking up soils, leaves intercepting precipitation); however, there are few evidence-based studies to support their use as a method of NFM. Moreover, the lack of collected infiltration data from planted trees may be a result of the awkwardness of collecting infiltration data via traditional methods (personnel, water and time required), which is discussed in greater depth throughout section Chapter 3.

The findings of this literature review, and the identified areas of literature scarcity, have informed the aims and objectives of study (section 1.3). The following chapter (Chapter 3) discusses commonly acknowledged (regarding relevant literature) methods of infiltration data collection and flood modelling in greater depth, and the findings of both chapters have informed the methodology of this study, which are outlined in Chapter 5.

## Chapter 3 Review of Previous Studies, Methods, and Tools

This chapter discusses commonly used methods of infiltration data collection and hydraulic and hydrological modelling software. The aims and objectives of this study (section 1.3) indicate that infiltration data will be collected, then subsequently modelled, so an understanding of what methods exist and other authors who have investigated or utilised these tools is important for building the study methodology (Chapter 5). Model calibration and validation is discussed in addition to the Nash and Sutcliffe (1970) Efficiency (NSE) tool throughout section 3.3, and modelling limitations are outlined in section 3.4.

### **3.1 Infiltration Measurement**

Understanding infiltration is important to identify the response of an area to precipitation and has been investigated in the literature by several authors (Carroll *et al.*, 2004; Thomas and Nisbet, 2016; Chandler *et al.*, 2018) comparing the infiltration rate of woodland soils to that of other land cover (i.e. grasslands) to determine runoff reduction as a result of increasing woodland cover. Studies comparing the infiltration of urban land cover to rural land cover to better understand the implications of urbanisation (Yang and Zhang, 2011; Sun *et al.*, 2018). Studies assessing hillslope hydrology to gain insight about how slope influences infiltration rates and runoff (Harden and Scruggs, 2003; Archer *et al.*, 2013); and authors calibrating hydrological models to observed site conditions, i.e., infiltration rates need to be as accurate to the field as possible whilst building a hydrological model (Park and Parker, 2008).

Field work is an important element of infiltration data collection, particularly when evaluating the effectiveness of NFM methods (Wingfield *et al.*, 2019; Connelly *et al.*, 2020; Cooper *et al.*, 2021). Therefore, the following sections will evaluate the common methods of measuring infiltration in further detail, critically evaluating each based-on portability, useability, measurement, water usage, and derived measurement.

### 3.1.1 Single and Double Ring Infiltrometers

The single ring infiltrometer (SRI) is a metal tube, inserted into the soil surface to a depth of between 5 and 10 cm (Wahl *et al.*, 2003; Carroll *et al.*, 2004; Chandler *et al.*, 2018). Water is added to the tube and the level is recorded at consistent time intervals, defined by the user (Bátková *et al.*, 2020). Measurement continues until the water level remains constant for (commonly) three-time intervals, at which point the total and mean infiltration rate of the area can be calculated (Bagarello and Sgroi, 2004; Chandler *et al.*, 2018). Total infiltration is the sum amount of water that enters the soil over the measurement duration, and the infiltration rate (in minutes) is a division of the total sum by the measurement duration. The primary limitation of the SRI, however, is the lateral leakage (seepage), whereby infiltrating water travels laterally instead of vertically, which can lead to an overestimation of the infiltration rate (Muneer *et al.*, 2020).

Double ring infiltrometers (DRI) consist of two cylindrical tubes, one larger than the other inserted 5-10 cm into the sample soil (Fatehnia *et al.*, 2016; Folorunso and Aribisala, 2018). Whilst there is no guidance regarding the ratio of DRI ring sizes, it is common to use an outer ring with double the diameter of the inner (Lai and Ren, 2007; Zhang *et al.*, 2017a; Nestingen *et al.*, 2018). The outer ring of the DRI is filled and kept at a constant head throughout measurement, forming a 'bulb' around the infiltrating water from the inner-ring (Hornberger *et al.*, 2014). This encourages the vertical infiltration of inner-ring water and minimises lateral seepage and measurement inaccuracy, which is often inherent with SRI measurement (Folorunso and Aribisala, 2018; Rönnqvist, 2018; Zhang *et al.*, 2019b; Muneer *et al.*, 2020). The method of recording and deriving infiltration rate and capacity when using the DRI is the same as the SRI. The infiltration process of the SRI and the DRI are shown in Figure 3.1.

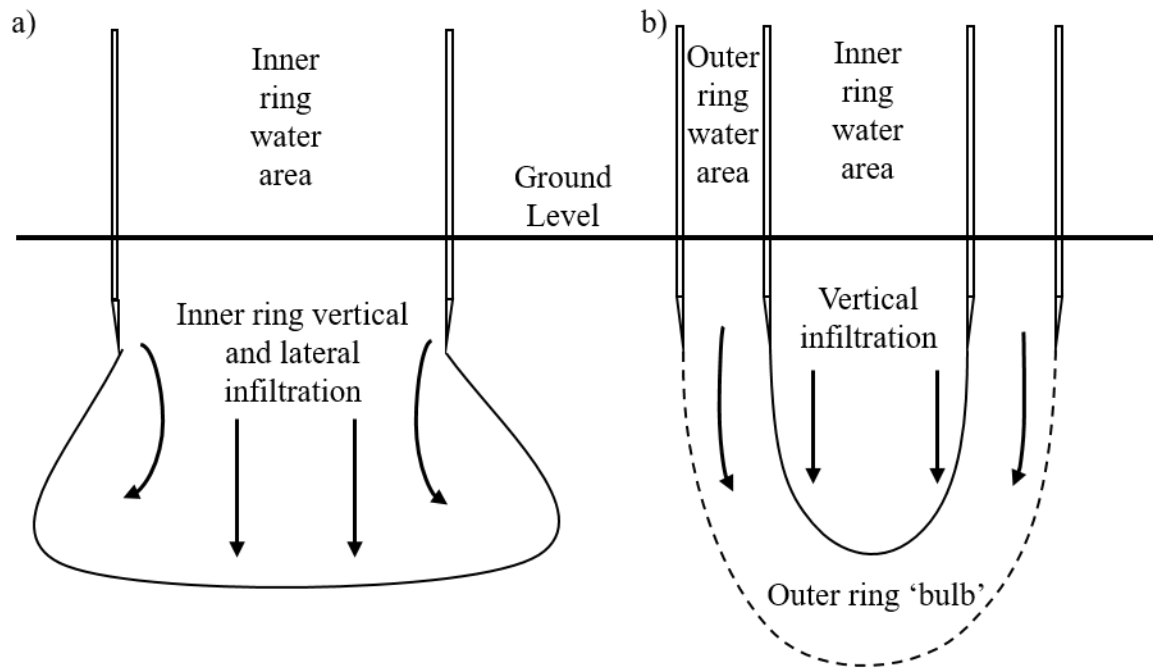


Figure 3.1. The infiltration processes of both a) SRI's and b) DRI's.

It is agreed within the literature that the size of SRI's and DRI's should be as large as possible to minimise lateral seepage and reduce edge effects (Bagarello and Sgroi, 2004; Lai and Ren, 2007; Khodaverdilo *et al.*, 2017; Nestingen *et al.*, 2018). Lateral seepage refers to water travelling laterally instead of vertically, leading to an overestimation of the infiltration rate (Muneer *et al.*, 2020); and edge effect is the phenomena of an external factor, or change in sampling consistency, influencing the process of consistent data collection or replication (Woo, 2004; Dai *et al.*, 2017). However, this is not always possible if transportation, personnel and water availability is limited in the field (Milla and Kish, 2006; Chen and Hsu, 2012; Kirkham, 2014b; Nestingen *et al.*, 2018). See Table 3.1.

Table 3.1. Studies utilising single and double ring infiltrometers with application and size noted.

<b>Single-Ring Infiltrimeters</b>		
<b>Author</b>	<b>Overview of study</b>	<b>Size (cm)</b>
Murphy <i>et al.</i> , (2021)	Woodland establishment and soil hydrological functioning	10
Xu <i>et al.</i> , (2012)	Comparing methods of deriving infiltration from SRI data	14
Hu <i>et al.</i> , (2020)	Field Assessment of the maintenance of permeable paving	30
Di Prima <i>et al.</i> , (2018)	transient and steady-state single-ring infiltrometer analysis	100
<b>Double-Ring Infiltrimeters</b>		
Nestingén <i>et al.</i> , (2018)	Laboratory comparison of field infiltrometers	20, 40
Mahapatra <i>et al.</i> , (2020)	Assessing Variability of Infiltration Characteristics in India	30, 60
Vand <i>et al.</i> , (2018)	Comparative Evaluation of Infiltration Models	30, 60
Zhang <i>et al.</i> , (2019b)	Method to partition preferential flow in forest soil	30, 60

One significant limitation associated with both the SRI and DRI is that they disrupt the soil (Bagarello *et al.*, 2014; Zhang *et al.*, 2019b). The intrusive insertion of the rings in to the soil can create macropores, leakage passages and distort the natural homogeneity of the soil making replication difficult and increasing measurement error (Bagarello and Sgroi, 2004; Zhang *et al.*, 2017a). Additionally, measurement of infiltration can be a time consuming process (in some cases up to six hours (Johnson, 1963)) dependent on desired result and soil type, making multiple site sampling challenging (Alagna *et al.*, 2016). Often, such equipment (SRI/DRI) is cumbersome to transport around the study site, and can require vast amounts of water for measurement and replication (which is not always easily attainable ‘in the field’); furthermore, they are expensive and outside the budgetary constraints for some projects (~£2000 for a DRI (Eijkelkamp, 2015)). These limitations can become more prominent depending on the desired outcome of SRI and DRI usage. If replication and time-on-site are not confining factors of the

study, then the SRI and DRI methods are appropriate; however, if access to the study site, water, personnel and budget are limited, then another method of deriving infiltration characteristics may be advisable (Milla and Kish, 2006; Chen and Hsu, 2012; Kirkham, 2014b; Nestingen *et al.*, 2018).

### 3.1.2 Minidisk Infiltrometer (MDI)

The Minidisk Infiltrometer (MDI), developed by METER® Group Inc., (2020), can measure the infiltration characteristics of a soil under a user-specified tension setting (Burguet *et al.*, 2016; Nestingen *et al.*, 2018; Bátková *et al.*, 2020; METER® Group Inc., 2020). See Figure 3.2.

This item has been removed due to 3rd Party Copyright. The unabridged version of the thesis can be found in the Lanchester Library, Coventry University.

*Figure 3.2. The Mini disk infiltrometer with parts labelled (Decagon Devices, 2006; Robichaud et al., 2008)*

The MDI has a measuring (soil contact) diameter of 4.5 cm and holds a total of 135 ml of water; 95 ml of which is for infiltration (the bubble chamber accounts for the additional 40 ml), 500% less than what is required by small SRI's or DRI's. The MDI is significantly smaller and is easier and quicker to operate in the field than the SRI and DRI (Kirkham, 2014b; Nestingen *et al.*, 2018). Furthermore, the method is non-intrusive - meaning measurements are taken from the soil surface which aids in measurement replication over time (Bagarello and Sgroi, 2004; Zhang *et al.*, 2019b). However, vegetation cover does have to be removed from the soil surface around the area of measurement before the MDI can be used, as full contact with the soil is

required (Robichaud *et al.*, 2008; Nestingen *et al.*, 2018; Naik *et al.*, 2019; METER® Group Inc., 2020).

The force that must be exerted on the base of the MDI by the soil to break the surface tension is controlled using the tension regulation tube. The user can select a desired tension, ranging from 0.5 cm (0.5 kPa) to 7 cm (7 kPa), in increments of 0.5 cm. The user manual suggests applying a higher tension when sampling more permeable soils and a lower tension when the soil is more compact (Naik *et al.*, 2019; METER® Group Inc., 2020). Despite these indications, there is limited guidance on the influence that different suction settings have on deriving infiltration, and therefore the impact of selecting dissimilar settings for various soil textures when calculating the infiltration (Fatehnia *et al.*, 2016; Nestingen *et al.*, 2018; Naik *et al.*, 2019). Furthermore, these values are typically not considered in studies that have used the MDI (Table 3.2).

Table 3.2. Mini Disk Infiltrometer application, objective, and selected suction.

Author and Reference	Overview of Study	Tension
Nesting et al. (2018)	A laboratory comparison of field infiltrometers	6
Robichaud et al. (2008)	A field assessment of post-fire soil infiltration using the MDI	1
Fatehnia et al. (2014)	A comparison of equations used to determine K	1, 2, 3
Matula et al. (2015)	A field comparison of K measurements from infiltrometers	0.5, 1, 3

Being a tension infiltrometer, the MDI allows the user to select the desired tension, which will act on infiltrating water to define the size of pores allowed to participate in infiltration. The higher tensions (closer to 7 cm) only allow infiltration via micro-pores, whereas lower tensions (closer to 0.5 cm) allow infiltration via macro-pores. The MDI user manual suggests a suction setting of 2 cm will sufficiently derive the infiltration characteristics of most geology textures (METER® Group Inc., 2020).

Compared with the SRI and DRI, the MDI is significantly smaller, uses less water, is easier and quicker to operate in the field and facilitates non-disruptive measurements, allowing for replication (Kirkham, 2014b; Nesting *et al.*, 2018). Ring-infiltrometer methods require insertion of between 5 and 10 cm into the sample soil to allow for the determination of infiltration characteristics (Bagarello *et al.*, 2014; Chandler *et al.*, 2018). This is a fundamental disadvantage of ring infiltrometers as the soil is not only disturbed when the ring is inserted, but also when the infiltrometer is removed; over time, the disturbance caused renders replication at the same location inaccurate as the soils structure is altered significantly (Bagarello and Sgroi, 2004; Zhang *et al.*, 2019b). Damage to the soil structure through this method renders all future infiltration measurements unreliable as they no longer represent the wider sample area (Zhang *et al.*, 2019b). This is an issue that is avoided by the MDI as the device does not need to be inserted into the soil, meaning replication can be undertaken multiple times from the sample location. A disadvantage of the MDI, however, is that repetitive

measurement with the MDI in the same location can result in soil compaction from the pressure of the MDI's base on the soil. Additionally, the MDI has a small measuring diameter, meaning lateral seepage and edge effect could influence MDI results in the same manner as the SRI. Furthermore, the sintered steel disk can clog when taking measurements from fine-textured sample areas (Kirkham, 2014b).

### 3.1.3 Chosen Method for Study

Based on what has been discussed with reference to SRI/DRI and MDI methods (sections 3.1.1 and 3.1.2), it is concluded that the MDI will be used to collect infiltration data for this study (in line with objective 1a); providing some validation is carried out (this is further described in Chapter 6). It is highlighted in section 3.1.1 that SRI and DRI methods are commonly employed by other studies (Di Prima *et al.*, 2018a; Nestingen *et al.*, 2018; Mahapatra *et al.*, 2020; Murphy *et al.*, 2021), however the intrusive method of measurement, the water requirements, the personnel requirements and their cost make these methods impractical for the objectives and desired outcomes of this study (Milla and Kish, 2006; Chen and Hsu, 2012; Kirkham, 2014b; Nestingen *et al.*, 2018). Replication is an imperative element of the infiltration data collection, as replication adds reliability to collected data (Prieksat *et al.*, 1994; Logsdon and Jaynes, 1996; Khodaverdiloo *et al.*, 2017), and it is discussed in section 3.1.1 that replication is not possible with SRI/DRI methods as the homogeneity of the soil core is disrupted with every measurement. Additionally, the equipment required to carry out SRI/DRI measurements across multiple sample areas whilst solo-working can pose a safety risk, in addition to the common constraints of access to water whilst in the field.

Use of the MDI will mitigate the key issues posed by the use of SRI/DRI methods. The MDI is significantly smaller than SRI/DRI methods, meaning it can be carried and operated across a study site by one person; uses less water, meaning the potential constraint of re-filling is mostly avoided (if re-filling is required, a large water bottle is often sufficient); is easier and

quicker to operate in the field; and facilitates non-disruptive measurements, allowing for replication (Kirkham, 2014b; Nestingen *et al.*, 2018). As discussed, SRI/DRI methods require 5 and 10 cm of insertion into the soil for measurement (Bagarello *et al.*, 2014; Chandler *et al.*, 2018), which is highly disruptive and ruins future replication; however this is avoided by the MDI as the device does not need to be inserted into the soil.

The MDI user manual suggests that 30-40ml of water needs to be infiltrated to collect an accurate and representative infiltration measurement, however it is unlikely that there will be enough time on site to allow this volume of water to infiltrate (inclusive of replication measurements). Therefore, a validation pilot study will need to be undertaken to validate MDI measurements over time, and a methodology devised to collect equally representative data over a shorter duration. This is described in Chapter 6.

### **3.2 Flood Modelling**

Simplistic methods of flood modelling were developed in the 1850's by Mulvaney (1850), who founded the rational method; a mathematical equation was used to determine peak discharge from small catchment areas, useful for assisting with the design of sewer and drainage systems (Todini, 2007; Mai and De Smedt, 2017). Advances in computing allowed for the development of more complex flood modelling software, able to comprehensively simulate the hydraulic processes (in-conduit), hydrological processes (loss mechanics of the whole catchment), or both (Barthélémy *et al.*, 2018; Li *et al.*, 2020). Hydraulic models can be categorised as 1-dimensional, 2-dimensional or linked (where both the 1-D and 2-D domains are utilized); hydrological (or rainfall-runoff) models often facilitate many other 'process models' that can be applied to a whole catchment, accounting for hydrological losses (Barthélémy *et al.*, 2018; Patil *et al.*, 2019). Hydrological models usually accommodate 1-D modelling, but the 2-D domain is less common.

### 3.2.1 Hydraulic Modelling

#### 3.2.1.1 1-Dimensional (1-D)

One-dimensional models (or routing models) assess water flowing in one directional plane (Pasquier *et al.*, 2019). They are normally constructed using a series of user-defined cross sections or pipes and can calculate in-channel flow level from a given rainfall event (Ng *et al.*, 2018; Pasquier *et al.*, 2019). Depending on the complexity of the modelling software, in-channel features and obstructions such as weirs, bridges or culvers can be added to test the 1-D response of a watercourse (Teng *et al.*, 2017; Stamataki and Kjeldsen, 2021). 1-D models are more simplistic compared with 2-D or linked models, require less input information to run effectively, complete simulations quickly and require less computing power (Moya Quiroga *et al.*, 2016; Barthélémy *et al.*, 2018). However, 1-D models lack the ability to compute overbank flow (as flow onto the floodplain is 2-dimensional), consider momentum or compute complex interactions between the floodplain and river channel – which are often of primary interest to the user (Kong *et al.*, 2017; Ngai *et al.*, 2017; Lea *et al.*, 2019).

#### 3.2.1.2 2-Dimensional (2-D)

Two-dimensional models simulate water flowing across two directional planes (watercourse and floodplain), making them naturally more complex however enabling both the input and resultant output to more comprehensive than that of a 1-D model (Brunner, 2016; Pasquier *et al.*, 2019). 2-D models are (most often) used to simulate water pooling, levee breach and flooding through (commonly urban) areas of interest to the study (Crispino *et al.*, 2015; Gharbi *et al.*, 2016; Pasquier *et al.*, 2019). Whereas 1-D river models require cross sectional data for topographical calibration, 2-D models require a continuous representation of surrounding topography which is commonly achieved using a user-defined active area (Betsholtz and Nordlöf 2017, Finaud-Guyot *et al.* 2011). To maximise the topographical accuracy of a 2-D

model, most offer the ability to import compatible (e.g. .ASCII or .TIF) GIS elevation files, meaning the model can automatically detect topography (Shahriparsa *et al.*, 2016; Pinos and Timbe, 2019). Compared with 1-D models, where flow is confined to the user-defined watercourse, a 2-D model will ‘fill up’ with water from a defined control point, highlighting any areas of flooding and often (depending on software capability) providing a visual representation of where, when and to what extent the area simulated will flood.

### *3.2.1.3 Linked Modelling (1-D/2-D)*

Linked hydraulic modelling offers an improved understanding of interactions between the 1-D and 2-D domains due to the representation of both 1-D and 2-D modelling domains, representing interactions between topography and hydraulic features and urban (e.g., buildings, walls, sewers) (Noh *et al.*, 2018; Cardoso *et al.*, 2020). Linked modelling is complex and computationally demanding, as are the equations involved in computing linkages, which vary in complexity and required/assumed data depending on user requirements (linked model equations are comprehensively detailed by (Lin *et al.*, 2006; Finaud-Guyot *et al.*, 2011a, 2011b; Aricò *et al.*, 2016; Morales-Hernández *et al.*, 2016; Geng and Wang, 2020; Yang *et al.*, 2020). Linked modelling can be of value (depending on study requirements) due to its ability to represent flows both in the river channel, and on the floodplain (Pasquier *et al.*, 2019; Li *et al.*, 2020), and have been used in academic studies (Barthélémy *et al.*, 2018; Lea *et al.*, 2019; Pasquier *et al.*, 2019; Cardoso *et al.*, 2020). However linked modelling remains a relatively unexplored area (Lea *et al.*, 2019; Pasquier *et al.*, 2019).

#### 3.2.1.4 Selected Hydraulic Models

##### 3.2.1.4.1 MicroDrainage

MicroDrainage is a hydraulic modelling software commonly used by practitioners to design and simulate hydraulic features (storm-water sewers, foul-water sewers, culverted watercourses) (Innovyze, 2021). The software allows for the integration of GIS software, allowing the user to visualise the design process, compare with solely relying on spread-sheet outputs (Innovyze, 2021); MicroDrainage has been used to design and test SuDS for new-build and retrofit developments. Sañudo-Fontaneda *et al.*, (2017) compared the predictive ability of MicroDrainage to simulate discharge from highway filter drains when compared with laboratory testing under multiple rainfall scenarios, finding the simulated results to correlate closely from both methods. Lashford *et al.*, (2020) used MicroDrainage to simulate the reductions in discharge from multiple SuDS methods, finding results from all simulated methods to positively reduce flows over 720-minute duration storms of varying intensity. Literature involving the use of MicroDrainage is sparse, primarily due to the cost of licensing the software and stipulations from the developer regarding the publication of methods and processes. Regarding the scope of the aims and objectives of this study (section 1.3), MicroDrainage is outside the budgetary constraints, and only computes the 1-D domain, whereas this study intends to model the catchment scale.

##### 3.2.1.4.2 Hydrologic Engineering Centre's River Analysis System (HEC-RAS)

HEC-RAS is a freely available hydraulic modelling software capable of modelling 1-D and 2-D flow (US Army Corps of Engineers, 2021). The software supports GIS integration, and allows for river profile cross-sections to be created and imported from Arc-Map through a plug-in, HEC-GeoRAS (Zhou *et al.*, 2018a; Joshi *et al.*, 2019). Abdessamed and Abderrazak (2019) used HEC-RAS to analyse the flood extent of Ain Sefra city, Algeria, both with and without the implementation of concrete retaining walls, finding that the retaining walls decreased flood

extent, but could not mitigate against higher intensity storms. Lea *et al.*, (2019) test the efficiency of HEC-RAS to simulate 1-D/2-D linked models using the Baeksan river levee breach event in South Korea in 2011; result show a good correlation between aerial photography of the event and simulated flood extent, showing HEC-RAS to be effective when simulating flood inundation. Malik and Pal (2020) used HEC-RAS to generate ratings curves for limited observed telemetry points in an effort to predict the early signs of flooding in data-sparse areas of West Bengal, concluding that HEC-RAS was capable of simulating the ratings. Whilst HEC-RAS is capable of 1-D/2-D simulation, its predominant focus is in-channel geomorphology and obstruction, and there is no capability to inputting catchment hydrological data such as infiltration, interception and evapotranspiration. Thus, the use of HEC-HMS is infeasible when considering the aims and objectives and desired outcomes of this project (section 1.3).

### 3.2.2 Hydrological (Rainfall-Runoff) Modelling

Hydrological (or hydrologic/rainfall-runoff) models differ from hydraulic models as their primary objective is to account for hydrological processes throughout the catchment, compared with only assessing in-channel or floodplain flow (Ficchi *et al.*, 2019; Annis *et al.*, 2020). Rainfall is considered the primary component of the hydrological cycle (Tikhamarine *et al.*, 2020), and the hydrological process that can effect rainfall on its way to the receiving watercourse are where a hydrological model is of value (Sahraei *et al.*, 2020). Hydrological models are valuable when assessing the modelled impacts of land use change (infiltration change, vegetation planting) (Asadi *et al.*, 2019), and investigating the hydrological changes throughout a catchment as a result of changing precipitation and/or weather patterns (which is of value considering climate change) (Rubinato *et al.*, 2019).

### 3.2.2.1 Selected Hydrological Models

#### 3.2.2.1.1 HYSIM

HYSIM is a hydrological model owned and licensed by Water Resource Associates (2021), and is capable of simulating interception, surfacer runoff, infiltration, soil-water exchange, baseflow, groundwater abstraction, and in-channel flow. HYSIM does not incorporate common methods of simulating (i.e.) precipitation, infiltration, surface roughness or evapotranspiration; instead, the total loss from all selected features are subtracted from the total precipitation to predict an outflow from the study site (Water Resource Associates, 2021). This makes the model less comprehensive than others (e.g.) HEC-HMS, due to the rigidity of parameter selection and output. Adeloye and Dau (2019) utilised a calibrated HYSIM model to simulate the hydrological and hydraulic impact of nearby hedging operations on the reliability of irrigation water supply on the Pong reservoir, India. Remesan *et al.* (2019) built and calibrated two contrasting HYSIM models to determine the impact of model perimeter selection on output, using the River Beas catchment in the western Himalayan region of India. However, the use of the model in academic studies (and publication of its use) is sparse due to its common use in industry, licensing agreements, and the cost of licensing and using the software.

#### 3.2.2.1.2 Hydrologic Engineering Centre's Hydrological Modelling System, HEC-HMS

HEC-HMS can simulate multiple hydrological processes throughout the rainfall-runoff process, and is commonly used in the literature to assess the impacts of catchment changes (land used, climate, weather) on overall hydrology (Derdour *et al.*, 2018; Al-Mukhtar and Al-Yaseen, 2019; Joshi *et al.*, 2019; Nkwunonwo *et al.*, 2020; Rangari *et al.*, 2020). HEC-HMS allows the application of various numerical 'process models' to be applied to each stage of the rainfall-runoff process, meaning a model can be tailored to serve a very specific purpose dependent on the required output. On the hydrological side, HMS supports 10 infiltration/loss models, 7 transform methods and 5 baseflow methods (Scharffenberg, 2016). Additionally,

HEC-HMS supports hydraulic element simulation allowing watercourses to be inputted as either user-defined open channels, or various shaped culvers/pipes. Six routing methods can be applied to the hydraulic elements to reflect either open-channel flow, or pipe flow. appendix A.1 outlines the specific process models supported by HEC-HMS. Table 3.3 shows the element selection of authors who have undertaken projects using HEC-HMS.

Table 3.3. Literature uses of HEC-HMS with selected loss (L), transform (T), baseflow (B) and routing (R) models specified.

Author	Study Purpose	L	T	B	R
Zeleelew and Melesse, (2018)	The applicability of a spatially semi-distributed hydrological model for runoff estimation in Northwest Ethiopia	Initial and Constant / SCS Curve Number	SCS Unit Hydrograph / Clark Unit Hydrograph	Constant / Monthly	Muskingum
Koneti <i>et al.</i> , (2018)	Modelling land-use and land-cover change runoff dynamics in the Godavari River basin	SCS Curve Number	SCS Unit Hydrograph	Constant / Monthly	Muskingum / Cunge
Derdour <i>et al.</i> , (2018)	Rainfall runoff modelling using HEC-HMS in Ain Sefra watershed, Ksour Mountains	SCS Curve Number	SCS Unit Hydrograph	-	-
Kafle, (2019)	Rainfall-runoff modelling of the Koshi River basin using HEC-HMS	Deficit and Constant	Clark Unit Hydrograph	Constant / Monthly	Muskingum
Joshi <i>et al.</i> , (2019)	Simulating rainfall-runoff characteristics in the Cache River Basin, Illinois	SCS Curve Number	SCS Unit Hydrograph	-	Muskingum / Cunge
Cahyono and Adidarma, (2019)	Influence analysis of peak rate factor in the event calibration process using HEC-HMS	SCS Curve Number	SCS Unit Hydrograph	Recession	-
Al-Mukhtar and Al-Yaseen, (2019)	Testing the ability of HEC-HMS to simulate flow in the Gilgel Abay Catchment, Upper Blue Nile Basin, Ethiopia.	SCS Curve Number	SCS Unit Hydrograph	-	Muskingum

---

Rangari <i>et al.</i> , (2020)	Urban area rainfall-runoff modelling of Hyderabad City using HEC-HMS	Green and Ampt	SCS Unit Hydrograph	-	Muskingum Cunge
Ramly <i>et al.</i> , (2020)	Evaluating the performance of the Stormwater Management and Road Tunnel (SMART) in Kuala Lumpur	SCS Curve Number	SCS Unit Hydrograph	-	Muskingum
Hamdan <i>et al.</i> , (2021)	Rainfall-Runoff Modelling Using the HEC-HMS Model for the Al-Adhaim River Catchment, Northern Iraq	SCS Curve Number	SCS Unit Hydrograph	-	Muskingum
Hussain <i>et al.</i> , (2021)	Application of Physically Based Semi-Distributed HEC-HMS Model for Flow Simulation in Tributary Catchments of Kaohsiung Area Taiwan	SCS Curve Number	SCS Unit Hydrograph	-	Muskingum

---

Studies have been undertaken to validate the accuracy of HEC-HMS and the included process models. Halwatura and Najim (2013) undertook a validation of the accuracy of HMS and the included ‘process models’, finding that HMS can be reliably used to simulate flow providing prior calibration and validation has been performed (section 0). Gumindoga *et al.* (2017) used HMS to simulate flows from ten ungauged catchments in Zimbabwe, concluding that HMS can be accurately used to simulate flows from multiple subbasins and reaches over large areas. Oleyiblo and Li (2010) concluded that HEC-HMS is suitable for the simulation of study catchments, and added that whilst the structure of HEC-HMS is simple, it is a powerful tool for flood forecasting. Overall, the process models available in HEC-HMS, combined with the free to use ethos and abundance of technical and applied support makes it a desirable software for hydrological study, as has been presented in Table 3.3.

### 3.2.3 Chosen Flood Model for Study

As discussed regarding both MicroDrainage and HEC-RAS, they are hydraulic models focussing on 1-D and 1-D/2-D in-channel and floodplain simulations. Whilst they are powerful tools and have been used in the literature for a variety of applications, they will not be able to provide results of value in the scope of the aims and objectives of this study, as this study aims to investigate hydrological processes (section 1.3). Therefore, the modelling elements of this study, and the representation of the collected infiltration data, will be done-so using a hydrological model. HYSIM is discussed to be a powerful tool, with various add-ons that can aid in varying geomorphological and hydrological applications, however published literature using the software is scarce primarily due to the cost of attaining a licence and the stipulations on what can and cannot be published. HEC-HMS is discussed to be capable of simulating whole-catchment hydrology, inclusive of infiltration, runoff, interception and evapotranspiration; and is therefore chosen to build the hydrological rainfall-runoff model for this study (Derdour *et al.*, 2018; Al-Mukhtar and Al-Yaseen, 2019; Joshi *et al.*, 2019; Rangari

*et al.*, 2020). This study focusses on catchment-based woodland-influenced hydrological processes and is less concerned with mapping in-channel features and the resulting flood events. The process models available in HEC-HMS, combined with it being free to use with freely available technical support, combine with its abundant use in the literature (Gunathilake *et al.*, 2020; Sahoo *et al.*, 2020; Sharu, 2020; Hussain *et al.*, 2021), make the software the most viable modelling software for this study.

### **3.3 Flood Model Calibration and Validation**

Model calibration is the process of gradually and methodologically adjusting model parameter values so the simulated output of the model matches the observed output as closely as possible across multiple events (Sahraei *et al.*, 2020; Othman *et al.*, 2021). Models are commonly calibrated using observed and simulated streamflow or stage data (Kumarasamy and Belmont, 2018; Al-Mukhtar and Al-Yaseen, 2019; Cahyono and Adidarma, 2019). The end goal of model calibration is to produce a set of model parameters that will consistently produce the best possible outputs over any simulated event (Othman *et al.*, 2021). The number of parameters available for adjustment during calibration depends on both the complexity of the model, and the number of observed parameters across the study area (Kumar and Sherring, 2021). The more observed hydrological parameters of an area, the fewer parameters that will be available for calibration. Models should be calibrated such that the modelled output best represents the observed output, however model parameters must only be adjusted to within a tolerance that still represents the hydrological characteristics of an area (Al-Mukhtar and Al-Yaseen, 2019; Sharu, 2020). For example, adjusting the infiltration of a single sub-catchment to reduce the output of the model is a poor representation, even if infiltration data is ungauged; a more acceptable method is to spread infiltration over the ‘most realistic’ areas (Gholami and Khaleghi, 2021).

Hydrological models should be calibrated to the highest possible standard to ensure that future outputs are of a representative consistency (Othman *et al.*, 2021). However, this is sometimes a difficult constraint to overcome, as good calibration is dependent on model complexity, observed and unobserved data, the methods used within the modelling software to determine hydrology, and the desired output and intended use of the model.

Model validation is the process of analysing a model's performance when simulating and forecasting events to within a pre-determined scope (Gumindoga *et al.*, 2017; Patil *et al.*, 2019). Model validation follows model calibration, and the (now) calibrated model is given new input parameters differing from those used in calibration (infiltration, precipitation, storm duration); the correlation is measured statistically to demine an overall accuracy of the calibrated model (Patil *et al.*, 2019; Sahoo *et al.*, 2020). Separate datasets from the same catchment are often used for calibration and validation, as validating a model using the same event as was used in calibration would show an identical relationship, and not achieve the aim of testing the models capability to simulate independent events without user interference (Al-Mukhtar and Al-Yaseen, 2019; Sharu, 2020; Kumar and Sherring, 2021). No parameters are changed during validation (as this is done throughout the calibration stage), and once complete, validation indicates the final ability of the model to simulate events, both observed and unobserved.

### 3.3.1 Nash and Sutcliffe Efficiency (NSE)

To assess the ability of the model to simulate observed flow, the Nash and Sutcliffe Efficiency (1970) (NSE) method was used. The NSE method is a statistical method of comparing the mean variance, per specified timestep, of two comparable sets of continuous data; and is commonly used in the calibration and validation of hydrological modelling to indicate 'goodness of fit' (Derdour *et al.*, 2018; Al-Mukhtar and Al-Yaseen, 2019; Cahyono and Adidarma, 2019; Paul *et al.*, 2019). The NSE equation shows:

$$NSE = 1 - \left[ \frac{\sum_{i=1}^n (Y_i^{obs} - Y_i^{sim})^2}{\sum_{i=1}^n (Y_i^{obs} - Y^{mean})^2} \right] \quad EQ 3.1$$

Where  $Y_i^{obs}$  is the observed discharge,  $Y_i^{sim}$  is the simulated discharge and  $Y^{mean}$  is the mean of observed discharge.

The NSE method produces a value between 0 and 1, as an indication of how well the simulated dataset ( $Y_i^{sim}$ ) fits the observed dataset ( $Y_i^{obs}$ ). A value of 1 indicates a perfect fit between the two datasets, whereas a value of 0 (or a negative value) indicates a poor fit. The accuracy of the NSE method has been tested in the literature, concluding that if interpreted correctly, the method can be a reliable indication of model goodness-of-fit (McCuen *et al.*, 2006). Model calibration and validation, play a crucial role in reducing model output ambiguity, reducing uncertainty and acting as indicators for the reliability of modelled results (Sharu, 2020). When statistical methods of correlation have been undertaken and shown results of an acceptable tolerance, it is fair to presume that any future modelled outputs are an acceptable representation of site hydrology (Othman *et al.*, 2021).

### **3.4 Limitations and Uncertainties of Flood Modelling**

Whilst flood modelling software is commonly used to detect, analyse and predict the hydraulic and hydrological response of a catchment to changes in input, there are limitations with modelling methods (Nkwunonwo *et al.*, 2020). Hydrology is complex (Sy *et al.*, 2019), and a large majority of it is unobserved and/or difficult to monitor without the use of expensive and extensive (and often intrusive) monitoring methods (Sy *et al.*, 2019; Zhu *et al.*, 2020c). To account for this complexity and lack of observed data, modelling software (such as those introduced throughout sections 3.2.1.4 and 3.2.2) utilises equations and simplifications of movement processes (routing methods, transform methods, baseflow method) to simulate a ‘most likely’ response (Li *et al.*, 2010; Beven, 2019). Additionally, modelling is often limited by the quality and quantity of collected field data (infiltration, flow data, cross sectional

measurement), however the collection of such data is commonly sparse due to time/budgetary constraints (Sy *et al.*, 2019). The accuracy and availability of remotely sensed data can also influence the accuracy of flood modelling; the misrepresentation, availability and resolution of DTM data used in model build can distort or impede the final result, making results from the model less-reliable (Sy *et al.*, 2019). Moreover, the cost of modelling software and the expenditure that can be attributed to collecting and processing field data can have an impact on overall model output (David and Schmalz, 2020; Rampinelli *et al.*, 2020). However, regardless of the limitations highlighted, hydrological modelling is abundantly used in both academic and industry settings to investigate and assess the implications of (i.e.) development, land use change and flood intervention methods to a catchment, and the resulting hydrological changes as a result; and many authors have conducted studies relying on flood modelling software (Ahmadian *et al.*, 2018; Zelelew and Melesse, 2018; David and Schmalz, 2020; Deng *et al.*, 2020). Flood modelling should not be interpreted as an exact representation of what will happen across a catchment, however it is a vital tool in using what is known and observed, to mathematically produce a ‘most likely’ response (Rampinelli *et al.*, 2020; Kumar and Sherring, 2021).

### **3.5 Chapter Summary**

This chapter has identified the primary differences in commonly utilised methods of infiltration data collection, and assessed them in line with the aims and objectives of this study. The primary observations are that the SRI/DRI methods of infiltration data collection require large amounts of water during operation, are expensive, cumbersome to carry across large areas, and measurements are non-replicable due to the disruption caused to the soil column. The MDI, however compensates for the primary issues with the SRI/DRI methods; the MDI is lightweight, portable, requires less water in comparison, and allows for measurement

replication due to its non-intrusive nature. The MDI has been chosen to collect infiltration data for this study.

Different hydraulic and hydrological modelling software has been discussed, and appropriate literature regarding each has been identified. MicroDrainage and HEC-RAS are used as example hydraulic modelling software, and HYSIM and HEC-HMS are used as example hydrological modelling software. It is discussed in sections 3.2.1.4.1 and 3.2.1.4.2 that hydraulic modelling software is not appropriate for the desired study outcomes as they are only capable of simulating flow in one domain. Therefore, hydrological software should be used to best represent both the input data and desired outputs of the study, namely HEC-HMS (this is discussed in greater detail throughout section 5.3).

Model calibration and validation are valuable processes that can assist in improving the predictive output of flood models, and the NSE method of deriving a numerical figure is useful throughout this process for a numerical indication of model performance. The HEC-HMS model is calibrated and validated, the process of which are outlined in sections 5.4 and 5.5.

## Chapter 4 Study Site

This section discusses the rationale for study site selection, highlights the desired requirements, and explains the reasoning for choosing the selected site. Section 4.1 outlines the desired requirements of any potential study site based on the desired outcomes of this project, section 4.2 explains the reasons for study site selection, which is followed by further study site investigation in sections 4.2.1 (watershed delineation), section 4.2.2 (topographical analysis), section 4.2.3 (hydrological analysis) and section 4.2.4 (geological analysis).

### **4.1 Characterising the Study Site**

Both aim 1 and aim 3 focus on the collection and simulation of infiltration data, meaning a study site needed to be identified for study. It is discussed in section (3.1) that the MDI would be used for infiltration data collection, and the MDI is further explored throughout Chapter 6. As per the requirements of objective 1a (section 1.3), the sampling of the chosen study site would need to be achievable in a single day to keep weather conditions as constant as possible - if data collection was to be split across several days, issues would arise regarding the changing antecedent conditions of the sample plots, particularly if there was rainfall between days (Chen *et al.*, 2015; Bois *et al.*, 2020). Accommodating data collection over a single day was also a requirement of the health and safety and ethical agreements of this project (see Appendix B.9). As data collection was to continue throughout summer and winter, it was unsafe to sample the site alone during the shorter and darker winter days. Furthermore, the study site would also need to be safely navigable by foot, i.e., not be obscured by fences / private land / impassable areas (wetlands etc.). This is both for the benefit of the health and safety requirements of this project regarding lone working (see Appendix B.9), but also due to the lack of access to vehicular travel whilst on site. In addition, the chosen study site would ideally contain plots of woodland planted in different (known) years, which would accommodate objective 1b of this

project, which is to sample the effects of woodland planting due to both tree proximity and maturity. In addition, the study site would include an area of grassland (as a control and for hydrological modelling), and an area of mature woodland, for comparison against newer planted trees. Finally, the chosen study site would ideally contain a watercourse, which is accessible enough to install monitoring equipment and take cross-sectional measurements for the benefit of hydrological modelling. A rain gauge in close proximity to the site would also be beneficial for the purposes of model calibration and validation.

Upon identifying the desirable requirements of any potential study site, the Heart of England Forest (HofE) charity were approached to see if any sites matching these criteria were under their ownership. The HofE forest are introduced below (section 4.1.1).

#### *4.1.1 The Heart of England Forest and Planted Tree Species*

The Heart of England (HofE) Forest's owned areas primarily fall within the catchment area of the Arrow and Alne Rivers in Warwickshire. Figure 4.1 shows the Arrow and Alne catchment area with reference to the UK as a whole.

*Figure 4.1. The catchment area of the Arrow and Alne rivers, shown in reference to the UK  
(Data from Ordnance Survey, 2021, 2022).*

To date, the HofE Forest have planted 1,883,928 trees across 2832 hectares of Warwickshire and Worcestershire, and aim to eventually plant and maintain 12,140 hectares of forest across the English Midlands for the benefit CO<sub>2</sub> mitigation, public amenity, habitat creation, wildlife and biodiversity (The Heart of England Forest Charity, 2020, 2021). The HofE forest plant new areas of woodland in a random pattern, the only stipulation being trees be planted between 1 and 6 meters from the next, with occasional 10 – 15 m wide walkways left unplanted to aid visitors access (Felix Dennis Trust, 2019; Heart of England Forest, 2020; The Heart of England Forest Charity, 2021). Grasslands areas are only mown twice throughout the summer, but are

left mostly untouched with the intention of the areas gradually becoming more suitable for wild flower and small shrub species (Felix Dennis Trust, 2019; The Heart of England Forest Charity, 2021) (Figure 4.3 and Figure 4.2)



*Figure 4.2. Newly planted area of HofE woodland showing planting populations and walkways.*



*Figure 4.3. HofE owned grassland area*

Planted tree species is dictated by the National Vegetation Classification (NVC), developed in 1991 by the Joint Nature Conservation Committee (2003), defining the suggested distribution of vegetation species throughout the UK (JNCC, 2003; Rodwell, 2006). The HofE forests fall in to the NVC category ‘mature lowland broadleaved woodland’; the exact permissible species included under this classification are listed in appendix B.1. The HofE forest do not intent to replicate every aspect of mature broadleaved woodland, but to instead plant the key species to allow the woodlands to develop naturally (Felix Dennis Trust, 2019).

To further characterise and understand the topography and hydrology of the Arrow-Alne catchment boundary (Figure 4.1), a 2m resolution digital terrain model (DTM) was generated using data from the Environment Agency *et al.*, (2020) (see appendix Table B.16). This DTM was used to perform a flow direction analysis (Li *et al.*, 2019) as a precursor to a watershed delineation, which would define the study site (Brunda and Nyamathi, 2015; Li *et al.*, 2019). These processes are described in detail in Appendix B.2.

## ***4.2 Spernal Study Site***

Discussions were held with the head forester of the HofE forest, in which the study site requirements (section 4.1) were outlined. The intention here was to find an area of HofE owned land that best matched the requirements study, and would best facilitate the aims and objectives of study (section 1.3). Outcomes of these discussions led to a HofE owned area at Spernal Farm; Spernal Farm and the surrounding area is shown in Figure 4.4.

This item has been removed due to 3rd Party Copyright. The unabridged version of the thesis can be found in the Lanchester Library, Coventry University.

*Figure 4.4. HofE Spernal site, tributary and river Arrow (aerial photography courtesy of Ordnance Survey, 2020).*

The HofE forest were in full support of the collection of continuous data from their Spernal study site, and allowed for the private car park to be used when collecting data from the study site. In addition to this, the Spernal site is entirely navigable by foot, as the HofE forest aim to promote woodland walks. This meant that there are signposted footpaths and no boundary fences throughout the site, meaning getting from sample area to sample area is direct and efficient. This is an advantage from the point of view of the health and safety of this project

(lone working and uneven terrain), but also from the perspective of keeping antecedent ground and weather conditions as constant as possible (Chen *et al.*, 2015; Bois *et al.*, 2020). Furthermore, the ease and efficiency of traversing the site allowed more time on site to collect data, as opposed to having to travel long distances from site-to-site. Moreover, the Sernal site was the first (formerly agricultural) area purchased by the HofE forest, and the first area to host multiple plots planted in sequential years from 2006 to 2012. It being the first planted area, combined with trees being planted sequentially, means that collected data will be representative of the most mature and the most recently planted woodland, which would allow for trends between infiltration and maturity to be detected, as per objective 1b. The Sernal site also hosts an area of woodland planted *ca.* 1900 site, which was in-situ before the HofE forest owned the site, and can be sampled as an indication of the ability of more mature trees to influence infiltration. Additionally, the site contains grassland areas that pre-exists the HofE forest, and can be sampled for comparison against woodland areas, these areas will also be valuable throughout hydrological modelling to compare woodland infiltration and grassland infiltration (section 7.2) (Leung *et al.*, 2018). Further to this, Figure 4.4 (and later Figure 4.5) shows that the Sernal site is intersected by a tributary flowing from east-to-west, discharging into the river Arrow (see section 4.2.3). This was an additional benefit of sampling at the Sernal site; as discussed in section 4.1, access to a tributary would allow for monitoring equipment to be installed (section 5.3.1) which could be used in the calibration and validation of the hydrological model (sections 5.4 and 5.5), as required for objective 2a. Furthermore, the tributary was accessible from the banks and had several bridges, which allowed for cross sectional data to be collected (for the benefit of hydrological modelling) and also allowed for the watercourse to be crossed (allowing for easier site navigation). In addition to the tributary, a rain gauge was also accessible at the nearby NextGen (2020) water treatment plant; again, this was for use throughout the hydrological modelling phase of the study (see section 5.3.1).

Upon the selection of the study site (Spernal), further spatial analysis was required to define the boundary of the study area through watershed delineation (section 4.2.1), and investigate the topography (section 4.2.2), hydrology (section 4.2.3) and geology of the study site (section 4.2.4). This information would be used to develop a sampling method for infiltration data collection (section 5.2), and also form the basis for hydrological modelling (section 5.3).

#### *4.2.1 Watershed Delineation*

In order to define a hydrological boundary for infiltration data collection (section 5.2) and hydrological modelling (section 5.3), the tributary running through the Spernal site was digitised using OS data (Ordnance Survey, 2021), and a flow direction raster was generated using the Arrow-Alne catchment DTM (section B.2.1). After digitisation, the Arrow-Alne catchments DTM and flow direction raster (Figure B.1 and Figure B.4) were used in conjunction with the watershed delineation tool in ArcMap, which defined the extent of the study site catchment using the digitised tributary polyline (ESRI, 2020) (Dixon and Uddameri, 2016; Bajjali, 2018). Figure 4.5 presents the output extent for the Spernal study site, and Figure 4.6 shows the Spernal study site in proximity to Alcester and Redditch.

This item has been removed due to 3rd Party Copyright. The unabridged version of the thesis can be found in the Lanchester Library, Coventry University.

*Figure 4.5. Output catchment following watershed delineation. The study site area is 220 Ha (2.2 km<sup>2</sup>) (aerial photography courtesy of Ordnance Survey, 2020).*

This item has been removed due to 3rd Party Copyright. The unabridged version of the thesis can be found in the Lanchester Library, Coventry University.

*Figure 4.6. The Arrow-Alne catchment area, with Spernal study site highlighted (in red), in proximity to Alcester and Redditch (Data from Ordnance Survey, 2021, 2022).*

Defining the study area based on the watershed delineation method is beneficial as it defines a justified area in which a sampling method for field work can be undertaken and will act as the bounds for hydrological modelling (Dixon and Uddameri, 2016; Bajjali, 2018; Li *et al.*, 2019). The output from the watershed delineation will be used as the study site boundary throughout this study, and all field data collection and hydrological modelling will be undertaken within the confines of the area defined.

#### 4.2.2 *Study Area: Topography*

Upon definition of the hydrological catchment boundary, more specific topographical analysis of the study area was undertaken in addition to the DTM shown in Figure B.1. An understanding of the study site at a higher resolution would enable the production of the flow direction analysis (section 4.2.3), which would aid in the definition of flow pathways and hydrological node allocation throughout hydrological modelling (section 5.3.2) (Annis *et al.*; Jeziorska, 2019; Deng *et al.*, 2020). The area was surveyed using a drone capable of capturing LiDAR data at 14cm resolution (in comparison to the EA DTM of 2m resolution). See Figure 4.7.

This item has been removed due to 3rd Party Copyright. The unabridged version of the thesis can be found in the Lanchester Library, Coventry University.

*Figure 4.7. Extent of LiDAR data collected by the drone (Boundary data from Ordnance Survey, 2021, 2022)..*

Only 156Ha (70%) of the 220Ha study area could be surveyed by the drone due to permissive issues; to in-fill the remaining 30%, the 2 m DTM (Figure B.1) was mosaiced to the drone DTM using ArcMap. It was specified when using the mosaic tool that as much of the high-

resolution drone data should be used as possible, ensuring that the lower resolution data was used only in areas where higher resolution was not available. Figure 4.8 shows the final mosaiced output DTM for the study area.

This item has been removed due to 3rd Party Copyright. The unabridged version of the thesis can be found in the Lanchester Library, Coventry University.

*Figure 4.8. Elevation model of the study catchment as a result of merging drone and prior topographical (2 m) data (Data from Environment Agency et al., 2020; Ordnance Survey, 2021, 2022).*

Whilst this method allowed for the creation of an elevation model for the whole study area, which would be of use in later hydrological modelling, there are limitations caused by the inconsistency of data resolution and the time between the collection dates of both datasets. The coarser resolution is less descriptive of small changes in topography, meaning that the higher resolution areas could represent overland flow more accurately, possibly leading to overestimation in the model (Liu et al., 2019). However, only 30% of the catchment is comprised of coarser imagery, 50% of which is not owned or maintained by the HofE forest – meaning that little hydrological information would be derived from these areas to inform the

model, regardless of the impact of coarser imagery (Ng *et al.*, 2018; Li *et al.*, 2019; Pinos and Timbe, 2019). Additionally, the EA 2m resolution data was collected in 2017 and the drone data was collected in 2019 – this discrepancy in datasets may lead to changes in detectable topography over time (differences in field cover, development, cover from larger trees) (Lopes Bento *et al.*, 2022). However, the discrepancies in data collection periods were a constraint of using secondary data, and the less of the 2m resolution data was used (30%), meaning the more consistent, high resolution data could be used to inform the hydrological model with little impact (Li *et al.*, 2019; Lopes Bento *et al.*, 2022).

#### 4.2.3 *Study Area: Hydrology*

An additional flow direction analysis was undertaken on the defined study site using the newly created elevation model (Figure 4.8) to better understand hydrological details of the study site, such as overland flow pathways and water-flow directions, in preparation for the hydrological modelling. See Figure 4.9 and Figure 4.10.

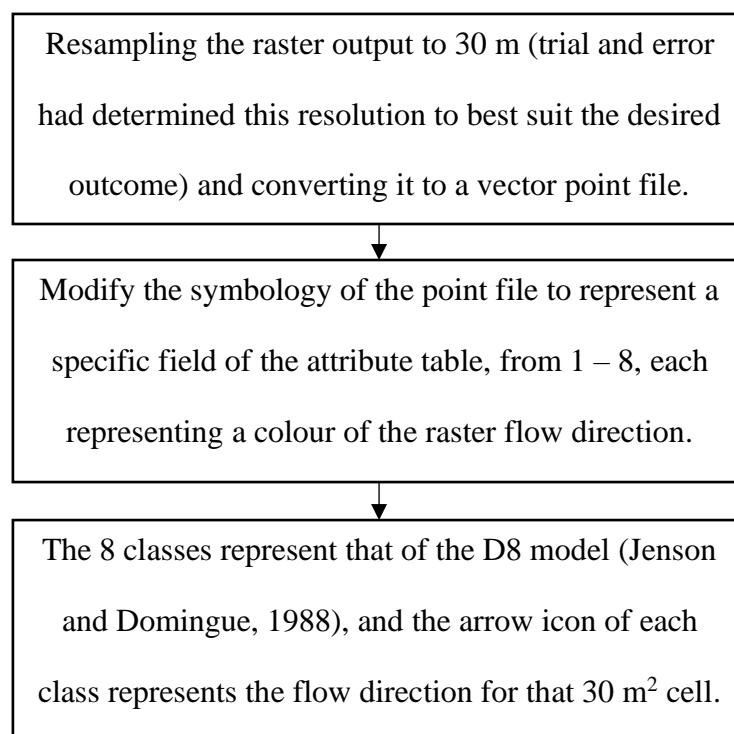


Figure 4.9. Process of creating the study site flow direction analysis vector overlay

*Figure 4.10. The resultant output of the flow direction analysis described (aerial photography courtesy of Ordnance Survey, 2020).*

To generate Figure 4.10, the output arrow point file was overlain with the study catchment elevation model to produce a clear representation of overland flow direction across the catchment. This step was particularly beneficial for reference during the hydrological modelling stage of the project, as the output allowed for a thorough, high-resolution interpretation of the overland flow pathways (Mockler *et al.*, 2016; Metcalfe *et al.*, 2018).

#### 4.2.4 Study Area: Geology

To develop a deeper understanding of the study site in preparation for hydrological modelling, the bedrock and superficial geology of the study area was determined in addition to the

topographical and hydrological information (Archer *et al.*, 2013; Folorunso and Aribisala, 2018). 1:10,000 resolution geology data for the study catchment was downloaded under special permission from the British Geological Survey (BGS), seen in Figure 4.11. This item has been removed due to 3rd Party Copyright. The unabridged version of the thesis can be found in the Lanchester Library, Coventry University.

*Figure 4.11. Bedrock and superficial geology of the study area (Geology data from British Geological Survey, 2019).*

The bedrock geology of the study area is primarily mudstone with small areas of siltstone, the superficial deposits include clay and silt with localised areas of sand and gravel (broadly following the tributary), with an area of diamicton to the north. Whilst the 1:10,000 geology data is valuable, it is important to note that this is still a coarse resolution and the smaller, localised geology types may vary more frequently than shown in Figure 4.11 (Lovat *et al.*, 2019; Ding *et al.*, 2020). Additionally, the BGS map does not represent surface soil texture or soil type, only underlying superficial and bedrock geology. The specific determination of sample site soil texture is discussed in section 5.2.1.1.

### ***4.3 Chapter Summary***

This section has introduced the desired characteristics of any chosen study site, in addition to introducing and describing the characteristics of the chosen HofE owned site at Sernal. The Sernal study site has been presented in reference to the wider Arrow/Alne catchment (Figure 4.6) and additional spatial analysis has been undertaken to further investigate the study site, namely; a watershed delineation (section 4.2.1), a topographical evaluation (section 4.2.2), a hydrological evaluation (flow direction analysis) (section 4.2.3) and a geological evaluation. In addition to these processes providing further information about the study site, this information will be used to develop a sampling method for infiltration data collection (section 5.2), and inform the build of the HEC-HMS model (section 5.3).

## Chapter 5 Research Design and Methodology

This chapter introduces and evaluates the study methodology. Section 5.1 introduces the research philosophy and hypotheses of study; section 5.2 introduces the sampling methodology and the processes used in sample site design, section 5.3 introduces the processes involved in hydrological model build, and sections 5.4 and 5.5 present the processes and results of model calibration and validation. Section 5.6 introduces the methods involved in present-day study site simulations, and section 5.7 presents the data and methods used in projecting future hydrological outputs.

Table 5.1 below presents a summary table indicating where, in the following chapters and sections, the aims and objectives of this study are met. Figure 5.1 to Figure 5.4 below present several conceptual methods frameworks outlining how this chapter is structured, and how elements interlink.

*Table 5.1. Sections in which the primary requirements of the aims and objectives are met.*

<b>Aim 1:</b>			
<b><i>Through field investigation, determine to what extent woodland planting by the Heart of England Forest has influenced infiltration, with reference to tree proximity and tree maturity.</i></b>			
<b>Objectives</b>	Methods section(s)	Results section(s)	Discussion Section(s)
<b>1a:</b> <i>Define suitable sampling locations and methods for infiltration data collection and gather data.</i>	3.1; 4.2; 5.2	6.1	-
<b>1b:</b> <i>Using data collected in objective 1a, derive any relationships between infiltration and tree proximity and maturity.</i>	-	7.1	8.1

### **Aim 2:**

***Using HEC-HMS, build, calibrate, and validate two-separate hydrological models using spatial and hydrometric data collected from the study site.***

<b>Objective</b>	<b>Methods section(s)</b>	<b>Results section(s)</b>	<b>Discussion Section(s)</b>
<b>2a:</b> <i>Build, calibrate and validate two hydrological models in HEC-HMS</i>	5.3; 5.4; 5.5	-	-

**Aim 3:**

*Using the HEC-HMS model, simulate outflow hydrology from the study site dependent on changing storm intensity, duration, land cover, tree maturity and climate change; and determine to what extent HofE woodland planting has influenced infiltration, runoff and river flows.*

<b>Objectives</b>	<b>Methods section(s)</b>	<b>Results section(s)</b>	<b>Discussion Section(s)</b>
<b>3a:</b> <i>Using both field data collected in aim 1a, and the HEC-HMS model, simulate the hydrological responses of the HofE study site to varying land cover, tree maturity, storm duration and intensity.</i>	5.6	7.2	8.2.1
<b>3b:</b> <i>Use recent Environment Agency climate change allowances, in conjunction with the HEC-HMS model, to predict the likely future changes to site hydrology considering developing tree maturity and climate change.</i>	5.7	7.3	8.2.2
<b>3c:</b> <i>Using the empirical and simulated results of this study, evaluate the hydrological effects of tree planting as a method of NFM.</i>	-	-	8.2.3

**Aim 4:**

**Assess the implications of study findings, and provide recommendations and suggestions for relevant stakeholders and future policy.**

<b>4a:</b> <i>Using the findings of both aim 1 and aim 3, provide recommendations and suggestions for relevant stakeholders and future policy.</i>	-	-	9.1
--	---	---	-----

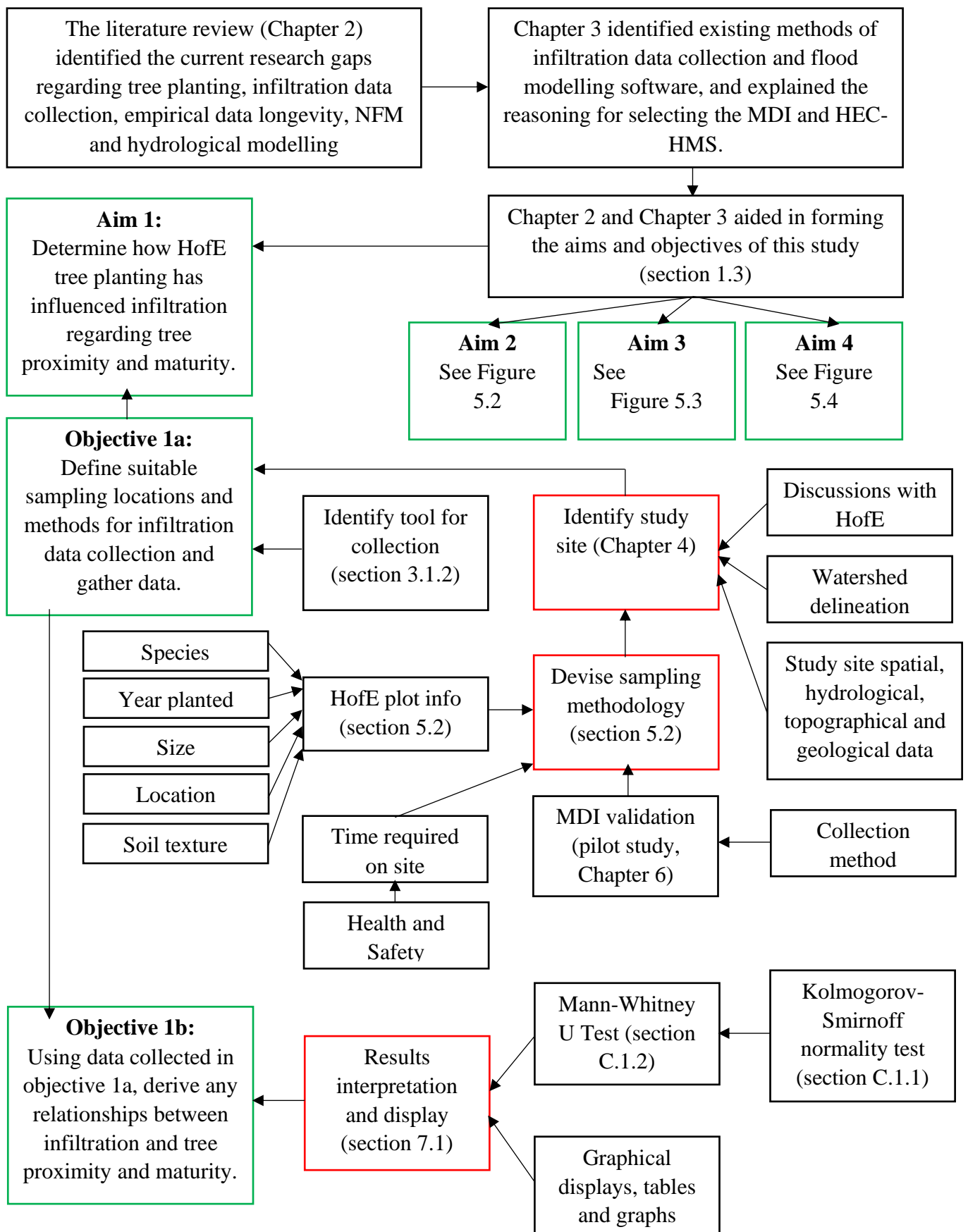


Figure 5.1. Conceptual methods framework outlining how previous chapters, and the upcoming methodology interlink with the aims and objectives of study. This Figure describes Aim 1 of this stud. Green boxes indicate aims/objectives, and red boxes indicate key processes.

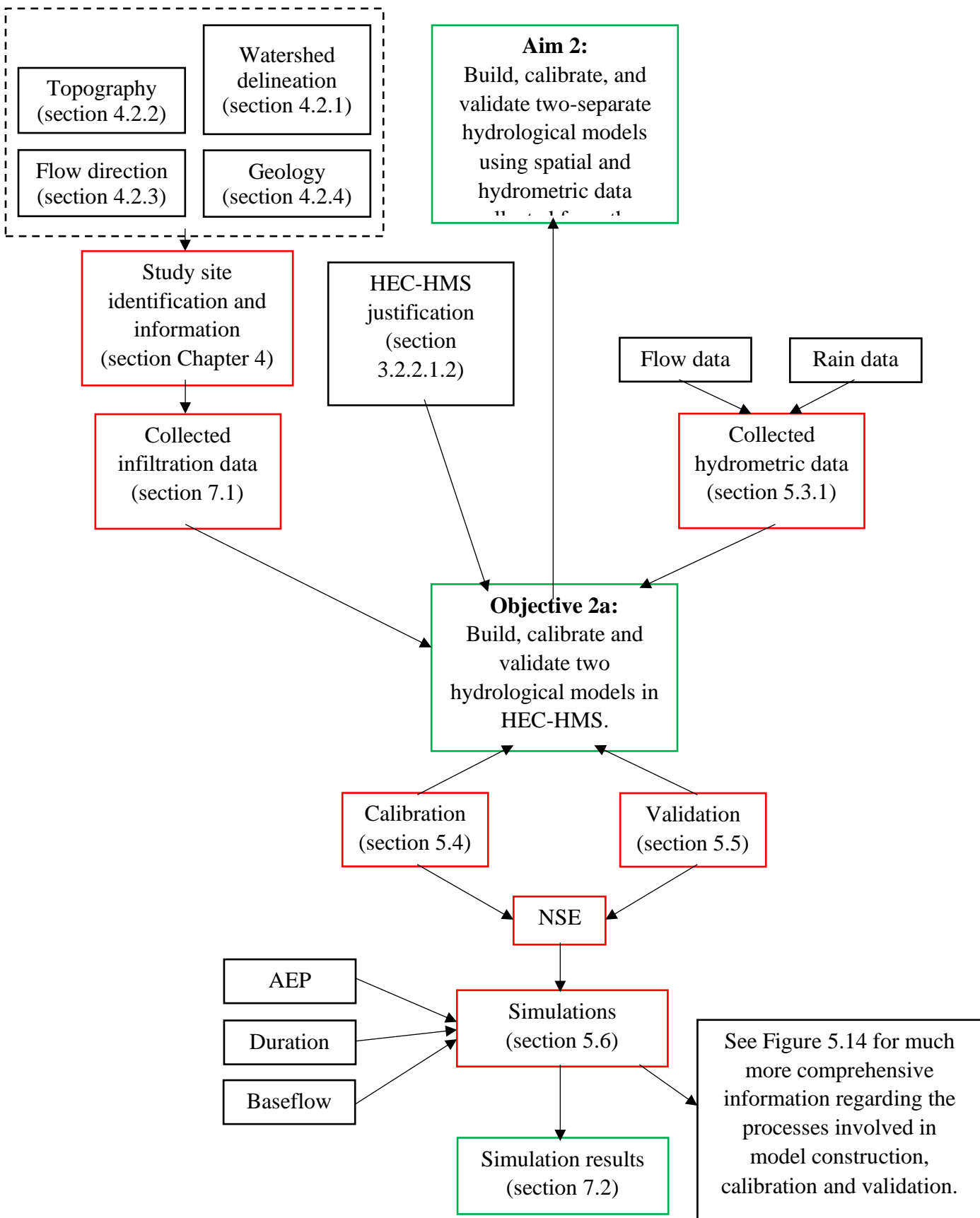


Figure 5.2. Conceptual methods framework outlining how previous chapters, and the upcoming methodology interlink with the aims and objectives of study. This Figure describes Aim 2 of this study. Green boxes indicate aims/objectives, and red boxes indicate key processes.

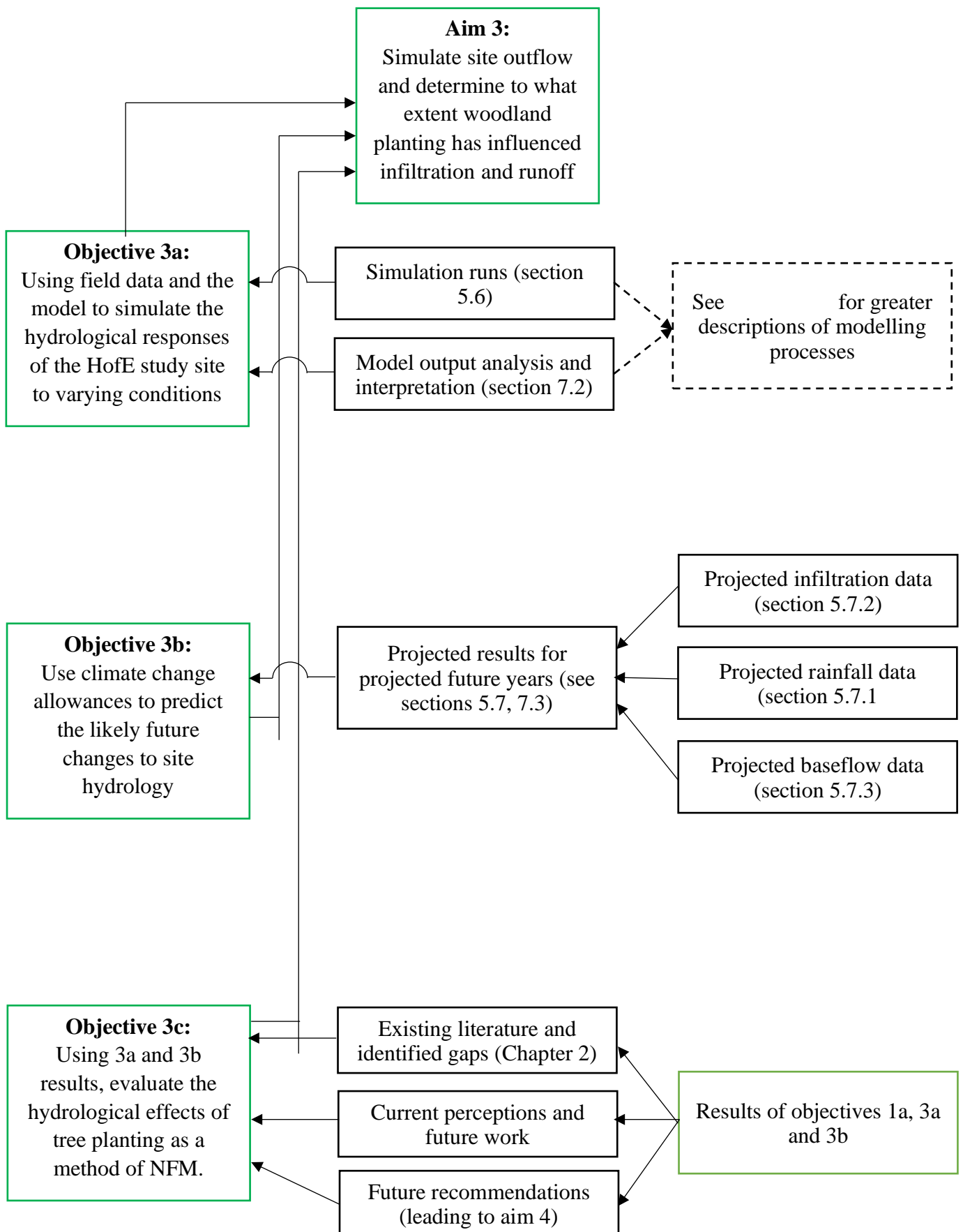


Figure 5.3. Conceptual methods framework outlining how previous chapters, and the upcoming methodology interlink with the aims and objectives of study. This Figure describes Aim 3 of this study. Green boxes indicate aims/objectives, and red boxes indicate key processes.

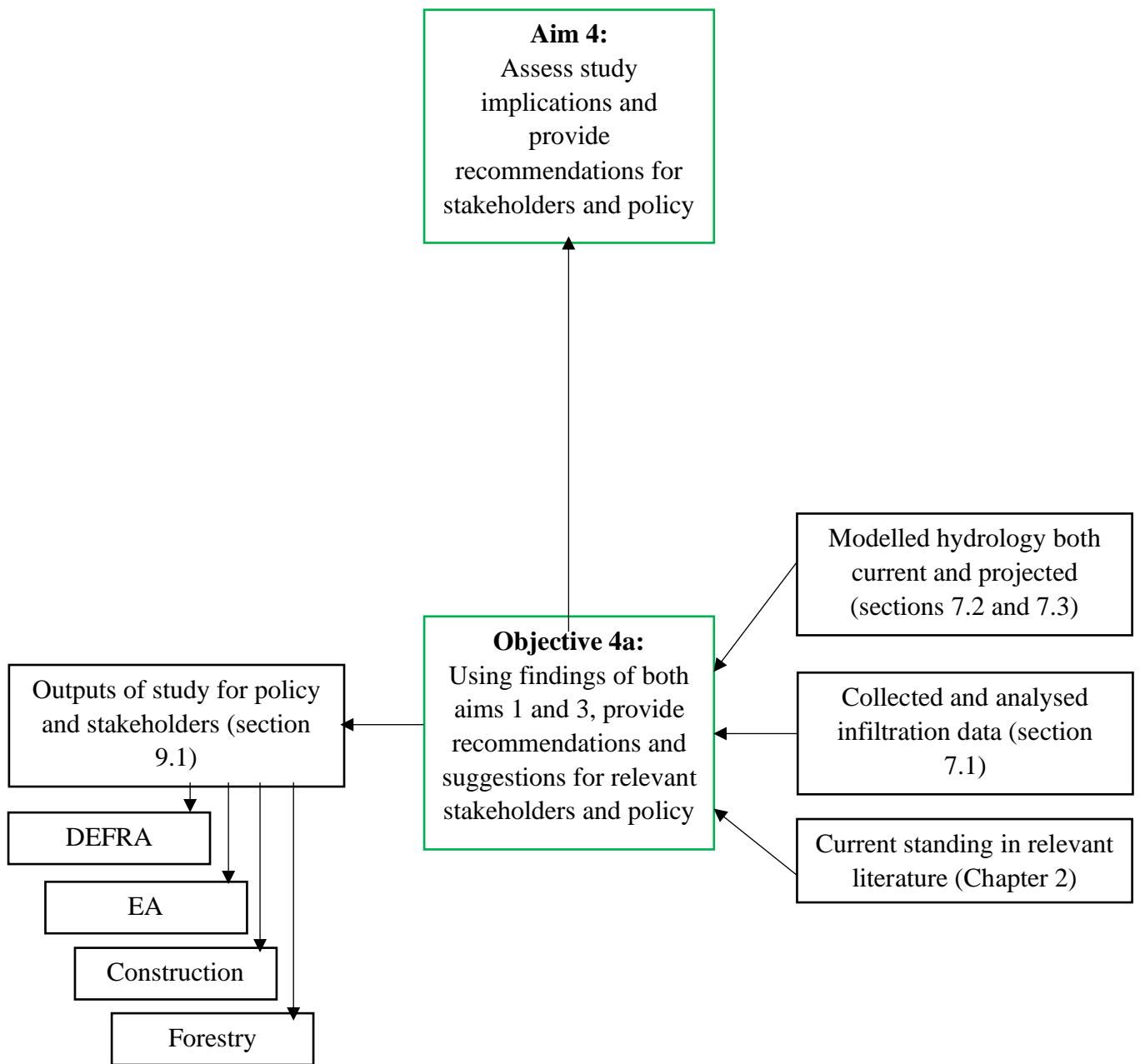


Figure 5.4. Conceptual methods framework outlining how previous chapters, and the upcoming methodology interlink with the aims and objectives of study. This Figure describes Aim 4 of this study. Green boxes indicate aims/objectives, and red boxes indicate key processes.

### **5.1 Research Philosophy and Hypotheses**

Research philosophy refers to a system of approaches and beliefs about the way in which data should be gathered, analysed, and used (Saunders *et al.*, 2019). All research is prone to some form of philosophical assumption (Burrell and Morgan, 2016), namely, ontological (assumptions about reality), epistemological (assumptions about human knowledge), and axiological (assumptions about personal belief) (Alvesson and Skoldberg, 2009; Saunders *et al.*, 2019). An acknowledgement of both assumptions and research philosophy, and the influence they can have on research methods and results interpretation, is important when evaluating the impact of a contribution to the wider subject area (Crotty, 1998; Johnson and Clark, 2006; Saunders *et al.*, 2019).

The research onion was presented by (Saunders *et al.*, 2019) as a model to demonstrate the different stages of organising and constructing a methodology, symbolically illustrating the ways in which elements of the research could be examined to inform the final research design. The research onion is presented in Figure 5.5.

*Figure 5.5. The research onion model by (Saunders et al., 2019) outlining the layered approach to study design and data collection.*

Shown in Figure 5.5, the research onion consists of six 'layers' demonstrating the scales at which principles should be considered, from right-to-left; philosophy, approach to theory development, methodological choice, strategy(ies), time horizon and techniques and procedures (Saunders et al., 2019). Much deeper explanation and analysis into the details of each layer of the research onion are discussed by (Melnikovas, 2018; Saunders et al., 2019); however, for the purposes of this study, Table 5.2 presents the approaches adopted for use throughout this study methodology.

Table 5.2. Categories of the research onion with regard to the philosophy, hypothesis and methodology of this study.

Onion 'layer'	Relevant classification/ category for this project	Additional Information
<b>Philosophy</b>	Positivism	Positivism bases its ideologies around working with an observable reality to produce law-like generalisations (Melnikovas, 2018). The philosophy aims to deliver and interpret unambiguous and accurate knowledge, focussing solely on scientifically observed parameters, uninfluenced by human interpretation or bias (Crotty, 1998; Saunders <i>et al.</i> , 2019).
<b>Philosophical Assumption</b>	Epistemology	Scientific method, favours observable and measurable facts, provides law-like generalisations, involvement of numbers, contributions are commonly causal explanations and predictions
<b>Approach</b>	Deduction	Deductive research starts with an existing theory based on observation and data collection, then intends to form, accept, or reject a hypothesis to form a theory after conducting deeper analysis (Crotty, 1998; Burrell and Morgan, 2016). The deductive approach is usually applied to the testing of existing theories – in this case, infiltration testing and hydrological modelling (sections 5.2 and 5.3). The study hypotheses are introduced below this table.
<b>Methodological choice</b>	Quantitative	Data collected and expressed as a measurable quantity, common for measurements units to be associated with the data.
<b>Strategies</b>	Case study	Referring to a defined area in which a sampling method will be structured, and data will be collected. The case study for this project is introduced in Chapter 4.

<b>Time horizon</b>	Longitudinal	Data will be collected for the maximum possible duration for this study (multiple years). It is discussed in section 5.2.2.1 that data was collected over a 2-year period.
<b>Techniques and procedures</b>	Infiltration data collection	Infiltration data will be collected following the sampling method discussed in section 5.2. The infiltration data will be statistically analysed (section 7.1) and inform a hydrological model (section 7.2).
	Hydrological modelling	Hydrological data will be collected (section 5.3), which will, alongside the infiltration data, inform a hydrological model (section 5.6) to produce results in line with the aims and objectives of this study (section 1.3).

As outlined in Table 5.2, hypotheses are required for deductive study approaches, therefore this study methodology is designed to test the following hypotheses:

- 1) *If woodland planting can influence infiltration, dependent on tree proximity and tree maturity.*
- 2) *If woodland planting can reduce river flows compared to grassland and impermeable surfaces.*
- 3) *If woodland planting has the potential to mitigate future river flows considering the predicted increase in precipitation expected due to climate change.*

### **5.2 Field Sample Plots, Sampling Methods, Data Collection and Data Recording**

Once the study site had been identified, and the boundary defined (section 4.2), a sampling method for infiltration data collection (objective 1a) could be devised. Any sampling method would need to ensure that the collected data would be replicable and representative of the wider study area to produce accurate results (Prieksat *et al.*, 1994; Logsdon and Jaynes, 1996; Khodaverdiloo *et al.*, 2017) and inform the hydrological modelling phase of study (section 5.6). Outlined in section 4.1:

1. The sampling of the site needed to be achievable in a single day to keep weather conditions as constant as possible (Chen *et al.*, 2015; Bois *et al.*, 2020), but also as a pre-requisite of the health and safety and ethical agreements of this project (see Appendix B.9).
2. Methods and equipment used in the field could not be too expensive due to budgetary constraints; and any equipment for measuring infiltration needed to be lightweight, portable and require reasonable amounts of water to operate as the study site could only be navigated on foot, and water was not available on the site.
3. Infiltration testing needed to be replicable on a week-by-week basis, so intrusive methods of infiltration data collection were ruled out. Replication was an important requirement for the data collected throughout this study, as the aim of infiltration data collection was to detect any change in infiltration due to proximity over time. This ruled out SRI and DRI methods due to their use requiring the insertion of the ring into the soil core, and then the subsequent destruction of the soil core upon removal (Bagarello and Sgroi, 2004; Zhang *et al.*, 2017a).

Considering the criteria discussed and the sampling methods employed by other authors conducting similar research (Chandler *et al.* 2018, Marshall *et al.* 2013 and Sanou *et al.* 2010), a sampling method was devised and is discussed throughout the following sections.

### *5.2.1 Infiltration Sampling Sites (Spernal)*

The first phase of designing a sampling method was to identify the maturity and species of wooded areas at Spernal. See Figure 5.6.

*Figure 5.6. Study area showing the tributary, owned HofE woodland and the year areas were planted (plot data was provided by the HofE Forest Charity, aerial photography courtesy of Ordnance Survey, 2020).*

Figure 5.6 shows the oldest trees at the study site were planted *ca.*1900, before the Heart of England Forest purchased the Sernal site, the oldest trees planted by the HofE forest were planted in 2006, and the youngest trees were planted in 2012. The unrecorded categories represent areas of grassland that were in-situ prior to the HofE Forest moving to the site. Whilst there is only a six-year difference between the youngest and oldest (HofE planted) trees across the site, this will still allow for an analysis of the influence of maturity and proximity on infiltration over time. Additionally, the sample areas being in close proximity and situated throughout the same watershed, allowed for the trees to be sampled in one day and results to be representative of hydrological processes throughout the catchment (compared with driving to different areas to collect data). Both of these factors were particularly advantageous when collecting results from the study site, and when contextualising the results of this study with

existing literature and policy; also of use when extrapolating the study site characteristics to the whole study site for hydrological modelling and future climate projection. Species groups of the planted wooded areas are shown in Figure 5.7.

This item has been removed due to 3rd Party Copyright. The unabridged version of the thesis can be found in the Lanchester Library, Coventry University.

*Figure 5.7. Species group of wooded areas across the study area (aerial photography courtesy of Ordnance Survey, 2020).*

The trees planted by the HofE forest in 2006 were sampled as they would represent the oldest area of HofE planted woodland for comparison against more recently planted areas. To accommodate the sampling requirements discussed in (section 5.2), more specifically the restraints regarding the time on site required for sufficient data collection, areas planted in 2008, 2010 and 2012 were sampled in addition to the 2006 plot. If woodland planted in every sequential year from 2006 were to be sampled, the time alone on site required to collect data (particularly when allowing time for measurement replication) would exceed the rules specified by the health and safety agreement of this project. In addition to measurements taken at plots planted in 2006, 2008, 2010 and 2012; a *ca.* 1900 plot would be included in the sampling for a

comparison of the effect of an established (mature) tree on infiltration, as would a grassland control to represent the infiltration characteristics of land that had not been wooded (Hepner *et al.*, 2020; Tinya *et al.*, 2020; Zhu *et al.*, 2020a). The largest plot-areas of each sample year were selected as to reduce edge effects - the process of an external factor, or change in sampling consistency, influencing the process of consistent data collection or replication (Baddeley, 2019; Hatfield *et al.*, 2020). Edge effects need to be carefully interpreted as failing to identify the process could lead to inaccurate data collection (Baddeley, 2019; Hatfield *et al.*, 2020). Information provided by the HofE forest was used to determine the coordinates of the centre of the plots on ArcMap. The centre coordinates of each planting area were uploaded to a handheld GPS device to allow the same location to be identified in the field, and the tree closest to this location would be the sample tree for that area. However, after a site visit it was apparent that sampling the centre of the *ca.*1900 or control sites was not possible; the *ca.*1900 site has deer-fencing around the centre, and the middle of the control plot fell in the gravel car park. Therefore, the sampling locations of these plots were moved slightly to best represent plot infiltration, but still consider the sensitivity of edge effects (Razafindratsima *et al.*, 2018; Baddeley, 2019; Hatfield *et al.*, 2020). Whilst this may have slightly influenced the data collected from these sites, sampling parameters were considered (consistency and location representation) and relevant literature consulted (Bonell *et al.*, 2010; Chandler *et al.*, 2018) before finalising the new sampling locations. The final sampling locations would stay constant throughout the duration of data collection in the interests of measurement consistency and replication. Figure 5.8 shows the sample plots selected along with the exact locations of MDI measurement, further information regarding the specific sample trees can be seen in Appendix B.2.

*Figure 5.8. Woodland areas, year planted and sample points for sampling (aerial photography courtesy of Ordnance Survey, 2020).*

#### 5.2.1.1 Additional Infiltration Sampling Sites, Soil Texture and Sample Tree Species

As all trees were planted at the Sernal site by 2012, two newer sites (also owned by the HofE forest) were included for infiltration sampling; one planted in 2014, and one in 2020. Data collected from these additional sites would represent the influence of more recently planted trees, and further determine how tree planting has affected local infiltration over time. The locations of the 2014/2020 sites are shown in proximity to Sernal in Figure 5.9.

This item has been removed due to 3rd Party Copyright. The unabridged version of the thesis can be found in the Lanchester Library, Coventry University.

*Figure 5.9. Additional 2014 and 2020 sample areas. 2014 is to the southeast of Studley, 2.5 km north of the Spernal site; and 2020 is to the south of Newnham, 6 km southeast of the Spernal (aerial photography courtesy of Ordnance Survey, 2020).*

Whilst the inclusion of the 2014 and 2020 sites was valuable for the comparison of newly planted woodland against woodland planted in earlier years (at Spernal), the main advantage of collecting infiltration data from these sites was for hydrological modelling (section 5.3). Information from 2014 and 2020 allowed for the projection of future infiltration changes, regarding tree growth and increased precipitation due to climate change. This is explained in greater detail in section 5.7.

It should be noted that data collection from the 2014 and 2020 sample sites took place on alternate weeks to data collection at Spernal, which means considerations must be made when interpreting the data. Antecedent moisture and atmospheric temperatures varied between data collection at Spernal and the 2014 and 2020 sites (appendix C.2). This is a potential area of limitation as changing antecedent conditions can influence soil conditions and subsequent

infiltration data collection (Chen *et al.*, 2015; Bois *et al.*, 2020) due to variations in hydraulic conductivity, soil saturation and (potential) frost cover (see section 5.2.2). However, soil texture classifications were the same between both 2014 and 2020, and most of the Sperial sites (aside from *ca.* 1900, 2010 and control), meaning that the sites were comparable from the perspective of infiltration data collection. To determine the soil texture of all infiltration sample locations, a LaMotte (2020) soil texture test kit was used. This required 1 ml of soil texture dispersing reagent and 45 ml of water to be added to a 15 ml soil sample, shaken, left to settle, and transferred to several different test tubes representing separate percentage. The LaMotte method was used over alternate methods of soil texture analysis ('press-and-roll' method, water suspension method) due to its use in other studies, and its increased reliability compared with methods involving only touch or water (Itoh *et al.*, 2003; Rasmussen *et al.*, 2018; Oliveira-Jr *et al.*, 2020). The soil textures of all sample sites are shown in Table 5.3.

*Table 5.3. Separate percentiles and UK soil classification of sample site soil textures.*

Sample Site	Sand %	Silt %	Clay %	UK Soil Classification	
Control	53	20	27	SaCL	Sandy clay loam
<i>ca.</i> 1900	47	40	13	SSL	Sandy silt loam
2006	20	20	60	C	Clay
2008	13	20	67	C	Clay
2010	53	33	14	SaL	Sandy Loam
2012	33	13	54	C	Clay
2014	7	13	80	C	Clay
2020	13	23	77	C	Clay

The control, *cc.*1900 and 2010 sites to consist of a slightly sandier geology compared with the other sample sites, consisting of primarily clay particles. Discussed in section 2.5, clay-heavy soil textures inherit lower infiltration, conductivity and porosity due to the smaller, more

rounded particles (<0.002 mm) fitting tightly together (Rabot *et al.*, 2018). Sand particles are larger (0.06 mm – 2.0 mm) and more angular, meaning larger pores are left between the particles, allowing for greater infiltration and conductivity in sandier-textured soils (section 2.5) (Rabot *et al.*, 2018; Meyer *et al.*, 2019; Bátková *et al.*, 2020; Mahapatra *et al.*, 2020). The difference in soil texture is acknowledged and accounted for throughout the analysis of study results (Chapter 7 and Chapter 8). In addition to soil texture, there were variations in sampled tree species, see

Table 5.4.

*Table 5.4. Sample tree species and sample area for all plots.*

Year Planted	Group	Species Name		Size (Ha)
Unrecorded	Grassland			8.6
ca.1900	Mixed Broadleaf	Sessile Oak	Quercus Petraea	2.6
2006	Native Mixed Broadleaf	Silver Birch	Betula Pendula	6.5
2008	Native Mixed Broadleaf	Aspen	Populus Tremula	8.5
2010	Native Mixed Broadleaf	Silver Birch	Betula Pendula	14.3
2012	Native Mixed Broadleaf	Aspen	Populus Tremula	13.7
2014	Native Mixed Broadleaf	Aspen	Populus Tremula	2.6
2020	Native Mixed Broadleaf	Aspen	Populus Tremula	17.7
Total				70.5

The variation in species is due to two factors: 1) the method of sampling from the closest tree to the centre of the sample site (discussed in section 5.2.1), and 2) the HofE forest planting following the NVC (see appendix B.1). The ca.1900 site was in-situ before the HofE forest owned the site and will be used as an indication of the ability of more mature trees to influence infiltration. The grassland site was used as a control, and will be valuable throughout hydrological modelling to compare woodland infiltration and grassland infiltration (section

7.2) (Leung *et al.*, 2018). Whilst the ideal sample design would collect infiltration data from only one species of woodland throughout the duration of study, this was not possible due to the above reasons (the NVC and the decision to collect data from the centre of the sample plots). However, the collection of infiltration data from the selected study sites would allow for data analysis, and contribute to the identified research gap and justification of this study (sections 1.3 and 2.6). Results from the Birch and Aspen sites will be analysed together, however their physical differences (expected age, growth rates, size) will be accounted for throughout the climatic projection methods (section 5.7). The collection of the 2014 and 2020 infiltration data added to the study robustness and acted as an additional empirical anchor point throughout hydrological modelling and results interpretation compared with if the values were to be derived from published values. Details of the locations used for sampling in this study are presented in appendix B.2.

### 5.2.2 Field Sampling Methods and Data Collection

As outlined above, the 2014/20 sites were sampled on alternate weeks to the Sernal sites. The sampling of Sernal and 2014/2020 took a day each. A day was allocated due to the amount of time required to sample each plot at both locations, in addition to allowing enough time to travel to every plot on foot, collect the required amount of data, and keep climate and weather conditions as consistent as possible between and during measurement. Variations in (e.g.) soil moisture, dew or frost between sample sites could influence the collected infiltration data for that sample, and skew the results during analysis (Harden and Scruggs, 2003; Baiamonte, 2019). If data collection was to be split across several days, issues would arise regarding the changing antecedent conditions of the sample plots, particularly if there was rainfall between days (Chen *et al.*, 2015; Bois *et al.*, 2020). The chosen method was also advantageous from a health and safety point of view, concerned with being on uneven terrain, near a watercourse in the dark (during the winter months). To ensure the infiltration data collection was

representative of the issues that can arise due to varying weather (e.g., heavy dew, overnight rainfall site saturation and soil moisture), the sites were sampled in reverse order from week-to-week (Harden and Scruggs, 2003; Miller and Hess, 2017; Baiamonte, 2019). Meaning at the start of a new sample week, the last site sampled on the previous visit would be the first sampled on the current visit, this is visualised and discussed in appendix B.4.

#### *5.2.2.1 Mini Disk Infiltrometer Measurement*

Regarding the equipment used to measure infiltration, it is discussed by Alagna et al. (2016) and Khodaverdiloo et al. (2017) that several factors should be considered; the accuracy of measurement, the speed and simplicity of measurement, the cost of the device, the portability of the equipment and the required recourses of each individual measurement (water, person-power). SRI and DRI methods of infiltration data collection (section 3.1) were considered; however, these methods do not allow for consistent replication (due to the disruption of the soil core), they are cumbersome to transport around the study site, they require vast amounts of water for measurement (which was not easily attainable at any sample site), and they are expensive (~£2000 for a DRI). Therefore, the Mini Disk Infiltrometer (MDI) was used for all infiltration data collection throughout this project; due to its portability, low water requirements, speed of set up and ease of (solo) measurement and data recording. Both methods are discussed and evaluated in more detail throughout sections 3.1.1 and 3.1.2; the reasoning for selecting the MDI is discussed in section 3.1.3.

Infiltration measurements were taken from both 10 cm and 200 cm away from the base of the tree. The 10 cm proximity was chosen during a pre-sampling visit to the study site where it was determined that 10 cm was as close as the MDI could get to the base of the tree without interference from the root system or growths around the base. Infiltration data collected from the 10 cm proximity would also act as a direct representation of the change in infiltration because of the tree – this would later be used in hydrological modelling to represent the closer

proximity in the model (section 5.6). The 200 cm proximity was chosen after assessing the exiting literature regarding tree lateral root spread (section 2.3.1), but also literature specifically regarding the tree species sampled (Perry, 1982; Mauer and Palátová, 2003; Hepner *et al.*, 2020), suggesting that the lateral root spread would surpass the 200 cm measuring distance (meaning a greater chance of collecting infiltration data in an area affected by roots). The 200 cm would also be used for hydrological modelling but will act as a comparison to the 10 cm proximity in addition, allowing for the influence of tree proximity on infiltration to be delineated.

It is well regarded in the literature that infiltration measurements taken in the field inherit high spatial variability, and replication is imperative for attaining accurate results (Prieksat *et al.*, 1994; Logsdon and Jaynes, 1996; Khodaverdiloo *et al.*, 2017). There are no definitive suggestions regarding how many replicas are required, however the number of repetitions should best represent field conditions at the time of measurement. Thus, every measurement taken with the MDI was replicated twice (in addition to the first measurement) and all replicates were averaged to give a final averaged total for that site. The decision to replicate three times at each proximity was primarily driven by the time that would be required for each measurement, and the ability of three measurements to allow for a mean average to be calculated. Figure 5.10 shows the method in which infiltration measurements were taken in proximity to the tree.

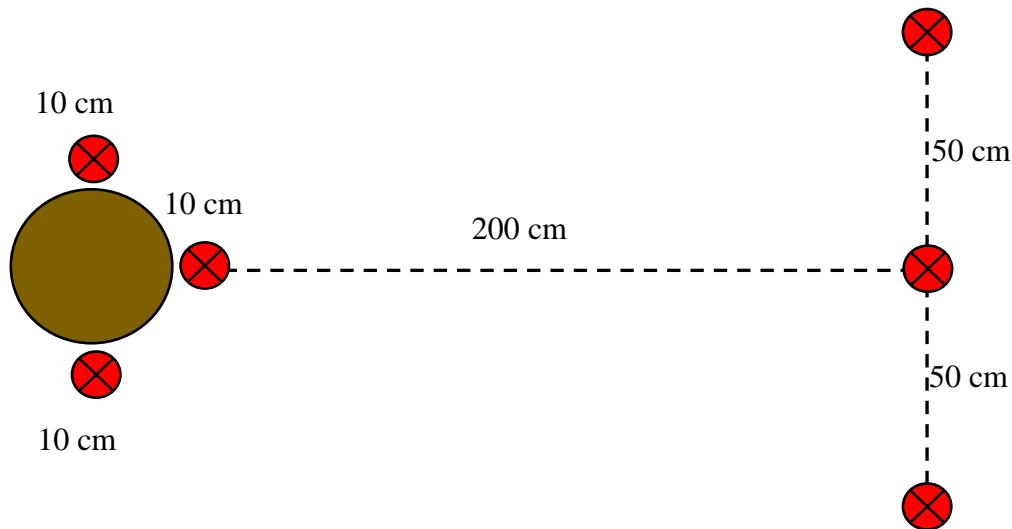


Figure 5.10. MDI measurements in proximity to the sample tree. Black/red crosses indicate measurement location.

Although the rationale for sampling infiltration at 10 and 200 cm was to determine the influence of tree planting on infiltration regarding proximity and tree root spread, determining where tree roots were at the 200 cm proximity was challenging. Measurements and replicas for the 10 cm proximity were simple - three measurements from 10 cm away in a triangular pattern (Figure 5.11); however, the 200 cm proximity was more complex. Some authors have identified tree root locations through use of GPR (section 2.3.1) (Alani and Lantini, 2020; Zou *et al.*, 2020; Aboudourib *et al.*, 2021); however, this was outside the budgetary limitations of this project. An alternative method would be to dig around the tree until roots are found and mark their location, however this would spoil the in-situ soil core and deem all future infiltration measurements invaluable (Romero-Ruiz *et al.*, 2018; Adekanmbi *et al.*, 2020). Therefore, once the 10 cm datums had been marked, a line was measured 200 cm from the base of the tree in the direction of least obstruction (i.e., no other trees, undergrowth or shrubbery intruding the area). It was important that the 200 cm measurements did not fall within proximity to any other tree than the sample tree, as this may influence the collected measurements and roots from the other tree may influence the collected infiltration data. 50 cm was then measured both left and right of the end of the 200 cm line, which then became the locations for the 200 cm replica

measurements. Replication could not take place in the exact same location as the initial infiltration measurement as any measurements would be skewed due to previous saturation of the soil. Therefore 50 cm was chosen as it is far enough away from the previous measurement to avoid lateral seepage - where infiltrating water travels laterally instead of vertically often leading to the overestimation of vertical infiltration values - but close enough to the initial measurement to be representative of the sample area (Folorunso and Aribisala, 2018; Rönnqvist, 2018; Muneer *et al.*, 2020).

There are potential areas of limitation with this study design: additional infiltration samples could have been taken at differing intervals to solely the 10 cm and 200 cm proximities to portray a greater cross section of root spread; infiltration measurements could have been collected in a radius around the tree for the same effect as mentioned above; and infiltration could have been taken from different depths throughout the soil column (however not replicable) to further interrogate influence between root spread and infiltration. However, these methods would have required too much time on site than was allocated, and would have pushed the project slightly outside of the defined scope, presented in section 1.3. Whilst the chosen sampling method does not guarantee that the 200 cm proximity measurements will be recorded in areas affected by root spread, nor take into account the effected radius around the tree, it is a justified method based on the desired outcomes of this project and the difficulties in locating tree root spread non-intrusively. Additionally, this method of infiltration data collection, the study design, and the repetitive and prolonged use of the MDI had not been attempted in existing literature, so this design was partially designed to fill the gap in literature regarding infiltration data collection, within the confines of time and budget. See Figure 5.11 displaying an image of the sample method in the field.



*Figure 5.11. Overview of MDI sampling locations at 10 and 200 cm proximities.*

The method of testing for the grassland control and the 2020 planting site (until it was planted in 24/03/2020) was slightly different due to the absence of trees. Therefore, infiltration at these sites was carried out in a triangular format, with every infiltration location being 50 cm apart from the last. See Figure 5.12.

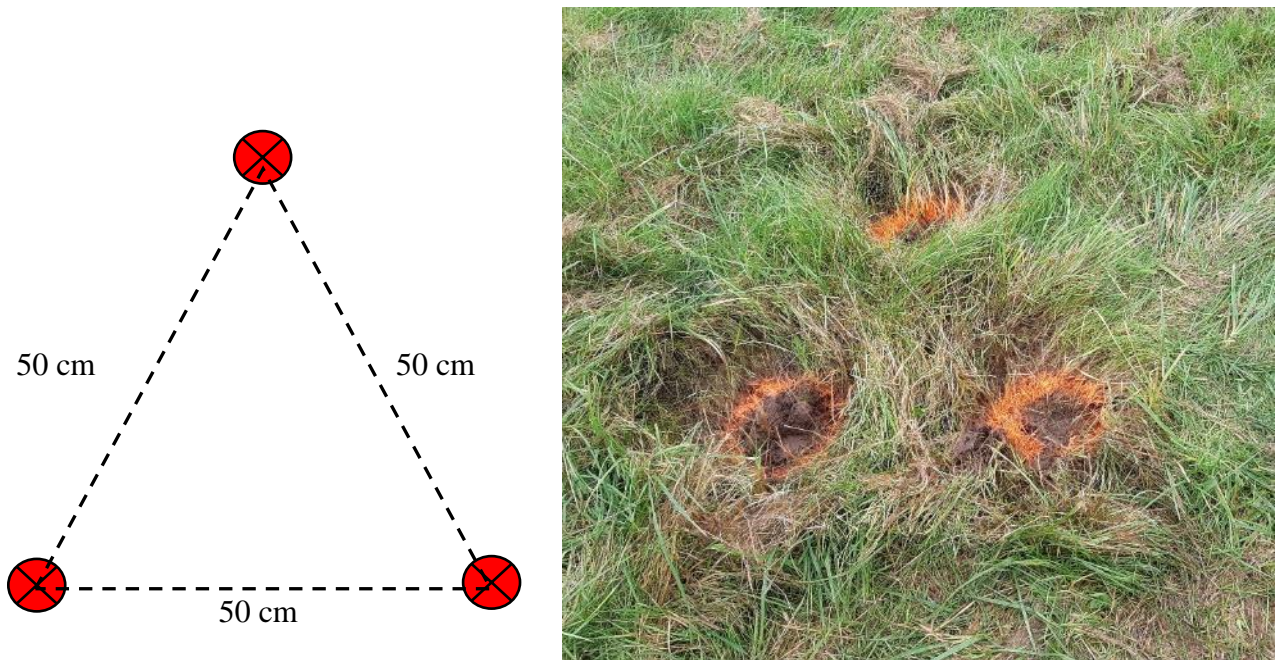


Figure 5.12. Infiltration sampling method for the control and 2020 sample areas.

Every MDI measurement was taken three times at each proximity, meaning six measurements for wooded sites, and three for the control (and 2020 until it was planted on 24/03/2020). Initially, MDI measurements were taken following the advice of the user guide (METER® Group Inc., 2020), however, it became apparent that this method was impractical for the study site and the longevity of the data collection period.

Relevant literature indicates the tension setting of the MDI is altered from study-to-study in existing literature (Robichaud *et al.*, 2008; Matula *et al.*, 2015; Fatehnia *et al.*, 2016; Nestingen *et al.*, 2018) (see section 3.1.2), therefore a tension setting of 2 cm was selected following the suggestion of the MDI user manual (METER® Group Inc., 2020). However, the user manual suggests that at least 30 to 40 ml of water needs to infiltrate the soil to provide an accurate measure of infiltration. The soil texture of all sample sites, excluding *ca.*1900, 2010 and the control, is clay which inherently exhibits a low permeability (Folorunso and Aribisala, 2018). Additionally, site hydrology varies significantly from summer to winter and the clay textures are completely saturated in the winter, however dry and cracking in the summer, shown in Figure 5.13.



Figure 5.13. a) and b) saturation of the 2006 sample site, c) and d) cracking of the 2006 and 2008 sample sites.

Replication was important to ensure field data collection was as representative of field conditions as possible (Khodaverdiloo *et al.*, 2017), and the number of sample areas was required to gather enough data to evaluate the aims and objectives (section 1.3). Therefore, the MDI user manual's suggestion of 30-40 ml of infiltrated water per measurement was adjusted for this project; primarily as the time required for volume is dependent on antecedent moisture conditions, rainfall, and soil saturation. This methodology was tested in the field as part of the pilot study, and the methodology and subsequent outputs of study are presented in Chapter 6. Infiltration sampling started on the 05<sup>th</sup>-November-2019 and continued every week at alternate sites until the 24<sup>th</sup>-March-2020, at which time the UK Government enforced the first national COVID-19 lockdown. Field work resumed on the 1<sup>st</sup> of July 2020 and data was collected until the 25<sup>th</sup> of August 2021. In total 1686 infiltration measurements were taken: 900 from the 10

cm proximity (including replicas and including the control) and 786 from the 200 cm proximity. Using the three consecutive/10-minute measurement methodology (adopted as a result of the pilot study, Chapter 6), data collection of wooded sample areas took one hour each (30 minutes at both the 10 and 200 cm proximities), and sampling at the control and 2020 (until it was planted in 24/03/2020) took 30 minutes each.

#### *5.2.2.2 Temperature Data Collection*

Air, ground (land surface) and soil temperatures were collected throughout the infiltration data collection period, to derive any relationships between temperature variables and infiltration and identify any effect that variations in temperature may have had on infiltration data collection:

- Air temperature was recorded at each sample site using a Kestrel 5000 series handheld anemometer (accuracy  $\pm 0.40^{\circ}\text{C}$ ).
- Land surface (ground) temperature was recorded at each sample site at both 10 and 200 cm proximities using a Helect handheld infrared thermometer (accuracy  $\pm 2\%^{\circ}\text{C}$ ).
- Soil temperature was recorded at each sample site at both 10 and 200 cm proximities using a soil infiltrometer.

These results are summarised in section 7.1.1 and analysed and discussed in greater detail throughout appendix C.2.

### **5.3 Hydrometric Data and HEC-HMS modelling**

This section describes the processes and methods used to build, calibrate, and validate the hydrological model used to generate the modelled results presented in sections 7.2 and 7.3. Figure 5.14 shows a flow diagram outlining the processes undertaken, and how these methods fit with previous and upcoming methodological processes.

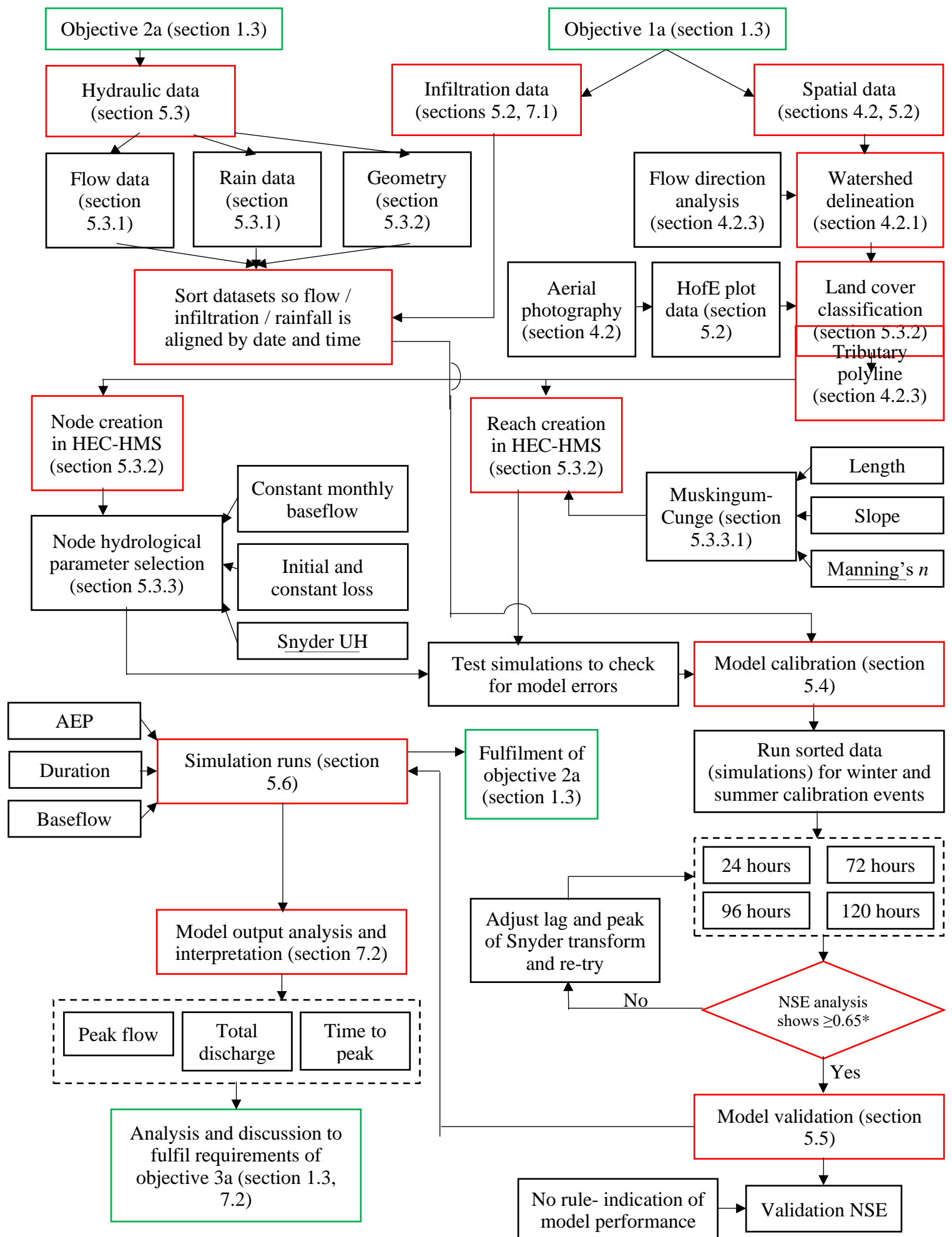


Figure 5.14. The methods and processes undertaken to build the hydrological models, leading on from the spatial data collected throughout

*aforementioned sections. The primary processes are outlined in red, processes relating to aims and objectives are outlined in green. \*indicates accordance with Environment Agency (2008) guidance, which are most commonly followed and accepted by practitioners and academics alike.*

### 5.3.1 Collected Hydrometric Data for Modelling

Rainfall data for the area (in mm) was collected in 5 minute intervals via a tipping bucket rain gauge (accuracy  $\pm 4\%$  between 0.2 and 50 mm) located at the NextGen (2020) waste water treatment plant 1 km north of the HofE Sernal site (Figure 5.15). It is widely acknowledged that rainfall is highly heterogeneous over scale, time and space (Chen *et al.*, 2015; Terink *et al.*, 2018; Mazzoleni *et al.*, 2019; Bois *et al.*, 2020). However, the NextGen rain gauge is within visible distance of the study site, and the surrounding area is topographically similar, with no obtuse characteristics within proximity. For these reasons, the rain gauge was considered to be representative of rainfall effecting the HofE site, additionally it is the only nearby rain gauge in the area (Terink *et al.*, 2018; Mazzoleni *et al.*, 2019; Maier *et al.*, 2020). The stage (in mm) and flow (in l/s) of the tributary that flows through the Sernal study site was recorded every 15 minutes via a pressure transducer (accuracy  $\pm 0.05\%$  FS) lain on the bed of the tributary at the downstream end, see Figure 5.15.

This item has been removed due to 3rd Party Copyright. The unabridged version of the thesis can be found in the Lanchester Library, Coventry University.

*Figure 5.15. Locations of the downstream flow gauge and the rain gauge located at the NextGen (2020) waste treatment plant to the north of the study site (Data from Ordnance Survey, 2020, 2021).*

The transducer, being downstream of the tributary, represented the final outflow volume of the site, and always had continuous flow, meaning that baseflow and hydraulic variations could be identified and accounted for through calibration and validation. Upon installation, the transducer was calibrated by Environmental Monitoring Solutions Ltd (2020) (EMS) to record the water stage based on the amount of pressure on the transducer. Additionally, the location of the transducer was fitted with a temporary flow gauge for 4-weeks to generate a ratings curve, allowing for the discharge flow of the river (in l/s) to be determined from the stage, recorded by the pressure transducers. A ratings curve is only an approximation of the relationship between stage and flow based on a (in this case) small quantity of observed data, therefore, rating curves are not always representative of the intricate variations in flow patterns

over time (Horner *et al.*, 2018; Rampinelli *et al.*, 2020). Additionally, in flood frequency analysis, rating curve uncertainty can be exaggerated as a larger proportion of the curve is extrapolated (Horner *et al.*, 2018; Mansanarez *et al.*, 2019; McMahon and Peel, 2019; Rampinelli *et al.*, 2020). However, regardless of uncertainty, pressure transducers are more cost effective, easier to install and maintain, and have been widely used in hydrological and hydraulic studies (Shahriparsa *et al.*, 2016; Afshari *et al.*, 2018; Dittrich *et al.*, 2019; Malik and Pal, 2020; Rampinelli *et al.*, 2020).

Alternative streamflow monitoring methods are comprehensively described and assessed by Davids *et al.*, (2019), namely; Bernoulli, current meter, deflection rod, float, Manning-Strickler, pitot tube, salt dilution (constant-rate injection) and salt dilution (slug). Whilst these methods are all viable for the determination of streamflow, they are either expensive, derive discrete data, or require a constant presence at the sample site (meaning collecting streamflow for a 96-hour event would require multiple measurements to derive a comprehensive dataset). The pressure transducer method used in this project allowed for a cost effective, near real-time (15 minute) representation of streamflow, allowing for accurate calibration and validation (see sections 5.4 and 5.5).

### 5.3.2 Model GIS Preparation and Cross Section Design

As the aim of the model was to simulate the collected infiltration data and determine to what extent woodland planting by the HofE forest was influencing runoff from the site, it was important to create a hydrological model that represented the area scale, as accurately as possible. The HofE planted areas are not entirely comprised of dense woodland, this can be seen in Figure 5.16, instead the woodland areas comprise of grassland meadows and walkways, along with areas of grass between planted trees. Neglecting to represent the grassland and instead modelling the whole area as woodland would be a hydrological misrepresentation, and results from this model would inaccurately represent the variations in infiltration and land

cover. In addition to this, the infiltration data collected from 10 and 200 cm proximities would need to be separately inputted into the model, as infiltration varies. Therefore, a method of representing the infiltration data from the 10 cm proximity, the 200 cm proximity and the grassland walkways/meadows in each plot of HofE owned land across the defined watershed (study area) was required. Ordnance Survey (2020) aerial imagery of the site was digitised using ArcMap to identify ponds, watercourses, grassland, woodland, and impermeable areas. To account for both measured proximities (aim 1), the derived woodland area was further divided in two; this was so the 10 cm proximity (closest to the tree trunk), and the 200 cm proximity would represent 50% of the remaining woodland area each. This method was utilised as infiltration data was not collected between the two proximities, so dividing the area in-half and allocating a known infiltration value to each (for 10 cm and 200 cm proximity) represented all land cover (as was required for the modelling software). Figure 5.16 shows an example woodland plot before and after the digitisation process, and Figure 5.17 shows the watershed area after land cover digitisation.



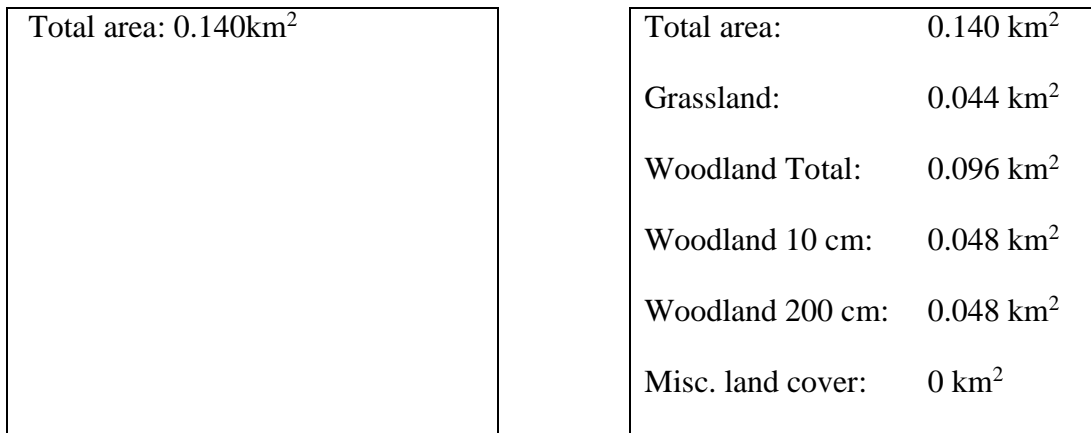
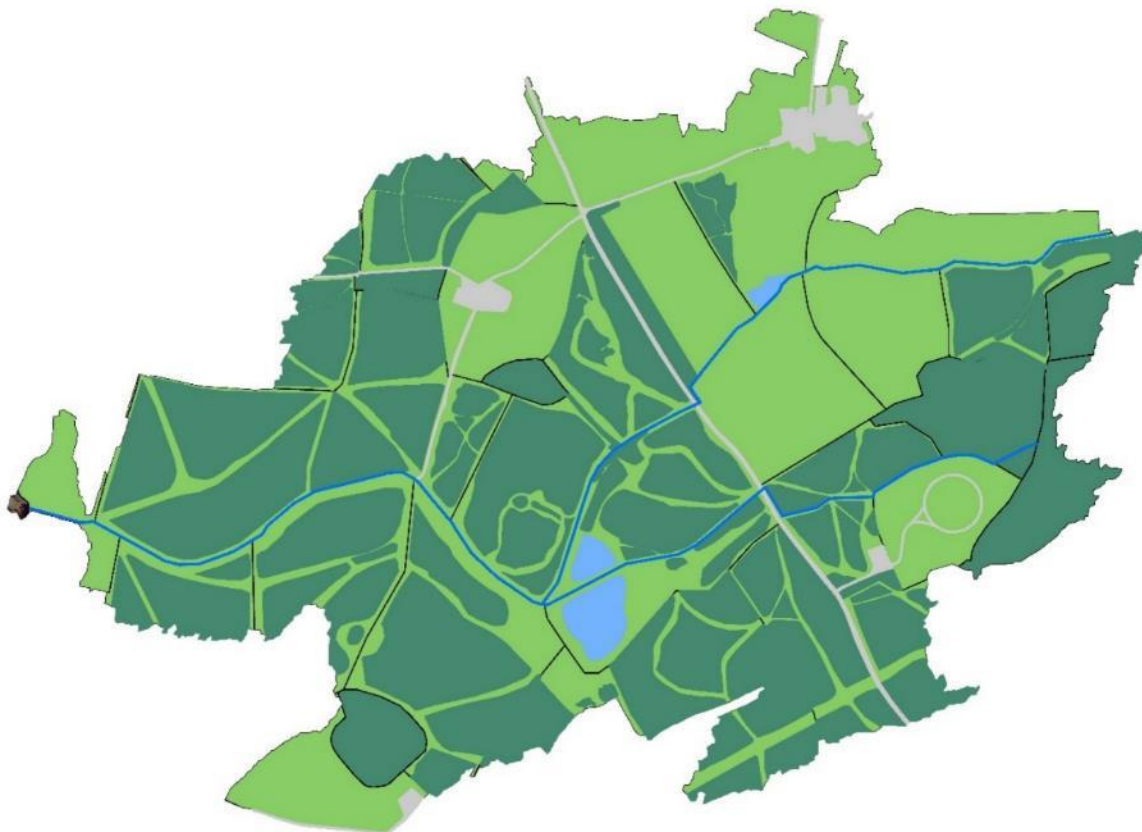


Figure 5.16. 2010\_2 plot before woodland and grassland area calculation (left), and after woodland (10 and 200 cm) and grassland area calculation (right). Tables below indicate the difference in land cover area calculation.

Figure 5.17 shows the complete digitised interpretation of the study site. This was used to define the land cover types of each planting plot across the study area and could be used in conjunction with the study site DTM and flow direction analysis (see section 4.2) to construct the spatial elements of the HEC-HMS model.



*Figure 5.17. The study catchment area after land cover digitisation. Grey = impermeable surface, dark green = woodland, light green = grassland, and blue = water.*

After the land cover was manually classified (Figure 5.17) the hydrological model could be built. HEC-HMS version 4.6.1 was chosen to build the hydrological rainfall-runoff model due to reasonings discussed in sections 3.2.2.1.2 and 3.2.3. To build the model, the shapefiles of the individual plots were imported, along with the 14 cm / 2 m resolution study catchment DTM layer (see section 4.2.2). The tributary was added first, as all sub-catchments would connect to this, and the measurement tool on ArcGIS was used to ensure that the length and course of the watercourse was to scale (Ramly *et al.*, 2020; Hamdan *et al.*, 2021). The river reaches had to be connected to junctions to turn corners, and a junction was used to converge the two upstream tributaries into one watercourse in the middle of the site Figure 5.18. Cross-sectional measurements of the tributary were collected in the field, which allowed the watercourse in the model to represent the real-dimension of the watercourse in the field (Stamataki and Kjeldsen, 2021). This was an important step as the accuracy of watercourse cross-sectional dimensions influences the modelled output of the river (i.e., the parameters of in-channel routing method, see section 5.3.3). Figure 5.18 shows the cross-sectional geometry for upstream and downstream watercourse profiles.

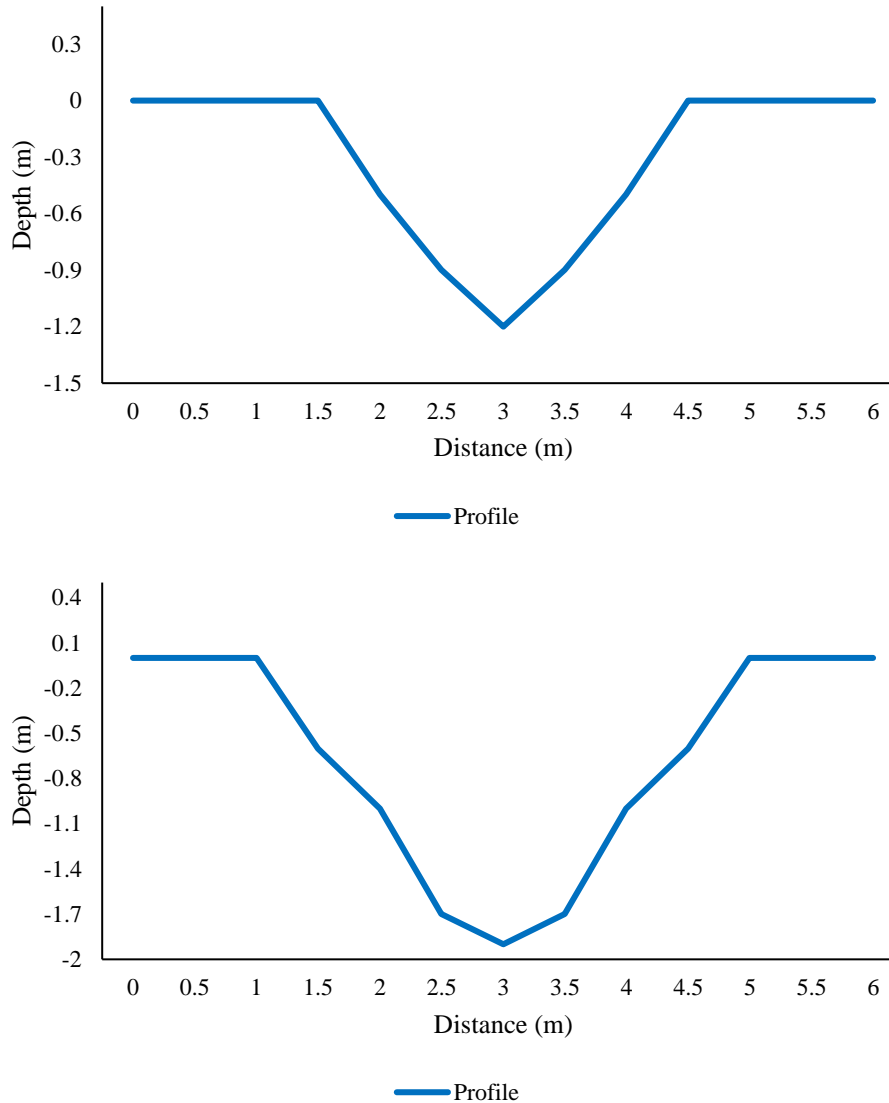


Figure 5.18. (top) upstream and (bottom) downstream river profile cross-sections in HEC-HMS.

The upstream profile is steeper than the downstream profile with a narrower bed, this profile was applied to the reaches above the converging of the two upstream tributaries. The downstream profile is wider and wider-bedded than the upstream profile, and this was applied to the watercourse after the convergence of the two upstream tributaries. The resolution of the cross-sectional measurements are relatively coarse (0.5 m), however, the empirical observations add reliability to model outputs as empirical cross-sectional data is often difficult to attain for modelling studies (Neal *et al.*, 2015).

Once the tributary had been drawn to scale, the nodes (computational representations of hydrological model input parameters) to represent the area of each land cover type in each plot were added. There were as many as three nodes required by each plot, one to represent woodland at the 10 cm proximity, one to represent woodland at the 200 cm proximity, and one to represent the grassland – any impermeable area contained within the plot was deducted from the grassland area and inputted as ‘percentage impermeable’ in the model interface. To connect the nodes, the flow direction analysis (Figure 4.10) was manually assessed alongside the high resolution (14 / 200 cm) study site DTM (Figure 4.8) to identify both overland flow pathways, and obstructions between sample area plots and the tributary. It is a requirement within HEC-HMS that nodes be connected to ‘junctions’, which are features in the model indicating the end of one ‘reach’ (watercourse section) and the start of another (junctions are also required for the watercourse to turn corners). Upon identifying where plots (nodes) would flow into the watercourse, a junction was created to allow a computational input. The watercourse already hosted junctions at each change in direction, however, more junctions were added when needed to allow all nodes to connect. The resultant hydrological model is shown in Figure 5.19.

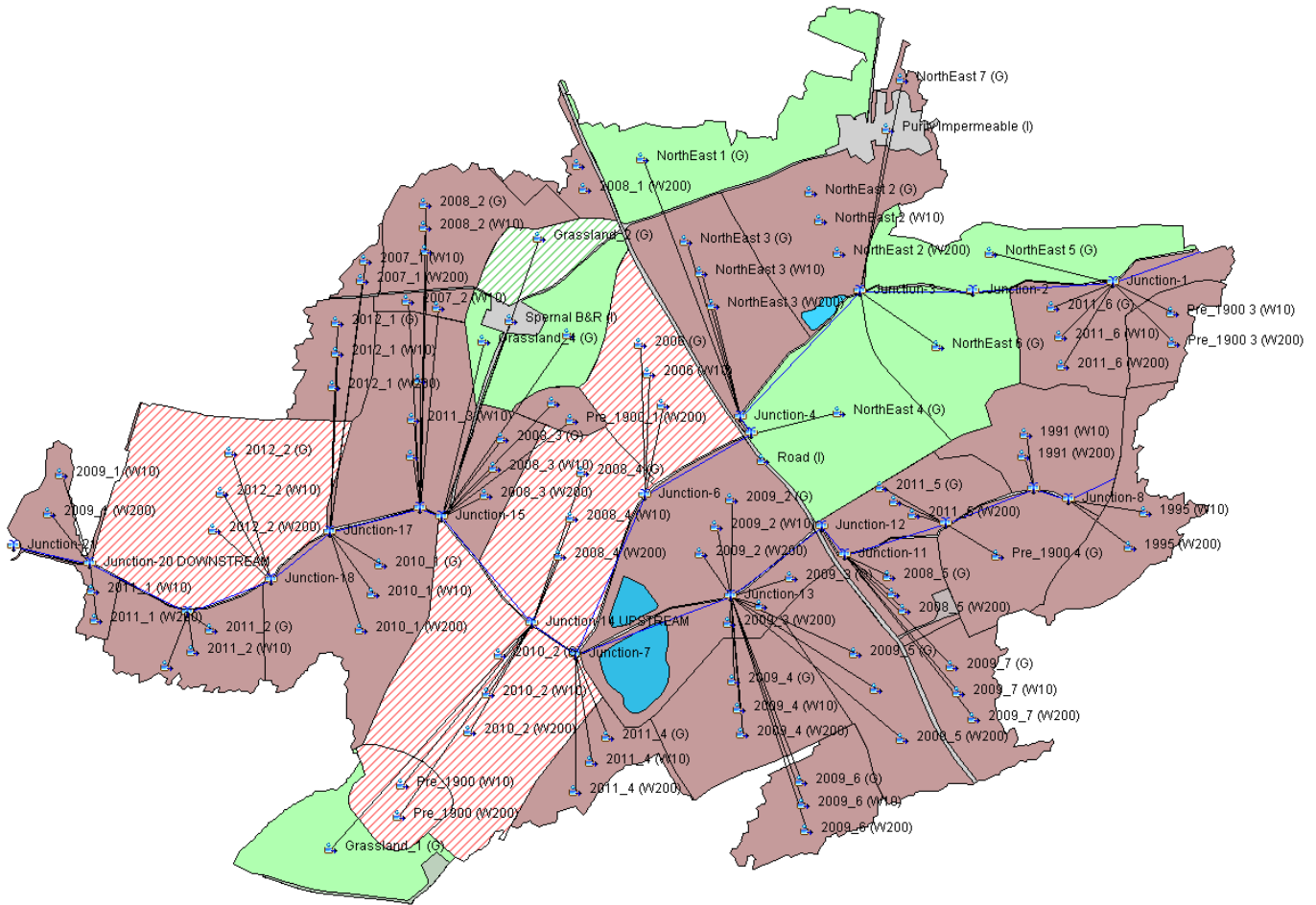


Figure 5.19. Final HEC-HMS hydrological model. The brown areas indicate woodland plots, the green areas indicate grassland only plots, the grey areas indicate impermeable surfaces, and the cross-hatched areas represent infiltration sample areas.  denotes a node (subbasin node),  denotes a reach (watercourse reach), and  denotes a junction.

5.3.3 Selected Model Parameters

The ‘process models’ available in HEC-HMS for each hydrological process are presented in appendix A.1. In the HEC-HMS model used for this project, the Muskingum-Cunge routing method was used for modelling tributary flow (Kafle, 2019; Ramly *et al.*, 2020; Rangari *et al.*, 2020). The initial and constant loss method was used to simulate the collected infiltration data (section 5.2), the Snyder unit hydrograph transform was used to simulate the observed runoff and lag times of the catchment areas, and the constant monthly baseflow method was used to

simulate antecedent baseflow of the site (Koneti *et al.*, 2018; Zelelew and Melesse, 2018; Kafle, 2019). These models are discussed in the following sections.

### 5.3.3.1 Muskingum-Cunge Routing Method

The Muskingum-Cunge routing method builds upon the Muskingum method, and is used for simulating in-channel flow based on cross-sectional geometry (Cunge, 1969; Ponce, 1991). The Muskingum-Cunge method combines a simplified form of the continuity equation and a simplified form of the momentum equation to determine the predictable propagation of flow waves based on cross-sectional dimensions (Cunge, 1969; Ponce, 1991). The Muskingum-Cunge method can re-calculate flow at every timestep perimeters based on changing channel properties and flow depth.

The Muskingum-Cunge method states:

$$Q_{j+1}^{n+1} = C_0 Q_j^{n+1} + C_1 Q_j^n + C_2 Q_{j+1}^n \quad EQ 5.1$$

Where  $Q$  is discharge,  $j$  is a spatial index,  $n$  is time index.  $C_0$ ,  $C_1$  and  $C_2$  are calculated as follows (Cunge, 1969):

$$C_0 = \frac{\Delta t - 2KX}{2K(1 - X) + \Delta t} \quad EQ 5.2$$

$$C_1 = \frac{\Delta t + 2KX}{2K(1 - X) + \Delta t} \quad EQ 5.3$$

$$C_2 = \frac{2K(1 - X) - \Delta t}{2K(1 - X) + \Delta t} \quad EQ 5.4$$

and K and X are calculated as follows (Cunge, 1969):

$$K = \frac{\Delta x}{c} \quad EQ 5.5$$

$$X = \frac{1}{2} \left( 1 - \frac{q}{S_o c \Delta x} \right) \quad EQ 5.6$$

Where  $\Delta x$  is reach length,  $c$  is flood wave celerity,  $q$  is unit width discharge, and  $S_o$  is channel bed slope (Cunge, 1969)

The Muskingum-Cunge method was chosen for use in the HEC-HMS model due to its inclusion of the data collected from the study site (cross sectional geometry). Additionally, it has been used in similar studies (Kafle, 2019; Ramly *et al.*, 2020; Rangari *et al.*, 2020) and produces an accurate representation of in-channel flow for analysis throughout Chapter 7 (Ibrahim-Bathis and Ahmed, 2016).

### 5.3.3.2 Initial and Constant Loss Method

A loss model calculates the loss of total precipitation due to infiltration (and can also be used for evaporation/evapotranspiration loss). In the HEC-HMS model built for this project, the initial and constant loss method was used to simulate the collected infiltration data (section 2.1), the constant rate element is calculated as follows:

$$pe_t = \begin{cases} p_t - f_c & \text{if } p_t > f_c \\ 0 & \text{otherwise} \end{cases} \quad EQ 5.7$$

Where  $f_c$  is the maximum potential rate of precipitation loss,  $p_t$  is the mean areal precipitation depth during a time interval, and  $pe_t$  is the excess overland flow. The initial loss is calculated as follows:

$$pe_t \begin{cases} 0 & \text{if } \sum p_i < I_a \\ p_1 - f_c & \text{if } \sum p_i > I_a \text{ and } p_t > f_c \\ 0 & \text{if } \sum p_i > I_a \text{ and } p_t < f_c \end{cases} \quad EQ 5.8$$

Where  $pe_t$  is excess overland flow,  $p_1$  is precipitation depth,  $f_c$  is the maximum potential rate of precipitation, and  $I_a$  is initial loss.

The requirements of the initial and constant loss model within HEC-HMS matched the data that had been collected from the study site, meaning no criteria had to be assumed, nor inferred from external data (Razmkhah, 2016). This was advantageous as all collected data from the HofE site could be included in the model, and the initial and loss method was chosen for use in the model due to this. Additionally, the initial and constant loss method has been used in other HEC-HMS models for similar applications to this project (Zezelew and Melesse, 2018; Sharu, 2020). It is worth considering, however, that whilst the initial and constant method was adopted here due to the requirements matching the collected data, it is a simplification of the infiltration process and cannot account for complex flows after the infiltration process has occurred. However, as discussed in section 3.4, hydrology is complex, and no hydrological model is capable of modelling exact hydrological and hydraulic processes with 100% accuracy, which is why calibration is valuable (see section 5.4).

### 5.3.3.3 Snyder Unit Hydrograph Transform

In HEC-HMS, the transform model dictates how sub-catchment precipitation is converted to (and from) overland flow, and then to in-channel flow after all losses have been deducted from the input (precipitation) (Kafle, 2019; Ramly *et al.*, 2020). The Snyder unit hydrograph

transform was used to simulate the observed runoff and lag times of the catchment areas, Snyder's equation for lag time is (Fedorova *et al.*, 2018):

$$T_{lag} = C_t(LL_c)^{0.2} \quad EQ\ 5.9$$

Where  $T_{lag}$  is the catchment lag time (hours),  $C_t$  is the catchment gradient coefficient,  $L$  is flow path length (km) and  $L_c$  is length of flow path from outlet to closest point of the catchment centroid (km).

And for peak discharge is (Fedorova *et al.*, 2018):

$$Q_p = \frac{2.78 \times C_p \times A}{T_{lag}} \quad EQ\ 5.10$$

Where  $Q_p$  is peak discharge related to 1cm of effective rainfall ( $m^3/s$ ),  $A$  is catchment area ( $km^2$ ) and  $C_p$  is an empirical coefficient of peak intensity.

Use of the Snyder unit hydrograph method was chosen for the models used in this project due the method requiring input information that could be derived through using the observed data from the site (the pressure transducer) (US Army Corps of Engineers, 2000; Gumindoga *et al.*, 2017; Fedorova *et al.*, 2018). The method calculates the expected lag time based on the slope, observed lag and peaking coefficient of the watercourse. Discussed in section 5.4, empirical observations of in-channel flow were recorded, and these were used alongside a 'trial-and-error' method to calculate the lag times and peaking coefficients of overland flow for each node during summer and winter. The discussed trial and error method involved using observed and simulated flows from the study site until a balance could be struck between both datasets; this was crucial for model calibration and is discussed in much more detail throughout section 5.4. Other methods of simulating hydrological transforms in HEC-HMS are outlined in appendix A.1, however the Snyder method required input information that could be extracted from site observations, and has been used in other studies (De Silva *et al.*, 2014; Derdour *et al.*, 2018; Ma *et al.*, 2018). Alternative transform methods required data that had/could not be collected or required additional observations for equivalent outputs to the Snyder method.

#### **5.3.3.4 Constant Monthly Baseflow**

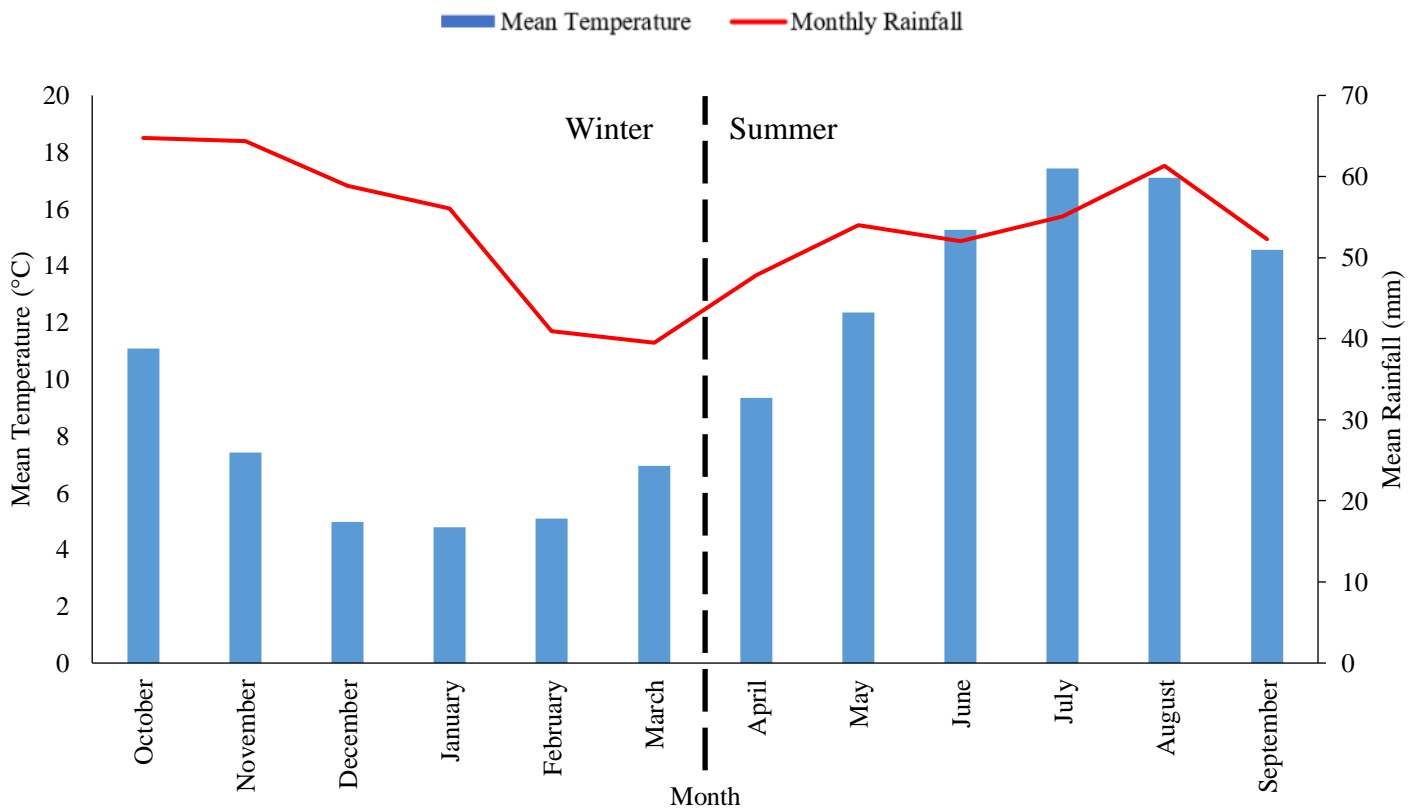
The constant monthly baseflow method was used to simulate antecedent baseflow of the site, which applied a user-defined constant flow to all models as required. This method was chosen due to the ability of the method to maintain a defined baseflow from the site (see section 5.6.4), and for its ability to allow an observed baseflow to be added to the model to account for changes both seasonally, and due to climate change (Koneti *et al.*, 2018; Zelelew and Melesse, 2018; Kafle, 2019). Alternative methods of simulating baseflow can be seen in appendix A.1, however the constant monthly method was used as this study is less about baseflow value, and more about the influence of woodland planting on peak flows and total discharge. Additionally, using the constant monthly baseflow model meant that if baseflow was found to be different, it could be adjusted without changing the shape of the output hydrograph. HEC-HMS model parameter values are presented in appendix B.5.

#### **5.4 Model Calibration**

The end goal of model calibration is to produce a set of model parameters that will consistently produce the best possible outputs over any simulated event (section 0). It would be inaccurate to represent the site using one set of calibrated parameters as empirical observation of the site throughout the data collection highlighted the variability of study site conditions throughout the year (see section 5.2.2). The site varied hydrologically between summer and winter, during the summer, grass developed across the soil surface, the clay-heavy soil texture began to crack creating macropores, and the trees were blooming. This is the opposite to winter, where the soil was bare and saturated, and the trees had shed their leaves. These changes influence the lag times, infiltration rates, interception and surface roughness of the site (Chandler *et al.*, 2018; Dittrich *et al.*, 2019; Zhang *et al.*, 2019a; Murphy *et al.*, 2021). To accommodate these variations, separate winter and summer models were created to best represent likely response

of site soil conditions in both wet and cold, and warm and dry periods. Metrologically, December, January and February are defined as winter, and June, July and August are defined as summer by the UK met office (The Met Office, 2021a, 2021b). However, for this project, the winter model included data ranging from October to March, and the summer model included data ranging from April to September. This was decided based on preliminary data collection from the site, and mean (1990 – 2020) annual temperature and rainfall data from the Met Office (2021). This data is shown in Figure 5.20.

Figure 5.20. Average monthly rainfall and temperature, used to define the sample periods for winter and summer.



Mean annual temperature and rainfall between October and March is 6.7°C and 55 mm respectively, mean annual temperature and rainfall between April and September is 14.4°C and 54 mm respectively. Whilst mean winter and summer rainfall differs only slightly, the change in atmospheric temperature was a key driver in infiltration rate, and subsequently the development of two hydrological models.

Model calibration involved setting the initial baseflow of the model to match that of the observed event (this was to account for antecedent flow already in the watercourse at the beginning of the calibration event), then systematically adjusting the unobserved model parameters (through process of trial-and-error). Empirically observed parameters could not be adjusted during calibration, these parameters were:

- Infiltration - the key parameter for the hydrological model, and this parameter could not be changed during the calibration process as infiltration was a known parameter.

- Rainfall and baseflow - been observed through use of the rain gauge and in-channel telemetry (section 5.3.1).
- In-channel hydraulics (including parameters used in the Muskingum-Cunge models) - these had been inputted using observed measurements from the study site.

Thus meaning, the only adjustable parameters were the lag times and peaking coefficients of the Snyder unit hydrograph transform (EQ 5.9 and EQ 5.10). These parameters were adjusted until one set of Snyder values could be used across all events and produce a similar outcome to the observed flow. The NSE method (EQ 3.1) was used to determine the efficiency and predictability of both the calibration and validation events. The root mean squared error (RMSE) of each calibration and validation event was calculated in addition, to further indicate the efficiency and capability of the model – a RMSE value closer to 0 indicates a good-fit between the observed and simulated datasets at each timestep, whereas a value further from 0 indicates a poor-fit between the datasets (Naik *et al.*, 2019; O’Loughlin *et al.*, 2020). This process was undertaken for both the summer and winter models. The variations in winter and summer calibration parameters are shown throughout appendix B.5.2. An explanation of RMSE values for calibration and (validation) is presented in appendix B.5.3.

To calibrate, the rainfall and flow data from the site (section 5.3.1) were combined and large rainfall events (identified through sorting data from the flow gauge) and the surrounding flow data were extracted and saved as individual events (either as a summer or a winter event depending on when they occurred). As infiltration is a key input to the model, and infiltration data at the HofE site has been collected since November 2019, the infiltration data collected from the HofE site at the closest date to the selected rainfall/flow event was used as the input for the sampled plots. Infiltration data for plots planted in years that were not sampled was extrapolated from the observed data, for example, infiltration data was collected from plots planted in 2008 and 2010, but not 2009 – so the 2009 infiltration value was determined from the median of the values collected in 2008 and 2010. This method is based on the mathematical

extrapolation of observed values and was adopted due to the lack of literature regarding how infiltration changes around trees, and how such data should be extrapolated. Four events were chosen for both summer and winter, the durations of which were 24 hours, 72 hours, 96 hours, and 120 hours. These calibration durations were chosen to test the ability of the model to represent flows from short duration to high duration events and based on the availability of continuous flow data from the site. However, it should be noted that the telemetry data became intermittent, and then unusable towards the end of this project due to the failure of data collection hardware and the hindered maintenance schedule of the installers due to the COVID-19 pandemic. Table 5.5 shows the rainfall events and infiltration data collection dates used in calibration.

Table 5.5. Calibration event timeframes and rainfall volumes for winter and summer storms

Calibration Simulation Event Timeframe								Infiltration data collection date	
Event	Duration	W/S	Start Date	Start Time	End Date	End Time	Rainfall (mm)	ca. 1900 - 2012	2014 - 2020
1	24 hrs	W	16 January 2021	04:00	17 January 2021	04:00	1.8	20 January 2021	14 January 2021
2	72 hrs	W	17 January 2021	16:00	20 January 2021	16:00	10.60	20 January 2021	14 January 2021
3	96 hrs	W	30 November 2019	04:00	04 December 2019	04:00	0.80	04 December 2019	26 November 2019
4	120 hrs	W	08 October 2020	07:00	13 October 2020	07:00	6.70	08 October 2020	14 October 2020
5	24 hrs	S	09 September 2020	03:00	10 September 2020	03:00	1.20	09 September 2020	02 September 2020
6	72 hrs	S	19 August 2020	07:00	22 August 2020	07:00	19.60	12 August 2020	19 August 2020
7	96 hrs	S	01 August 2020	01:00	05 August 2020	01:00	7.90	29 July 2020	05 August 2020
8	120 hrs	S	28 August 2020	07:00	02 September 2020	07:00	13.40	26 August 2020	02 September 2020

### 5.4.1 Winter Calibration Events

Output results from the winter model calibrations show the most accurate model outputs are achieved using Snyder values of 6 hours and 0.8 (lag time and peaking respectively) for impermeable surfaces; values of 18 hours and 0.5 (lag time and peaking respectively) all other catchments (see appendix B.5.2). Both a constant baseflow and a recession baseflow was applied and adjusted to each event, however the recession ratio was not adjusted – only the initial discharge was altered to account for varying antecedent flows between the calibration events. The results of the winter calibration are shown in Figure 5.21 to Figure 5.24, an explanation of RMSE values are shown in appendix B.5.3.

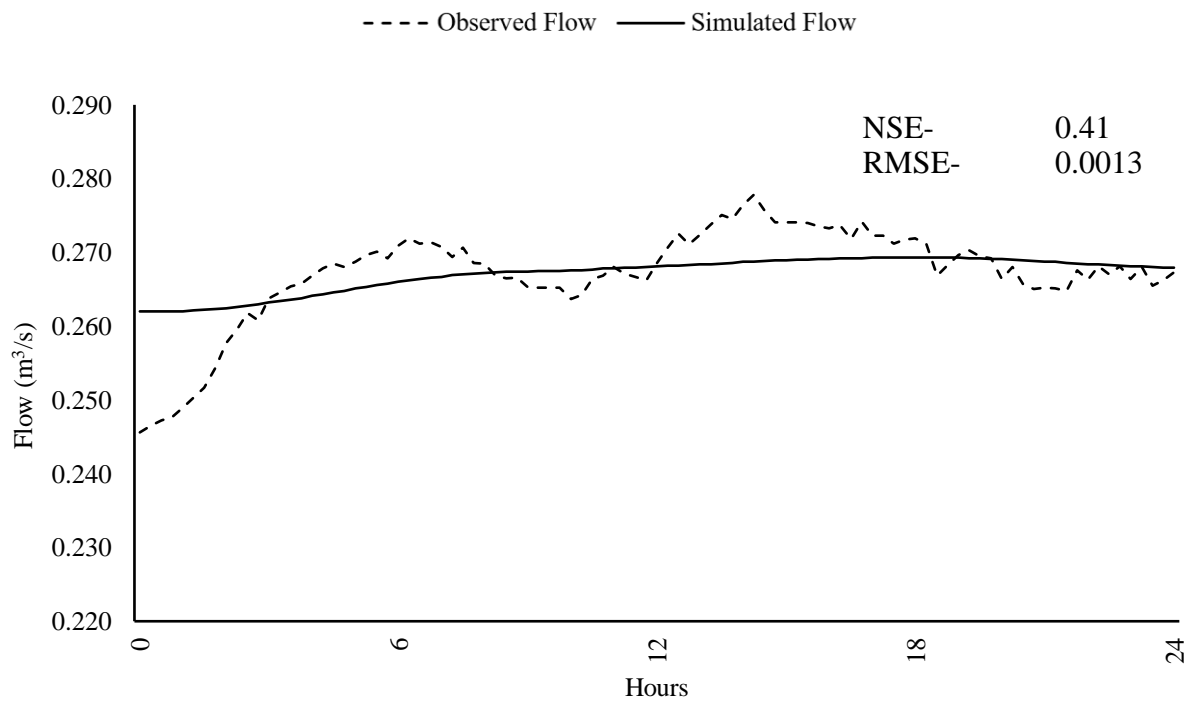


Figure 5.21. Observed and simulated flow the 24-hour winter calibration event

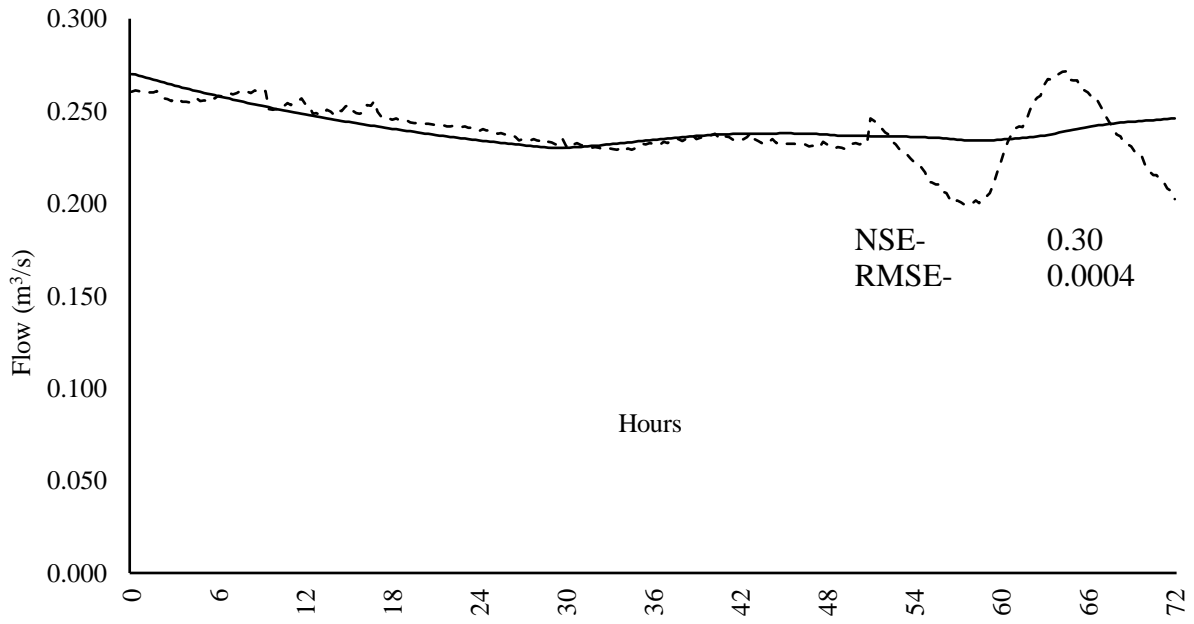


Figure 5.22. Observed and simulated flow the 72-hour winter calibration event

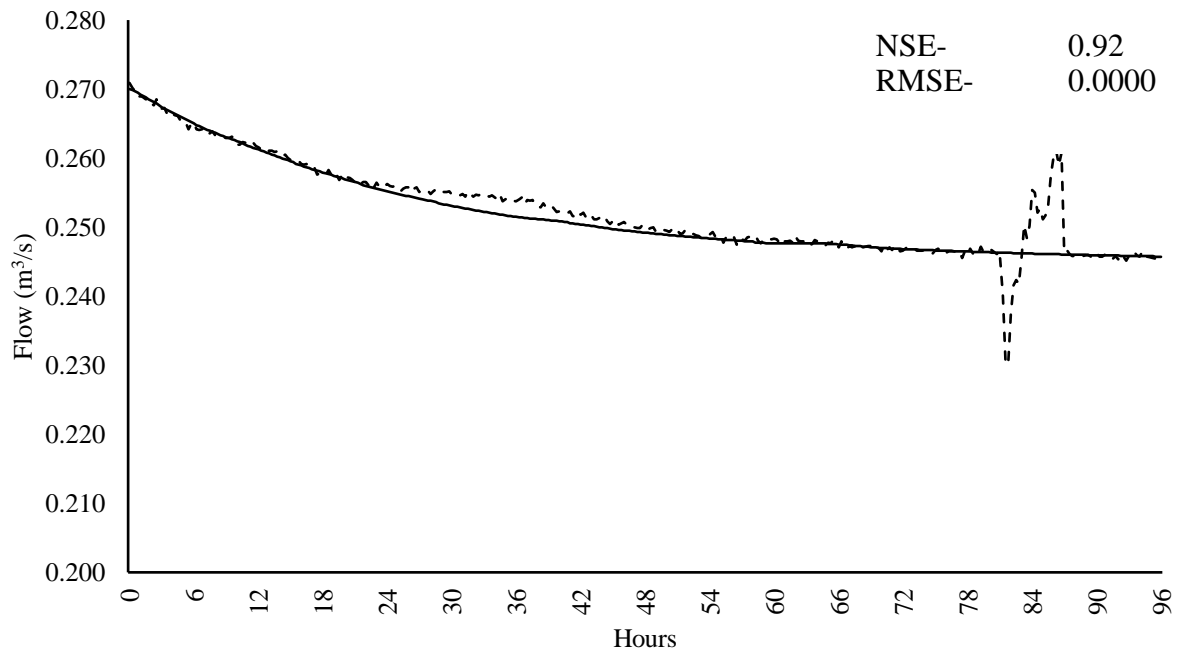


Figure 5.23. Observed and simulated flow the 96-hour winter calibration event

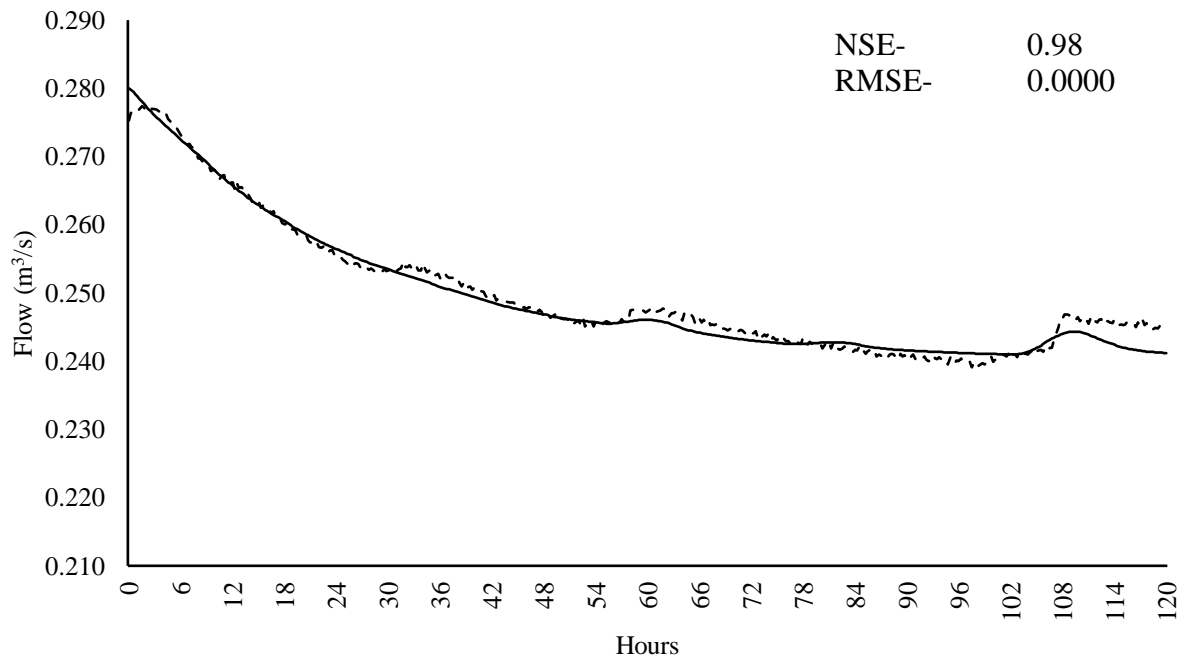


Figure 5.24. Observed and simulated flow the 120-hour winter calibration event

The mean NSE of the winter calibration events is 0.65, and the mean RMSE is 0.0004. The winter model can simulate low flows and returns to base but does not peak as highly as the observed flows. The winter model is less responsive to sharp changes in observed flow, this is highlighted in both the 24 and 72-hour storm durations. The slow responsiveness of the model may be due to the antecedent conditions of the site (i.e., if the ground was wet, runoff would be significantly higher due to the clay-geology of the site) (Folorunso and Aribisala, 2018). The 96 and 120-hour duration events resulted in above-acceptable NSE values, and it was the under-prediction of the 24 and 72-hour duration that reduced the overall average. The RMSE values are not as reflective of the lower NSE's as they are in the summer calibrations, all sites demonstrated a low RMSE, aside from the 24 and 72-hour durations, that were slightly higher.

#### 5.4.2 Summer Calibration Events

Output results from the summer model calibrations show the most accurate model outputs are achieved using Snyder values of 4 hours and 0.8 (lag time and peaking respectively) for impermeable surfaces; values of 6 hours and 0.5 (lag time and peaking respectively) all other

catchments (see appendix B.5.2). Both a constant baseflow and a recession baseflow was applied and adjusted to each event, however the recession ratio was not adjusted – only the initial discharge was altered to account for varying antecedent flows between the calibration events. The results of the winter calibration are shown in Figure 5.25 to Figure 5.28.

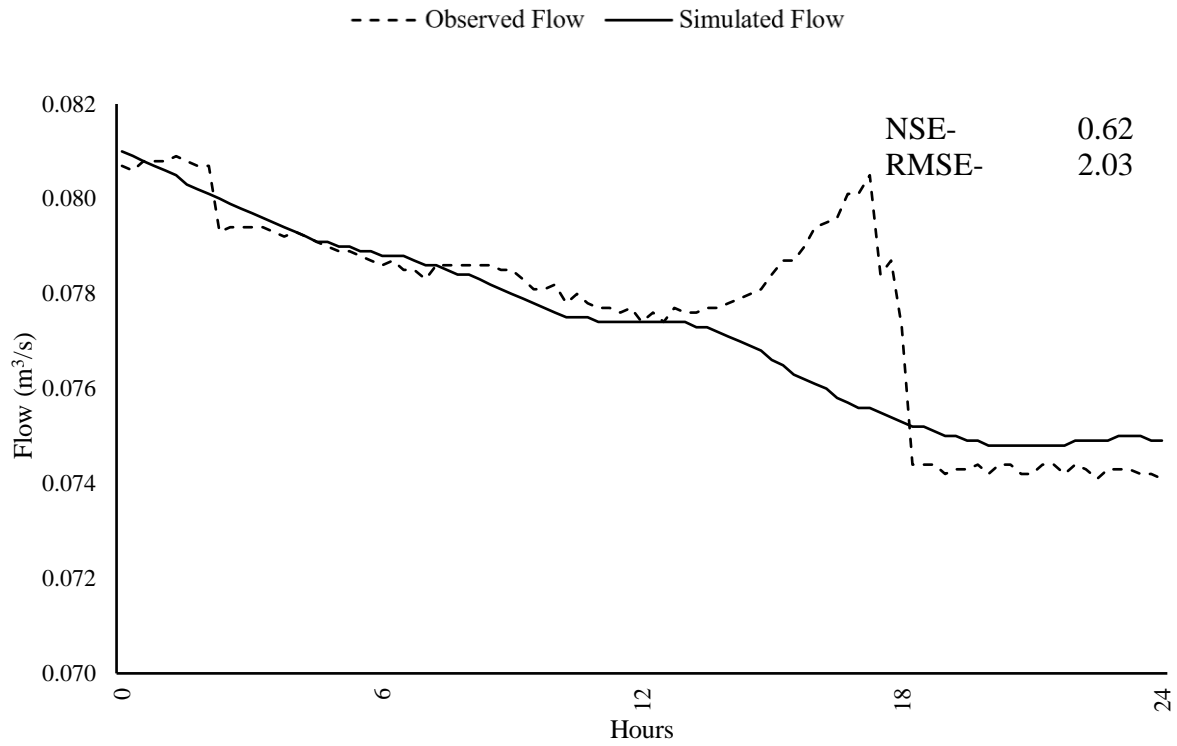


Figure 5.25. Observed and simulated flow the 24-hour summer calibration event

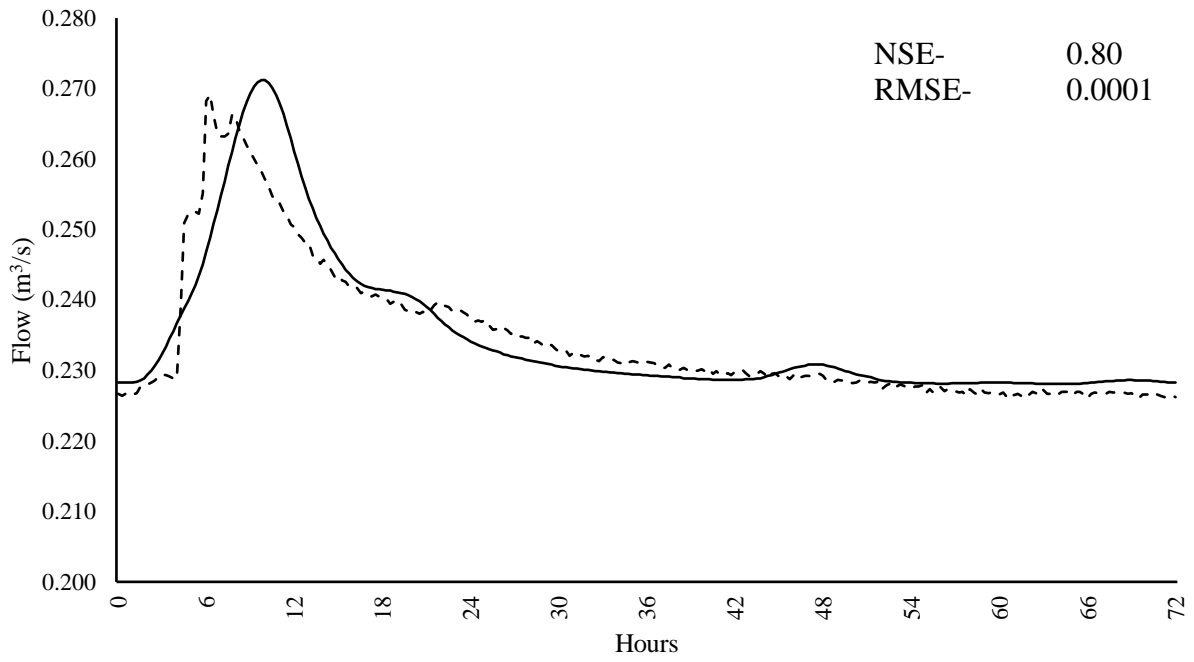


Figure 5.26. Observed and simulated flow the 72-hour summer calibration event

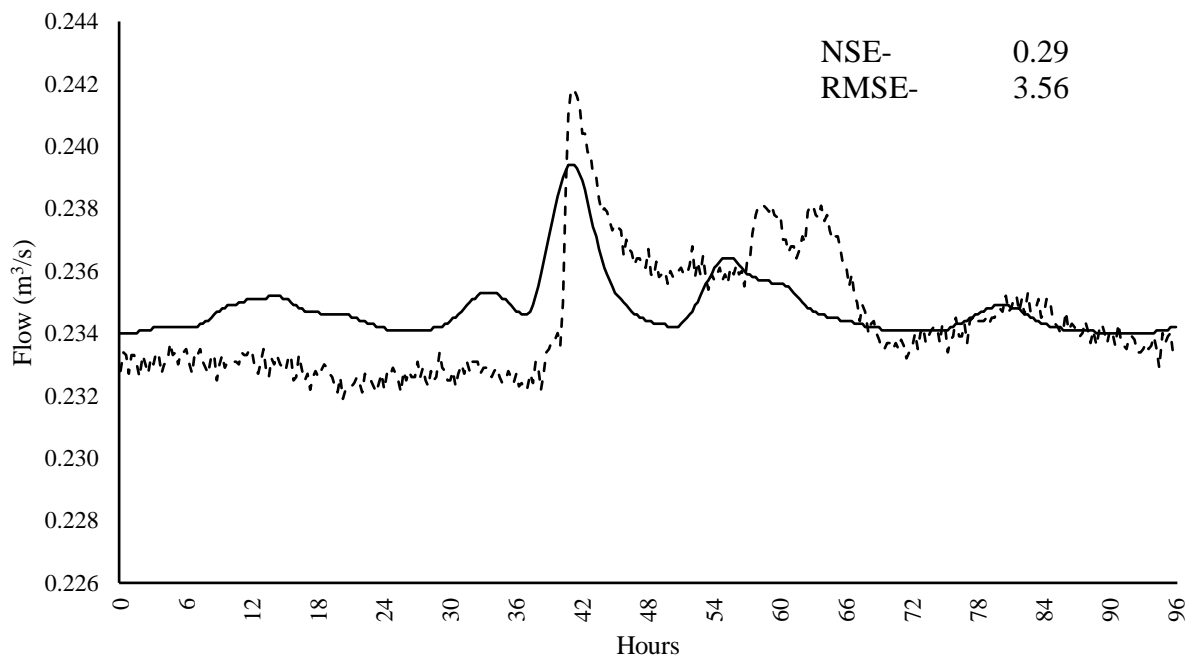


Figure 5.27. Observed and simulated flow the 96-hour summer calibration event

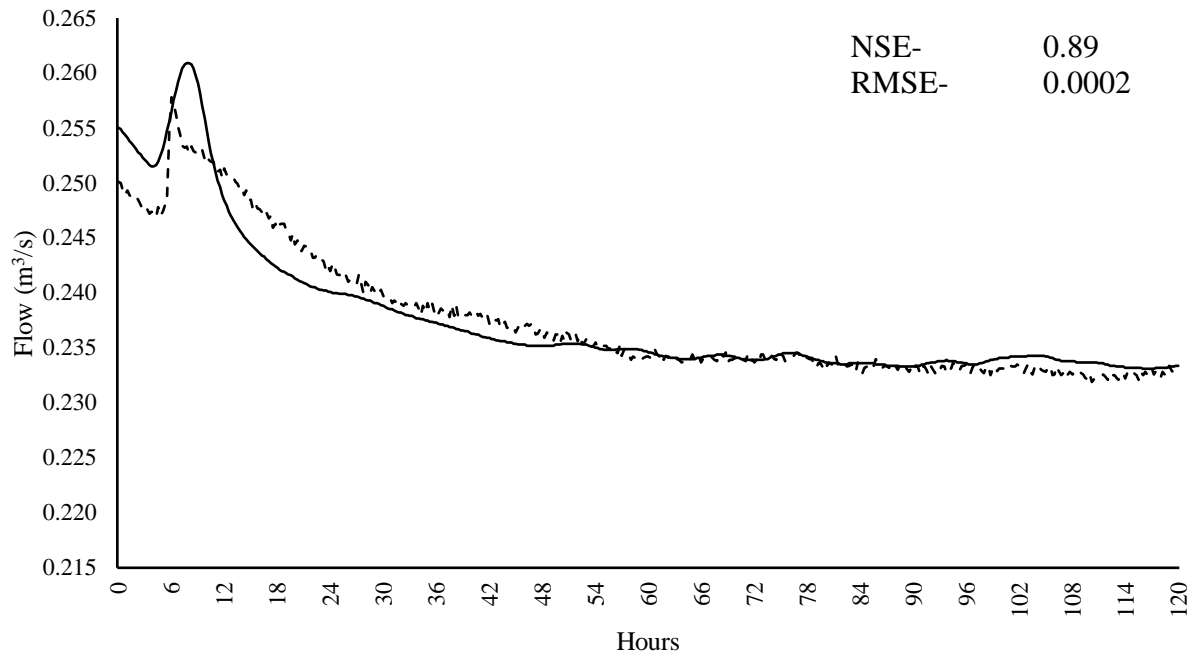


Figure 5.28. Observed and simulated flow the 120-hour summer calibration event

The mean NSE of the summer calibration events is 0.65, and the mean RMSE is 1.39. The summer model can simulate low flows and returns to base but does not peak as highly as the observed flows. This could be due to hydrological inputs to the observed flows not being accounted for in the model; as discussed in section 3.4, catchment hydrology is complex and hydrological modelling is only a best representation and often a simplification of much more complex processes (Sy *et al.*, 2019; Nkwunonwo *et al.*, 2020; Zhu *et al.*, 2020c). The 72 and 120-hour durations resulted in above-acceptable NSE values, and it was the under-prediction of the 24 and 96-hour duration that reduced the overall average. The NSE is reflected in the RMSE values, the 96 and 120-hour durations demonstrated very low RMSE, however the 24 and 96 hours were higher than 1, showing the error to be significant across all timesteps.

### 5.5 Model Validation

Model validation is undertaken after model calibration to determine the ability of the model to replicate observed parameters without further modifications from the user (Patil *et al.*, 2019; Sahoo *et al.*, 2020). Entirely new data was used in validation compared with calibration; it was

decided that using the same events as used in calibration would not be effective as the model is already calibrated to those events. Additionally, validating the model to other events tests the wider applicability of the model, reflecting its ability to simulate rainfall events independently (Al-Mukhtar and Al-Yaseen, 2019; Sharu, 2020; Kumar and Sherring, 2021). The validation event timeframes for winter and summer are shown in Table 5.6.

Table 5.6. Validation event timeframes and rainfall volumes for winter and summer storms

Validation Simulation Event Timeframe								Infiltration data collection date	
Event	Duration	W/S	Start Date	Start Time	End Date	End Time	Rainfall (mm)	ca.1900 - 2012	2014 - 2020
1	24 hrs	W	14 January 2021	04:30	15 January 2021	04:30	1.10	06 January 2021	14 January 2021
2	72 hrs	W	06 December 2020	07:00	09 December 2020	07:00	2.70	09 December 2020	02 December 2020
3	96 hrs	W	02 November 2020	01:00	06 November 2020	01:00	6.70	28 October 2020	05 November 2020
4	120 hrs	W	13 October 2020	07:00	18 October 2020	07:00	4.50	8 October 2020	14 October 2020
5	24 hrs	S	04 September 2020	02:00	05 September 2020	02:00	0.70	10 September 2020	02 September 2020
6	72 hrs	S	09 September 2020	22:00	12 September 2020	22:00	1.00	10 September 2020	16 September 2020
7	96 hrs	S	04 September 2020	22:00	08 September 2020	22:00	4.20	10 September 2020	02 September 2020
8	120 hrs	S	30 August 2020	02:00	04 September 2020	02:00	8.00	26 August 2020	02 September 2020

### 5.5.1 Winter Validation Events

Figure 5.29 to Figure 5.32 show the results of the winter model validation events.

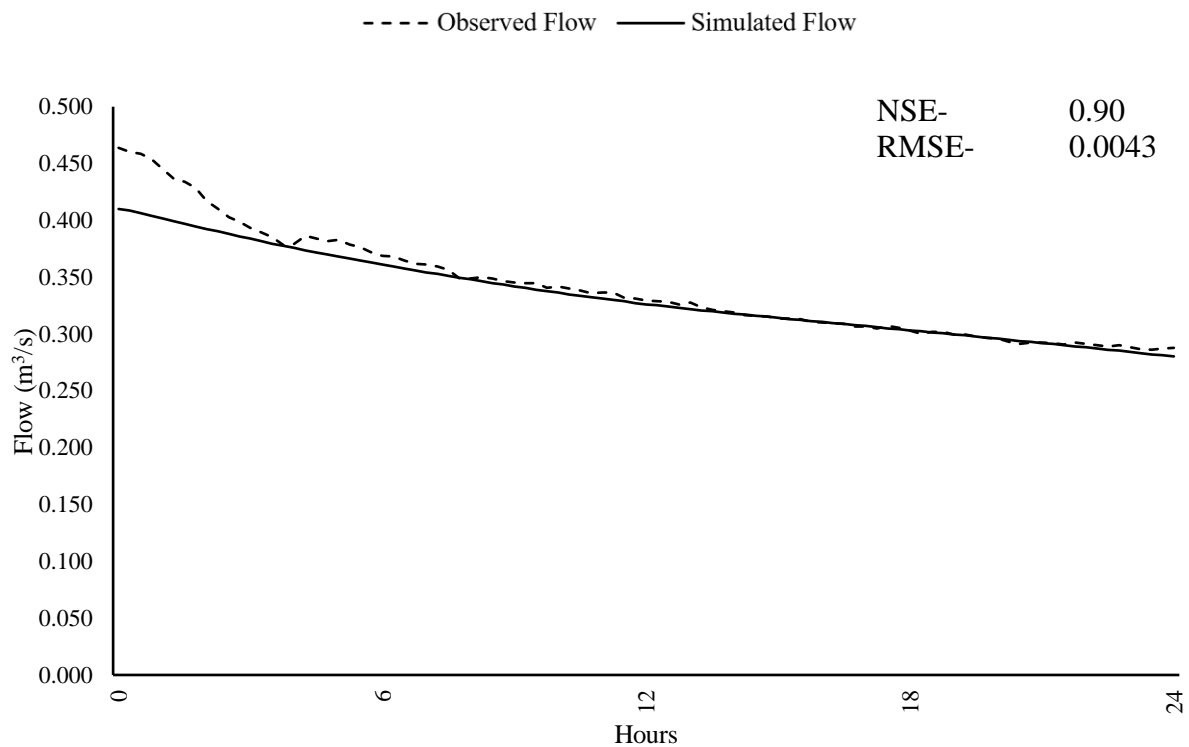


Figure 5.29. Observed and simulated flow the 24-hour winter validation event

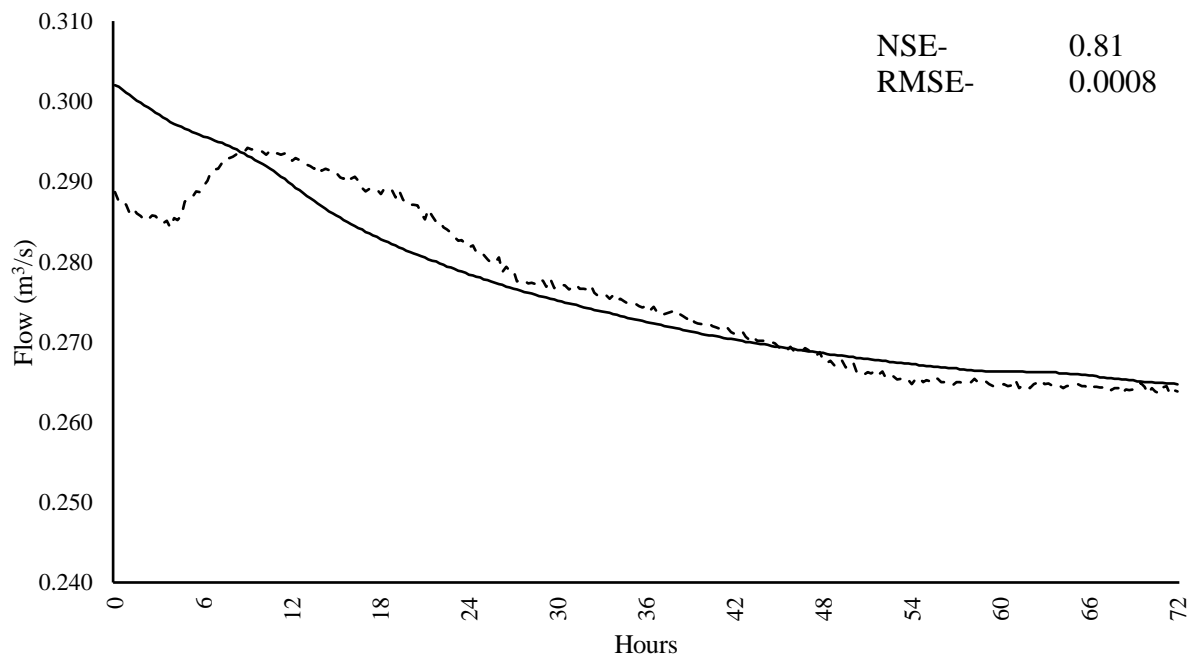


Figure 5.30. Observed and simulated flow the 72-hour winter validation event

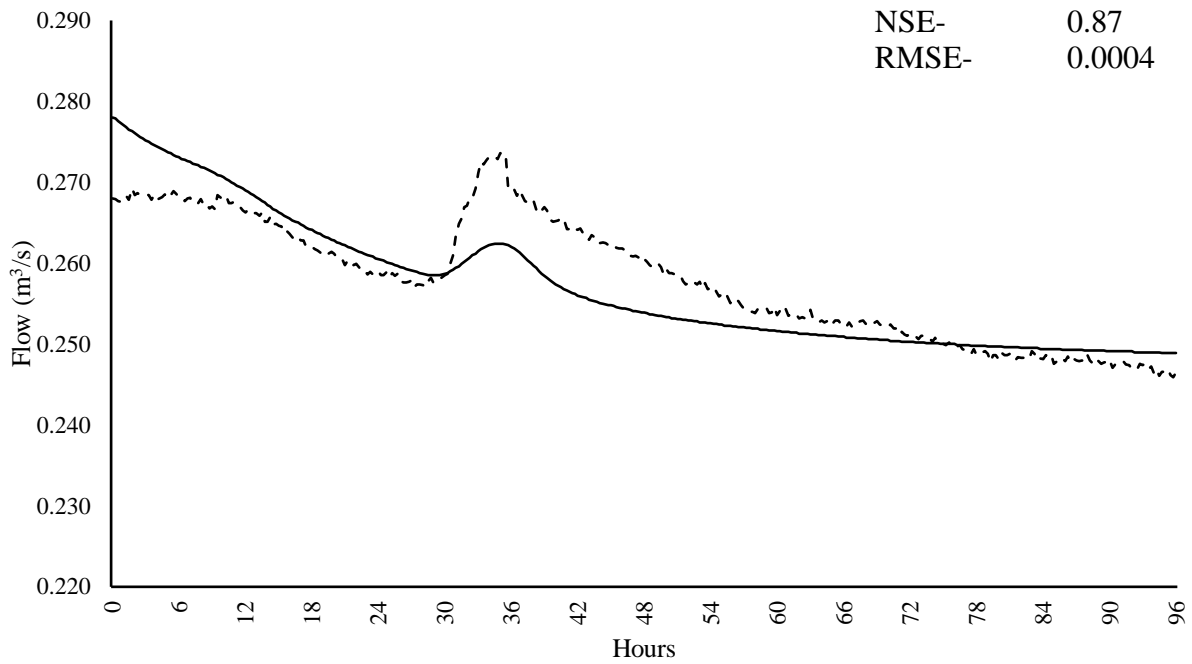


Figure 5.31. Observed and simulated flow the 96-hour winter validation event

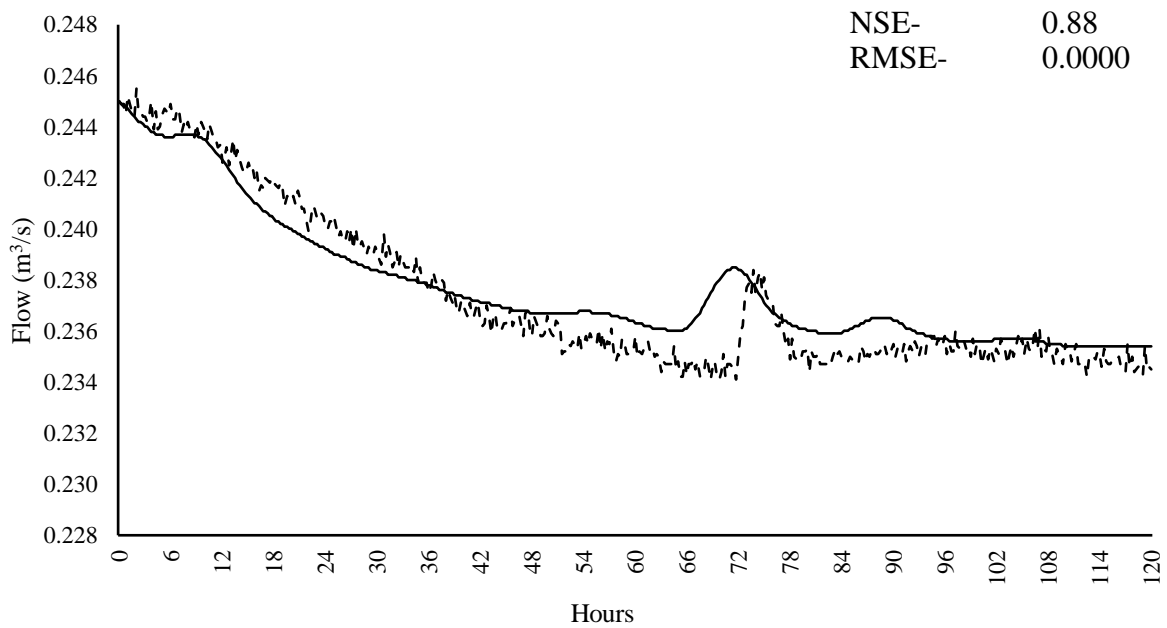


Figure 5.32. Observed and simulated flow the 120-hour winter validation event

The mean NSE value of the winter model validations is 0.87, meaning the model is a very good representation of the hydrological processes occurring across the study area, based on the observed data. The validation NSE is significantly higher than the 0.65 NSE achieved in calibration, again indicating that the model parameters defined throughout calibration are near-

representations of the hydrological response of the site during a storm event. The mean RMSE of the winter validations is 0.0014, showing very little error between each timestep of both the observed and simulated data used in validation (Naik *et al.*, 2019; O’Loughlin *et al.*, 2020).

### 5.5.2 Summer Validation Events

Winter validation events are shown throughout Figure 5.33 to Figure 5.36.

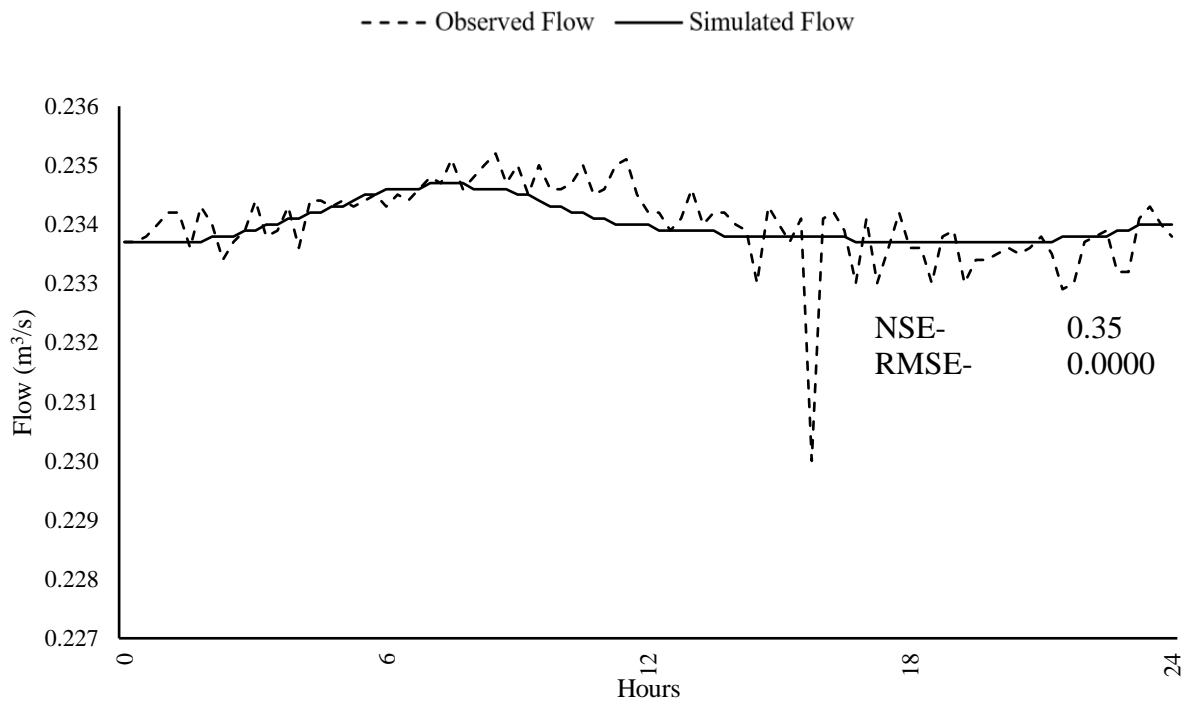


Figure 5.33. Observed and simulated flow the 24-hour summer validation event

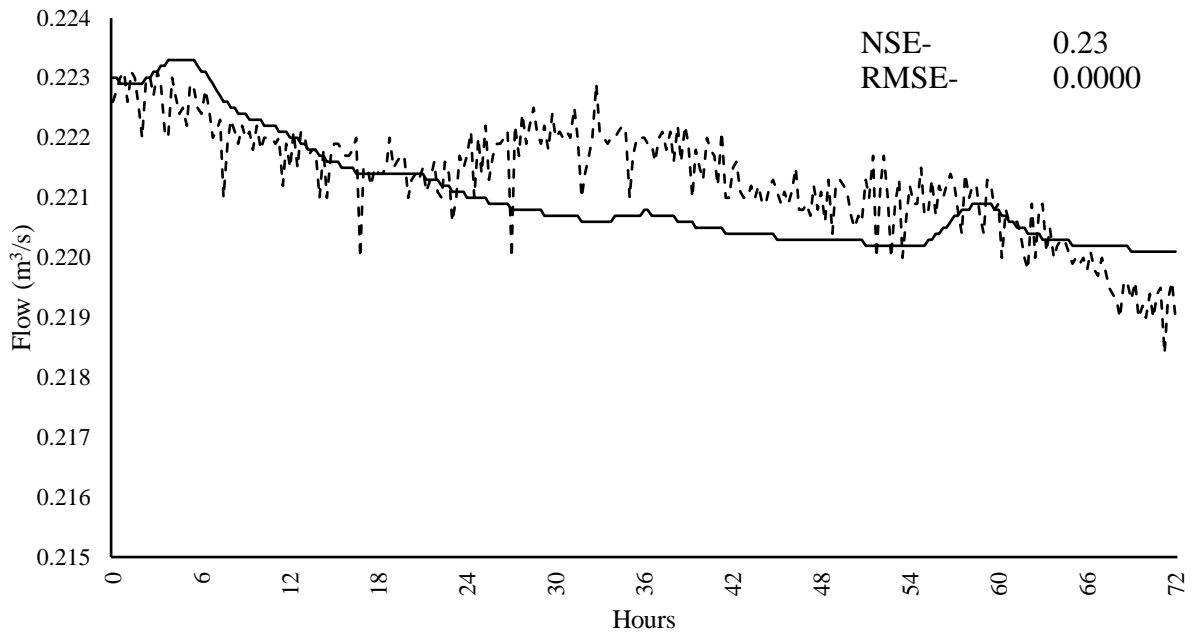


Figure 5.34. Observed and simulated flow the 72-hour summer validation event

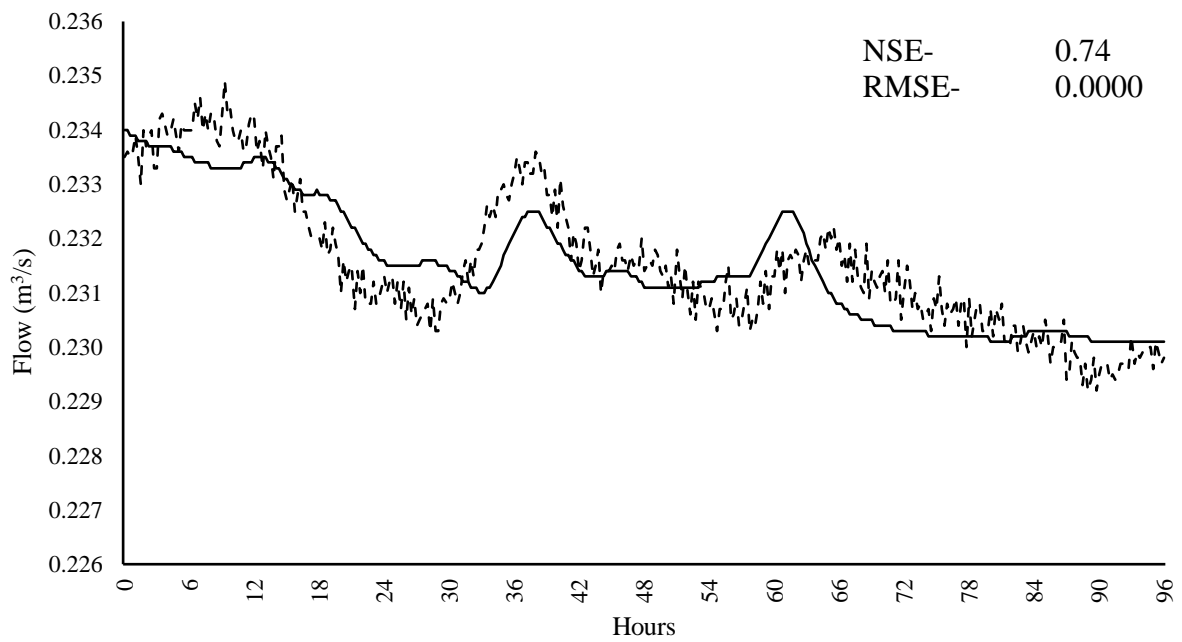
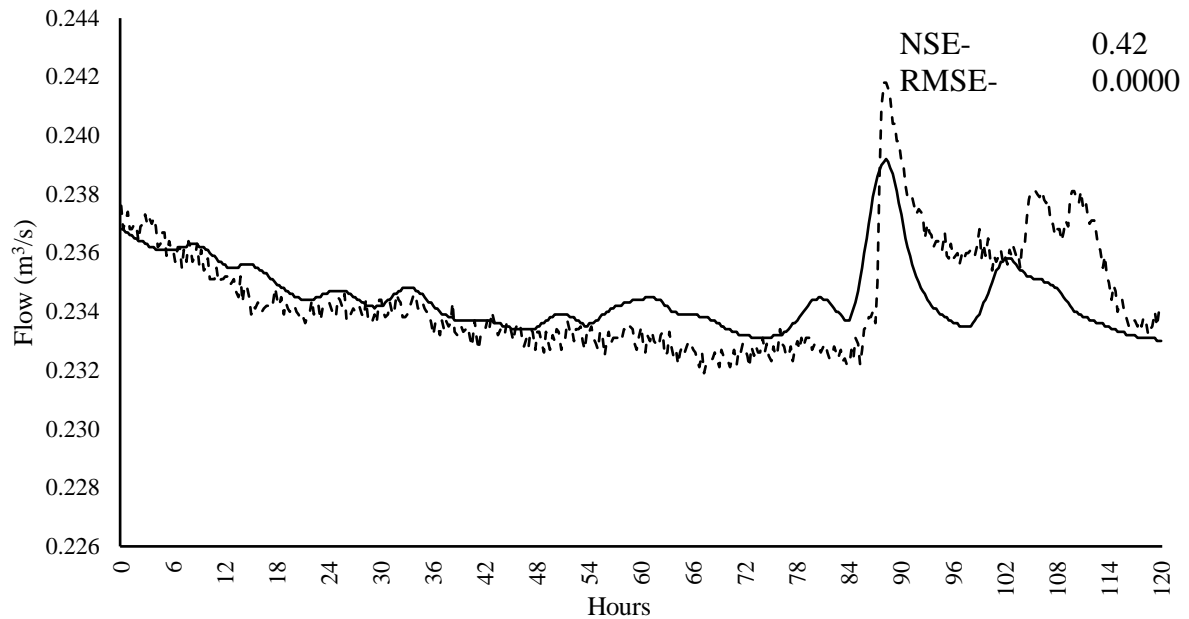


Figure 5.35. Observed and simulated flow the 96-hour summer validation event



*Figure 5.36. Observed and simulated flow the 120-hour summer validation event*

The mean NSE of the summer model after validation is 0.44. This value is significantly lower than the winter calibration, and 0.21 lower than the NSE that indicated a ‘good’ hydrological model (Nash and Sutcliffe, 1970). This value is the highest possible NSE for the summer model and multiple simulations and changes to the baseflows were undertaken to try and increase the NSE (no other parameters could be altered due to the successful calibration of the summer model), however any alteration only seemed to worsen the NSE, therefore, the NSE of 0.44 was accepted. The RMSE of the summer validation events, however, have a mean RMSE of 0 (an explanation of RMSE values can be seen in Appendix B.5.3).

The chosen calibration and validation datasets were selected primarily due to the scarcity of collected telemetry data from the study site and the timescales from which the data needed to be collected. Therefore, replication of calibration and validation events for the purposes of increased accuracy was not possible in this instance. Data scarcity for calibration and hydrological modelling is a common occurrence in this study discipline, and models are often calibrated using telemetry data from outside the catchment of study (Ibrahim-Bathis and Ahmed, 2016; Jiang *et al.*, 2020). The methods presented throughout this section could be

adopted by other researchers in the discipline aiming to simulate similar scenarios to those presented here.

## **5.6 Post-Validation Model Parameters and Simulations**

This section describes the processes used to simulate design storm scenarios from the study site, and how collected field data was interpreted to simulate events across the study area.

### **5.6.1 Simulation Durations and Intensities**

For every infiltration scenario, 50%, 10%, 2% and 1% annual exceedance probability (AEP) rainfall events were simulated over 6, 24 and 96-hour durations. 24 and 96-hour durations were chosen to test the short-to-medium scale impacts of tree planting on infiltration. The 6 hour duration was chosen due to the requirement of all sustainable drainage systems (SuDS) (Local Authority SuDS Officer Organisation (LASOO), 2016) to be tested to this level; it is hoped in the future that NFM and SuDS will be treated as a coherent entity, so consideration was given to this when planning the modelled storm scenarios (Dittrich *et al.*, 2019; Cooper *et al.*, 2021). The rainfall intensities were chosen for similar reasons: the modelled results would enable further understanding regarding the true ability of tree planting to mitigate runoff from low intensity (50% AEP) to very high intensity (1% AEP) events, offering insight in to its use as a method of NFM, and fulfil the partial requirements of aim 3 (objectives 3a and 3c) (Metcalf *et al.*, 2017b; Dittrich *et al.*, 2019).

Three scenarios were simulated using both the winter and summer models: (1) where the collected infiltration data was simulated to give a ‘current HofE land cover’ representation of site discharge; (2) where infiltration was altered to represent sites discharge if it was impermeable land cover (developed); and (3) where the control site infiltration value was used to represent the site if only grassland had been planted. For the impermeable cover, the ‘impermeability’ criteria in HEC-HMS was set to 99% for every sub-catchment, as

impermeable cover is never 100% impermeable due to depression storage, cracks in the surface allowing infiltration into the sub-base (Hornberger *et al.*, 2014; Elbasit *et al.*, 2020; Grimm and Chu, 2020; Cieśliński, 2021). However, for the purpose of the hydrological model, 99% was a compromise as it was intended to simulate the site as if the entire area had just been developed, this would unlikely be the case in the real-world, but acted as a comparison for grassland and woodland values.

The aforementioned scenarios were chosen for use throughout hydrological simulations due to the information the derived results would provide. The ‘current’ representation would provide an insight into the hydrological characteristics of the site at present, considering all collected infiltration data, and accounting for the variations in soil conditions and interception (see sections 5.4 and 5.6.2). The grassland simulations were undertaken using only the control sample site infiltration data, and these results would act as a comparison point when comparing the impacts of tree planting. Simulating the site as if it was completely developed acts as a comparison point for both ‘current’ and grassland simulations, indicating the variations in peak flow and total discharge as a result of developing the entire site. This was prompted as a result of the increase in urbanisation, as discussed throughout Chapter 1.

### 5.6.2 Rainfall Data, Design Storms, and Interception

The Flood Estimation Handbook (FEH) consists of five volumes containing information regarding the hydrological characteristics and predicted rainfall severity (relating to a given AEP) of every catchment across the UK (UK Centre for Ecology and Hydrology, 2021). The FEH provides the information needed to generate a design storm - a synthetic hyetograph that disperses total rainfall based on catchment descriptors (given by the FEH), in a way to test drainage infrastructure during hydrological modelling (Alfieri *et al.*, 2008; Krvavica and Rubinić, 2020). To generate the design storms for the durations and intensities outlined in 0, the hydrology tools on Flood Modeller (Jacobs, 2021) were used; the FEH catchment

descriptors were imported, required storm duration and AEP specified, and the resulting design storm exported.

As discussed in 5.4, two models were built to account for hydrological variations of the site throughout summer and winter. Interception and the influence it can have on reducing runoff is discussed in sections 2.3.3 and 2.4, with regards to its importance when considering NFM (Lunka and Patil, 2016; Ngai *et al.*, 2017). In this study, interception needed to be considered as the sampled tree species are deciduous (

Table 5.4), meaning interception is variable throughout the year. Interception loss was not empirically monitored for this study due to it falling beyond the scope; however, it was accounted for throughout the modelling phase using published values (Calder, 2003; Nisbet, 2005; Lunka and Patil, 2016; Ngai *et al.*, 2017). See Table 5.7.

*Table 5.7. Mean interception loss from grassland and broadleaf trees.*

Land cover	Suggested loss	Central loss (per annum)	Reference
Grassland	Negligible	< 0 %	(Ngai <i>et al.</i> , 2017)
	Negligible	< 0 %	(Nisbet, 2005)
Broadleaf	28-34%	21 %	(Lunka and Patil, 2016)
	10-25%	17.5 %	(Calder, 2003)
	Mean Average	24.25 %	

The ranges (28-34%, 10-25%) of broadleaf interception loss were averaged to give a single figure (24.25%) to apply to FEH rainfall for the summer model, grassland interception values are shown in the literature to be negligible (<0%). It is acknowledged that there will be less precipitation entering the model throughout the summer simulations due to the discussed loss due to interception. This further supports the decision to create both summer and winter models and simulate separately.

Table 5.8 shows the FEH values before (for winter) and after (for summer) interception loss.

Table 5.8. Total FEH values before (for winter) and after (for summer) interception loss.

<b>Duration (hours)</b>	<b>AEP %</b>	<b>Winter precipitation (mm)</b>	<b>Summer precipitation (after interception loss) (mm)</b>
6	50	22.34	16.92
6	10	35.37	26.79
6	2	52.94	40.10
6	1	62.77	47.55
24	50	36.66	27.77
24	10	54.37	41.18
24	2	76.83	58.20
24	1	88.91	67.35
96	50	56.04	42.45
96	10	77.74	58.89
96	2	103.80	78.63
96	1	117.16	88.75

The FEH values shown were used to simulate rainfall in the winter and summer models respectively. This is a method accounts for interception loss without the use of specialised equipment or continuous monitoring, and was an important process as the influence of interception loss would vary seasonally across the site both at present and in the future (Iida *et al.*, 2020).

### 5.6.3 Simulating Infiltration

The infiltration data collected as part of objective 1a needed to be interpreted and included as a critical part of the modelling process and needed to be sorted in to winter and summer (section 5.4). The collected infiltration data from every sample site at 10 and 200 cm proximity was ordered by collection month over collection years, for example, winter infiltration data was collected in 2019/2020 and 2020/2021, so the total infiltration for the same sample sites over both winter durations were recorded.

To account for the infiltration values of sites that were not observed but were required in the hydrological model for an accurate representation of the site (1991, 1995, 2007, 2009, 2011, 2013, 2015, 2016, 2017 2018 and 2019), the median value was calculated from the observed data. For example, the infiltration for 2007 was taken from the median value of 2006 and 2008, and the median value from 2008 and 2010 was used to produce the infiltration value for 2009 (etc.). This method was simplistic for planting years that fell between observed years, however, became slightly more complicated between 2014 and 2020 as there was no observed infiltration data. Instead, the median between 2014 and 2020 was used as the 2017 value, and then these values used to calculate the median for 2015, 16, 18 and 19 respectively. Whilst the method of deriving the infiltration values for the unobserved sites is mathematically based on observed data, it is reasonable to assume that the infiltration would follow the trend due to similarities in soil texture and tree species (Jarvis, 2007; Folorunso and Aribisala, 2018; Rahman *et al.*, 2019; Mahapatra *et al.*, 2020). It is also advantageous that the only unobserved values between 2014 and 2020 to be used in the model are two small plots planted in 2018, meaning the extrapolation did not have to be extensively employed.

#### 5.6.4 Baseflow and Antecedent River Conditions

For any simulation to be representative of current site hydrology, baseflow had to be approximated (Schütte and Schulze, 2017; Onyutha, 2019). If baseflow was overlooked, then the total discharge from each simulated storm would neglect the water volume of the river before simulation, and therefore not represent true site conditions (Cahyono and Adidarma, 2019; Gholami and Khaleghi, 2021). To calculate the baseflow, telemetry data collected via the pressure transducer (accuracy  $\pm 0.05\%$  FS) (see section 5.3.1) starting at the date that the equipment was calibrated on-site (09/04/2019), was collected and split into summer and winter (Section 5.4). This data was then averaged, and the result was used as the baseflow input for the model when simulating the current flow at the study site. See Figure 5.37

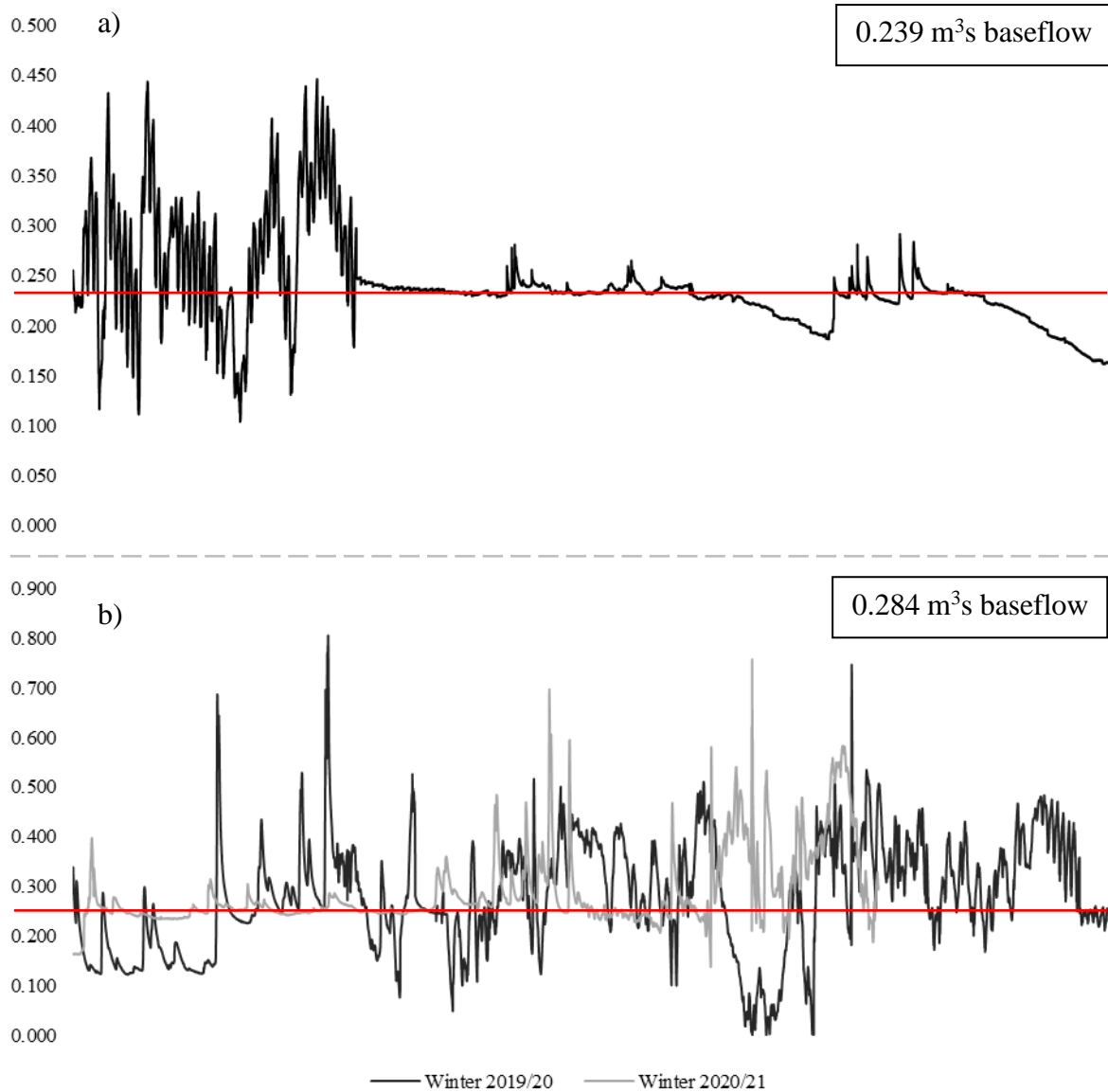


*Figure 5.37. Collected telemetry data for a) summer and b) winter, red line indicates mean flow (taken as baseflow for hydrological modelling)*

The winter mean baseflow was  $0.284\text{m}^3\text{s}$  and the summer mean baseflow is  $0.239\text{m}^3\text{s}$ . It should be noted that the summer mean was based only on data collected from April to September 2020 as no data was available before these dates, and a fault with the pressure transducer meant that data after these dates could not be recovered.

## **5.7 Precipitation, Infiltration and Baseflow Projections**

This section describes the processes of projecting precipitation, infiltration and baseflow to account for future climate change; and how these methods were utilised to fulfil objective 3b.

### **5.7.1 Projected Variations in Precipitation due to Climate Change**

The UK Climate Projections 2018 (UKCP18) toolkit provides independently peer reviewed future climate change projections at 60 km scale globally, and at 12 and 2.2 km scale for the UK (The Met Office, 2019). Climate projections in the UKCP toolkit are used by the EA to anticipate change to hydrometric datasets due to climate change over the next century (Environment Agency, 2021a). Each data allowance is based on a percentile of climate data collected from 1961-1990; the central allowance based on the 50<sup>th</sup> percentile, the and the upper allowance based on the 90<sup>th</sup> percentile (Environment Agency, 2021a). Table 5.9 shows national precipitation increase allowances for catchments smaller than 5km<sup>2</sup>.

*Table 5.9. Percentage increase for total event rainfall for given timescales.*

<b>Allowance</b>	<b>Anticipated Increase</b>		
	<b>2015 - 2039</b>	<b>2040 - 2069</b>	<b>2070 - 2115</b>
<b>Upper end</b>	10%	20%	40%
<b>Central</b>	5%	10%	20%

Percentage increase for the central 2071-2115 and the upper 2041-2070 are both 20%, and the upper 2015-2040 and the central 2040-2069 are both 10%. Simulating these individually would result in the same values being produced, contributing no additional information to the study. To comprehensively simulate all projected future changes to precipitation, FEH rainfall values were increased by 5, 10, 20 and 40% over each duration and AEP. This allowed for all likely precipitation increase scenarios to be accounted for, and eventually provide a range of output results shown throughout section 7.3.

As discussed in section 5.6.2, interception loss was subtracted from summer FEH values for the ‘current day’ models. To account for precipitation changes throughout the summer due to climate change, the post-interception loss rainfall values were multiplied by the values shown in Table 5.9.

### 5.7.2 Projected Variation to Infiltration Values due to Climate Change

Projecting infiltration for the purposes of modelling the hydrological characteristics of the site considering climate change posed a unique challenge to this study. As reflected in section 3.5, there are no past or ongoing projects that have collected infiltration data to the frequency or duration of what has been collected for this project; meaning literature and guidance is sparse for this area. Whilst authors acknowledge that tree planting increases infiltration over time (Chandler *et al.*, 2018; Zhang *et al.*, 2019a; Murphy *et al.*, 2021) and is of benefit when reducing flood risk (Lacob *et al.*, 2014; Dittrich *et al.*, 2019; Murphy *et al.*, 2021), very little data is available to project values in to the future. Due to the novelty of this attempt, and the lack of external data to use for justification, any method selected for the projection of data would need to be built on reasonable assumption and/or mathematics or statistics. In total, three methods of projecting infiltration data were tested; however, the method chosen utilised published information (maturity, growth rates) in addition to collected infiltration data to cumulatively increase the infiltration year-on-year until maturity. This would be applied to observed sites, and unobserved sites would be extrapolated from averaging observed values (in the same method discussed in section 5.6.3). The results of the alternative methods tested for infiltration projection are shown in appendix B.6.

The first step was to find the ages at which the sample trees mature and reach their average maximum dimensions. Infiltration increases as a result of tree roots breaking up the surrounding soil; the larger the tree, the larger the roots and the larger the area for potential increased infiltration (Silber, 2019; Tzioutzios and Kastridis, 2020; Martinez *et al.*, 2021).

When a tree reaches its maximum dimensions (and maturity), root growth slows to a quasi-steady state, indicating infiltration would remain at a constant value until the decline and gradual death of the tree (Alvarez-Uria and Körner, 2007; Muller *et al.*, 2019). The tree species of the sample sites (section 5.2.1) are shown again in Table 5.10.

Table 5.10. Species of sampled woodland.

Planting year	Species Name	
Pre – 1900	Sessile Oak	<i>Quercus Petraea</i>
2006, 2010	Silver Birch	<i>Betula Pendula</i>
2008, 2012, 2014, 2020	Aspen	<i>Populus Tremula</i>

Regarding the *ca.*1900 site, Sessile Oak (*Quercus Petraea*) can live for 600 - 1000 years, and all Oak species are classed as ancient from 400 years onwards. A Sessile Oak reaches its ultimate height in 50 years, at which point growing slows (The Royal Horticultural Society, 2021; Woodland Trust, 2021). Using this information and applying to the *ca.*1900 site at Sernal, it is reasonable to assume that infiltration will unlikely change significantly from now until the last simulated year (2120), so mean infiltration will be used for both the 10 and 200 cm proximities for all projection years. The Silver Birch (*Betula Pendula*), planted at the 2006 and 2010 sites, grows rapidly for the first 50-60 years (Hynynen *et al.*, 2010), but usually reaches its maturity and ultimate height around 60 years (Kuparinen *et al.*, 2010; Lee *et al.*, 2015; Zeltiņš *et al.*, 2018). A Silver Birch can live for 60-70 years and usually become more susceptible to decay and other defects before reaching 100 (Hynynen *et al.*, 2010). Aspen trees (*Populus Tremula*), planted at the 2008, 2012, 2014 and 2020, sites grow rapidly for the first 25-30 years. Growth slows at around 30 years, and their mean lifespan is 100-120 years (MacKenzie, 2010; CAB International, 2013; Savill, 2019). Like the *ca.*1900 site, the infiltration rates collected from the grassland control are likely to stay the same through all projection years; aerial imagery (appendix Table B.16) shows that area has been grassland for

over 100 years, so is unlikely to change in infiltration unless provoked through development/agricultural practice, of which the HofE are not planning on undertaking for the foreseeable future (The Heart of England Forest Charity, 2021).

Once information about the sample trees had been derived, it was used in conjunction with the mean infiltration data for both summer and winter to project future changes. The age of each tree was calculated based on the year it was planted (in 2021, the 2006 trees would be 15 years old), the mean infiltration value was then divided by this value, which would give the mean infiltration for the tree if it was 1 year old. This was then used to cumulatively increase the infiltration year-on-year, until the year that the tree would mature was reached. This is shown in EQ 5.11

$$\text{Infiltration per year} = \left( \frac{\text{Mean infiltration}}{\text{Years planted}} \right) \times \text{years until maturity age} \quad \text{EQ 5.11}$$

The results of this method are shown for 10 and 200 cm proximity winter and summer in appendix B.7. Figure B.32 to Figure B.39 (appendix B.7) show the projected values for 2014 and 2020 to be higher than other values for the same proximity and season; this is due to the amount of observed data available for use in projections. This is a result of the projection method used; as the 2014 and 2020 planting areas are relatively new, there were less ‘established years’ to divide the mean infiltration by. This meant that when infiltration was divided and multiplied to account for growth over time until maturity, the growth rate was faster for trees newer trees of younger maturity. As mentioned in section 5.6.3, the 2014 and 2020 datasets were only used for the benefit of a small section of land (planted in 2017 and 2018), not owned by the HofE forest, so the use of these infiltration projections in modelling will not influence results as substantially as they would if the entire site was reliant on the 2014 and 2020 projections. The need for devising such methods further emphasises the novelty and uniqueness of this project, few other catchments in the UK has such comprehensive infiltration data, so this method was chosen based on trial and error, and the required outcome. After

projections had been extrapolated for the observed infiltration years, infiltration data for unobserved sites needed to be projected to account for likely future change. For this, the median values were derived (following the method explained in section 5.6.3), and this value was then calculated using EQ 5.11.

Figure B.32 to Figure B.39 (appendix B.7) show a taper in infiltration as the trees reach their maturity. Whilst this is possibly not representative of infiltration trends observed in the field, it is important to remember that these projections have been extrapolated from observed data using statistical methods. Additionally, they are based on the tree growing consistently year-on-year and in reality, trees are much more complicated. Tree growth is dependent on soil texture, soil nutrients, biological activity, resistance to illness, sunlight, rain patterns and atmospheric temperatures (Alvarez-Uria and Körner, 2007; Skovsgaard *et al.*, 2018; Muller *et al.*, 2019). However, as mentioned above, the presented infiltration projections are for the purpose of producing a likely peak flow and total discharge range based on the collected infiltration field data, and will contribute to the knowledge base regarding the role of woodland a method of NFM.

### 5.7.3 Projected Variation to Baseflow due to Climate Change

Projecting the changes to baseflow as a result of climate change is of significance to the hydrological modelling stage of this project. There is very little literature regarding baseflow changes for catchments across the UK due to its unpredictability and variability from catchment to catchment (Yusop *et al.*, 2007; Onyutha, 2019). The method used in this study is based on the method used regularly by water practitioners and hydrological consultancies, and uses the EA's peak flow projections, which are based on UKCP18 climate projection data (Lowe *et al.*, 2019; Environment Agency, 2021a, 2021b; JBA Personal Communication and PCC Personal Communication, 2021). Table 5.11 shows the peak flow uplifts for the study site tributary (Severn, Avon Warwickshire).

*Table 5.11. Percentage increase for baseflow for specified future year range*

<b>Allowance</b>	<b>Anticipated Increase</b>		
	<b>2020 - 2049</b>	<b>2050 - 2079</b>	<b>2080 +</b>
<b>Upper end</b>	22%	31%	59%
<b>Central</b>	7%	8%	21%

The conversion from the percentage uplifts in Table 5.11 to baseflow is shown in EQ 5.12.

$$\text{Baseflow uplift} = \text{observed baseflow} \times 1.x \quad \text{EQ 5.12}$$

Where  $x$  = the percentage increase as defined by the EA for the desired timescale (Table 5.11).

The results of the uplifted baseflow for higher and central projections for each timeframe can be seen in Table 5.12.

Table 5.12. Baseflow values after applying EA uplifts

	2020 - 2049	2050 - 2079	2080 +
Winter – Current mean baseflow: <b>0.284m<sup>3</sup>s</b>			
<b>Upper end</b>	0.346	0.372	0.452
<b>Central</b>	0.304	0.307	0.344
Summer– Current mean baseflow: <b>0.239m<sup>3</sup>s</b>			
<b>Upper end</b>	0.292	0.313	0.380
<b>Central</b>	0.256	0.258	0.289

Upper end and central projections refer to the percentage of possible scenarios that fall above and below an allowance level. The central allowance is based on the 50th percentile, meaning 50% of possible flow scenarios fall both above and below this point; and the upper end allowance is based on the 90<sup>th</sup> percentile, meaning 90% of likely flow events fall below this value, and 10% above (Environment Agency, 2021a). The EA also issue a H++ scenario for river flows, however these are based on there being no mitigative actions taken against climate change and are rarely used in hydrological modelling due to their speculative nature. Therefore, H++ was not included here, but central and upper were simulated to produce a range of possible outcomes for future flows from the study site based on EA data (see section 7.3).

### **5.8 Summary of Simulations and Data Used**

Table 5.13 is a list of completed hydrological simulations, detailing the duration, AEP and data and information used for each. In total 448 simulations were undertaken, 324 in winter and 324 in summer.

Table 5.13. Simulations and data used for each. Each simulation was computed for both winter and summer.

Duration (hours) AEP (%)	6, 24, 96				Notes
	50	10	2	1	
HofE site	✓	✓	✓	✓	Collected winter and summer infiltration data
Impermeable	✓	✓	✓	✓	99% impermeable
100% Grassland	✓	✓	✓	✓	Control site (grassland) infiltration value winter and summer
Site in 20 years (2040), 5% rainfall, central baseflow.	✓	✓	✓	✓	Current site in future years (defined in column 1), using precipitation, infiltration and baseflow projections (discussed throughout section 5.7)
Site in 20 years (2040), 5% rainfall, upper baseflow.	✓	✓	✓	✓	
Site in 50 years (2070), 10% rainfall, central baseflow.	✓	✓	✓	✓	
Site in 50 years (2070), 10% rainfall, upper baseflow.	✓	✓	✓	✓	
Site in 100 years (2120), 20% rainfall, central baseflow.	✓	✓	✓	✓	
Site in 100 years (2120), 20% rainfall, upper baseflow.	✓	✓	✓	✓	
Site in 100 years (2120), 40% rainfall, central baseflow.	✓	✓	✓	✓	
Site in 100 years (2120), 40% rainfall, upper baseflow.	✓	✓	✓	✓	
Grassland site in 20 years (2040), 5% rainfall, central baseflow.	✓	✓	✓	✓	Grassland site in future years (defined in column 1), using precipitation, infiltration and baseflow projections (discussed throughout section 5.7)
Grassland site in 20 years (2040), 5% rainfall, upper baseflow.	✓	✓	✓	✓	
Grassland site in 50 years (2070), 10% rainfall, central baseflow.	✓	✓	✓	✓	
Grassland site in 50 years (2070), 10% rainfall, upper baseflow.	✓	✓	✓	✓	
Grassland site in 100 years (2120), 20% rainfall, central baseflow.	✓	✓	✓	✓	
Grassland site in 100 years (2120), 20% rainfall, upper baseflow.	✓	✓	✓	✓	
Grassland site in 100 years (2120), 40% rainfall, central baseflow.	✓	✓	✓	✓	
Grassland site in 100 years (2120), 40% rainfall, upper baseflow.	✓	✓	✓	✓	
Impermeable site in 20 years (2040), 5% rainfall, central baseflow.	✓	✓	✓	✓	Impermeable site in future years (defined in column 1), using precipitation, infiltration and baseflow projections (discussed throughout section 5.7)
Impermeable site in 20 years (2040), 5% rainfall, upper baseflow.	✓	✓	✓	✓	
Impermeable site in 50 years (2070), 10% rainfall, central baseflow.	✓	✓	✓	✓	
Impermeable site in 50 years (2070), 10% rainfall, upper baseflow.	✓	✓	✓	✓	
Impermeable site in 100 years (2120), 20% rainfall, central baseflow.	✓	✓	✓	✓	
Impermeable site in 100 years (2120), 20% rainfall, upper baseflow.	✓	✓	✓	✓	
Impermeable site in 100 years (2120), 40% rainfall, central baseflow.	✓	✓	✓	✓	
Impermeable site in 100 years (2120), 40% rainfall, upper baseflow	✓	✓	✓	✓	

## **5.9 Chapter Summary**

This chapter has introduced the research philosophy and hypotheses of study (section 5.1), and described and critically assessed the methods selected for in producing study results in line with the study aims and objectives (section 1.3). Upon defining the study site in Chapter 4, infiltration sample plots were identified following the criteria outlined in section 5.2. Infiltration was collected with the MDI from plots planted in 2006, 2008, 2010, 2012 (in addition to a grassland control and area of woodland planted *ca.*1900) at Spernal; additional data was collected from 2014 and 2020 sites on alternate weeks to Spernal. This data is presented and analysed in section 7.1.

Two hydrological models were built, calibrated, and validated using hydraulic data from the site, and the NSE method was used to determine the accuracy of the models. Two models were created to better represent study site conditions throughout winter and summer respectively, and these models were used to generate the present-day response of the site to varying rainfall events. The results are presented in section 7.2.

The collected infiltration data, and the required hydrometric data (precipitation and baseflow) were projected using appropriate methods (comprehensively discussed in section 5.7) to project the influence of woodland planting in the future, considerate to the predicted changes due to climate change. These results are presented throughout section 7.3.

## **Chapter 6 Pilot Results and Reflection for Infiltration Tests**

It is outlined in section 5.2.2.1 that, due to the importance of infiltration measurement replication for this study, the MDI user manual's suggestion of 30-40 ml of infiltrated water per measurement was adjusted. This methodology was tested at the HofE site as part of a preliminary pilot study, and the processes and results of this adaptation are discussed throughout this chapter, along with how this method was up scaled to the whole study site.

### **6.1 Mini Disk Infiltrometer Testing and Validation**

A tension setting of 2 cm was selected following the suggestion of the MDI user manual (METER® Group Inc., 2020), however the manual also notes that 30 to 40 ml of water should infiltrate the soil for accurate measurement. The soil texture of most sample sites at Sernal is clay, which inherently exhibits a low permeability (Folorunso and Aribisala, 2018), thus indicating that allowing 30-40 ml of water to infiltrate would surpass the allotted time on site each week (accounting for replication, and the requirements of the health and safety agreement). Therefore, for further justification and to quantify the 'time on site' that would be required to collect the desired data (and replicates) from all sample sites using the suggested 30-40 ml of water, a pilot study was undertaken.

The MDI was filled and placed at the *ca.*1900, 2006, 2008, control and 2010 sites, and monitored until 40 ml of water infiltrated the soil, at which point, the measurement ended. Measurements took place over two days at the HofE Sernal study site, and the results are shown in Figure 6.1 and Table 6.1.

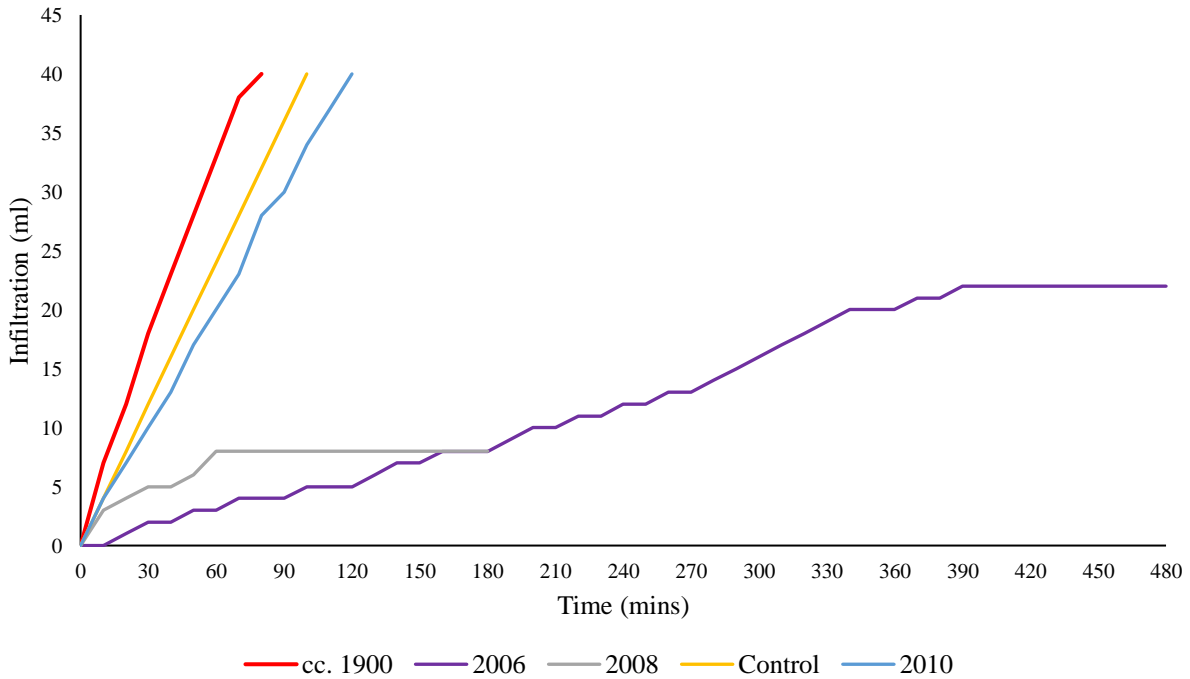


Figure 6.1. Graphical display of infiltration / duration results from the MDI validation.

Table 6.1. Tabulated results of the MDI validation showing time to infiltrate, infiltration volume and reasons for measurement conclusion.

Site	Sample day	Time		Infiltration (ml)	Note
		Mins	Hours		
ca.1900	1	80	01:20	40	40 ml infiltrated
2006	1	480	08:00	22	Getting dark
Control	2	100	01:40	40	40 ml infiltrated
2010	2	120	02:00	40	40 ml infiltrated
2008	2	180	03:00	8	Getting dark

As seen, 40 ml of infiltration was reached at the *ca.*1900, control and 2010 sites in 1:20, 1:40 and 2:00 hours respectively. The 2006 sample could not be completed due to the daylight fading and the sample having run for 8 hours (1:30 hours of which remaining at 22 ml). The 2008 sample could not be completed as light was fading and infiltration had remained the same for 2:00 hours (8 ml). Results of Figure 6.1 and Table 6.1 show that collecting infiltration following the user manual’s suggestion is impractical for the overall aim of the infiltration data collection. For example, the measurement of both proximities including replication of the *ca.*1900 site (the quickest site to reach the 40 ml threshold) would take 8 hours; and the

collection of the same data at the slowest site (2006) would take 48 hours (it is also worth noting that the 2006 failed to reach the user manual 40 ml threshold).

Using the above information, it was decided that the user manual recommendation not be followed, and instead measurement would end when consecutive infiltration measurements were recorded for three sequential timesteps (in line with Bagarello and Sgroi (2004) and Chandler *et al.*, (2018)), or when measurement duration reached 10 minutes. To verify this method, an additional MDI measurement was recorded 50 cm away from the location of those shown in Table 6.1, however this measurement was limited to 10 minutes. The results in Table 6.1 were then divided to show the infiltration per minute, and per 10 minutes (columns A), and compared to the 10-minute duration measurements, as shown in Table 6.2 (columns B).

*Table 6.2. 10-minute MDI measurement (columns B) compared to the data displayed in Table 6.1 (columns A).*

Site	A			B	
	Total Infiltration (ml)	Infiltration per minute (ml)	Infiltration per 10- minutes (ml)	Observed 10-minute infiltration (ml)	% +/- 10-minute value
ca.1900	40	0.50	5.00	5.73	+14.60
2006	22	0.05	0.46	1.08	+135.64
Control	40	0.40	4.00	3.4	-15.00
2010	40	0.33	3.33	3.28	-1.60
2008	8	0.04	0.44	3.01	+100.67

Results show that there is variation between the 10-minute values in infiltration at all sites, the 2006 site shows the highest variation, followed by 2008, Control ca. 1900, and 2010. It is important to consider that whilst there is variation between columns A and B, the 10-minute infiltration in column A is a division of a larger dataset, whereas column B data was taken at one measurement over 10 minutes, therefore there is less data to be divisible by in column B. The findings presented as a result of the pilot study were valuable in the shaping of the sampling method used for infiltration data collection (in line with objective 1a) (section 1.3). The results show that the MDI user manual recommendation of 30-40 ml of infiltrated water could not be

followed for this study due to the amount of time that would be required on site, but also that comparable results could be collected over a 10-minute duration at all sites. Using the newly formed methodology of collecting infiltration data over a 10- minute period (or until 3 consecutive measurements were collected, following Chandler *et al.*, (2018) allowed for measurements to be collected and replicated at all Sperial sites, in one site visit. This was beneficial for allowing all sites to be sampled in one site visit (keeping external conditions as consistent as possible and for allowing replications to be collected, which further enforces the reliability of infiltration measurements (see section 4.1). The tension setting of 2 cm was used for all infiltration measurement in the field, following the suggestion of the MDI user manual (METER® Group Inc., 2020).

## **6.2 Chapter Summary**

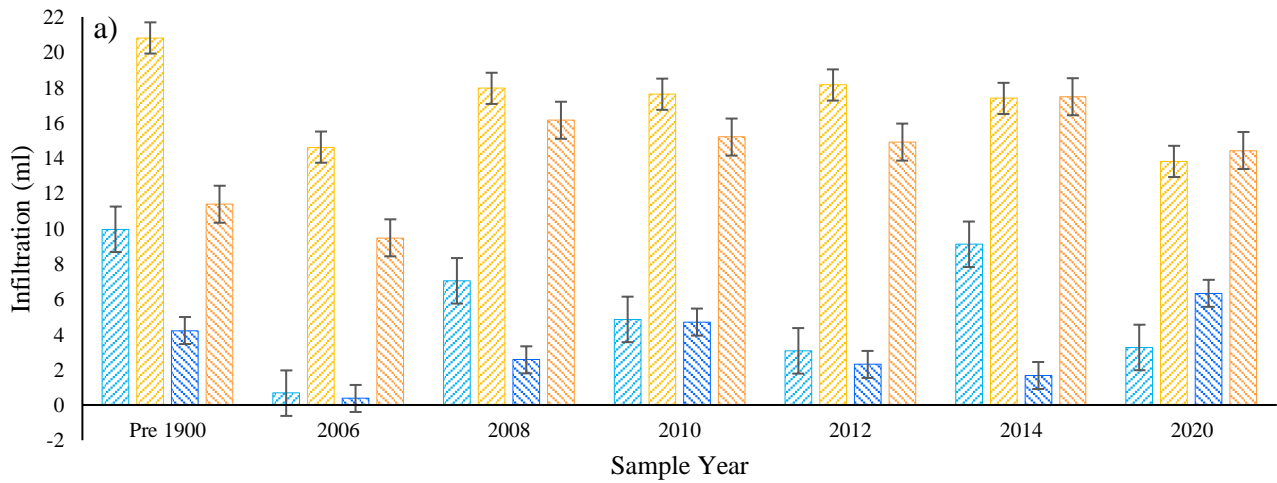
This chapter has introduced the pilot study, conducted to test both the suitability of the existing guidance regarding MDI measurement, and the effectiveness of upscaling the adapted method to the wider study site. Figure 6.1 and Table 6.1 show that following the MDI user manual guidance of allowing 30-40 ml of water to infiltrate is unfeasible at the study site due to both the inherently low permeability of clay soils, and the requirement of replication for this study, as defined in section 6.1, the alternative methodology of sampling infiltration for 10 minutes or until three consecutive measurements are recorded (whichever is first) could be extrapolated for sampling the whole study site, and was ultimately the method used to collect the infiltration data in line with objective 1a (section 1.3).

## **Chapter 7 Results and Analysis**

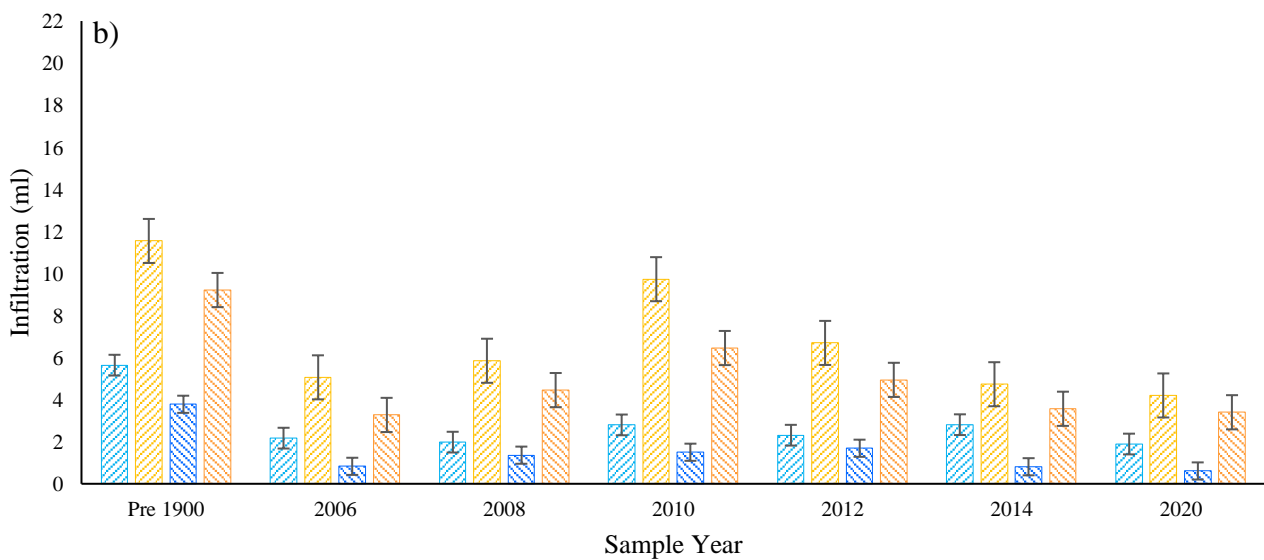
This section presents and interprets the results of the study, generated via the methods discussed throughout Chapter 5. Section 7.1 presents and statistically analyses the collected infiltration data collection, with regard to proximity and maturity. Section 7.2 presents the results of the hydrological modelling of the HofE site at present in both summer and winter. Section 7.3 presents the simulated peak flow and total discharge projections from the site throughout both summer and winter.

### ***7.1 Tree Proximity, Infiltration and Maturity***

Objective 1b was to analyse the collected field data to identify a correlation between infiltration and tree proximity and maturity (section 1.3). Figure 7.1 and Table 7.1 show the mean infiltration values for each sample site throughout winter and summer 2019/20 and 2020/21. Note control has been excluded from figure and tables due to this section being a comparison of infiltration change due to proximity.



▨ 2019/20 10 cm Winter      ▨ 2019/20 10 cm Summer  
▩ 2019/20 200 cm Winter      ▨ 2019/20 200 cm Summer



▨ 2020/21 10 cm Winter      ▨ 2020/21 10 cm Summer  
▩ 2020/21 200 cm Winter      ▨ 2020/21 200 cm Summer

*Figure 7.1 Comparison of mean infiltration data from 10 and 200 cm proximity throughout summer and winter in a) 2019/2020 and b) 2020/2021.*

Table 7.1. Mean infiltration for 10 and 200 cm proximities throughout both winter and summer sample periods. The control site infiltration values are shown here for reference. S.D. refers to the standard deviation of infiltration values, and n indicates the values included in measurement.

	Control	ca. 1900		2006		2008		2010		2012		2014		2020	
		(ml)	S.D.												
<b>2019/20 10 cm</b>		9.96 (n=27)	17.90	0.67 (n=27)	1.05	7.04 (n=27)	17.43	4.85 (n=27)	11.62	3.07 (n=27)	4.36	9.11 (n=27)	18.68	3.26 (n=27)	6.24
<b>2020/21 10 cm</b>	3.4	5.64 (n=36)	3.54	2.17 (n=36)	1.71	1.98 (n=36)	1.61	2.80 (n=36)	3.36	2.31 (n=36)	1.53	2.81 (n=36)	1.94	1.89 (n=36)	1.50
<b>2019/20 200 cm</b>	(n=21)	4.22 (n=27)	7.18	0.37 (n=27)	0.89	2.56 (n=27)	5.96	4.70 (n=27)	11.20	2.30 (n=27)	4.62	1.67 (n=27)	4.07	6.33 (n=3)	6.33
<b>2020/21 200 cm</b>		3.78 (n=36)	3.23	0.83 (n=36)	1.28	1.36 (n=36)	1.18	1.50 (n=36)	1.34	1.69 (n=36)	1.32	0.81 (n=36)	0.72	0.61 (n=36)	0.63
<b>2019/20 10 cm</b>		20.81 (n=21)	25.61	14.62 (n=21)	14.94	17.95 (n=21)	24.94	17.62 (n=21)	28.45	18.14 (n=21)	20.83	17.38 (n=21)	33.55	13.81 (n=21)	17.59
<b>2020/21 10 cm</b>	12.35	11.54 (n=33)	6.85	5.06 (n=33)	3.25	5.85 (n=33)	3.51	9.73 (n=33)	6.34	6.70 (n=33)	4.55	4.73 (n=30)	2.47	4.20 (n=30)	3.51
<b>2019/20 200 cm</b>	(n=18)	11.38 (n=21)	7.94	9.48 (n=21)	8.20	16.14 (n=21)	29.76	15.19 (n=21)	23.34	14.90 (n=21)	16.09	17.48 (n=21)	29.70	14.43 (n=21)	20.17
<b>2020/21 200 cm</b>		9.21 (n=33)	6.55	3.27 (n=33)	2.67	4.45 (n=33)	3.20	6.45 (n=33)	4.70	4.94 (n=33)	3.60	3.57 (n=30)	2.33	3.40 (n=30)	3.01

Table 7.2 and Table 7.3 present the percent difference in infiltration varying by both proximity and seasonality.

*Table 7.2. Percent variation in infiltration measurement at 10 cm and 200 cm proximity varying by measurement period*

<b>Season</b>	<b>+/- 10 cm proximity infiltration higher than 200 cm proximity infiltration</b>
<b>Winter 2019/20</b>	+ 71.38 %
<b>Winter 2020/21</b>	+ 85.26 %
<b>Summer 2019/20</b>	+ 21.55 %
<b>Summer 2020/21</b>	+ 35.48 %
<b>Winter Mean</b>	+ <b>75.87 %</b>
<b>Summer Mean</b>	+ <b>25.19 %</b>

*Table 7.3. Overall mean percent difference in infiltration measurements at 10 cm and 200 cm proximity.*

<b>Measurement</b>	<b>+/- higher in summer compared with winter</b>
<b>10 cm</b>	+ 192 %
<b>200 cm</b>	+ 310 %

Table 7.2 shows that in winter, mean 10 cm infiltration was 75.87% higher than mean 200 cm infiltration over both sample years; and in summer, mean 10 cm infiltration was 25.19% higher than 200 cm. Table 7.3 shows that mean 10 cm infiltration is 192% higher in summer compared with winter, and mean 200 cm infiltration is 310% higher in summer compared with winter. There is more variation between the 10 and 200 cm proximities in winter compared with summer; however, summer 10 cm infiltration is still higher than 200 cm by 21.55% and 35.48% in 2019/20 and 2020/21 respectively.

To further test the significance of the difference in infiltration values collected at the same proximity in both winter and summer (i.e., 10 cm winter vs 10 cm summer and 200 cm winter vs 200 cm summer), statistical analysis was undertaken. A Kolmogorov-Smirnoff normality test was performed using all infiltration data (Gadian *et al.*, 2018; Mishra *et al.*, 2019) finding the data to be non-parametric (see appendix C.1.1); additionally, the collected infiltration data is unpaired data, as the relationship between the data is not related by any other relationship other than the nature of measurement, therefore a Mann-Whitney U test were undertaken (Mishra *et al.*, 2019; Kamis *et al.*, 2021). The Mann-Whitney U test was chosen over other nonparametric statistical tests (Kruskal-Wallis, Mood's median, Wilcoxon signed rank) as it produces results equivalent to the (parametric) independent samples t-test (Fay and Proschan, 2010; Mishra *et al.*, 2019; Kamis *et al.*, 2021). The methodology of the Mann-Whitney U test is presented in appendix C.1.2, and additional statistical information is shown in appendix C.1.3. Results of the Mann-Whitney U tests are shown in Table 7.4.

Table 7.4. Mann-Whitney U test results from comparing equivalent infiltration proximity data from winter and summer

Test Criteria	P-value	Significant difference? ( $P \leq 0.05$ )
All 10 cm winter vs 10 cm summer	<0.00	YES
All 200 cm winter vs 200 cm summer	<0.00	YES
<i>ca.</i> 1900 10 cm winter vs 10 cm summer	0.01	YES
<i>ca.</i> 1900 200 cm winter vs 200 cm summer	<0.00	YES
2006 10 cm winter vs 10 cm summer	<0.00	YES
2006 200 cm winter vs 200 cm summer	<0.00	YES
2008 10 cm winter vs 10 cm summer	<0.00	YES
2008 200 cm winter vs 200 cm summer	<0.00	YES
2010 10 cm winter vs 10 cm summer	<0.00	YES
2010 200 cm winter vs 200 cm summer	<0.00	YES
2012 10 cm winter vs 10 cm summer	<0.00	YES
2012 200 cm winter vs 200 cm summer	<0.00	YES
2014 10 cm winter vs 10 cm summer	0.01	YES
2014 200 cm winter vs 200 cm summer	<0.00	YES
2020 10 cm winter vs 10 cm summer	0.05	YES
2020 200 cm winter vs 200 cm summer	1.00	NO

Results of the Mann-Whitney U tests support the findings displayed in Table 7.1. There is a statistically significant difference in infiltration data collected from the same proximities between winter and summer. Most tests showed a p value <0.00 (alpha), some samples showed a higher p value of 0.01 – 0.05 (*ca.* 1900 10 cm, 2014 10 cm, 2020 10 cm); the only site to show a p-value significantly higher than 0.05 (indicating no significant difference between summer and winter) was 2020 200 cm. The results presented in Table 7.4 are a further indication of the variability of study site hydro-geological conditions throughout summer and winter, and further supports the decision to build, calibrate and simulate two models independently for more representative results (section 5.4).

Referring back to Table 7.1, when considering any correlations between tree maturity and infiltration, it would be expected that the discrepancy between infiltration at the 10 cm and 200 cm proximity would become greater, as tree roots develop laterally, breaking up the surrounding soil matrix, reducing compaction and increasing porosity (Mölder *et al.*, 2019; Zhang *et al.*, 2019a; Xie *et al.*, 2020; Martinez *et al.*, 2021) (section 2.3.1). Considering this, it would be expected that the most recently planted trees (2020/2014), would show a lower mean infiltration at both proximities, and older (HofE) planted trees (2006/2008) would show higher mean infiltration values; however, this is not the case. Table 7.5 shows the mean infiltration of each sample site, sorted in ascending order, in winter and summer at both measured proximities.

*Table 7.5. Sample sites ordered in ascending order based on mean infiltration (ml) in winter and summer at both 10 and 200 cm proximity. n indicates the number of values used to calculate the mean.*

	<b>ca. 1900</b>	<b>2014</b>	<b>2008</b>	<b>2010</b>	<b>2012</b>	<b>2020</b>	<b>2006</b>
<b>Winter 10 cm</b>	7.80 (n=63)	5.96 (n=63)	4.51 (n=63)	3.83 (n=63)	2.69 (n=63)	2.58 (n=63)	1.42 (n=63)
	<b>ca. 1900</b>	<b>2010</b>	<b>2012</b>	<b>2008</b>	<b>2020</b>	<b>2014</b>	<b>2006</b>
<b>Summer 10 cm</b>	16.18 (n=42)	13.68 (n=42)	12.42 (n=42)	11.90 (n=42)	11.06 (n=21)	9.84 (n=42)	9.01 (n=42)
	<b>ca. 1900</b>	<b>2020</b>	<b>2010</b>	<b>2012</b>	<b>2008</b>	<b>2014</b>	<b>2006</b>
<b>Winter 200 cm</b>	4.00 (n=63)	3.47 (n=39)	3.10 (n=63)	2.00 (n=63)	1.96 (n=63)	1.24 (n=63)	0.60 (n=63)
	<b>2010</b>	<b>2014</b>	<b>ca. 1900</b>	<b>2008</b>	<b>2012</b>	<b>2020</b>	<b>2006</b>
<b>Summer 200 cm</b>	10.82 (n=54)	10.53 (n=51)	10.30 (n=54)	10.30 (n=54)	9.92 (n=54)	8.92 (n=51)	6.38 (n=54)

Table 7.5 shows that the sorted mean infiltration data does not follow the chronological order expected (as discussed), aside from the 2006 site which consistently shows the lowest mean infiltration regardless of season or proximity. The *ca.* 1900 site shows the highest mean

infiltration for winter (10 and 200 cm) and summer 10 cm, however is displaced by 2010 at the summer 200 cm proximity. There is no obvious trend between the highest and lowest infiltration values, with no consistent chronology, as would be expected based on the existing literature (Mölder *et al.*, 2019; Zhang *et al.*, 2019a; Xie *et al.*, 2020; Martinez *et al.*, 2021). Whereas Table 7.5 displays mean infiltration change relative to proximity and maturity, this alone is not an accurate representation of the observed trends. As discussed (in section 5.2.1.1), the soil texture of the 2006 site is (almost) entirely clay, meaning infiltration is lower (Folorunso and Aribisala, 2018). However, this does not necessarily mean that the differences in infiltration due to proximity and maturity are less significant. To derive further trends required to fulfil objective 1b, Mann-Whitney U tests were undertaken to define the significance of relationships between infiltration relative to both woodland proximity and woodland maturity, following the criteria shown in Table 7.6.

Table 7.6. Test criteria, P values and significance levels of Mann-Whitney U testing. Green indicates a significant difference; red indicates a significance level higher than 0.05.

Test Criteria	P-value	Significant difference? ( $P \leq 0.05$ )
All 10 cm vs 200 cm	<0.00	YES
All winter 10 cm vs 200 cm	<0.00	YES
All summer 10 cm vs 200 cm	0.02	YES
<i>ca.</i> 1900 10 cm vs 200 cm winter	0.03	YES
2006 10 cm vs 200 cm winter	0.02	YES
2008 10 cm vs 200 cm winter	0.15	NO
2010 10 cm vs 200 cm winter	0.23	NO
2012 10 cm vs 200 cm winter	0.07	NO
2014 10 cm vs 200 cm winter	0.01	YES
2020 10 cm vs 200 cm winter	0.09	NO
<i>ca.</i> 1900 10 cm vs 200 cm summer	0.26	NO
2006 10 cm vs 200 cm summer	0.07	NO
2008 10 cm vs 200 cm summer	0.08	NO
2010 10 cm vs 200 cm summer	0.17	NO
2012 10 cm vs 200 cm summer	0.17	NO
2014 10 cm vs 200 cm summer	0.25	NO
2020 10 cm vs 200 cm summer	0.31	NO

It is seen in Table 7.6 that there is a significant difference between all combined infiltration data at 10 cm and 200 cm, with the 10 cm showing higher mean infiltration rates across all sampled sites, regardless of age or sampling season. Additionally, there is still a significant difference between 10 cm and 200 cm proximity infiltration values when all sample sites are separated into winter and summer; replicating the visual trends displayed in Figure 7.1. However, whilst the overall trends from proximity infiltration data show that 10 cm is significantly different compared with 200 cm, this trend is not seen to be significant on the individual site-by-site basis. The only sites to show a p-value lower than the 0.05 threshold are the *ca.* 1900, 2006 and 2014 sites in winter; no sites show a significant difference between 10

cm and 200 cm infiltration data in the summer. The results seen here highlight the importance of this testing, as based on mean infiltration, the 2006 and 2014 sites showed no obvious trends. Whilst only a few values are below that significant threshold (0.05), the p-values can still be used as an indication of how woodland maturity may be influencing infiltration. As discussed, it would be expected that the more recently planted trees (2020/2014), would show less discrepancy (higher p-values) between infiltration at both proximities, and older (HofE) planted trees (2006/2008) would show more discrepancy (lower p-values). The sample sites sorted (in ascending order) by infiltration p-values are shown in Table 7.7.

*Table 7.7. Sample sites sorted in ascending order of the relationship between infiltration change at 10 cm and 200 cm for winter and summer*

Winter	P-value	Summer	P-value
<b>2014</b>	0.01	<b>2006</b>	0.07
<b>2006</b>	0.02	<b>2008</b>	0.08
<b>ca. 1900</b>	0.03	<b>2010</b>	0.17
<b>2012</b>	0.07	<b>2012</b>	0.17
<b>2020</b>	0.09	<b>2014</b>	0.25
<b>2008</b>	0.15	<b>ca. 1900</b>	0.26
<b>2010</b>	0.23	<b>2020</b>	0.31

The values in Table 7.7 do not follow the expected chronological increase of 10 cm and 200 cm infiltration data, as would be expected based on existing literature, however this trend may be due to varying soil textures, sample days and antecedent atmospheric conditions. This is discussed in more detail in sections 8.1 and 8.2.

### 7.1.1 Summary of Collected Field Data

Objective 1b (section 1.3) is to analyse the collected data to derive any relationships between infiltration and tree proximity and maturity. Sections 7.1 to 7.3 have demonstrated that overall, infiltration at the 10 cm proximity is higher than the 200 cm proximity in both summer and winter. In winter, mean infiltration at the 10 cm proximity is on average 76% higher than the 200 cm proximity, and in summer, infiltration at the 10 cm proximity is on average 25% higher than the 200 cm proximity. This therefore indicates that the presence of the tree is overall influencing infiltration and is an indication that the tree is making the soil more porous, allowing for soil-water storage and faster infiltration (see section 2.5). Regarding seasonality, infiltration is on average 235% higher thought the site in summer compared with winter, with summer infiltration being 180% and 290% higher in summer than winter at the 10 cm and 200 cm proximities respectively. This highlights the seasonal variability of the study site, indicating that soil texture and antecedent moisture conditions may be influencing seasonal infiltration; this discovery also further supports the decision to build and calibrate two hydrological models to best represent the study site (see section 5.4).

Regarding maturity, there is no evidence to suggest a correlation between tree maturity and increase infiltration at this stage in the lifecycle of the sample trees. Whilst Table 7.1 shows that the *ca.* 1900 sample site demonstrated the highest infiltration at the 200 cm proximity in the winter, and the 10 cm proximity in both winter and summer (somewhat supporting the literature suggesting that maturity results in greater infiltration (Birkinshaw *et al.*, 2014; Lacob *et al.*, 2017; Chandler *et al.*, 2018; Xiao *et al.*, 2021)); infiltration is lowest at the 2006 site, which is the oldest (HofE planted) sample area. According to chronology, it would be expected that 2006 site would inherit the next highest infiltration (after *ca.* 1900). This is not the case and may be an indication that external conditions are influencing the collected infiltration data, which is discussed in greater detail throughout sections 8.1 and 8.2.

Additional analysis was undertaken regarding the influence of atmospheric, soil and land surface temperature on the collected infiltration data. These results are presented in appendix C.2. Results show that there is a positive correlation between all measured temperatures and infiltration, however it is important to note that none of the derived correlation coefficients are particularly strong – the highest being 0.58 (for soil temperature at the *ca.* 1900 site). Mean average correlation was higher for all measured temperatures at the 200 cm proximity than the 10 cm proximity, being 0.31 (+0.02), 0.35 (+0.05) and 0.37 (+0.06) for air, soil, and ground respectively. Regarding the results of the regression analysis, ground temperature at the *ca.* 1900 site (at both proximities) is demonstrated to be directly influencing infiltration (10 cm =  $p = 0.04\%$ , 200 cm =  $p = 0.03\%$ ). However, *ca.* 1900 is the exception, and all  $p$ -values for other sample areas are significantly higher than 0.05%, indicating temperature does not directly influence infiltration overall.

## 7.2 Modelled Results

Objective 3a was to use the calibrated the HEC-HMS model to simulate the hydrological response of the HofE study site to varying land cover, tree maturity and storm duration and intensity. The methods of the model creation and simulated storm duration and intensity are described in section 5.6, and this section will present and analyse the results of each. The following sections present the results of both summer and winter hydrological modelling.

### 7.2.1 6-hour storm Duration

Figure 7.2 shows the peak discharge and total flow of the 6-hour summer and winter simulation, Table 7.8 shows the tabulated data with the discrepancy between land cover types shown in comparison to the current HofE site as a percentage.

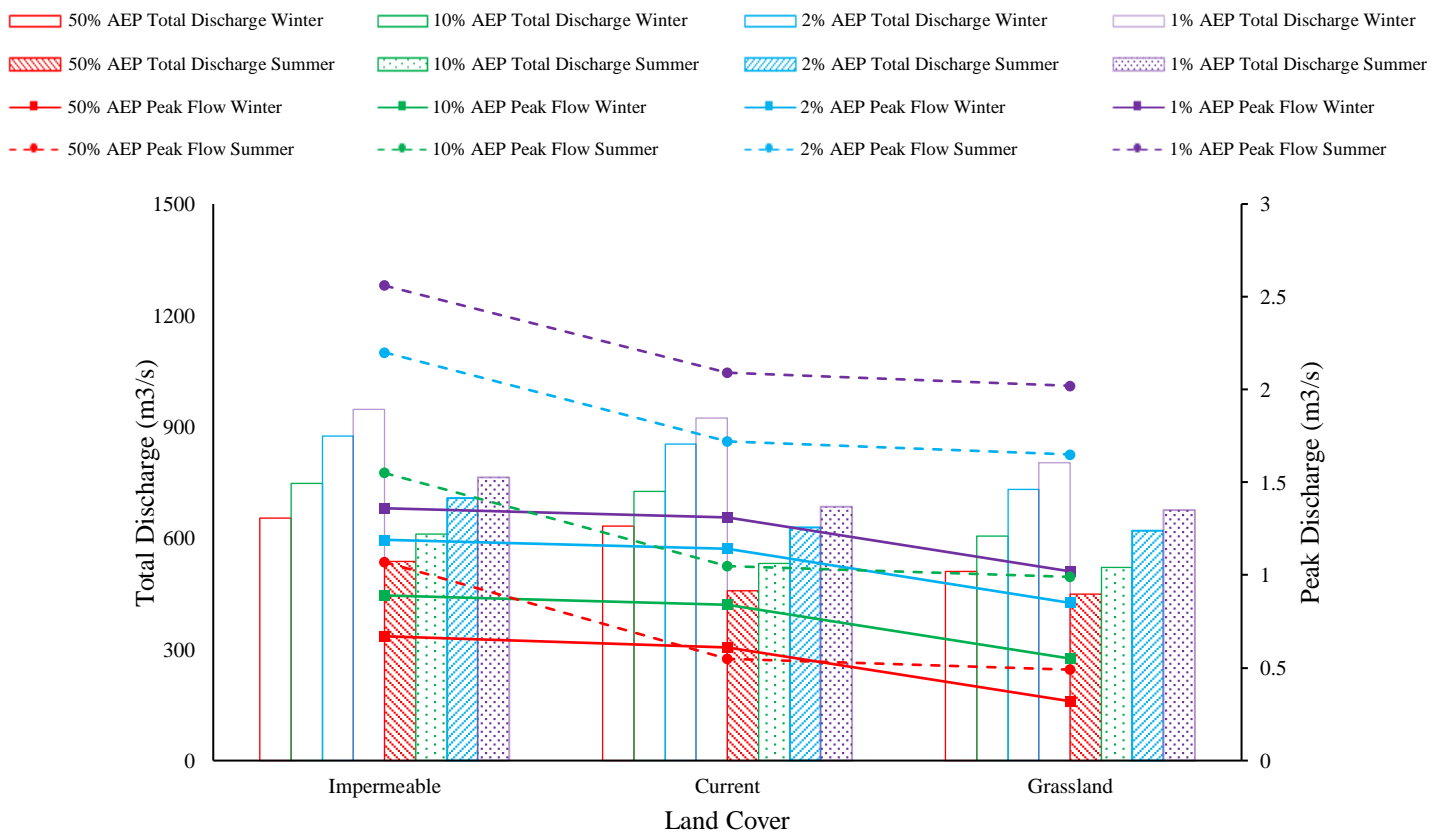


Figure 7.2. Peak flow and total discharge values for winter and summer 6-hour 50%, 10%, 2% and 1% AEP events over each landcover type

Table 7.8. Peak flow, time to peak and total discharge for winter and summer 6-hour 50%, 10%, 2% and 1% AEP events over HofE, impermeable and grassland land cover.

6-hour	AEP (%)	HofE	Imperm.	% +/- Current	Grassland	% +/- Current
<b>Winter</b>						
<b>Time to peak (mins)</b>	50	1200	1185	-1.25	570.00	-52.50
	10	1205	1210	0.41	1245.00	3.32
	2	1210	1200	-0.83	1250.00	3.31
	1	1210	1205	-0.41	1235.00	2.07
<b>Peak volume (m3/s)</b>	50	0.61	0.67	9.84	0.32	-47.54
	10	0.84	0.89	5.95	0.55	-34.52
	2	1.14	1.19	4.39	0.85	-25.44
	1	1.31	1.36	3.82	1.02	-22.14
<b>Total Discharge (m3/s)</b>	50	631.29	653.57	3.53	509.87	-19.23
	10	725.56	747.85	3.07	604.16	-16.73
	2	852.59	874.9	2.62	731.21	-14.24
	1	923.75	946.03	2.41	802.35	-13.14
<b>Summer</b>						
<b>Time to peak (mins)</b>	50	585	540	-7.69	600.00	2.56
	10	565	540	-4.42	575.00	1.77
	2	560	535	-4.46	565.00	0.89
	1	555	535	-3.60	560.00	0.90
<b>Peak volume (m3/s)</b>	50	0.55	1.07	94.55	0.49	-10.91
	10	1.05	1.55	47.62	0.99	-5.71
	2	1.72	2.20	27.91	1.65	-4.07
	1	2.09	2.56	22.49	2.02	-3.35
<b>Total Discharge (m3/s)</b>	50	458.2	537.07	17.21	448.46	-2.13
	10	530.99	609.81	14.84	521.25	-1.83
	2	629.07	707.84	12.52	619.33	-1.55
	1	683.98	762.75	11.52	674.25	-1.42

Figure 7.2 and Table 7.8 show that peak runoffs from the impermeable land cover simulations were higher than HofE and grassland simulations across all modelled storm events in both summer and winter, however the discrepancy in winter was slight. Peak flows from HofE land cover were 9.84%, 5.95%, 4.39% and 3.82% lower than impermeable for a 50, 10, 2 and 1% AEP event respectively. However, in summer this difference was higher, with peak flows being 94.55%, 47.62%, 27.91% and 22.49% greater across 50, 10, 2 and 1% AEP events for impermeable land cover compared to current. In winter, grassland shows a 47.54%, 34.52%,

25.44% and 22.14% reduction in peak flows compared to current land cover; this reduction is less in summer, being 10.91%, 5.71%, 4.07% and 3.35% for 50, 10, 2 and 1% AEP storms.

Throughout all simulations, the summer events show the highest peak flows across all land covers compared to winter, indicating that the site is more responsive, and runoff is quicker during the summer period. This is further reflected by the time to peak of all summer simulations being significantly shorter than the equivalent winter simulations. In winter, the time to peak of HofE and impermeable land cover is fairly consistent, ranging by 10 minutes across all AEP's (50% AEP being the shortest, 2% and 1% AEP being the longest), the impermeable cover is similar, ranging by 25 minutes across all AEP's (50% AEP being the shortest, and 10% being the longest). The grassland land cover, however, shows a range of 680 minutes, with the 50% AEP duration being significantly shorter than other events, peaking at 570 minutes compared with 1245, 1250, 1235 for the 10, 2 and 1% AEP events respectively. This value was re-tested for confirmation and delivered the same results and is likely due to the lower volume of rainfall for this event (

Table 5.8), combined with the higher infiltration of the grassland simulation, resulting in there being little-to-no water in the system. This may also be a result of the Snyder transform method, forcing the water to peak at a specified time regardless of water volume (discussed in section 5.3.3.3). Time to peak of the impermeable land cover ranges by 5 minutes (540 for 50% and 10%, and 535 for 2 and 1% AEPs), current HofE land cover ranges by 30 minutes (585, 565, 560 and 555 for 50, 10, 2 and 1% AEPs respectively), and grassland ranges by 40 minutes (600, 575, 565 and 560 for 50, 10, 2 and 1% AEPs respectively).

Total discharge is lower throughout all summer simulations compared with winter by 26.60%, 18.69% and 14.26% throughout HofE, impermeable and grassland simulations respectively. Thought both winter and summer, total discharge was highest from impermeable land cover compared to HofE land cover by on average 2.91% (winter) and 14.02% (summer); and

grassland was the lowest, being 15.84% (summer) and 1.73% (winter) lower than the HofE site at present.

### 7.2.2 24-hour storm Duration

Figure 7.3 shows the peak discharge and total flow of the 6-hour summer and winter simulations, Table 7.9 shows the tabulated data with the discrepancy between land cover types shown in comparison to the HofE site as a percentage.

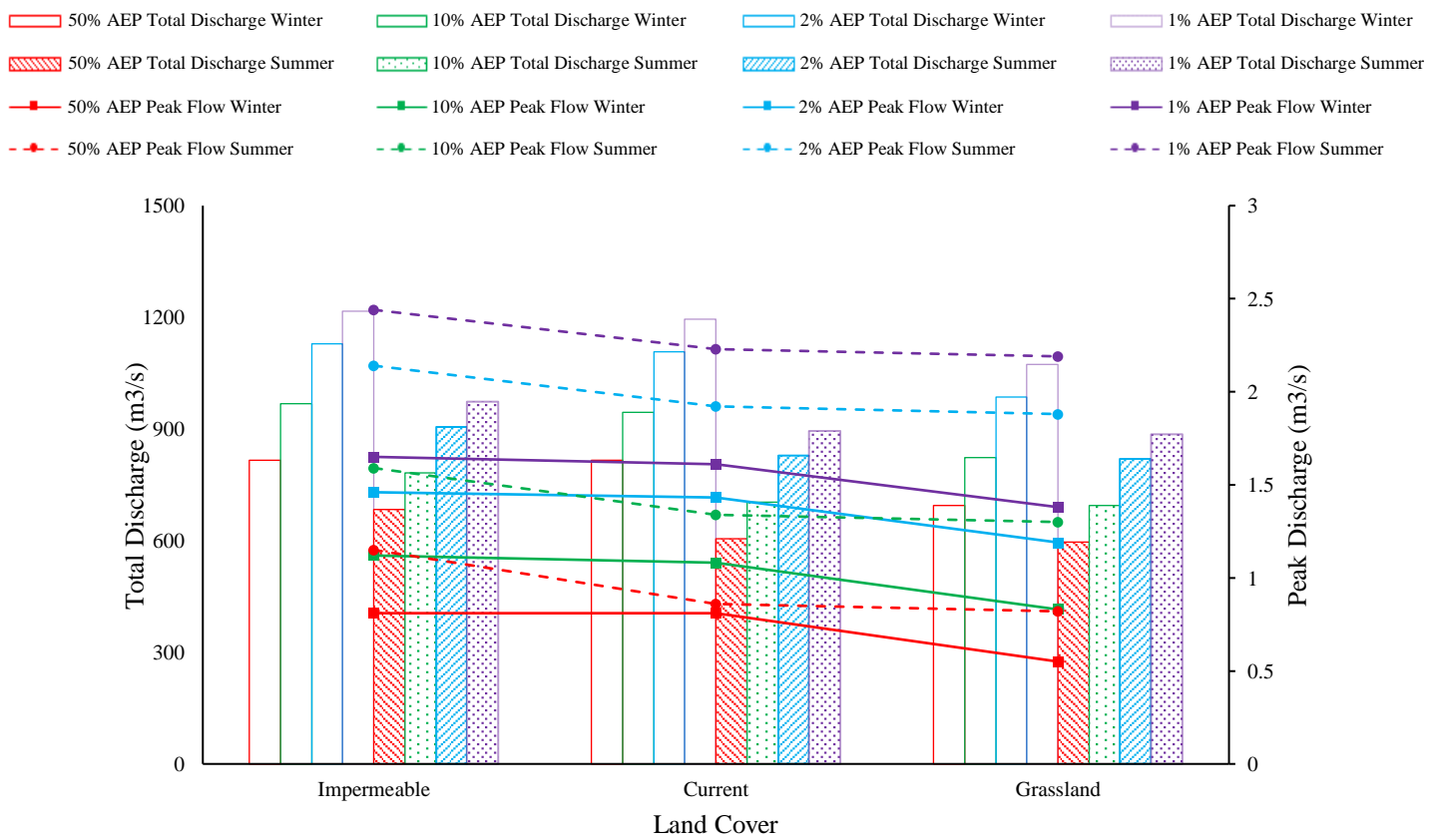


Figure 7.3. Peak flow and total discharge values for winter and summer 24-hour 50%, 10%, 2% and 1% AEP events over each landcover type

Table 7.9. Peak flow, time to peak and total discharge for winter and summer 24-hour 50%, 10%, 2% and 1% AEP events over HofE, impermeable and grassland land cover.

24-hour	AEP (%)	HofE	Imperm.	% +/- Current	Grassland	% +/- Current
<b>Winter</b>						
<b>Time to peak (mins)</b>	50	1785.00	1785.00	0.00	1935.00	8.40
	10	1790.00	1770.00	-1.12	1870.00	4.47
	2	1790.00	1770.00	-1.12	1855.00	3.63
	1	1800.00	1770.00	-1.67	1835.00	1.94
<b>Peak volume (m3/s)</b>	50	0.81	0.81	0.00	0.55	-32.10
	10	1.08	1.12	3.70	0.83	-23.15
	2	1.43	1.46	2.10	1.19	-16.78
	1	1.61	1.65	2.48	1.38	-14.29
<b>Total Discharge (m3/s)</b>	50	816.65	816.65	0.00	695.26	-14.86
	10	944.78	967.07	2.36	823.36	-12.85
	2	1107.22	1129.52	2.01	985.81	-10.97
	1	1194.59	1216.88	1.87	1073.21	-10.16
<b>Summer</b>						
<b>Time to peak (mins)</b>	50	1230.00	1140.00	-7.32	1255.00	2.03
	10	1195.00	1140.00	-4.60	1215.00	1.67
	2	1175.00	1145.00	-2.55	1190.00	1.28
	1	1170.00	1145.00	-2.14	1180.00	0.85
<b>Peak volume (m3/s)</b>	50	0.86	1.15	33.72	0.82	-4.65
	10	1.34	1.59	18.66	1.30	-2.99
	2	1.92	2.14	11.46	1.88	-2.08
	1	2.23	2.44	9.42	2.19	-1.79
<b>Total Discharge (m3/s)</b>	50	605.89	683.85	12.87	596.16	-1.61
	10	704.07	781.94	11.06	694.32	-1.38
	2	828.39	906.20	9.39	818.66	-1.17
	1	895.32	973.09	8.69	885.56	-1.09

Figure 7.3 and Table 7.9 show similar trends to the 6-hour duration simulations. The highest peak runoff of all simulated land cover types over both winter and summer is generated by the impermeable land cover; being on average 2.07% higher than HofE land cover in winter, and 18.31% higher in summer over all AEPs. The impermeable cover, however, produces the same peak runoff as the HofE site for the 50% AEP in winter, and peak flows for the impermeable land cover for 10%, 2% and 1% AEPs in winter are on average higher than that of the HofE

site land cover by only 1.39%. This is possibly due to the saturation of the ground in winter compared with the drying of the ground in summer, discussed further in sections 8.1 and 8.2. A similar trend is seen in summer, where peak flows from the HofE land cover are only 0.24% lower than impermeable values for all AEPs. All 24-hour events show less of a discrepancy between the HofE and impermeable land covers in the winter compared to the 6-hour simulations, showing that as storm duration increases, the flows from impermeable and HofE land cover become more similar in the winter months. Similar to the 6-hour duration, grassland peak flows are lower than impermeable and HofE site land cover throughout the winter, however HofE site and grassland peak flows vary less in the summer. In the winter, grassland peak flow is 32.10%, 23.15%, 16.78% and 14.29% lower than HofE land cover for 50, 10, 2 and 1% AEPs; however, in the summer grassland is only 4.65%, 2.99%, 2.08% and 1.79% lower than the HofE site for all respective AEPs.

Total discharge is less across grassland compared with both impermeable and HofE land cover, by an average of 13% (vs. HofE) and 15% (vs. impermeable) in winter and 1.3% (vs. HofE) and 11.7% (vs. impermeable) in summer. Total discharge from impermeable land cover is unchanged between HofE and impermeable land cover in winter for the 50% AEP event, and higher than HofE land cover by 2.36%, 2.01% and 1.87% for the 10, 2 and 1% AEPs respectively. In summer, total discharge for impermeable cover is higher than winter values, being 12.87%, 11.06%, 9.39% and 8.69% for 50, 10, 2 and 1% AEP events respectively.

Similar to the 6-hour duration, all summer duration events show a quicker time to peak compared with winter values by an average of 48% (52.29% HofE, 45.47% impermeable and 47.37% grassland). The time to peak of the impermeable surface is quickest (1206 minutes in winter, 575 minutes in summer), followed by the HofE land cover (1200 minutes in winter, 654 minutes in summer), and grassland (1075 minutes in winter, 565 minutes in summer) in both summer and winter.

### 7.2.3 96-hour storm Duration

Figure 7.4 shows the peak discharge and total flow of the 6-hour summer and winter simulations, Table 7.10 shows the tabulated data with the discrepancy between land cover types shown in comparison to the HofE site as a percentage.

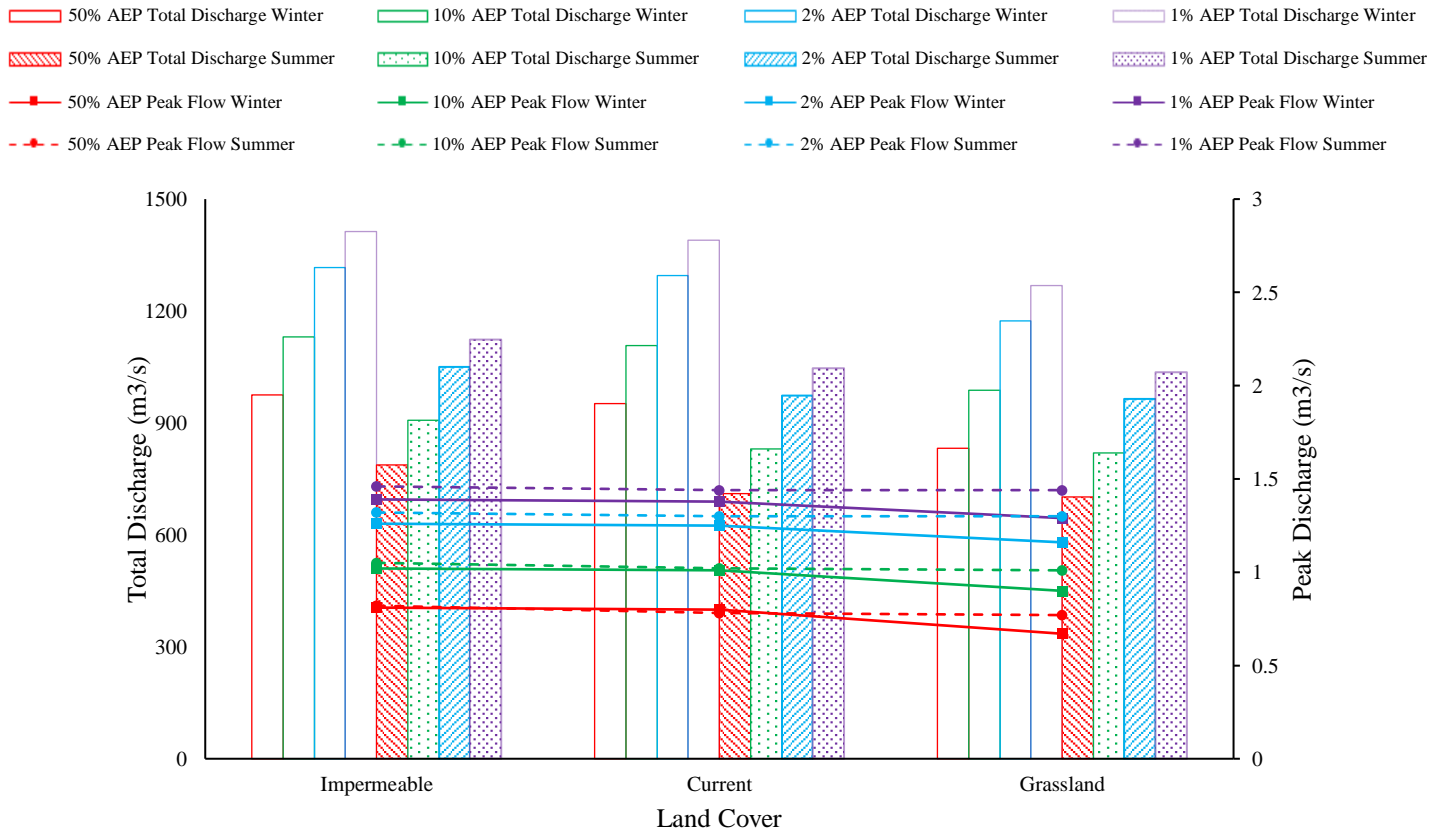


Figure 7.4. Peak flow and total discharge values for winter and summer 96-hour 50%, 10%, 2% and 1% AEP events over each landcover type

Table 7.10. Peak flow, time to peak and total discharge for winter and summer 50%, 10%, 2% and 1% AEP events over HofE, impermeable and grassland land cover.

96-hour	AEP (%)	HofE	Imperm.	% +/- Current	Grassland	% +/- Current
<b>Winter</b>						
<b>Time to peak (mins)</b>	50	4165.00	4125.00	-0.96	4485.00	7.68
	10	4165.00	4135.00	-0.72	4320.00	3.72
	2	4165.00	4145.00	-0.48	4275.00	2.64
	1	4165.00	4135.00	-0.72	4270.00	2.52
<b>Peak volume (m3/s)</b>	50	0.80	0.81	1.25	0.67	-16.25
	10	1.01	1.02	0.99	0.90	-10.89
	2	1.25	1.26	0.80	1.16	-7.20
	1	1.38	1.39	0.72	1.29	-6.52
<b>Total Discharge (m3/s)</b>	50	952.79	975.05	2.34	831.62	-12.72
	10	1108.18	1130.46	2.01	986.86	-10.95
	2	1294.74	1317.04	1.72	1173.40	-9.37
	1	1390.39	1412.67	1.60	1269.03	-8.73
<b>Summer</b>						
<b>Time to peak (mins)</b>	50	3460.00	3375.00	-2.46	3465.00	0.14
	10	3400.00	3390.00	-0.29	3465.00	1.91
	2	3385.00	3390.00	0.15	3435.00	1.48
	1	3385.00	3390.00	0.15	3435.00	1.48
<b>Peak volume (m3/s)</b>	50	0.78	0.82	5.13	0.77	-1.28
	10	1.02	1.05	2.94	1.01	-0.98
	2	1.30	1.32	1.54	1.30	0.00
	1	1.44	1.46	1.39	1.44	0.00
<b>Total Discharge (m3/s)</b>	50	710.85	788.09	10.87	701.12	-1.37
	10	830.10	907.35	9.31	820.36	-1.17
	2	973.27	1050.51	7.94	963.53	-1.00
	1	1046.04	1123.28	7.38	1036.30	-0.93

Figure 7.4 and Table 7.10 is that results from the 96-hour simulations show similar trends to 6 and 24-hour simulations, however the discrepancy in peak flow between land cover simulations are less notable, as are the seasonal variations in peak flows. Impermeable cover exhibits the highest peak flows compared to HofE and grassland landcover, however this difference is marginal. Impermeable peak flows are 1.25%, 0.99%, 0.80% and 0.72% higher in winter, and 5.13%, 2.94%, 1.54% and 1.39% higher in summer than HofE landcover for 50, 10, 2 and 1% AEP events respectively.

There is more variation between HofE land cover and grassland in the winter than the summer; peak flows from the grassland cover are 16.25%, 10.89%, 7.20% and 6.52% higher than the HofE site in the winter for 50, 10, 2 and 1% AEP events respectively; however only show a difference of 1.28%, 0.98% for 50 and 10% AEP events, and 0 change for the 2% and 1% AEPs in the summer. Peak flows show less variation between summer and winter for all land cover types, compared to the trends seen in the 6- and 24-hour duration simulations.

All simulations show a higher total discharge in winter compared with summer; discharge from HofE land cover is 25% lower, impermeable surfaces are 20% lower and grassland is 17% lower in summer compared with winter. Total discharge from the impermeable surface is the highest throughout both winter and summer, being on average 1.92% higher than HofE land cover in the winter, and 8.87% higher than HofE land cover in the summer. Grassland shows the lowest total discharge compared to the HofE site, being 10.44% lower in the winter, and 1.12% lower in the summer.

Time to peak of the simulated 96-hour events show similar findings to that of the 6- and 24-hour duration events. All summer duration events show a quicker time to peak compared with winter values by an average of 78% (78.63% HofE, 76.61% impermeable and 79.70% grassland). The time to peak of the impermeable surface is quickest (4165 minutes in winter, 890 minutes in summer), followed by the HofE land cover (4135 minutes in winter, 967 minutes in summer), and grassland (4337 minutes in winter, 880 minutes in summer) in both summer and winter.

#### 7.2.4 Summary of Model Results

The modelled results presented throughout this section show all winter simulations to produce a higher total discharge compared with summer models, however summer simulations show a higher peak flow. The higher winter total discharge can be attributed to interception not being accounted for (as it was in summer simulations) due to the tree across the HofE site being

deciduous, therefore shedding leaves in the winter. Regarding the higher summer peak flows, this is due to the method of model calibration (see section 5.4), and the used empirical data indicating that the site is ‘flashier’ in the summer.

Peak flows are greatest throughout the 24-hour duration storms, compared with both 6- hour and 96-hour in both winter and summer; however, peak flows become less variable across all land cover types throughout the 96-hour duration storms. Of all duration and land cover simulations, the impermeable land cover showed the highest peak volume and total discharge, followed by the HofE site, and finally the grassland land cover. Impermeable cover generating the highest peak flows and total discharge is unsurprising, as it is known that the increase in impermeable surface cover is driving the push towards NFM (Burgess-Gamble *et al.*, 2018; Ferguson and Fenner, 2020a; Ellis *et al.*, 2021), and is a key motivator for the aims and objectives created for this study.

Overall, it is demonstrated that, at present, woodland planting cannot reduce peak flow or total discharge in either winter or summer below the values of grassland. However, these results must be interpreted considering the likely influences of soil texture and antecedent conditions during infiltration data collection. This is discussed throughout section 8.2

### **7.3 Seasonal Model Projections**

As defined by objective 3b, the collected infiltration data (section 5.2.2) was used in conjunction with published values to project the likely changes to infiltration in the future (section 5.7). Published values were used to derive the likely future changes to rainfall and baseflow in light of climate change, and this information, combined with the projected infiltration data was modelled using the HEC-HMS models (section 5.3). The peak flow results of the simulated runoff projections are shown throughout this section; the HofE peak flow is shown as ‘2020 peak discharge’ as are the intensities for 2040, 2070 and 2120 respectively. 2120 is included twice as the ‘high rainfall’ series simulates the maximum rainfall increase expected in 2120 (40% increase from present, represented as 2120 H). Peak and total flows are presented as a range of possible outputs for all land cover types (woodland, grassland, impermeable) based on the baseflow scenarios defined in section 5.7.3.

#### **7.3.1 Winter Modelled Projections**

The following sections present the results of the winter 6-, 24- and 96-hour duration modelled projections. These results were produced using the methods discussed throughout section 5.7. The tabulated result ranges are presented throughout appendix C.3.

##### **7.3.1.1 Winter 6-Hour Storm Duration Projections**

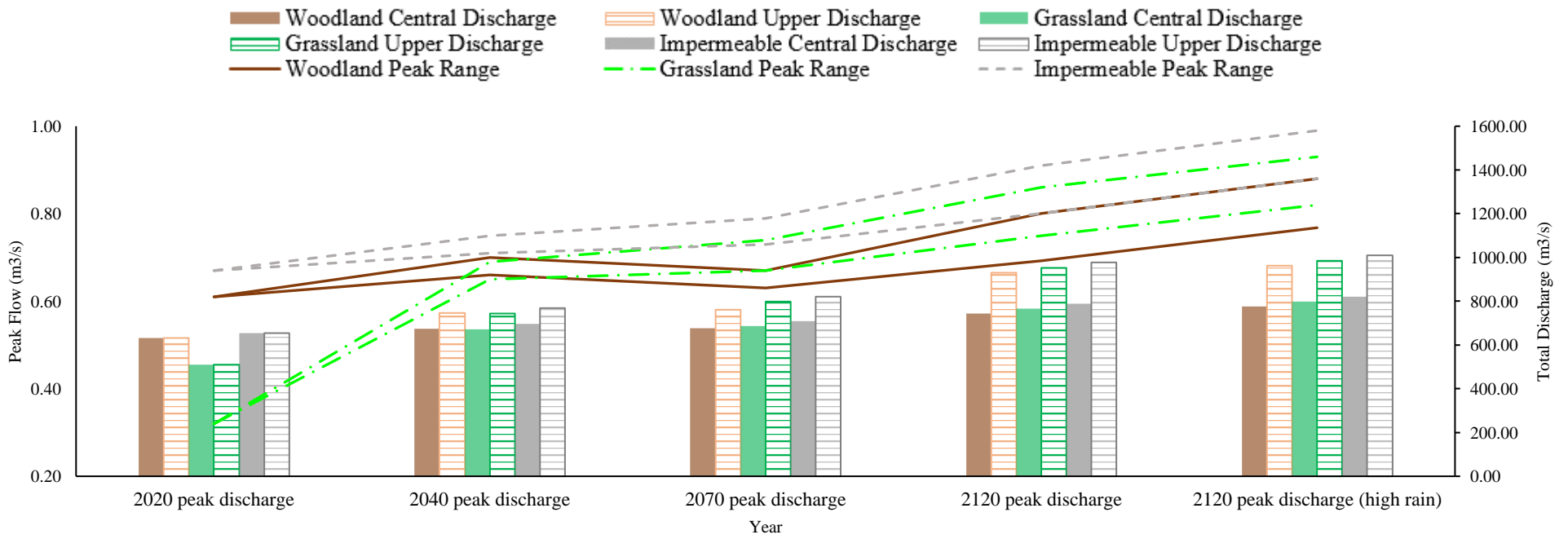


Figure 7.5. 50% AEP 6-hour peak flow and total discharge ranges winter. Please note the variable y-axis values.

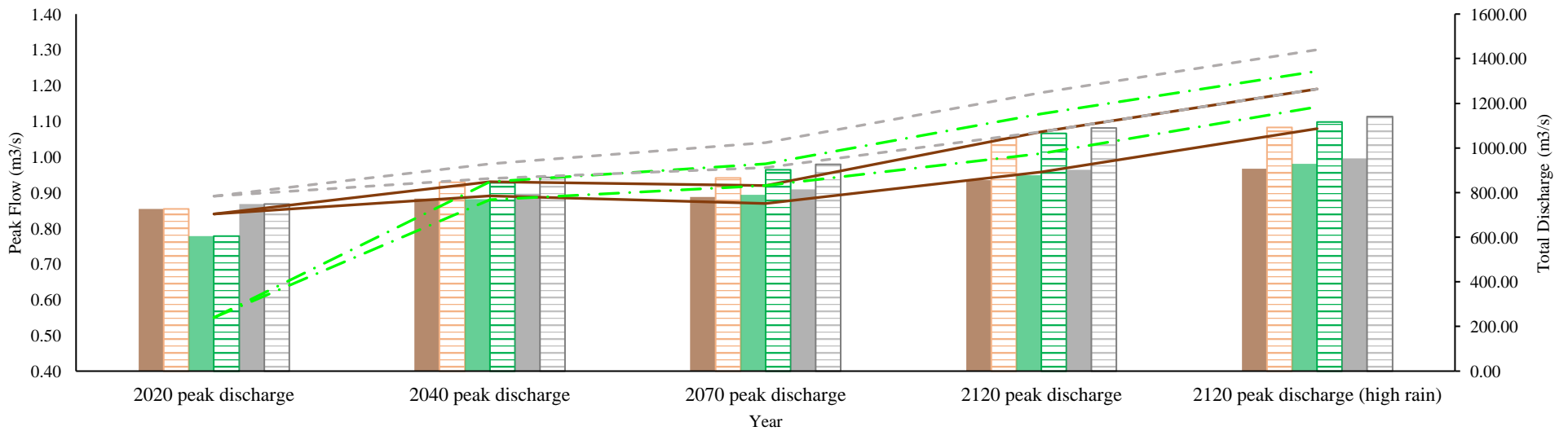


Figure 7.6. 10% AEP 6-hour peak flow and total discharge ranges winter. Please note the variable y-axis values.

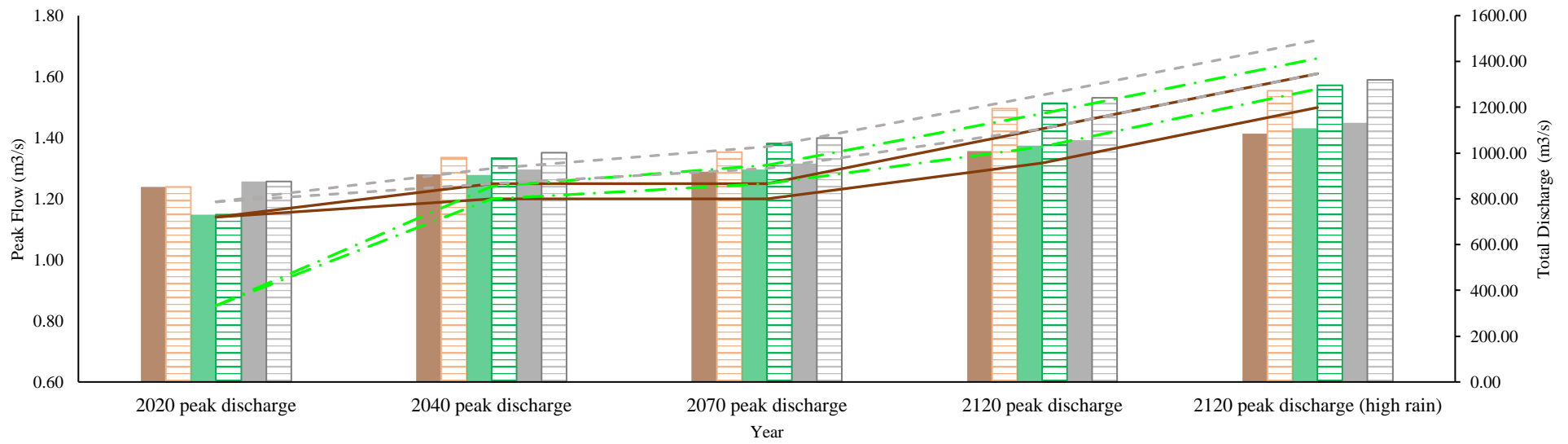


Figure 7.7. 2% AEP 6-hour peak flow and total discharge ranges winter. Please note the variable y-axis values.

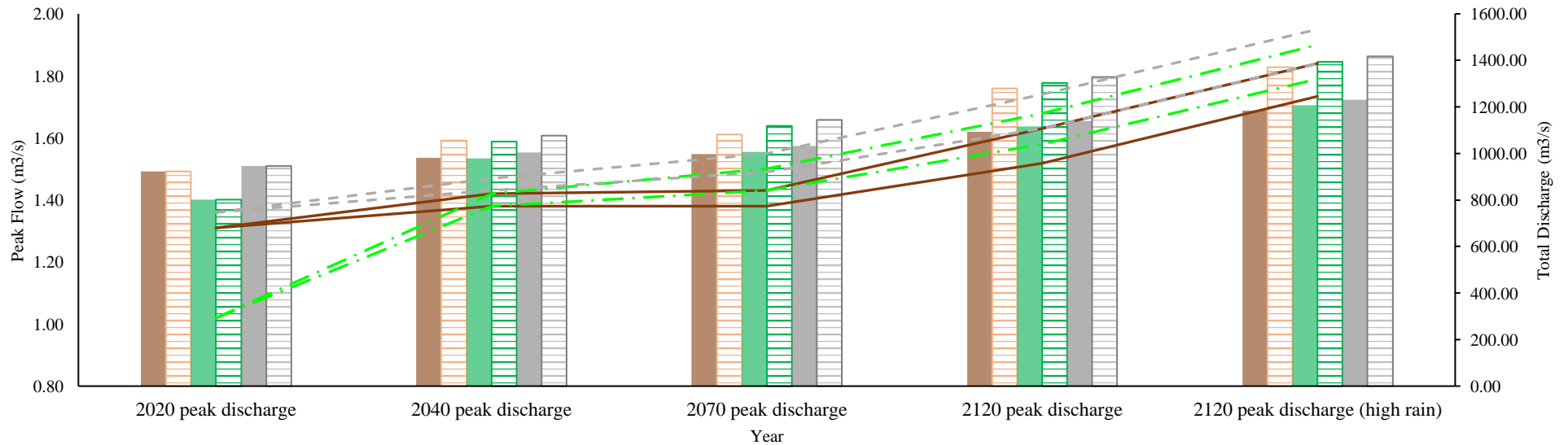


Figure 7.8. 1% AEP 6-hour peak flow and total discharge ranges winter. Please note the variable y-axis values.

Figure 7.5 to Figure 7.8 show that across all projection years for 6-hour duration storms, no land cover type will reduce peak flow below 2020 values, however, it is noticeable that certain land cover types are more able to mitigate peak flow compared to others.

The mean peak flow ranges of woodland are consistently the lowest (1.05 m<sup>3</sup>/s for 2040, 1.04 m<sup>3</sup>/s for 2070, 1.18 m<sup>3</sup>/s for 2120 and 1.32 m<sup>3</sup>/s for 2120 H), followed by grassland (1.05 m<sup>3</sup>/s for 2040, 1.10 m<sup>3</sup>/s for 2070, 1.23 m<sup>3</sup>/s for 2120 and 1.38 m<sup>3</sup>/s for 2120 H) and impermeable (1.10 m<sup>3</sup>/s for 2040, 1.15 m<sup>3</sup>/s for 2070, 1.29 m<sup>3</sup>/s for 2120 and 1.43 m<sup>3</sup>/s for 2120 H) land cover respectively. Woodland shows the lowest percentage increase in peak flows compared with 2020 values, being 8.22% in 2040, 7.19% in 2070, 20.81% in 2120 and 36.04% in 2120 H. Grassland showed the second-lowest increase, being 7.65%, 12.95%, 26.53% and 41.74% higher than 2020 values for 2040, 2070, 2120 and 2120 H respectively. The highest increase was the impermeable cover, being 13.28%, 18.62%, 32.19% and 47.39% higher than 2020 values for 2040, 2070, 2120 and 2120 H respectively.

The percent-change of woodland peak flow compared to 2020 values is slightly lower in 2070 (7.19%) compared with 2040 (8.22%). This change is of note as it coincides with when the HofE planted woodland is projected to reach its maximum infiltration potential due to tree maturity (see section 5.7.2). This indicates that the projected changes to woodland infiltration will reduce woodland peak flows when HofE trees mature, however this impact is limited, and is outweighed by the projected increases to precipitation due to climate change (see section 5.7.1).

Total discharge shows a similar increasing trend to peak flows. Mean woodland total discharge increases from current values by 11.16%, 13.06%, 29.97% and 37.97% for 2040, 2070, 2120 and 2120 H respectively. Impermeable land cover shows a percentage increase from 2020 of 10.75%, 15.81%, 32.25% and 40.04% in 2040, 2070, 2120 and 2120 H respectively. Mean grassland peak flow is 31.17% higher in 2040, 37.33% higher in 2070, 57.35% higher in 2120 and 66.82% higher in 2120 H. Grassland shows the largest percentage increase to total

discharge compared to 2020, however, this is due to the initial values being lower for grassland in 2020. The above peak flow and total discharge values, represented in Figure 7.5 to Figure 7.8 and discussed throughout this section, are tabulated in appendix C.3.1. Additionally, the percent increase/decrease of peak flow and total discharge compared with 2020 values for 50%, 10%, 2% and 1% AEPs over 6-, 24- and 96-hour storms are presented in appendix C.3.2.

7.3.1.2 Winter 24-Hour Storm Duration Projections

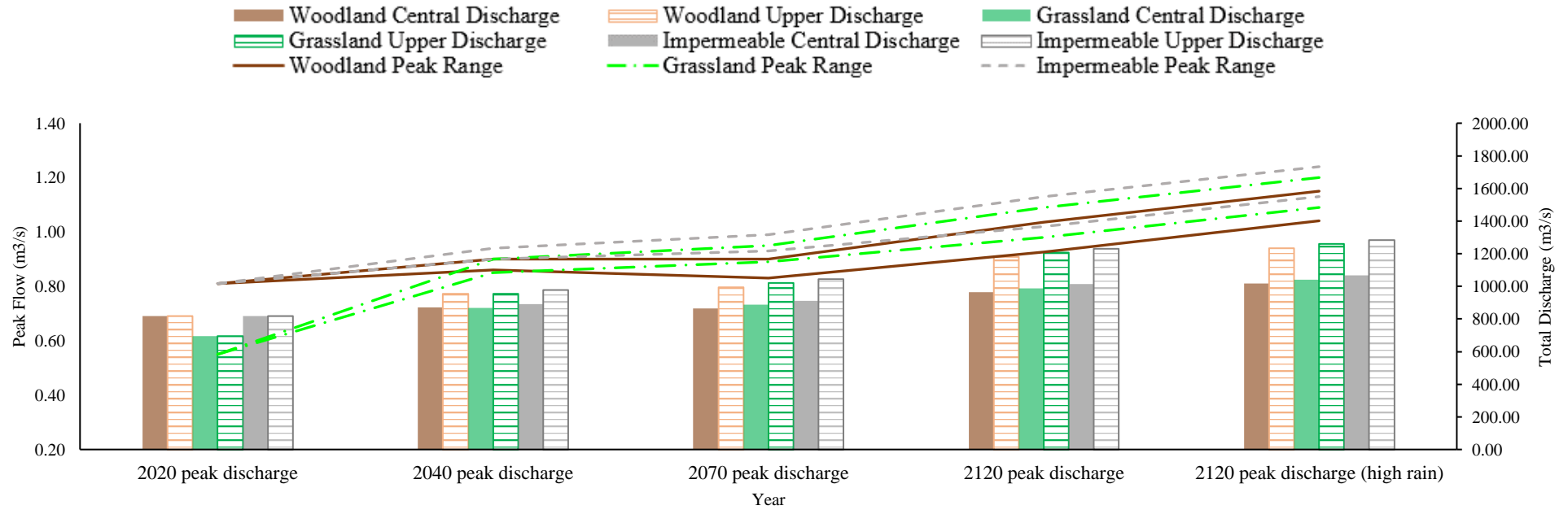


Figure 7.9. 50% AEP 24-hour peak flow and total discharge ranges winter. Please note the variable y-axis values.

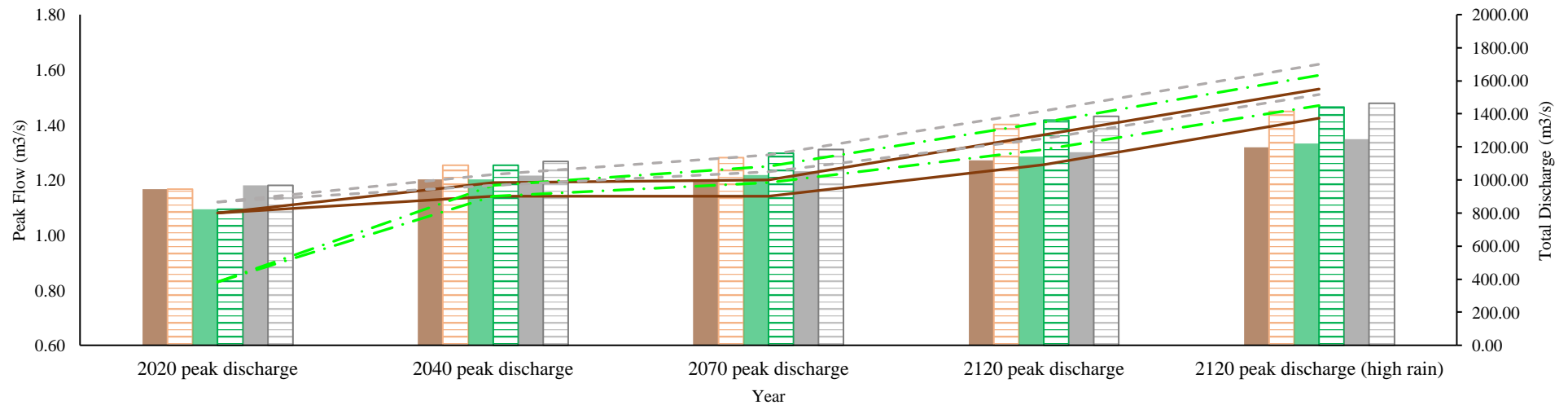


Figure 7.10. 10% AEP 24-hour peak flow and total discharge ranges winter. Please note the variable y-axis values.

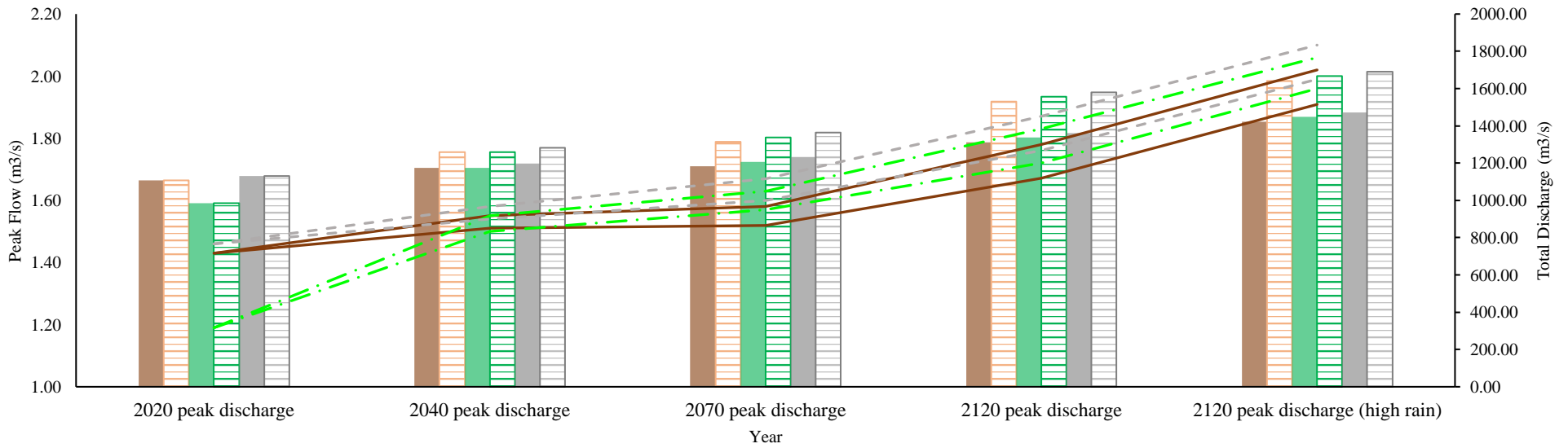


Figure 7.11. 2% AEP 24-hour peak flow and total discharge ranges winter. Please note the variable y-axis values.

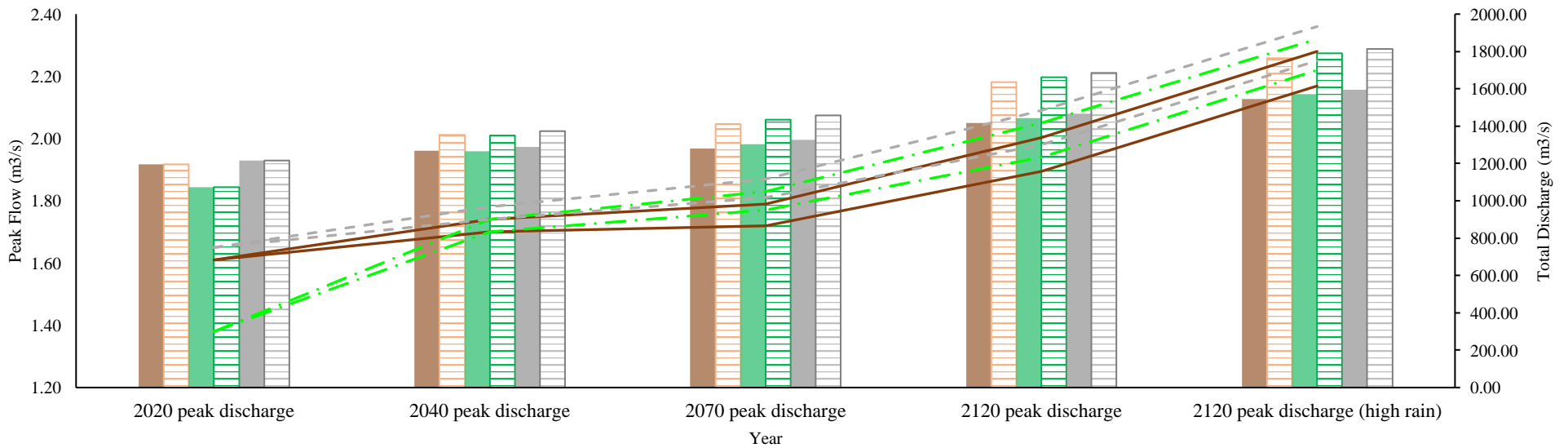


Figure 7.12. 1% AEP 24-hour peak flow and total discharge ranges winter. Please note the variable y-axis values.

Figure 7.9 to Figure 7.12 show the 24-hour duration winter storms display a similar trend to the 6-hour durations. The mean peak flow ranges of woodland are consistently the lowest (1.32 m<sup>3</sup>/s for 2040, 1.33 m<sup>3</sup>/s for 2070, 1.49 m<sup>3</sup>/s for 2120 and 1.69 m<sup>3</sup>/s for 2120 H), followed by grassland (1.32 m<sup>3</sup>/s for 2040, 1.38 m<sup>3</sup>/s for 2070, 1.54 m<sup>3</sup>/s for 2120 and 1.74 m<sup>3</sup>/s for 2120 H) and impermeable (1.36 m<sup>3</sup>/s for 2040, 1.42 m<sup>3</sup>/s for 2070, 1.58 m<sup>3</sup>/s for 2120 and 1.78 m<sup>3</sup>/s for 2120 H) land cover respectively. Woodland shows the lowest percentage increase in peak flows compared with 2020 values, being 7.35% in 2040, 8.34% in 2070, 21.09% in 2120 and 37.18% in 2120 H. Impermeable cover showed the second-lowest increase, being 7.96%, 13.03%, 25.46% and 41.08% for 2040, 2070, 2120 and 2120 H respectively. The highest increase was the grassland cover, being 33.65%, 40.14%, 56.01% and 75.99% higher than 2020 values for 2040, 2070, 2120 and 2120 H respectively, however as with the results in section 0, this is primarily due to the lower values exhibited by grassland in 2020 (see section 0). Differing from the 6-hour projections, there are no obvious reductions in peak flow in 2070, which is when the HofE woodland is projected to reach maturity and maximum infiltration potential. This is likely due to the increased volume of rainfall throughout the 24-hour storms (see

Table 5.8), further emphasised by the FEH precipitation increases discussed in section 5.7.1.

Total discharge shows a similar increasing trend to peak flows. Mean woodland total discharge increases from current values by 10.43%, 12.97%, 29.14% and 38.28 for 2040, 2070, 2120 and 2120 H respectively. Grassland shows the largest percentage increase to total discharge compared to 2020, however, this is due to the initial values being lower for grassland in 2020. Mean grassland peak flow is 25.24% higher in 2040, 31.11% higher in 2070, 49.48% higher in 2120 and 59.86% higher in 2120 H; impermeable land cover shows a percentage increase from 2020 of 10.80%, 15.89%, 31.81% and 40.80% in 2040, 2070, 2120 and 2120 H respectively. The above peak flow and total discharge values, represented in Figure 7.9 to Figure 7.12 and discussed throughout this section, are tabulated in appendix C.3.1. Additionally, the percent

increase/decrease of peak flow and total discharge compared with 2020 values for 50%, 10%, 2% and 1% AEPs over 6-, 24- and 96-hour storms are presented in appendix C.3.2.

7.3.1.3 *Winter 96-Hour Storm Duration Projections*

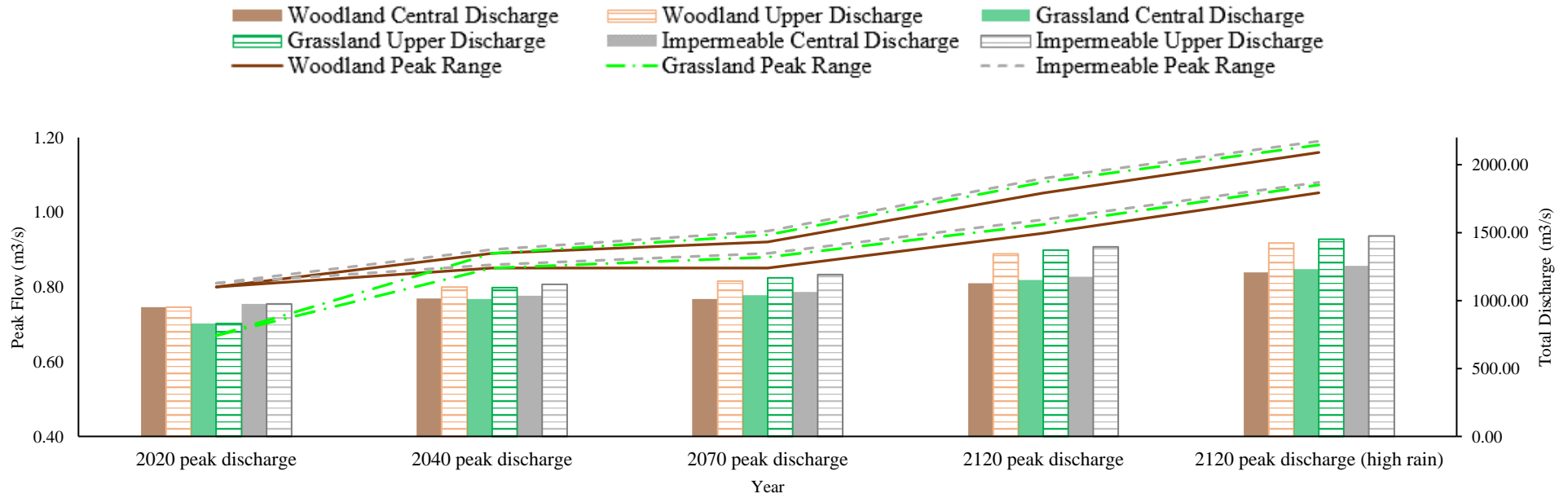


Figure 7.13. 50% AEP 96-hour peak flow and total discharge ranges winter. Please note the variable y-axis values.

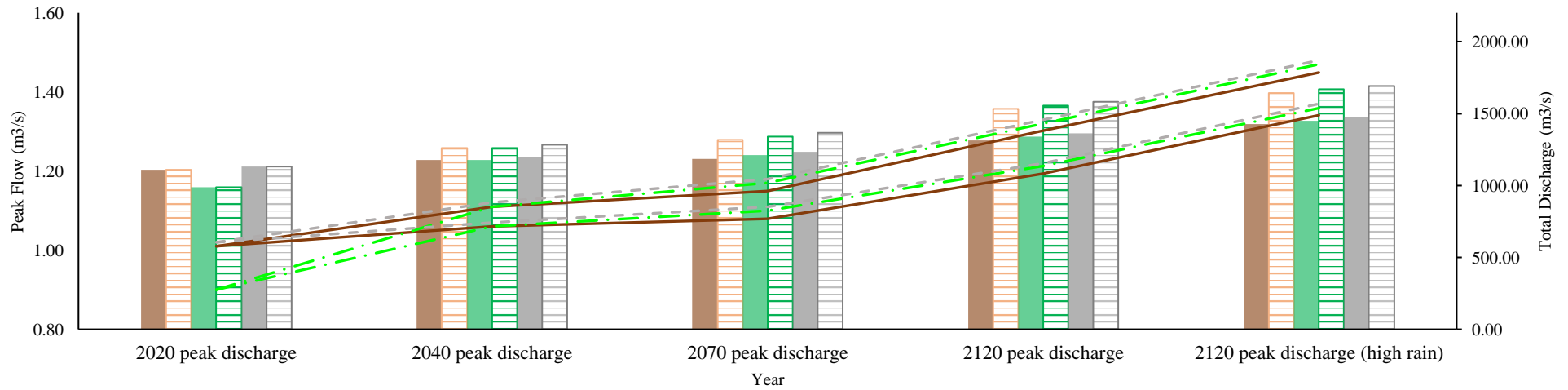


Figure 7.14. 10% AEP 96-hour peak flow and total discharge ranges winter. Please note the variable y-axis values.

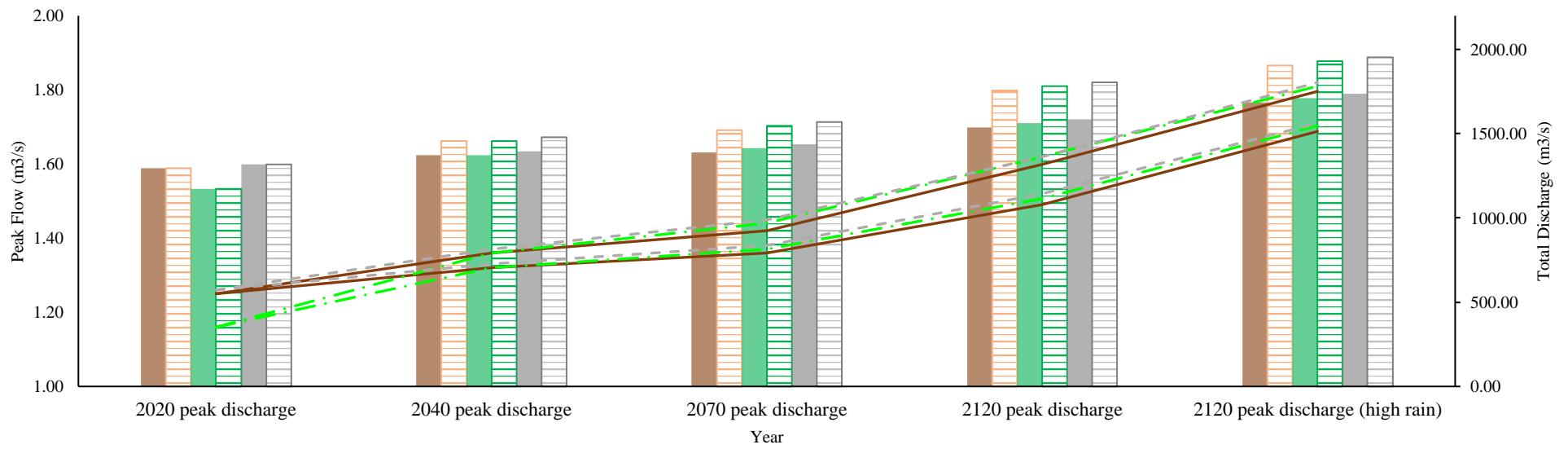


Figure 7.15. 2% AEP 96-hour peak flow and total discharge ranges winter. Please note the variable y-axis values.

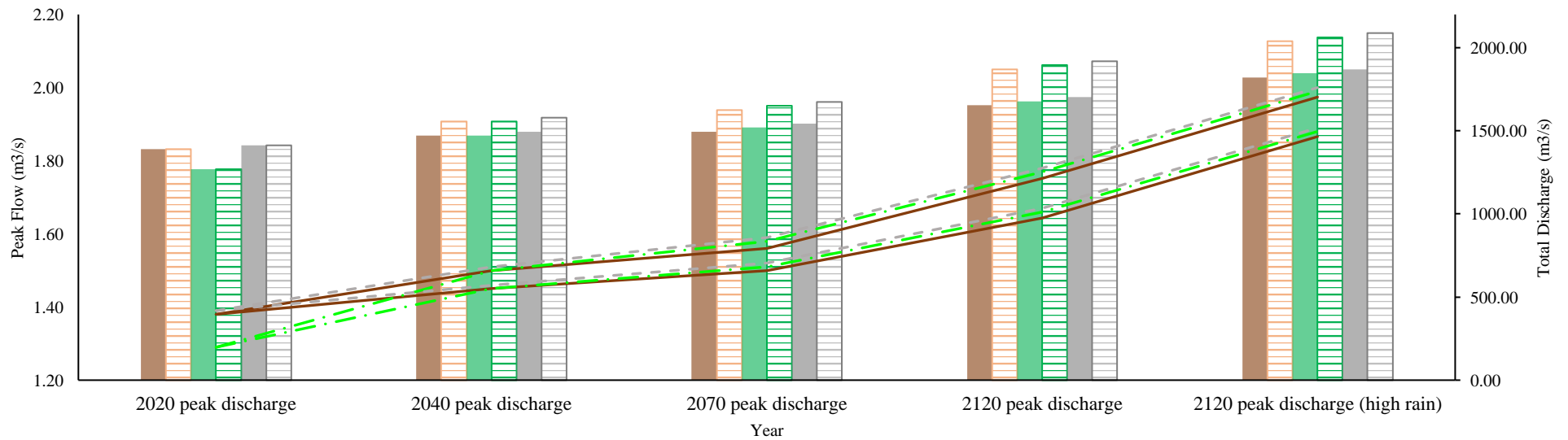


Figure 7.16. 1% AEP 96-hour peak flow and total discharge ranges winter. Please note the variable y-axis values.

Figure 7.13 to Figure 7.16 show the results of the 96-hour winter climate projections. Differing from the 6- and 24-hour simulation results, there is less noticeable discrepancy between the peak and total flow projection ranges of differing land covers.

Mean woodland peak flow is 1.19 m<sup>3</sup>/s, 1.23 m<sup>3</sup>/s, 1.37 m<sup>3</sup>/s and 1.54 m<sup>3</sup>/s for 2040, 2070, 2120 and 2120 H, which is an increase from 2020 values of 7.48%, 10.74%, 23.63% and 38.81% for the projected years respectively. Grassland is the second lowest average peak, being 1.19 m<sup>3</sup>/s (in 2040), 1.25 m<sup>3</sup>/s (in 2070), 1.39 m<sup>3</sup>/s (in 2120) and 1.56 m<sup>3</sup>/s (in 2120 H), however the percentage increase is greater for grassland due to the lower 2020 value: 18.83% in 2040, 24.46% in 2070, 38.59% in 2120 and 55.23% in 2120 H. Impermeable cover shows the highest average peak flows, being 1.20 m<sup>3</sup>/s, 1.26 m<sup>3</sup>/s, 1.40 m<sup>3</sup>/s and 1.57 m<sup>3</sup>/s for 2040, 2070, 2120 and 2120 H, which is an increase of 7.44%, 12.49%, 25.11% and 40.04% compared with 2020 values for each projection year.

Woodland shows the lowest total discharge, being 1301.34 m<sup>3</sup>/s (for 2040), 1335.50 m<sup>3</sup>/s (for 2070), 1516.66 m<sup>3</sup>/s (for 2120) and 1643.76 m<sup>3</sup>/s (for 2120 H); this is a percentage change from 2020 values of 9.68%, 12.56%, 27.82% and 38.54% for respective projection years. Grassland shows the next-highest total discharge, being 1299.69 m<sup>3</sup>/s, 1360.67 m<sup>3</sup>/s, 1541.83 m<sup>3</sup>/s and 1668.91 m<sup>3</sup>/s for 2040, 2070, 2120 and 2120 H, which is an increase from 2020 values of 22.01%, 27.73%, 44.74% and 56.67% for the respective projected years. Impermeable simulations produce the highest total discharge, being 1323.62 m<sup>3</sup>/s (in 2040), 1384.59 m<sup>3</sup>/s (in 2070), 1565.76 m<sup>3</sup>/s (in 2120) and 1692.87 m<sup>3</sup>/s (in 2120 H), which is an increase of 9.50%, 14.54%, 29.53% and 40.04%. The above peak flow and total discharge values, represented in Figure 7.13 to Figure 7.16 and discussed throughout this section, are tabulated in appendix C.3.1. Additionally, the percent increase/decrease of peak flow and total discharge compared with 2020 values for 50%, 10%, 2% and 1% AEPs over 6-, 24- and 96-hour storms are presented in appendix C.3.2.

### *7.3.2 Summer Modelled Projections*

The following sections present the results of the summer 6-, 24- and 96-hour duration modelled projections. These results were produced using the methods discussed throughout section 5.7.

The tabulated result ranges are presented throughout appendix C.3.

7.3.2.1 Summer 6-Hour Storm Duration Projections

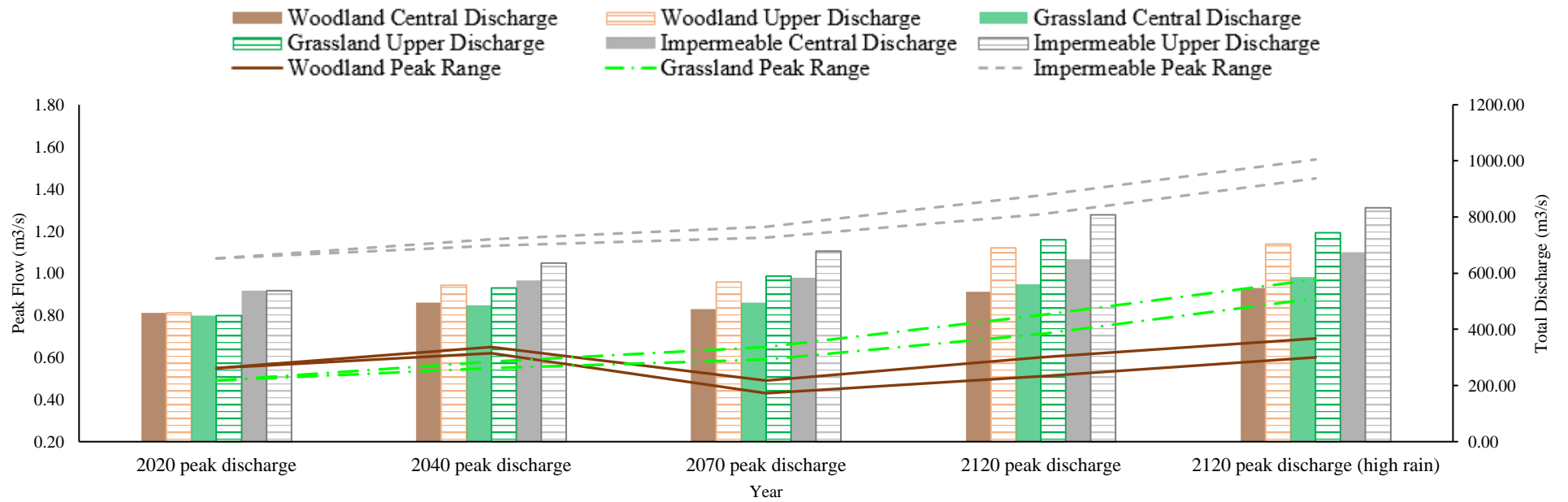


Figure 7.17. 50% AEP 6-hour peak flow and total discharge ranges summer. Please note the variable y-axis values.

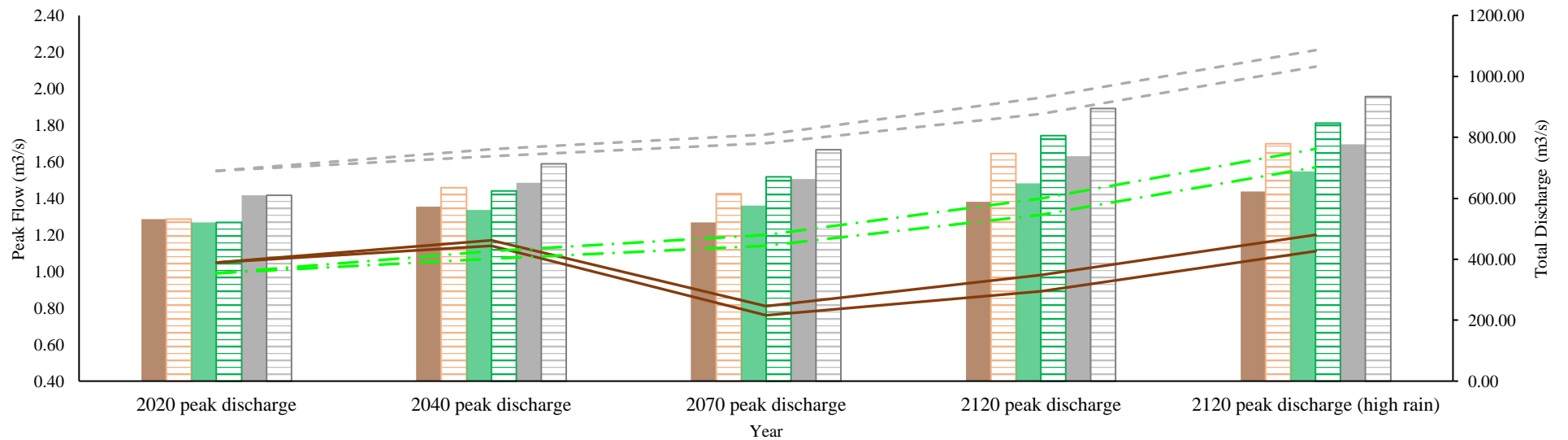


Figure 7.18. 10% AEP 6-hour peak flow and total discharge ranges summer. Please note the variable y-axis values.

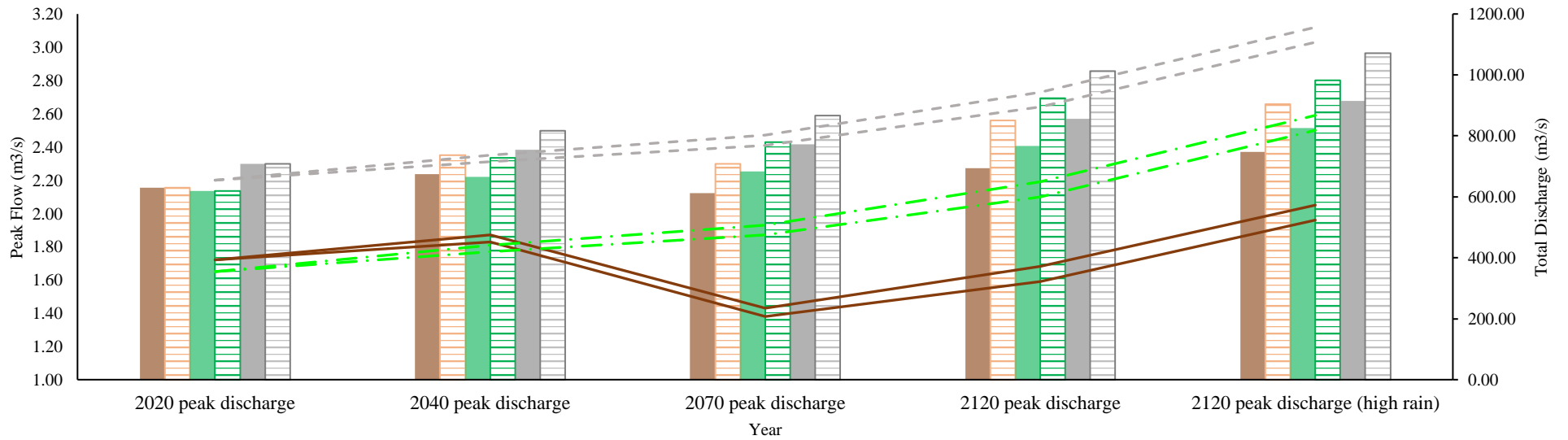


Figure 7.19. 2% AEP 6-hour peak flow and total discharge ranges summer. Please note the variable y-axis values.

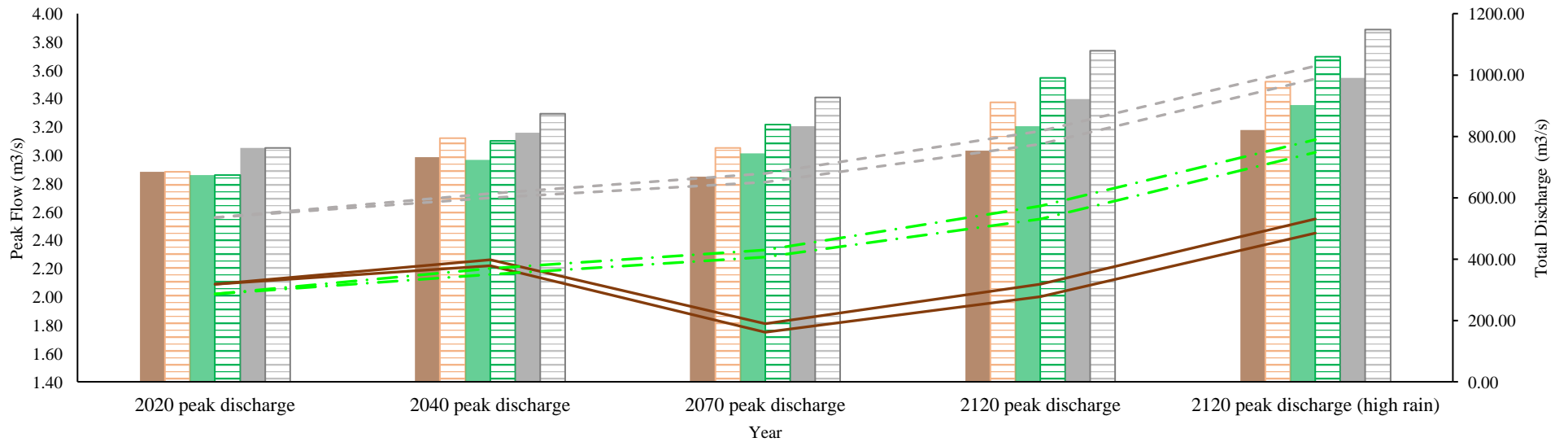


Figure 7.20. 1% AEP 6-hour peak flow and total discharge ranges summer. Please note the variable y-axis values.

Figure 7.17 to Figure 7.20 show that across all AEP events, impermeable land cover produces the highest peak flow, whereas woodland and grassland vary. Impermeable cover shows a mean peak flow of 1.96 m<sup>3</sup>/s in 2040, 2.05 m<sup>3</sup>/s in 2070, 2.26 m<sup>3</sup>/s in 2120 and 2.58 m<sup>3</sup>/s in 2120 H, increasing from 2020 values by 6.29%, 1.25%, 22.61% and 40.01%. Grassland shows the lowest peak flow range until 2040, at which point it is surpassed by woodland, showing a significant reduction in peak and total discharge. Grassland peak flow is 1.41 m<sup>3</sup>/s, 1.50 m<sup>3</sup>/s, 1.71 m<sup>3</sup>/s and 2.04 m<sup>3</sup>/s for 2040, 2070, 2120 and 2120 H respectively: differing from 2020 values by 9.17%, 16.43%, 32.98% and 58.35% for the respective projection years. As seen in Figure 7.17 to Figure 7.20, woodland peak flow reduces notably in 2070 – peak flows for woodland are 1.47 m<sup>3</sup>/s in 2040, 1.11 m<sup>3</sup>/s in 2070, 1.29 m<sup>3</sup>/s in 2120 and 1.58 m<sup>3</sup>/s in 2120 H, which varies from 2020 values by 8.69%, -18.13%, -4.36% and 16.58% across respective projection years.

The most noticeable difference between winter and summer projections, is the drop in woodland peak flow and total discharge values in the summer 2070 projections. The sudden reduction in projected woodland peak flow can be explained by referring to section 5.7.2, regarding the years in which planted trees across the HofE site will reach maturity. It is shown that trees across the HofE site will have matured and reached their ultimate heights around 2050 (Hynynen *et al.*, 2010; MacKenzie, 2010; Lee *et al.*, 2015; Zeltinš *et al.*, 2018; Savill, 2019), at which point, root spread will be a maximum, as will infiltration. The next modelled projection interval is 2070, so these results are inclusive of the final infiltration projections of the site, whereas the 2040 projections are not. This explains why there is a significant fall in infiltration between the two projection intervals (Figure 7.17 to Figure 7.20), and 2070 shows a lower runoff and peak flow for woodland compared with grassland and impermeable land cover. This reduction is not as obvious throughout the winter projections; the shorter duration winter simulations do show a reduction in woodland peak flow and total discharge in 2070,

however it is not as obvious as summer projections. This is discussed more throughout section 8.2.2.

Regarding total discharge, summer impermeable cover is the highest being 649.90 m<sup>3</sup>/s, 615.99 m<sup>3</sup>/s, 720.94 m<sup>3</sup>/s and 762.81 m<sup>3</sup>/s for 2040, 2070, 2120 and 2120 H respectively, which is 12.92%, 7.02%, 25.26% and 32.53% higher than 2020 values. Grassland flows with mean discharges of 640.16 m<sup>3</sup>/s for 2040, 672.13 m<sup>3</sup>/s for 2070, 781.09 m<sup>3</sup>/s for 2120 and 829.49 m<sup>3</sup>/s for 2120 H: being 11.22%, 16.78%, 35.71% and 44.12% higher than 2020 values for the projected years. Woodland showed the lowest total discharge, being 728.71 m<sup>3</sup>/s, 760.67 m<sup>3</sup>/s, 869.62 m<sup>3</sup>/s and 918.00 m<sup>3</sup>/s for 2040, 2070, 2120 and 2120 H, which is an increase from 2020 values of 26.61%, 32.16%, 51.09% and 59.50% for respective projected years. Total discharge in summer is lower compared with winter and can be explained by the lower FEH rainfall values due to the increased likelihood of interception (see section 5.7.1). As discussed in section 5.6.2, interception loss was accounted for throughout the summer months to account for the deciduous nature of the sample site woodland (Lunka and Patil, 2016; Ngai *et al.*, 2017; Rahman *et al.*, 2019). The above peak flow and total discharge values, represented in Figure 7.17 to Figure 7.20 and discussed throughout this section, are tabulated in appendix C.3.1. Additionally, the percent increase/decrease of peak flow and total discharge compared with 2020 values for 50%, 10%, 2% and 1% AEPs over 6-, 24- and 96-hour storms are presented in appendix C.3.2.

7.3.2.2 Summer 24-Hour Storm Duration Projections

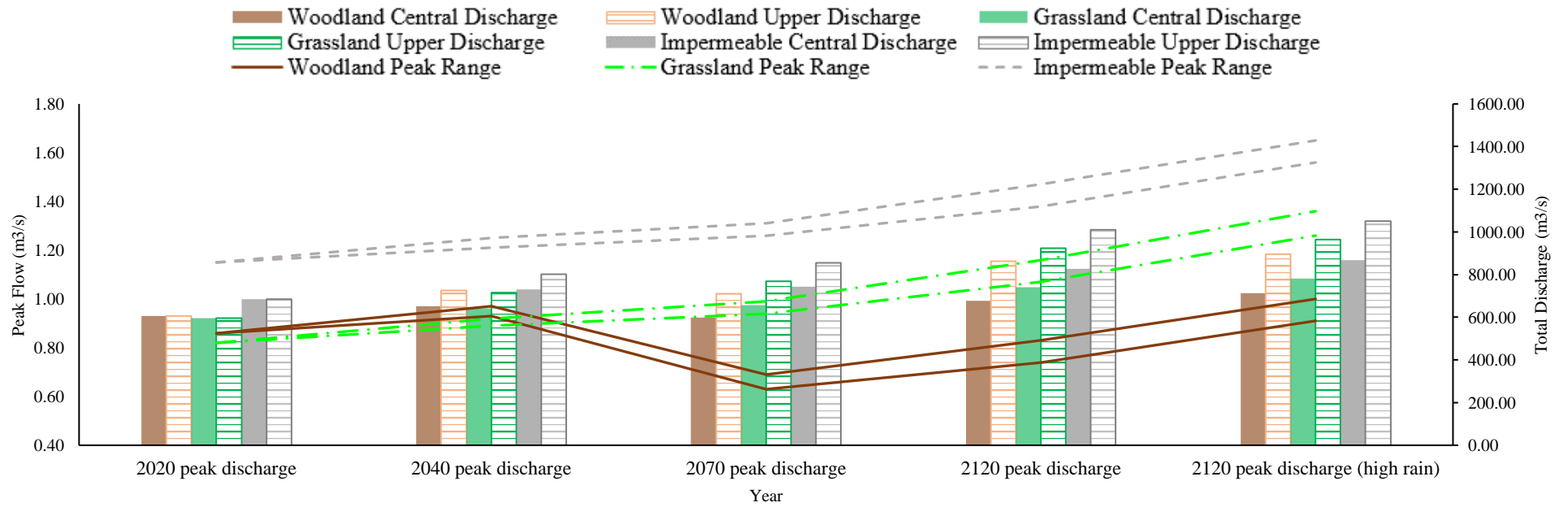


Figure 7.21. 50% AEP 24-hour peak flow and total discharge ranges summer. Please note the variable y-axis values.

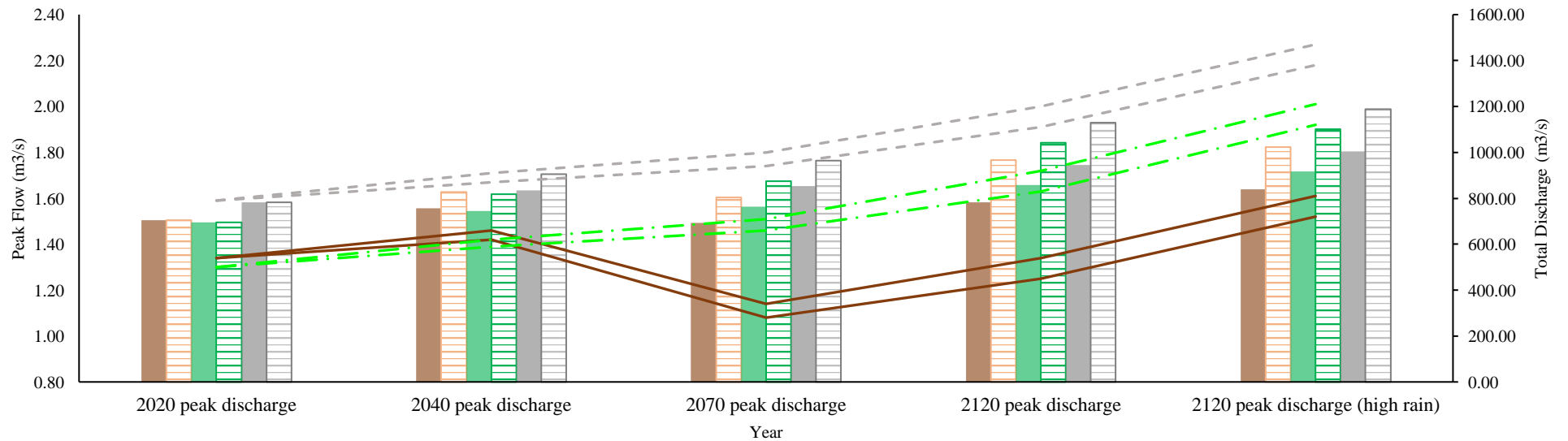


Figure 7.22. 10% AEP 24-hour peak flow and total discharge ranges summer. Please note the variable y-axis values.

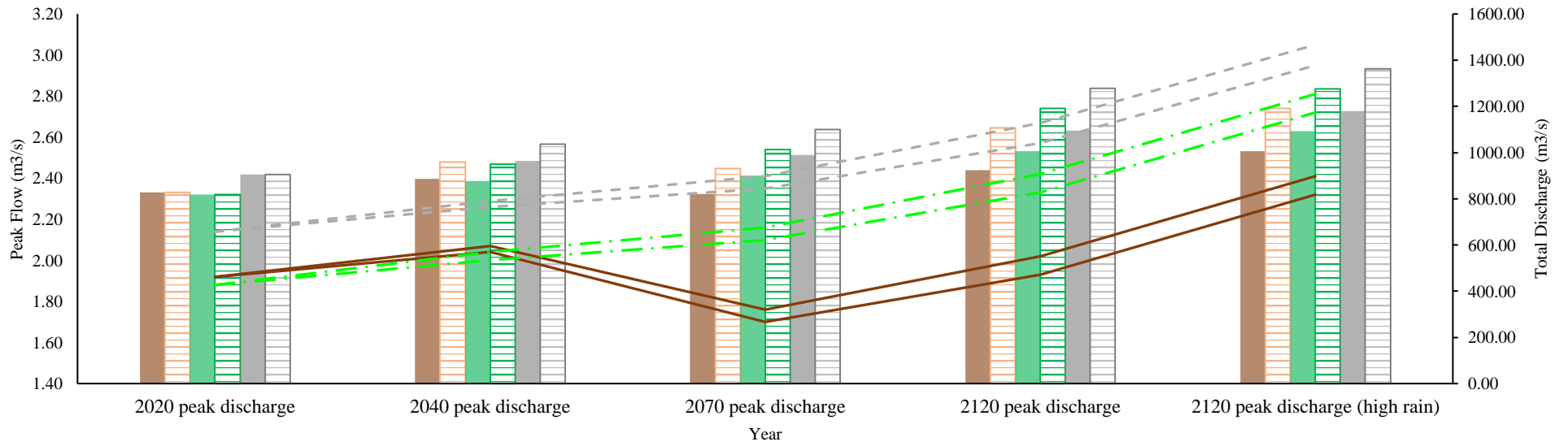


Figure 7.23. 2% AEP 24-hour peak flow and total discharge ranges summer. Please note the variable y-axis values.

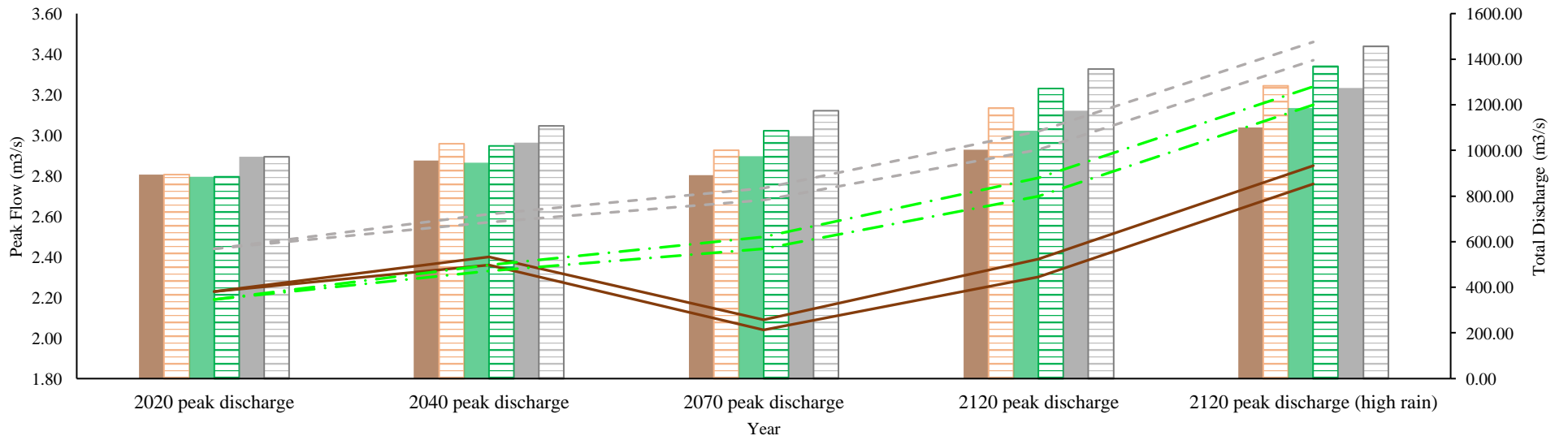


Figure 7.24. 1% AEP 24-hour peak flow and total discharge ranges summer. Please note the variable y-axis values.

Figure 7.21 to Figure 7.24 show similar trends to those seen throughout the 6-hour projections, including the reduction in woodland peak flow and total discharge from 2070 onwards. Impermeable land cover shows the highest peak flow range throughout all projection years, being 1.94 m<sup>3</sup>/s, 2.04 m<sup>3</sup>/s, 2.24 m<sup>3</sup>/s and 2.56 for 2040, 2070, 2120 and 2120 H respectively; these values are 6.31%, 11.28%, 22.69% and 40.05% high than 2020 values. Grassland showed the second-highest peak flow range, with mean discharge being 1.67 m<sup>3</sup>/s for 2040, 1.76 m<sup>3</sup>/s for 2070, 1.98 m<sup>3</sup>/s for 2120 and 2.31 m<sup>3</sup>/s for 2120 H; this is an increase of 7.72%, 13.85%, 27.81% and 49.17% for respective storm projections. Woodland showed the lowest peak flow range, with mean discharge being 1.71 m<sup>3</sup>/s for 2040, 1.39 m<sup>3</sup>/s for 2070, 1.60 m<sup>3</sup>/s for 2120 and 1.92 m<sup>3</sup>/s for 2120 H: 7.52%, -12.30%, 0.79%, and 21.20% higher than 2020 values respectively. The peak flow intensities are higher throughout the larger 24-hour AEP events (2% and 1%) compared with the 6-hour equivalent storms; however, this is somewhat to be expected as modelled FEH rainfall is greater in comparison (see Table 5.8).

Regarding total discharge, impermeable landcover continually shows the highest discharge, being 926.65 m<sup>3</sup>/s, 967.48 m<sup>3</sup>/s, 1102.03 m<sup>3</sup>/s, and 1173.08 m<sup>3</sup>/s for 2040, 2070, 2120 and 2120 H projections respectively (10.81%, 15.69%, 31.78% and 40.28% higher than 2020 values respectively). Grassland and woodland total discharge are non-discrepant until 2070, where they deviate; grassland discharge is 839.07 m<sup>3</sup>/s, 879.91 m<sup>3</sup>/s, 1014.47 m<sup>3</sup>/s and 1085.54 m<sup>3</sup>/s, and woodland discharge is 848.80 m<sup>3</sup>/s, 806.39 m<sup>3</sup>/s, 938.69 m<sup>3</sup>/s and 1006.36 m<sup>3</sup>/s for 2040, 2070, 2120 and 2120 H projections respectively. The above peak flow and total discharge values, represented in Figure 7.21 to Figure 7.24 and discussed throughout this section, are tabulated in appendix C.3.1. Additionally, the percent increase/decrease of peak flow and total discharge compared with 2020 values for 50%, 10%, 2% and 1% AEPs over 6-, 24- and 96-hour storms are presented in appendix C.3.2.

7.3.2.3 *Summer 96-Hour Storm Duration Projections*

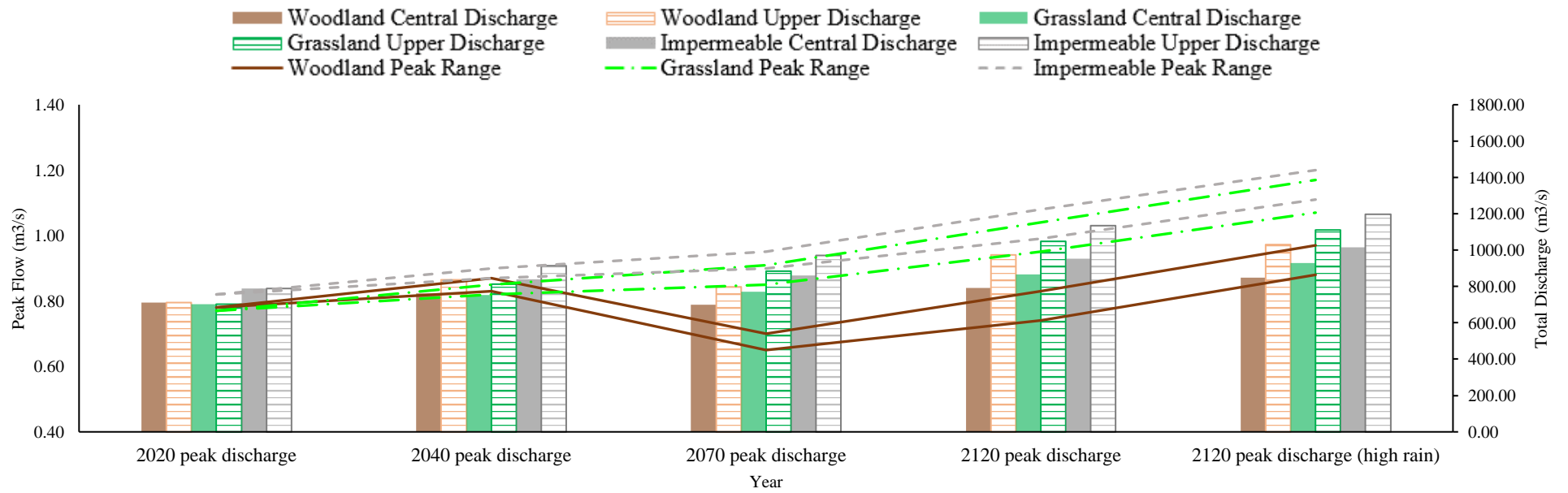


Figure 7.25. 50% AEP 96-hour peak flow and total discharge ranges summer. Please note the variable y-axis values.

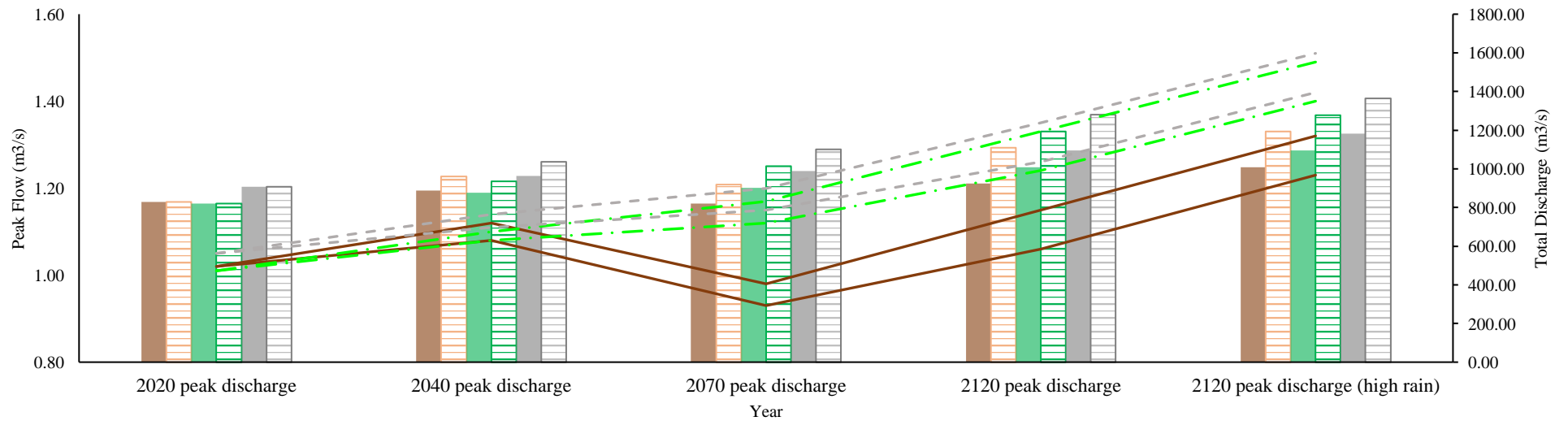


Figure 7.26. 10% AEP 96-hour peak flow and total discharge ranges summer. Please note the variable y-axis values.

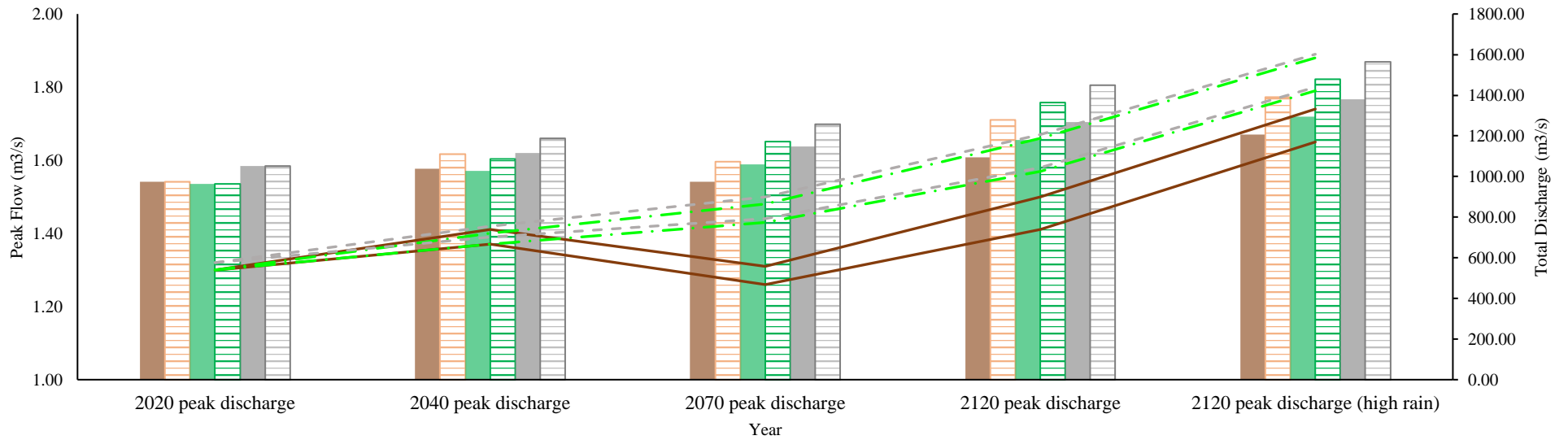


Figure 7.27. 2% AEP 96-hour peak flow and total discharge ranges summer. Please note the variable y-axis values.

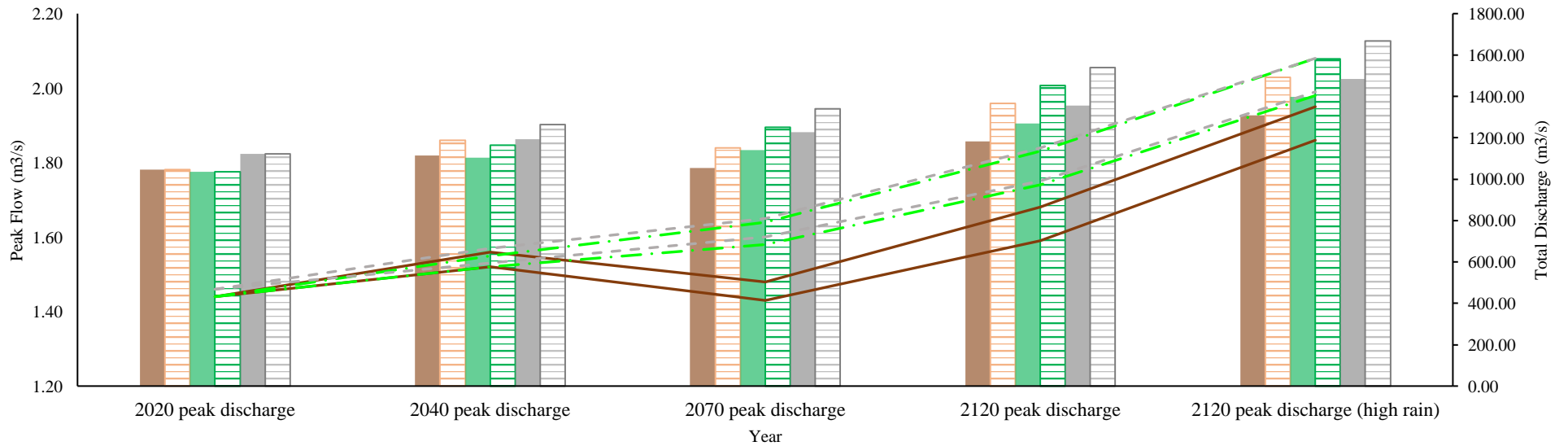


Figure 7.28. 1% AEP 96-hour peak flow and total discharge ranges summer. Please note the variable y-axis values.

Trends throughout the 96-hour duration modelled projections (Figure 7.25 to Figure 7.28) differ from those seen through the 6 and 24-hour duration simulations; there is less contrast between the peak flows of impermeable and grassland land cover. Impermeable land cover shows mean peak flows of 1.24 m<sup>3</sup>/s, 1.30 m<sup>3</sup>/s, 1.44 m<sup>3</sup>/s and 1.62 m<sup>3</sup>/s for 2040, 2070, 2120 and 2120 H (an increase of 7.05%, 12.01%, 24.21% and 40.10% for respective projection years). Grassland cover shows mean peak flows of 1.21 m<sup>3</sup>/s for 2040, 1.27 m<sup>3</sup>/s for 2070, 1.42 m<sup>3</sup>/s for 2120 and 1.61 m<sup>3</sup>/s for 2120 H, which is an increase of 7.13%, 12.73%, 25.58% and 42.32% for the projection years respectively. Woodland still shows a reduction in peak flow in 2070, values being 1.22 m<sup>3</sup>/s, 1.09 m<sup>3</sup>/s, 1.25 m<sup>3</sup>/s and 1.45 m<sup>3</sup>/s for 2040, 2070, 2120 and 2120 H, respectively 7.37%, -3.90%, 9.73% and 27.78% lower than 2020 values for each projection year. The trend seen throughout woodland peak flows is the same trend seen in the 6- and 24-hour durations (the reduction in woodland peak flow and total discharge from 2070 onwards), however the difference is less significant throughout the 96-hour simulations compared with previous durations. These results indicate that woodland struggles to mitigate the effects of climate change on local hydrology over sustained rainfall durations.

As with all modelled projections, impermeable land cover shows the highest total discharge, being 1064.00 m<sup>3</sup>/s for 2040, 1111.43 m<sup>3</sup>/s for 2070, 1259.36 m<sup>3</sup>/s for 2120 and 1356.79 m<sup>3</sup>/s for 2120 H, higher than 2020 values by 10.00%, 14.90%, 30.19% and 40.26% for the respective modelled outputs. Grassland showed the next highest total discharge, being 969.96 m<sup>3</sup>/s, 1024.45 m<sup>3</sup>/s, 1172.37 m<sup>3</sup>/s and 1269.81 m<sup>3</sup>/s for 2040, 2070, 2120 and 2120 H respectively (10.18%, 16.37%, 33.18% and 44.24% higher than 2020 values respectively). Woodland showed the lowest total discharge, being 986.76 m<sup>3</sup>/s, 936.20 m<sup>3</sup>/s, 1089.77 m<sup>3</sup>/s and 1185.30 m<sup>3</sup>/s for 2040, 2070, 2120 and 2120 H storms (10.86%, 5.18%, 22.44% and 33.17% higher than 2020 values respectively). The above peak flow and total discharge values, represented in Figure 7.25 to Figure 7.28 and discussed throughout this section, are tabulated in appendix C.3.1. Additionally, the percent increase/decrease of peak flow and total discharge compared with

2020 values for 50%, 10%, 2% and 1% AEPs over 6-, 24- and 96-hour storms are presented in appendix C.3.2.

### 7.3.3 Summary of Modelled Projections

Overall, the projected results presented throughout sections 7.3.1 and 7.3.2 show that woodland planting is unlikely to mitigate future projected peak flow and total discharge from the HofE site throughout the winter, however is more likely to have an impact throughout summer.

#### 7.3.3.1 Winter

Winter model projections show that woodland, whilst able to reduce peak flow and total discharge compared with impermeable and grassland land cover simulations, will not reduce peak flow and total discharge compared with current values in any projected year throughout winter (section 7.3.1). This is likely a result of the projected increase in rainfall across the site, combined with the lower infiltration values (due to the influence of soil texture and antecedent conditions (sections 5.2 and 8.1)) influencing infiltration projections (section 5.7.2). Winter projections show that woodland is more effective at reducing peak flows in shorter duration storms compared with longer duration storms, demonstrated by the discrepancy between peak flow and total discharge becoming less as storm duration increases (section 7.3.1). Grassland continually shows the highest percentage increase (from 2020 values) in peak flow and total discharge throughout the winter; however, this only represents that grassland values have changed from the 2020 simulated value, and not that grassland shows higher values. Grassland produces the second-lowest peak flow and total discharge behind woodland. Impermeable cover shows the highest peak flow and total discharge throughout winter, however, this is to be expected as it is known that the increase in impermeable surface cover is driving the push towards NFM (Burgess-Gamble *et al.*, 2018; Ferguson and Fenner, 2020a; Ellis *et al.*, 2021). This result is also seen in the ‘current’ simulations of the HofE site seen throughout section 7.2.

### 7.3.3.2 Summer

Overall, summer projections show lower total discharge compared with winter values, but higher peak flow. The higher peak flow is a result of the calibration parameters used to represent summer hydrology (section 5.4), and the lower total discharge is a result of the inclusion of interception – which reduced the rainfall received in summer by 24.25% (Calder, 2003; Nisbet, 2005; Lunka and Patil, 2016; Ngai *et al.*, 2017).

The most significant variation between winter and summer projections, is the reduction in peak flow and total discharge values from 2070 onwards. Mentioned in section 7.3.2.1, this is a result of the infiltration projections (i.e., when the trees would reach maturity = maximum infiltration (section 5.7.2)), and the inclusion of interception – meaning there is less precipitation to be infiltrated overall in the summer projections. This trend is observed throughout woodland peak flows and total discharges in winter, however is much more subtle than the summer projections, being more noticeable in shorter duration events (sections 7.2.1 and 7.2.2). This is explained further in section 8.2.2

Similar to winter projections, impermeable land cover produces the highest peak and total flow volumes, however, the peak flows from grassland and impermeable land cover become more similar as storm duration increases. Throughout shorter duration storms, grassland shows a lower peak flow compared with grassland until 2070 (where woodland shows to reduce peak flow significantly). This relationship is less distinguishable in longer duration events, where impermeable and grassland peak flows become more similar. Regardless of the reduction of woodland peak flow and total discharge in 2070, results from the longer duration projections show that woodland, whilst still showing a reduction in peak flow and total volume compared with grassland and impermeable surfaces, does not mitigate the variables to the same magnitude as it does in shorter duration events. This is primarily due to increased precipitation.

## Chapter 8 Discussion

Chapter 7 presents and analyses the results of the study, derived through using the methods presented throughout Chapter 5, which were influenced by the current state of the literature (Chapter 2) and the wider background of the study topic (Chapter 1). This chapter contextualises the results presented throughout Chapter 7 considering the wider literature and the aims of this project, emphasising the findings and applications of this work. Note that aim 2 is not thoroughly discussed here due to the requirements of aim 2 being achieved throughout sections 5.3, 5.4 and 5.5 (see Table 5.1).

### **8.1 Aim 1: Determine to what extent tree planting by the Heart of England Forest has influenced infiltration, with reference to tree proximity and tree maturity.**

Aim 1 intended to determine to what extent woodland planting by the Heart of England Forest has influenced infiltration, with reference to tree proximity and tree maturity. Objective 1b was to use the data collected as required by objective 1a and derive any relationships between infiltration dependent on both woodland proximity and woodland maturity. It is presented in section 7.1 that mean infiltration is higher at the 10 cm proximity compared with the 200 cm proximity by 75.87% in winter and 25.19% in summer. Further to this, mean 10 cm infiltration is 192% higher in summer compared with winter, and mean 200 cm infiltration is 310% higher in summer compared with winter. These results conclude that overall, the presence of the tree, and particularly the developing root system, is influencing infiltration through increasing soil porosity, allowing for soil-water storage and faster infiltration. When tree roots develop, they grow outwards from the base of the trunk, their course guided primarily by following the path of least resistance through the soil matrix (Dobson, 1995; Crow, 2005). Section 2.3.1 highlights that tree roots connect flow pathways, reduce compaction, influence porosity and change soil structure (Jarvis, 2007; Zhang *et al.*, 2017b, 2019a; Chandler *et al.*, 2018; Leung *et al.*, 2018;

Malik *et al.*, 2019; Xie *et al.*, 2020; Guo *et al.*, 2021); and the results of this study support this and indicate that infiltration nearer the tree (and subsequently the origin of the root system) is higher. Further to this, section 7.1 demonstrates the seasonal variation in infiltration, showing infiltration to be 235% higher overall in summer compared with winter (180% higher at the 10 cm proximity, and 290% at the 200 cm proximity). These results show that woodland is capable of increasing infiltration regardless of the naturally low permeability of the sample site soil (Folorunso and Aribisala, 2018), and indicate that soil variability (texture and structure) and antecedent moisture conditions have an influence on seasonal infiltration. These results can be further contextualised when considering the influence of soil texture across the study site (Groenendyk *et al.*, 2015; Folorunso and Aribisala, 2018; Leung *et al.*, 2018). Seen in Table 5.3, the 2006, 2008, 2012, 2014 and 2020 sites are clay textured, and the control, *ca.* 1900 and 2010 sites are sandier-textured. Clay-heavy soil textures (such as the aforementioned) inherit lower infiltration, conductivity and porosity due to the smaller, rounded particle size of clay (<0.002 mm) fitting tightly together (Rabot *et al.*, 2018). Sand particles are larger (0.06 mm – 2.0 mm) and more angular, meaning larger pores are left between the particles, allowing for infiltration and conductivity (section 2.5) (Groenendyk *et al.*, 2015; Folorunso and Aribisala, 2018; Leung *et al.*, 2018). Common across the less permeable clay textured sample sites, was surface water pooling during and after rainfall, see Figure 8.1.

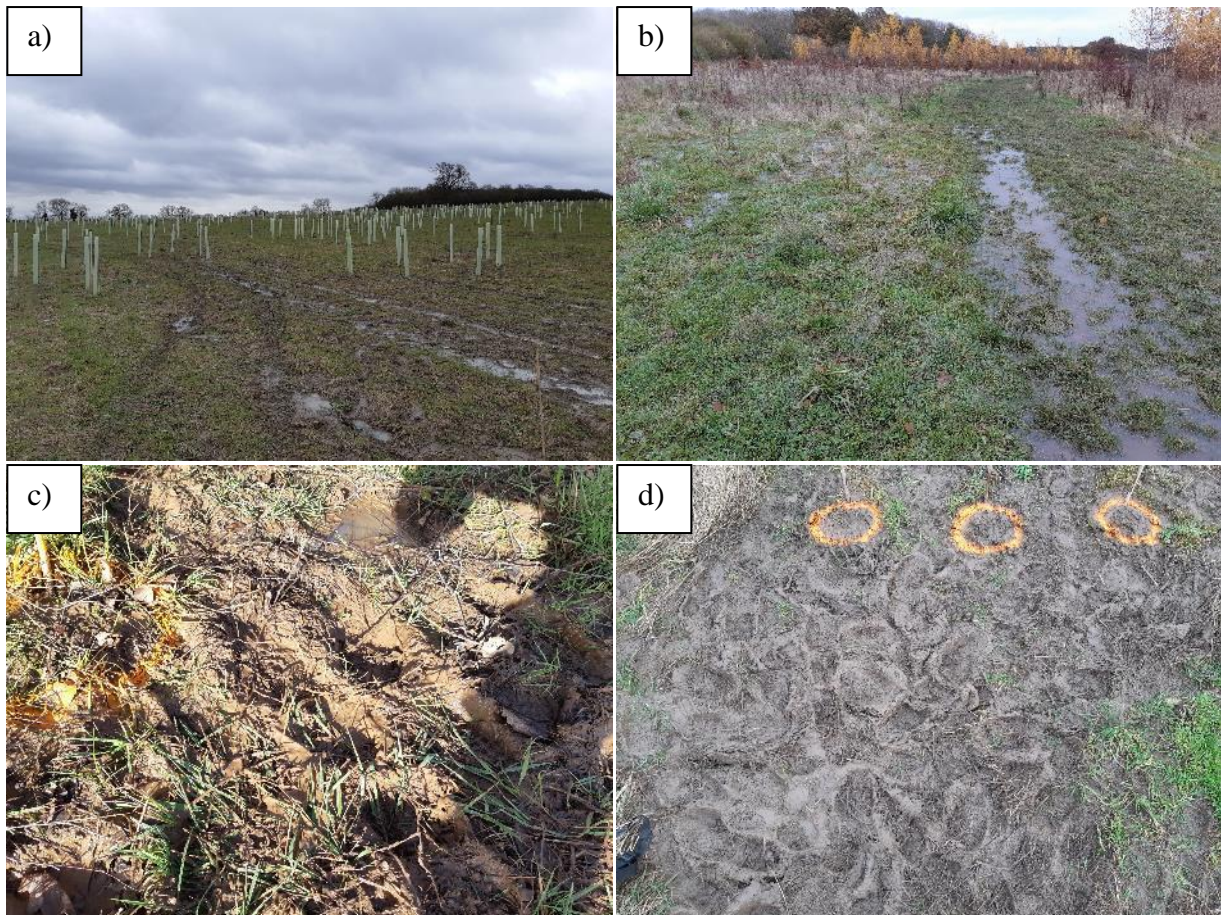


Figure 8.1. Surface pooling of clay-textured sites. a) 2020, b) 2014, c) 2006 and d) 2012

Infiltration data could not be collected (although was always attempted) during surface pooling; and it is this phenomenon that may account for recorded low permeability during the winter period (section 7.1). Surface pooling was also exaggerated by the winter of 2020 being the fifth wettest on record (329.4 mm/143% higher than the 1981–2010 baseline), and the February of 2020 being the wettest ever recorded, with 155 mm of precipitation (258% higher than the 1981–2010 baseline) (The Met Office, 2020; Davies *et al.*, 2021a). Whilst the influences of antecedent rainfall and clay-textured sample soils may have contributed to the lower infiltration values collected throughout winter; the results of this study have shown that infiltration was still higher at the 10 cm proximity compared with the 200 cm proximity. The wider implications of this are discussed throughout sections 9.1.3, 8.2.2 and 8.2.3.

There is no evidence to suggest a correlation between woodland maturity and increase infiltration at either proximity over time, this has been determined through use of the Mann-

Whitney U testing presented in section 7.1. Whilst this finding does predominantly dispute what was identified regarding woodland maturity in the literature (section 5.7.2) (Lacob *et al.*, 2014; Dittrich *et al.*, 2019; Julich *et al.*, 2021; Murphy *et al.*, 2021), it is important to consider these results in the context of the current age of sample woodland. Aside from the *ca.*1900 site, the oldest trees sampled were planted in 2006 and the youngest in 2020. Thus the 2006 woodland had only been in-situ for 15 years, and the 2020 woodland for 1 year (at the time of analysis). The maturity ages of the sampled woodland species are discussed in section 5.7.2, concluding that birch and aspen trees can live for 100-120 years, reaching their final heights (where infiltration will be at a maximum) at 60 and 30 years respectively (Perry, 1982; Mauer and Palátová, 2003; Hepner *et al.*, 2020). Considering this, the sampled woodlands are still early in their development and the maturity-relationship results presented in section 7.1 are only representative of the early stages of the likely effects that the sampled woodland will have on infiltration. Whilst there are no obvious trends between infiltration and maturity, Table 7.1 does show that the *ca.*1900 sample site demonstrated the highest infiltration at the 200 cm proximity in the winter, and the 10 cm proximity in both winter and summer. This is likely a result of the soil texture at the *ca.*1900 site being predominantly sand (sand 47%, silt 40%, clay 13%, see Table 5.3) meaning it is naturally more porous, leading to higher pore conductivity and infiltration. However, may also be a result of tree root spread – further increasing porosity and increasing conductivity and infiltration, which would account for the higher infiltration at the 200 cm proximity compared with other sites. This supports the existing literature regarding infiltration and maturity (Birkinshaw *et al.*, 2014; Lacob *et al.*, 2017; Chandler *et al.*, 2018; Julich *et al.*, 2021; Xiao *et al.*, 2021). According to chronology and based on the existing literature, it would be expected that the 2006 site would demonstrate the next highest infiltration (after *ca.* 1900). The presumption for this is based on the area being the first planted by the HofE forest, therefore having the most time to grow (of the HofE planted woodland) and develop a root system that would now be influencing porosity; however, this is not the

case. Table 7.1 shows the 2006 site to consistently show the lowest infiltration at both proximities regardless of seasonality. Referring back to the age of woodland planted at the site (section 5.2.1), particularly in comparison to their discussed maturity age and lifespan, this study has focussed primarily on young woodland (15 to 1 year(s) old). The results of the infiltration data analysis have indicated that very mature trees (*ca.*1900) promote infiltration in comparison to less mature trees, likely due to their increase root spread, and the influence of this on increasing porosity and increasing hydraulic conductivity within the measured proximities (Lacob *et al.*, 2014; Dittrich *et al.*, 2019; Cui *et al.*, 2021; Julich *et al.*, 2021; Murphy *et al.*, 2021). This is an insight into what could potentially be expected from the HofE planted trees across the site as all woodland develops into the future, and this has been tested in the infiltration projections and future climate models presented in sections 5.7.2 and 7.3. This research has demonstrated that trees can influence infiltration at varying proximity, with some early trends indicating that maturity may yet play a future part in this increase (Cui *et al.*, 2021; Julich *et al.*, 2021; Wu *et al.*, 2021). However, whilst tree planting can be hydrologically beneficial, instant increases in infiltration should not be expected as the findings of this research suggest that hydrological improvements are unlikely for a minimum of 15 years (as this is the oldest age of the trees sampled across the HofE site). This conclusion has connotations regarding the way in which woodland is currently handled, with reference to development, construction, and forestry. The following sections investigate this in further detail.

### 8.1.1 Summary of Aim 1 Findings

Aim 1 was to determine to what extent HofE woodland planting has influenced infiltration, dependent on proximity and tree maturity, through defining sampling locations and methods (objective 1a) and analysing the collected data to identify trends (objective 1b). Results of the collected infiltration data show that woodland planting increases infiltration at the 10 cm proximity in both summer and winter compared with the respective 200 cm sample. Mean

infiltration is higher at the 10 cm proximity compared with the 200 cm proximity by 75.87% in winter and 25.19% in summer; and mean 10 and 200 cm infiltration is 192% and 310% higher in summer compared with winter respectively. Regarding the influence of woodland maturity on infiltration, no significant trends were identified based on data collected from recently planted HofE woodland (2006 – 2020). However, the sampled *ca.*1900 site consistently showed the highest mean infiltration indicating that, whilst the recently planted HofE trees may not be notably influencing infiltration, they are early in their lifecycle and will likely influence infiltration when the root systems have developed (Archer *et al.*, 2016; Song *et al.*, 2018; Zhang *et al.*, 2019a, 2020). It is discussed that antecedent moisture and the influence of (clay) soil texture may have influenced data collection (i.e., not given a representative sample at all sites).

The results collected as part of aim 1 have contributed to the mostly sparse literature reserve regarding the current value of trees on hydrology, and the future hydrological impacts of woodland planting (Thomas and Nisbet, 2016; Chandler *et al.*, 2018; Cooper *et al.*, 2021; Murphy *et al.*, 2021). The results and presented discussion points can be used to inform current and future tree planting and NFM policy, which is discussed in greater detail throughout section 9.1. Additionally, the methods, results and discussions involved in the fulfilment of aim 1 were used in the development of an academic paper published by *Water MDPI* (see appendix D.2.2).

### **8.2 Aim 3: Simulate current and future hydrology from the study site and determine to what extent HofE woodland planting has influenced runoff and flood risk.**

To fulfil aim 3, objective 3a required the use of the HEC-HMS models to simulate the outflow of the study site dependent on changing storm intensity, duration, land cover and tree maturity. Objective 3b required the use of recent climate resources and the HEC-HMS models to predict the likely future changes to site hydrology regarding to developing tree maturity and climate change. Objective 3c required the culmination of existing literature and the results of aims 1

and objectives 3a and 3b to evaluate the value of tree planting as a method of NFM. This section discusses the outcomes of aim 3; objective 3a is discussed in section 8.2.1, objective 3b in 8.2.2, objective 3c in 8.2.3, and aim 3 is summarised in section 8.2.4.

### 8.2.1 Present Day (current) Hydrological Simulations

Results of the HEC-HMS modelling (section 7.2) show that HofE woodland planting has reduced winter peak runoff compared with impermeable land cover by a mean of 6%, 2% and 1% for 6-, 24- and 96-hour storms, and summer peak runoff by 48%, 18%, and 2.7% for 6-, 24-, and 96-hour storms. Whilst results show that woodland can reduce peak runoff in comparison with impermeable land cover, this is unsurprising as it is long-established that the increase in impermeable surface cover is driving the push towards NFM and is a key motivator for the aims of this project (Burgess-Gamble *et al.*, 2018; Ferguson and Fenner, 2020a; Ellis *et al.*, 2021). Discussed throughout section 7.2 is that grassland continually shows the lowest peak flow, being 32%, 21%, and 10% lower than the current site in the winter, and 6%, 2%, and 0.5% lower than the HofE site in the summer for 6-, 24-, and 96-hour duration storms respectively. This somewhat contradicts what has been discussed throughout section 8.1 regarding the observed increase in infiltration as a result of woodland planting; however, these results can be further explained when considering infiltration sample locations (objective 1a), soil texture, and the construction of the HMS model.

Outlined in section 5.2, infiltration sampling locations were chosen based on accessibility, size and landcover; the map of final sampling locations is shown in Figure 5.8. Table 5.3 presents the soil textures of infiltration sample sites, showing that the 2006, 2008, 2012, 2014 and 2020 sites are clay textured (naturally less permeable, section 2.5), whereas the *ca.*1900, 2010 and control sites host a sandier-texture (naturally more permeable, 2.5) (Groenendyk *et al.*, 2015; Leung *et al.*, 2018). This variation is insignificant throughout wooded and impermeable landcover simulations, as empirical (or extrapolated, section 5.6.3) infiltration data was

available for use; however, it is significant when simulating the grassland land cover scenarios. As discussed in section 5.6, to simulate grassland cover the infiltration from the control site was uniformly applied to all sub-catchments of the HMS model, and the results taken from these simulations were used in forming results in section 7.2. This process of grassland extrapolation resulted in the site being altered to represent the values of the sandier-textured control site, instead of maintaining the variations in soil texture observed at each sample location (Table 5.3) (Rabot *et al.*, 2018; Sun *et al.*, 2018; Silber, 2019). Whilst this method of grassland representation may have led to the over-prediction of infiltration for the entire site, it was the best possible method of deriving modelled results using empirical observations from the study site and is representative of the collected field data. These results should also be considered in the context of the general nature of field work and hydrological modelling. It is discussed (Prieksat *et al.*, 1994; Logsdon and Jaynes, 1996; Khodaverdiloo *et al.*, 2017) that spatial variability is inherent with fieldwork; and additional considerations had to be accounted for throughout this project (i.e.) budgetary constraints, health and safety, time on site and travelling time (section 5.2). Additionally, section 3.4 discusses that hydrology is complex (Sy *et al.*, 2019), and hydrological modelling is a mathematical simplification of the most likely response to given input parameters (Rampinelli *et al.*, 2020; Kumar and Sherring, 2021).

Apparent throughout all simulations presented in section 7.2, summer simulations show a lower total discharge, but a higher peak flow compared with their corresponding winter values (see sections 7.2.1 to 7.2.3). Noticeable, is that woodland seems to be more capable of mitigating lower intensity, shorter duration storms, compared with the longer duration AEP events; this is most obvious through comparing the ‘percentage difference’ columns of Table 7.8, Table 7.9 and Table 7.10. Table 7.8, shows the mean difference between the peak and total discharges of woodland and grassland to be -32.41% and -15.83% respectively in winter, and -6.01% and -1.73% respectively in summer. The same values for winter and summer over the 24-hour duration storms (Table 7.9) are -21.58% and -12.21% (winter) and -2.87% and -1.31%

(summer); and results of the 96-hour duration storms (Table 7.10) are -10.21% and -10.44% (winter) and -0.56% and 1.11% (summer). Obvious, is that the mean differences between grassland and woodland peak flow and total discharges diminish as storm duration increases. Furthermore, the same trends can be seen when investigating these changes on an ‘AEP-by-AEP’ basis. It is observed in every simulation that as AEP increases (50% to 1%), the differences between woodland and grassland peak flow become less. Discrepancies are also seen to diminish as storm duration increases across the same AEP, for example, the differences in peak flow and total discharge of the 50% AEP reduce as storm duration increases. This can be seen in Figure 7.2, Figure 7.3 and Figure 7.4 where peak flows and total discharges become more similar as duration increases. These results conclude that whilst woodland can mitigate the effects of lower intensity short duration storms in both winter and summer; their ability diminishes with increased intensity and duration, which is commonly observed in other studies (Chandler *et al.*, 2018; Carrick *et al.*, 2019; Ferguson and Fenner, 2020a; Xiao *et al.*, 2021). This indicates that woodland planting is effective at increasing soil porosity and infiltration (sections 2.3.1 and 7.1), and contributing to catchment FMR; however, a limitation of woodland is the inability to store excess amounts of precipitation. This therefore suggests that woodland planting may be most effective when used in conjunction with other methods of FRM, conventional or natural, and should be viewed as another valuable asset in a wider arsenal of NFM methods (Carrick *et al.*, 2019; Xiao *et al.*, 2021). This approach is discussed in greater detail throughout section 8.2.3.

The above results presented in fulfilment of objective 3a, in addition to the considerations that have been made to ensure reliability and accuracy in results, have contributed to the lack of empirically based tree planting and infiltration studies (Carrick *et al.*, 2019). These processes have provided a methodology for future authors to simulate woodland planting in similar catchments.

### 8.2.1.1 The Influence of Precipitation, Interception, Soil Texture and Model Calibration

As outlined in section 5.2 and reiterated in section 8.1, the majority of sample sites were comprised of clay-textured soils. Clay-heavy soil textures inherit lower infiltration, conductivity and porosity due to the smaller particle size of clay (Rabot *et al.*, 2018); compared with sand particles, which are larger and more angular allowing greater porosity, infiltration and conductivity (section 2.5) (Groenendyk *et al.*, 2015; Folorunso and Aribisala, 2018; Leung *et al.*, 2018; Rabot *et al.*, 2018). Due to this, seasonal infiltration data collection was highly variable (see section 8.1), which is the primary justification for the two hydrological models (section 5.4). The clay sample sites were prone to complete saturation throughout the winter, and cracking throughout the summer, see Figure 8.2.



*Figure 8.2. Saturation of the (a) 2006 and (b) 2008 sample sites during winter data collection, (c) cracking of the 2006 and (d) 2008 sample sites in the summer*

In the winter, the increase in surface pooling of the sample sites (Figure 8.2, section 8.1) likely helped hold water in place across the study site, slowing infiltration and overland flow and

creating more of a lag between precipitation and peak flow (Groenendyk *et al.*, 2015; Leung *et al.*, 2018). In the summer, however, the cracking of the dry clay caused the clay-textured areas to act similarly to an impermeable surface, resulting in a shorter lag time and a higher peak. Additionally, increased peak flow throughout the summer may have been influenced by the parameters of the chosen Snyder transform method. Discussed in section 5.3.3.3, the Snyder method allows for the lag and peaking coefficient to be adjusted to match observed hydrological values. The peaking coefficient (the value that determined the profile of the transform hydrograph) was set to 0.5 for both winter and summer, however empirical observations and the calibration process has determined the lag of the summer transform to be 6 hours, whereas winter is much longer at 18 hours. Regardless of this, both hydrological models were extensively and comprehensively calibrated to empirical values, resulting in final calibration and validation NSE values of 0.65 and 0.44 for summer, and 0.65 and 0.87 for winter (sections 5.4 and 5.5). The calibration of the HMS models adds validity to the results produced throughout section 7.2, as it is not always common practice for modelling studies to involve such comprehensive calibration. It is common for modelling studies to use gauged data from far-away instruments, or to use arbitrary ‘rainfall – outflow’ methods during model calibration (Revilla-Romero *et al.*, 2015; Gumindoga *et al.*, 2017; Komi *et al.*, 2017; Fedorova *et al.*, 2018; Muhammad and Lu, 2020).

The results and discussions presented in partial fulfilment of aim 3 throughout sections 7.2, 8.2.1 and 8.2.1.1 have added to the current state of literature regarding the construction, calibration and validation of the hydrological models, and the impacts of tree planting at influencing hydrological processes; and have allowed for the development of an academic paper published by *Water* MDPI (appendix D.2.1).

### 8.2.2 Modelled Future Impacts of Woodland Planting

The global climate is changing (Lowe *et al.*, 2019) (section 1.1), and it is discussed in section 2.2.2 that the future hydrological effectiveness of NFM methods (in light of climate change) is uncertain due to a lack of projected/recorded data (Lacob *et al.*, 2014, 2017; Carrick *et al.*, 2019; Black *et al.*, 2021). Woodland planting is not exempt from this hydrological uncertainty; however, it is generally regarded that woodland is overall beneficial as a climate mitigation tool due to its carbon sequestration potential (Carrick *et al.*, 2019; Fletcher *et al.*, 2021). This is discussed in greater detail throughout section 8.2.3.2, this section, however, contextualises the results of hydrological projections presented throughout section 7.3.

Results from the winter projections show that woodland planting will not reduce peak or total discharge below that of the current HofE site across any simulated storm duration. However, it can be seen throughout Figure 7.5 to Figure 7.16 that woodland will produce lower peak and total discharges than both grassland and impermeable cover. The results produced for winter are insightful as they show that woodland planting, although second-to-grassland in the present-day simulations (section 7.2), will surpass grassland once the root systems have developed. The reasoning for this is discussed further throughout sections 2.3.1, 2.5, 5.7.2 and 8.1; tree roots break up the surrounding soil matrix, increasing porosity, pore connectivity and infiltration (Jarvis, 2007; Zhang *et al.*, 2017b, 2019a; Chandler *et al.*, 2018; Leung *et al.*, 2018; Malik *et al.*, 2019; Xie *et al.*, 2020; Guo *et al.*, 2021). All projected peak and total discharges increase from 2020 values throughout winter simulations, due to a combination of the steady projected increase in infiltration as a result of the aforementioned impacts of root spread, and the equally progressive increase in precipitation (section 5.7.1). This is also likely an influence of the notably low values of infiltration data collected from the study site (discussed in section 8.1), combined with the method of infiltration projection. The method of infiltration projection, detailed in section 5.7.2, involved cumulatively increasing observed infiltration values until the trees reached their maturity age (see appendix B.7). As presented in section 7.1, infiltration

data throughout the winter was notably low due to a combination of antecedent moisture and soil texture (see Figure 8.1); this meant that when these values were cumulatively extrapolated, the output values were lower. A good comparison of the effects of this is to view the summer projections, which are more exponential due to the higher initial infiltration, leading to a higher cumulative increase (see section 5.7.2 and appendix B.7)

The summer projected peak and total discharge values show differing trends to that of winter simulations. Similarly, to the present-day summer modelled values, peak flows are higher and total discharge is lower than equivalent winter events. This is due to the inclusion of interception throughout the projected simulations, and these similarities are expected as the same calibration parameters were used for both the 'current' and projected simulations to maintain consistency and represent the site (Shinohara *et al.*, 2015; Krysanova *et al.*, 2018; Ficchi *et al.*, 2019; Nguyen *et al.*, 2020; Cooper *et al.*, 2021). The most notable difference between winter and summer projections is the drop in projected woodland peak flow and total discharge values in 2070. Figure 7.17 to Figure 7.28 show that across all durations and AEPs, the woodland projections drop in 2070, and remain consistently lower than grassland and impermeable outputs until 2120. As with winter projections, this is due to the infiltration projection method - all sample trees are predicted to reach their maximum infiltration potential (due to maturity) between 2040 and 2070 (see appendix B.7), reducing runoff, which is reflected in the drop in peak flow and total discharge of summer simulations (Lacob *et al.*, 2017; Krysanova *et al.*, 2018; Dittrich *et al.*, 2019; Kay *et al.*, 2019; Hosseinzadehtalaei *et al.*, 2020; Black *et al.*, 2021). This is also compounded by the higher summer infiltration values compared with winter (due to increased sample site porosity, see section 7.1, Figure 8.1 and Figure 8.2), and interception loss. An interception loss of 24.25% (section 5.6.2) was derived from the literature (Calder, 2003; Nisbet, 2005; Lunka and Patil, 2016; Ngai *et al.*, 2017) and applied to the increasing FEH precipitation values; thus meaning less precipitation in 2070, combined with higher infiltration and maximum tree maturity.

Overall, the projected results shown that in winter, even when factoring in the possible changes in infiltration and precipitation (and interception in the summer), woodland will not be able to mitigate peak flows or total discharge below the values determined by the present-day models. Woodland, however, is projected to show a lower peak flow and total discharge than grassland and impermeable land cover in all projected years (section 7.3). In the summer, projected results show that woodland will have a significant influence on peak flow and total discharge in 2070, and woodland peak flow and total discharge will be lower than both grassland and impermeable land cover (Kay *et al.*, 2019; Black *et al.*, 2021).

### 8.2.3 Woodland Planting as a Method of NFM

The overarching theme derived from the collected field data and both present and future hydrological models, is that woodland planting can influence hydrology through increasing soil porosity and increasing interception; however, trees need time to establish and grow before any impactful hydrological implications can be empirically observed (Kay *et al.*, 2019; Black *et al.*, 2021; Cooper *et al.*, 2021; Xiao *et al.*, 2021). The findings are impactful when assessing tree planting as a method of NFM, and its likely capabilities, advantages and disadvantages (Dittrich *et al.*, 2019; Cooper *et al.*, 2021; Murphy *et al.*, 2021). The implementation and operation of NFM methods are inherently different from conventional FRM methods (section 2.2.3) (Ngai *et al.*, 2017; Waylen *et al.*, 2018; Wilkinson *et al.*, 2019). Conventional methods can mitigate flooding from the day of completion, are designed to a specified AEP and withstand predicted future flow increases, and can respond in real-time to allow their mitigating effect to be adjusted dependent on hydrological conditions (e.g., the Thames Barrier) (Lacob *et al.*, 2014; Ferguson and Fenner, 2020a; Environment Agency, 2022). An additional advantage of conventional methods is their common obviousness, which instils a level of trust amongst the public, as the structure can be associated with reducing flooding (Lacob *et al.*, 2014; Waylen *et al.*, 2018). By nature, the benefits of NFM methods differ to the listed benefits

of conventional methods; NFM methods are dependent on soil texture, topography, vegetation growth, vegetation type and interception increase (see section 2.2) (Burgess-Gamble *et al.*, 2018; Shuttleworth *et al.*, 2019; Ferguson and Fenner, 2020b; Ellis *et al.*, 2021). Additionally, there is less research surrounding the current and future benefits of NFM, and methods commonly need time to establish and function as they are intended (Kay *et al.*, 2019; Wingfield *et al.*, 2019; Ferguson and Fenner, 2020a; Ellis *et al.*, 2021).

The results of this study show that the impacts of woodland planting are less noticeable throughout winter, which questions the capabilities of woodland to mitigate larger winter storm events. UK winters are wet (the wettest ever February was observed throughout the course of this study) and are projected to become even wetter under the influences of climate change (Chapter 1). It is shown in section 7.2 and discussed by Xiao *et al.*, (2021) that woodland planting is valuable for increasing infiltration and reducing runoff following smaller-scale storm events, but woodland should solely not be used to mitigate against larger events due to their limited capability. This is also discussed throughout sections 8.2.1 and 8.2.2., highlighting that woodland lacks the required hydrological storage to mitigate larger-scale precipitation events. This is a main limitation of woodland planting (and other vegetation planting-based methods of NFM) compared with conventional FRM methods; all of which are designed with sufficient storage capacity in order to mitigate large rainfall events (attenuation ponds, soakaways, storage tanks) (Butler and Davies, 2011; Shaw *et al.*, 2011). In response to this, it is generally acknowledged that NFM methods should be viewed holistically throughout a catchment, and multiple NFM methods, both in-channel and throughout the catchment, should be employed to achieve the best possible mitigative results on FRM (Forbes *et al.*, 2016; Ngai *et al.*, 2017; Lavers and Charlesworth, 2018; Nicholson *et al.*, 2019; Ellis *et al.*, 2021). The combination of NFM methods at varying catchment scales are comparable to a commonly promoted method in the field of sustainable drainage (SuDS) coined ‘management trains’ (Booth and Charlesworth, 2014; Lamond *et al.*, 2015; Lashford *et al.*, 2020). Examples of

where multiple methods (a ‘train’) of NFM methods have been utilised to mitigate flood risk (in addition to the Hills to Levels project, section 2.2.1) include: the re-meandering of the (previously artificial) Swindale Beck in Cumbria, where livestock activity was reduced, trees were planted, floodplains were reconnected, and temporary flood storage was installed (Wightman and Schofield). The Beam urban watercourse, London, where 12ha of ponds, reedbeds, and woodland were installed, in addition to 150 m of realignment, 600 m of reprofiling and 300 m of in-channel features (creating an additional 25,660 m<sup>3</sup> of flood storage) (Burgess-Gamble, 2012); and the Eye Brook, Stonton Brook, Barkby Brooks in Leicestershire, where permeable dams and field-edge wetlands have been installed – this in addition to support for farmers regarding improving soil management (Biggs *et al.*, 2017).

Relevant literature (Short *et al.*, 2019; Wells *et al.*, 2020; Bark *et al.*, 2021; Ellis *et al.*, 2021) discusses that NFM methods can contribute to an areas overall flood mitigation, however their effectiveness is increases when employed alongside (new or) pre-existing ‘hard’ conventional structures (Wilkinson *et al.*, 2019). It is often discussed that there should be a trade-off between the use of conventional methods, to mitigate against the ever-increasing occurrence of high intensity rainfall and extreme weather events, and NFM methods, for mitigation against lower-intensity storms and for their demonstrated abilities in CO<sub>2</sub> sequestration, biodiversity and habitat creation (Lacob *et al.*, 2017; Collentine and Futter, 2018; Seddon *et al.*, 2020; Ellis *et al.*, 2021). Conventional methods can be utilised for their excess storage and flow control ability (attenuation ponds, flood walls), whereas NFM methods, such as vegetation and woodland planting can reduce the volume of water entering the watercourse to begin with (Wilkinson *et al.*, 2019). This methodology supports the findings of this study, which have shown that woodland planting struggles to mitigate the peak flows and total discharge volumes of the HofE site in comparison to grassland alone (see section 8.2).

### 8.2.3.1 UK Soil Texture and Tree Planting

The results of this study have shown that trees (and subsequently woodland) are valuable as a method of NFM as they can increase infiltration at close proximity, and become more capable of doing so with increased maturity; this in addition to the associated benefits regarding carbon sequestration, biodiversity, habitat creation and public amenity (Lacob *et al.*, 2017; Collentine and Futter, 2018; Seddon *et al.*, 2020; Ellis *et al.*, 2021). Referred to throughout Chapter 7 and Chapter 8, the HofE site is predominantly clay-textured, which is known to demonstrate low permeability and infiltration (Groenendyk *et al.*, 2015; Folorunso and Aribisala, 2018). This therefore indicates that the derived results are a low-end representation of what the impacts of tree planting could be over a more permeable geology. Area calculations of superficial alluvium, clay, peat and fluvial deposits throughout the UK show 15% (36,374.25 km<sup>2</sup>) to be similar in geology to the HofE site (British Geological Survey, 2021). See Figure 8.3.

*Figure 8.3. 1:625k superficial geology map of the UK with the Arrow-Alne River catchment highlighted by red circle (British Geological Survey, 2021).*

This can be interpreted to infer that this 15% demonstrates similar infiltration characteristics to those presented throughout section 7.1, therefore, the results of this study are representative of 15% of UK geology. However, this statistic can also be interpreted to show that 85% (206,120.75 km<sup>2</sup>) of the UK is non-clay textured; indicating that the low-end results derived throughout this study will likely be increased if applied to other areas of the UK (Folorunso and Aribisala, 2018; Anderson *et al.*, 2020). Infiltration may be higher, and differing trends may be identified regarding seasonality and woodland maturity (Zhang *et al.*, 2019a; Xie *et al.*, 2020). This highlights the wider applicability of the collected data, emphasising the impact of

study results and proving the applicability of the methodology to other areas across the UK. This also presents an opportunity for this research to be extrapolated and applied to other geologies and soil textures, to potentially aid in justifying the use of woodland planting as a method of NFM.

#### *8.2.3.2 Perceptions of Woodland*

The above sections have focussed primarily on the hydrological implications of woodland planting (infiltration, soil, antecedent conditions, and interception), however the additional benefits of woodland planting (as introduced in section 2.3) should be highlighted. Woodland is beneficial to the oxygen cycle as it absorbs and stores CO<sub>2</sub>, and recirculates O<sub>2</sub>, they are amenable, and they create and preserve habitats for fauna and flora (Lacob *et al.*, 2014; Ellison *et al.*, 2017; Forestry Commission, 2018). These benefits in addition to the presented results regarding the impacts of tree planting on soil porosity, infiltration, and interception (sections 8.1, 8.2.1 and 8.2.2) indicate woodland to be an ‘ideal’ method of NFM (Burgess-Gamble *et al.*, 2018; Hankin *et al.*, 2018; Dittrich *et al.*, 2019; Tzioutzios and Kastridis, 2020; Ellis *et al.*, 2021; Murphy *et al.*, 2021). However, when considering the ways in which woodland planting is often presented and conveyed by relevant authorities (DEFRA, The UK Government, EA) - the extensive benefits are often overshadowed and reduced-down to the ‘need’ for woodland to sequester CO<sub>2</sub> considering a changing climate. This is emphasised in recent documentation published by the UK Government: the England Trees Actions Plan 2021-24 (UK Government, 2021a), and the Path to Net Zero (Climate Assembly UK and House of Commons, 2020) Roadmap. Both documents emphasise the need to plant woodland for carbon sequestration and biodiversity, however neither mention the need to plant woodland for their hydrological benefits, as has been the focus throughout this study. The emphasis on woodland CO<sub>2</sub> storage and removal may be the influence of increasing public interest and understanding of the effects and influences of climate change (Taylor *et al.*, 2014; Whitmarsh and Capstick, 2018; Hasan

and Kumar, 2019). Public interest and understanding of local climate change is changing, and this has been accelerated in the UK through the observed changes in flood frequency and severity (the flash-floods of summer 2021, see Chapter 1) and increased news coverage of climate related issues (referring to the summer flooding in Germany (Bosseler *et al.*, 2021) and the COP26 climate assembly (for example, BBC News, (2021)). Public understanding may be influencing the government to tailor new climate policies at reducing and sequestering CO<sub>2</sub> to resonate with public understanding, making the policy more favourable. An additional reason for this may also be to ‘sell’ the idea of woodland planting only for its benefits in CO<sub>2</sub> sequestration, however, to not explain the additional benefits of woodland planting (particularly when they are of direct impact in light of climate change) is interesting. Overall, it seems few policy documents investigate or present all benefits of woodland planting (the hydrological factors investigated throughout this project), and place emphasis on the carbon sequestration potential. The findings derived throughout this chapter indicate that woodland planting is valuable as a method of NFM due to its ability to increase nearby infiltration and subsequent storage (section 8.1). Additionally, woodland planting is predicted to mitigate future flows from the HofE site in comparison to grassland and impermeable surfaces (section 8.2.2). These findings can be used to inform upcoming and existing UK woodland and environmental policy, and evidence that woodland planting is hydrologically valuable, in addition to the currently emphasised benefits of carbon sequestration. It is understood by organisations such as the EA and the Forestry Commission that woodland planting is overall beneficial regardless of the planting motive (as was discussed at the EA/HofE feedback presentation, section D.1). However, it seems unnecessary to overlook the hydrological benefits from new documentation and policy supporting the increase in tree planting (Climate Assembly UK and House of Commons, 2020; UK Government, 2021a) only focus on CO<sub>2</sub> and biodiversity – instead, the hydrological benefits that come hand-in-hand with all other advantages should be included. A reason for the lack of emphasis regarding the hydrologic

benefits of trees may be the lack of empirically based studies in the UK, or a lack of long-term investigations in to the useability of woodland for future climate change (Nicholson *et al.*, 2019; Black *et al.*, 2021; Ellis *et al.*, 2021; Revell *et al.*, 2021). Numerous studies exist both nationally and internationally, proving that tree planting is beneficial to carbon sequestration (Carrick *et al.*, 2019; Fletcher *et al.*, 2021); however, few studies have empirically tested the impacts of woodland planting on infiltration over sustained periods. Ongoing woodland planting case studies do exist in the UK, however infiltration nor interception are ever the sole focus, and these parameters are often inferred through rainfall/runoff relationships (Kirby *et al.*, 1991; Birkinshaw *et al.*, 2014; Marshall *et al.*, 2014). The aforementioned lack of empirically based infiltration studies may be the reason that carbon sequestration is made the primary focus of emerging policy, and more data needs to be collected regarding tree hydrology to reinforce its importance as a method of NFM (Carrick *et al.*, 2019). However, regardless of the circumstances for planting, woodland is positive on multiple fronts (section 2.3) and the findings of this study further demonstrate that the 25-year Environment Plan (HM Government, 2018), the England Trees Action Plan 2021 – 2024 (UK Government, 2021a) and the Woodland for Water scheme (GOV.UK *et al.*, 2019) will be beneficial for flood risk reduction. Furthermore, the findings of this study also demonstrate the value of mature trees on hydrological processes, bolstering the recent amendments to the Environment Act, offering more protection to mature woodland (UK Government, 2021b). The implications and recommendations of this study are discussed in greater detail throughout Chapter 9.

The findings of aims 1 and 3 (Chapter 7) indicate that woodland planting is valuable as a method of NFM due to its ability to increase nearby infiltration and subsequent storage. Additionally, it is shown that whilst woodland is not reducing peak flow and total discharge in comparison to grassland at present, the effects will be more significant in the future throughout both summer and winter. The applications of these findings have been discussed in the context

of UK policy above, but these findings can also be used to inform international policy regarding tree planting and NFM (see section 9.1.5).

#### *8.2.4 Summary of Aim 3 Findings*

Aim 3 was to use the calibrated HEC-HMS model to simulate hydrology from the HofE site dependent on changing storm intensity, duration, land cover, tree maturity and climate change; and determine to what extent HofE woodland planting has influenced discharge. This section summarises the findings of objectives 3a, 3b and 3c.

The collected infiltration data, discussed throughout section 7.1, has shown that tree planting does influence infiltration. Coupling the present-day field data with the hydrological model has produced results indicating that, whilst woodland can increase infiltration at the 10 cm proximity in comparison with the 200 cm proximity, grassland still shows greater reductions in peak flow and total discharge (section 7.2). It is discussed in sections 8.1 and 8.2.1 that the influences of antecedent rainfall and varying soil textures of the control in comparison to the sample sites were likely the primary influence of these findings. Aside from the discussed discrepancies in soil texture, the present-day modelled results demonstrate that the mitigative influences of younger woodland are second-to grassland at this scale. However, considering the discussions in section 8.1 regarding the influence of maturity on infiltration, and the literature-wide acknowledgement that tree root systems increase infiltration over time, it is likely that woodlands will become more hydrologically impactful in future. This was demonstrated throughout the modelled projections.

Modelled projections are presented and discussed in sections 7.3 and 8.2.2. The projections are promising from a FRM perspective as they show that trees can mitigate peak flows and total discharge when their maximum growth, and subsequent root spread/infiltration is attained. The results are less prominent throughout winter, and it is discussed in (section 8.2.2) that this is likely a result of site conditions during winter infiltration data collection; however, summer

values show woodland to be promising into the future, taking into account the projected increase in precipitation (section 5.7.1). Section 8.2.3 evaluates the effectiveness and wider applications and considerations of woodland planting as a method of NFM.

## **Chapter 9 Implications and Recommendations for Stakeholders**

This section will discuss the implications of the study results with regards to the HofE forest, the forestry industry, the construction industry, and DEFRA policy. This section will also make recommendations, where fitting, based on the results and discussions presented throughout Chapter 7 and Chapter 8.

### **9.1 Aim 4: The Implications, Applications and Recommendations of Study Findings**

The following sections focus on the specific applications impacts and recommendations of this study regarding the HofE Forest Charity, the construction industry, the forestry (woodland) industry and current and future flood risk management policy, specifically policy relating to DEFRA and the EA.

#### **9.1.1 The Heart of England Forest**

The findings of this study can instil a level of confidence in the methods and mentality of tree planting adopted by the HofE forest. The study results have proven that the work they are doing is positively influencing infiltration, reducing flood risk, and is expected to carry on influencing hydrology into the future. Additionally, the HofE forest have been working towards their goal of creating 12,140 hectares of new woodland (section 4.1.1) (The Heart of England Forest Charity, 2020, 2021), and have ‘accidentally’ been improving infiltration and changing local hydrology as a by-product. This can be used to evidence how easy (and altogether beneficial) tree planting can be across any scale, particularly when considering that 85% of the UK hosts a more permeable soil texture than the study site (section 8.2.3.1). To maximise infiltration and hydrological impact, that the HofE forest could consider planting in a lattice pattern with no tree more than 200 cm from the next in all directions (this is discussed in greater detail in section 9.1.3). This would ensure infiltration in all directions around the tree would be at a

maximum, and would be of use should the charity want to profit from lumber sales. However, this would never be considered (at present) by the HofE forest, as their primary intention is to plant woodland to create a continuous forest, and for the benefit of public amenity and biodiversity (see section 4.1.1).

### 9.1.2 Woodland and Construction

Development and increased impermeable surfaces significantly alter the hydrology of an area and seal-off once permeable areas, excluding them from participating in infiltration processes (Chandler *et al.*, 2018; Chappell *et al.*, 2018; Cooper *et al.*, 2021; Julich *et al.*, 2021; Murphy *et al.*, 2021; Patra *et al.*, 2022). However, paragraph 180 c) of the National Planning Policy Framework (NPPF) 2021 (Ministry of Housing Communities & Local Government, 2021) states that development where the deterioration of ancient or veteran trees is a possibility should be refused unless there are wholly exceptional reasons. The NPPF defines an exceptional reason as ‘where a need for affordable housing is identified’, however stresses that a suitable compensation strategy must exist. Such strategies could include the translocation (movement) or felling-and-replanting of trees in a new location. As they grow, tree roots encroach into the surrounding soil, increasing its porosity, permeability and subsequent infiltration – this has been demonstrated and discussed throughout sections 2.3.1, 7.1 and 8.1 (Chappell *et al.*, 2018; Cooper *et al.*, 2021; Julich *et al.*, 2021; Murphy *et al.*, 2021; Patra *et al.*, 2022). Infiltration increases as proximity to the tree decreases; infiltration is also influenced by maturity, with fully established trees (trees that have been in-situ long enough to reach their maximum height and age) showing greater infiltration compared with younger woodlands (section 7.1). It is discussed throughout sections 2.5 and 8.1, that soil texture and structure have an overarching influence on infiltration, with more clayey soils inheriting lower permeability and subsequent infiltration compared with sandier soils (Jarvis, 2007; Scholl *et al.*, 2014; Folorunso and Aribisala, 2018). These influences, combined with the influences of woodland

maturity on infiltration, are significant when discussing the actual usefulness of felling or translocating/re-planting trees to a new location to make way for development. Replanted and translocated trees will not have a comparable moderating impact on flood risk compared with the felled mature trees, as younger trees have not yet developed the root systems nor influenced surrounding infiltration rates to the likely extent they will with maturity (Archer *et al.*, 2016; Song *et al.*, 2018; Zhang *et al.*, 2019a, 2020). This is demonstrated throughout section 7.1, where the 10 cm proximity mean is consistently greater than the 200 cm mean (Hynynen *et al.*, 2010; Archer *et al.*, 2013; Cooper *et al.*, 2021). Additionally, the removal and translocation of mature woodland is detrimental to the effects of interception. If a tree is removed, interception loss is no longer a factor, meaning more rainfall reaches ground surface to contribute to infiltration and overland flow (Deng *et al.*, 2020; Xie *et al.*, 2020; Kitsikoudis *et al.*, 2021). The significance of interception loss is demonstrated throughout present-day and future simulations (sections 7.2 and 7.3), showing that summer models demonstrate a lower total discharge compared with winter simulations. This is discussed throughout sections 5.6.2 and 5.7.1, and is due to the deciduous sample trees growing leaves in the winter, and shedding them throughout the summer (Komatsu *et al.*, 2011; Klamerus-Iwan, 2015; Cerdà *et al.*, 2021). In addition, removing or translocating trees can be detrimental to carbon sequestration, which is something the UK Government are trying to alleviate through woodland planting (UK Government, 2021a).

The findings of aim 1 show that mature trees are beneficial to their surrounding hydrology (infiltration, interception), however need time to reach their full hydrological potential (Chappell *et al.*, 2018; Cooper *et al.*, 2021; Julich *et al.*, 2021; Murphy *et al.*, 2021; Patra *et al.*, 2022). This indicates that the removal and replanting / translocations of trees in the wake of construction is hydrologically detrimental to an area, which supports the wording of the NPPF (Ministry of Housing Communities & Local Government, 2021), suggesting that ancient or veteran trees (defined in annex 2: glossary of the NPPF 2021) should not be disturbed or

removed during construction unless exceptional circumstances are met and a compensation strategy exists. However, sometimes permission can be given to large-scale construction projects regardless of the damage posed to ancient woodland, one example of note is High-Speed 2 (HS2).

HS2 aims to connect London, Birmingham, Nottingham and Manchester through 330 miles of new high-speed rail track (HS2, 2021a). It is hoped that HS2 will contribute towards the UK Governments' goal of achieving net zero carbon emissions by 2050 across all sectors (GOV.UK, 2021). However, whilst HS2 promises to be an essential tool in reducing air pollution and CO<sub>2</sub> emissions, some methods employed in its construction could be seen to be against the promoted environmental ethos (Razzaque and Lester, 2021). The Woodland Trust (2022) highlight that 51 areas of ancient woodland (established for over 1600 years (Ministry of Housing Communities & Local Government, 2021)) will be removed/partially removed to make way for the line, and a further 39 will be indirectly affected (disturbance/noise/pollution). The removal of ancient woodland is against the suggestions of paragraph 180 c) of the NPPF, however, whilst the removal of ancient woodland still looks inevitable for the construction of HS2, the project has set up a ~£1.2m 'Woodland Fund' to plant 7 million new trees (33 km<sup>2</sup>) along the route from the West Midlands to London. As of the 5<sup>th</sup> July, the project had planted 700,000 of these trees (in addition to new areas of grassland, ponds and wetlands) over 118 sites, including Finham Brook, Stoneleigh Park and South Cubbington Wood in Warwickshire, and Bernwood in Buckinghamshire (HS2, 2021b). Regardless, the removal of ancient woodland and their replacement with new saplings will not have the same level of hydrological mitigation for some time (Kay *et al.*, 2019; Wingfield *et al.*, 2019; Ferguson and Fenner, 2020a; Ellis *et al.*, 2021).

### 9.1.3 Woodland Management Practice: Planting, Felling and Woodland Structure

As discussed in section 4.1.1, the HofE forest do not plant new areas of woodland in any pre-determined pattern, nor do they harvest their woodland; however, the results presented in section 7.1 can be applied to organisations that do. Coppicing is the process of felling trees at their base, and is desirable compared with felling and replanting as coppiced trees develop similar root systems to those of more mature trees, making regrowth quicker (2-25 years) (Collentine and Futter, 2018; Siegmeier *et al.*, 2019; Hepner *et al.*, 2020; Tullus *et al.*, 2020). The collected infiltration data (section 7.1) shows that at all sample sites (aside from 2020 in the winter), infiltration was greater at the 10 cm proximity compared with the 200 cm proximity, and from this, it can be derived that there is a gradual decrease in infiltration as distance away from the tree increases (section 7.1). Considering this and the already largely employed woodland management method of coppicing (to maximise lumber production and minimise growing times), it can be deduced that planting woodland in a lattice pattern could maximise a wooded areas overall infiltration (this is briefly outlined with reference to the HofE forest in section 9.1.1). Planting in a lattice pattern would capitalise on what is known about the lateral spread of roots (Perry, 1982; Crow, 2005; Day and Wiseman, 2009; Myking *et al.*, 2011; Alani and Lantini, 2020), and over time, the roots of woodland planted in this pattern would form a ‘mat’ of roots under the soil surface. Coppicing a tree forces the root system to continually grow and develop as if the tree is maturing, regardless of felling (Siegmeier *et al.*, 2019), so the continual growth of the roots system coupled with the increase in infiltration with tree maturity (sections 7.1 and 8.1) would indicate that the ‘mat’ of roots would eventually break-up the surrounding soils increasing porosity, hydraulic conductivity and infiltration (Jarvis, 2007; Zhang *et al.*, 2017b, 2019a; Chandler *et al.*, 2018; Leung *et al.*, 2018; Malik *et al.*, 2019; Xie *et al.*, 2020; Guo *et al.*, 2021). For the forestry industry, this would maximise lumber production (as coppicing would be encouraged), whilst simultaneously making the entire woodland area more capable of mitigating heavy precipitation events, and maximising

flood risk mitigation (Lozano-Baez *et al.*, 2019; Ferguson and Fenner, 2020a). It is also suggested by Collentine and Futter (2018) that rotation times (the time from felling, through growth to harvesting) and required specialised harvesting machinery vary by species, broadening the horizons of how applicable this method could be to forestry and FRM.

So far, this section has outlined several key impacts as a direct result of the results presented in section 7.1. However, whilst lattice planting and coppicing would be beneficial to lumber production and the maximisation of infiltration (from an NFM perspective), there are limitations to be considered. For a lumber-production forest, planting in a lattice pattern with limited space between trees would increase disease susceptibility (Ashton and Kelty, 2018; Singer *et al.*, 2019), and the limited accessibility for heavy harvesting machinery would outweigh any hydrological benefit from the perspective of the forestry industry (Ballard, 2011; Al-Dousari *et al.*, 2019). Additionally, the compaction caused by vehicles and machinery travelling between the trees would influence the porosity induced through root-spread of latticed trees, defeating the purpose of planting for hydrological benefit (see section 2.5 on compaction). Moreover, planting in the rigid lattice structure would defer from the natural amenity of woodland, and the lack of sunlight reaching the forest floor would limit the growth of additional vegetation, influencing interception, additional infiltration, and biodiversity (all of which are main ambitions of NFM, section 2.2) (Ashton and Kelty, 2018; Singer *et al.*, 2019). Relating the discussed to the HofE forest, it is unlikely that they will invest in the discussed methods, as they do not correlate with their key values of wildlife, biodiversity and public enjoyment and engagement (section 4.1.1). For the HofE forest to peruse these recommendations in the interest of maximising infiltration: community planting days would stop and public access throughout HofE owned forests would be limited due to health and safety concerns, and the woodland areas would lose their abundant amenity and biodiversity potentials.

This section has discussed the ways in which woodland can be planted to maximise hydrological impact and infiltration. However, the usability of the methods proposed have shown to be mostly limiting to the public enjoyment of woodland areas and biodiversity, which are key values of the HofE forest. Limitations aside, whilst planting wooded areas purely in the interest of maximising infiltration and runoff reduction is mostly impractical for the reasons discussed above, the wider benefits of woodland planting on surrounding hydrology should be explored on a larger scale. The HofE forest do not intend to grow and harvest lumber, and the woodland planting they are doing is contributing to the local hydrology, more-so than doing nothing at all, and infiltration results and modelled projections show that they are contributing to the future climate resilience of the catchment.

#### 9.1.4 Department for Environment, Food and Rural Affairs (DEFRA) and the Environment Agency

The findings of this study are of particular interest to the Department for Environment, Food and Rural Affairs (DEFRA) and the Environment Agency (EA) as these organisations are due to become responsible for the selection and planting of woodland areas for the benefit of both flood risk reduction and CO<sub>2</sub> sequestration. Additionally, DEFRA and the EA are working cooperatively towards the Governments ‘Net Zero by 2050 plan’ and are already promoting schemes and policies regarding woodland planting (see section 2.4). Furthermore, the EA have a vested interest in NFM research, and are undertaking NFM projects throughout the UK to test the feasibility of such approaches (see ‘case studies’ section of the GOV.UK *et al.*, (2021) website); the results presented throughout this study will aid in their justification of tree planting to stakeholders. The infiltration and future climate change projection elements of this project were of particular interest to the EA during the feedback presentation (appendix D.1), quoting that future work could involve turning these results into an ‘off-the-shelf’ saleable

product. This section introduces more specific DEFRA policy and schemes and highlights the impacts and recommendations of this work on such schemes.

#### *9.1.4.1 The Environment Act (2021)*

The Environment Act (UK Government, 2021b) aims to improve air and water quality, tackle waste, improve biodiversity and make other positive changes to the way the environment is handled. With regards to trees, the most recent revisions to the environment act included additional protection to established trees, stating that the unnecessary or illegal felling of trees could result in prosecution or fines (UK Government, 2021b).

The findings of this study, particularly those indicating that trees influence infiltration more-so as they mature, support the recent amendments to the environment act. It is discussed throughout Chapter 8 that mature(ing) woodland has the greatest influence on infiltration (in addition to positively influencing surrounding biological and ecological processes and public amenity), as the root systems have had ample time to develop and influence porosity and subsequent infiltration. Therefore, the increased protection warranted through the Environment Act will allow mature trees to remain throughout a catchment, and positively influence hydrological processes (infiltration) as they mature.

#### *9.1.4.2 The Agriculture Act (2020) and Environmental Land Management Schemes (ELMS)*

The Agricultural Act, introduced in 2020, is a post-Brexit alternative to the previously inefficient policy instated by the EU (Defra, 2020). The Act defines how land managers in England will be rewarded with public money for public goods, such as initiatives to improve air, soil and water quality, reduce flood risk and mitigate the adverse effects of climate change; applicable under the Environmental Land Management Scheme (ELMS) (Defra, 2020; The UK Government, 2020).

There are three defined ELMS (Defra and Rural Payments Agency, 2021):

- Sustainable farming schemes (launched in 2022) - comprised of a set of customisable and adoptable standards based on natural features (i.e., hedgerows, grassland), that govern how each should be managed. Payment is attained upon adhering to the standard management technique agreed upon.
- Local nature recovery schemes (piloting in 2022 and launching in 2024) – payment for actions that support and promote local nature recovery and environmental priorities. The added intention is to encourage collaboration between land owners, peers and the community.
- Landscape recovery schemes (piloting in 2022 and launching in 2024) – payment for long-term schemes that support landscape and ecosystem recovery, such as rewilding, large-scale tree planting, and peatland and saltmarsh restoration.

Throughout these schemes, land managers will be encouraged (and will be paid for) delivering and enhancing (e.g.): clean and plentiful water, clean air, thriving plants and wildlife, protection from environmental hazards, reduction of and adaptation to climate change, beauty, heritage and engagement with the environment. A seven-year transition period from the EU framework to the new agricultural system introduced by the Act began in 2021, and it is believed that these financial incentives will aid in achieving the goals of the government’s 25 Year Environment Plan (see section 9.1.4.3), and DEFRA’s commitment to reach net zero emissions by 2050 (see section 9.1.4).

When contextualising the results of this study with regard to the Agricultural act and ELMS, it can be suggested that this study has provided preliminary evidence that the ELMS will contribute to improving air, soil and water quality, reducing flood risk and mitigating the adverse effects of climate change. It is discussed throughout section 2.4 that woodland planting is seen to be beneficial from the perspective of carbon sequestration, biodiversity and ecology; and the positive hydrological influences of woodland planting (both present and future) are

presented and discussed throughout Chapter 7 and Chapter 8. The encouragement of land owners to implement management schemes to enhance the sustainability, biodiversity and carbon sequestration potential of their land will contribute towards the 25 Year Environment Plan (see section 9.1.4.3) and DEFRA's commitment to reach net zero emissions by 2050 (see section 9.1.4). Additionally, it is proven throughout section 7.1 that long-term schemes (such as those posed by the landscape recovery schemes), will improve infiltration and soil storage, reducing the likelihood and severity of flooding.

#### *9.1.4.3 DEFRA 25-Year Environment Plan (2018)*

As has been referred to in above sections, the 25-year environmental plan sets out the goals and philosophies of DEFRA for improving and future-proofing the environment through using more sustainable management methods (Defra, 2021). The plan sets out targets to aid in improving: air quality, water quality, encouraging wildlife and biodiversity, improved sustainability and encouraging methods of future climate resilience (Defra, 2021).

Woodland planting is mentioned numerous times throughout the 25-year plan, however the primary focus is in regards to increasing woodland coverage for the benefits of carbon sequestration and biodiversity. A recommendation of this study for consideration by the 25-year plan would be that woodland can should be viewed not only for the positive implications regarding the above points, but also from a hydrological perspective. Chapter 7 and Chapter 8 demonstrate and discuss that woodland planting can increase infiltration, and this combined with the increase in root-growth over time can be hydrologically beneficial in light of climate change. Therefore, a greater emphasis on this throughout the 25-year plan would allow for the hydrological implications of woodland planting to be further explored and quantified by academics and practitioners, and aid when justifying both the short and long-term hydrological (and other discussed (section 2.3)) benefits of woodland planting to stakeholders in light of a changing climate.

#### 9.1.4.4 England Trees Action Plan (2021 – 2024)

The England Trees Action Plan defines the current government's vision for extensive and opportunistic future woodland planting across England by 2050 and beyond. The plan details a framework for implementing the Nature for Climate Fund, and outlines over 80 policy actions the current government is taking to deliver these objectives (UK Government, 2021a).

The primary focus of the plan is to increase woodland coverage for the benefit of carbon sequestration, biodiversity, wildlife and public amenity; the hydrological benefits and flood risk mitigation potentials of trees, whilst featured, are not the focus of the document (UK Government, 2021a). However, the plan does detail how responsible authorities (DEFRA) should aim to support land owners with tree planting, and the benefits this can have from both the perspective of flood risk management, and ELMS payments (for the land owner) (section 9.1.4.2).

A recommendation to the action plan as a result of the results detailed and discussed throughout Chapter 7 and Chapter 8 is to increase the reference to literature supporting the use of woodland planting (as a method of NFM) to reduce the frequency and severity of flood events (Chandler *et al.*, 2018; Revell *et al.*, 2021, 2022). This would add further justification and applicability to woodland planting, and would enable other researchers to justify investigating the hydrological implications of woodland planting on infiltration and reducing flood severity. Providing enough future quantification regarding the hydrological advantages of woodland planting, this newfound data could be used when justifying the use of woodland as a method of NFM to reduce the frequency and severity of flooding (alongside the commonly noted advantages to biodiversity, public amenity, habitat creation and carbon sequestration).

### 9.1.5 International and Domestic Flood Risk Management Policy and NFM

UK policy regarding NFM, and tree planting have been introduced and discussed throughout sections 2.4, 8.2.3.2 and 9.1.1 - 9.1.4.4. The findings of this study (Chapter 7) can inform these policies, and support the use of tree planting as a method of NFM due to its multiple benefits, inclusive of the purely hydrological (section 8.2.3.2); however, the study findings also have international applications. On the 16<sup>th</sup> September 2021, the United States Army Corps of Engineers (USACE) published an international guide on using NFM (however referred to as Natural and Nature Based Features (NNBF), see Table 2.1) to aid international policymakers with the application and uses of such devices (Bridges *et al.*, 2021). Rijkswaterstaat – a department of the Dutch Ministry of Infrastructure and Water Management - aided in the development of the guide, and the UK Environment Agency were involved in the authorship of chapters, supplying 10 UK case study examples (Environment Agency, 2021c); the publication had over 4,200 downloads as of February 2022, showing that the sharing of NFM methods, case studies and knowledge is being capitalised upon internationally. Furthermore, the European Commission, (2011) have published guidance for member states regarding the benefits of NFM, and how NFM and NWRM (natural water retention methods, Table 2.1) can be integrated across a catchment to achieve ‘greener’ outcomes compared with conventional methods.

The international application of NFM methods is promising for the more widespread uptake of such methods, and now the findings of this study can be used to inform both UK policy and international policy with regards to the positive impacts of tree planting on hydrology, and their use as a method of NFM. With further developments and evidence emerging from around the UK regarding the benefits of NFM, including the results presented as part of this study, it is hoped that international collaborations and contributions to the international knowledge base will continue. With continued development and collaboration, NFM (and tree planting) will become common practice when mitigating the adverse effects of flooding and a changing

climate internationally, whilst simultaneously aiding in biodiversity, preservation, habitat creation and CO<sub>2</sub> sequestration.

#### 9.1.6 Summary of Aim 4 Findings

This section has discussed the findings and discussions of Chapter 7 and Chapter 8 in the context of its wider implications regarding the HofE forest, woodland and construction, and woodland management. Further to this, outcomes have been contextualised and recommendations been posed regarding current and future water policies and water-governing authorities, namely; DEFRA, the Agricultural Act, the 25-year plan, the England trees action plan, and other international policy.

The overarching conclusions of this section are that tree planting and woodland area creation are featuring more prominently in recent and upcoming policy. The ability of woodland to sequester carbon and improve biodiversity seem to be the main drivers (in light of climate change and the recent COP26 conference); however, more emphasis should be targeted towards the hydrological benefits of trees – as has been proven throughout this work. This study has shown that woodland planting can increase infiltration, improve soil porosity and increase catchment-water storage potential in forests (Chapter 7) – and this is only projected to increase in impact as trees mature, which will contribute towards mitigating the adverse effects of climate change. The inclusion and emphasis of the hydrological impacts of trees would aid in the further justification of large-scale and targeted tree planting, and would also have the effect of encouraging more research both from academia and the water industry. However, this being said, tree planting, as with many other methods of NFM (Kay *et al.*, 2019; Wells *et al.*, 2020; Ellis *et al.*, 2021), lacks empirical and quantifiable support, and whilst this study does quantify and present the hydrological benefits of trees for the study site, further research needs to be conducted to build the empirical body of knowledge before policy can encourage woodland for this benefit alone.



## Chapter 10 Conclusion

This chapter summarises the main research findings and reviews how and where the aims and objectives (section 1.3) were met. The contributions to knowledge are identified, as are any sources of error and opportunities for future work.

### ***10.1 Review of Aims and Objectives***

Aim 1 and the associated objectives determined the structure and methods for the collection of infiltration data and aim 2 determined how such data should be hydrologically modelled. Aim 3 compiled both field and modelled data to simulate the hydrological responses of the site both at present, and in the future, and then assessed the feasibility of woodland planting as a method of NFM. Aim 4 was to apply and contextualise the findings of this research to shareholders and policy, providing recommendations for both. The following sections conclude each aim individually.

#### ***10.1.1 Aim 1***

Aim 1 was to determine to what extent tree planting by the HofE forest has influenced infiltration regarding proximity and maturity. This was to be achieved through defining suitable sampling locations and methods for infiltration data collection (objective 1a) and using the collected data to derive any relationships (objective 1b).

The methodology for sample site selection, along with the finalised sample site locations are discussed throughout sections 5.2; as is information regarding the rationale for the use of MDI, infiltration data collection points and the interpretation of data. Section 7.1 presents and analyses the results of the collected infiltration data, showing that mean infiltration is higher at the 10 cm proximity compared with the 200 cm proximity by 75.87% in winter and 25.19% in summer. Further to this, 10 cm infiltration is 192% higher in summer compared with winter

and mean 200 cm infiltration is 310% higher in summer compared with winter. These results conclude that overall, the presence of the tree, and particularly the developing root system, is influencing infiltration through increasing soil porosity, allowing for soil-water storage and faster infiltration. Regarding the influence of tree maturity on infiltration, there is no evidence in the collected field data to suggest a correlation, however the *ca.*1900 site did continually show the highest infiltration (aside from at the 200 cm proximity in summer 2020/2021). The conclusions of this are discussed comprehensively throughout section 8.1, where it is determined that the reason for the lack of correlation is simply the young age of the sample trees.

The results collected show that tree planting does influence infiltration, and infiltration is higher at the 10 cm proximity compared with the 200 cm proximity. Whilst there is no obvious correlation between infiltration and maturity, these results contribute to the growing literature base regarding tree planting as a method of NFM.

The construction of the infiltration data collection methodology and the subsequent collection of infiltration data formed an imperative element of study result generation, which then allowed the production of both present-day and future hydrological models to be produced. The methods involved were also used in the development of an academic paper published by *Water MDPI* (appendix D.2.2).

### *10.1.2 Aim 2*

Aim 2 was to use HEC-HMS to build, calibrate, and validate two-separate hydrological models using spatial and hydrometric data collected from the study site. This was to be achieved through the fulfilment of objective 2a, requiring the construction, calibration, and validation of two hydrological models.

HEC-HMS was chosen for all hydrological modelling due to its common use in similar studies (Derdour *et al.*, 2018; Al-Mukhtar and Al-Yaseen, 2019; Joshi *et al.*, 2019; Rangari *et al.*,

2020), its reliability, and the supported ‘process models’ - allowing for the intricate representation of site hydrology based on the available input data (see sections 3.2.2.1.2 and 5.3.3). The model was constructed using multiple GIS methods to delineate the catchment, specify likely overland flow pathways, (manually) classify landcover, and define catchment and river geomorphology (these methods are compressively discussed throughout sections 4.2.2, 4.2.3 and 5.3.2). Representing study site hydrology through use of two models (summer and winter) allowed for more accurate representation of the seasonal variations in study site hydrology (which had been observed throughout data collection) (see section 5.4). Calibration was undertaken using empirical and simulated flow data from the study site; unobserved model variables were adjusted until consistent parameters could emulate empirical flow in all calibration storm events (see section 5.4 and appendix B.5.2). The winter and summer models both showed a calibration NSE of 0.65. The models were validated following a similar methodology to calibration however no parameters were adjusted; different storm events (varying by magnitude and duration) were selected, and the simulated and empirical outflows were observed. The validation NSE’s of winter and summer models are 0.87 and 0.44 respectively.

The construction, calibration and validation of the hydrological models formed an imperative element of study result generation, which then allowed the fulfilment of aim 3. The methods involved were also used in the development of an academic paper published by *Water* MDPI (appendix D.2.1).

### 10.1.3 Aim 3

Aim 3 was to simulate outflow from the HofE site dependent on changing storm intensity, duration, land cover, tree maturity and climate change; and determine to what extent HofE woodland planting has influenced runoff and flood risk. This was to be achieved through simulating the hydrological responses of the HofE study site to varying land cover, tree

maturity, storm duration and intensity (objective 3a). Using recent climate resources to predict the likely future changes to site hydrology regarding to developing tree maturity and climate change (objective 3b); and evaluating how valuable tree planting is as a method of NFM using both the empirical and simulated results of the study (objective 3c).

Present-day simulations of the HofE site show that woodland planting has reduced winter peak runoff compared to impermeable cover by a mean of 6%, 2% and 1% for 6-, 24- and 96-hour storms, and summer peak runoff by 48%, 18%, and 2.7% for 6-, 24-, and 96-hour storms (section 7.2). However, grassland simulations show the lowest peak flow, being 32%, 21%, and 10% lower than the current site in the winter, and 6%, 2%, and 0.5% lower than the HofE site in the summer for 6-, 24-, and 96-hour duration storms respectively. Although this contradicts what would maybe be expected (based on the literature, and the results of aim 1 showing woodland to increase infiltration), the soil texture of the grassland site was more-permeable, meaning a higher infiltration when extrapolated to the whole site in the model (this is discussed in section 8.2). These results can also be interpreted using the conclusions of aim 1, discussing that the sample trees are early in their development, and infiltration will likely surpass that of grassland over time; however, this is an area of future work (section 10.4). The methods and results involved in the present-day hydrological models have contributed towards the publication of a peer reviewed journal article in *Water MDPI* (see section D.2).

Results of the likely future changes to study site hydrology (section 7.3) were based on existing EA precipitation increase (due to climate change) information, infiltration data extrapolation, and baseflow projections (section 5.7). The modelled impacts of tree planting on infiltration and subsequent overland flow reduction were investigated, as an extension of the results derived regarding the current day impacts (objective 3a). Results showed that in winter, woodland is predicted to reduce peak flow and total discharge below that of grassland and woodland, however, will not reduce it below present-day simulated values (but does come close in 2070). The summer projections show similar results to winter (woodland with a lower peak

flow and total discharge compared with grassland and impermeable), however a significant difference is the reduction of woodland flow in 2070. The reduction is the result of HofE woodland maturing (see section 7.3.2.1). The results derived in fulfilment of objective 3b indicate that woodland is a valuable method of reducing the adverse hydrological effects of climate change (throughout the summer) once tree maturity is reached.

Objective 3c required the culmination of existing literature and the results of aims 1 and 3 to evaluate the value of tree planting as a method of NFM - this is discussed comprehensively throughout section 8.2.3 (see also sections 9.1.1, 9.1.3, 8.2 and 8.2.2). It is concluded that tree planting is a valuable method of NFM as it increases nearby infiltration and is projected to be useful at mitigating adverse hydrology as a result of climate change. However, it is discussed in section 8.2.3.2 that woodland (similarly to other methods of NFM) should not be used alone – it should be used in conjunction with other methods (NFM or conventional) to maximise effectiveness (Burgess-Gamble *et al.*, 2018; Wilkinson *et al.*, 2019; Xiao *et al.*, 2021). Woodland planting is advantageous from the perspectives of CO<sub>2</sub> mitigation, biodiversity, habitat creation and public amenity, and relevant authorities are beginning to encourage woodland creation in current and upcoming policy (summarised in section 10.1.4).

#### *10.1.4 Aim 4*

Aim 4 was to assess the implications of study findings, and provide recommendations and suggestions for relevant stakeholders and future policy; this was to be achieved in part through objective 4a, which required contextualising the findings of both aims 1 and 3 to provide recommendations and suggestions for relevant stakeholders and future policy.

This aim is fulfilled in detail through Chapter 9, where the results and key discussion topics of this study are used to assess and provide recommendations for; the HofE forest, the woodland and construction industry, and woodland management bodies. Additionally, current and future

policy is discussed with regard to the findings of this study, namely; DEFRA, the Agricultural Act, the 25-year plan, the England trees action plan, and other international policy.

In summary of aim 4, it is concluded that whilst woodland planting is beginning to feature more prominently in recent and upcoming policy for the ability to sequester carbon and improve biodiversity, there is little reference to the influence that woodland can have on reducing flood severity. It is unsurprising that policies regarding woodland planting are tailored towards their climate mitigation potential, as some were published ahead of / slightly after the COP26 conference, additionally, the public are more aware of the impacts of climate change, so tailoring policies to these audiences will rally support. Recommendations as a result of Chapter 7, Chapter 8 and Chapter 9 of this study to organisations, governing bodies, and policymakers in the water industry, is to focus on increasing the publicization of the benefits of woodland planting on infiltration increase and flood risk. This will allow for greater understanding of the hydrological benefits of woodland planting (in addition to the alternatives previously mentioned), and will encourage more research regarding the quantification and implementation of woodland planting as a method of NFM. It is noted in section 2.2.3 that NFM (inclusive of woodland planting) struggles with a lack of empirical evidence (Kay *et al.*, 2019; Wells *et al.*, 2020; Ellis *et al.*, 2021), so encouraging further research is both an outcome of this study, and a recommendation to those in the water industry.

## **10.2 Contributions to Knowledge**

The research methods, hydrological modelling and derived results of this study have contributed to the current state of knowledge regarding the use of trees as a method of NFM. This study has shown that tree planting increases nearby infiltration, showing that the tree is influencing the permeability and influencing porosity. No correlation between infiltration and tree maturity was detected, however, the sample trees are still early in development, and a correlation may be identifiable in future years (discussed throughout section 8.1). These

findings are significant when applied to the handling of trees during construction (section 9.1.2), and how woodlands can be managed to maximise infiltration (section 9.1.3). Additionally, these findings support the recent Governmental policy shift towards increasing tree planting (see section 2.4) and show that there are positive hydrological implications also (in addition to the CO<sub>2</sub> sequestration). The impacts of this work have been discussed with respect to flood risk management policy, the HofE Forest Charity, the forestry industry, the construction industry, and DEFRA and the Environment Agency in Chapter 9.

An additional contribution of this study is the methodologies employed throughout infiltration data collection, and hydrological model calibration and validation. As discussed in sections 3.1.2 and 5.2.2.1, one of the many advantages of the MDI compared with ring-infiltrometer methods is the opportunity for replication. This study has demonstrated that similar studies to this one (requiring continuous replicable infiltration data collection) are achievable through use of the instrument, and such information has been published as a result of this work (section D.2.2). Useable academic guidance on the specific processes of model calibration and validation is sparse, therefore the full disclosure and explanation of these processes throughout sections 5.4 and 5.5 can be used by other authors wishing to calibrate and validate hydrological models. Both the use of the MDI and the thorough explanation of model calibration and validation enable other authors to use this project as a framework when contributing to the knowledge base regarding infiltration, NFM, woodland planting, and hydrology as a whole.

The method of infiltration projection (section 5.7.2) has provided a framework for other authors to project the likely changes to infiltration in the future, using empirical values and published literature regarding the maturity ages of sample trees. Additionally, the resultant hydrological projections (section 7.3) can be used to support the hydrological benefits of woodland planting in future years (accounting for climate change) when presenting to stakeholders; and an element of future research is to develop these projections further. The projections were of particular interest to the EA, during the feedback presentation, see section D.1.

Chapter 9 highlights the various contributions and recommendations of this work to organisations and industries of interest (the HofE forest, the woodland and construction industry, and woodland management bodies), and current and future policy (DEFRA, the Agricultural Act, the 25-year plan, the England trees action plan, and other international policy). The findings of this study support the current drive to increase woodland cover, however it is recommended that future policies focus on increasing the publicization of the benefits of woodland planting on infiltration increase and flood risk. In turn, this would allow for greater understanding of the hydrological benefits of woodland planting, and would encourage more research regarding the quantification and implementation of woodland planting as a method of NFM, contributing to the known knowledge gap in this area.

In addition to the contributions, the methods and results of this project have been continually fed-back into the academic and practitioner community through use of posters, presentations, conferences, and peer reviewed publications. These can be seen in Appendix D.

### ***10.3 Limitations and Sources of Uncertainty***

The following factors have been identified as having a potential influence on the study results

#### ***10.3.1 Data and Data Collection***

It is discussed in section 3.1.2 that vegetation was removed from all MDI measurement areas prior to collection. It is possible that this process may have influenced the accuracy of infiltration measurement, i.e., more precipitation was reaching the soil surface from this moment forward due to there being no surface vegetation to intercept incoming rain. This may have influenced the saturation of the collection points (mainly through winter); however, this would have been negligible. Additionally, vegetation removal is a pre-requisite for ring-infiltrometer methods (Eijkelkamp, 2015), so vegetation removal would have been a limitation with any infiltrometer method.

Mentioned in section 5.2.2.1. Infiltration data was not collected between the 24<sup>th</sup>-March-2020 and the 1<sup>st</sup> of July 2020 due to both UK Government and Coventry University restrictions regarding travel during the COVID-19 pandemic. This resulted in 15 sample days being missed (348 individual infiltrometer collection points) from the beginning of summer 2020 data collection, and this caused the mean summer infiltration (section 5.4) to be based on one year of collection (2021) compared with two. Whereas this limitation was unavoidable, it is worth considering as a potential influencing factor on infiltration results.

### *10.3.2 Methods and Modelling*

The first methodological limitation regards how unobserved infiltration data was predicted for the hydrological modelling of the study catchment. These values were calculated by using the median of observed values (see section 5.6.3) and this method may have over/underestimated infiltration for unobserved sites. Whilst this may have influenced model output, it is important to consider the lack of literature regarding specific infiltration rates for wooded areas, and that the models were calibrated and validated by this point – indicating that they could replicate empirical study site hydrology (see sections 5.4 and 5.5). Additionally, this section of the methodology has been peer reviewed and published (see appendix D.2) showing its overall acceptability.

On a similar note, there are limitations regarding the methods used to project infiltration for future hydrological projections of the site. It is comprehensively discussed throughout section 5.7.2 that existing literature and tree maturity was used to determine the rate of infiltration increase; however, it should be noted that trees do not grow uniformly, and their growth is influenced by numerous internal and external factors (section 2.3.1) (Dobson, 1995; Crow, 2005; Jarvis, 2007; Guo *et al.*, 2021). Whilst this may be the case, statistical testing (appendix C.1) showed the chosen method was the only one to show a positive infiltration increase over

time, and it was based on empirical data. Regardless, the output projections present a method that can be refined and adopted by other authors and is of interest to the EA (Appendix D.1).

#### **10.4 Further Work and Recommendations**

The methods and results used throughout this study have highlighted areas of potential future research. The first area being the application of this studies' methodology to other similar sized catchments (both in the UK, or internationally), however with differing soil texture. A study of this nature would add further evidence to what has been derived throughout this study regarding tree planting and infiltration and would add further context regarding different impacts dependent on soil texture. Secondly (as discussed in section 8.2.4), further research could be undertaken to refine and expand the climate projections presented throughout section 7.3. This could involve sampling more trees in different areas of the UK and would help in delivering a saleable tool for tree planting (as wished by the EA, see appendix D.1). Furthermore, from an academia perspective, information regarding the processes involved in model calibration and validation should be more readily available for authors looking to undertake their own hydrological simulations. It was found throughout this project that calibration and validation is referred to a great deal in modelling studies, however there is very little specific information on the process involved.

## Chapter 11 References

- Abdessamed D, Abderrazak B. 2019. Coupling HEC-RAS and HEC-HMS in rainfall–runoff modeling and evaluating floodplain inundation maps in arid environments: case study of Ain Sefra city, Ksour Mountain. SW of Algeria. *Environmental Earth Sciences* **78** (19): 586 DOI: 10.1007/s12665-019-8604-6
- Aboudourib A, Serhir M, Lesselier D. 2021. A Processing Framework for Tree-Root Reconstruction Using Ground-Penetrating Radar under Heterogeneous Soil Conditions. *IEEE Transactions on Geoscience and Remote Sensing* **59** (1): 208–219 DOI: 10.1109/TGRS.2020.2993719
- Adekanmbi AA, Shaw LJ, Sizmur T. 2020. Effect of Sieving on Ex Situ Soil Respiration of Soils from Three Land Use Types. *Journal of Soil Science and Plant Nutrition* **20** (3): 912–916 DOI: 10.1007/s42729-020-00177-2
- Adeloye AJ, Dau Q V. 2019. Hedging as an adaptive measure for climate change induced water shortage at the Pong reservoir in the Indus Basin Beas River, India. *Science of The Total Environment* **687**: 554–566 DOI: 10.1016/j.scitotenv.2019.06.021
- Afshari S, Tavakoly AA, Rajib MA, Zheng X, Follum ML, Omranian E, Fekete BM. 2018. Comparison of new generation low-complexity flood inundation mapping tools with a hydrodynamic model. *Journal of Hydrology* **556**: 539–556 DOI: 10.1016/j.jhydrol.2017.11.036
- Ahmadian R, Falconer RA, Wicks J. 2018. Benchmarking of flood inundation extent using various dynamically linked one- and two-dimensional approaches. *Journal of Flood Risk Management* **11**: S314–S328 DOI: 10.1111/jfr3.12208
- Aksoy H, Wittenberg H. 2011. Nonlinear baseflow recession analysis in watersheds with intermittent streamflow. *Hydrological Sciences Journal* **56** (2): 226–237 DOI: 10.1080/02626667.2011.553614
- Al-Dousari AM, Alsaleh A, Ahmed M, Misak R, Al-Dousari N, Al-Shatti F, Elrawi M, William T. 2019. Off-Road Vehicle Tracks and Grazing Points in Relation to Soil Compaction and Land Degradation. *Earth Systems and Environment* **3** (3): 471–482 DOI: 10.1007/s41748-019-00115-y
- Al-Mukhtar M, Al-Yaseen F. 2019. Modeling water quality parameters using data-driven models, a case study Abu-Ziriq marsh in south of Iraq. *Hydrology* **6** (1) DOI: 10.3390/hydrology6010021
- Alagna V, Bagarello V, Di Prima S, Giordano G, Iovino M. 2016. Testing infiltration run effects on the estimated water transmission properties of a sandy-loam soil. *Geoderma* **267**: 24–33 DOI: 10.1016/j.geoderma.2015.12.029
- Alani AM, Lantini L. 2020. Recent Advances in Tree Root Mapping and Assessment Using Non-destructive Testing Methods: A Focus on Ground Penetrating Radar. *Surveys in Geophysics* **41** (3): 605–646 DOI: 10.1007/s10712-019-09548-6
- Alfieri L, Laio F, Claps P. 2008. A simulation experiment for optimal design hyetograph selection. *Hydrological Processes* **22** (6): 813–820 DOI: 10.1002/hyp.6646
- Alvarez-Uria P, Körner C. 2007. Low temperature limits of root growth in deciduous and evergreen temperate tree species. *Functional Ecology* **21** (2): 211–218 DOI: 10.1111/j.1365-2435.2007.01231.x
- Alvesson M, Skoldberg K. 2009. *Reflexive Methodology: New Vistas For Qualitative Research*. SAGE: London, UK.
- Anderson RL, Brye KR, Wood LS. 2020. Landuse and soil property effects on infiltration into Alfisols in the Lower Mississippi River Valley, USA. *Geoderma Regional* **22**: e00297 DOI: 10.1016/j.geodrs.2020.e00297

- Annis A, Nardi F, Petroselli A, Apollonio C, Arcangeletti E, Tauro F, Belli C, Bianconi R, Grimaldi S. UAV-DEMs for Small-Scale Flood Hazard Mapping
- Annis A, Nardi F, Volpi E, Fiori A. 2020. Quantifying the relative impact of hydrological and hydraulic modelling parameterizations on uncertainty of inundation maps. *Hydrological Sciences Journal* **65** (4): 507–523 DOI: 10.1080/02626667.2019.1709640
- Archer NAL, Bonell M, Coles N, MacDonald AM, Auton CA, Stevenson R. 2013. Soil characteristics and landcover relationships on soil hydraulic conductivity at a hillslope scale: A view towards local flood management. *Journal of Hydrology* **497**: 208–222 DOI: 10.1016/j.jhydrol.2013.05.043
- Archer NALL, Otten W, Schmidt S, Bengough AG, Shah N, Bonell M. 2016. Rainfall infiltration and soil hydrological characteristics below ancient forest, planted forest and grassland in a temperate northern climate. *Ecohydrology* **9** (4): 585–600 DOI: 10.1002/eco.1658
- Aricò C, Filianoti P, Sinagra M, Tucciarelli T. 2016. The FLO diffusive 1D-2D model for simulation of river flooding. *Water (Switzerland)* **8** (5) DOI: 10.3390/w8050200
- Asadi H, Shahedi K, Jarihani B, Sidle RC. 2019. Rainfall-runoff modelling using hydrological connectivity index and artificial neural network approach. *Water (Switzerland)* **11** (2) DOI: 10.3390/w11020212
- Ashton MS, Kelty MJ. 2018. *The Practice of Silviculture: Applied Forest Ecology*. John Wiley and Sons: Hoboken, NJ, USA.
- Avery BW. 1973. Soil Classification in the Soil Survey of England and Wales. *Journal of Soil Science* **24** (3): 324–338 DOI: 10.1111/j.1365-2389.1973.tb00769.x
- Avery LM. 2012. Rural Sustainable Drainage Systems (RSuDS). Bristol. Available at: [https://assets.publishing.service.gov.uk/government/uploads/system/uploads/attachment\\_data/file/291508/scho0612buwh-e-e.pdf](https://assets.publishing.service.gov.uk/government/uploads/system/uploads/attachment_data/file/291508/scho0612buwh-e-e.pdf)
- Baddeley AJ. 2019. Spatial sampling and censoring. In *Stochastic Geometry* Routledge; 37–78. DOI: 10.1201/9780203738276-2
- Bagarello V, Sgroi A. 2004. Using the single-ring infiltrometer method to detect temporal changes in surface soil field-saturated hydraulic conductivity. *Soil and Tillage Research* **76** (1): 13–24 DOI: 10.1016/j.still.2003.08.008
- Bagarello V, Baiamonte G, Castellini M, Di Prima S, Iovino M. 2014. A comparison between the single ring pressure infiltrometer and simplified falling head techniques. *Hydrological Processes* **28** (18): 4843–4853 DOI: 10.1002/hyp.9980
- Baiamonte G. 2019. SCS Curve Number and Green-Ampt Infiltration Models. *Journal of Hydrologic Engineering* **24** (10): 04019034 DOI: 10.1061/(ASCE)HE.1943-5584.0001838
- Bajjali W. 2018. Watershed Delineation. In *ArcGIS for Environmental and Water Issues* Springer International Publishing; 235–245. DOI: 10.1007/978-3-319-61158-7\_14
- Ballard CE. 2011. The role of physics based models for simulating runoff responses to rural land management scenarios. *Department of Civil and Environmental Engineering*: 340
- Bark RH, Martin-Ortega J, Waylen KA. 2021. Stakeholders’ views on natural flood management: Implications for the nature-based solutions paradigm shift? *Environmental Science and Policy* **115** (October 2020): 91–98 DOI: 10.1016/j.envsci.2020.10.018
- Barthélémy S, Ricci S, Morel T, Goutal N, Le Pape E, Zaoui F. 2018. On operational flood forecasting system involving 1D/2D coupled hydraulic model and data assimilation. *Journal of Hydrology* **562** (July 2017): 623–634 DOI: 10.1016/j.jhydrol.2018.05.007
- Bátková K, Miháliková M, Matula S. 2020. Hydraulic properties of a cultivated soil in temperate continental climate determined by mini disk infiltrometer. *Water (Switzerland)* **12** (3): 1–21 DOI: 10.3390/w12030843
- BBC News. 2019. South Yorkshire flooding: Defences ‘reduce impact’ Available at: <https://www.bbc.co.uk/news/uk-england-south-yorkshire-50345553> [Accessed 11 May 2022]

- BBC News. 2021. COP26 News. COP26 Available at: <https://www.bbc.co.uk/news/topics/cgdwpywgeegt/cop26> [Accessed 20 December 2021]
- Beddoes DW, Booth CA, Lamond JE. 2018. Towards complete property-level flood protection of domestic buildings in the UK. *WIT Transactions on the Built Environment* **184**: 27–38 DOI: 10.2495/FRIAR180031
- Bennett TH, Peters JC. 2004. Continuous soil moisture accounting in the Hydrologic Engineering Center Hydrologic Modeling System (HEC-HMS). *Joint Conference on Water Resource Engineering and Water Resources Planning and Management 2000: Building Partnerships* **104** (1): 1–10 DOI: 10.1061/40517(2000)149
- Betsholtz A, Nordlöf B. 2017. Potentials and limitations of 1D, 2D and coupled 1D-2D flood modelling in HEC-RAS A case study on Hölje river. *Lund University*: 128 DOI: 10.1016/S0300-9440(03)00139-5
- Beven K. 2004. Robert E. Horton's perceptual model of infiltration processes. *Hydrological Processes* **18** (17): 3447–3460 DOI: 10.1002/hyp.5740
- Beven K. 2019. How to make advances in hydrological modelling. *Hydrology Research* **50** (6): 1481–1494 DOI: 10.2166/nh.2019.134
- Biggs J, Bonney S, Stoate C. 2017. Case study 33. Water Friendly Farming Project. (Photo 1): 1–11 Available at: <https://www.gov.uk/government/publications/working-with-natural-processes-to-reduce-flood-risk>
- Birkinshaw SJ, Bathurst JC, Robinson M. 2014. 45 years of non-stationary hydrology over a forest plantation growth cycle, Coalburn catchment, Northern England. *Journal of Hydrology* **519**: 559–573 DOI: 10.1016/j.jhydrol.2014.07.050
- Black A, Peskett L, MacDonald A, Young A, Spray C, Ball T, Thomas H, Werritty A. 2021. Natural flood management, lag time and catchment scale: Results from an empirical nested catchment study. *Journal of Flood Risk Management* **14** (3): 1–16 DOI: 10.1111/jfr3.12717
- Blengino Albrieu JL, Reginato JC, Tarzia DA. 2015. Modeling water uptake by a root system growing in a fixed soil volume. *Applied Mathematical Modelling* **39** (12): 3434–3447 DOI: 10.1016/j.apm.2014.11.042
- Blok C, De Kreij C, Baas R, Wever G. 2008. *Analytical methods used in soilless cultivation*. Elsevier Ltd. DOI: 10.1016/B978-044452975-6.50009-5
- Bois B, Pauthier B, Brillante L, Mathieu O, Leveque J, Van Leeuwen C, Castel T, Richard Y. 2020. Sensitivity of grapevine soil-water balance to rainfall spatial variability at local scale level. *Frontiers in Environmental Science* **8** (August): 1–14 DOI: 10.3389/fenvs.2020.00110
- Bonell M, Purandara BK, Venkatesh B, Krishnaswamy J, Acharya HAK, Singh UV, Jayakumar R, Chappell N. 2010. The impact of forest use and reforestation on soil hydraulic conductivity in the Western Ghats of India: Implications for surface and sub-surface hydrology. *Journal of Hydrology* **391** (1–2): 47–62 DOI: 10.1016/j.jhydrol.2010.07.004
- Booth CA, Charlesworth SM. 2014. *Water Resources in the Built Environment*. DOI: 10.1002/9781118809167
- Bosseler B, Salomon M, Schlüter M, Rubinato M. 2021. Living with Urban Flooding: A Continuous Learning Process for Local Municipalities and Lessons Learnt from the 2021 Events in Germany. *Water* **13** (19): 2769 DOI: 10.3390/w13192769
- Bracken LJ, Oughton EA, Donaldson A, Cook B, Forrester J, Spray C, Cinderby S, Passmore D, Bissett N. 2016. Flood risk management, an approach to managing cross-border hazards. *Natural Hazards* **82** (2): 217–240 DOI: 10.1007/s11069-016-2284-2
- Bridges T, King J, Simm J, Beck M, Collins G, Lodder Q, Mohan R. 2021. *International Guidelines on Natural and Nature-Based Features for Flood Risk Management*. Available at: <https://hdl.handle.net/11681/41946>
- British Geological Survey. 2019. DiGMapGB: Onshore Digital Geological Map of Great

- Britain Data Available at: [https://www.bgs.ac.uk/products/digitalmaps/dataInfo.html#\\_625](https://www.bgs.ac.uk/products/digitalmaps/dataInfo.html#_625) [Accessed 24 March 2019]
- British Geological Survey. 2021. 1:625k Bedrock and Superficial UK Geology. *BGS Geology 625K* Available at: <https://www.bgs.ac.uk/datasets/bgs-geology-625k-digmapgb/> [Accessed 15 June 2021]
- Broadbridge P, Daly E, Goard J. 2017. Exact Solutions of the Richards Equation With Nonlinear Plant-Root Extraction. *Water Resources Research* **53** (11): 9679–9691 DOI: 10.1002/2017WR021097
- Brookes A. 1987. Restoring the sinuosity of artificially straightened stream channels. *Environmental Geology and Water Sciences* **10** (1): 33–41 DOI: 10.1007/BF02588003
- Brunda GS, Nyamathi SJ. 2015. Derivation and Analysis of Dimensionless Hydrograph and S Curve for Cumulative Watershed Area. *Aquatic Procedia* **4** (Icwrcoe): 964–971 DOI: 10.1016/j.aqpro.2015.02.121
- Brunner GW. 2016. HEC-RAS River Analysis System User’s Manual
- Burgess-Gamble L. 2012. Case study 19. Beam Washlands: 1–8
- Burgess-Gamble L, Ngai R, Wilkinson M, Nisbet T, Pontee N, Harvey R, Kipling K, Addy S, Rose S, Maslen S, et al. 2018. *Working with Natural Processes – Evidence Directory*. Environment Agency, Horizon House, Deanery Road, Bristol, BS1 5AH.
- Burguet M, Di Prima S, Prosdocimi M, Taguas E V., Cerdà A. 2016. Minidisk against ring infiltrometer measurements to assess the saturated hydraulic conductivity in Mediterranean vineyards (*Vitis vinifera* L.) under Tillage and No-Tillage managements. *Solid Earth* **18**
- Burrell G, Morgan G. 2016. *Sociological Paradigms and Organisational Analysis*. Routledge: New York, NY, USA. DOI: 10.4324/9781315609751
- Butler D, Davies JW. 2011. *Urban Drainage*. Spon Press: Abingdon. DOI: 10.1017/CBO9781107415324.004
- CAB International. 2013. *The CABI Encyclopedia of Forest Trees*. CABI Publishing, United Kingdom.
- CaBA. 2022. Catchment Based Approach. *About CaBA* Available at: <https://catchmentbasedapproach.org/> [Accessed 10 May 2022]
- Cahyono C, Adidarma WK. 2019. Influence analysis of peak rate factor in the flood events’ calibration process using HEC–HMS. *Modeling Earth Systems and Environment* **5** (4): 1705–1722 DOI: 10.1007/s40808-019-00625-8
- Calder IR. 2003. Assessing the water use of short vegetation and forests: Development of the Hydrological Land Use Change (HYLUC) model. *Water Resources Research* **39** (11): 1–8 DOI: 10.1029/2003WR002040
- Cardoso MA, Almeida MC, Brito RS, Gomes JL, Beceiro P, Oliveira A. 2020. 1D/2D stormwater modelling to support urban flood risk management in estuarine areas: Hazard assessment in the Dafundo case study. *Journal of Flood Risk Management* **13** (4): 1–15 DOI: 10.1111/jfr3.12663
- Carrick J, Abdul Rahim MSA Bin, Adjei C, Ashraa Kalee HHH, Banks SJ, Bolam FC, Campos Luna IM, Clark B, Cowton J, Domingos IFN, et al. 2019. Is planting trees the solution to reducing flood risks? *Journal of Flood Risk Management* **12** (July 2018): 1–10 DOI: 10.1111/jfr3.12484
- Carroll ZL, Carroll ZL, Bird SB, Emmett BA, Reynolds B, Sinclair FL, Carroll ZL, Bird SB, Emmett BA, Reynolds B, et al. 2004. Can tree shelterbelts on agricultural land reduce flood risk? *Soil Use and Management* **20** (3): 357–359 DOI: 10.1079/sum2004266
- CBEC, Environment Agency. 2017. Natural Flood Management Toolbox: Guidance for working with natural processes in flood management schemes
- Centre for Ecology and Hydrology. 2014. Plynlimon Experimental Catchments. *CEH Projects* Available at: <https://www.ceh.ac.uk/our-science/projects/plynlimon-experimental->

- catchments [Accessed 28 January 2019]
- Cerdà A, Lucas-Borja ME, Franch-Pardo I, Úbeda X, Novara A, López-Vicente M, Popović Z, Pulido M. 2021. The role of plant species on runoff and soil erosion in a Mediterranean shrubland. *Science of the Total Environment* **799** DOI: 10.1016/j.scitotenv.2021.149218
- Chandler KR, Stevens CJ, Binley A, Keith AM. 2018. Influence of tree species and forest land use on soil hydraulic conductivity and implications for surface runoff generation. *Geoderma* **310** (August 2017): 120–127 DOI: 10.1016/j.geoderma.2017.08.011
- Chappell NA, Hankin B, Bielby S, Leeson P. 2018. Reducing surface flow during floods in the Upper Eden by scrub planting on Mallerstang West Common, Cumbria. Technical Report EAA7570/R1. Lancaster (UK).
- Chatterton J, Viviattene C, Morris J, Penning-Rowsell EC, Tapsell SM. 2010. *The costs of the summer 2007 floods in England*. DOI: 978-1-84911-146-1
- Chen CT, Hsu KC. 2012. Use of falling-head infiltration to estimate hydraulic conductivity at various depths. *Soil Science* **177** (9): 543–553 DOI: 10.1097/SS.0b013e318267ed7f
- Chen Y, Liu H, An J, Görssdorf L, Berger FH. 2015. A field experiment on the small-scale variability of rainfall based on a network of micro rain radars and rain gauges. *Journal of Applied Meteorology and Climatology* **54** (1): 243–255 DOI: 10.1175/JAMC-D-13-0210.1
- Chesworth W, Camps Arbestain M, Macías F, Spaargaren O, Spaargaren O, Mualem Y, Morel-Seytoux HJ, Horwath WR, Almendros G, Chesworth W, et al. 2008. *Encyclopedia of Soil Science* (W Chesworth, ed.). Springer Netherlands: Dordrecht. DOI: 10.1007/978-1-4020-3995-9
- Chow V Te, Maidment DR, Mays LW. 1988. *Applied Hydrology*. McGraw-Hill Book Company: Singapore.
- Cieśliński R. 2021. Determination of retention value using Mike She model in the area of young glacial catchments. *Applied Water Science* **11** (1): 1–18 DOI: 10.1007/s13201-020-01337-6
- Ciulla G, D’Amico A. 2019. Building energy performance forecasting: A multiple linear regression approach. *Applied Energy* **253** (April): 113500 DOI: 10.1016/j.apenergy.2019.113500
- Climate Assembly UK, House of Commons. 2020. Climate Assembly UK - The path to net zero: 1–15 Available at: file:///Volumes/750G/%23 setting/%23 Papers2 Library/Papers2/Files/pathtonetzerocourt2 - Wei Zhi.pdf%5Cpapers2://publication/uuid/8AA56729-9F2D-4363-922E-7FF5050B13A4
- Coffey SPC. 2021. Tree Species and Woodland Planting
- Collentine D, Futter MN. 2018. Realising the potential of natural water retention measures in catchment flood management: trade-offs and matching interests. *Journal of Flood Risk Management* **11** (1): 76–84 DOI: 10.1111/jfr3.12269
- Connelly A, Snow A, Carter J, Lauwerijssen R. 2020. What approaches exist to evaluate the effectiveness of UK-relevant natural flood management measures? A systematic map protocol. *Environmental Evidence* **9** (1): 1–13 DOI: 10.1186/s13750-020-00192-x
- Cooper MMD, Patil SD, Nisbet TR, Thomas H, Smith AR, McDonald MA. 2021. Role of forested land for natural flood management in the UK: A review. *Wiley Interdisciplinary Reviews: Water* **8** (5): 1–16 DOI: 10.1002/wat2.1541
- Crispino G, Gisonni C, Iervolino M. 2015. Flood hazard assessment: comparison of 1D and 2D hydraulic models. *International Journal of River Basin Management* **13** (2): 153–166 DOI: 10.1080/15715124.2014.928304
- Crotty M. 1998. *The Foundations of Social Research*. SAGE: London, UK.
- Crow P. 2005. The Influence of Soils and Species on Tree Root Depth. Edinburgh.
- Cui Z, Huang Z, Liu Y, López-Vicente M, Wu GL. 2021. Natural compensation mechanism of soil water infiltration through decayed roots in semi-arid vegetation species. *Science of the Total Environment* (26): 151985 DOI: 10.1016/j.scitotenv.2021.151985

- Cunge JA. 1969. On the subject of a flood propagation computation method (Maskingum method). *Journal of Hydraulic Research* **7** (2): 205–230
- Dadson SJ, Hall JW, Murgatroyd A, Acreman M, Bates P, Beven K, Heathwaite L, Holden J, Holman IP, Lane SN, et al. 2017. A restatement of the natural science evidence concerning catchment-based ‘natural’ flood management in the UK. *Royal Society Publishing* **473** (2199) DOI: 10.1098/rspa.2016.0706
- Dai Q, Peng X, Yang Z, Zhao L. 2017. Runoff and erosion processes on bare slopes in the Karst Rocky Desertification Area. *Catena* **152**: 218–226 DOI: 10.1016/j.catena.2017.01.013
- Darwish MM, Tye MR, Prein AF, Fowler HJ, Blenkinsop S, Dale M, Faulkner D. 2021. New hourly extreme precipitation regions and regional annual probability estimates for the UK. *International Journal of Climatology* **41** (1): 582–600 DOI: 10.1002/joc.6639
- David A, Schmalz B. 2020. Flood hazard analysis in small catchments: Comparison of hydrological and hydrodynamic approaches by the use of direct rainfall. *Journal of Flood Risk Management* **13** (4): 1–26 DOI: 10.1111/jfr3.12639
- Davids JC, Rutten MM, Pandey A, Devkota N, David Van Oyen W, Prajapati R, Van De Giesen N. 2019. Citizen science flow-an assessment of simple streamflow measurement methods. *Hydrology and Earth System Sciences* **23** (2): 1045–1065 DOI: 10.5194/hess-23-1045-2019
- Davies PA, McCarthy M, Christidis N, Dunstone N, Fereday D, Kendon M, Knight JR, Scaife AA, Sexton D. 2021a. The wet and stormy UK winter of 2019/2020. *Weather* (February): 1–7 DOI: 10.1002/wea.3955
- Davies PA, McCarthy M, Christidis N, Dunstone N, Fereday D, Kendon M, Knight JR, Scaife AA, Sexton D. 2021b. The wet and stormy UK winter of 2019/2020. *Weather*: wea.3955 DOI: 10.1002/wea.3955
- Day SD, Wiseman PE. 2009. At The Root of It: 20–22 Available at: [http://www.boneandjoint.org.uk/highwire/filestream/13335/field\\_highwire\\_article\\_pdf/0/741.full-text.pdf](http://www.boneandjoint.org.uk/highwire/filestream/13335/field_highwire_article_pdf/0/741.full-text.pdf)
- Decagon Devices. 2006. Mini Disk Infiltrometer User’s Manual. Pullman, WA. Available at: <https://www.metergroup.com/environment/products/mini-disk-infiltrometer/> [Accessed 11 September 2019]
- Defra. 2010. Surface Water Management Plan Technical Guidance. (March): 90
- Defra. 2014. Draft National Standards and Specified Criteria for Sustainable Drainage
- Defra. 2020. Landmark Agriculture Bill becomes law. *Common Agricultural Policy reform* Available at: <https://www.gov.uk/government/news/landmark-agriculture-bill-becomes-law> [Accessed 28 June 2022]
- Defra. 2021. At a glance: summary of targets in our 25 year environment plan. London, UK. Available at: <https://www.gov.uk/government/publications/25-year-environment-plan/25-year-environment-plan-our-targets-at-a-glance>
- Defra, Rural Payments Agency. 2021. Environmental Land Management schemes: overview. *Guidance for ELMS* Available at: <https://www.gov.uk/government/publications/environmental-land-management-schemes-overview/environmental-land-management-scheme-overview> [Accessed 28 June 2022]
- Deng J, Yin H, Kong F, Chen J, Dronova I, Pu Y. 2020. Determination of runoff response to variation in overland flow area by flow routes using UAV imagery. *Journal of Environmental Management* **265** (June 2019): 109868 DOI: 10.1016/j.jenvman.2019.109868
- Department for Environment Food & Rural Affairs. 2020. LIDAR Composite DTM. *LIDAR Composite DTM 2020 - 1m* Available at: <https://environment.data.gov.uk/dataset/668881ad-4f8f-42bd-b835-89acf0269496> [Accessed 16 July 2021]

- Derdour A, Bouanani A, Babahamed K. 2018. Modelling rainfall runoff relations using HEC-HMS in a semi-arid region: Case study in Ain Sefra watershed, Ksour Mountains (SW Algeria). *Journal of Water and Land Development* **36** (1): 45–55 DOI: 10.2478/jwld-2018-0005
- Difonzo F V., Masciopinto C, Vurro M, Berardi M. 2021. Shooting the Numerical Solution of Moisture Flow Equation with Root Water Uptake Models: A Python Tool. *Water Resources Management* **35** (8): 2553–2567 DOI: 10.1007/s11269-021-02850-2
- Ding X, Zhao Z, Yang Q, Chen L, Tian Q, Li X, Meng FR. 2020. Model prediction of depth-specific soil texture distributions with artificial neural network: A case study in Yunfu, a typical area of Udufts Zone, South China. *Computers and Electronics in Agriculture* **169** (December 2019): 105217 DOI: 10.1016/j.compag.2020.105217
- Dittrich R, Ball T, Wreford A, Moran D, Spray CJ. 2019. A cost-benefit analysis of afforestation as a climate change adaptation measure to reduce flood risk. *Journal of Flood Risk Management* **12** (4): 1–11 DOI: 10.1111/jfr3.12482
- Dixon B, Uddameri V. 2016. Watershed Delineation. In *GIS and Geocomputation for Water Resource Science and Engineering* John Wiley & Sons, Ltd: Chichester, UK; 297–312. DOI: 10.1002/9781118826171.ch20
- Dixon SJ, Sear DA, Odoni NA, Sykes T, Lane SN. 2016. The effects of river restoration on catchment scale flood risk and flood hydrology. *Earth Surface Processes and Landforms* **41** (7): 997–1008 DOI: 10.1002/esp.3919
- Dobson M. 1995. Tree Root Systems
- Dohnal M, Černý T, Votrubová J, Tesař M. 2014. Rainfall interception and spatial variability of throughfall in spruce stand. *Journal of Hydrology and Hydromechanics* **62** (4): 277–284 DOI: 10.2478/johh-2014-0037
- Dollinger J, Lin CH, Udawatta RP, Pot V, Benoit P, Jose S. 2019. Influence of agroforestry plant species on the infiltration of S-Metolachlor in buffer soils. *Journal of Contaminant Hydrology* **225** (May): 103498 DOI: 10.1016/j.jconhyd.2019.103498
- Dong X. 2016. How to put plant root uptake into a soil water flow model. *F1000Research* **5**: 1–9 DOI: 10.12688/f1000research.7686.1
- Eden Rivers Trust. 2021. Cairn Beck NFM project. *Natural Flood Management* Available at: <https://www.edenriverstrust.org.uk/projects/natural-flood-management/cairn-beck/> [Accessed 11 February 2022]
- Eijkelkamp. 2015. Double Ring Infiltrometer User's Manual. *Double Ring Infiltrometer*: 1–9
- Elbasit MAA, Abu-Zreig MM, Ojha CSP, Yasuda H, Gang L. 2020. Estimation of surface depression storage capacity from random roughness and slope. *Water SA* **46** (3): 404–409 DOI: 10.17159/wsa/2020.v46.i3.8650
- Ellis N, Anderson K, Brazier R. 2021. Mainstreaming natural flood management: A proposed research framework derived from a critical evaluation of current knowledge. *Progress in Physical Geography: Earth and Environment*: 1–23 DOI: 10.1177/0309133321997299
- Ellison D, Morris CE, Locatelli B, Sheil D, Cohen J, Murdiyarso D, Gutierrez V, Noordwijk M van, Creed IF, Pokorny J, et al. 2017. Trees, forests and water: Cool insights for a hot world. *Global Environmental Change* **43**: 51–61 DOI: 10.1016/j.gloenvcha.2017.01.002
- Environment Agency. 2007. Review of 2007 summer floods. *Environment* (December): 1–58
- Environment Agency. 2008. *Continuous Estimation of River Flows (CERF)*. Environment Agency: Bristol.
- Environment Agency. 2010. Working with Natural Processes to Manage Flood and Coastal Erosion Risk. (March): 74
- Environment Agency. 2017. Working with Natural Processes - the evidence base - Project Summary
- Environment Agency. 2021a. Flood risk assessments: climate change allowances. *Guidance* Available at: <https://www.gov.uk/guidance/flood-risk-assessments-climate-change-allowances> [Accessed 22 May 2020]

- Environment Agency. 2021b. Climate change allowances for peak river flow in England: map Available at: <https://environment.maps.arcgis.com/apps/webappviewer/index.html?id=363522b846b842a4a905829a8d8b3d0c> [Accessed 13 August 2021]
- Environment Agency. 2021c. Working with international partners to promote natural flood management. *Blog - Flood* Available at: <https://environmentagency.blog.gov.uk/2021/09/20/working-with-international-partners-to-promote-natural-flood-management/> [Accessed 15 February 2022]
- Environment Agency. 2021d. LIDAR Composite 1m DTM. *DEFRA Survey Data Download* Available at: <https://environment.data.gov.uk/DefraDataDownload/?Mode=survey> [Accessed 13 October 2018]
- Environment Agency. 2022. The Thames Barrier. *The Thames Barrier* Available at: <https://www.gov.uk/guidance/the-thames-barrier> [Accessed 28 February 2022]
- Environment Agency, CAPITA, AECOM. 2017. Slowing the Flow in the Rivers Ouse and Foss: Appendix A - Natural Flood Management Literature Review
- Environment Agency, NERC SW, Blue Sky, Get Mapping, Airbus. 2020. Environment Agency Intergrated Height Model (IHM). *The Environment Agency (EA) Intergrated Height Model (IHM) DTM*
- Environmental Monitoring Solutions Ltd. 2020. Environmental Monitoring Solutions. *EMS products* Available at: <https://www.em-solutions.co.uk/>
- Ezezi Isaac O, Eric Chikweru A. 2018. Test for Significance of Pearson's Correlation Coefficient (r). *International Journal of Innovative Mathematics, Statistics & Energy Policies* **1** (1): 11–23 Available at: <http://seahipaj.org/journals-ci/mar-2018/IJIMSEP/full/IJIMSEP-M-2-2018.pdf>
- ESRI. 2019. Flow Direction Function. *Flow Direction Toolset Overview* Available at: <https://pro.arcgis.com/en/pro-app/help/data/imagery/flow-direction-raster-function.htm> [Accessed 18 May 2020]
- ESRI. 2020. Watershed Tool - ArcGIS. *Hydrology Toolset Tool Reference* Available at: <https://desktop.arcgis.com/en/arcmap/10.3/tools/spatial-analyst-toolbox/watershed.htm>
- European Centre for River Restoration. 2022. River Restoration. *Healthy rivers provide a quality environment* Available at: <https://www.ecrr.org/River-Restoration/Social-benefits-of-river-restoration> [Accessed 11 May 2022]
- European Commission. 2011. Towards Better Environmental Options for Flood risk management, DG ENV D.1. *International journal of integrated care* **1**: 23 Available at: <http://www.ncbi.nlm.nih.gov/pubmed/16896409> <http://www.pubmedcentral.nih.gov/articlerender.fcgi?artid=PMC1484409>
- European Commission. 2014. Natural Water Retention Measures Available at: [https://circabc.europa.eu/sd/a/2457165b-3f12-4935-819a-c40324d22ad3/Policy Document on Natural Water Retention Measures\\_Final.pdf](https://circabc.europa.eu/sd/a/2457165b-3f12-4935-819a-c40324d22ad3/Policy Document on Natural Water Retention Measures_Final.pdf) [Accessed 10 May 2022]
- European Commission. 2022. The forms and functions of green infrastructure. *What is green infrastructure?* Available at: [https://ec.europa.eu/environment/nature/ecosystems/benefits/index\\_en.htm#:~:text=Green infrastructure is a strategically,and climate mitigation and adaptation](https://ec.europa.eu/environment/nature/ecosystems/benefits/index_en.htm#:~:text=Green infrastructure is a strategically,and climate mitigation and adaptation) [Accessed 10 May 2022]
- Farming and Wildlife Advisory Group. 2020. Hills to Levels. *Hills to Levels* Available at: <https://www.fwagsw.org.uk/hills-to-levels> [Accessed 29 April 2020]
- Fatehnia M, Tawfiq K, Abichou T. 2014. Comparison of the methods of hydraulic conductivity estimation from mini disk infiltrometer. *Electronic Journal of Geotechnical Engineering* **19 E** (December 2015): 1047–1063
- Fatehnia M, Tawfiq K, Ye M. 2016. Estimation of saturated hydraulic conductivity from double-ring infiltrometer measurements. *European Journal of Soil Science* **67** (2): 135–147 DOI: 10.1111/ejss.12322

- Fay MP, Proschan MA. 2010. Wilcoxon-Mann-Whitney or t-test? On assumptions for hypothesis tests and multiple interpretations of decision rules. *Statistics Surveys* **4** (none): 1–37 DOI: 10.1214/09-SS051
- Fazio JR. 2012. How Trees Can Retain Stormwater Runoff. Nebraska City. Available at: [http://www.northlandnemo.org/images/800TreeCityUSABulletin\\_55.pdf](http://www.northlandnemo.org/images/800TreeCityUSABulletin_55.pdf)
- Fedorova D, Kovár P, Gregar J, Jelínková A, Novotná J, Darya F, Pavel K, Jan G, Andrea J, Jana N, et al. 2018. The use of Snyder synthetic hydrograph for simulation of overland flow in small ungauged and gauged catchments. *Soil and Water Research* **13** (4): 185–192 DOI: 10.17221/237/2017-SWR
- Felix Dennis Trust. 2019. Felix Dennis Available at: <http://felixdennis.com/Default.aspx> [Accessed 13 March 2019]
- Ferguson C. 2020. The effects of upstream Natural Flood Management on urban surface drainage performance. (September) Available at: <https://www.repository.cam.ac.uk/handle/1810/312038>
- Ferguson C, Fenner R. 2020a. The impact of Natural Flood Management on the performance of surface drainage systems: A case study in the Calder Valley. *Journal of Hydrology* **590** (July): 125354 DOI: 10.1016/j.jhydrol.2020.125354
- Ferguson CR, Fenner RA. 2020b. The potential for natural flood management to maintain free discharge at urban drainage outfalls. *Journal of Flood Risk Management* **13** (3): 1–15 DOI: 10.1111/jfr3.12617
- Fernandez A, Adamowski J, Petroselli A. 2016. Analysis of the behavior of three digital elevation model correction methods on critical natural scenarios. *Journal of Hydrology: Regional Studies* **8**: 304–315 DOI: 10.1016/j.ejrh.2016.09.009
- Ficchì A, Perrin C, Andréassian V. 2019. Hydrological modelling at multiple sub-daily time steps: Model improvement via flux-matching. *Journal of Hydrology* **575** (May): 1308–1327 DOI: 10.1016/j.jhydrol.2019.05.084
- Field RH, Buchanan GM, Hughes A, Smith P, Bradbury RB. 2020. The value of habitats of conservation importance to climate change mitigation in the UK. *Biological Conservation* **248** (May): 108619 DOI: 10.1016/j.biocon.2020.108619
- Finaud-Guyot P, Delenne C, Guinot V. 2011a. Coupling of 1D and 2D models for river flow modelling. *La Houille Blanche* (3): 23–28 DOI: 10.1051/lhb/2011028
- Finaud-Guyot P, Delenne C, Guinot V, Llovel C. 2011b. 1D-2D coupling for river flow modeling. *Comptes Rendus - Mécanique* **339** (4): 226–234 DOI: 10.1016/j.crme.2011.02.001
- Fletcher TI, Scott CE, Hall J, Spracklen D V. 2021. The carbon sequestration potential of Scottish native woodland. *Environmental Research Communications* **3** (4): 041003 DOI: 10.1088/2515-7620/abf467
- Folorunso O, Aribisala J. 2018. Effect of Soil Texture on Soil Infiltration Rate. *Archives of Current Research International* **14** (3): 1–8 DOI: 10.9734/ACRI/2018/41974
- Food and Agriculture Organisation of the United Nations (FAO). 2020. Global Forest Resources Assessment. Rome. DOI: 10.4324/9781315184487-1
- Forbes H, Ball K, McLay F. 2016. *Natural Flood Management Handbook*. Scottish Environment Protection Agency Strathallan House Castle Business Park Stirling. DOI: 10.13140/RG.2.1.4956.1444
- Forest Research. 2020. Provisional Woodland Statistics 2020 Edition. Edinburgh. Available at: [https://www.forestresearch.gov.uk/documents/7647/PWS\\_2020\\_ggXAYhv.pdf](https://www.forestresearch.gov.uk/documents/7647/PWS_2020_ggXAYhv.pdf)
- Forestry Commission. 2018. Forestry Statistics 2018 Available at: <https://www.forestresearch.gov.uk/tools-and-resources/statistics/forestry-statistics/forestry-statistics-2018/>
- Franzluebbers AJ. 2002. Water infiltration and soil structure related to organic matter and its stratification with depth. *Soil and Tillage Research* **66** (2): 197–205 DOI: 10.1016/S0167-1987(02)00027-2

- Gadian AM, Blyth AM, Bruyere CL, Burton RR, Done JM, Groves J, Holland G, Mobbs SD, Pozo JT, Tye MR, et al. 2018. A case study of possible future summer convective precipitation over the UK and Europe from a regional climate projection. *International Journal of Climatology* **38** (5): 2314–2324 DOI: 10.1002/joc.5336
- Gee GW, Or D. 2018. 2.4 Particle-Size Analysis. In *Astronomy & Astrophysics* 255–293. DOI: 10.2136/sssabookser5.4.c12
- Geng Y fen, Wang Z li. 2020. An Implicit Coupled 1D/2D Model for Unsteady Subcritical Flow in Channel Networks and Embayment. *China Ocean Engineering* **34** (1): 110–118 DOI: 10.1007/s13344-020-0011-y
- Geograph. 2015. River Medlock emerges from culvert Available at: <https://www.geograph.org.uk/photo/4734144> [Accessed 11 May 2022]
- Gharbi M, Soualmia A, Dartus D, Masbernat L. 2016. Comparison of 1D and 2D hydraulic models for floods simulation on the medjerda river in tunisia. *Journal of Materials and Environmental Science* **7** (8): 3017–3026
- Gholami V, Khaleghi MR. 2021. A simulation of the rainfall-runoff process using artificial neural network and HEC-HMS model in forest lands. *Journal of Forest Science* **67** (No. 4): 165–174 DOI: 10.17221/90/2020-JFS
- Glińska-Lewczuk K, Burandt P. 2011. Effect of river straightening on the hydrochemical properties of floodplain lakes: Observations from the Łyna and Drwęca Rivers, N Poland. *Ecological Engineering* **37** (5): 786–795 DOI: 10.1016/j.ecoleng.2010.07.028
- Google. 2022. Google Earth Available at: [https://www.google.co.uk/intl/en\\_uk/earth/](https://www.google.co.uk/intl/en_uk/earth/) [Accessed 16 March 2022]
- GOV.UK. 2020. £3.9 million to drive innovative tree planting. *UK Gov Press Release* Available at: <https://www.gov.uk/government/news/39-million-to-drive-innovative-tree-planting> [Accessed 13 July 2021]
- GOV.UK. 2021. UK becomes first major economy to pass net zero emissions law. *News Story* Available at: <https://www.gov.uk/government/news/uk-becomes-first-major-economy-to-pass-net-zero-emissions-law> [Accessed 18 October 2021]
- GOV.UK, Environment Agency, Flood and Coastal Erosion Risk Management Research and Development Programme. 2021. Working with natural processes to reduce flood risk. *Flood and Coastal Erosion Risk Management (FCERM) research reports* Available at: <https://www.gov.uk/flood-and-coastal-erosion-risk-management-research-reports/working-with-natural-processes-to-reduce-flood-risk> [Accessed 28 February 2022]
- GOV.UK, Environment Agency, Forestry Commission. 2019. Reduce Flood Risk with the Woodland for Water Scheme Available at: <https://www.gov.uk/government/news/reduce-flood-risk-with-the-woodlands-for-water-scheme> [Accessed 27 October 2021]
- Graham CB, Lin H. 2012. *Subsurface Flow Networks at the Hillslope Scale: Detection and Modeling*. DOI: 10.1016/B978-0-12-386941-8.00018-6
- Grimm K, Chu X. 2020. Depression threshold control proxy to improve HEC-HMS modeling of depression-dominated watersheds. *Hydrological Sciences Journal* **65** (2): 200–211 DOI: 10.1080/02626667.2019.1690148
- Groenendyk DG, Ferré TPA, Thorp KR, Rice AK. 2015. Hydrologic-Process-Based Soil Texture Classifications for Improved Visualization of Landscape Function (AC Singer, ed.). *PLoS ONE* **10** (6): e0131299 DOI: 10.1371/journal.pone.0131299
- Güçlü YS, Şen Z. 2016. Hydrograph estimation with fuzzy chain model. *Journal of Hydrology* **538**: 587–597 DOI: 10.1016/j.jhydrol.2016.04.057
- Gumindoga W, Rwasoka DT, Nhapi I, Dube T. 2017. Ungauged runoff simulation in Upper Manyame Catchment, Zimbabwe: Application of the HEC-HMS model. *Physics and Chemistry of the Earth* **100**: 371–382 DOI: 10.1016/j.pce.2016.05.002
- Gunathilake MB, Panditharathne P, Gunathilake AS, Warakagoda ND. 2020. Application of a hec-hms model on event-based simulations in a tropical watershed. *Engineering and*

- Applied Science Research* **47** (4): 349–360 DOI: 10.14456/easr.2020.38
- Guo FX, Wang YP, Hou TT, Zhang L Sen, Mu Y, Wu F yong. 2021. Variation of soil moisture and fine roots distribution adopts rainwater collection, infiltration promoting and soil anti-seepage system (RCIP-SA) in hilly apple orchard on the Loess Plateau of China. *Agricultural Water Management* **244** (September 2020) DOI: 10.1016/j.agwat.2020.106573
- Hale K, Spencer M, Peterken GF, Mountford EP, Bradshaw RHW. 2019. Rapid carbon accumulation within an unmanaged, mixed, temperate woodland. *Scandinavian Journal of Forest Research* **34** (3): 208–217 DOI: 10.1080/02827581.2019.1575975
- Halwatura D, Najim MMM. 2013. Application of the HEC-HMS model for runoff simulation in a tropical catchment. *Environmental Modelling and Software* **46**: 155–162 DOI: 10.1016/j.envsoft.2013.03.006
- Hamdan ANA, Almuktar S, Scholz M. 2021. Rainfall-Runoff Modeling Using the HEC-HMS Model for the Al-Adhaim River Catchment, Northern Iraq. *Hydrology* **8** (2): 58 DOI: 10.3390/hydrology8020058
- Hankin B, Chappell N, Page T, Kipling K, Whitling M, Burgess-Gamble L. 2018. Mapping the potential for Working with Natural Processes-technical report. Available at: <https://www.gov.uk/government/organisations/environment-agency/about/research>.
- Hankin B, Metcalfe P, Beven K, Chappell NA. 2019. Integration of hillslope hydrology and 2D hydraulic modelling for natural flood management. *Hydrology Research* **50** (6): 1535–1548 DOI: 10.2166/nh.2019.150
- Hankin B, Metcalfe P, Johnson D, Chappell NA, Page T, Craigen I, Lamb R, Beven K. 2017. Strategies for Testing the Impact of Natural Flood Risk Management Measures. *Flood Risk Management*: 1–40 DOI: 10.5772/intechopen.68677
- Harden CP, Scruggs PD. 2003. Infiltration on mountain slopes: A comparison of three environments. *Geomorphology* **55** (1–4): 5–24 DOI: 10.1016/S0169-555X(03)00129-6
- Hasan MK, Kumar L. 2019. Comparison between meteorological data and farmer perceptions of climate change and vulnerability in relation to adaptation. *Journal of Environmental Management* **237** (January): 54–62 DOI: 10.1016/j.jenvman.2019.02.028
- Hashim M, Watson A, Thomas M. 2004. An approach for correcting inhomogeneous atmospheric effects in remote sensing images. *International Journal of Remote Sensing* **25** (22): 5131–5141 DOI: 10.1080/01431160410001712971
- Hatfield JH, Barlow J, Joly CA, Lees AC, Parruco CH de F, Tobias JA, Orme CDL, Banks-Leite C. 2020. Mediation of area and edge effects in forest fragments by adjacent land use. *Conservation Biology* **34** (2): 395–404 DOI: 10.1111/cobi.13390
- Heart of England Forest. 2020. Heart of England Forest Tree Guide. *Get to know the native broadleaf trees that make up the Heart of England Forest.*: 10 Available at: [https://www.heartofenglandforest.com/wp-content/uploads/2017/03/Tree\\_Guide.pdf](https://www.heartofenglandforest.com/wp-content/uploads/2017/03/Tree_Guide.pdf)
- Hepner H, Lutter R, Tullus A, Kanal A, Tullus T, Tullus H. 2020. Effect of Early Thinning Treatments on Above-Ground Growth, Biomass Production, Leaf Area Index and Leaf Growth Efficiency in a Hybrid Aspen Coppice Stand. *Bioenergy Research* **13** (1): 197–209 DOI: 10.1007/s12155-020-10111-0
- Hessel R, Jetten V, Guanghui Z. 2003. Estimating Manning’s n for steep slopes. *Catena* **54** (1–2): 77–91 DOI: 10.1016/S0341-8162(03)00058-4
- HM Government. 2009. The Flood Risk Regulations 2009. *Environmental Protection* **2008** (3042)
- HM Government. 2018. A Green Future: Our 25 Year Plan to Improve the Environment. London, UK. Available at: [https://assets.publishing.service.gov.uk/government/uploads/system/uploads/attachment\\_data/file/693158/25-year-environment-plan.pdf](https://assets.publishing.service.gov.uk/government/uploads/system/uploads/attachment_data/file/693158/25-year-environment-plan.pdf)
- Hohensinner S, Hauer C, Muhar S. 2018. River Morphology, Channelization, and Habitat Restoration. In *Riverine Ecosystem Management* Springer International Publishing:

- Cham; 41–65. DOI: 10.1007/978-3-319-73250-3\_3
- Hornberger GM, Wiberg PL, Raffensperger JP, D’Odorico P. 2014. *Elements of Physical Hydrology*. John Hopkins University Press: Baltimore.
- Horner I, Renard B, Le Coz J, Branger F, McMillan HK, Pierrefeu G. 2018. Impact of Stage Measurement Errors on Streamflow Uncertainty. *Water Resources Research* **54** (3): 1952–1976 DOI: 10.1002/2017WR022039
- Hosseinzadehtalaei P, Tabari H, Willems P. 2020. Climate change impact on short-duration extreme precipitation and intensity–duration–frequency curves over Europe. *Journal of Hydrology* **590** (June): 125249 DOI: 10.1016/j.jhydrol.2020.125249
- HS2. 2021a. HS2: About Us. *About Us* Available at: <https://www.hs2.org.uk/about-us/> [Accessed 18 October 2021]
- HS2. 2021b. HS2 announces new landmark as 700,000 trees planted and over 100 new habitats thriving on Phase One of the project. *HS2 News* Available at: <https://mediacentre.hs2.org.uk/news/hs2-announces-new-landmark-as-700-000-trees-planted-and-over-100-new-habitats-thriving-on-phase-one-of-the-project> [Accessed 14 February 2022]
- Hu N, Zhang J, Xia S, Han R, Dai Z, She R, Cui X, Meng B. 2020. A field performance evaluation of the periodic maintenance for pervious concrete pavement. *Journal of Cleaner Production* **263**: 121463 DOI: 10.1016/j.jclepro.2020.121463
- Huntington TG, Weiskel PK, Wolock DM, McCabe GJ. 2018. A new indicator framework for quantifying the intensity of the terrestrial water cycle. *Journal of Hydrology* **559**: 361–372 DOI: 10.1016/j.jhydrol.2018.02.048
- Hussain F, Wu R-S, Yu K-C. 2021. Application of Physically Based Semi-Distributed Hec-Hms Model for Flow Simulation in Tributary Catchments of Kaohsiung Area Taiwan. *Journal of Marine Science and Technology* **29** (1) DOI: 10.51400/2709-6998.1003
- Hynynen J, Niemisto P, Vihera-Aarnio A, Brunner A, Hein S, Velling P. 2010. Silviculture of birch (*Betula pendula* Roth and *Betula pubescens* Ehrh.) in northern Europe. *Forestry* **83** (1): 103–119 DOI: 10.1093/forestry/cpp035
- Ibrahim-Bathis K, Ahmed SA. 2016. Rainfall-runoff modelling of Doddahalla watershed—an application of HEC-HMS and SCN-CN in ungauged agricultural watershed. *Arabian Journal of Geosciences* **9** (3): 1–16 DOI: 10.1007/s12517-015-2228-2
- Iida S, Shimizu T, Tamai K, Kabeya N, Shimizu A, Ito E, Ohnuki Y, Chann S, Levia DF. 2020. Evapotranspiration from the understory of a tropical dry deciduous forest in Cambodia. *Agricultural and Forest Meteorology* **295** (September): 108170 DOI: 10.1016/j.agrformet.2020.108170
- Innovyze. 2021. MicroDrainage. *MicroDrainage* Available at: <https://www.innovyze.com/en-us/products/microdrainage> [Accessed 8 November 2021]
- Itoh A, Yamakura T, Ohkubo T, Kanzaki M, Palmiotto PA, LaFrankie J V., Ashton PS, Lee HS. 2003. Importance of topography and soil texture in the spatial distribution of two sympatric dipterocarp trees in a Bornean rainforest. *Ecological Research* **18** (3): 307–320 DOI: 10.1046/j.1440-1703.2003.00556.x
- Jačka L, Walmsley A, Kovář M, Frouz J. 2021. Effects of different tree species on infiltration and preferential flow in soils developing at a clayey spoil heap. *Geoderma* **403** (August) DOI: 10.1016/j.geoderma.2021.115372
- Jacobs. 2021. Flood Modeller. *Flood Modeller Product Information* Available at: <https://www.floodmodeller.com/products/software/flood-modeller/> [Accessed 7 May 2020]
- Janes VJ, Grabowski RC, Mant J, Allen D, Morse JL, Haynes H. 2017. The Impacts of Natural Flood Management Approaches on In-Channel Sediment Quality. *River Research and Applications* **33** (1): 89–101 DOI: 10.1002/rra.3068
- Jarvis NJ. 2007. A review of non-equilibrium water flow and solute transport in soil macropores: Principles, controlling factors and consequences for water quality. *European*

- Journal of Soil Science* **58** (3): 523–546 DOI: 10.1111/j.1365-2389.2007.00915.x
- JBA Personal Communication, PCC Personal Communication. 2021. Climate Baseflow Uplifts JBA Risk Management. 2021. A Retrospective Look at London Surface Water Flash Floods. *Event Response* Available at: <https://www.jbarisk.com/flood-services/event-response/a-retrospective-look-at-summer-2021-london-flash-floods/> [Accessed 20 December 2021]
- Jenson SK, Domingue JO. 1988. Extracting Topographic Structure from Digital Elevation Data for Geographic Information System Analysis. *Photogrammetric Engineering and Remote Sensing* **54** (11): 1593–1600
- Jeziorska J. 2019. UAS for wetland mapping and hydrological modeling. *Remote Sensing* **11** (17) DOI: 10.3390/rs11171997
- Jiang L, Wu H, Tao J, Kimball JS, Alfieri L, Chen X. 2020. Satellite-based evapotranspiration in hydrological model calibration. *Remote Sensing* **12** (3) DOI: 10.3390/rs12030428
- JNCC. 2003. *National Vegetation Classification - Ten years experience using the woodland section* (E Goldberg, ed.). JNCC: Monkstone House, City Road, Peterborough.
- Johnson AI. 1963. A Field Method for Measurement of Infiltration: USGS Water-Supply Paper 1544-F. *Geological Survey Water-Supply Paper* **1544-F**: 27
- Johnson P, Clark M. 2006. *Business and Management Research Methodologies*. SAGE: London, UK.
- Jordon MW. 2021. Does mixed vs separate sheep and cattle grazing reduce soil compaction? *Soil Use and Management* **37** (4): 822–831 DOI: 10.1111/sum.12659
- Joshi N, Bista A, Pokhrel I, Kalra A, Ahmad S. 2019. Rainfall-Runoff Simulation in Cache River Basin, Illinois, Using HEC-HMS. In *World Environmental and Water Resources Congress 2019* American Society of Civil Engineers: Reston, VA; 348–360. DOI: 10.1061/9780784482339.035
- Julich S, Kreiselmeier J, Scheibler S, Petzold R, Schwärzel K, Feger KH. 2021. Hydraulic properties of forest soils with stagnic conditions. *Forests* **12** (8): 1–13 DOI: 10.3390/f12081113
- Kafle MR. 2019. Rainfall-Runoff Modelling of Koshi River Basin Using HEC-HMS. *Journal of Hydrogeology & Hydrologic Engineering* **8** (1): 1–9
- Kamis AS, Ahmad Fuad AF, Ashaari A, Mohd Noor CW. 2021. Development of WOP mathematical model for efficient course alteration: LNG tanker manoeuvring analysis and Mann-Whitney U test. *Ocean Engineering* **239** (April): 109768 DOI: 10.1016/j.oceaneng.2021.109768
- Kay AL, Old GH, Bell VA, Davies HN, Trill EJ. 2019. An assessment of the potential for natural flood management to offset climate change impacts. *Environmental Research Letters* **14** (4) DOI: 10.1088/1748-9326/aafdbe
- Kay AL, Rudd AC, Fry M, Nash G, Allen S. 2021. Climate change impacts on peak river flows: Combining national-scale hydrological modelling and probabilistic projections. *Climate Risk Management* **31** (December 2020): 100263 DOI: 10.1016/j.crm.2020.100263
- Kay AL, Watts G, Wells SC, Allen S. 2020. The impact of climate change on U. K. river flows: A preliminary comparison of two generations of probabilistic climate projections. *Hydrological Processes* **34** (4): 1081–1088 DOI: 10.1002/hyp.13644
- Khodaverdiloo H, Khani Cheraghbdal H, Bagarello V, Iovino M, Asgarzadeh H, Ghorbani Dashtaki S. 2017. Ring diameter effects on determination of field-saturated hydraulic conductivity of different loam soils. *Geoderma* **303** (May): 60–69 DOI: 10.1016/j.geoderma.2017.04.031
- Kim J, Ivanov VY, Katopodes ND. 2012. Hydraulic resistance to overland flow on surfaces with partially submerged vegetation. *Water Resources Research* **48** (10): 1–19 DOI: 10.1029/2012WR012047
- Kirby C, Newson MD, Gilman K. 1991. Plynlimon research: the first two decades
- Kirkham MB. 2014a. Water Movement in Saturated Soil. In *Principles of Soil and Plant Water Relations* Elsevier; 85–100. DOI: 10.1016/C2013-0-12871-1

- Kirkham MB. 2014b. Infiltration. In *Principles of Soil and Plant Water Relations* Elsevier; 201–227. DOI: 10.1016/C2013-0-12871-1
- Kitsikoudis V, Erpicum S, Rubinato M, Shucksmith JD, Archambeau P, Piroton M, Dewals B. 2021. Exchange between drainage systems and surface flows during urban flooding: Quasi-steady and dynamic modelling in unsteady flow conditions. *Journal of Hydrology* **602** (March): 126628 DOI: 10.1016/j.jhydrol.2021.126628
- Klamerus-Iwan A. 2014. Different views on tree interception process and its determinants. *Forest Research Papers* **75** (3): 291–300 DOI: 10.2478/frp-2014-0028
- Klamerus-Iwan A. 2015. Rainfall parameters affect canopy storage capacity under controlled conditions. *Forest Research Papers* **75** (4): 353–358 DOI: 10.2478/frp-2014-0032
- Komatsu H, Kume T, Otsuki K. 2011. Increasing annual runoff-broadleaf or coniferous forests? *Hydrological Processes* **25** (2): 302–318 DOI: 10.1002/hyp.7898
- Komi K, Neal J, Trigg MA, Diekkrüger B. 2017. Modelling of flood hazard extent in data sparse areas: a case study of the Oti River basin, West Africa. *Journal of Hydrology: Regional Studies* **10**: 122–132 DOI: 10.1016/j.ejrh.2017.03.001
- Koneti S, Sunkara SL, Roy PS. 2018. Hydrological modeling with respect to impact of land-use and land-cover change on the runoff dynamics in Godavari river basin using the HEC-HMS model. *ISPRS International Journal of Geo-Information* **7** (6) DOI: 10.3390/ijgi7060206
- Kong F, Ban Y, Yin H, James P, Dronova I. 2017. Modelling stormwater management at the city district level in response to changes in land use and low impact development. *Environmental Modelling and Software* **95**: 132–142 DOI: 10.1016/j.envsoft.2017.06.021
- Krvavica N, Rubinić J. 2020. Evaluation of design storms and critical rainfall durations for flood prediction in partially urbanized catchments. *Water (Switzerland)* **12** (7) DOI: 10.3390/w12072044
- Krysanova V, Donnelly C, Gelfan A, Gerten D, Arheimer B, Hattermann F, Kundzewicz ZW. 2018. How the performance of hydrological models relates to credibility of projections under climate change. *Hydrological Sciences Journal* **63** (5): 696–720 DOI: 10.1080/02626667.2018.1446214
- Kuhlmann A, Neuweiler I, Van Der Zee SEATM, Helmig R. 2012. Influence of soil structure and root water uptake strategy on unsaturated flow in heterogeneous media. *Water Resources Research* **48** (2): 1–16 DOI: 10.1029/2011WR010651
- Kumar P, Sherring A. 2021. Modelling of rainfall and runoff using HEC-HMS in Oghani Micro-watershed of Azamgarh District Uttar Pradesh. *International Journal of Chemical Studies* **9** (1): 3476–3482 DOI: 10.22271/chemi.2021.v9.i1aw.11772
- Kumarasamy K, Belmont P. 2018. Calibration parameter selection and watershed hydrology model evaluation in time and frequency domains. *Water (Switzerland)* **10** (6) DOI: 10.3390/w10060710
- Kuparinen A, Savolainen O, Schurr FM. 2010. Increased mortality can promote evolutionary adaptation of forest trees to climate change. *Forest Ecology and Management* **259** (5): 1003–1008 DOI: 10.1016/j.foreco.2009.12.006
- Lacob O, Brown I, Rowan J. 2017. Natural flood management, land use and climate change trade-offs: the case of Tarland catchment, Scotland. *Hydrological Sciences Journal* **62** (12): 1931–1948 DOI: 10.1080/02626667.2017.1366657
- Lacob O, Rowan JS, Brown I, Ellis C. 2014. Evaluating wider benefits of natural flood management strategies: an ecosystem-based adaptation perspective. *Hydrology Research* **45** (6): 774–787 DOI: 10.2166/nh.2014.184
- Lai J, Ren L. 2007. Assessing the size dependency of measured hydraulic conductivity using double-ring infiltrometers and numerical simulation. *Soil Science Society of America Journal* **71** (6): 1667–1675 DOI: 10.2136/sssaj2006.0227
- Lamond JE, Rose CB, Booth CA. 2015. Evidence for improved urban flood resilience by sustainable drainage retrofit. *Proceedings of the Institution of Civil Engineers: Urban*

- Design and Planning* **168** (2): 101–111 DOI: 10.1680/udap.13.00022
- LaMotte. 2020. Soil Texture Test Kit. *Individual Soil & Plant Tissue Test Kits* Available at: <https://lamotte.com/products/soil/individual-soil-plant-tissue-test-kits/soil-texture-test-1067> [Accessed 15 October 2020]
- Landhäuser SM, Pinno BD, Mock KE. 2019. Tamm Review: Seedling-based ecology, management, and restoration in aspen (*Populus tremuloides*). *Forest Ecology and Management* **432** (July 2018): 231–245 DOI: 10.1016/j.foreco.2018.09.024
- LandIS. 2020. UK Soil Texture Triangle. *Soil Survey of England and Wales* Available at: <http://www.landis.org.uk/data/nmtopsoiltexture.cfm> [Accessed 18 March 2019]
- Lashford C, Charlesworth S, Warwick F, Blackett M. 2020. Modelling the role of SuDS management trains in minimising flood risk, using microDrainage. *Water (Switzerland)* **12** (9): 1–13 DOI: 10.3390/w12092559
- Lashford C, Lavers T, Reaney S, Charlesworth S, Burgess-Gamble L, Dale J. 2022. Sustainable Catchment-Wide Flood Management: A Review of the Terminology and Application of Sustainable Catchment Flood Management Techniques in the UK. *Water* **14** (8): 1204 DOI: 10.3390/w14081204
- Lavers T, Charlesworth SM. 2016. Natural Flood Risk Management and its Role in Working with Natural Processes. In *Sustainable Surface Water Management*, Charlesworth SM, , Booth CA (eds). Wiley; 157–176. DOI: 10.1002/9781118897690.ch12
- Lavers T, Charlesworth S. 2018. Opportunity mapping of natural flood management measures: a case study from the headwaters of the Warwickshire-Avon. *Environmental Science and Pollution Research* **25** (20): 19313–19322 DOI: 10.1007/s11356-017-0418-z
- Lea D, Yeonsu K, Hyunuk A. 2019. Case study of HEC-RAS 1D-2D coupling simulation: 2002 Baeksan flood event in Korea. *Water (Switzerland)* **11** (10): 1–14 DOI: 10.3390/w11102048
- Lee SJ, Connolly T, Wilson SM, Malcolm DC, Fonweban J, Worrell R, Hubert J, Sykes RJ. 2015. Early height growth of silver birch (*Betula pendula* Roth) provenances and implications for choice of planting stock in Britain. *Forestry* **88** (4): 484–499 DOI: 10.1093/forestry/cpv018
- Leung AK, Boldrin D, Liang T, Wu ZY, Kamchoom V, Bengough AG. 2018. Plant age effects on soil infiltration rate during early plant establishment. *Geotechnique* **68** (7): 646–652 DOI: 10.1680/jgeot.17.T.037
- Li CZ, Wang H, Liu J, Yan DH, Yu FL, Zhang L. 2010. Effect of calibration data series length on performance and optimal parameters of hydrological model. *Water Science and Engineering* **3** (4): 378–393 DOI: 10.3882/j.issn.1674-2370.2010.04.002
- Li L, Yang J, Wu J. 2019. A Method of Watershed Delineation for Flat Terrain Using Sentinel-2A Imagery and DEM: A Case Study of the Taihu Basin. *ISPRS International Journal of Geo-Information* **8** (12): 528 DOI: 10.3390/ijgi8120528
- Li Q, Liang Q, Xia X. 2020. A novel 1D-2D coupled model for hydrodynamic simulation of flows in drainage networks. *Advances in Water Resources* **137** (January): 103519 DOI: 10.1016/j.advwatres.2020.103519
- Li Z, Schneider RL, Morreale SJ, Xie Y, Li C, Li J. 2018. Woody organic amendments for retaining soil water, improving soil properties and enhancing plant growth in desertified soils of Ningxia, China. *Geoderma* **310** (August 2017): 143–152 DOI: 10.1016/j.geoderma.2017.09.009
- Lili M, Bralts VF, Yinghua P, Han L, Tingwu L. 2008. Methods for measuring soil infiltration: State of the art. *International Journal of Agricultural and Biological Engineering* **1** (1): 22–30 DOI: 10.3965/j.issn.1934-6344.2008.01.022-030
- Limpert KE, Carnell PE, Trevathan-Tackett SM, Macreadie PI. 2020. Reducing Emissions From Degraded Floodplain Wetlands. *Frontiers in Environmental Science* **8** (February): 1–18 DOI: 10.3389/fenvs.2020.00008
- Lin B, Wicks JM, Falconer RA, Adams K. 2006. Integrating 1D and 2D hydrodynamic models

- for flood simulation. *Proceedings of the Institution of Civil Engineers: Water Management* **159** (1): 19–25 DOI: 10.1680/wama.2006.159.1.19
- Liu Z, Zhang H, Liang Q. 2019. A coupled hydrological and hydrodynamic model for flood simulation. *Hydrology Research* **50** (2): 589–606 DOI: 10.2166/nh.2018.090
- Lo HW, Smith M, Klaar M, Woulds C. 2021. Potential secondary effects of in-stream wood structures installed for natural flood management: A conceptual model. *WIREs Water* **8** (5) DOI: 10.1002/wat2.1546
- Local Authority SuDS Officer Organisation (LASOO). 2016. Non-statutory technical standards for sustainable drainage
- Logsdon SD, Jaynes DB. 1996. Spatial variability of hydraulic conductivity in a cultivated field at different times. *Soil Science Society of America Journal* **60**: 703–709
- Lopes Bento N, Araújo E Silva Ferraz G, Alexandre Pena Barata R, Santos Santana L, Diennévan Souza Barbosa B, Conti L, Becciolini V, Rossi G. 2022. Overlap influence in images obtained by an unmanned aerial vehicle on a digital terrain model of altimetric precision. *European Journal of Remote Sensing* **55** (1): 263–276 DOI: 10.1080/22797254.2022.2054028
- Lovat A, Vincendon B, Ducrocq V. 2019. Assessing the impact of resolution and soil datasets on flash-flood modelling. *Hydrology and Earth System Sciences* **23** (3): 1801–1818 DOI: 10.5194/hess-23-1801-2019
- Lowe JA, Bernie D, Bett P, Bricheno L, Brown S, Calvert D, Clark R, Edwards T, Fosser G, Fung F, et al. 2019. UKCP18 Science Overview Report
- Lozano-Baez SE, Cooper M, Meli P, Ferraz SFB, Rodrigues RR, Sauer TJ. 2019. Land restoration by tree planting in the tropics and subtropics improves soil infiltration, but some critical gaps still hinder conclusive results. *Forest Ecology and Management* **444** (April): 89–95 DOI: 10.1016/j.foreco.2019.04.046
- Lunka P, Patil SD. 2016. Impact of tree planting configuration and grazing restriction on canopy interception and soil hydrological properties: Implications for flood mitigation in silvopastoral systems. *Hydrological Processes* **30** (6): 945–958 DOI: 10.1002/hyp.10630
- Ma H, Dong X, Chang W. 2018. Application of Synthetic Unit Hydrograph on HEC-HMS Model for Flood Forecasting. *MATEC Web of Conferences* **246** DOI: 10.1051/mateconf/201824601076
- MacKenzie NA. 2010. Ecology, conservation and management of Aspen: A Literature Review. Aberfeldy, UK.
- Mahapatra S, Jha MK, Biswal S, Senapati D. 2020. Assessing Variability of Infiltration Characteristics and Reliability of Infiltration Models in a Tropical Sub-humid Region of India. *Scientific Reports* **10** (1): 1–18 DOI: 10.1038/s41598-020-58333-8
- Mai DT, De Smedt F. 2017. A combined hydrological and hydraulic model for flood prediction in Vietnam applied to the Huong river basin as a test case study. *Water* **9** (11) DOI: 10.3390/w9110879
- Maier R, Krebs G, Pichler M, Muschalla D, Gruber G. 2020. Spatial Rainfall Variability in Urban Environments—High-Density Precipitation Measurements on a City-Scale. *Water* **12** (4): 1157 DOI: 10.3390/w12041157
- Malik I, Pawlik Ł, Ślęzak A, Wistuba M. 2019. A study of the wood anatomy of *Picea abies* roots and their role in biomechanical weathering of rock cracks. *Catena* **173** (October 2018): 264–275 DOI: 10.1016/j.catena.2018.10.018
- Malik S, Pal SC. 2020. Application of 2D numerical simulation for rating curve development and inundation area mapping: a case study of monsoon dominated Dwarkeswar river. *International Journal of River Basin Management* **0** (0): 1–11 DOI: 10.1080/15715124.2020.1738447
- Mann HB, Whitney DR. 1947. On a Test of Whether one of Two Random Variables is Stochastically Larger than the Other. *The Annals of Mathematical Statistics* **18** (1): 50–60 DOI: 10.1214/aoms/1177730491

- Mansanarez V, Westerberg IK, Lam N, Lyon SW. 2019. Rapid Stage-Discharge Rating Curve Assessment Using Hydraulic Modeling in an Uncertainty Framework. *Water Resources Research* **55** (11): 9765–9787 DOI: 10.1029/2018WR024176
- Marcotullio PJ, Braimoh AK, Onishi T. 2008. The Impact of Urbanization on Soils. In *Land Use and Soil Resources* Springer Netherlands: Dordrecht; 201–250. DOI: 10.1007/978-1-4020-6778-5\_10
- Marshall M. 2016. Tree planting and reducing flooding : will it work ? 12–13
- Marshall MR, Ballard CE, Frogbrook ZL, Solloway I, McIntyre N, Reynolds B, Wheater HS. 2014. The impact of rural land management changes on soil hydraulic properties and runoff processes: results from experimental plots in upland UK. *Hydrological Processes* **28** (4): 2617–2629 DOI: 10.1002/hyp.9826
- Martinez P, Buurman P, do Nascimento DL, Almquist V, Vidal-Torrado P. 2021. Substantial changes in podzol morphology after tree-roots modify soil porosity and hydrology in a tropical coastal rainforest. *Plant and Soil* **463** (1–2): 77–95 DOI: 10.1007/s11104-021-04896-y
- Mason DC, Trigg M, Garcia-Pintado J, Cloke HL, Neal JC, Bates PD. 2016. Improving the TanDEM-X Digital Elevation Model for flood modelling using flood extents from Synthetic Aperture Radar images. *Remote Sensing of Environment* **173**: 15–28 DOI: 10.1016/j.rse.2015.11.018
- Matula S, Miháliková M, Lufinková J, Bátková K. 2015. The role of the initial soil water content in the determination of unsaturated soil hydraulic conductivity using a tension infiltrometer. *Plant, Soil and Environment* **62** (11): 515–521 DOI: 10.17221/527/2015-PSE
- Mauer O, Palátová E. 2003. The role of root system in silver birch (*Betula pendula* Roth) dieback in the air-polluted area of Krušné hory Mts. *Journal of Forest Science* **49** (5): 191–199 DOI: 10.17221/4693-jfs
- Mayor of London. 2021. London Flood Awareness Week 2021. *LONDONASSEMBLY* Available at: <https://www.london.gov.uk/city-hall-blog/london-flood-awareness-week-2021> [Accessed 20 December 2021]
- Mazzoleni M, Brandimarte L, Amaranto A. 2019. Evaluating precipitation datasets for large-scale distributed hydrological modelling. *Journal of Hydrology* **578** (December 2018): 124076 DOI: 10.1016/j.jhydrol.2019.124076
- McCuen RH, Knight Z, Cutter AG. 2006. Evaluation of the Nash–Sutcliffe Efficiency Index. *Journal of Hydrologic Engineering* **11** (6): 597–602 DOI: 10.1061/(ASCE)1084-0699(2006)11:6(597)
- McLean L, Beever L, Pender G, Haynes H, Wilkinson M. 2013. Natural Flood Management in the UK: Developing a Conceptual Management Tool. *35th IAHR World Congress* (January 2015): 12 DOI: 10.1039/a800340h
- McMahon TA, Peel MC. 2019. Uncertainty in stage–discharge rating curves: application to Australian Hydrologic Reference Stations data. *Hydrological Sciences Journal* **64** (3): 255–275 DOI: 10.1080/02626667.2019.1577555
- McMillan HK, Booker DJ, Cattoën C. 2016. Validation of a national hydrological model. *Journal of Hydrology* **541**: 800–815 DOI: 10.1016/j.jhydrol.2016.07.043
- Melnikovas A. 2018. Towards an explicit research methodology: Adapting research onion model for futures studies. *Journal of Futures Studies* **23** (2): 29–44 DOI: 10.6531/JFS.201812\_23(2).0003
- Merz B, Hall J, Disse M, Schumann A. 2010. Fluvial flood risk management in a changing world. *Natural Hazards and Earth System Science* **10** (3): 509–527 DOI: 10.5194/nhess-10-509-2010
- Met Office. 2021. UK Climate Averages. *UK Climate Averages for Pershore (Worcestershire)* Available at: <https://www.metoffice.gov.uk/research/climate/maps-and-data/uk-climate-averages/gcq89t680>

- Metcalf P, Beven K, Hankin B, Lamb R. 2017a. Simplified representation of runoff attenuation features within analysis of the hydrological performance of a natural flood management scheme. *Earth Syst. Sci. Discuss. Earth Syst. Sci. Discussion started* **13** (July) DOI: 10.5194/hess-2017-398
- Metcalf P, Beven K, Hankin B, Lamb R. 2017b. A modelling framework for evaluation of the hydrological impacts of nature-based approaches to flood risk management, with application to in-channel interventions across a 29-km<sup>2</sup> scale catchment in the United Kingdom. *Hydrological Processes* **31** (9): 1734–1748 DOI: 10.1002/hyp.11140
- Metcalf P, Beven K, Hankin B, Lamb R. 2018. A new method, with application, for analysis of the impacts on flood risk of widely distributed enhanced hillslope storage. *Hydrology and Earth System Sciences* **22** (4): 2589–2605 DOI: 10.5194/hess-22-2589-2018
- METER® Group Inc. 2020. *Mini Disk Infiltrometer User's Manual*. METER Group, Inc. USA: 2365 NE Hopkins Court, Pullman, WA.
- Meyer N, Welp G, Amelung W. 2019. Effect of sieving and sample storage on soil respiration and its temperature sensitivity (Q<sub>10</sub>) in mineral soils from Germany. *Biology and Fertility of Soils* **55** (8): 825–832 DOI: 10.1007/s00374-019-01374-7
- Milla K, Kish S. 2006. A low-cost microprocessor and infrared sensor system for automating water infiltration measurements. *Computers and Electronics in Agriculture* **53** (2): 122–129 DOI: 10.1016/j.compag.2006.05.001
- Miller JD, Hess T. 2017. Urbanisation impacts on storm runoff along a rural-urban gradient. *Journal of Hydrology* **552**: 474–489 DOI: 10.1016/j.jhydrol.2017.06.025
- Ministry of Housing Communities & Local Government. 2021. *National Planning Policy Framework*. Ministry of Housing, Communities and Local Government: London, UK. Available at: [https://assets.publishing.service.gov.uk/government/uploads/system/uploads/attachment\\_data/file/1005759/NPPF\\_July\\_2021.pdf](https://assets.publishing.service.gov.uk/government/uploads/system/uploads/attachment_data/file/1005759/NPPF_July_2021.pdf)
- Mishra P, Pandey C, Singh U, Keshri A, Sabaretnam M. 2019. Selection of appropriate statistical methods for data analysis. *Annals of Cardiac Anaesthesia* **22** (3): 297–301 DOI: 10.4103/aca.ACA\_248\_18
- Mishra SK, Tyagi J V., Singh VP. 2003. Comparison of infiltration models. *Hydrological Processes* **17** (13): 2629–2652 DOI: 10.1002/hyp.1257
- Mockler EM, O'Loughlin FE, Bruen M. 2016. Understanding hydrological flow paths in conceptual catchment models using uncertainty and sensitivity analysis. *Computers and Geosciences* **90**: 66–77 DOI: 10.1016/j.cageo.2015.08.015
- Mölder A, Sennhenn-Reulen H, Fischer C, Rumpf H, Schönfelder E, Stockmann J, Nagel RV. 2019. Success factors for high-quality oak forest (*Quercus robur*, *Q. petraea*) regeneration. *Forest Ecosystems* **6** (1) DOI: 10.1186/s40663-019-0206-y
- Morales-Hernández M, Petaccia G, Brufau P, García-Navarro P. 2016. Conservative 1D-2D coupled numerical strategies applied to river flooding: The Tiber (Rome). *Applied Mathematical Modelling* **40** (3): 2087–2105 DOI: 10.1016/j.apm.2015.08.016
- Moya Quiroga V, Kure S, Udo K, Mano A. 2016. Application of 2D numerical simulation for the analysis of the Bolivian Amazonia flood: Application of the new HEC-RAS version 5. *RIBAGUA - Revista Iberoamericana del Agua* **3** (1): 25–33 DOI: 10.1016/j.riba.2015.12.001
- Muhammad M, Lu Z. 2020. Estimating the UK Index Flood: an Improved Spatial Flooding Analysis. *Environmental Modeling and Assessment* **25** (5): 731–748 DOI: 10.1007/s10666-020-09713-x
- Muller B, Guédon Y, Passot S, Lobet G, Nacry P, Pagès L, Wissuwa M, Draye X. 2019. Lateral Roots: Random Diversity in Adversity. *Trends in Plant Science* **24** (9): 810–825 DOI: 10.1016/j.tplants.2019.05.011
- Mulvany T. 1850. The use of self registering rain and flood gauges. *Institute of Civil Engineers* **4** (2): 1–8

- Muneer AS, Sayl KN, Kamal AH. 2020. A Comparative Study to Assess the Suitable Models for Predicting the Infiltration Rate in an Arid Region. *Iraqi Journal of Civil Engineering* **14** (1): 29–38
- Murphy T. 2021. Optimising oak woodland establishment into UK upland pastures in the context of climate change ; and the role of oak woodland in soil hydrological recovery for natural flood management
- Murphy TR, Hanley ME, Ellis JS, Lunt PH. 2021. Native woodland establishment improves soil hydrological functioning in UK upland pastoral catchments. *Land Degradation and Development* **32** (2): 1034–1045 DOI: 10.1002/ldr.3762
- Myking T, Bøhler F, Austrheim G, Solberg EJ. 2011. Life history strategies of aspen (*Populus tremula* L.) and browsing effects: A literature review. *Forestry* **84** (1): 61–71 DOI: 10.1093/forestry/cpq044
- Nachar N. 2008. The Mann-Whitney U: A Test for Assessing Whether Two Independent Samples Come from the Same Distribution. *Tutorials in Quantitative Methods for Psychology* **4** (1): 13–20 DOI: 10.20982/tqmp.04.1.p013
- Naik AP, Ghosh B, Pekkat S. 2019. Estimating soil hydraulic properties using mini disk infiltrometer. *ISH Journal of Hydraulic Engineering* **25** (1): 62–70 DOI: 10.1080/09715010.2018.1471363
- Nash JE, Sutcliffe JV. 1970. River flow forecasting through conceptual models Part I-A discussion of principles. *Journal of Hydrology* **10**: 282–290 DOI: 10.3917/difa.012.0161
- National River Flow Archive. 2019. NRFA Hydrometric Data Search. 54907 - Arrow at Broom Available at: <https://nrfa.ceh.ac.uk/data/station/spatial/54907> [Accessed 15 February 2019]
- Neal JC, Odoni NA, Trigg MA, Freer JE, Garcia-Pintado J, Mason DC, Wood M, Bates PD. 2015. Efficient incorporation of channel cross-section geometry uncertainty into regional and global scale flood inundation models. *Journal of Hydrology* **529**: 169–183 DOI: 10.1016/j.jhydrol.2015.07.026
- Nesting R, Asleson BC, Gulliver JS, Hozalski RM, Nieber JL. 2018. Laboratory Comparison of Field Infiltrimeters. *Journal of Sustainable Water in the Built Environment* **4** (3): 1–6 DOI: 10.1061/JSWBAY.0000857
- NextGen. 2020. NextGen Sernal, UK. *Demonstration Cases, Sernal, United Kingdom* Available at: <https://nextgenwater.eu/demonstration-cases/spernal/> [Accessed 16 March 2020]
- Ng ZF, Gisen JI, Akbari A. 2018. Flood Inundation Modelling in the Kuantan River Basin using 1D-2D Flood Modeller coupled with ASTER-GDEM. *IOP Conference Series: Materials Science and Engineering* **318** (1): 012024 DOI: 10.1088/1757-899X/318/1/012024
- Ngai R, Wilkinson M, Nisbet T, Harvey R, Addy S, Burgess-Gamble L, Rose S, Maslen S, Nicholson A, Page T, et al. 2017. *Working with Natural Processes-Evidence Directory Appendix 2: Literature review*. Environment Agency, Horizon House, Deanery Road, Bristol, BS1 5AH. Available at: <http://www.gov.uk/government/organisations/environment-agency/publications/working-with-natural-processes-evidence-directory>
- Nguyen NT, He W, Zhu Y, Lü H. 2020. Influence of calibration parameter selection on flash flood simulation for small to medium catchments with misdc-2l model. *Water (Switzerland)* **12** (11) DOI: 10.3390/w12113255
- Nicholson AR, O'Donnell GM, Wilkinson ME, Quinn PF. 2019. The potential of runoff attenuation features as a Natural Flood Management approach. *Journal of Flood Risk Management* **13** (S1): 1–14 DOI: 10.1111/jfr3.12565
- Nisbet T. 2005. Water Use by Trees - Forestry Commission Information Note FCIN065: 1–8 Available at: [https://www.forestry.gov.uk/pdf/FCIN065.pdf/\\$file/FCIN065.pdf](https://www.forestry.gov.uk/pdf/FCIN065.pdf/$file/FCIN065.pdf)
- Nkwunonwo UC, Whitworth M, Baily B. 2020. A review of the current status of flood

- modelling for urban flood risk management in the developing countries. *Scientific African* **7**: e00269 DOI: 10.1016/j.sciaf.2020.e00269
- Noh SJ, Lee JH, Lee S, Kawaike K, Seo DJ. 2018. Hyper-resolution 1D-2D urban flood modelling using LiDAR data and hybrid parallelization. *Environmental Modelling and Software* **103**: 131–145 DOI: 10.1016/j.envsoft.2018.02.008
- Norbury M, Phillips H, Macdonald N, Brown D, Boothroyd R, Wilson C, Quinn P, Shaw D. 2021. Quantifying the hydrological implications of pre- and post-installation willowed engineered log jams in the Pennine Uplands, NW England. *Journal of Hydrology* **603** (PC): 126855 DOI: 10.1016/j.jhydrol.2021.126855
- Nutt N, Perfect C. 2011. Allan Water Natural Flood Management: Scoping Study. Stirling, SEPA.
- O’Loughlin FE, Neal J, Schumann GJP, Beighley E, Bates PD. 2020. A LISFLOOD-FP hydraulic model of the middle reach of the Congo. *Journal of Hydrology* **580** (September 2019): 124203 DOI: 10.1016/j.jhydrol.2019.124203
- Odoni NA, Lane SN. 2010. Assessment of the Impact of Upstream Land Management Measures on Flood Flows in Pickering Beck Using Overflow
- Oleyiblo JO, Li ZJ. 2010. Application of HEC-HMS for flood forecasting in Misai and Wan’an catchments in China. *Water Science and Engineering* **3** (1): 14–22 DOI: 10.3882/j.issn.1674-2370.2010.01.002
- Oliveira-Jr A, Resende C, Pereira A, Madureira P, Gonçalves J, Moutinho R, Soares F, Moreira W. 2020. IoT Sensing Platform as a Driver for Digital Farming in Rural Africa. *Sensors* **20** (12): 3511 DOI: 10.3390/s20123511
- Onyutha C. 2019. Hydrological model supported by a step-wise calibration against sub-flows and validation of extreme flow events. *Water (Switzerland)* **11** (2) DOI: 10.3390/w11020244
- Ordnance Survey. 2020. Ordnance Survey MasterMap Imagery Layer. *OS MasterMap Imagery Layer* Available at: <https://www.ordnancesurvey.co.uk/business-and-government/products/imagery-layer.html> [Accessed 15 February 2019]
- Ordnance Survey. 2021. Ordnance Survey Open Data Download. *OS OpenData* Available at: <https://www.ordnancesurvey.co.uk/opendatadownload/products.html> [Accessed 15 February 2019]
- Ordnance Survey. 2022. OS VectorMap District. *Free OS Open Data* Available at: <https://osdatahub.os.uk/downloads/open/VectorMapDistrict> [Accessed 14 December 2021]
- Osman KT. 2013. *Forest soils: Properties and management*. Springer: New York, USA.
- Othman N, Romali NS, Samat SR, Ahmad AM. 2021. Calibration and validation of hydrological model using HEC-HMS for Kuantan River Basin. *IOP Conference Series: Materials Science and Engineering* **1092** (1): 012028 DOI: 10.1088/1757-899X/1092/1/012028
- Pan F, Stieglitz M, McKane RB. 2012. An algorithm for treating flat areas and depressions in digital elevation models using linear interpolation. *Water Resources Research* **48** (2): 1–13 DOI: 10.1029/2011WR010735
- Park E, Parker JC. 2008. A simple model for water table fluctuations in response to precipitation. *Journal of Hydrology* **356** (3–4): 344–349 DOI: 10.1016/j.jhydrol.2008.04.022
- Pasquier U, He Y, Hooton S, Goulden M, Hiscock KM. 2019. An integrated 1D–2D hydraulic modelling approach to assess the sensitivity of a coastal region to compound flooding hazard under climate change. *Natural Hazards* **98** (3): 915–937 DOI: 10.1007/s11069-018-3462-1
- Patil VK, Saraf VR, Karad O V., Ghodke SB, Gore D, Dhekale SS. 2019. Simulation of Rainfall Runoff Process Using HEC-HMS Model for Upper Godavari Basin Maharashtra, India. *European Journal of Engineering Research and Science* **4** (4): 102–107 DOI:

- 10.24018/ejers.2019.4.4.927
- Patra S, Kaushal R, Singh D, Kumar R, Gadedjisso-Tossou A, Durai J. 2022. Surface soil hydraulic conductivity and macro-pore characteristics as affected by four bamboo species in North-Western Himalaya, India. *Ecohydrology and Hydrobiology* **22** (1): 188–196 DOI: 10.1016/j.ecohyd.2021.08.012
- Pattison I, Lane SN, Hardy RJ, Reaney SM. 2014. The role of tributary relative timing and sequencing in controlling large floods. *Water Resources Research* **50** (7): 5444–5458 DOI: 10.1002/2013WR014067
- Paul PK, Gaur S, Kumari B, Panigrahy N, Mishra A, Singh R. 2019. Diagnosing Credibility of a Large-Scale Conceptual Hydrological Model in Simulating Streamflow. *Journal of Hydrologic Engineering* **24** (4): 04019004 DOI: 10.1061/(asce)he.1943-5584.0001766
- Perry TO. 1982. Tree Roots : Facts and Fallacies. *Journal of Arboriculture* **8**: 197–211
- Petchko K. 2018. Results, Discussion, and Conclusion. In *How to Write About Economics and Public Policy* Elsevier; 271–300. DOI: 10.1016/B978-0-12-813010-0.00014-4
- Peukert S, Uglow J, Langdon A, Thorne B. 2017. Case study 31 . Hills to Levels Project Available at: <https://www.gov.uk/government/publications/working-with-natural-processes-to-reduce-flood-risk>
- Pinos J, Timbe L. 2019. Performance assessment of two-dimensional hydraulic models for generation of flood inundation maps in mountain river basins. *Water Science and Engineering* **12** (1): 11–18 DOI: 10.1016/j.wse.2019.03.001
- Pitt M. 2008. Learning Lessons from the 2007 Floods: An Independent Review by Sir Michael Pitt. London. DOI: 10.1007/s13398-014-0173-7.2
- Planchon O, Darboux F. 2002. A fast, simple and versatile algorithm to fill the depressions of digital elevation models. *Catena* **46** (2–3): 159–176 DOI: 10.1016/S0341-8162(01)00164-3
- Ponce VM. 1991. Kinematic Wave Controversy. *Journal of Hydraulic Engineering* **117** (4): 511–525 DOI: 10.1061/(ASCE)0733-9429(1991)117:4(511)
- Prieksat MA, Kaspar TC, Ankeny MD. 1994. Positional and temporal changes in ponded infiltration in a corn field. *Soil Science Society of America Journal* **58**: 181–184
- Di Prima S, Concialdi P, Lassabatere L, Angulo-Jaramillo R, Pirastru M, Cerdà A, Keesstra S. 2018a. Laboratory testing of Beerkan infiltration experiments for assessing the role of soil sealing on water infiltration. *Catena* **167** (October 2017): 373–384 DOI: 10.1016/j.catena.2018.05.013
- Di Prima S, Lassabatere L, Rodrigo-Comino J, Marrosu R, Pulido M, Angulo-Jaramillo R, úbeda X, Keesstra S, Cerdà A, Pirastru M. 2018b. Comparing transient and steady-state analysis of single-ring infiltrometer data for an abandoned field affected by fire in Eastern Spain. *Water (Switzerland)* **10** (4) DOI: 10.3390/w10040514
- Putro B, Kjeldsen TR, Hutchins MG, Miller J. 2016. An empirical investigation of climate and land-use effects on water quantity and quality in two urbanising catchments in the southern United Kingdom. *Science of the Total Environment* **548–549**: 164–172 DOI: 10.1016/j.scitotenv.2015.12.132
- Rabot E, Wiesmeier M, Schlüter S, Vogel HJ. 2018. Soil structure as an indicator of soil functions: A review. *Geoderma* **314** (June 2017): 122–137 DOI: 10.1016/j.geoderma.2017.11.009
- Rahman M, Ennos R. 2016. What we know and don't know about the surface runoff reduction potential of urban trees: 1–14
- Rahman MA, Moser A, Anderson M, Zhang C, Rötzer T, Pauleit S. 2019. Comparing the infiltration potentials of soils beneath the canopies of two contrasting urban tree species. *Urban Forestry and Urban Greening* **38** (November 2018): 22–32 DOI: 10.1016/j.ufug.2018.11.002
- Ramly S, Tahir W, Abdullah J, Jani J, Ramli S, Asmat A. 2020. Flood Estimation for SMART Control Operation Using Integrated Radar Rainfall Input with the HEC-HMS Model.

- Water Resources Management* DOI: 10.1007/s11269-020-02595-4
- Rampinelli CG, Knack I, Smith T. 2020. Flood mapping uncertainty from a restoration perspective: A practical case study. *Water (Switzerland)* **12** (7): 1–20 DOI: 10.3390/w12071948
- Randrup TB. 2001. A review of tree root conflicts with sidewalks, curbs, and roads. *Urban Ecosystems* **5** (3): 209–225 DOI: 10.1023/A:1024046004731
- Rangari VA, Sridhar V, Umamahesh N V., Patel AK. 2020. Rainfall Runoff Modelling of Urban Area Using HEC-HMS: A Case Study of Hyderabad City., AlKhaddar R, , Singh RK, , Dutta S, , Kumari M (eds).Springer Singapore: Singapore; 113–125. DOI: 10.1007/978-981-13-8181-2\_9
- Rashed M. 2016. Rolling ball algorithm as a multitask filter for terrain conductivity measurements. *Journal of Applied Geophysics* **132**: 17–24 DOI: 10.1016/j.jappgeo.2016.06.016
- Rasmussen AL, Busby RR, Hoeksema JD. 2018. Host preference of ectomycorrhizal fungi in mixed pine–oak woodlands. *Canadian Journal of Forest Research* **48** (2): 153–159 DOI: 10.1139/cjfr-2017-0227
- Rath S, Tripathy A, Tripathy AR. 2020. Prediction of new active cases of coronavirus disease (COVID-19) pandemic using multiple linear regression model. *Diabetes and Metabolic Syndrome: Clinical Research and Reviews* **14** (5): 1467–1474 DOI: 10.1016/j.dsx.2020.07.045
- Razafindratsima OH, Brown KA, Carvalho F, Johnson SE, Wright PC, Dunham AE. 2018. Edge effects on components of diversity and above-ground biomass in a tropical rainforest. *Journal of Applied Ecology* **55** (2): 977–985 DOI: 10.1111/1365-2664.12985
- Razmkhah H. 2016. Comparing performance of different loss methods in rainfall-runoff modeling. *Water Resources* **43** (1): 207–224 DOI: 10.1134/S0097807816120058
- Razzaque J, Lester C. 2021. Why Protect Ancient Woodland in the UK? Rethinking the Ecosystem Approach. *Transnational Environmental Law* **10** (1): 135–158 DOI: 10.1017/S2047102520000333
- Remesan R, Begam S, Holman IP. 2019. Effect of baseline snowpack assumptions in the HySIM model in predicting future hydrological behaviour of a Himalayan catchment. *Hydrology Research* **50** (2): 691–708 DOI: 10.2166/nh.2018.069
- Ren X, Hong N, Li L, Kang J, Li J. 2020. Effect of infiltration rate changes in urban soils on stormwater runoff process. *Geoderma* **363** (December 2019) DOI: 10.1016/j.geoderma.2019.114158
- Revell N, Lashford C, Blackett M, Rubinato M. 2021. Modelling the Hydrological Effects of Woodland Planting on Infiltration and Peak Discharge Using HEC-HMS. *Water* **13** (21): 3039 DOI: 10.3390/w13213039
- Revell N, Lashford C, Rubinato M, Blackett M. 2022. The Impact of Tree Planting on Infiltration Dependent on Tree Proximity and Maturity at a Clay Site in Warwickshire, England. *Water* **14** (6): 892 DOI: 10.3390/w14060892
- Revilla-Romero B, Beck HE, Burek P, Salamon P, de Roo A, Thielen J. 2015. Filling the gaps: Calibrating a rainfall-runoff model using satellite-derived surface water extent. *Remote Sensing of Environment* **171**: 118–131 DOI: 10.1016/j.rse.2015.10.022
- Roberts N. 2008. Assessing the spatial and temporal variation in the skill of precipitation forecasts from an NWP model. *Meteorological Applications* **15** (1): 163–169 DOI: 10.1002/met.57
- Robichaud PR, Lewis SA, Ashmun LE. 2008. New procedure for sampling infiltration to assess post-fire soil water repellency. *USDA Forest Service - Research Note RMRS-RN* (33 RMRS-RN): 1–14
- Robinson M, Newson MD. 1986. Comparison of forest and moorland hydrology in an upland area with peat soils. *International Peat Journal* **1**: 49–68
- Rodwell JS. 2006. *National Vegetation Classification : Users handbook*. JNCC: Monkstone

- House, City Road, Peterborough.
- Romero-Ruiz A, Linde N, Keller T, Or D. 2018. A Review of Geophysical Methods for Soil Structure Characterization. *Reviews of Geophysics* **56** (4): 672–697 DOI: 10.1029/2018RG000611
- Rönnqvist H. 2018. Double-Ring Infiltrometer for In-Situ Permeability Determination of Dam Material. *Engineering* **10** (06): 320–328 DOI: 10.4236/eng.2018.106022
- Rossi MJ, Ares JO, Jobbágy EG, Vivoni ER, Vervoort RW, Schreiner-McGraw AP, Saco PM. 2018. Vegetation and terrain drivers of infiltration depth along a semiarid hillslope. *Science of the Total Environment* **644**: 1399–1408 DOI: 10.1016/j.scitotenv.2018.07.052
- Rubinato M, Nichols A, Peng Y, Zhang J min, Lashford C, Cai Y peng, Lin P zhi, Tait S. 2019. Urban and river flooding: Comparison of flood risk management approaches in the UK and China and an assessment of future knowledge needs. *Water Science and Engineering* **12** (4): 274–283 DOI: 10.1016/j.wse.2019.12.004
- Sahoo N, Panigrahi B, Das DM, Das DP. 2020. Simulation of runoff in baitarani basin using composite and distributed curve number approaches in HEC-HMS model. *Mausam* **71** (4): 675–686
- Sahraei S, Asadzadeh M, Unduche F. 2020. Signature-based multi-modelling and multi-objective calibration of hydrologic models: Application in flood forecasting for Canadian Prairies. *Journal of Hydrology* **588** (November 2019): 125095 DOI: 10.1016/j.jhydrol.2020.125095
- Sanou J, Zougmore R, Bayala J, Teklehaimanot Z. 2010. Soil infiltrability and water content as affected by Baobab (*Adansonia digitata* L.) and Néré (*Parkia biglobosa* (Jacq.) Benth.) trees in farmed parklands of West Africa. *Soil Use and Management* **26** (1): 75–81 DOI: 10.1111/j.1475-2743.2009.00250.x
- Sañudo-Fontaneda LA, Jato-Espino D, Lashford C, Coupe SJ. 2017. Simulation of the hydraulic performance of highway filter drains through laboratory models and stormwater management tools. *Environmental Science and Pollution Research* **25** (May): 1–10 DOI: 10.1007/s11356-017-9170-7
- Sarkar R, Dutta S, Panigrahy S. 2008. Characterizing overland flow on a preferential infiltration dominated hillslope: Case study. *Journal of Hydrologic Engineering* **13** (7): 563–569 DOI: Doi 10.1061/(Asce)1084-0699(2008)13:7(563)
- Saunders MNK, Lewis P, Thornhill A. 2019. *Research Methods for Business Students*. Pearson: Harlow.
- Savill P. 2019. *The Silviculture of Trees Used in British Forestry*. CABI Publishing, United Kingdom.
- Scharffenberg W. 2016. Hydrologic Modelling System HEC-HMS, User's Manual. *US Army Corps of Engineers, Hydrologic Engineering Center* (August) DOI: CDP-74A
- Schober P, Boer C, Schwarte LA. 2018. Correlation Coefficients. *Anesthesia & Analgesia* **126** (5): 1763–1768 DOI: 10.1213/ANE.0000000000002864
- Scholl P, Leitner D, Kammerer G, Loiskandl W, Kaul HP, Bodner G. 2014. Root induced changes of effective 1D hydraulic properties in a soil column. *Plant and Soil* **381** (1–2): 193–213 DOI: 10.1007/s11104-014-2121-x
- Schütte S, Schulze RE. 2017. Projected impacts of urbanisation on hydrological resource flows: A case study within the uMngeni Catchment, South Africa. *Journal of Environmental Management* **196**: 527–543 DOI: 10.1016/j.jenvman.2017.03.028
- Seddon N, Chausson A, Berry P, Girardin CAJ, Smith A, Turner B. 2020. Understanding the value and limits of nature-based solutions to climate change and other global challenges. *Philosophical Transactions of the Royal Society B: Biological Sciences* **375** (1794) DOI: 10.1098/rstb.2019.0120
- Shahiriparsa A, Noori M, Heydari M, Rashidi M. 2016. Floodplain zoning simulation by using HEC-RAS and CCHE2D models in the Sungai Maka river. *Air, Soil and Water Research* **9** (April): 55–62 DOI: 10.4137/ASWR.S36089

- Sharu EH. 2020. Development of HEC-HMS Model for Flow Simulation at Dungun River Basin Malaysia. *Advances in Agricultural and Food Research Journal* **1** (December 2020): 1–16 DOI: 10.36877/aafrrj.a0000169
- Shaw EM. 1988. *Hydrology in Practice*.
- Shaw EM, Beven KJ, Chappell NA, Lamb R. 2011. *Hydrology in Practice*. Spon Press: Oxford.
- Shinohara Y, Levia DF, Komatsu H, Nogata M, Otsuki K. 2015. Comparative modeling of the effects of intensive thinning on canopy interception loss in a Japanese cedar (*Cryptomeria japonica* D. Don) forest of western Japan. *Agricultural and Forest Meteorology* **214–215**: 148–156 DOI: 10.1016/j.agrformet.2015.08.257
- Short C, Clarke L, Carnelli F, Uttley C, Smith B. 2019. Capturing the multiple benefits associated with nature-based solutions: Lessons from a natural flood management project in the Cotswolds, UK. *Land Degradation and Development* **30** (3): 241–252 DOI: 10.1002/ldr.3205
- Shuttleworth EL, Evans MG, Pilkington M, Spencer T, Walker J, Milledge D, Allott TEH. 2019. Restoration of blanket peat moorland delays stormflow from hillslopes and reduces peak discharge. *Journal of Hydrology X* **2** DOI: 10.1016/j.hydroa.2018.100006
- Siegmeier T, Blumenstein B, Möller D. 2019. Bioenergy Production and Organic Agriculture. In *Organic Farming* Elsevier; 331–359. DOI: 10.1016/B978-0-12-813272-2.00012-4
- Silber A. 2019. Chemical Characteristics of Soilless Media. In *Soilless Culture* Elsevier; 113–148. DOI: 10.1016/B978-0-444-63696-6.00004-9
- De Silva M, Weerakoon SB, Herath S. 2014. Modeling of Event and Continuous Flow Hydrographs with HEC-HMS: Case Study in the Kelani River Basin, Sri Lanka. *Journal of Hydrologic Engineering* **19** (4): 800–806 DOI: 10.1061/(ASCE)HE.1943-5584.0000846
- Singer JA, Turnbull R, Foster M, Bettigole C, Frey BR, Downey MC, Covey KR, Ashton MS. 2019. Sudden aspen decline: A review of pattern and process in a changing climate. *Forests* **10** (8): 1–17 DOI: 10.3390/f10080671
- Singer MB, Dunne T. 2004. An empirical-stochastic, event-based program for simulating inflow from a tributary network: Framework and application to the Sacramento River basin, California. *Water Resources Research* **40** (7): 1–19 DOI: 10.1029/2003WR002725
- Skovsgaard JP, Ols C, Mc Carthy R. 2018. High-pruning of silver birch (*Betula pendula* Roth): work efficiency as a function of pruning method, pole saw type, slash removal, operator, pruning height and branch characteristics. *International Journal of Forest Engineering* **29** (2): 117–127 DOI: 10.1080/14942119.2018.1462593
- Smith RE, Parlange J -Y. 1978. A parameter-efficient hydrologic infiltration model. *Water Resources Research* **14** (3): 533–538 DOI: 10.1029/WR014i003p00533
- Solloway I. 2012. Effects of tree shelterbelts on the hydrology of upland areas. Imperial College London.
- Song X, Gao X, Dyck M, Zhang W, Wu P, Yao J, Zhao X. 2018. Soil water and root distribution of apple tree (*Malus pumila* Mill) stands in relation to stand age and rainwater collection and infiltration system (RWCI) in a hilly region of the Loess Plateau, China. *Catena* **170** (June): 324–334 DOI: 10.1016/j.catena.2018.06.026
- Stamatakis I, Kjeldsen TR. 2021. Reconstructing the peak flow of historical flood events using a hydraulic model: The city of Bath, United Kingdom. *Journal of Flood Risk Management* **14** (3): 1–15 DOI: 10.1111/jfr3.12719
- Suffolk Wildlife Trust. 2020. Woodland Creation. *Woodlands and Hedgerows* Available at: <https://www.suffolkwildlifetrust.org/conservationadvice/woodlands-and-hedgerows/woodland-creation> [Accessed 11 February 2022]
- Sun D, Yang H, Guan D, Yang M, Wu J, Yuan F, Jin C, Wang A, Zhang Y. 2018. The effects of land use change on soil infiltration capacity in China: A meta-analysis. *Science of the Total Environment* **626**: 1394–1401 DOI: 10.1016/j.scitotenv.2018.01.104
- Sy B, Frischknecht C, Dao H, Consuegra D, Giuliani G. 2019. Flood hazard assessment and

- the role of citizen science. *Journal of Flood Risk Management* **12** (February 2018): 1–14 DOI: 10.1111/jfr3.12519
- Szilagyi J, Parlange MB. 1998. Baseflow separation based on analytical solutions of the Boussinesq equation. *Journal of Hydrology* **204** (1–4): 251–260 DOI: 10.1016/S0022-1694(97)00132-7
- Taylor AL, Dessai S, Bruine de Bruin W. 2014. Public perception of climate risk and adaptation in the UK: A review of the literature. *Climate Risk Management* **4**: 1–16 DOI: 10.1016/j.crm.2014.09.001
- Teng J, Jakeman AJ, Vaze J, Croke BFW, Dutta D, Kim S. 2017. Flood inundation modelling: A review of methods, recent advances and uncertainty analysis. *Environmental Modelling and Software* **90**: 201–216 DOI: 10.1016/j.envsoft.2017.01.006
- Terink W, Leijnse H, van den Eertwegh G, Uijlenhoet R. 2018. Spatial resolutions in areal rainfall estimation and their impact on hydrological simulations of a lowland catchment. *Journal of Hydrology* **563** (May): 319–335 DOI: 10.1016/j.jhydrol.2018.05.045
- The Heart of England Forest Charity. 2020. All the latest from the Heart of England Forest. *All the latest from the Heart of England Forest (email newsletter)*
- The Heart of England Forest Charity. 2021. The Heart of England Forest Available at: <https://www.heartofenglandforest.com/> [Accessed 13 March 2019]
- The Met Office. 2019. About UKCP18. *About UKCP18* Available at: <https://www.metoffice.gov.uk/research/approach/collaboration/ukcp/about> [Accessed 22 May 2020]
- The Met Office. 2020. Record Breaking Rainfall. *Wettest February on record and 5th wettest Winter* Available at: <https://www.metoffice.gov.uk/about-us/press-office/news/weather-and-climate/2020/2020-winter-february-stats> [Accessed 11 June 2021]
- The Met Office. 2021a. When does summer start? *When does summer start?* Available at: <https://www.metoffice.gov.uk/weather/learn-about/weather/seasons/summer/when-does-summer-start>
- The Met Office. 2021b. When does winter start? *When does winter start?* Available at: <https://www.metoffice.gov.uk/weather/learn-about/weather/seasons/winter/when-does-winter-start>
- The Royal Horticultural Society. 2021. Quercus petraea. *Woodland Classifications* Available at: <https://www.rhs.org.uk/Plants/14280/Quercus-petraea/Details> [Accessed 23 March 2021]
- The UK Government. 2020. Agriculture Act 2020 Available at: <https://www.legislation.gov.uk/ukpga/2020/21/2021-01-01>
- The World Health Organisation. 2021. Floods. *Health Topics* Available at: [https://www.who.int/health-topics/floods#tab=tab\\_1](https://www.who.int/health-topics/floods#tab=tab_1) [Accessed 12 October 2021]
- Thomas H, Nisbet TR. 2016. Slowing the flow in pickering: quantifying the effect of catchment Woodland planting on flooding using the soil conservation service curve number method. *International Journal of Safety and Security Engineering* **6** (3): 466–474 DOI: 10.2495/SAFE-V6-N3-466-474
- Tikhamarine Y, Souag-Gamane D, Ahmed AN, Sammen SS, Kisi O, Huang YF, El-Shafie A. 2020. Rainfall-runoff modelling using improved machine learning methods: Harris hawks optimizer vs. particle swarm optimization. *Journal of Hydrology* **589** (May): 125133 DOI: 10.1016/j.jhydrol.2020.125133
- Tinya F, Kovács B, Aszalós R, Tóth B, Csépanyi P, Németh C, Ódor P. 2020. Initial regeneration success of tree species after different forestry treatments in a sessile oak-hornbeam forest. *Forest Ecology and Management* **459** (January): 117810 DOI: 10.1016/j.foreco.2019.117810
- Todini E. 2007. Hydrological catchment modelling: past, present and future. *Hydrological Earth System Science* **11** (1): 468–482 DOI: 10.5194/hess-11-468-2007
- Tullus A, Rosenvald K, Lutter R, Kaasik A, Kupper P, Sellin A. 2020. Coppicing improves the

- growth response of short-rotation hybrid aspen to elevated atmospheric humidity. *Forest Ecology and Management* **459** (December 2019): 117825 DOI: 10.1016/j.foreco.2019.117825
- Tzioutzios C, Kastridis A. 2020. Multi-criteria evaluation (MCE) method for the management of Woodland plantations in floodplain areas. *ISPRS International Journal of Geo-Information* **9** (12) DOI: 10.3390/ijgi9120725
- UK Centre for Ecology and Hydrology. 2021. The Flood Estimation Handbook. *The FEH* Available at: <https://www.ceh.ac.uk/services/flood-estimation-handbook>
- UK Data Service Census Support. 2011. Census Boundary Data. *Get Census Data* Available at: <https://census.ukdataservice.ac.uk/get-data/boundary-data.aspx> [Accessed 15 March 2019]
- UK Government. 2021a. *The England Trees Action Plan 2021 - 2024*. APS Group: Defra, Seacole Building, 2 Marsham Street, London. Available at: [www.nationalarchives.gov.uk/doc/open-](http://www.nationalarchives.gov.uk/doc/open-)
- UK Government. 2021b. Environment Act 2021 Available at: <https://www.legislation.gov.uk/ukpga/2021/30/contents/enacted>
- UK Met Office. 2018. UKCP18 Guidance: Representative Concentration Pathways: 18–20 Available at: <https://www.metoffice.gov.uk/research/approach/collaboration/ukcp/guidance-science-reports>
- US Army Corps of Engineers. 1993. Introduction and application of kinematic wave routing techniques using HEC-1. Davis, CA.
- US Army Corps of Engineers. 2000. Hydrologic modeling system HEC-HMS, Technical Reference Manual. *Technical Reference Manual* (March): 145 DOI: CDP-74B
- US Army Corps of Engineers. 2021. HEC-RAS. *HEC-RAS Features* Available at: <https://www.hec.usace.army.mil/software/hec-ras/features.aspx> [Accessed 8 November 2021]
- US Army Corps of Engineers. 2022. HEC-HMS Technical Reference Manual Available at: <https://www.hec.usace.army.mil/confluence/hmsdocs/hmstrm/introduction>
- Vand AS, Sihag P, Singh B, Zand M. 2018. Comparative Evaluation of Infiltration Models. *KSCE Journal of Civil Engineering* **22** (10): 4173–4184 DOI: 10.1007/s12205-018-1347-1
- Vergani C, Graf F. 2016. Soil permeability, aggregate stability and root growth: a pot experiment from a soil bioengineering perspective. *Ecohydrology* **9** (5): 830–842 DOI: 10.1002/eco.1686
- Wagner FH, Ferreira MP, Sanchez A, Hirye MCM, Zortea M, Gloor E, Phillips OL, de Souza Filho CR, Shimabukuro YE, Aragão LEOC. 2018. Individual tree crown delineation in a highly diverse tropical forest using very high resolution satellite images. *ISPRS Journal of Photogrammetry and Remote Sensing* **145** (September): 362–377 DOI: 10.1016/j.isprsjprs.2018.09.013
- Wahl NA, Bens O, Schäfer B, Hüttl RF. 2003. Impact of changes in land-use management on soil hydraulic properties: Hydraulic conductivity, water repellency and water retention. *Physics and Chemistry of the Earth* **28** (33–36): 1377–1387 DOI: 10.1016/j.pce.2003.09.012
- Warwick F. 2017. Surface Water Strategy, Policy and Legislation. In *Sustainable Surface Water Management: A Handbook for SuDS*, Charlesworth S, , Booth C (eds). John Wiley & Sons, Inc.; 31–44. DOI: 10.1002/9781118897690
- Water Resource Associates. 2021. HYSIM Model. *HSIM* Available at: <https://www.watres.com/software/HYSIM/> [Accessed 8 November 2021]
- Waylen KA, Holstead KL, Colley K, Hopkins J. 2018. Challenges to enabling and implementing Natural Flood Management in Scotland. *Journal of Flood Risk Management* **11** (May): S1078–S1089 DOI: 10.1111/jfr3.12301

- Wells J, Labadz JC, Smith A, Islam MM. 2020. Barriers to the uptake and implementation of natural flood management: A social-ecological analysis. *Journal of Flood Risk Management* **13** (S1): 1–12 DOI: 10.1111/jfr3.12561
- West Cumbria Rivers Trust. 2018. Natural flood management measures: A practical guide for farmers Available at: <http://doi.wiley.com/10.1002/wat2.1211>
- Whitmarsh L, Capstick S. 2018. *Perceptions of climate change*. Elsevier Inc. DOI: 10.1016/B978-0-12-813130-5.00002-3
- Wightman S, Schofield L. Case study 23. Swindale Valley, Haweswater: 1–8
- Wilkinson ME, Addy S, Quinn PF, Stutter M. 2019. Natural flood management: small-scale progress and larger-scale challenges. *Scottish Geographical Journal* **135** (1–2): 23–32 DOI: 10.1080/14702541.2019.1610571
- Wingfield T, Macdonald N, Peters K, Spees J, Potter K. 2019. Natural Flood Management: Beyond the evidence debate. *Area* **51** (4): 743–751 DOI: 10.1111/area.12535
- Wobus C, Gutmann E, Jones R, Rissing M, Mizukami N, Lorie M, Mahoney H, Wood A, Mills D, Martinich J. 2017. Modeled changes in 100 year Flood Risk and Asset Damages within Mapped Floodplains of the Contiguous United States. *Natural Hazards and Earth System Sciences Discussions*: 1–21 DOI: 10.5194/nhess-2017-152
- Woo M. 2004. Boundary and border considerations in hydrology. *Hydrological Processes* **18** (7): 1185–1194 DOI: 10.1002/hyp.1399
- Woodland Trust. 2021. Ancient Tree Inventory. *Oak Species* Available at: <https://ati.woodlandtrust.org.uk/how-to-record/species-guides/oak/> [Accessed 23 March 2021]
- Woodland Trust. 2022. Woods Under Threat from HS2 Available at: [https://www.google.com/maps/d/viewer?mid=13Gep69V\\_tKpagkcbVgJnixNdOfTe\\_wd8&ll=52.617963728404426%2C-1.172413994067072&z=8](https://www.google.com/maps/d/viewer?mid=13Gep69V_tKpagkcbVgJnixNdOfTe_wd8&ll=52.617963728404426%2C-1.172413994067072&z=8)
- Woodland Trust, Cymru C, Group TPF. 2013. The Pontbren Project: A farmer-led approach to sustainable land management in the uplands
- Wu GL, Cui Z, Huang Z. 2021. Contribution of root decay process on soil infiltration capacity and soil water replenishment of planted forestland in semi-arid regions. *Geoderma* **404** (26): 115289 DOI: 10.1016/j.geoderma.2021.115289
- Xiao L, Robinson M, O'Connor M. 2021. Woodland's role in natural flood management: Evidence from catchment studies in Britain and Ireland. *Science of the Total Environment* (xxxx): 151877 DOI: 10.1016/j.scitotenv.2021.151877
- Xie C, Cai S, Yu B, Yan L, Liang A, Che S. 2020. The effects of tree root density on water infiltration in urban soil based on a Ground Penetrating Radar in Shanghai, China. *Urban Forestry and Urban Greening* **50** (March): 126648 DOI: 10.1016/j.ufug.2020.126648
- Xu X, Lewis C, Liu W, Albertson JD, Kiely G. 2012. Analysis of single-ring infiltrometer data for soil hydraulic properties estimation: Comparison of BEST and Wu methods. *Agricultural Water Management* **107**: 34–41 DOI: 10.1016/j.agwat.2012.01.004
- Yang JL, Zhang GL. 2011. Water infiltration in urban soils and its effects on the quantity and quality of runoff. *Journal of Soils and Sediments* **11** (5): 751–761 DOI: 10.1007/s11368-011-0356-1
- Yang Y, Sun L, Li R, Yin J, Yu D. 2020. Linking a Storm Water Management Model to a Novel Two-Dimensional Model for Urban Pluvial Flood Modeling. *International Journal of Disaster Risk Science* **11** (4): 508–518 DOI: 10.1007/s13753-020-00278-7
- Yusop Z, Chan CH, Katimon A. 2007. Runoff characteristics and application of HEC-HMS for modelling stormflow hydrograph in an oil palm catchment. *Water Science and Technology* **56** (8): 41–48 DOI: 10.2166/wst.2007.690
- Zeleeuw DG, Melesse AM. 2018. Applicability of a spatially semi-distributed hydrological model for watershed scale runoff estimation in Northwest Ethiopia. *Water (Switzerland)* **10** (7): 10–12 DOI: 10.3390/w10070923
- Zeltniš P, Gailis A, Jansons J, Katrevičs J, Jansons Ā. 2018. Genetic Parameters of Growth

- Traits and Stem Quality of Silver Birch in a Low-Density Clonal Plantation. *Forests* **9** (2): 52 DOI: 10.3390/f9020052
- Zhang D, Dai Y, Wang L, Chen L. 2020. Influence of living and dead roots of gansu poplar on water infiltration and distribution in soil. *Applied Sciences (Switzerland)* **10** (10) DOI: 10.3390/app10103593
- Zhang D, Wang Z, Guo Q, Lian J, Chen L. 2019a. Increase and Spatial Variation in Soil Infiltration Rates Associated with Fibrous and Tap Tree Roots. *Water* **11** (8): 1700 DOI: 10.3390/w11081700
- Zhang J, Lei T, Qu L, Chen P, Gao X, Chen C, Yuan L, Zhang M, Su G. 2017a. Method to measure soil matrix infiltration in forest soil. *Journal of Hydrology* **552**: 241–248 DOI: 10.1016/j.jhydrol.2017.06.032
- Zhang J, Lei T, Qu L, Zhang M, Chen P, Gao X, Chen C, Yuan L. 2019b. Method to quantitatively partition the temporal preferential flow and matrix infiltration in forest soil. *Geoderma* **347** (17): 150–159 DOI: 10.1016/j.geoderma.2019.03.026
- Zhang J, Xu Z, Li F, Hou R, Ren Z. 2017b. Quantification of 3D macropore networks in forest soils in Touzhai valley (Yunnan, China) using X-ray computed tomography and image analysis. *Journal of Mountain Science* **14** (3): 474–491 DOI: 10.1007/s11629-016-4150-9
- Zhang X, Hu M, Guo X, Yang H, Zhang Z, Zhang K. 2018. Effects of topographic factors on runoff and soil loss in Southwest China. *Catena* **160** (September 2017): 394–402 DOI: 10.1016/j.catena.2017.10.013
- Zhou K, Duan JG, Rosenberg ; Abigail, Shim J. 2018a. World Environmental and Water Resources Congress: 489
- Zhou Q, Leng G, Peng J. 2018b. Recent changes in the occurrences and damages of floods and droughts in the United States. *Water (Switzerland)* **10** (9): 27–30 DOI: 10.3390/w10091109
- Zhu P, Zhang G, Wang H, Zhang B, Wang X. 2020a. Land surface roughness affected by vegetation restoration age and types on the Loess Plateau of China. *Geoderma* **366** (January): 114240 DOI: 10.1016/j.geoderma.2020.114240
- Zhu P zong, Zhang G hui, Zhang B jun, Wang H xiao. 2020b. Variation in soil surface roughness under different land uses in a small watershed on the Loess Plateau, China. *Catena* **188** (January): 104465 DOI: 10.1016/j.catena.2020.104465
- Zhu R, Croke BFW, Jakeman AJ. 2020c. Diffuse groundwater recharge estimation confronting hydrological modelling uncertainty. *Journal of Hydrology* **584** (January): 124642 DOI: 10.1016/j.jhydrol.2020.124642
- Zou L, Wang Y, Giannakis I, Tosti F, Alani AM, Sato M. 2020. Mapping and assessment of tree roots using ground penetrating radar with low-cost GPS. *Remote Sensing* **12** (8) DOI: 10.3390/RS12081300

## Chapter 12 Appendices

This appendix contains additional explanations, technical information, figures, and graphs in support/addition to the work included throughout the main body. The structure of this appendix is as follows:

---

<b>Appendix A</b>	Literature Review
<b>Appendix B</b>	Methodology
<b>Appendix C</b>	Results
<b>Appendix D</b>	Academic Engagement and Extracurricular Engagement

---

## APPENDIX TABLE OF CONTENTS

<b>Appendix A. Literature Review .....</b>	<b>12-1</b>
A.1 Process Models Included in HEC-HMS 4.6.1 .....	12-1
<b>Appendix B. Methodology .....</b>	<b>12-13</b>
B.1 HofE Planted Tree Species Defined by the NVC .....	12-13
B.2 Spatial Analysis of the Arrow-Alne Catchment Area.....	12-14
B.2.1 Arrow-Alne Catchment: Topography .....	12-14
B.2.2 Arrow-Alne Catchment: Flow Direction .....	12-16
B.3 Individual Sampling Locations and Information .....	12-20
B.3.1 Control .....	12-20
B.3.2 ca. 1900.....	12-23
B.3.3 2006 .....	12-25
B.3.4 2008 .....	12-27
B.3.5 2010 .....	12-29
B.3.6 2012 .....	12-31
B.3.7 2014 .....	12-33
B.3.8 2020 .....	12-35
B.4 Maps and Routes around Sample site from Week-to-week.....	12-37
B.5 Model Information .....	12-40
B.5.1 HEC-HMS Model Node Area Calculations .....	12-40
B.5.2 Model Calibration Parameters for Winter and Summer Models .....	12-41
B.5.3 RMSE Values for Calibration and Validation .....	12-44
B.6 Tested Methods for Infiltration Projection .....	12-45
B.6.1 Disused Infiltration Projection Method 1 .....	12-45
B.6.2 Disused Infiltration Projection Method 2 .....	12-46
B.7 Projected Increases to Infiltration due to Climate Change .....	12-47
B.7.1 Empirical Site Infiltration Projections .....	12-47
B.7.2 Non-Empirical Site Infiltration Projections.....	12-52
B.8 Data Sources, Permissions and Uses .....	12-57
B.9 Ethical Approvals.....	12-59
<b>Appendix C. Results.....</b>	<b>12-60</b>
C.1 Statistical Testing .....	12-60
C.1.1 Kolmogorov-Smirnov (Normality) Testing.....	12-60
C.1.2 Mann-Whitney U Test .....	12-65
C.1.3 Selection of Statistical Tests for Results Analysis .....	12-66
C.2 Temperature and Infiltration .....	12-67
C.3 Modelled Climate Projections.....	12-70

C.3.1	Data Tables .....	12-70
C.3.2	Percent difference between projected peak flow and total discharge...	12-77
<b>Appendix D.</b>	<b>Extracurricular Academic Engagement.....</b>	<b>12-79</b>
D.1	HofE and EA Feedback Presentation.....	12-79
D.2	Peer Reviewed Publications.....	12-81
D.2.1	Modelling the Hydrological Effects of Woodland Planting on Infiltration and Peak Discharge Using HEC-HMS .....	12-81
D.2.2	The Impact of Tree Planting on Infiltration Dependent on Tree Proximity and Maturity at a Clay Site in Warwickshire, England .....	12-102
D.3	Conferences, Presentations and Posters .....	12-118
D.3.1	AGU Fall 2020 Conference, San Francisco (Poster and Presentation) ....	12-119
D.3.2	ICUD Conference, Melbourne (Presentation) .....	12-120
D.3.3	Coventry University Postgraduate Research Seminar (Oral Presentation)	12-121
D.3.4	Cov-Unovi (Oral Presentation).....	12-121
D.3.5	Coventry University Doctoral College Trailblazer Showcase (Poster Presentation)	12-122
D.4	Additional Development and Engagement .....	12-123
D.4.1	Development Activity Log .....	12-123
D.4.2	Mini-Disk Infiltrometer App Development.....	12-124

## LIST OF APPENDIX FIGURES

<u>Figure</u>	<u>Page</u>
Figure B.1. Digital Terrain Model (DTM) of the Arrow Alne catchment (Data from the Environment Agency et al., 2020). .....	12-15
Figure B.2. Process of creating flow direction raster.....	12-17
Figure B.3. (left) colours and numbers associated with flow to any of the 8 given directions from the centre cell. (right) associated directional relevance of colour allocation (Adapted from Pan et al., 2012; ESRI, 2019).....	12-18
Figure B.4. Output flow direction raster of whole catchment with the Arrow and Alne highlighted. Directional colours correspond to the D8 model. ....	12-19
Figure B.5. Overview map of all sample sites (image retrieved from Google Earth (Google, 2022)). .....	12-20
Figure B.6. Aerial imagery of the Control site, marked with red circle (image retrieved from Google Earth (Google, 2022)).....	12-21
Figure B.7. MDI replication locations at the control site, outlined in orange. ....	12-22
Figure B.8. A view of the grassland control site (looking towards middle Spernal farm)	12-22
Figure B.9. Aerial imagery of the ca.1900 site, marked with red circle (image retrieved from Google Earth (Google, 2022)).....	12-23
Figure B.10. MDI replication locations at the ca. 1900 sample site .....	12-24
Figure B.11. ca.1900 sample site surrounding area, sample tree can be seen to the left (denoted by orange cross) .....	12-24
Figure B.12. Aerial imagery of the 2006 site, marked with red circle (image retrieved from Google Earth (Google, 2022)).....	12-25
Figure B.13. MDI replication locations at the 2006 sample site. ....	12-26
Figure B.14. 2006 sample site surrounding area.....	12-26
Figure B.15. Aerial imagery of the 2008 site, marked with red circle (image retrieved from Google Earth (Google, 2022)).....	12-27
Figure B.16. MDI replication locations at the 2008 sample site .....	12-28
Figure B.17. 2008 sample site surrounding area.....	12-28
Figure B.18. Aerial imagery of the 2010 site, marked with red circle (image retrieved from Google Earth (Google, 2022)).....	12-29
Figure B.19. MDI replication locations at the 2010 sample site. ....	12-30
Figure B.20. 2010 sample site surrounding area.....	12-30

Figure B.21. Aerial imagery of the 2012 site, marked with red circle (image retrieved from Google Earth (Google, 2022)).....	12-31
Figure B.22. MDI replication locations at the 2012 sample site. ....	12-32
Figure B.23. 2012 sample site surrounding area.....	12-32
Figure B.24. Aerial imagery of the 2014 site, marked with red circle (image retrieved from Google Earth (Google, 2022)).....	12-33
Figure B.25. MDI replication locations at the 2014 sample site. Orange circles indicate MDI measurement locations.....	12-34
Figure B.26. 2014 sample site surrounding area.....	12-34
Figure B.27. Aerial imagery of the 2020 site, marked with red circle (image retrieved from Google Earth (Google, 2022)).....	12-35
Figure B.28. MDI replication locations at the 2020 sample site. Orange circles indicate MDI measurement locations.....	12-36
Figure B.29. 2020 sample site surrounding area.....	12-36
Figure B.30. Route 1: Start, control, 2006, 2008, 2010, ca.1900, 2012, finish. ....	12-38
Figure B.31. Route 2: Start, ca.1900, 2010, 2008, 2012, 2006, control, finish. ....	12-39
Figure B.32. Mean winter infiltration projections for all empirical sample sites at 10 cm proximity.....	12-48
Figure B.33. Mean winter infiltration projections for all empirical sample sites at 200 cm proximity.....	12-49
Figure B.34. Mean summer infiltration projections for all empirical sample sites at 10 cm proximity.....	12-50
Figure B.35. Mean summer infiltration projections for all empirical sample sites at 200 cm proximity.....	12-51
Figure B.36. Mean winter infiltration projections for all non-empirical sample sites at 10 cm proximity.....	12-53
Figure B.37. Mean winter infiltration projections for all non-empirical sample sites at 200 cm proximity.....	12-54
Figure B.38. Mean summer infiltration projections for all non-empirical sample sites at 10 cm proximity.....	12-55
Figure B.39. Mean summer infiltration projections for all non-empirical sample sites at 200 cm proximity.....	12-56
Figure B.40. Original CU Ethics application (project P96879).....	12-59
Figure B.41. Updated CU Ethics approval with added procedures to account for the COVID-19 pandemic (project P108617).....	12-59

Figure C.1. Distribution of all infiltration data regardless of proximity and season. ....	12-61
Figure C.2. Distribution of all 10 cm infiltration regardless of season.....	12-62
Figure C.3. Distribution of all 200 cm infiltration regardless of season.....	12-62
Figure C.4. Distribution of all winter 10 cm infiltration data .....	12-63
Figure C.5. Distribution of all winter 200 cm infiltration data .....	12-63
Figure C.6. Distribution of all summer 10 cm infiltration data .....	12-64
Figure C.7. Distribution of all summer 200 cm infiltration data .....	12-64

## LIST OF APPENDIX TABLES

<u>Table</u>	<u>Page</u>
Table A.1. Loss models supported by HEC-HMS. Note the E/C column specifies if the loss method should be used in event or continuous simulations. Gridded models have not been included, as discussed below (adapted from US Army Corps of Engineers, 2000, 2022; Scharffenberg, 2016).....	12-2
Table A.2. Transform models supported by HEC-HMS (adapted from US Army Corps of Engineers, 2000, 2022; Scharffenberg, 2016). .....	12-5
Table A.3. Baseflow models supported by HEC-HMS (adapted from US Army Corps of Engineers, 2000, 2022; Scharffenberg, 2016). .....	12-8
Table A.4. Routing models supported by HEC-HMS (adapted from US Army Corps of Engineers, 2000, 2022; Scharffenberg, 2016). .....	12-10
Table B.1. Woodland species included under NVC classification. ....	12-13
Table B.2. Geographical location, size, and soil texture of the control sample site .....	12-21
Table B.3. Geographical location, size, and soil texture of the ca. 1900 sample site.....	12-23
Table B.4. Geographical location, size, and soil texture of the 2006 sample site .....	12-25
Table B.5. Geographical location, size, and soil texture of the 2008 sample site .....	12-27
Table B.6. Geographical location, size, and soil texture of the 2010 sample site. ....	12-29
Table B.7. Geographical location, size, and soil texture of the 2012 sample site .....	12-31
Table B.8. Geographical location, size, and soil texture of the 2014 sample site .....	12-33
Table B.9. Geographical location, size, and soil texture of the 2020 sample site .....	12-35
Table B.10. Land cover calculations for each HMS node .....	12-40
Table B.11. Final Snyder parameters for winter and summer model calibration. ....	12-41
Table B.12. RMSE values for calibration events, shown to 10 significant figures. ....	12-44
Table B.13. RMSE values for validation events, shown to 10 significant figures. ....	12-44
Table B.14. Projected infiltration for 2120 using method 1 .....	12-45
Table B.15. Projected infiltration for 2120 using method 2. ....	12-46
Table B.16. Data sources and special permissions for project .....	12-57
Table C.1. Test metrics and output P-values for KS tests .....	12-61
Table C.2. Statistical tests for non-parametric data .....	12-66
Table C.3. Correlation coefficients for air, ground, and soil temperatures .....	12-67
Table C.4. Resultant P-values from the multiple regression analysis.....	12-68

Table C.5. Peak flow and total discharge change ranges for woodland (W), grassland (G) and impermeable (I) land cover, compared with 2020 values for 6-hour 50%, 10%, 2% and 1% AEP events in winter .....	12-71
Table C.6. Peak flow and total discharge change ranges for woodland (W), grassland (G) and impermeable (I) land cover, compared with 2020 values for 24-hour 50%, 10%, 2% and 1% AEP events in winter .....	12-72
Table C.7. Peak flow and total discharge change ranges for woodland (W), grassland (G) and impermeable (I) land cover, compared with 2020 values for 96-hour 50%, 10%, 2% and 1% AEP events in winter .....	12-73
Table C.8. Peak flow and total discharge change ranges for woodland (W), grassland (G) and impermeable (I) land cover, compared with 2020 values for 6-hour 50%, 10%, 2% and 1% AEP events in summer.....	12-74
Table C.9. Peak flow and total discharge change ranges for woodland (W), grassland (G) and impermeable (I) land cover, compared with 2020 values for 24-hour 50%, 10%, 2% and 1% AEP events in summer.....	12-75
Table C.10. Peak flow and total discharge change ranges for woodland (W), grassland (G) and impermeable (I) land cover, compared with 2020 values for 96-hour 50%, 10%, 2% and 1% AEP events in summer.....	12-76
Table C.11. Winter peak flow and percent difference compared with 2020. W=woodland, G=grassland, I=impermeable land cover .....	12-77
Table C.12. Winter total discharge and percent difference compared with 2020. W=woodland, G=grassland, I=impermeable land cover .....	12-77
Table C.13. Summer peak flow and percent difference compared with 2020. W=woodland, G=grassland, I=impermeable land cover .....	12-78
Table C.14. Summer total discharge and percent difference compared with 2020. W=woodland, G=grassland, I=impermeable land cover .....	12-78
Table D.1. Extracurricular additional activities undertaken throughout the course of study	12-123

## **Appendix A. Literature Review**

This appendix contains additional and supporting information relating to the literature review in Chapter 2.

### **A.1 Process Models Included in HEC-HMS 4.6.1**

Outlined in sections 3.2.2.1.2 and 5.3.3, HEC-HMS is capable of simulating hydrological processes via a number of ‘process models’. HMS supports 10 infiltration/loss models (Table A.1), 7 transform models (Table A.2), 5 baseflow models (Table A.3) and 6 routing models (Table A.4). This section outlines the available models within HEC-HMS, their uses and the assumptions and limitations of each.

Table A.1. Loss models supported by HEC-HMS. Note the E/C column specifies if the loss method should be used in event or continuous simulations. Gridded models have not been included, as discussed below (adapted from US Army Corps of Engineers, 2000, 2022; Scharffenberg, 2016).

Loss method	E/C	Overview	Requirements	Information and Limitations
Deficit and Constant	C	<ul style="list-style-type: none"> <li>–Good at simulating total infiltration loss.</li> <li>–Infiltration/runoff calculated as single layer.</li> <li>–Precipitation input during storm. evapotranspiration withdraws during dry periods.</li> <li>–Infiltration process is Hortonian (Beven, 2004).</li> </ul>	<ul style="list-style-type: none"> <li>–Initial soil infiltration capacity (mm).</li> <li>–Soil layer thickness (mm).</li> <li>–Constant infiltration (mm/hr).</li> <li>–Impervious area (%).</li> </ul>	<ul style="list-style-type: none"> <li>–Assumes soil to be homogenous.</li> <li>–Assumes precipitation is infinite until soil saturation.</li> <li>–Difficulty applying to ungauged areas due to lack of direct physical relationship of parameters and watershed properties.</li> <li>–Sometimes too simple to predict losses throughout longer events.</li> </ul>
Exponential	E	<ul style="list-style-type: none"> <li>–Represents infiltration as a decreasing function of infiltration capacity.</li> <li>–Can facilitate increased initial infiltration capacity for use in dry soils.</li> </ul>	<ul style="list-style-type: none"> <li>–Initial infiltration capacity (mm).</li> <li>–Initial loss rate coefficient <math>((\text{mm/hr})^{(1-x)})</math>.</li> <li>–Loss coefficient curve.</li> <li>–Precipitation exponent (0.0 to 1.0).</li> <li>–Impervious area (%).</li> </ul>	<ul style="list-style-type: none"> <li>–Advised that this method is not used without calibration.</li> <li>–Consideration should be given to Green and Ampt as an alternative, due to the use of better physical interpretation.</li> </ul>
Green and Ampt	E	<ul style="list-style-type: none"> <li>–Calculated as initial content (user specifies initial soil moisture content), or initial deficit (specified as a volume ratio, calculated as the difference between the saturated content and initial content).</li> <li>–Soil infiltration capacity is governed by the Richards equation, which is derived by combining unsaturated flow from Darcy’s law with mass conservation (Baiamonte, 2019).</li> </ul>	<ul style="list-style-type: none"> <li>–Initial soil infiltration capacity</li> <li>–Initial soil moisture as a ratio.</li> <li>–Maximum water holding capacity of soil as a ratio.</li> <li>–Soil suction (mm).</li> <li>–Hydraulic conductivity (mm/hr).</li> <li>–Impervious area (%).</li> </ul>	<ul style="list-style-type: none"> <li>–Uses porosity, hydraulic conductivity and wetting front suction values from the literature if not known. This can impact results, so should only be used if all parameters are known and entered on a site-by-site basis by the user.</li> <li>–Not widely used, so less mature, not as much experience in professional community.</li> <li>–Has been compared with other physically based infiltration models by (Mishra <i>et al.</i>, 2003), finding it to show poor efficiency (<math>\geq 75\%</math>).</li> </ul>

Initial and Constant	E	<ul style="list-style-type: none"> <li>-Maximum potential rate of precipitation loss is constant throughout an event.</li> <li>-No runoff occurs until precipitation exceeds initial loss volume (Hortonian, (Beven, 2004)).</li> </ul>	<ul style="list-style-type: none"> <li>-Initial infiltration loss (mm).</li> <li>-Constant infiltration rate (mm/hr).</li> <li>-Impervious area (%).</li> </ul>	<ul style="list-style-type: none"> <li>-SCS approximate loss rates can be substituted to calculate constant rate, if not known.</li> <li>-More commonly applied to empirical areas due to the reliance on physical parameters and watershed properties.</li> </ul>
SCS Curve Number	E	<ul style="list-style-type: none"> <li>-Estimate precipitation excess as a function of cumulative precipitation, soil cover, land use and antecedent moisture</li> <li>-Runoff is zero until the accumulated rainfall exceeds initial abstraction</li> <li>-An empirical relationship was developed between initial abstraction and potential maximum retention, allowing a calculation of excess flow at time t</li> <li>-A curve number (CN) can be empirically estimated or derived from literature, ranging from 254 (for impermeable surfaces) to 25400 (for water bodies).</li> <li>-Approximates the Richard's equation by assuming the wetting front can be represented with an exponential scaling of the saturated conductivity</li> </ul>	<ul style="list-style-type: none"> <li>-Initial abstraction (mm).</li> <li>-The SCS curve number.</li> <li>-Impervious area (%).</li> <li>-Initial soil saturation as a volume ratio</li> <li>-Ratio of water remaining in soil after all drainage has ceased</li> <li>-Ratio of soil water holding capacity</li> <li>-Wetting front suction (mm)</li> <li>-Total pore space and distribution</li> <li>-Hydraulic conductivity (mm/hr)</li> <li>-Impervious area (%).</li> </ul>	<ul style="list-style-type: none"> <li>-Infiltration rate will approach zero during a storm of long duration, rather than constant rate as expected.</li> <li>-Developed with data from small agricultural watersheds in midwestern US, so applicability elsewhere is uncertain.</li> <li>-Initial abstraction does not scale with storm characteristics or timing. Thus, same number would be applied to both 50% and 1% AEP storms.</li> <li>-Rainfall intensity and ground slope not considered (Al-Mukhtar and Al-Yaseen, 2019)</li> <li>-Delivers reasonable approximations of the wetting front and infiltration loss (Smith and Parlange, 1978) and has been compared with other physically based infiltration models by (Mishra <i>et al.</i>, 2003), finding it to be <math>\geq 95\%</math> efficient.</li> </ul>
Soil Moisture Accounting	C	<ul style="list-style-type: none"> <li>-Simulates both wet and dry weather behaviour (continuous).</li> </ul>	<ul style="list-style-type: none"> <li>-Soil storage (%).</li> <li>-Groundwater layer 1 storage (%).</li> <li>-Groundwater layer 2 storage (%).</li> </ul>	<ul style="list-style-type: none"> <li>-Developed by HEC-HMS, so not widely applicable outside the software.</li> </ul>

---

<ul style="list-style-type: none"> <li>-Developed by (Bennett and Peters, 2004) – simulates water movement, storage, interception and groundwater storage.</li> <li>-Can compute evapotranspiration (ET), surface runoff, groundwater (GW) flow, and aquifer percolation.</li> </ul>	<ul style="list-style-type: none"> <li>-Maximum infiltration (mm/hr).</li> <li>-Impervious area (%).</li> <li>-Soil storage (mm).</li> <li>-Tension storage (mm).</li> <li>-Soil percolation (mm/hr).</li> <li>-Groundwater layer 1 storage (mm).</li> <li>-Groundwater layer 1 percolation (mm/hr).</li> <li>-Groundwater layer 1 coefficient (hr).</li> <li>-Groundwater layer 2 storage (mm).</li> <li>-Groundwater layer 2 percolation (mm/hr).</li> <li>-Groundwater layer 2 coefficient (hr).</li> </ul>	<ul style="list-style-type: none"> <li>-Complex and requires large volumes of very specific soil profile and infiltration data.</li> </ul>
--	--	--

---

Note that gridded loss models (gridded deficit constant, gridded SCS curve number, and gridded soil moisture accounting) have not been included in Table A.1. This is because HMS gridded models divide the sub-basin in to (minimum) 10x10 m cells and individual cell initial parameters are specified by the user; in comparison to non-gridded methods, which simulate the whole sub-basin area with one set of defined parameters. The minimum resolution of gridded data input is too coarse for the size of the study catchment, additionally, gridded data requires vast amounts of telemetered hydrometric and spatial data to compute. Such information was not available for this project, and due to the design of the model (section 5.3), a more specific representation of empirical infiltration could be derived through use of the chosen loss method (section 5.3.3.2 ).

Table A.2. Transform models supported by HEC-HMS (adapted from US Army Corps of Engineers, 2000, 2022; Scharffenberg, 2016).

Transform method	Overview	Requirements	Information and Limitations
Clark Unit Hydrograph	<ul style="list-style-type: none"> <li>–Hydrograph based on time-area histogram.</li> <li>–Uses the linear reservoir method (the lumped impacts of all inputted watershed storage) to account for storage in the subbasin.</li> <li>–The movement of water through the catchment to the outlet is calculated with the absence of attenuation, and instead through the provided histogram.</li> </ul>	<ul style="list-style-type: none"> <li>–For standard:                             <ul style="list-style-type: none"> <li>–Time of concentration (hr).</li> <li>–Storage coefficient (hr).</li> </ul> </li> <li>–For Variable:                             <ul style="list-style-type: none"> <li>–Time of concentration (hr).</li> <li>–Storage coefficient (hr).</li> <li>–Index excess (mm/hr).</li> <li>–Concentration curve.</li> <li>–Storage curve.</li> </ul> </li> <li>–For Maricopa County:                             <ul style="list-style-type: none"> <li>–Flow path length (km).</li> <li>–Flow path slope (m/km).</li> <li>–Resistance coefficient.</li> </ul> </li> </ul>	<ul style="list-style-type: none"> <li>–Can be used to simulate both translation (movement of water from the origin to outlet), or attenuation (the reduction of the volume of discharged water due to attenuation).</li> <li>–Assumes that all water is heading to the outlet at varying times.</li> <li>–Parameters required for the Clark method can be implied implicitly through calibration and observed data.</li> </ul>
Kinematic Wave	<ul style="list-style-type: none"> <li>–Represents the watershed as an open channel, with inflow to the channel equal to the excess precipitation.</li> <li>–HMS solves the transform equations (i.e., the momentum and continuity equations) as shallow unsteady in-channel flow to generate a transform hydrograph.</li> <li>–Method is ideal for smaller catchments where most hydrological parameters are empirical.</li> </ul>	<ul style="list-style-type: none"> <li>–For comprehensive required input parameters, see US Army Corps of Engineers (2000, 2022) and Scharffenberg, (2016).</li> </ul>	<ul style="list-style-type: none"> <li>–Due to numerical limitations of the equations, it is suggested by Ponce (1991) that KW should only be used for small watersheds of (2.5km<sup>2</sup> or less) as to not compromise the deterministic nature of the equations.</li> </ul>
SCS Unit Hydrograph	<ul style="list-style-type: none"> <li>–Developed based on collected rainfall and runoff data from small agricultural watersheds throughout the US.</li> </ul>	<ul style="list-style-type: none"> <li>–Graph type (peak rate factor (PRF))</li> <li>–Lag time (min)</li> </ul>	<ul style="list-style-type: none"> <li>–Method assumes that the resultant transform hydrograph is single-peaked, so should not</li> </ul>

	<ul style="list-style-type: none"> <li>-The peak rate factor (PRF) is specified, as is the lag time, and the model uses a dimensionless, single-peaked hydrograph to calculate runoff from the subbasin.</li> </ul>		<ul style="list-style-type: none"> <li>be used when multiple peaks are observed throughout the subbasin.</li> <li>-The requirement to specify the best fitting hydrograph is not always inclusive of more intricate hydrology across varying sites.</li> </ul>
<p style="text-align: center;">Snyder Unit Hydrograph</p>	<ul style="list-style-type: none"> <li>-Uses the lag, peak and time to base of a subbasin to calculate discharge over time.</li> </ul>	<ul style="list-style-type: none"> <li>-For Standard: <ul style="list-style-type: none"> <li>-Lag (hr)</li> <li>-Peaking coefficient</li> </ul> </li> <li>-For FT Worth District: <ul style="list-style-type: none"> <li>-Length (km)</li> <li>-Centroid length (km)</li> <li>-Weighted slope (m/km)</li> <li>-Impermeable area (%)</li> <li>-Sand (%)</li> <li>-Peaking coefficient</li> </ul> </li> <li>-For Tulsa District: <ul style="list-style-type: none"> <li>-Length (km)</li> <li>-Centroid length (km)</li> <li>-Weighted slope (m/km)</li> <li>-Channelisation (%)</li> </ul> </li> </ul>	<ul style="list-style-type: none"> <li>-Empirically based so can be tailored to suit observed flows during calibration.</li> <li>-Follows a similar process to SCS Unit hydrograph and User-specified unit hydrograph; however, the Snyder method allows for further user manipulation to variables.</li> <li>-Standard, Ft Worth and Tulsa allow for the inclusion of other parameters based on model requirements and empirical data availability.</li> </ul>
<p style="text-align: center;">User-Specified S Graph</p>	<ul style="list-style-type: none"> <li>-Exact empirical relationship between one unit of excess rainfall and the resulting direct runoff to be specified.</li> <li>-Defined in terms of % unit flow versus % of lag time, meaning that the S-graph can be used in multiple subbasins to define different lag times to discharge.</li> </ul>	<ul style="list-style-type: none"> <li>-S-graph import</li> <li>-Standard method: <ul style="list-style-type: none"> <li>-Lag time (hr)</li> </ul> </li> <li>-Regression method: <ul style="list-style-type: none"> <li>-Length (km)</li> <li>-Centroid length (km)</li> <li>-Slope (m/km)</li> <li>-Roughness</li> <li>-M exponent</li> <li>-P exponent</li> </ul> </li> </ul>	<ul style="list-style-type: none"> <li>-Similar in theory to the unit hydrograph method, however the method requires a 'percentage curve' to be selected from a list of pre-loaded curves.</li> <li>-This method is exclusive to HEC-HMS, and therefore very little supporting literature exists beyond the user manuals and technical reference guides.</li> </ul>

---

User-Specified  
Unit Hydrograph

–Allows for the direct entry of known (flow/time) data for a catchment/watershed. –Unit hydrograph import

- A hydrograph must be created for every subbasin.
  - Uncommon due to data availability and the amount of observed data required (coupled with the lack thereof in many watersheds).
  - Each subbasin hydrograph requires extensive calibration to ensure it replicates observed data (Chow *et al.*, 1988)
- 

Note that the ModClark transform method has not been included in Table A.2 due to it being a gridded parameter. As discussed below Table A.1, gridded methods divide the sub-basin in to (minimum) 10x10 m cells, and the minimum resolution of gridded data input is too coarse for the size of the study catchment. Additionally, gridded data requires vast amounts of telemeted hydrometric and spatial data to compute. Such information was not available for this project, and due to the design of the model (section 5.3), a more specific representation of empirical infiltration could be derived through use of the chosen loss method (section 5.3.3.2 ).

Table A.3. Baseflow models supported by HEC-HMS (adapted from US Army Corps of Engineers, 2000, 2022; Scharffenberg, 2016).

Baseflow method	Overview	Requirements	Information and Limitations
Recession	<ul style="list-style-type: none"> <li>–Suggests that baseflow decays over time as a ration of the starting flow value.</li> <li>–The starting baseflow is defined as an initial condition of the model and can be specified as flow rate or flow per area.</li> </ul>	<ul style="list-style-type: none"> <li>–Initial type (discharge/discharge per area).</li> <li>–Initial discharge (<math>\text{m}^3/\text{s}</math> or <math>\text{m}^3/\text{s per km}^2</math>).</li> <li>–Regression constant.</li> <li>–Threshold type (ratio to peak/threshold discharge).</li> <li>–Ratio.</li> </ul>	<ul style="list-style-type: none"> <li>–Method is beneficial when a decay of baseflow is observed or is frequent at the study site.</li> <li>–This method has applications regarding abstraction or can be used to represent the influence of flow control measures (flap gates allowing water into the channel at a specified volume).</li> <li>–The recession ratio can be defined as the ration of baseflow at the current time, compared with the ration one day earlier.</li> </ul>
Bounded Recession	<ul style="list-style-type: none"> <li>–Uses same principles as recession, however, allows the user to input a bounded recession volume for each month.</li> <li>–This method is beneficial for longer simulations, where baseflow is variable from month-to-month.</li> </ul>	<ul style="list-style-type: none"> <li>–Initial type (discharge/discharge per area).</li> <li>–Initial discharge (<math>\text{m}^3/\text{s}</math> or <math>\text{m}^3/\text{s per km}^2</math>).</li> <li>–Regression constant.</li> <li>–Monthly baseflow (<math>\text{m}^3/\text{s}</math> or <math>\text{m}^3/\text{s per km}^2</math>).</li> </ul>	<ul style="list-style-type: none"> <li>–Ideally used in real time or near real-time simulations.</li> <li>–This method is a combination of recession baseflow (meaning baseflow decays following a specified ration over time) and constant monthly baseflow (as monthly values can be specified).</li> <li>–The recession ratio can be defined as the ration of baseflow at the current time, compared with the ration one day earlier.</li> </ul>
Constant Monthly	<ul style="list-style-type: none"> <li>–Represents baseflow as a constant volume, specified on a month-by-month basis</li> <li>–A user specified flow is added to the direct runoff and computed per timestep during the simulation.</li> </ul>	<ul style="list-style-type: none"> <li>–Monthly baseflow (<math>\text{m}^3/\text{s}</math>).</li> </ul>	<ul style="list-style-type: none"> <li>–Effective when baseflow is empirically monitored and varies monthly.</li> </ul>

	<ul style="list-style-type: none"> <li>–Monthly baseflows are best simulated using empirical data.</li> </ul>	
Linear Reservoir	<ul style="list-style-type: none"> <li>–Should be used in conjunction with the soil moisture accounting (SMA) loss method (Table A.1).</li> <li>–Simulates baseflow as storage and movement of water through reservoirs.</li> <li>–The outflow from GW 1 of the SMA method is inflow to one baseflow reservoir, and the same for GW 2 of the SMA. The outflow is combined to compute total subbasin outflow.</li> </ul>	<ul style="list-style-type: none"> <li>–Reservoirs.</li> <li>–Initial type (discharge/discharge per area).</li> <li>–Groundwater 1 initial (<math>m^3/s</math>).</li> <li>–Groundwater 1 fraction.</li> <li>–Groundwater 1 coefficient (hr).</li> <li>–Groundwater 1 steps.</li> </ul>
Nonlinear Boussinesq	<ul style="list-style-type: none"> <li>–Uses a simplified assumption that a horizontal impermeable layer underlies an aquifer, which is drained by a fully penetrating stream.</li> <li>–The baseflow maximum and baseflow recession can be estimated using observed discharge from past flood events. The hydrograph rising limb is assumed to be linear for simplicity (Szilagyi and Parlange, 1998; Aksoy and Wittenberg, 2011).</li> </ul>	<ul style="list-style-type: none"> <li>–Initial type (discharge/discharge per area).</li> <li>–Initial discharge (<math>m^3/s</math> or <math>m^3/s</math> per <math>km^2</math>).</li> <li>–Threshold type (ratio to peak/threshold discharge).</li> <li>–Ratio.</li> <li>–Length (m).</li> <li>–Conductivity (mm/hr).</li> <li>–Porosity.</li> </ul>
		<ul style="list-style-type: none"> <li>–Beneficial when the study area is comprehensively empirically monitored.</li> <li>–Can represent the influence of groundwater and aquifer flows when used in combination with the SMA loss method.</li> <li>–Useful for simulating the influences of surface water/groundwater pollution.</li> </ul>
		<ul style="list-style-type: none"> <li>–Ideal when aiming to simulate the behaviours of baseflow following a simulated event.</li> <li>–Can be used in event or continues simulation, as parameters can be reset after each event.</li> <li>–Operates similarly to the recession method, however only applying the recession once the simulated event has subsided.</li> </ul>

Table A.4. Routing models supported by HEC-HMS (adapted from US Army Corps of Engineers, 2000, 2022; Scharffenberg, 2016).

Routing method	Overview	Requirements	Information and Limitations
Kinematic Wave	<ul style="list-style-type: none"> <li>–Calculated based upon finite difference approximations of the continuity equation (section 3.2), and a simplification of the momentum equation.</li> <li>–More information regarding the applications and uses of the Kinematic Wave routing method in HEC-HMS can be found in (US Army Corps of Engineers, 1993).</li> </ul>	<ul style="list-style-type: none"> <li>–Initial type (Specified discharge/ discharge = inflow)</li> <li>–Length (m)</li> <li>–Slope (m/m)</li> <li>–Manning’s <math>n</math></li> <li>–Sub-reaches</li> <li>–Index method (celerity/flow)</li> <li>–Index flow (<math>m^3/s</math>)</li> <li>–Cross-sectional shape (Circle, eight-point, rectangle, trapezoid, triangle)</li> <li>–Bottom width (m)</li> <li>–Side slope (xH:1V)</li> <li>–Invert (m)</li> </ul>	<ul style="list-style-type: none"> <li>–Requires vast amounts of empirical data including for set up, however large proportions of this can be derived from maps and imagery.</li> <li>–Commonly used to simulate 1-D flow in open-channels or large closed channels (conduits).</li> <li>–Should not be used when watercourse slope exceeds 0.002 (km), an alternative is the Muskingum-Cunge method.</li> </ul>
Lag	<ul style="list-style-type: none"> <li>–Outflow hydrograph is a replication of the input hydrograph, but with all components lagged by a user specified amount.</li> <li>–Flow is not attenuated, so hydrograph shape does not change throughout simulation.</li> </ul>	<ul style="list-style-type: none"> <li>–Initial type (Specified discharge/discharge = inflow).</li> <li>–Lag (min).</li> </ul>	<ul style="list-style-type: none"> <li>–commonly used in urban drainage channels or pipe networks where flow pathways are simplistic with minute losses due to storage and resistance.</li> <li>–Lag can be derived empirically or determined through calibration using past observed data.</li> </ul>
Lag and K	<ul style="list-style-type: none"> <li>–Identical to the lag routing method; however, accounts for hydrograph peak attenuation as water moves downstream.</li> <li>–The reduction in peak can be estimated, however it is commonly achieved through empirical and historically recorded data.</li> </ul>	<ul style="list-style-type: none"> <li>–Initial type (Specified discharge/discharge = inflow)</li> <li>–Lag method (constant lag/variable lag)</li> <li>–K method (constant K/variable K)</li> </ul>	<ul style="list-style-type: none"> <li>–Only works effectively when dealing with slowly varying flood waves</li> <li>–Does not account for backwater, constrictions, bridges, ice, or tidal-influenced river reaches.</li> </ul>

	<ul style="list-style-type: none"> <li>-This is ideally used for channels with a very gradual change downstream.</li> </ul>		
Modified Puls (a.k.a. storage routing, level-pool routing)	<ul style="list-style-type: none"> <li>-Calculated based upon finite difference approximations of the continuity equation (section 3.2), coupled with an empirical representation of the momentum equation.</li> <li>-Does not consider cross-sectional width.</li> <li>-Method should be calibrated through empirical flood events, then applied to the rest of the cross-sectional areas before simulation.</li> </ul>	<ul style="list-style-type: none"> <li>-Initial type (Specified discharge/discharge = inflow).</li> <li>-Sub-reaches.</li> <li>-Invert (m).</li> </ul>	<ul style="list-style-type: none"> <li>-Require a large amount of pre-processing before use: requires a storage-outflow relationship to be defined through use of hydraulic modelling, historical observations, or inflow and outflow hydrographs. This can be beyond the scope and processing power of smaller-scale simulations.</li> <li>-Requires extensive calibration if observed data is not extensively available.</li> </ul>
Muskingum	<ul style="list-style-type: none"> <li>-Uses finite difference approximations of the continuity equation (similar to the Modified Puls method).</li> <li>-Storage is represented as the sum of prism storage (volume defined by flow water profile), and wedge storage (additional water volume under the flood wave profile). During inflow, wedge storage is added to prism storage, during outflow, wedge storage is subtracted from prism storage to wedge storage.</li> </ul>	<ul style="list-style-type: none"> <li>-Initial type (Specified discharge/discharge = inflow).</li> <li>-Muskingum K (hr).</li> <li>-Muskingum X.</li> <li>-Sub-reaches.</li> </ul>	<ul style="list-style-type: none"> <li>-Includes parameters that are not physically based, and are not always replicated in natural channels, thus are difficult to estimate (prism and wedge).</li> <li>-K and X parameters are essential to accuracy, however difficult to predict.</li> <li>-Can be calibrated using observed flows and inflow and outflow hydrographs to determine the difference in flow between two identical points on each hydrograph.</li> </ul>
Muskingum-Cunge	<ul style="list-style-type: none"> <li>-Includes adaptations to the Muskingum method to overcome the limitations with predicting K and X.</li> <li>-Based upon the continuity equation and the diffusion form of the momentum equation, used in conjunction with the linear approximation.</li> </ul>	<ul style="list-style-type: none"> <li>-Initial type (Specified discharge/ discharge = inflow)</li> <li>-Length (m)</li> <li>-Slope (m/m)</li> <li>-Manning's <math>n</math></li> <li>-Sub-reaches</li> </ul>	<ul style="list-style-type: none"> <li>-If the channel is complex, reaches may need to be sub-divided and modelled as a series of linked reaches.</li> <li>-Backflow and pooling can influence results if undetected, as the Muskingum-Cunge method cannot account for these influences.</li> </ul>

- 
- Time steps and distance coefficients must be selected and influence outcomes.
  - Cross-sectional shape must be specified by the user – however the model does allow an eight-point channel to be inputted.
  - Space-time method (auto DX auto DT, specified DX auto DT, Specified DX specified DT)
  - Index method (celerity/flow)
  - Index flow (m<sup>3</sup>/s)
  - Cross-sectional shape (Circle, eight-point, rectangle, trapezoid, triangle)
  - Bottom width (m)
  - Side slope (xH:1V)
  - Invert (m)
  - Parameters required for simulations can be derived through imagery, maps, and site walks.
  - Can simulate slowly rising flood waves.
-

## Appendix B. Methodology

This appendix contains additional and supporting information relating to the methods presented throughout Chapter 5.

### **B.1** *HofE Planted Tree Species Defined by the NVC*

The HofE forest fall into the NVC category ‘mature lowland broadleaved woodland’ (see section 4.1.1), the species included under this classification are displayed in Table B.1 (Heart of England Forest, 2020; Coffey, 2021).

*Table B.1. Woodland species included under NVC classification.*

English oak	Quercus robur	Cherry	Prunus avium
Alder	Alnus glutinosa	Whitebeam	Sorbus aria
Birch	Betula pendula	White poplar	Populus alba
Sycamore	Acer psuedoplatanus	Holly	Ilex aquifolium
Sesile oak	Quercus petraea	Hazel	Corylus avellana
Aspen	Populus tremula	Dogwood	Cornus sanguinia
Lime	Tilia cordata	Common privet	Lingustrum vulgare
Sweet chestnut	Castanea sativa	Guelder rose	Viburnum opulus
Hornbeam	Carpinus betulus	Wayfaring tree	Viburnum lantana
Wild service	Sorbus torminalis	Spindle	Euonymous europeas
Beech	Fagus sylvatica	Buckthorn	Rhamnus catharticus
Rowan	Sorbus aucuparia	Mixed Willow	Salix cinerea, Salix
Field maple	Acer campestre		purpurea, Salix viminalis

## **B.2 Spatial Analysis of the Arrow-Alne Catchment Area**

As discussed in section 4.1.1, topographical and hydrological analysis was undertaken using the Arrow-Alne catchment area; namely, a flow direction analysis, and a watershed delineation. An understanding of these parameters aid in the identification of the study site (section 4.2), allowing for a deeper understanding of study site characteristics. This section describes these processes in greater detail.

### **B.2.1 Arrow-Alne Catchment: Topography**

A comprehensive understanding of catchment topography is necessary for gaining further insight in to the hydrological response of a catchment, and is also of use in both GIS and hydrological modelling (Zhang *et al.*, 2018). Topographical data is commonly acquired through light detection and ranging (LiDAR) and can be outputted as a digital surface model (DSM - inclusive of above-terrain features such as houses and trees), or a digital terrain model (DTM - a 'bare earth' representation excluding above-surface features) (Mason *et al.*, 2016). A 2 m resolution DTM was created for the River Arrow catchment using data downloaded from the EA (see appendix Table B.16). The Arrow-Alne DTM is shown in Figure B.1.

*Figure B.1. Digital Terrain Model (DTM) of the Arrow Alne catchment (Data from the Environment Agency et al., 2020).*

The creation of the Arrow-Alne catchment DTM (Figure B.1) was required to allow for an accurate flow direction analysis (Li *et al.*, 2019). The flow direction analysis was performed as a necessary precursor to the watershed delineation process, which would allow for the hydrological boundary of the study site to be defined (Brunda and Nyamathi, 2015; Li *et al.*, 2019). The flow direction and watershed delineation processes are discussed below.

### B.2.2 Arrow-Alne Catchment: Flow Direction

A flow direction analysis allows for watershed delineation, which will be the method used for defining the hydrological study catchment for this study, however, before flow direction, further processing of the elevation model (Figure B.1) was required (Brunda and Nyamathi, 2015; Li *et al.*, 2019). Elevation models often contain ‘sinks’, or areas of depression resulting from genuine topography changes or incorrect data (Fernandez *et al.*, 2016; Rashed, 2016). A flow direction cannot be assigned to a sink cell as a two-cell loop is created, resulting in an inaccurate flow direction raster output, so sinks need to be filled correctly before the flow direction can be calculated (Rashed, 2016; Wagner *et al.*, 2018; Li *et al.*, 2019).

The ‘sink’ tool in ArcGIS was utilised to identify areas of negative or impossible flow. Few sinks were present in the elevation model; however, all were cross referenced against aerial photography and elevation data from Google Earth (Google, 2022), determining that the sinks were a result of no data, and therefore could be rectified through use of the ‘fill’ tool in ArcMap; this method is in line with those commonly adopted in relevant literature (Planchon and Darboux, 2002; Pan *et al.*, 2012; Fernandez *et al.*, 2016). outlines the steps taken to prepare the elevation model for flow direction analysis.

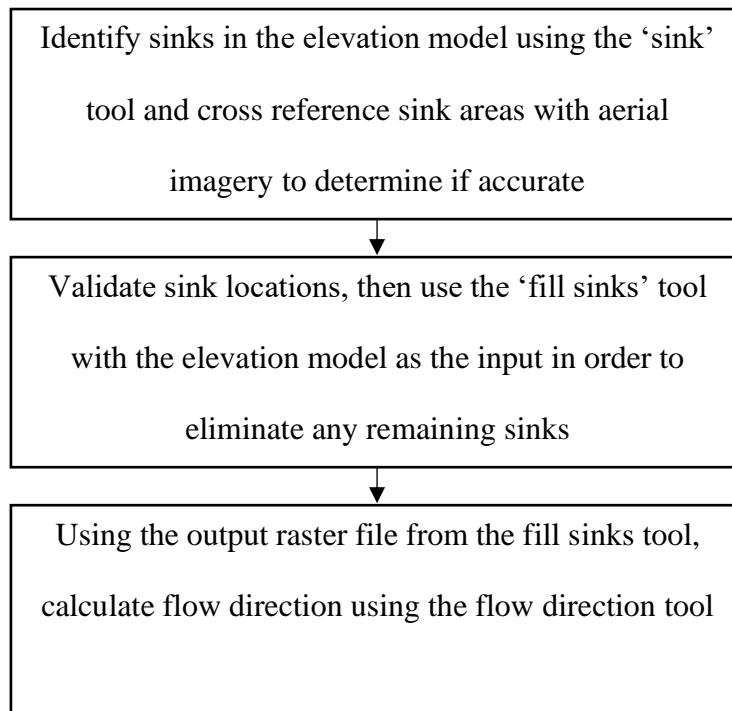


*Figure B.2. Process of creating flow direction raster*

Once filled, a flow direction analysis of the catchment elevation model could be undertaken. The ArcGIS flow direction tool operates following the rolling ball technique, where the direction of steepest decent throughout the elevation model is calculated on a cell-by-cell basis (Hashim *et al.*, 2004; Rashed, 2016; Wagner *et al.*, 2018). The calculation is:

$$\text{Maximum drop} = \frac{\Delta Z}{d} \times 100 \quad \text{EQ 12.1}$$

Where  $\Delta Z$  is the change in elevation, and  $d$  is the distance (cell size). After applying EQ 12.1 to every cell in the elevation model, the tool numbers and colour codes of each cell to represent the direction of flow from that cell to the next, in line with Jenson and Domingue's (1988) D8 model, see Figure B.3.

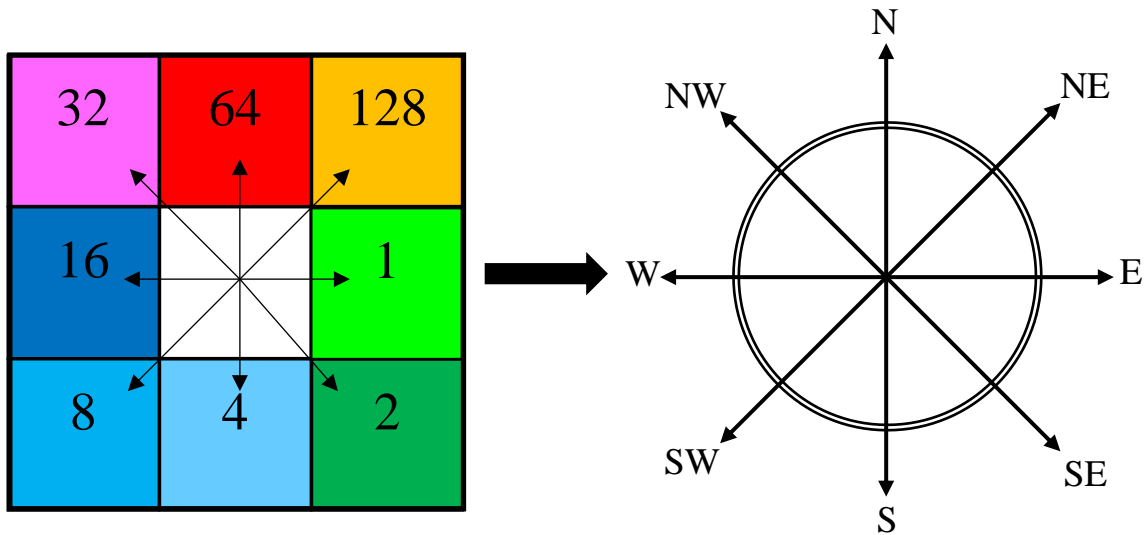


*Figure B.3. (left) colours and numbers associated with flow to any of the 8 given directions from the centre cell. (right) associated directional relevance of colour allocation (Adapted from Pan et al., 2012; ESRI, 2019).*

The output of the flow direction analysis for the whole catchment elevation model is shown in Figure B.3.

*Figure B.4. Output flow direction raster of whole catchment with the Arrow and Alne highlighted. Directional colours correspond to the D8 model.*

The general movement of flow for the Arrow-Alne catchment is to the south/south-west/west, which aligns with the direction of flow of the Arrow and Alne Rivers. There are significant areas of red on the map, indicating that water is flowing north, however, north flowing water then reverts downslope in to either the River Arrow or Alne (dependent on closest proximity). This is particularly evident towards the north and east of Figure B.4.

### **B.3 Individual Sampling Locations and Information**

The following sections display and describe the characteristics of each infiltration sample area (as discussed throughout section 5.2) in turn. Figure B.5 shows an overview map of all sample sites.

This item has been removed due to 3rd Party Copyright. The unabridged version of the thesis can be found in the Lanchester Library, Coventry University.

*Figure B.5. Overview map of all sample sites (image retrieved from Google Earth (Google, 2022)).*

#### **B.3.1 Control**

Table B.2 shows the location and soil texture of the control sample site. Figure B.6 to Figure B.8 show additional photographs of the sample site and surrounding area.

*Table B.2. Geographical location, size, and soil texture of the control sample site*

<b>Site</b>	<b>Latitude</b>	<b>Longitude</b>	<b>Grid Ref</b>	<b>East (X)</b>	<b>North (Y)</b>	<b>Size (Ha)</b>
Control	52.253906,	-1.860428	SP0962561757	409625	261757	2.49
<b>Soil</b>	<b>Sand %</b>	<b>Silt %</b>	<b>Clay %</b>	<b>UK Soil Classification</b>		
<b>Texture</b>	53	20	27	SaCL	Sandy clay loam	

This item has been removed due to 3rd Party Copyright. The unabridged version of the thesis can be found in the Lanchester Library, Coventry University.

*Figure B.6. Aerial imagery of the Control site, marked with red circle (image retrieved from Google Earth (Google, 2022)).*



*Figure B.7. MDI replication locations at the control site, outlined in orange.*



*Figure B.8. A view of the grassland control site (looking towards middle Sernal farm)*

### B.3.2 *ca. 1900*

Table B.3 shows the location and soil texture of the *ca. 1900* sample site. Figure B.9 to Figure B.11 show additional photographs of the sample site and surrounding area.

*Table B.3. Geographical location, size, and soil texture of the ca. 1900 sample site*

	<b>Latitude</b>	<b>Longitude</b>	<b>Grid Ref</b>	<b>East (X)</b>	<b>North (Y)</b>	<b>Size (Ha)</b>
	52.244356,	-1.864804	SP0932860694	409328	260694	2.93
<b>Soil</b>	<b>Sand %</b>	<b>Silt %</b>	<b>Clay %</b>	<b>UK Soil Classification</b>		
<b>Texture</b>	47	40	13	SSL	Sandy silt loam	
<b>Species</b>	Sessile Oak			Quercus Petraea		

This item has been removed due to 3rd Party Copyright. The unabridged version of the thesis can be found in the Lanchester Library, Coventry University.

*Figure B.9. Aerial imagery of the ca. 1900 site, marked with red circle (image retrieved from Google Earth (Google, 2022))*



*Figure B.10. MDI replication locations at the ca. 1900 sample site*



*Figure B.11. ca.1900 sample site surrounding area, sample tree can be seen to the left  
(denoted by orange cross)*

### B.3.3 2006

Table B.4 shows the location and soil texture of the 2006 sample site. Figure B.12 to Figure B.14 show additional photographs of the sample site and surrounding area.

*Table B.4. Geographical location, size, and soil texture of the 2006 sample site*

	<b>Latitude</b>	<b>Longitude</b>	<b>Grid Ref</b>	<b>East (X)</b>	<b>North (Y)</b>	<b>Size (Ha)</b>
	52.251681,	-1.857476	SP0982761510	409827	261510	6.48
<b>Soil</b>	<b>Sand %</b>	<b>Silt %</b>	<b>Clay %</b>	<b>UK Soil Classification</b>		
<b>Texture</b>	20	20	60	C	Clay	
<b>Species</b>	Silver Birch			Betula Pendula		

This item has been removed due to 3rd Party Copyright. The unabridged version of the thesis can be found in the Lanchester Library, Coventry University.

*Figure B.12. Aerial imagery of the 2006 site, marked with red circle (image retrieved from Google Earth (Google, 2022))*



*Figure B.13. MDI replication locations at the 2006 sample site.*



*Figure B.14. 2006 sample site surrounding area.*

### B.3.4 2008

Table B.5 shows the location and soil texture of the 2008 sample site. Figure B.15 to Figure B.17 show additional photographs of the sample site and surrounding area.

*Table B.5. Geographical location, size, and soil texture of the 2008 sample site*

	<b>Latitude</b>	<b>Longitude</b>	<b>Grid Ref</b>	<b>East (X)</b>	<b>North (Y)</b>	<b>Size (Ha)</b>
	52.249425,	-1.859663	SP0967861259	409678	261259	8.9
<b>Soil</b>	<b>Sand %</b>	<b>Silt %</b>	<b>Clay %</b>	<b>UK Soil Classification</b>		
<b>Texture</b>	13	20	67	C	Clay	
<b>Species</b>	Aspen			Populus Tremula		

This item has been removed due to 3rd Party Copyright. The unabridged version of the thesis can be found in the Lanchester Library, Coventry University.

*Figure B.15. Aerial imagery of the 2008 site, marked with red circle (image retrieved from Google Earth (Google, 2022))*



*Figure B.16. MDI replication locations at the 2008 sample site*



*Figure B.17. 2008 sample site surrounding area*

### B.3.5 2010

Table B.6 shows the location and soil texture of the 2010 sample site. Figure B.18 to Figure B.20 show additional photographs of the sample site and surrounding area.

*Table B.6. Geographical location, size, and soil texture of the 2010 sample site.*

	<b>Latitude</b>	<b>Longitude</b>	<b>Grid Ref</b>	<b>East (X)</b>	<b>North (Y)</b>	<b>Size (Ha)</b>
	52.246350,	-1.862651	SP0947460916	409474	260916	13.8
<b>Soil</b>	<b>Sand %</b>	<b>Silt %</b>	<b>Clay %</b>	<b>UK Soil Classification</b>		
<b>Texture</b>	53	33	14	SaL	Sandy Loam	
<b>Species</b>	Silver Birch			Betula Pendula		

This item has been removed due to 3rd Party Copyright. The unabridged version of the thesis can be found in the Lanchester Library, Coventry University.

*Figure B.18. Aerial imagery of the 2010 site, marked with red circle (image retrieved from Google Earth (Google, 2022)).*



*Figure B.19. MDI replication locations at the 2010 sample site.*



*Figure B.20. 2010 sample site surrounding area.*

### B.3.6 2012

Table B.7 shows the location and soil texture of the 2012 sample site. Figure B.21 to Figure B.23 show additional photographs of the sample site and surrounding area.

*Table B.7. Geographical location, size, and soil texture of the 2012 sample site*

	<b>Latitude</b>	<b>Longitude</b>	<b>Grid Ref</b>	<b>East (X)</b>	<b>North (Y)</b>	<b>Size (Ha)</b>
	52.250039,	-1.869270	SP0902261326	409022	261326	13.2
<b>Soil</b>	<b>Sand %</b>	<b>Silt %</b>	<b>Clay %</b>	<b>UK Soil Classification</b>		
<b>Texture</b>	33	13	54	C	Clay	
<b>Species</b>	Aspen			Populus Tremula		

This item has been removed due to 3rd Party Copyright. The unabridged version of the thesis can be found in the Lanchester Library, Coventry University.

*Figure B.21. Aerial imagery of the 2012 site, marked with red circle (image retrieved from Google Earth (Google, 2022))*



*Figure B.22. MDI replication locations at the 2012 sample site.*



*Figure B.23. 2012 sample site surrounding area.*

### B.3.7 2014

Table B.8 shows the location and soil texture of the 2014 sample site. Figure B.24 to Figure B.26 show additional photographs of the sample site and surrounding area.

*Table B.8. Geographical location, size, and soil texture of the 2014 sample site*

	<b>Latitude</b>	<b>Longitude</b>	<b>Grid Ref</b>	<b>East (X)</b>	<b>North (Y)</b>	<b>Size (Ha)</b>
	52.272429,	-1.877509	SP0845563815	408455	263815	2.65
<b>Soil</b>	<b>Sand %</b>	<b>Silt %</b>	<b>Clay %</b>	<b>UK Soil Classification</b>		
<b>Texture</b>	7	13	80	C	Clay	
<b>Species</b>	Aspen			Populus Tremula		

This item has been removed due to 3rd Party Copyright. The unabridged version of the thesis can be found in the Lanchester Library, Coventry University.

*Figure B.24. Aerial imagery of the 2014 site, marked with red circle (image retrieved from Google Earth (Google, 2022)).*



*Figure B.25. MDI replication locations at the 2014 sample site. Orange circles indicate MDI measurement locations*



*Figure B.26. 2014 sample site surrounding area.*

### B.3.8 2020

Table B.9 shows the location and soil texture of the 2020 sample site. Figure B.27 to Figure B.29 show additional photographs of the sample site and surrounding area.

*Table B.9. Geographical location, size, and soil texture of the 2020 sample site*

	<b>Latitude</b>	<b>Longitude</b>	<b>Grid Ref</b>	<b>East (X)</b>	<b>North (Y)</b>	<b>Size (Ha)</b>
	52.234833,	-1.772749	SP1561759651	415617	259651	17.5
<b>Soil</b>	<b>Sand %</b>	<b>Silt %</b>	<b>Clay %</b>	<b>UK Soil Classification</b>		
<b>Texture</b>	13	23	77	C	Clay	
<b>Species</b>	Aspen			Populus Tremula		

This item has been removed due to 3rd Party Copyright. The unabridged version of the thesis can be found in the Lanchester Library, Coventry University.

*Figure B.27. Aerial imagery of the 2020 site, marked with red circle (image retrieved from Google Earth (Google, 2022))*



*Figure B.28. MDI replication locations at the 2020 sample site. Orange circles indicate MDI measurement locations.*



*Figure B.29. 2020 sample site surrounding area*

#### **B.4 Maps and Routes around Sample site from Week-to-week**

As discussed in section 5.2.2 data was collected from the sample sites in reverse order from week-to-week. This was to account for any implications that may arise regarding the sampling of the same site at the same time every week. For instance, if the control site was only ever sampled first, then it could be assumed that the control site was unfairly exposed to antecedent conditions or morning dew, which would impact data collection. Similar could be said if the control site was only ever sampled last – the site would have been thawing/during all day, meaning the results of data collection would be skewed. Figure B.30 and Figure B.31 show the routes taken between sample sites at the Sernal site.

Note that the routes taken were selected based on ease of access and efficiency. The sites were not sampled in exact reverse order every week (i.e., oldest – newest / newest – oldest) as this was not the most efficient way to traverse the site. This route was also selected due to health and safety concerns (lone working in the darker winter months).

Note the 2020 and 2014 sites (not mapped) were treated with the same method; one week would start at the 2014 site then travel to 2020, then next would start at 2020 and travel to 2014.

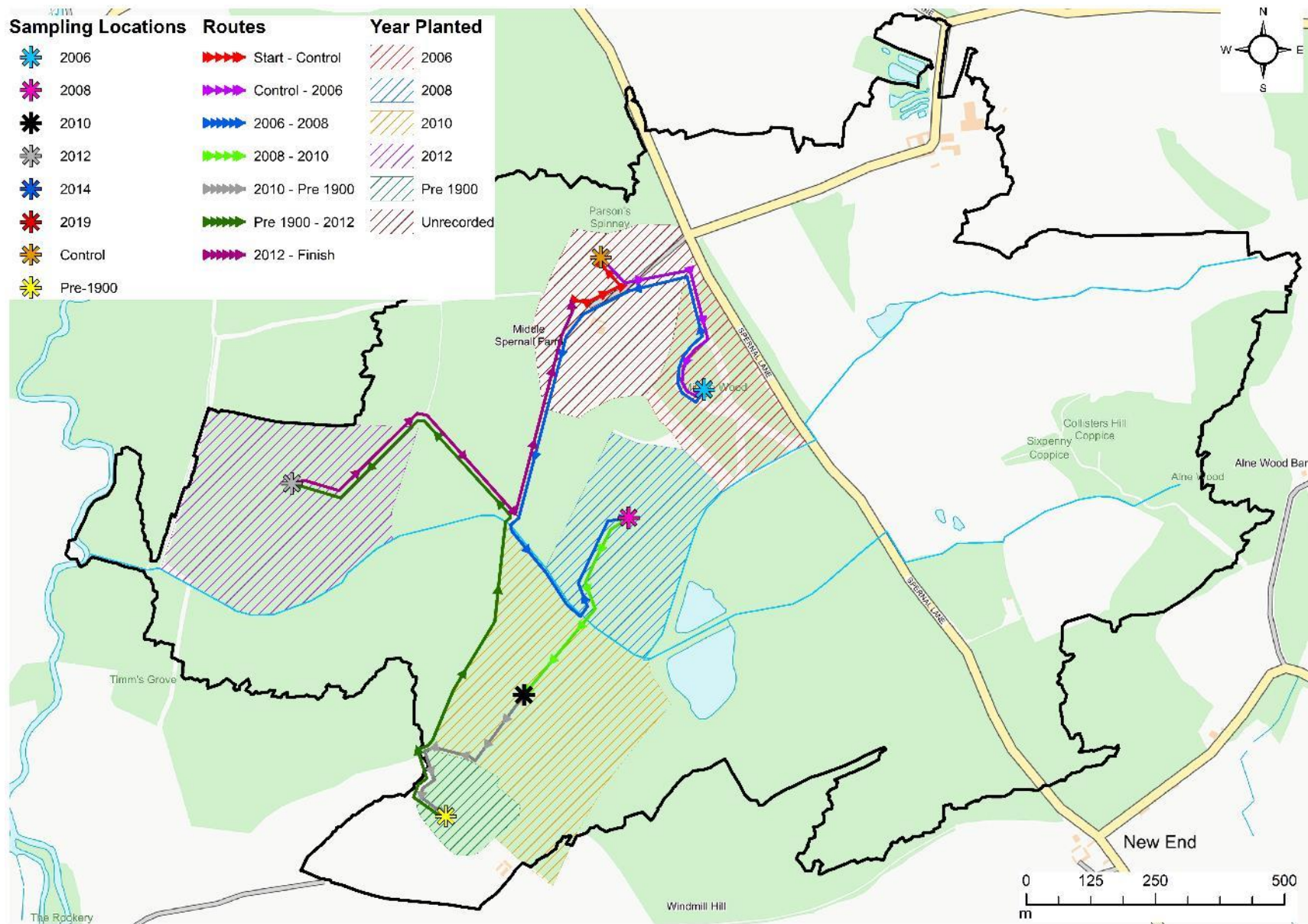


Figure B.30. Route 1: Start, control, 2006, 2008, 2010, ca.1900, 2012, finish.

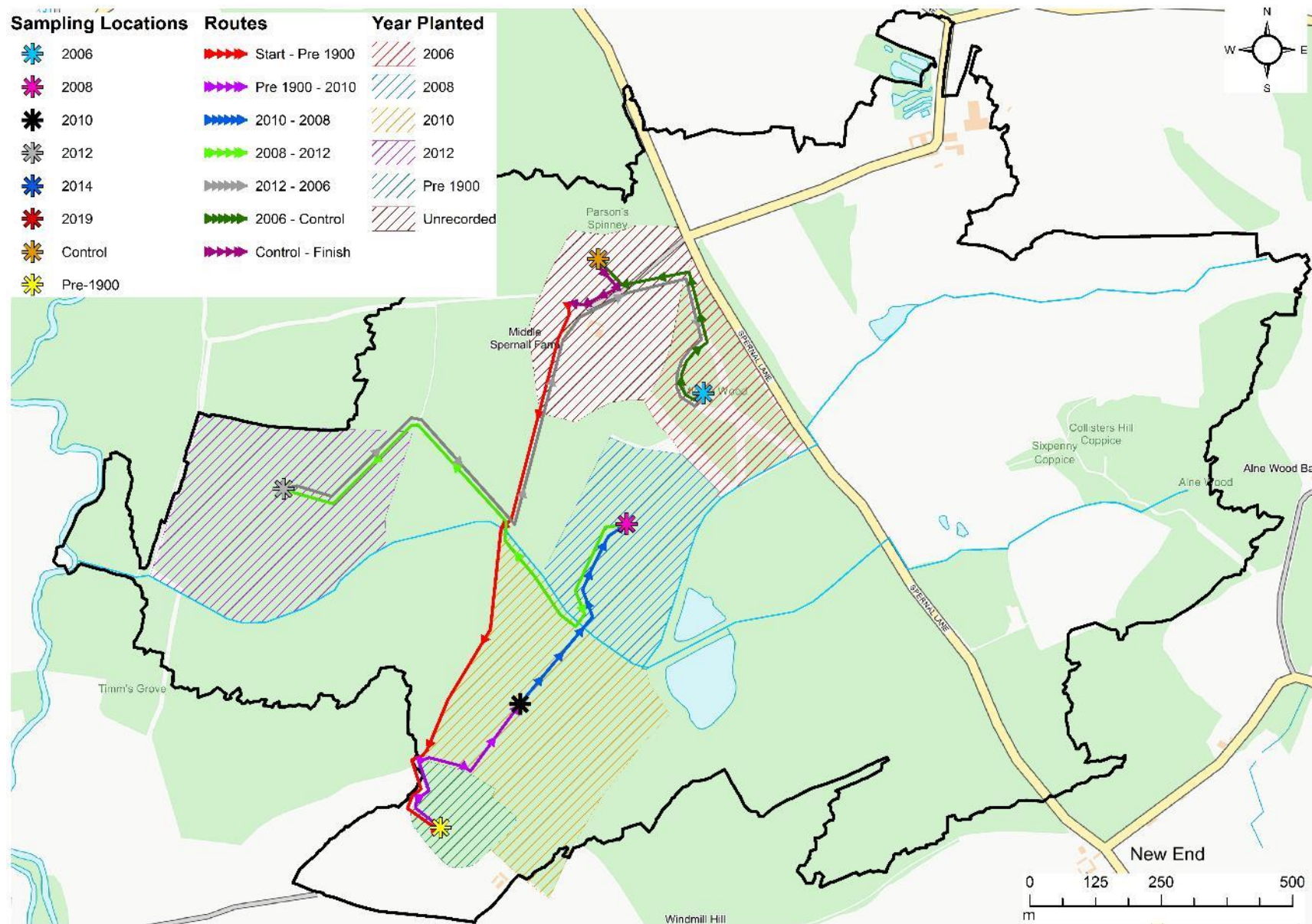


Figure B.31. Route 2: Start, ca.1900, 2010, 2008, 2012, 2006, control, finish.

## **B.5 Model Information**

This appendix contains information regarding the calculated total areas of HMS model nodes, the final calibration parameters, and an explanation of the calibration and validation RMSE values.

### **B.5.1 HEC-HMS Model Node Area Calculations**

Table B.10 shows the area calculations for each sub catchment/HMS model node as described throughout section 5.3.

*Table B.10. Land cover calculations for each HMS node*

<b>Plot</b>	<b>Total</b>	<b>Wood</b>	<b>10 cm</b>	<b>200 cm</b>	<b>Grass</b>	<b>Misc.</b>	<b>Misc. Detail</b>	<b>% Wood</b>	<b>% Grass</b>	<b>% Misc.</b>
1991	0.056	0.056	0.028	0.028	0.000	0.000		100.0	0.0	0.0
1995	0.046	0.046	0.023	0.023	0.000	0.000		100.0	0.0	0.0
2006	0.066	0.045	0.023	0.023	0.021	0.000		68.2	31.8	0.0
2007_1	0.006	0.005	0.003	0.003	0.001	0.000		83.3	16.7	0.0
2007_2	0.008	0.008	0.004	0.004	0.000	0.000		100.0	0.0	0.0
2008_1	0.013	0.013	0.007	0.007	0.000	0.000		100.0	0.0	0.0
2008_2	0.055	0.044	0.022	0.022	0.011	0.000		80.0	20.0	0.0
2008_3	0.029	0.017	0.009	0.009	0.012	0.000		58.6	41.4	0.0
2008_4	0.086	0.065	0.033	0.033	0.021	0.000		75.6	24.4	0.0
2008_5	0.030	0.016	0.008	0.008	0.012	0.002		53.3	40.0	6.7
2009_1	0.020	0.020	0.010	0.010	0.000	0.000		100.0	0.0	0.0
2009_2	0.086	0.054	0.027	0.027	0.027	0.005	Pond	62.8	31.4	5.8
2009_3	0.057	0.009	0.005	0.005	0.033	0.015	Pond	15.8	57.9	26.3
2009_4	0.074	0.064	0.032	0.032	0.010	0.000		86.5	13.5	0.0
2009_5	0.068	0.055	0.028	0.028	0.013	0.000		80.9	19.1	0.0
2009_6	0.043	0.033	0.017	0.017	0.010	0.000		76.7	23.3	0.0
2009_7	0.040	0.032	0.016	0.016	0.008	0.000		80.0	20.0	0.0
2010_1	0.091	0.060	0.030	0.030	0.031	0.000		65.9	34.1	0.0
2010_2	0.140	0.095	0.048	0.048	0.045	0.000		67.9	32.1	0.0
2011_3	0.083	0.071	0.036	0.036	0.012	0.000		85.5	14.5	0.0
2011_1	0.008	0.008	0.004	0.004	0.000	0.000		100.0	0.0	0.0
2011_2	0.048	0.034	0.017	0.017	0.014	0.000		70.8	29.2	0.0
2011_4	0.031	0.018	0.009	0.009	0.013	0.000		58.1	41.9	0.0
2011_5	0.037	0.030	0.015	0.015	0.007	0.000		81.1	18.9	0.0
2011_6	0.057	0.042	0.021	0.021	0.015	0.000		73.7	26.3	0.0
2012_1	0.031	0.025	0.013	0.013	0.006	0.000		80.6	19.4	0.0
2012_2	0.138	0.110	0.055	0.055	0.028	0.000		79.7	20.3	0.0

Grassland 1	0.052	0.000	0.000	0.000	0.049	0.003		0.0	94.2	5.8
Grassland 2	0.025	0.000	0.000	0.000	0.025	0.000		0.0	100.0	0.0
Grassland 3	0.042	0.000	0.000	0.000	0.042	0.000		0.0	100.0	0.0
Grassland 4	0.008	0.000	0.000	0.000	0.008	0.000		0.0	100.0	0.0
Northeast 1	0.078	0.000	0.000	0.000	0.078	0.000		0.0	100.0	0.0
Northeast 2	0.076	0.010	0.005	0.005	0.064	0.002	Lake	13.2	84.2	2.6
Northeast 3	0.075	0.015	0.008	0.008	0.060	0.000		20.0	80.0	0.0
Northeast 4	0.089	0.000	0.000	0.000	0.089	0.000		0.0	100.0	0.0
Northeast 5	0.060	0.000	0.000	0.000	0.060	0.000		0.0	100.0	0.0
Northeast 6	0.063	0.000	0.000	0.000	0.063	0.000		0.0	100.0	0.0
Northeast 7	0.004	0.000	0.000	0.000	0.004	0.000		0.0	100.0	0.0
Pre-1900_1	0.010	0.010	0.005	0.005	0.000	0.000		100.0	0.0	0.0
Pre-1900_2	0.027	0.027	0.014	0.014	0.000	0.000		100.0	0.0	0.0
Pre-1900_3	0.022	0.022	0.011	0.011	0.000	0.000		100.0	0.0	0.0
Pre-1900_4	0.053	0.000	0.000	0.000	0.052	0.001		0.0	98.1	1.9
Purity Area	0.017	0.000	0.000	0.000	0.000	0.017		0.0	0.0	100.0
Road	0.011	0.000	0.000	0.000	0.000	0.011	Road	0.0	0.0	100.0
Misc. Impermeable	0.009	0.000	0.000	0.000	0.000	0.009		0.0	0.0	100.0

### B.5.2 Model Calibration Parameters for Winter and Summer Models

Table B.11 presents the final values used to represent each HEC-HMS model node during model calibration for both winter and summer models (see section 5.4).

*Table B.11. Final Snyder parameters for winter and summer model calibration.*

HEC-HMS node name	Snyder Transform Parameters			
	Winter		Summer	
	Lag	Peaking	Lag	Peaking
Grassland_1 (G)	18	0.5	6	0.5
Grassland_2 (G)	18	0.5	6	0.5
Grassland_3 (G)	18	0.5	6	0.5
Grassland_4 (G)	18	0.5	6	0.5
Northeast 1 (G)	18	0.5	6	0.5
Northeast 2 (G)	18	0.5	6	0.5
Northeast 2 (W10)	18	0.5	6	0.5
Northeast 2 (W200)	18	0.5	6	0.5
Northeast 3 (G)	18	0.5	6	0.5
northeast 3 (W10)	18	0.5	6	0.5
Northeast 3 (W200)	18	0.5	6	0.5
Northeast 4 (G)	18	0.5	6	0.5
Northeast 5 (G)	18	0.5	6	0.5
Northeast 6 (G)	18	0.5	6	0.5
Northeast 7 (G)	18	0.5	6	0.5

Pond 1	18	0.5	6	0.5
Pond 2	18	0.5	6	0.5
Pre_1900 3 (W10)	18	0.5	6	0.5
Pre_1900 3 (W200)	18	0.5	6	0.5
Pre_1900 4 (G)	18	0.5	6	0.5
Pre_1900 (W10)	18	0.5	6	0.5
Pre_1900 (W200)	18	0.5	6	0.5
Pre_1900_1 (W10)	18	0.5	6	0.5
Pre_1900_1 (W200)	18	0.5	6	0.5
Purity Impermeable (I)	6	0.8	4	0.8
Road (I)	6	0.8	4	0.8
Sernal B&R (I)	6	0.8	4	0.8
1991 (W10)	18	0.5	6	0.5
1991 (W200)	18	0.5	6	0.5
1995 (W10)	18	0.5	6	0.5
1995 (W200)	18	0.5	6	0.5
2006 (G)	18	0.5	6	0.5
2006 (W10)	18	0.5	6	0.5
2006 (W200)	18	0.5	6	0.5
2007_1 (W10)	18	0.5	6	0.5
2007_1 (W200)	18	0.5	6	0.5
2007_2 (W10)	18	0.5	6	0.5
2007_2 (W200)	18	0.5	6	0.5
2008_1 (W10)	18	0.5	6	0.5
2008_1 (W200)	18	0.5	6	0.5
2008_2 (G)	18	0.5	6	0.5
2008_2 (W10)	18	0.5	6	0.5
2008_2 (W200)	18	0.5	6	0.5
2008_3 (G)	18	0.5	6	0.5
2008_3 (W10)	18	0.5	6	0.5
2008_3 (W200)	18	0.5	6	0.5
2008_4 (G)	18	0.5	6	0.5
2008_4 (W10)	18	0.5	6	0.5
2008_4 (W200)	18	0.5	6	0.5
2008_5 (G)	18	0.5	6	0.5
2008_5 (W10)	18	0.5	6	0.5
2008_5 (W200)	18	0.5	6	0.5
2009_1 (W10)	18	0.5	6	0.5
2009_1 (W200)	18	0.5	6	0.5
2009_2 (G)	18	0.5	6	0.5
2009_2 (W10)	18	0.5	6	0.5
2009_2 (W200)	18	0.5	6	0.5
2009_3 (G)	18	0.5	6	0.5
2009_3 (W10)	18	0.5	6	0.5
2009_3 (W200)	18	0.5	6	0.5
2009_4 (G)	18	0.5	6	0.5

2009_4 (W10)	18	0.5	6	0.5
2009_4 (W200)	18	0.5	6	0.5
2009_5 (G)	18	0.5	6	0.5
2009_5 (W10)	18	0.5	6	0.5
2009_5 (W200)	18	0.5	6	0.5
2009_6 (G)	18	0.5	6	0.5
2009_6 (W10)	18	0.5	6	0.5
2009_6 (W200)	18	0.5	6	0.5
2009_7 (G)	18	0.5	6	0.5
2009_7 (W10)	18	0.5	6	0.5
2009_7 (W200)	18	0.5	6	0.5
2010_1 (G)	18	0.5	6	0.5
2010_1 (W10)	18	0.5	6	0.5
2010_1 (W200)	18	0.5	6	0.5
2010_2 (G)	18	0.5	6	0.5
2010_2 (W10)	18	0.5	6	0.5
2010_2 (W200)	18	0.5	6	0.5
2011_1 (W10)	18	0.5	6	0.5
2011_1 (W200)	18	0.5	6	0.5
2011_2 (G)	18	0.5	6	0.5
2011_2 (W10)	18	0.5	6	0.5
2011_2 (W200)	18	0.5	6	0.5
2011_3 (G)	18	0.5	6	0.5
2011_3 (W10)	18	0.5	6	0.5
2011_3 (W200)	18	0.5	6	0.5
2011_4 (G)	18	0.5	6	0.5
2011_4 (W10)	18	0.5	6	0.5
2011_4 (W200)	18	0.5	6	0.5
2011_5 (G)	18	0.5	6	0.5
2011_5 (W10)	18	0.5	6	0.5
2011_5 (W200)	18	0.5	6	0.5
2011_6 (G)	18	0.5	6	0.5
2011_6 (W10)	18	0.5	6	0.5
2011_6 (W200)	18	0.5	6	0.5
2012_1 (G)	18	0.5	6	0.5
2012_1 (W10)	18	0.5	6	0.5
2012_1 (W200)	18	0.5	6	0.5
2012_2 (G)	18	0.5	6	0.5
2012_2 (W10)	18	0.5	6	0.5
2012_2 (W200)	18	0.5	6	0.5

### B.5.3 RMSE Values for Calibration and Validation

As outlined in section 5.4, RMSE was calculated for each calibration and validation event to further indicate the efficiency of the model. A RMSE closer to 0 indicates a good-fit between the observed and simulated data, whereas a value further from 0 indicates a poor-fit (Naik *et al.*, 2019; O’Loughlin *et al.*, 2020). Some calibration and validation results shown in sections 5.4 and 5.5 show a RMSE of 0. This is due to the values being defined to 4 significant figures. The actual RMSE values for each calibration and validation event are shown in Table B.12 and Table B.13.

*Table B.12. RMSE values for calibration events, shown to 10 significant figures.*

Duration	Winter	Summer
24	0.0013301035	0.0000203069
72	0.0004470588	0.0001000000
96	0.0000101929	0.0000356753
120	0.0000957518	0.0002188612

*Table B.13. RMSE values for validation events, shown to 10 significant figures.*

Duration	Winter	Summer
24	0.0043964489	0.0000507673
72	0.0008647059	0.0000176471
96	0.0004586825	0.0000000000
120	0.0000227980	0.0000091192

## **B.6 Tested Methods for Infiltration Projection**

A discussed in section 5.7.2, future infiltration across the site was extrapolated using published values of maturity and growth to cumulatively increase the infiltration year-on-year until maturity (these results can be seen in appendix section B.7). The other two methods tested for the projection of infiltration data are discussed in sections B.6.1 and B.6.2.

### **B.6.1 Disused Infiltration Projection Method 1**

Tested projection method 1 aimed to perform a regression analysis on the collected infiltration data for every observed site over both summer and winter, then use the slope and intercept of the regression line ( $Y = mx + c$ ) to project infiltration data into the future. The data for the years in between would be taken as the mean from this data. Results of this method showed the 2006, 2008, 2010 and 2012 sites to demonstrate negative infiltration, with only the 2014 and 2020 sites showing positive infiltration. See Table B.14.

*Table B.14. Projected infiltration for 2120 using method 1*

Planting year	2006	2008	2010	2012	2014	2020
2120 Infiltration rate (ml)	-575.88	-1602.87	-1638.80	-513.34	2193.77	960.60

Negative infiltration is a hydrological impossibility, and it is noted in the literature that infiltration around woodland increases over time (Chandler *et al.*, 2018; Zhang *et al.*, 2019a; Murphy *et al.*, 2021), so the results of this method were deemed unsuitable for the requirements of this project.

*B.6.2 Disused Infiltration Projection Method 2*

Tested projection method 2 used the same regression method as method 1, however treated the collected infiltration data as the data for sequential years. For example, providing the data collected in 2019 for each site is progressively older year-on-year, (i.e.) the 2006 site is interpreted as the tree being 13 years old in 2019, 14 in 2020, and 15 in 2021. Results of this method showed similar projections to method 1, with 2006, 2008, 2010, 2012 and 2015 showing negative infiltration, and only 2007, 2009, 2011, 2013, 2014, 2016, 2020 being positive infiltration, and even then, the positive values are deemed unrealistic based on what has been observed already. See Table B.15.

*Table B.15. Projected infiltration for 2120 using method 2.*

Planting year	2006	2007	2008	2009	2010	2011	2012	2013	2014	2015	2016	2020
2120 Infiltration rate (ml)	-2270	1196	-5638	594	-3472	1192	-1136	712	620	-2550	1902	1410

The same constraints are seen in the results of method 2 as were discussed regarding method 1, therefore, method 2 was deemed an unsuitable method of projecting infiltration for this project. The conclusions of both disused projection methods resulted in the selection of the chosen method for infiltration data projection (section B.7).

## **B.7 Projected Increases to Infiltration due to Climate Change**

A discussed in section 5.7.2, future infiltration across the site was extrapolated using published values of maturity and growth to cumulatively increase the infiltration year-on-year until maturity.

### **B.7.1 Empirical Site Infiltration Projections**

The results of infiltration data extrapolations for EMPIRICAL sites are shown throughout Figure B.32 to Figure B.35.

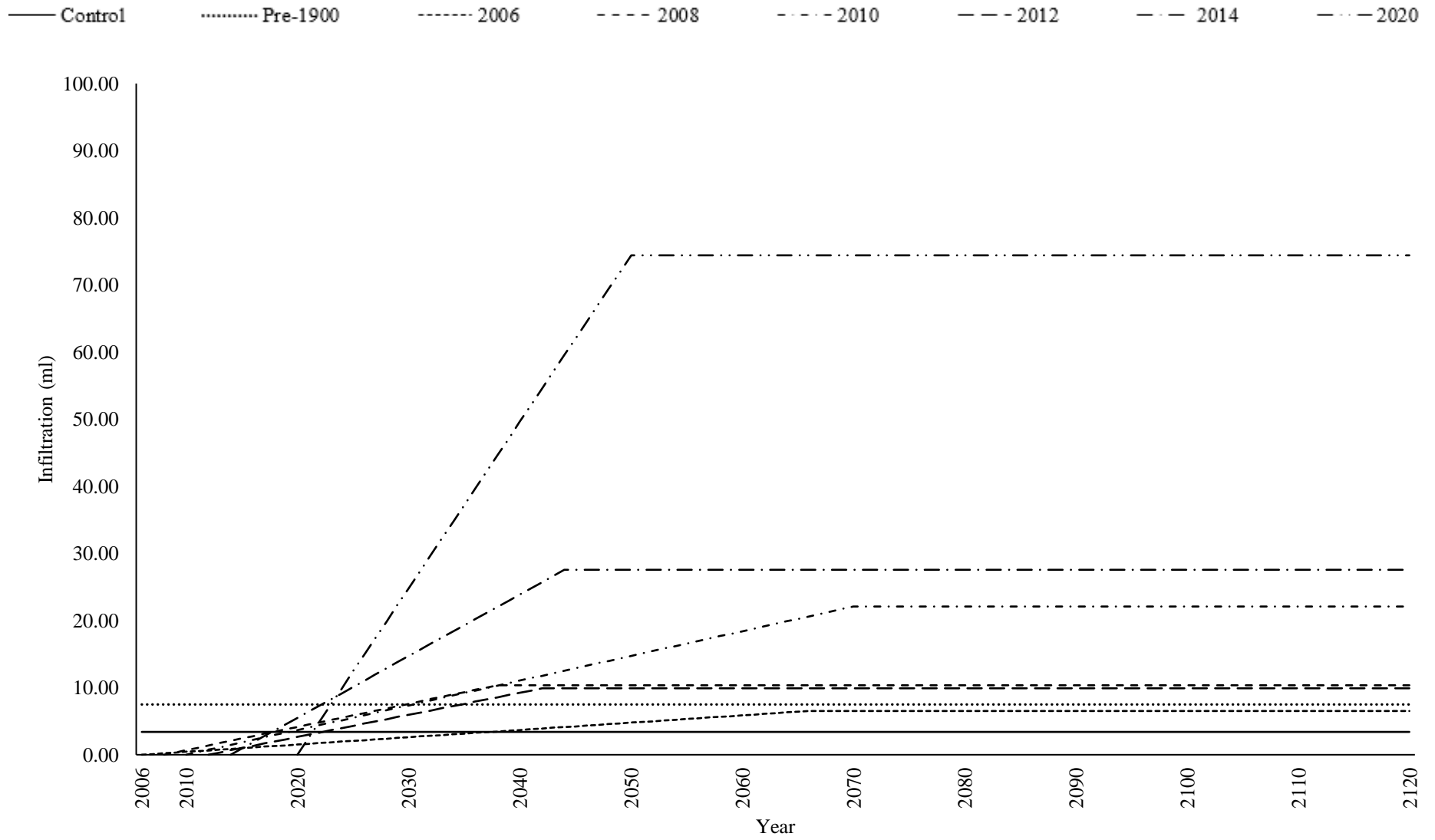


Figure B.32. Mean winter infiltration projections for all empirical sample sites at 10 cm proximity

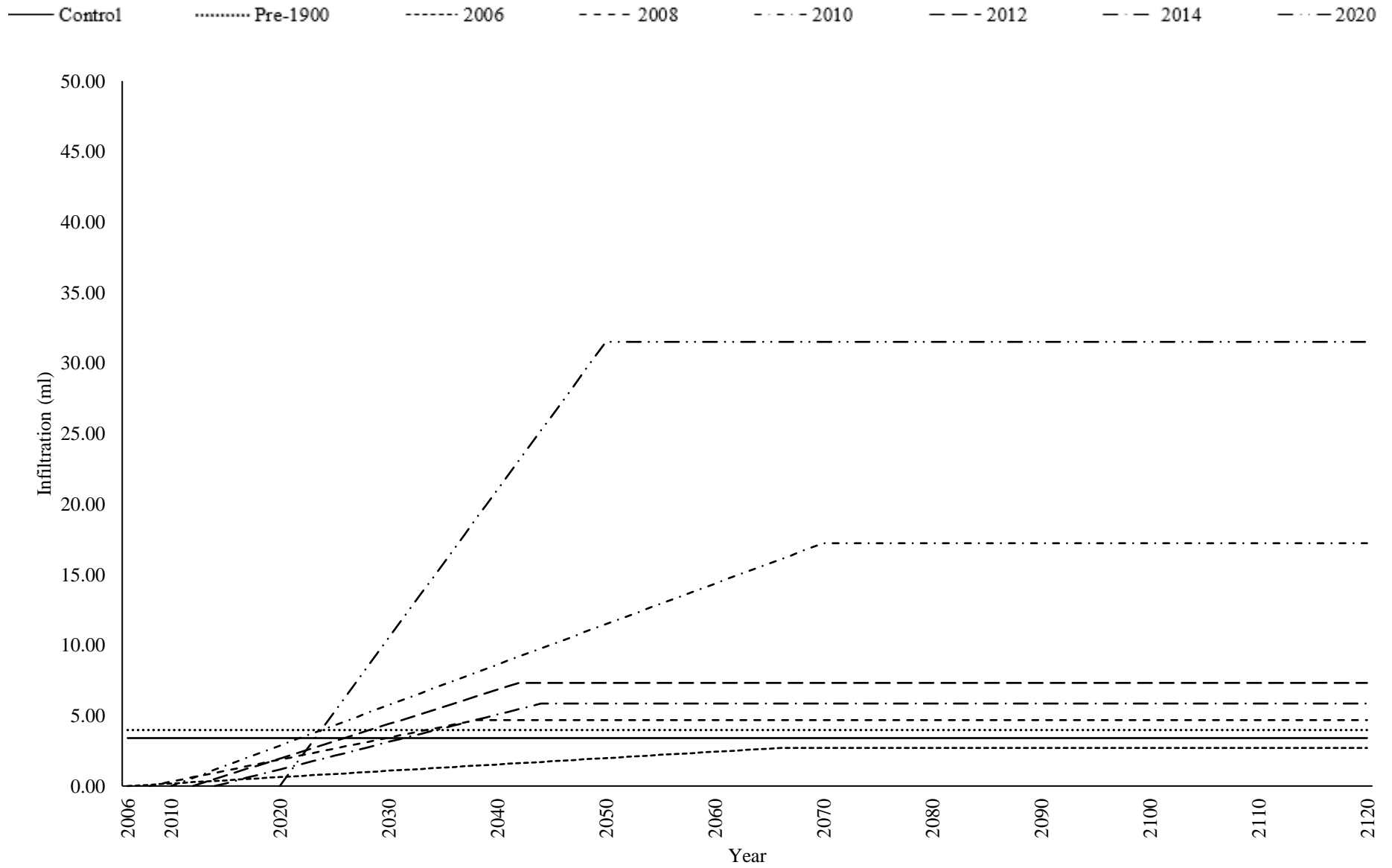


Figure B.33. Mean winter infiltration projections for all empirical sample sites at 200 cm proximity

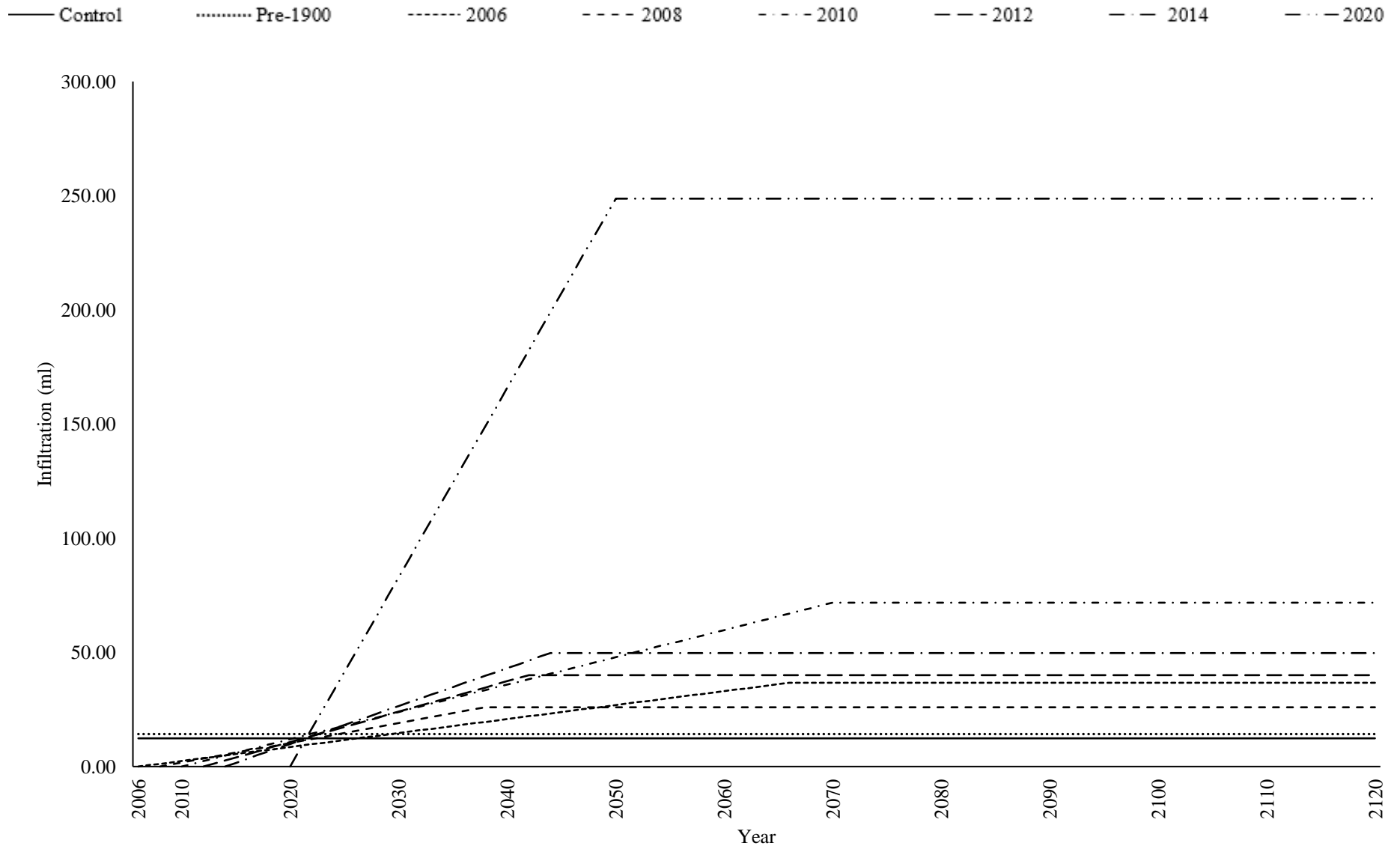


Figure B.34. Mean summer infiltration projections for all empirical sample sites at 10 cm proximity.

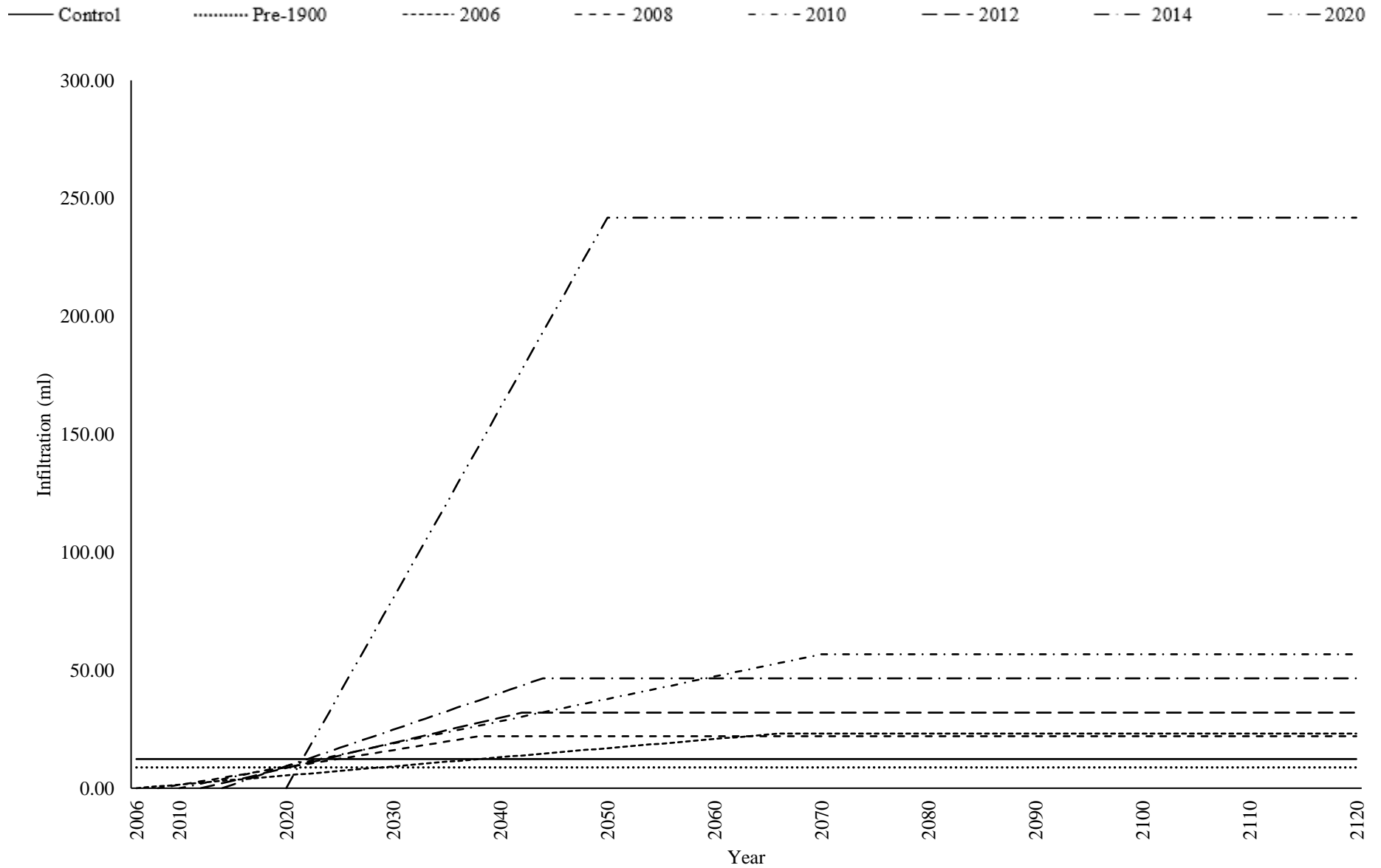


Figure B.35. Mean summer infiltration projections for all empirical sample sites at 200 cm proximity.

### *B.7.2 Non-Empirical Site Infiltration Projections*

The results infiltration data extractions for NON-EMPIRICAL values are shown throughout Figure B.36 to Figure B.39. These figures present values for sites within the study catchment where infiltration was not directly sampled with the MDI (section 5.2.2); and represent the results of the chosen infiltration projection method (discussed in section 5.7.2).

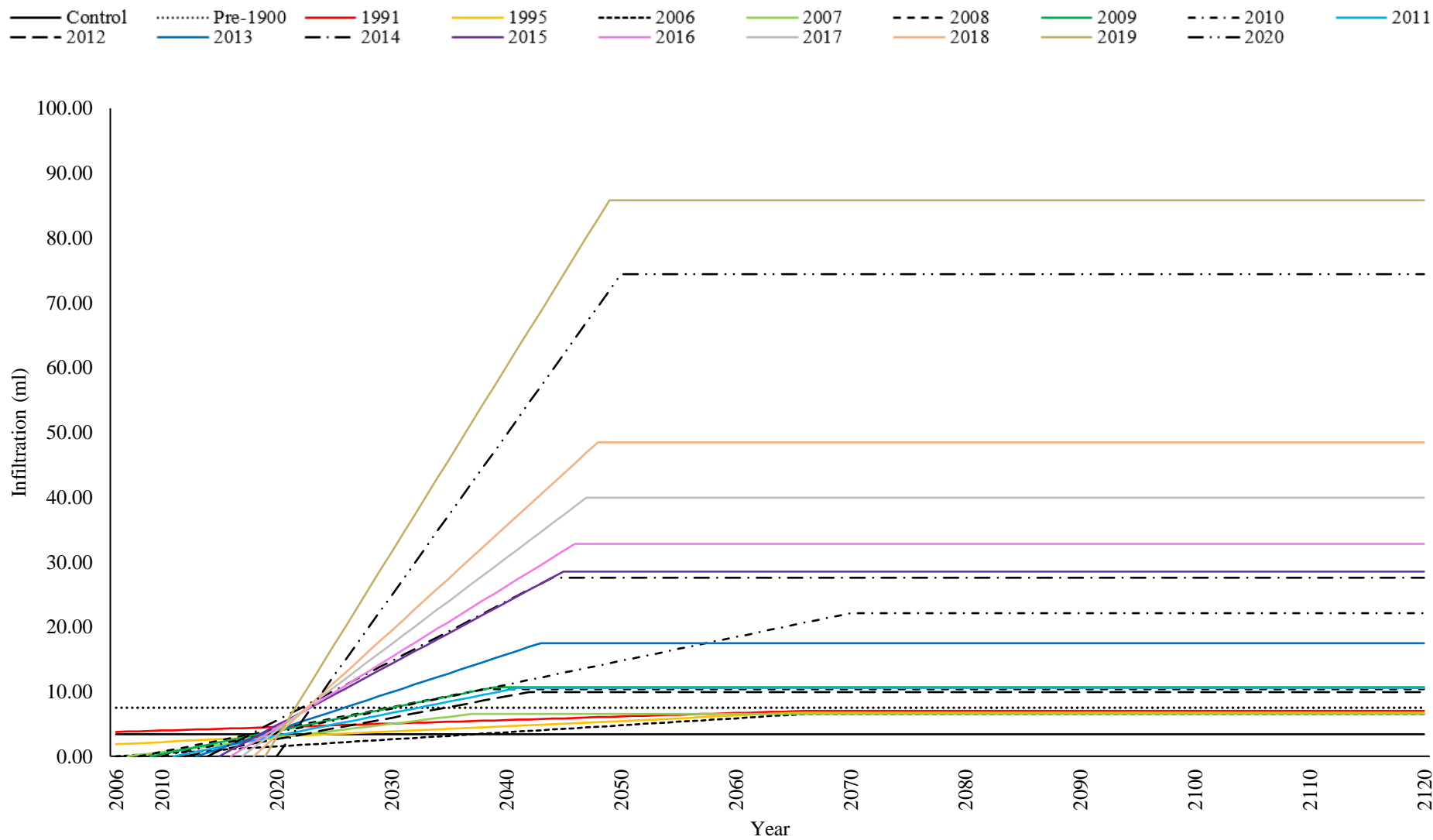


Figure B.36. Mean winter infiltration projections for all non-empirical sample sites at 10 cm proximity.

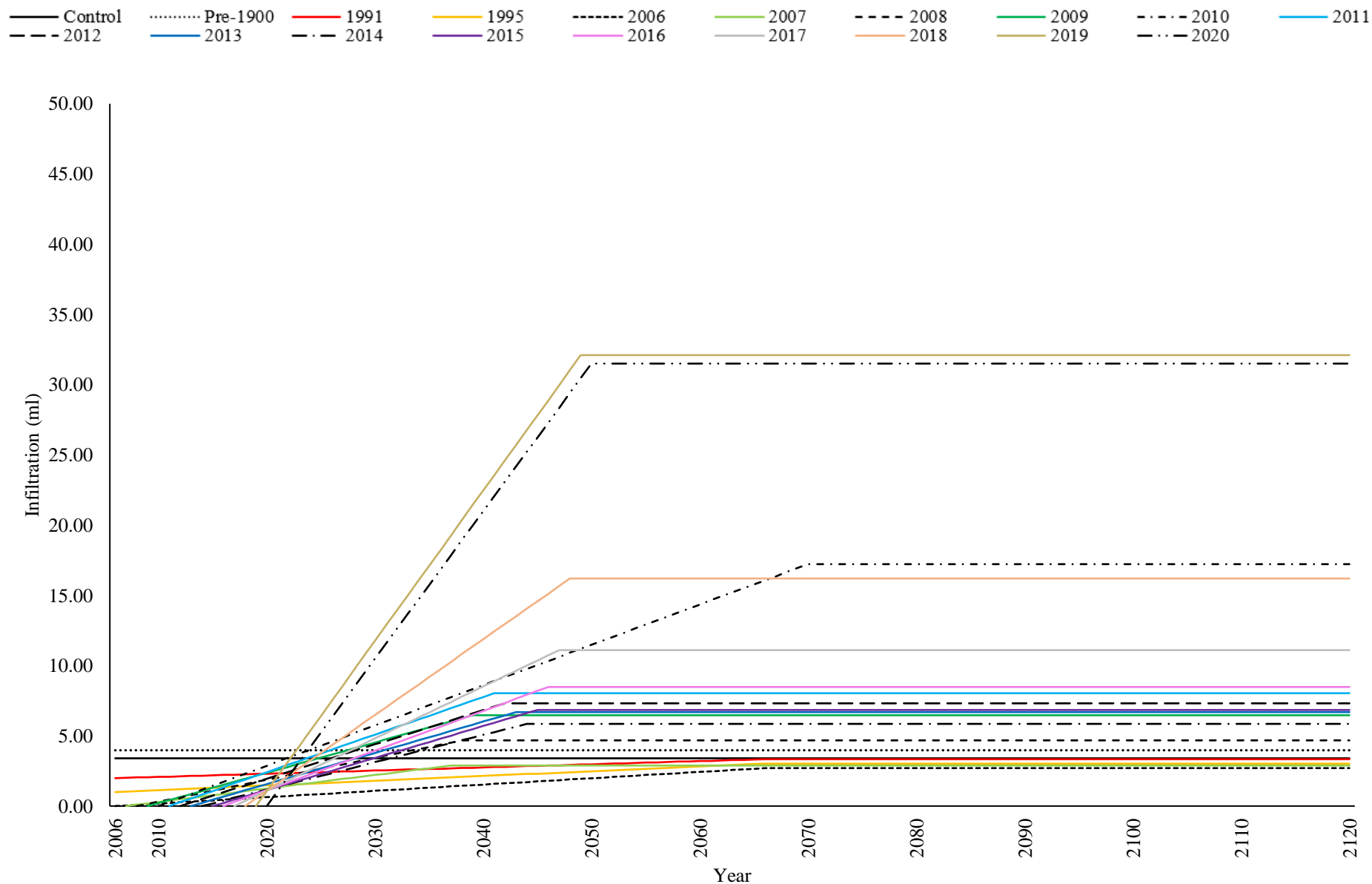


Figure B.37. Mean winter infiltration projections for all non-empirical sample sites at 200 cm proximity.

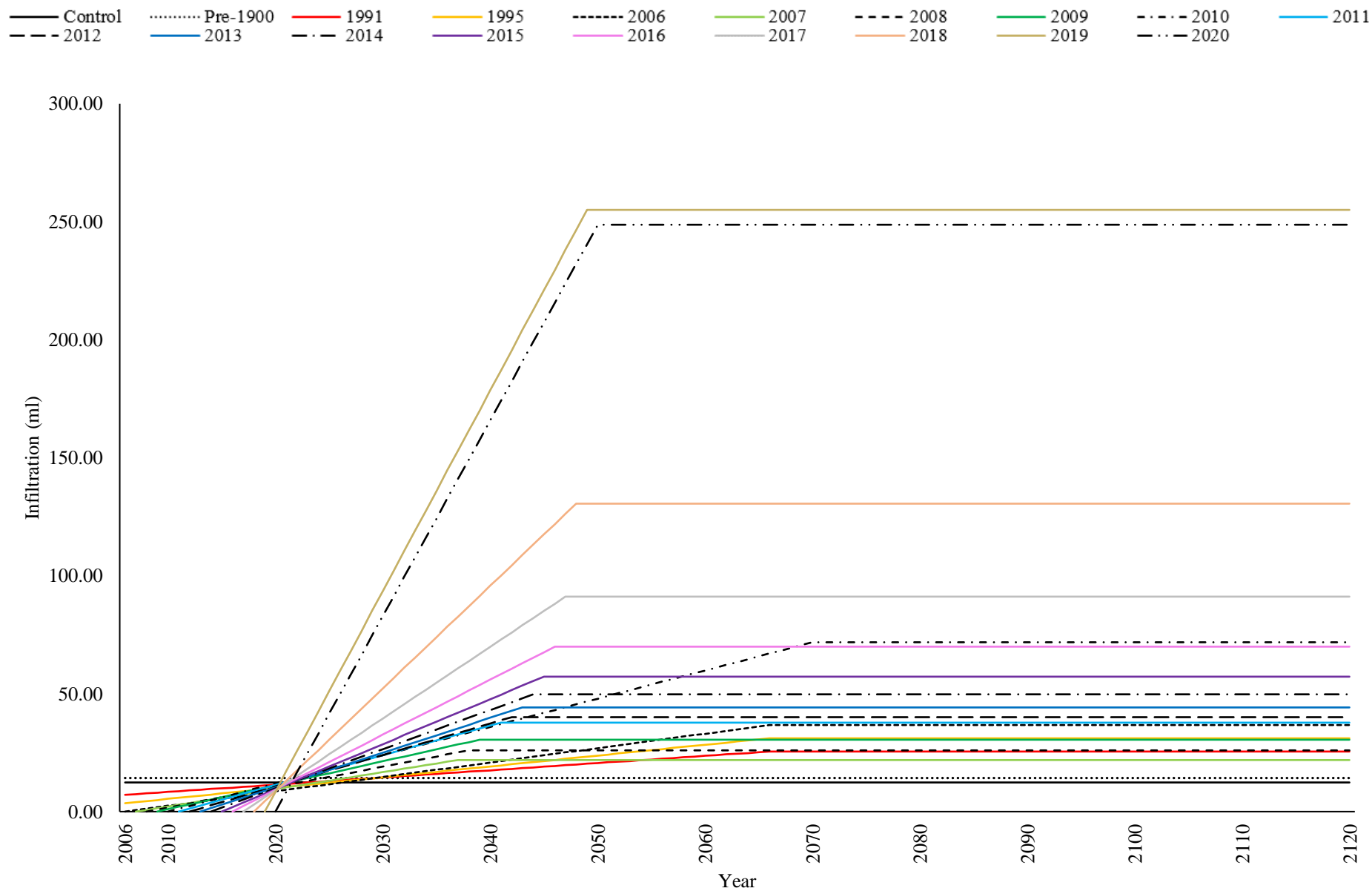


Figure B.38. Mean summer infiltration projections for all non-empirical sample sites at 10 cm proximity.

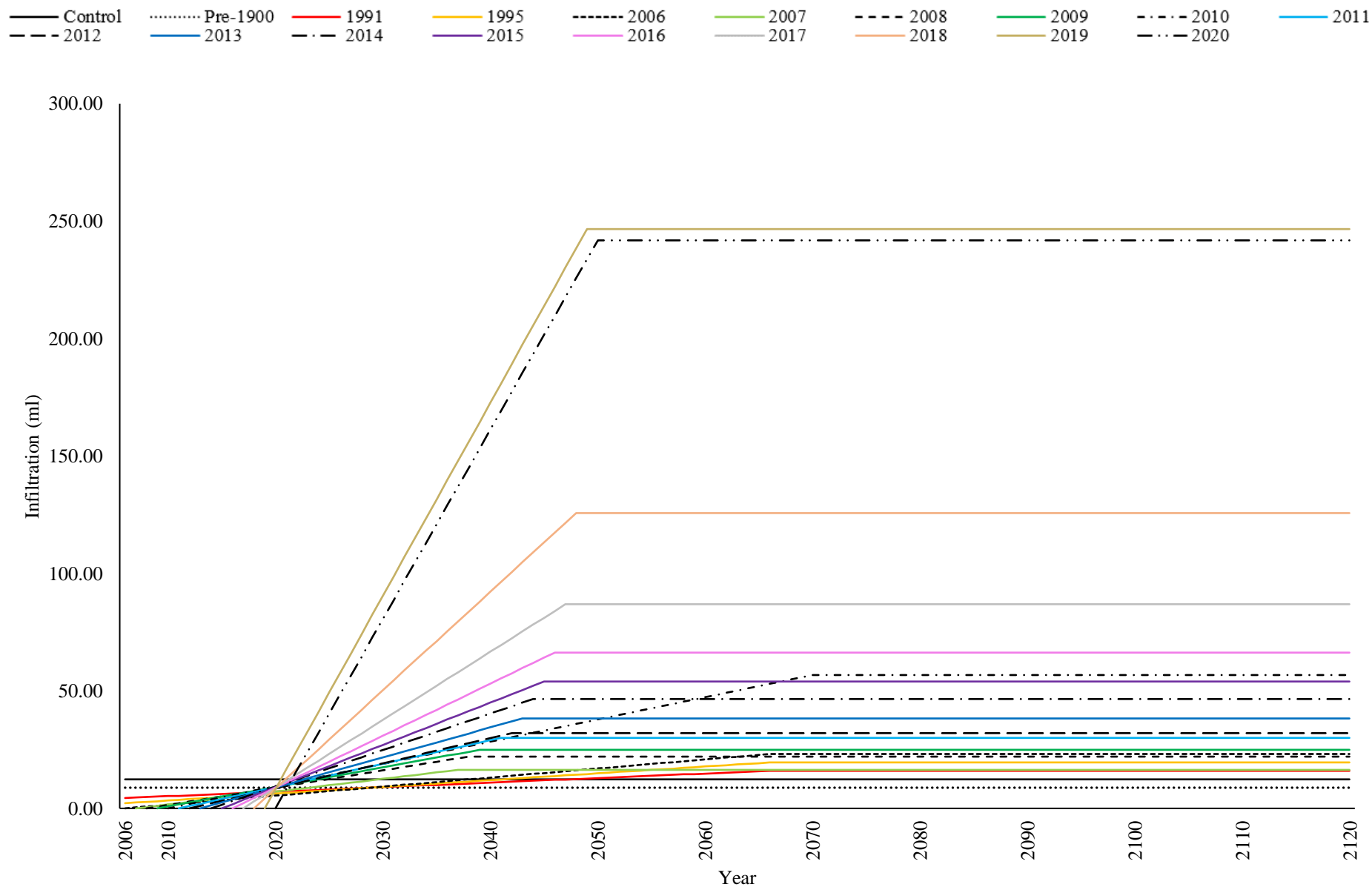


Figure B.39. Mean summer infiltration projections for all non-empirical sample sites at 200 cm proximity.

## **B.8 Data Sources, Permissions and Uses**

Table B.16 outlines the sources, year and uses of data used throughout this study.

*Table B.16. Data sources and special permissions for project*

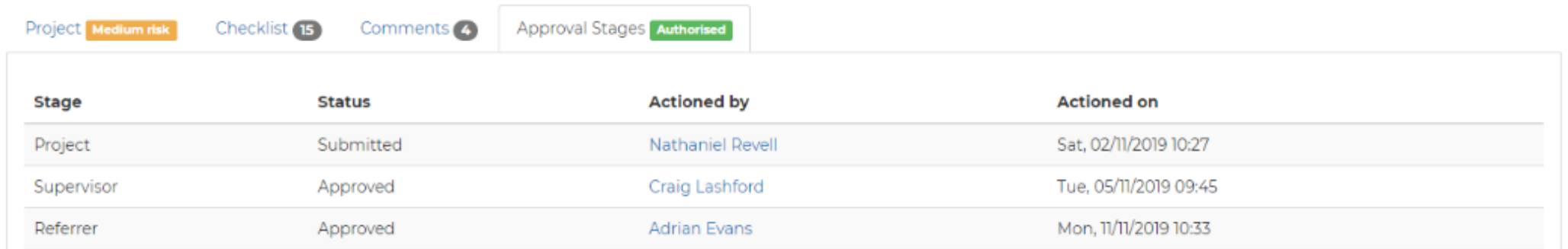
<b>Data</b>	<b>Year</b>	<b>Source / Permissions</b>	<b>Purpose/ Use</b>
Arrow-Alne catchment area north of Broom gaging station	2019	National River Flow Archive (NRFA) (2019)	To define the catchment boundary of the Arrow/Alne Catchment
Arrow/ordinary watercourse shapefiles	2019	Ordnance Survey open data download webpage (Ordnance Survey, 2021)	For use in the GIS map outputs presented throughout the study and for flood modelling
10k raster base map of Arrow catchment	2019	Ordnance Survey open data download webpage (Ordnance Survey, 2021)	To use as a base map for the GIS map outputs presented throughout the study
Environment Agency Integrated Height Model (IHM) 2m resolution LiDAR DTM of Broom catchment	2020	Granted under permission from the Environment Agency	For use in the whole catchment analysis in section... and for the creation of the study area elevation model
Owned Heart of England site location shapefiles and tree species detail	2019	Special permission from the Heart of England Forest charity	Used in the determination of sample sites and in GIS map outputs presented throughout the study
1:625,000 Scale Map of UK Bedrock and Superficial Geology	2019	British Geological Survey (BGS) data download portal (British Geological Survey, 2019)	Used for investigating bedrock and superficial geology of the whole/study catchments, and used in GIS map outputs presented throughout the study
25cm resolution aerial photography of Arrow catchment	2018	Special permission from (Ordnance Survey, 2020)	For use in the GIS map outputs presented throughout the study and for flood modelling
1m resolution LiDAR DTM of Broom catchment	2018	Department of Environment Food and Rural Affairs (DEFRA) download portal (Environment Agency, 2021d)	For use in the whole catchment elevation analysis in section...

Lower Super Output Areas (LSOA) of geographical census areas	2011	Census boundary data portal (UK Data Service Census Support, 2011)	For use in presenting the boundaries of Redditch and Alcester in figure...
Drone Imagery (14/100 cm DTM and aerial imagery)		Collected on site by Dr. Sim Reaney of Durham University with permission from Stephen Coffey, head forester at the Heart of England Forest	For use in the creation of the study area elevation model and flood modelling.
Rainfall Data	2019 - 2022	Collected by the rain gauge located at the NextGen wastewater treatment plant.	Used in the calibration and validation of the hydrological models
Flow and stage data of the study site tributary	2019 - 2022	Fitted in the tributary of the HofE Sernal site at the request of this project by Environmental Monitoring Solutions (EMS) Ltd, after permission from Stephen Coffey of the HofE forest Charity	Used in the calibration and validation of the hydrological models

## B.9 Ethical Approvals

Figure B.40 and Figure B.41 show the approvals of the required ethics applications for this study. The figures represent both the pre-pandemic approval, and revised approval including updated precautions as a result of the COVID-19 pandemic.

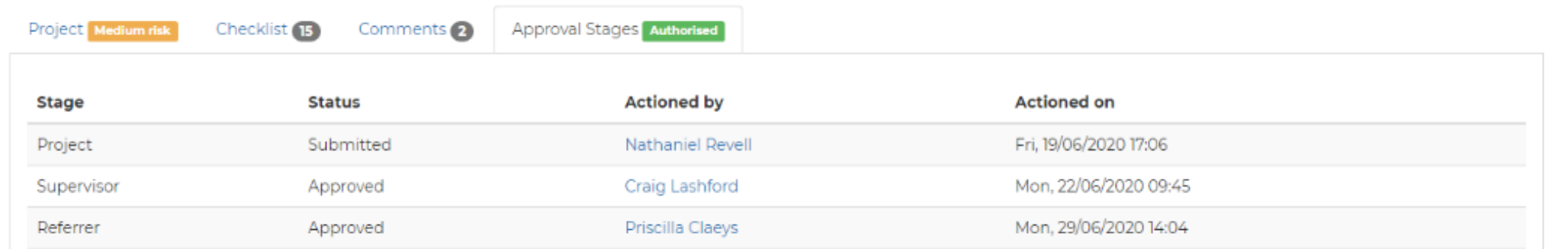
*Figure B.40. Original CU Ethics application (project P96879)*



The screenshot shows the approval stages for project P96879. At the top, there are navigation tabs: 'Project' (Medium risk), 'Checklist' (15), 'Comments' (4), and 'Approval Stages' (Authorised). Below the tabs is a table with the following data:

Stage	Status	Actioned by	Actioned on
Project	Submitted	Nathaniel Revell	Sat, 02/11/2019 10:27
Supervisor	Approved	Craig Lashford	Tue, 05/11/2019 09:45
Referrer	Approved	Adrian Evans	Mon, 11/11/2019 10:33

*Figure B.41. Updated CU Ethics approval with added procedures to account for the COVID-19 pandemic (project P108617)*



The screenshot shows the approval stages for project P108617. At the top, there are navigation tabs: 'Project' (Medium risk), 'Checklist' (15), 'Comments' (2), and 'Approval Stages' (Authorised). Below the tabs is a table with the following data:

Stage	Status	Actioned by	Actioned on
Project	Submitted	Nathaniel Revell	Fri, 19/06/2020 17:06
Supervisor	Approved	Craig Lashford	Mon, 22/06/2020 09:45
Referrer	Approved	Priscilla Claeys	Mon, 29/06/2020 14:04

## Appendix C. Results

This appendix contains additional and supporting information relating to the results presented in Chapter 7.

### **C.1** *Statistical Testing*

As discussed in section 7.1 statistical testing was undertaken to both determine the sorting of the collected infiltration data (parametric/non-parametric), and to conduct more thorough analysis. These are discussed further through the following sections.

#### *C.1.1 Kolmogorov-Smirnov (Normality) Testing*

A Kolmogorov-Smirnov (KS) test returns a value indicating if the sample data is parametric or non-parametric. A knowledge of this is important when deciding the correct statistical tests to perform across a dataset, as using a parametric statistical test using non-parametric data can yield inaccurate results, and visa-versa (Gadian *et al.*, 2018; Mishra *et al.*, 2019). The KS test outputs a numerical value, which is compared with a known value (derived from the sample size) to calculate the correct KS value for a P value of 0.05%, given by the equation:

$$\frac{1.36}{\sqrt{n}}$$

Where n is the number of samples used in the KS test. Table C.1 displays the input data for the seven KS tests undertaken, and the output P-values for each.

Table C.1. Test metrics and output P-values for KS tests

	KS Test Input Data	KS Value	P-Value
1	All infiltration data regardless of proximity and season	1.00	0.06
2	All summer infiltration regardless of proximity	0.87	0.07
3	All winter infiltration regardless of proximity	0.79	0.07
4	All winter 10 cm infiltration data	0.87	0.10
5	All winter 200 cm infiltration data	0.99	0.10
6	All summer 10 cm infiltration data	0.99	0.11
7	All summer 200 cm infiltration data	1.00	0.11

No tested input data showed a P-value less than alpha (0.05%), thus indicating that the data collected from the study site is not normally distributed (non-parametric), which will influence the type of statistical test used in data analysis. To visualise the distribution of the collected field data alongside the KS values shown (Table C.1), the distribution graphs for all seven scenarios are shown throughout Figure C.1 to Figure C.7

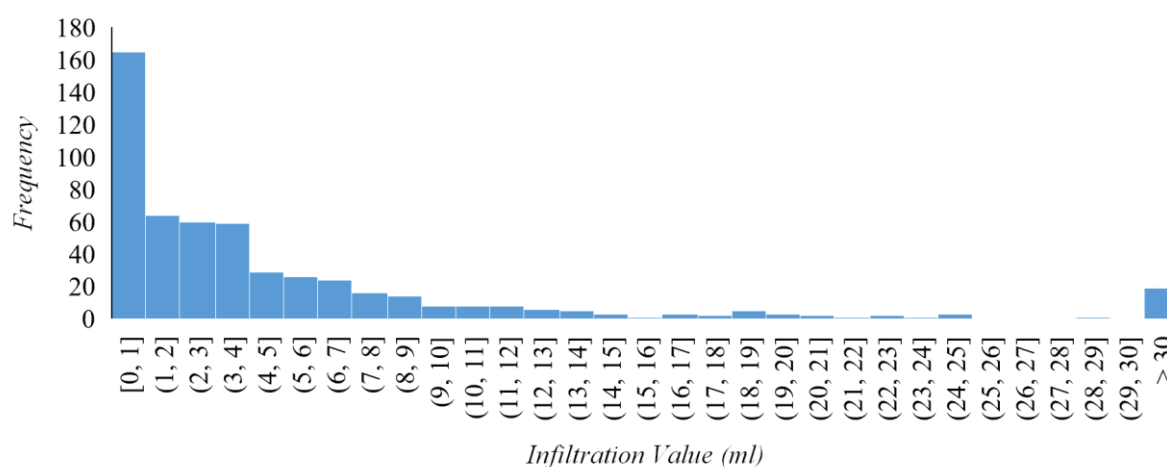


Figure C.1. Distribution of all infiltration data regardless of proximity and season.

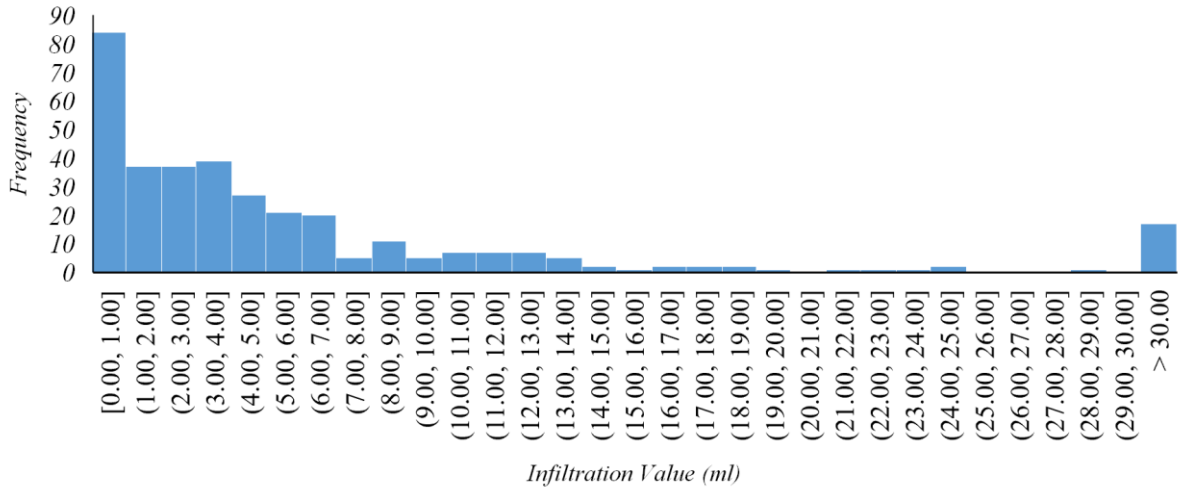


Figure C.2. Distribution of all 10 cm infiltration regardless of season

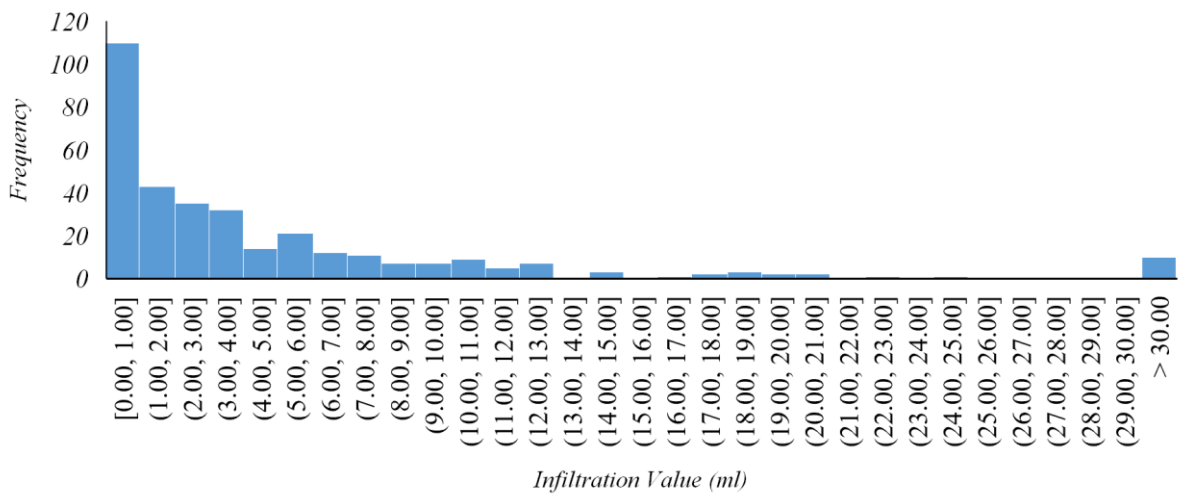


Figure C.3. Distribution of all 200 cm infiltration regardless of season

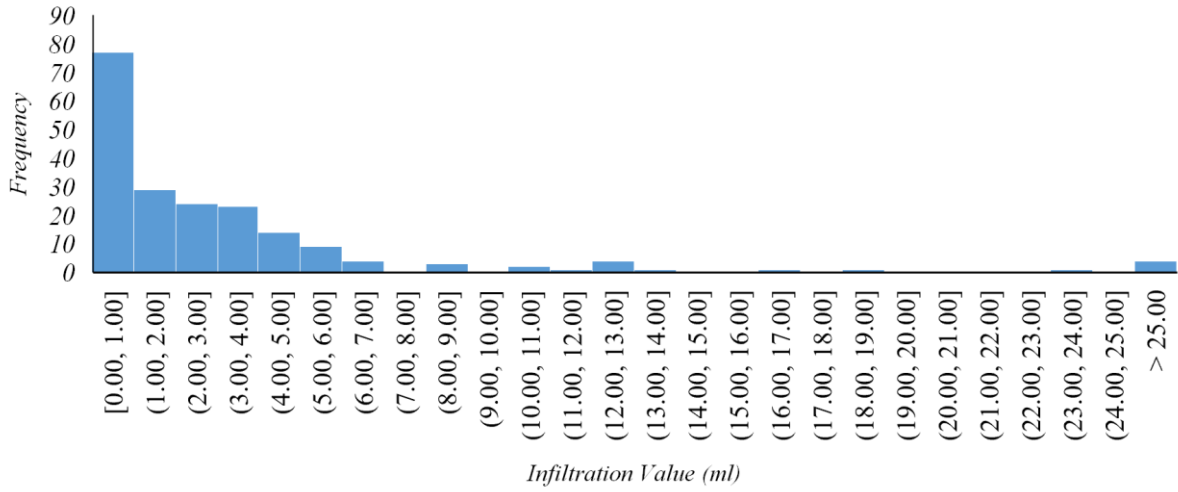


Figure C.4. Distribution of all winter 10 cm infiltration data

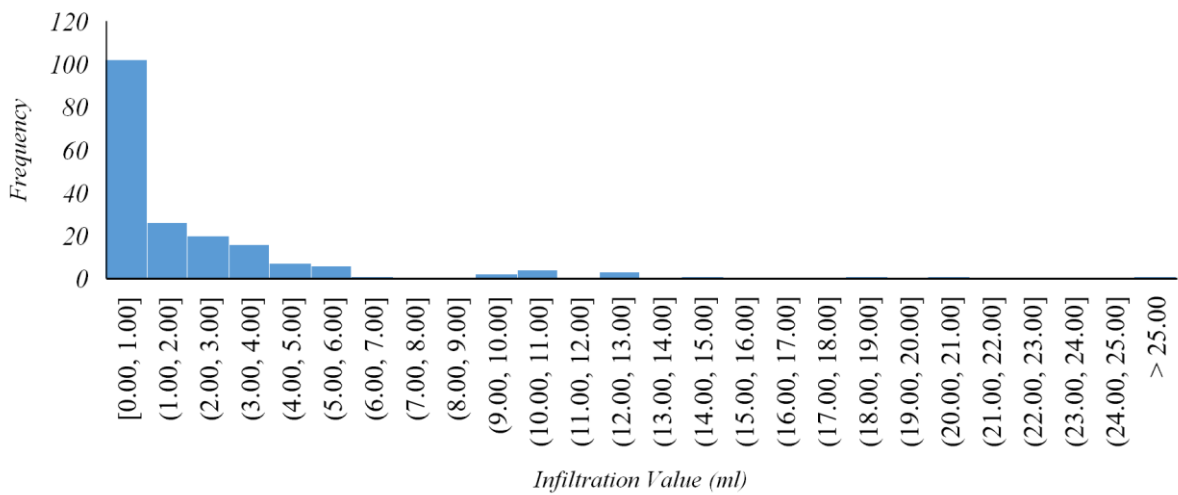


Figure C.5. Distribution of all winter 200 cm infiltration data

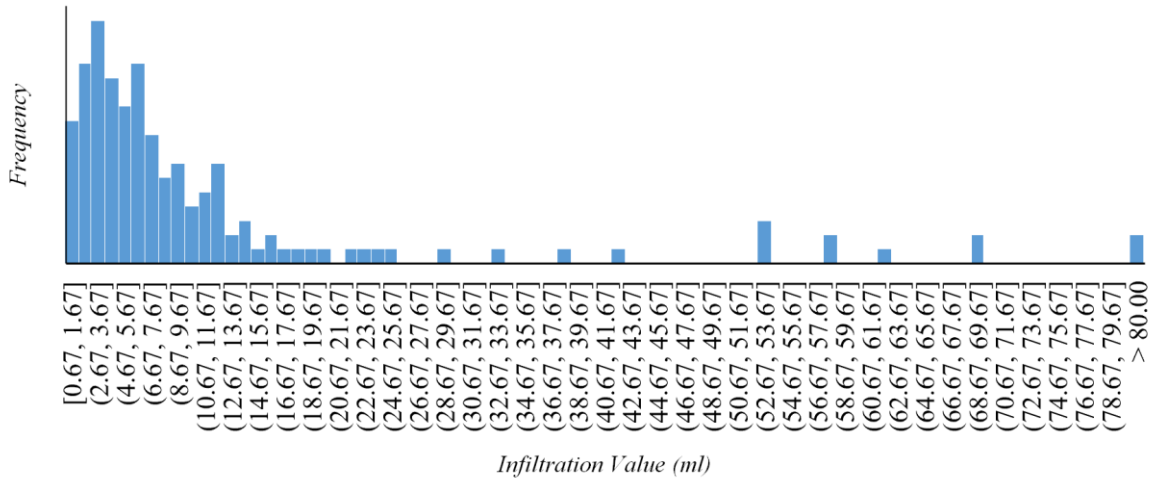


Figure C.6. Distribution of all summer 10 cm infiltration data

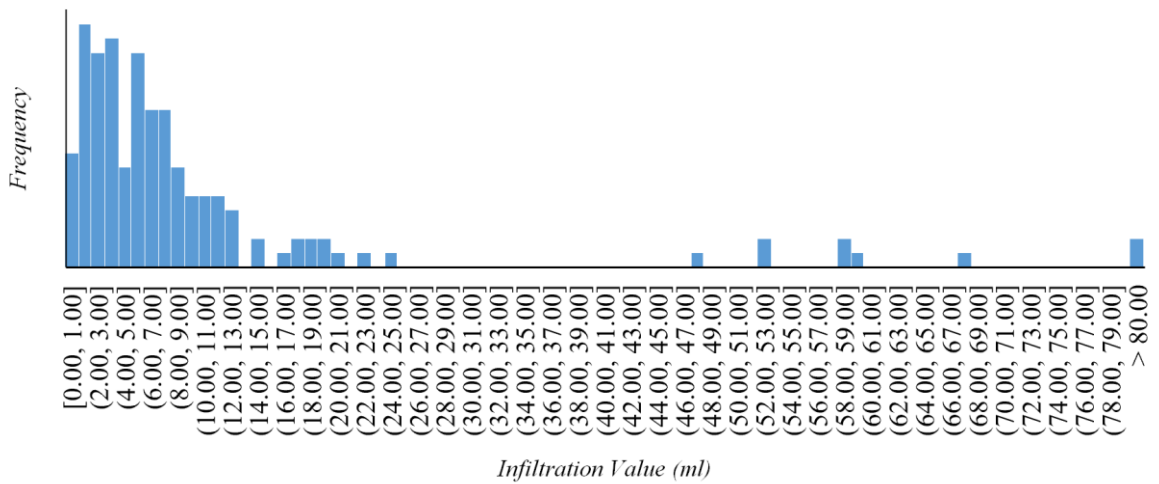


Figure C.7. Distribution of all summer 200 cm infiltration data

### C.1.2 Mann-Whitney U Test

As discussed in section 7.1 Mann-Whitney U tests were undertaken following the Kolmogorov-Smirnoff test (appendix C.1.1) to determine the significance of the relationships between infiltration and proximity, and infiltration and maturity (Fay and Proschan, 2010; Mishra *et al.*, 2019; Kamis *et al.*, 2021). The Mann-Whitney U test is the non-parametric equivalent of the independent samples t-test:

$$U_1 = n_1 n_2 + \frac{n_1(n_1+1)}{2} - R_1 \quad \text{EQ 12.2}$$

$$U_2 = n_1 n_2 + \frac{n_2(n_2+1)}{2} - R_2 \quad \text{EQ 12.3}$$

$n_1$  and  $n_2$  are the number of samples in group 1 and 2 respectively, and  $R_1$  and  $R_2$  are the sum of all ranks from the data in groups 1 and 2 respectively. Both  $U_1$  and  $U_2$  (EQ 12.2 and EQ 12.3) can be interpreted as the number of observations in a sample that precede or follow observations in the other sample when all samples are ranked in ascending order (Nachar, 2008). To determine significance ( $P$ -value), the normal approximation equation (Mann and Whitney, 1947) can be used:

$$P = \frac{|U_{min} - \frac{n_1 n_2}{2}|}{\sqrt{\frac{n_1 n_2 (n_1 n_2 + 1)}{12}}} \quad \text{EQ 12.4}$$

Where  $U_{min}$  is the smallest U value (of  $U_1$  and  $U_2$ ). The results of Mann-Whitney U testing can be seen throughout section 7.1.

### *C.1.3 Selection of Statistical Tests for Results Analysis*

It is determined in section C.1.1 that the collected data is non-parametric, meaning it does not follow a normal distribution, therefore influencing the type of statistical method that could be used during analysis. Furthermore, the collected infiltration data is unpaired. Paired data refers to measurements that have been taken from the same sample population/area both before and after a known change (i.e., infiltration both before and after rainfall, immune response both before and after taking prescribed medication). This contrasts with unpaired (independent) data, when the collected data is from separate populations/sample sites at different points in time, and with potentially different characteristics. The infiltration data collected throughout this study is unpaired, as measurements are taken from three separate areas (replicas, see section 5.2.2) at 10 cm and 200 cm proximities, and soil and moisture conditions can vary. Ultimately, the Mann-Whitney U test was chosen for use throughout this study (section C.1.2), however other commonly used nonparametric statistical tests are presented in Table C.2.

*Table C.2. Statistical tests for non-parametric data*

<b>Nonparametric Test</b>	<b>Parametric Equivalent</b>	<b>Description</b>
Kruskal-Wallis	One-way ANOVA	Compares <b>more than two</b> independent groups with ordinal (scaled/ordered/0-10(e.g.)) data.
Wilcoxon signed rank	Paired samples T-test	Compares two <b>dependent (paired)</b> samples with ordinal data.
Mann-Whitney U Test	Independent samples T-test	Analyses two <b>independent (unpaired)</b> samples that contain ordinal data.

## **C.2 Temperature and Infiltration**

A correlation analysis was undertaken to quantify the effect of air temperature, ground surface and soil temperature on the collected infiltration data. A correlation analysis derives a dimensionless value between -1 and 1, where a value closer to 1 indicates positive correlation, and a value closer to -1 indicates a negative correlation; a value closer to 0 indicates the absence of correlation (Esezi Isaac and Eric Chikweru, 2018; Schober *et al.*, 2018). The results of the correlation analysis are shown in Table C.3

*Table C.3. Correlation coefficients for air, ground, and soil temperatures*

	Control	ca.1900	2006	2008	2010	2012	2014	2020	Mean
10									
Air	0.36	0.30	0.45	0.19	0.31	0.35	0.16	0.22	0.29
Ground	0.36	0.30	0.44	0.18	0.33	0.40	0.17	0.31	0.31
Soil	0.38	0.30	0.45	0.20	0.31	0.34	0.15	0.26	0.30
200									
Air		0.46	0.50	0.22	0.28	0.40	0.18	0.13	0.31
Ground		0.57	0.55	0.15	0.29	0.47	0.24	0.31	0.37
Soil		0.58	0.55	0.13	0.32	0.41	0.17	0.26	0.35

Table C.3 shows there to be a positive correlation between all measured temperatures and infiltration at both proximities, however very few correlations are notably strong. At the 10 cm proximity, measured temperatures at the 2006 sample site showed the strongest correlation (however still relatively weak), being 0.45, 0.44 and 0.45 for air, ground, and soil respectively. The weakest positive correlation at the 10 cm proximity is between 2014 soil temperature and infiltration, being 15, followed by 2014 air and ground, being 16 and 17 respectively. The lowest mean positive correlation was seen between air temperature and infiltration (0.29), followed by soil (0.30), then by ground (0.31). Of the 200 cm proximity, air temperature of the 2020 site, and soil temperature of the 2008 site both show the lowest correlation value of 0.13; the highest correlation is seen between soil and infiltration at the *ca.* 1900 site. Most correlation values are higher for the 200 cm proximity than the 10 cm proximity, except for air temperature

in 2010 and 2020 (-0.03 and -0.09 respectively), ground temperature in 2008 and 2010 (-0.03 and -0.04 respectively), and soil temperature in 2008 (-0.07). Overall, the mean correlation of all measured temperatures for the 200 cm proximity were higher than that of 10 cm, being 0.31 (+0.02), 0.35 (+0.05) and 0.37 (+0.06) for air, soil, and ground respectively.

Whilst the results of the correlation analysis are valuable for indicating the relationship between infiltration and temperature values, a multiple linear regression was undertaken in addition to this, to investigate the influence of each temperature variable on infiltration. A multiple linear regression is used to assess the relationship between a dependent variable (in this case infiltration) and several predictor variables (in this case, air, ground and soil temperature) (Petchko, 2018; Ciulla and D’Amico, 2019; Rath *et al.*, 2020). Table C.4 shows the *P*-values for each temperature measure in relation to infiltration.

*Table C.4. Resultant P-values from the multiple regression analysis*

	Control	ca.1900	2006	2008	2010	2012	2014	2020	Mean
10 cm P-values									
Air	0.60	0.86	0.41	0.60	0.85	0.75	0.61	0.75	0.68
Ground	0.27	0.04	0.35	0.70	0.39	0.28	0.28	0.24	0.32
Soil	0.86	0.08	0.08	0.57	0.61	0.82	0.17	0.88	0.51
200 cm P-values									
Air		0.89	0.97	0.22	0.87	0.67	0.67	0.23	0.65
Ground		0.03	0.80	0.37	0.52	0.13	0.38	0.13	0.34
Soil		0.38	0.22	0.75	0.70	0.46	0.94	0.96	0.63

In Table C.4, a *P*-value smaller than 0.05 indicates the measured temperatures do effect infiltration, whereas a *P*-value higher than 0.05 indicates no relationship between variables. the only temperature with a *P*-value lower than alpha is ground temperature at both proximities at the ca. 1900 site (10 cm =*P*- 0.04, 200 cm = *P*-0.03). This indicates that out of all measured data, ground temperature at the ca. 1900 site is the only measured temperature that shows to have an influence on infiltration at the same site. The correlation analysis (Table C.3) combined with the multiple regression analysis (Table C.4) can be used to determine that, whilst there is

a positive correlation between all measured temperatures and infiltration, there is no evidence to suggest that temperature directly influences infiltration, aside from at the *ca.* 1900 site.

### **C.3** **Modelled Climate Projections**

The following sections present the raw data used to generate the projection figures throughout section 7.3, the mean projected future peak flow for the site throughout summer and winter, and the mean percent difference from current (2020) modelled values.

#### *C.3.1 Data Tables*

This section presents the results of the HEC-HMS modelled projections for future peak flow and total discharge throughout winter, inclusive of climate change projections defined by the EA and UKCP (section 5.7.1). Peak and total flows are presented as a range of possible outputs for all land cover types (woodland, grassland, impermeable) based on the baseflow scenarios defined in section 5.7.3. The HofE peak flow is shown as ‘2020 peak discharge’ as are the intensities for 2040, 2070 and 2120 respectively. 2120 is included twice as the ‘high rainfall’ series simulates the maximum rainfall increase expected in 2120 (40% increase from present, displayed at 2120H).

The following tables (Table C.5 to Table C.10) are of use for authors/organisations aiming to evaluate the likely reduction in peak flow as a result of woodland planting over a clay-textured sample site.

Table C.5. Peak flow and total discharge change ranges for woodland (W), grassland (G) and impermeable (I) land cover, compared with 2020 values for 6-hour 50%, 10%, 2% and 1% AEP events in winter

		AEP%	2040		2070		2120		2120 H	
			m3/s	% Change						
W	Peak Flow Range	50	0.66 - 0.70	8.20 - 14.75	0.63 - 0.67	3.28 - 9.84	0.69 - 0.80	13.11 - 31.15	0.77 - 0.88	26.23 - 44.26
		10	0.89 - 0.93	5.95 - 10.71	0.87 - 0.92	3.57 - 9.52	0.96 - 1.07	14.29 - 27.38	1.08 - 1.19	28.57 - 41.67
		2	1.20 - 1.25	5.26 - 9.65	1.20 - 1.25	5.26 - 9.65	1.32 - 1.43	15.79 - 25.44	1.50 - 1.61	31.58 - 41.23
		1	1.38 - 1.42	5.34 - 8.40	1.38 - 1.43	5.34 - 9.16	1.52 - 1.63	16.03 - 24.43	1.73 - 1.84	32.06 - 40.46
	Total Discharge Range	50	674.81 - 747.43	6.89 - 18.40	676.66 - 761.38	7.19 - 20.61	742.82 - 929.55	17.67 - 47.25	774.93 - 961.67	22.75 - 52.33
		10	773.79 - 846.41	6.65 - 16.66	779.70 - 864.42	7.46 - 19.14	855.35 - 1042.08	17.89 - 43.62	906.31 - 1093.06	24.91 - 50.65
		2	907.20 - 979.82	6.41 - 14.92	919.19 - 1003.91	7.81 - 17.75	1007.64 - 1194.38	18.19 - 40.09	1084.22 - 1270.96	27.17 - 49.07
		1	981.89 - 1054.51	6.29 - 14.16	997.47 - 1082.19	7.98 - 17.15	1092.96 - 1279.71	18.32 - 38.53	1183.78 - 1370.51	28.15 - 48.36
G	Peak Flow Range	50	0.65 - 0.69	103.13 - 115.63	0.67 - 0.74	109.38 - 131.25	0.75 - 0.86	134.38 - 168.75	0.82 - 0.93	156.25 - 190.63
		10	0.88 - 0.93	60.00 - 69.09	0.92 - 0.98	67.27 - 78.18	1.01 - 1.12	83.64 - 103.64	1.14 - 1.24	107.27 - 125.45
		2	1.20 - 1.24	41.18 - 45.88	1.25 - 1.31	47.06 - 54.12	1.37 - 1.48	61.18 - 74.12	1.56 - 1.66	83.53 - 95.29
		1	1.38 - 1.42	35.29 - 39.22	1.43 - 1.50	40.20 - 47.06	1.58 - 1.68	54.90 - 64.71	1.79 - 1.90	75.49 - 86.27
	Total Discharge Range	50	672.3 - 744.91	31.86 - 46.10	685.6 - 797.99	34.47 - 56.51	765.66 - 952.40	50.17 - 86.79	798.00 - 984.73	56.51 - 93.13
		10	771.3 - 843.91	27.66 - 39.68	789.25 - 901.63	30.64 - 49.24	878.83 - 1065.56	45.46 - 76.37	929.97 - 1116.7	53.93 - 84.84
		2	904.68 - 977.30	23.72 - 33.66	929.01 - 1041.39	27.05 - 42.42	1031.27 - 1218.01	41.04 - 66.57	1107.86 - 1294.6	51.51 - 77.05
		1	979.41 - 1052.02	22.07 - 31.12	1007.29 - 1119.68	25.54 - 39.55	1116.63 - 1303.36	39.17 - 62.44	1207.44 - 1394.17	50.49 - 73.76
I	Peak Flow Range	50	0.71 - 0.75	5.97 - 11.94	0.73 - 0.79	8.96 - 17.91	0.80 - 0.91	19.40 - 35.82	0.88 - 0.99	31.34 - 47.76
		10	0.94 - 0.98	5.62 - 10.11	0.97 - 1.04	8.99 - 16.85	1.07 - 1.18	20.22 - 32.58	1.19 - 1.30	33.71 - 46.07
		2	1.25 - 1.30	5.04 - 9.24	1.30 - 1.37	9.24 - 15.13	1.43 - 1.54	20.17 - 29.41	1.61 - 1.72	35.29 - 44.54
		1	1.43 - 1.47	5.15 - 8.09	1.49 - 1.55	9.56 - 13.97	1.63 - 1.74	19.85 - 27.94	1.84 - 1.95	35.29 - 43.38
	Total Discharge Range	50	696.24 - 768.86	6.53 - 17.64	709.54 - 821.92	8.56 - 25.76	789.61 - 976.34	20.81 - 49.39	821.93 - 1008.66	25.76 - 54.33
		10	795.23 - 867.85	6.34 - 16.05	813.21 - 925.60	8.74 - 23.77	902.77 - 1089.50	20.72 - 45.68	953.92 - 1140.66	27.55 - 52.53
		2	928.65 - 1001.27	6.14 - 14.44	952.95 - 1065.33	8.92 - 21.77	1055.23 - 1241.96	20.61 - 41.95	1131.81 - 1318.55	29.36 - 50.71
		1	1003.35 - 1075.98	6.06 - 13.74	1031.23 - 1143.61	9.01 - 20.89	1140.56 - 1327.29	20.56 - 40.30	1231.38 - 1418.11	30.16 - 49.90

Table C.6. Peak flow and total discharge change ranges for woodland (W), grassland (G) and impermeable (I) land cover, compared with 2020 values for 24-hour 50%, 10%, 2% and 1% AEP events in winter

		AEP%	2040		2070		2120		2120 H	
			m3/s	% Change						
W	Peak Flow Range	50	0.86 - 0.90	6.17 - 11.11	0.83 - 0.90	2.47 - 11.11	0.93 - 0.94	14.81 - 16.05	1.04 - 1.15	28.4 - 41.98
		10	1.14 - 1.19	5.56 - 10.19	1.14 - 1.20	5.56 - 11.11	1.26 - 1.19	16.67 - 10.19	1.42 - 1.53	31.48 - 41.67
		2	1.51 - 1.55	5.59 - 8.39	1.52 - 1.58	6.29 - 10.49	1.67 - 1.49	16.78 - 4.20	1.91 - 2.02	33.57 - 41.26
		1	1.70 - 1.74	5.59 - 8.07	1.72 - 1.79	6.83 - 11.18	1.90 - 1.64	18.01 - 1.86	2.17 - 2.28	34.78 - 41.61
	Total Discharge Range	50	870.29 - 955.00	6.57 - 16.94	863.05 - 994.16	5.68 - 21.74	964.03 - 1181.86	18.05 - 44.72	1016.89 - 1234.72	24.52 - 51.19
		10	1004.83 - 1089.55	6.36 - 15.32	1003.77 - 1134.87	6.24 - 20.12	1117.68 - 1335.52	18.30 - 41.36	1196.29 - 1414.12	26.62 - 49.68
		2	1175.42 - 1260.14	6.16 - 13.81	1182.59 - 1313.69	6.81 - 18.65	1312.56 - 1530.40	18.55 - 38.22	1423.71 - 1641.54	28.58 - 48.26
		1	1267.16 - 1351.88	6.07 - 13.17	1278.58 - 1409.69	7.03 - 18.01	1417.44 - 1635.28	18.65 - 36.89	1546.03 - 1763.88	29.42 - 47.66
G	Peak Flow Range	50	0.85 - 0.90	165.63 - 181.25	0.89 - 0.95	178.13 - 196.88	0.98 - 1.09	206.25 - 240.63	1.09 - 1.20	240.63 - 275.00
		10	1.14 - 1.18	107.27 - 114.55	1.19 - 1.25	116.36 - 127.27	1.31 - 1.41	138.18 - 156.36	1.47 - 1.58	167.27 - 187.27
		2	1.50 - 1.55	76.47 - 82.35	1.57 - 1.63	84.71 - 91.76	1.72 - 1.83	102.35 - 115.29	1.96 - 2.06	130.59 - 142.35
		1	1.70 - 1.74	66.67 - 70.59	1.77 - 1.83	73.53 - 79.41	1.94 - 2.05	90.20 - 100.98	2.22 - 2.32	117.65 - 127.45
	Total Discharge Range	50	868.64 - 953.35	24.94 - 37.12	888.00 - 1019.11	27.72 - 46.58	989.06 - 1206.90	42.26 - 73.59	1042.06 - 1259.90	49.88 - 81.21
		10	1003.17 - 1087.89	21.84 - 32.13	1028.93 - 1160.04	24.97 - 40.89	1142.87 - 1360.71	38.81 - 65.26	1221.46 - 1439.29	48.35 - 74.81
		2	1173.76 - 1258.48	19.07 - 27.66	1207.73 - 1338.83	22.51 - 35.81	1337.73 - 1555.58	35.70 - 57.80	1448.87 - 1666.70	46.97 - 69.07
		1	1265.52 - 1350.23	17.92 - 25.81	1303.77 - 1434.86	21.48 - 33.70	1442.60 - 1660.45	34.42 - 54.72	1571.19 - 1789.03	46.40 - 66.70
I	Peak Flow Range	50	0.90 - 0.94	34.33 - 40.30	0.93 - 0.99	38.81 - 47.76	1.02 - 1.13	52.24 - 68.66	1.13 - 1.24	68.66 - 85.07
		10	1.18 - 1.22	32.58 - 37.08	1.23 - 1.29	38.20 - 44.94	1.35 - 1.45	51.69 - 62.92	1.51 - 1.62	69.66 - 82.02
		2	1.54 - 1.58	29.41 - 32.77	1.60 - 1.67	34.45 - 40.34	1.76 - 1.87	47.90 - 57.14	1.99 - 2.10	67.23 - 76.47
		1	1.74 - 1.78	27.94 - 30.88	1.81 - 1.87	33.09 - 37.50	1.98 - 2.09	45.59 - 53.68	2.25 - 2.36	65.44 - 73.53
	Total Discharge Range	50	892.58 - 977.30	9.30 - 19.67	911.94 - 1043.04	11.67 - 27.72	1013.02 - 1230.85	24.05 - 50.72	1066.01 - 1283.84	30.53 - 57.21
		10	1027.12 - 1111.83	6.21 - 14.97	1052.87 - 1183.97	8.87 - 22.43	1166.80 - 1384.64	20.65 - 43.18	1245.38 - 1463.21	28.78 - 51.30
		2	1197.72 - 1282.43	6.04 - 13.54	1231.67 - 1362.78	9.04 - 20.65	1361.67 - 1579.52	20.55 - 39.84	1472.81 - 1690.64	30.39 - 49.68
		1	1289.46 - 1374.17	5.96 - 12.93	1327.70 - 1458.80	9.11 - 19.88	1466.54 - 1684.39	20.52 - 38.42	1595.15 - 1812.99	31.09 - 48.99

Table C.7. Peak flow and total discharge change ranges for woodland (W), grassland (G) and impermeable (I) land cover, compared with 2020 values for 96-hour 50%, 10%, 2% and 1% AEP events in winter

		AEP%	2040		2070		2120		2120 H	
			m3/s	% Change						
W	Peak Flow Range	50	0.85 - 0.89	6.25 - 11.25	0.85 - 0.92	6.25 - 15.00	1.04 - 1.05	30.00 - 31.25	1.05 - 1.16	31.25 - 45.00
		10	1.06 - 1.11	4.95 - 9.90	1.08 - 1.15	6.93 - 13.86	1.36 - 1.30	34.65 - 28.71	1.34 - 1.45	32.67 - 43.56
		2	1.32 - 1.36	5.60 - 8.80	1.36 - 1.42	8.80 - 13.60	1.78 - 1.60	42.40 - 28.00	1.69 - 1.80	35.20 - 44.00
		1	1.45 - 1.50	5.07 - 8.70	1.50 - 1.56	8.70 - 13.04	2.00 - 1.75	44.93 - 26.81	1.87 - 1.97	35.51 - 42.75
	Total Discharge Range	50	1013.96 - 1098.68	6.42 - 15.31	1012.94 - 1144.04	6.31 - 20.07	1127.13 - 1344.97	18.30 - 41.16	1207.45 - 1425.28	26.73 - 49.59
		10	1176.65 - 1261.37	6.18 - 13.82	1184.04 - 1315.14	6.85 - 18.68	1313.52 - 1531.36	18.53 - 38.19	1424.80 - 1642.64	28.57 - 48.23
		2	1372.52 - 1457.24	6.01 - 12.55	1388.86 - 1519.96	7.27 - 17.39	1537.51 - 1755.35	18.75 - 35.58	1686.67 - 1904.51	30.27 - 47.10
		1	1472.79 - 1557.50	5.93 - 12.02	1493.97 - 1625.08	7.45 - 16.88	1652.82 - 1870.65	18.87 - 34.54	1820.43 - 2038.27	30.93 - 46.60
G	Peak Flow Range	50	0.85 - 0.89	26.87 - 32.84	0.88 - 0.94	31.34 - 40.30	0.97 - 1.08	44.78 - 61.19	1.07 - 1.18	59.70 - 76.12
		10	1.06 - 1.11	17.78 - 23.33	1.10 - 1.17	22.22 - 30.00	1.21 - 1.32	34.44 - 46.67	1.36 - 1.47	51.11 - 63.33
		2	1.32 - 1.36	13.79 - 17.24	1.37 - 1.44	18.10 - 24.14	1.51 - 1.62	30.17 - 39.66	1.70 - 1.81	46.55 - 56.03
		1	1.45 - 1.50	12.40 - 16.28	1.51 - 1.58	17.05 - 22.48	1.66 - 1.77	28.68 - 37.21	1.88 - 1.99	45.74 - 54.26
	Total Discharge Range	50	1012.31 - 1097.02	21.73 - 31.91	1038.08 - 1169.19	24.83 - 40.59	1152.28 - 1370.12	38.56 - 64.75	1232.56 - 1450.40	48.21 - 74.41
		10	1174.98 - 1259.70	19.06 - 27.65	1209.21 - 1340.31	22.53 - 35.82	1338.69 - 1556.52	35.65 - 57.72	1449.97 - 1667.81	46.93 - 69.00
		2	1370.88 - 1455.59	16.83 - 24.05	1414.04 - 1545.14	20.51 - 31.68	1562.7 - 1780.53	33.18 - 51.74	1711.83 - 1929.68	45.89 - 64.45
		1	1471.14 - 1555.86	15.93 - 22.60	1519.13 - 1650.23	19.71 - 30.04	1678.00 - 1895.84	32.23 - 49.39	1845.60 - 2063.44	45.43 - 62.60
I	Peak Flow Range	50	0.86 - 0.90	6.17 - 11.11	0.89 - 0.95	9.88 - 17.28	0.98 - 1.09	20.99 - 34.57	1.08 - 1.19	33.33 - 46.91
		10	1.07 - 1.12	4.90 - 9.80	1.11 - 1.18	8.82 - 15.69	1.22 - 1.33	19.61 - 30.39	1.37 - 1.48	34.31 - 45.10
		2	1.33 - 1.37	5.56 - 8.73	1.38 - 1.45	9.52 - 15.08	1.52 - 1.62	20.63 - 28.57	1.71 - 1.82	35.71 - 44.44
		1	1.46 - 1.51	5.04 - 8.63	1.52 - 1.59	9.35 - 14.39	1.67 - 1.78	20.14 - 28.06	1.89 - 2.00	35.97 - 43.88
	Total Discharge Range	50	1036.24 - 1120.94	6.28 - 14.96	1062.00 - 1193.10	8.92 - 22.36	1176.21 - 1394.05	20.63 - 42.97	1256.55 - 1474.39	28.87 - 51.21
		10	1198.96 - 1283.67	6.06 - 13.55	1233.12 - 1364.22	9.08 - 20.68	1362.62 - 1580.46	20.54 - 39.81	1473.91 - 1691.74	30.38 - 49.65
		2	1394.79 - 1479.51	5.90 - 12.34	1437.97 - 1569.08	9.18 - 19.14	1586.63 - 1804.46	20.47 - 37.01	1735.77 - 1953.61	31.79 - 48.33
		1	1495.08 - 1579.79	5.83 - 11.83	1543.07 - 1674.17	9.23 - 18.51	1701.92 - 1919.76	20.48 - 35.90	1869.56 - 2087.40	32.34 - 47.76

Table C.8. Peak flow and total discharge change ranges for woodland (W), grassland (G) and impermeable (I) land cover, compared with 2020 values for 6-hour 50%, 10%, 2% and 1% AEP events in summer

		AEP%	2040		2070		2120		2120 H	
			m3/s	% Change	m3/s	% Change	m3/s	% Change	m3/s	% Change
W	Peak Flow Range	50	0.62 - 0.65	12.73 - 18.18	0.43 - 0.49	-21.82 - -10.91	0.51 - 0.60	-7.27 - 9.09	0.60 - 0.69	9.09 - 25.45
		10	1.14 - 1.17	8.57 - 11.43	0.76 - 0.81	-27.62 - -22.86	0.89 - 0.98	-15.24 - -6.67	1.11 - 1.20	5.71 - 14.29
		2	1.83 - 1.87	6.40 - 8.72	1.38 - 1.43	-19.77 - -16.86	1.59 - 1.68	-7.56 - -2.33	1.96 - 2.05	13.95 - 19.19
		1	2.22 - 2.26	6.22 - 8.13	1.75 - 1.81	-16.27 - -13.40	2.00 - 2.09	-4.31 - 0.00	2.45 - 2.55	17.22 - 22.01
	Total Discharge Range	50	495.59 - 557.83	8.16 - 21.74	472.75 - 567.84	3.18 - 23.93	532.84 - 690.18	16.29 - 50.63	546.41 - 703.74	19.25 - 53.59
		10	571.97 - 634.22	7.72 - 19.44	520.55 - 615.64	-1.97 - 15.94	589.23 - 746.57	10.97 - 40.60	622.11 - 779.45	17.16 - 46.79
		2	674.97 - 737.22	7.30 - 17.19	612.50 - 707.59	-2.63 - 12.48	693.24 - 850.58	10.20 - 35.21	747.48 - 904.82	18.82 - 43.83
		1	732.59 - 794.83	7.11 - 16.21	667.96 - 763.06	-2.34 - 11.56	753.76 - 911.11	10.20 - 33.21	820.56 - 977.90	19.97 - 42.97
G	Peak Flow Range	50	0.55 - 0.58	12.24 - 18.37	0.59 - 0.65	20.41 - 32.65	0.71 - 0.80	44.90 - 63.27	0.88 - 0.97	79.59 - 97.96
		10	1.07 - 1.11	8.08 - 12.12	1.14 - 1.20	15.15 - 21.21	1.31 - 1.40	32.32 - 41.41	1.57 - 1.67	58.59 - 68.69
		2	1.77 - 1.81	7.27 - 9.70	1.87 - 1.93	13.33 - 16.97	2.10 - 2.19	27.27 - 32.73	2.50 - 2.59	51.52 - 56.97
		1	2.16 - 2.20	6.93 - 8.91	2.28 - 2.33	12.87 - 15.35	2.55 - 2.64	26.24 - 30.69	3.02 - 3.11	49.50 - 53.96
	Total Discharge Range	50	485.85 - 548.09	8.34 - 22.22	495.47 - 590.56	10.48 - 31.69	561.64 - 718.98	25.24 - 60.32	586.54 - 743.88	30.79 - 65.87
		10	562.24 - 624.48	7.86 - 19.80	575.53 - 670.63	10.41 - 28.66	648.92 - 806.26	24.49 - 54.68	688.43 - 845.77	32.07 - 62.26
		2	665.23 - 727.48	7.41 - 17.46	683.45 - 778.54	10.35 - 25.71	766.63 - 923.97	23.78 - 49.19	825.74 - 983.08	33.33 - 58.73
		1	722.83 - 785.08	7.21 - 16.44	743.88 - 838.98	10.33 - 24.43	832.49 - 989.83	23.47 - 46.80	902.59 - 1059.92	33.87 - 57.20
I	Peak Flow Range	50	1.13 - 1.16	5.61 - 8.41	1.17 - 1.22	9.35 - 14.02	1.28 - 1.37	19.63 - 28.04	1.45 - 1.54	35.51 - 43.93
		10	1.63 - 1.67	5.16 - 7.74	1.70 - 1.75	9.68 - 12.90	1.86 - 1.95	20.00 - 25.81	2.12 - 2.21	36.77 - 42.58
		2	2.31 - 2.35	5.00 - 6.82	2.41 - 2.47	9.55 - 12.27	2.64 - 2.73	20.00 - 24.09	3.03 - 3.12	37.73 - 41.82
		1	2.70 - 2.73	5.47 - 6.64	2.81 - 2.87	9.77 - 12.11	3.08 - 3.17	20.31 - 23.83	3.54 - 3.63	38.28 - 41.80
	Total Discharge Range	50	574.46 - 636.70	6.96 - 18.55	584.06 - 679.15	8.75 - 26.45	650.22 - 807.56	21.07 - 50.36	675.11 - 832.45	25.70 - 55.00
		10	650.8 - 713.04	6.72 - 16.93	664.10 - 759.19	8.90 - 24.50	737.46 - 894.81	20.93 - 46.74	776.94 - 934.28	27.41 - 53.21
		2	753.75 - 815.99	6.49 - 15.28	771.96 - 867.06	9.06 - 22.49	855.13 - 1012.47	20.81 - 43.04	914.22 - 1071.55	29.16 - 51.38
		1	811.33 - 873.58	6.37 - 14.53	832.37 - 927.46	9.13 - 21.59	920.98 - 1078.31	20.74 - 41.37	991.04 - 1148.39	29.93 - 50.56

Table C.9. Peak flow and total discharge change ranges for woodland (W), grassland (G) and impermeable (I) land cover, compared with 2020 values for 24-hour 50%, 10%, 2% and 1% AEP events in summer

		AEP%	2040		2070		2120		2120 H	
			m3/s	% Change	m3/s	% Change	m3/s	% Change	m3/s	% Change
W	Peak Flow Range	50	0.93 - 0.97	8.14 - 12.79	0.63 - 0.69	-26.74 - -19.77	0.74 - 0.83	-13.95 - -3.49	0.91 - 1.00	5.81 - 16.28
		10	1.42 - 1.46	5.97 - 8.96	1.08 - 1.14	-19.4 - -14.93	1.25 - 1.34	-6.72 - 0.00	1.52 - 1.61	13.43 - 20.15
		2	2.04 - 2.07	6.25 - 7.81	1.70 - 1.76	-11.46 - -8.33	1.93 - 2.02	0.52 - 5.21	2.32 - 2.41	20.83 - 25.52
		1	2.36 - 2.40	5.83 - 7.62	2.04 - 2.09	-8.52 - -6.28	2.3 - 2.39	3.14 - 7.17	2.76 - 2.85	23.77 - 27.80
	Total Discharge Range	50	652.34 - 724.95	7.67 - 19.65	599.41 - 710.33	-1.07 - 17.24	678.53 - 862.08	11.99 - 42.28	712.78 - 896.32	17.64 - 47.93
		10	755.42 - 828.03	7.29 - 17.61	692.97 - 803.90	-1.58 - 14.18	783.25 - 966.80	11.25 - 37.32	838.66 - 1022.20	19.12 - 45.18
		2	885.98 - 958.59	6.95 - 15.72	820.31 - 931.24	-0.98 - 12.42	923.54 - 1107.09	11.49 - 33.64	1007.08 - 1190.63	21.57 - 43.73
		1	956.25 - 1028.86	6.81 - 14.92	891 - 1001.93	-0.48 - 11.91	1002.32 - 1185.87	11.95 - 32.45	1099.82 - 1283.37	22.84 - 43.34
G	Peak Flow Range	50	0.89 - 0.92	8.54 - 12.2	0.94 - 0.99	14.63 - 20.73	1.07 - 1.16	30.49 - 41.46	1.26 - 1.36	53.66 - 65.85
		10	1.39 - 1.42	6.92 - 9.23	1.46 - 1.51	12.31 - 16.15	1.63 - 1.72	25.38 - 32.31	1.92 - 2.01	47.69 - 54.62
		2	2.00 - 2.04	6.38 - 8.51	2.10 - 2.16	11.70 - 14.89	2.33 - 2.42	23.94 - 28.72	2.72 - 2.81	44.68 - 49.47
		1	2.33 - 2.36	6.39 - 7.76	2.44 - 2.50	11.42 - 14.16	2.70 - 2.79	23.29 - 27.40	3.15 - 3.24	43.84 - 47.95
	Total Discharge Range	50	642.61 - 715.22	7.79 - 19.97	656.68 - 767.62	10.15 - 28.76	739.70 - 923.25	24.08 - 54.87	780.30 - 963.85	30.89 - 61.68
		10	745.69 - 818.30	7.40 - 17.86	764.60 - 875.54	10.12 - 26.10	857.42 - 1040.97	23.49 - 49.93	917.60 - 1101.14	32.16 - 58.59
		2	876.25 - 948.85	7.03 - 15.90	901.44 - 1012.38	10.11 - 23.66	1006.70 - 1190.25	22.97 - 45.39	1091.75 - 1275.31	33.36 - 55.78
		1	946.5 - 1019.12	6.88 - 15.08	975.03 - 1085.97	10.10 - 22.63	1086.92 - 1270.49	22.74 - 43.47	1185.43 - 1368.98	33.86 - 54.59
I	Peak Flow Range	50	1.21 - 1.25	5.22 - 8.70	1.26 - 1.31	9.57 - 13.91	1.38 - 1.47	20.00 - 27.83	1.56 - 1.65	35.65 - 43.48
		10	1.67 - 1.71	5.03 - 7.55	1.74 - 1.80	9.43 - 13.21	1.91 - 2.00	20.13 - 25.79	2.18 - 2.27	37.11 - 42.77
		2	2.26 - 2.29	5.61 - 7.01	2.35 - 2.41	9.81 - 12.62	2.57 - 2.67	20.09 - 24.77	2.95 - 3.05	37.85 - 42.52
		1	2.57 - 2.61	5.33 - 6.97	2.68 - 2.74	9.84 - 12.30	2.93 - 3.02	20.08 - 23.77	3.37 - 3.46	38.11 - 41.80
	Total Discharge Range	50	730.31 - 802.92	6.79 - 17.41	744.35 - 855.28	8.85 - 25.07	827.35 - 1010.89	20.98 - 47.82	867.93 - 1051.48	26.92 - 53.76
		10	833.28 - 905.89	6.57 - 15.85	852.20 - 963.14	8.99 - 23.17	945.01 - 1128.57	20.85 - 44.33	1005.16 - 1188.70	28.55 - 52.02
		2	963.77 - 1036.38	6.35 - 14.37	988.96 - 1099.90	9.13 - 21.37	1094.22 - 1277.78	20.75 - 41.00	1179.25 - 1362.80	30.13 - 50.39
		1	1034.02 - 1106.63	6.26 - 13.72	1062.53 - 1173.46	9.19 - 20.59	1174.44 - 1357.98	20.69 - 39.55	1272.90 - 1456.45	30.81 - 49.67

Table C.10. Peak flow and total discharge change ranges for woodland (W), grassland (G) and impermeable (I) land cover, compared with 2020 values for 96-hour 50%, 10%, 2% and 1% AEP events in summer

		AEP%	2040		2070		2120		2120 H	
			m3/s	% Change	m3/s	% Change	m3/s	% Change	m3/s	% Change
W	Peak Flow Range	50	0.83 - 0.87	6.41 - 11.54	0.65 - 0.70	-16.67 - -10.26	0.74 - 0.83	-5.13 - 6.41	0.88 - 0.97	12.82 - 24.36
		10	1.08 - 1.12	5.88 - 9.80	0.93 - 0.98	-8.82 - -3.92	1.06 - 1.15	3.92 - 12.75	1.23 - 1.32	20.59 - 29.41
		2	1.37 - 1.41	5.38 - 8.46	1.26 - 1.31	-3.08 - 0.77	1.41 - 1.50	8.46 - 15.38	1.65 - 1.74	26.92 - 33.85
		1	1.52 - 1.56	5.56 - 8.33	1.43 - 1.48	-0.69 - 2.78	1.59 - 1.68	10.42 - 16.67	1.86 - 1.95	29.17 - 35.42
	Total Discharge Range	50	762.74 - 557.83	7.3 - -21.53	699.44 - 567.84	-1.61 - -20.12	790.37 - 690.18	11.19 - -2.91	847.98 - 703.74	19.29 - -1.00
		10	887.13 - 634.22	6.87 - -23.60	821.25 - 615.64	-1.07 - -25.84	925.22 - 746.57	11.46 - -10.06	1009.16 - 779.45	21.57 - -6.10
		2	1037.43 - 737.22	6.59 - -24.25	975.49 - 707.59	0.23 - -27.30	1094.52 - 850.58	12.46 - -12.61	1207.74 - 904.82	24.09 - -7.03
		1	1114.53 - 794.83	6.55 - -24.02	1054.99 - 763.06	0.86 - -27.05	1181.86 - 911.11	12.98 - -12.90	1309.23 - 977.90	25.16 - -6.51
G	Peak Flow Range	50	0.82 - 0.85	6.49 - 10.39	0.85 - 0.91	10.39 - 18.18	0.95 - 1.04	23.38 - 35.06	1.07 - 1.17	38.96 - 51.95
		10	1.08 - 1.10	6.93 - 8.91	1.12 - 1.17	10.89 - 15.84	1.24 - 1.33	22.77 - 31.68	1.40 - 1.49	38.61 - 47.52
		2	1.37 - 1.40	5.38 - 7.69	1.43 - 1.48	10.00 - 13.85	1.57 - 1.66	20.77 - 27.69	1.79 - 1.88	37.69 - 44.62
		1	1.52 - 1.55	5.56 - 7.64	1.58 - 1.64	9.72 - 13.89	1.74 - 1.83	20.83 - 27.08	1.98 - 2.08	37.50 - 44.44
	Total Discharge Range	50	753.01 - 548.09	7.40 - -21.83	771.92 - 590.56	10.10 - -15.77	865.46 - 718.98	23.44 - 2.55	927.58 - 743.88	32.3 - 6.10
		10	877.39 - 624.48	6.95 - -23.88	902.63 - 670.63	10.03 - -18.25	1008.69 - 806.26	22.96 - -1.72	1093.92 - 845.77	33.35 - 3.10
		2	1027.67 - 727.48	6.66 - -24.50	1060.61 - 778.54	10.08 - -19.20	1180.14 - 923.97	22.48 - -4.11	1294.18 - 983.08	34.32 - 2.03
		1	1104.80 - 785.08	6.61 - -24.24	1140.79 - 838.98	10.08 - -19.04	1268.12 - 989.83	22.37 - -4.48	1396.46 - 1059.92	34.75 - 2.28
I	Peak Flow Range	50	0.87 - 0.90	12.99 - 16.88	0.90 - 0.95	16.88 - 23.38	0.99 - 1.08	28.57 - 40.26	1.11 - 1.20	44.16 - 55.84
		10	1.11 - 1.14	9.90 - 12.87	1.15 - 1.20	13.86 - 18.81	1.26 - 1.35	24.75 - 33.66	1.42 - 1.51	40.59 - 49.50
		2	1.39 - 1.42	6.92 - 9.23	1.44 - 1.50	10.77 - 15.38	1.58 - 1.67	21.54 - 28.46	1.80 - 1.89	38.46 - 45.38
		1	1.53 - 1.57	6.25 - 9.03	1.60 - 1.65	11.11 - 14.58	1.75 - 1.84	21.53 - 27.78	1.99 - 2.08	38.19 - 44.44
	Total Discharge Range	50	574.46 - 636.70	-27.11 - -19.21	584.06 - 679.15	-25.89 - -13.82	650.22 - 807.56	-17.49 - 2.47	675.11 - 832.45	-14.34 - 5.63
		10	650.80 - 713.04	-28.27 - -21.42	664.10 - 759.19	-26.81 - -16.33	737.46 - 894.81	-18.72 - -1.38	776.94 - 934.28	-14.37 - 2.97
		2	753.75 - 815.99	-28.25 - -22.32	771.96 - 867.06	-26.52 - -17.46	855.13 - 1012.47	-18.60 - -3.62	914.22 - 1071.55	-12.97 - 2.00
		1	811.33 - 873.58	-27.77 - -22.23	832.37 - 927.46	-25.90 - -17.43	920.98 - 1078.31	-18.01 - -4.00	991.04 - 1148.39	-11.77 - 2.24

C.3.2 Percent difference between projected peak flow and total discharge

Table C.11 to Table C.14 present the mean projected peak flow and total discharge for winter and summer storms, in addition to the mean percent change from current (2020) modelled values.

*Table C.11. Winter peak flow and percent difference compared with 2020. W=woodland, G=grassland, I=impermeable land cover*

Duration		2020			2040		2070		2120		2120 H	
		m3/s	m3/s	± %								
6	W	0.97	1.05	8.22	1.04	7.19	1.18	20.81	1.32	36.04		
	G	0.68	1.05	7.65	1.10	12.95	1.23	26.53	1.38	41.74		
	I	1.02	1.10	13.28	1.15	18.62	1.29	32.19	1.43	47.39		
24	W	1.23	1.32	35.86	1.33	37.12	1.49	53.25	1.69	73.62		
	G	0.99	1.32	35.58	1.38	42.15	1.54	58.26	1.74	78.53		
	I	1.26	1.36	39.66	1.42	46.21	1.58	62.29	1.78	82.51		
96	W	1.11	1.19	7.48	1.23	10.74	1.37	23.63	1.54	38.81		
	G	1.00	1.19	7.43	1.25	12.52	1.39	25.29	1.56	40.34		
	I	1.12	1.20	8.31	1.26	13.40	1.40	26.13	1.57	41.17		

*Table C.12. Winter total discharge and percent difference compared with 2020.*

*W=woodland, G=grassland, I=impermeable land cover*

Duration		2020			2040		2070		2120		2120 H	
		m3/s	m3/s	± %								
6	W	783.30	870.73	11.16	885.62	13.06	1018.06	29.97	1080.68	37.97		
	G	661.90	868.23	31.17	908.98	37.33	1041.46	57.35	1104.18	66.82		
	I	805.59	892.18	10.75	932.92	15.81	1065.41	32.25	1128.13	40.04		
24	W	1015.81	1121.78	10.43	1147.55	12.97	1311.85	29.14	1404.65	38.28		
	G	894.41	1120.13	25.24	1172.66	31.11	1336.99	49.48	1429.81	59.86		
	I	1032.53	1144.08	10.80	1196.59	15.89	1360.93	31.81	1453.76	40.80		
96	W	1186.53	1301.34	9.68	1335.50	12.56	1516.66	27.82	1643.76	38.54		
	G	1065.23	1299.69	22.01	1360.67	27.73	1541.83	44.74	1668.91	56.67		
	I	1208.81	1323.62	9.50	1384.59	14.54	1565.76	29.53	1692.87	40.04		

Table C.13. Summer peak flow and percent difference compared with 2020. W=woodland, G=grassland, I=impermeable land cover

Duration		2020		2040		2070		2120		2120 H	
		m3/s	m3/s	± %	m3/s	± %	m3/s	± %	m3/s	± %	
6	W	1.35	1.47	8.69	1.11	-18.13	1.29	-4.36	1.58	16.58	
	G	1.29	1.41	9.17	1.50	16.43	1.71	32.98	2.04	58.35	
	I	1.84	1.96	6.29	2.05	11.25	2.26	22.61	2.58	40.01	
24	W	1.59	1.71	7.52	1.39	-12.30	1.60	0.79	1.92	21.20	
	G	1.55	1.67	7.72	1.76	13.85	1.98	27.81	2.31	49.17	
	I	1.83	1.94	6.31	2.04	11.28	2.24	22.69	2.56	40.05	
96	W	1.14	1.22	7.37	1.09	-3.90	1.25	9.73	1.45	27.78	
	G	1.13	1.21	7.13	1.27	12.73	1.42	25.58	1.61	42.32	
	I	1.16	1.24	7.05	1.30	12.01	1.44	24.21	1.62	40.10	

Table C.14. Summer total discharge and percent difference compared with 2020. W=woodland, G=grassland, I=impermeable land cover

Duration		2020		2040		2070		2120		2120 H	
		m3/s	m3/s	± %							
6	W	575.56	649.90	12.92	615.99	7.02	720.94	25.26	762.81	32.53	
	G	565.82	640.16	13.14	672.13	18.79	781.09	38.05	829.49	46.60	
	I	654.37	728.71	11.36	760.67	16.25	869.62	32.89	918.00	40.29	
24	W	758.42	848.80	11.92	806.39	6.32	938.69	23.77	1006.36	32.69	
	G	748.67	839.07	12.07	879.91	17.53	1014.47	35.50	1085.54	45.00	
	I	836.27	926.65	10.81	967.48	15.69	1102.03	31.78	1173.08	40.28	
96	W	890.06	986.76	10.86	936.20	5.18	1089.77	22.44	1185.30	33.17	
	G	880.32	969.96	10.18	1024.45	16.37	1172.37	33.18	1269.81	44.24	
	I	967.31	1064.00	10.00	1111.43	14.90	1259.36	30.19	1356.79	40.26	

## **Appendix D. Extracurricular Academic Engagement**

This section details all academic and extracurricular engagement undertaken throughout the course of the study duration.

### **D.1 HofE and EA Feedback Presentation**

Upon partial completion of the project (i.e., all infiltration, modelled and projected results had been produced and analysed), a feedback presentation was held with Roy Stokes (project manager in the EA's Midlands region), Stephen Coffey (head forester for the HofE forest charity), and Sophie Leszczynska (biodiversity manager for the HofE forest charity). The aim of this presentation was primarily to explain the motivations for the project, the methods employed, the determined results, the applications and reliability of findings, and the opportunities for future work across the HofE site and the Midlands in general. The presentation also acted as a productive environment to receive any feedback on the project and develop ideas that could be discussed throughout Chapter 8 to broaden the applicability and current relevance of study findings.

Overall feedback was highly positive. The HofE forest were happy that a side-effect of their motivations for woodland planting was an increase in infiltration (section 7.1). The EA were interested in continuing the development of the modelled projections to infiltration, peak flow, and total discharge – with primary interest revolving around the potential to make this data a saleable product. They were keen on learning about the methods used in infiltration data projection, future peak flow, and total discharge calculations, and think this is a valuable area of future research in the field of woodland planting and NFM. The HofE forest were happy with the research undertaken and pleased that they had contributed towards the publication of the peer reviewed paper (section D.2) and are keen to initiate future projects at the study site.

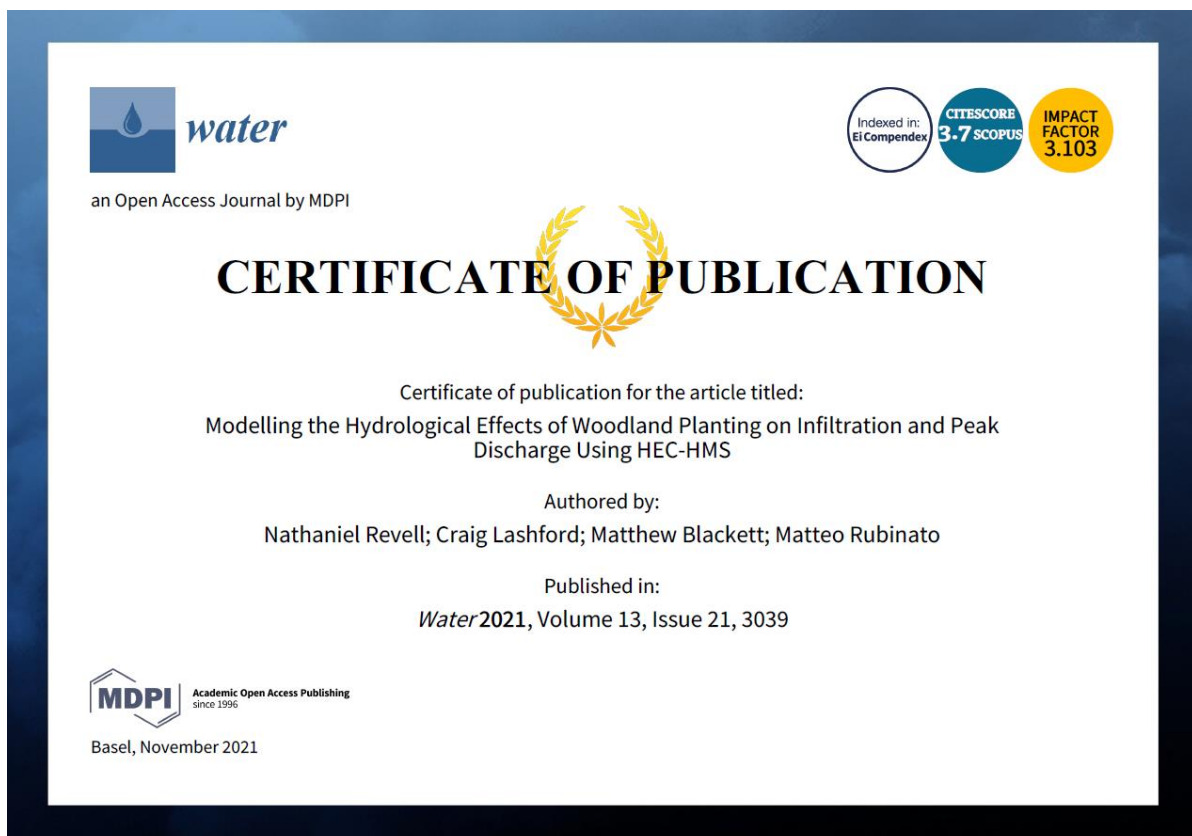
No fundamental floors, nor areas for large-scale modification/improvement were identified as a result of the presentation. However, discussions with the attendees did influence some of the discussion points outlined throughout section Chapter 8. Both the HofE forest and the EA emphasised the numerous benefits of woodland planting aside from the predominantly hydrological ones discussed throughout this study (carbon sequestration, biodiversity, public amenity, mental health, and fitness). This led to sections of this nature to be added to the discussion, placing more emphasis on the wider-scale impacts of woodland planting, and how there is a governmental shift towards woodland planting for the benefit of carbon sequestration, however this is also advantageous for flood risk, even if not specified by the policies themselves.

## **D.2 Peer Reviewed Publications**

This section presents the peer-reviewed publications, produced as a direct output of this work.

### **D.2.1 Modelling the Hydrological Effects of Woodland Planting on Infiltration and Peak Discharge Using HEC-HMS**

First author of the below article, published in the Water MDPI special issue ‘forms, functions and values of treescapes (natural and urban)’. The paper presents the methods and results of the hydrological modelling undertaken in partial fulfilment of this study, presented in sections 5.3 and 7.2 of this thesis.



The publication is inserted below.

# Modelling the Hydrological Effects of Woodland Planting on Infiltration and Peak Discharge Using HEC-HMS

Nathaniel Revell <sup>1,\*</sup>, Craig Lashford <sup>1,2</sup>, Matthew Blackett <sup>1,2</sup> and Matteo Rubinato <sup>1,2,3</sup>

<sup>1</sup> Centre for Agroecology, Water and Resilience, Coventry University, Wolston Lane, Coventry CV8 3LG, UK; ab0874@coventry.ac.uk (C.L.); aa8533@coventry.ac.uk (M.B.); ad2323@coventry.ac.uk (M.R.)

<sup>2</sup> Faculty of Engineering, Environment & Computing, School of Energy, Construction and Environment, Coventry University, Coventry CV1 5FB, UK

<sup>3</sup> IKT-Institute for Underground Infrastructure, Exterbruch 1, 45886 Gelsenkirchen, Germany

\* Correspondence: revelln@uni.coventry.ac.uk

**Abstract:** Woodland planting is gaining momentum as a potential method of natural flood management (NFM), due to its ability to break up soil and increase infiltration and water storage. In this study, a 2.2 km<sup>2</sup> area in Warwickshire, England, planted with woodland every year from 2006 to 2012, was sampled using a Mini Disk infiltrometer (MDI). Infiltration measurements were taken from 10 and 200 cm away from the trees, from November 2019 to August 2021. Two individual hydrological models were built using the US Hydraulic Engineering Center Hydrological Modelling System (HEC-HMS), to model the effects of infiltration change on peak flows from the site throughout the summer and winter. The models were calibrated and validated using empirical data; the Nash and Sutcliffe Efficiency (NSE) was used as an indicator of accuracy. Results from this study show that woodland planting reduced peak flow intensity compared to impermeable land cover by an average of 6%, 2%, and 1% for 6-h, 24-h, and 96-h winter storms, respectively, and 48%, 18%, and 3% for 6-h, 24-h, and 96-h summer storms, respectively. However, grassland simulations show the greatest reduction in peak flows, being 32%, 21%, and 10%, lower than woodland for 6-, 24-, and 96-h winter storms, respectively, and 6%, 3%, and 0.5% lower than woodland for 6-, 24-, and 96-h summer storms, respectively.

**Keywords:** infiltration; natural flood management; HEC-HMS; hydrological modelling; Nash and Sutcliffe efficiency; calibration; validation

**Citation:** Revell, N.; Lashford, C.; Blackett, M.; Rubinato, M. Modelling the Hydrological Effects of Woodland Planting on Infiltration and Peak Discharge Using HEC-HMS. *Water* **2021**, *13*, x. <https://doi.org/10.3390/w13213039>

**Publisher's Note:** MDPI stays neutral with regard to jurisdictional claims in published maps and institutional affiliations.



**Copyright:** © 2021 by the authors. Submitted for possible open access publication under the terms and conditions of the Creative Commons Attribution (CC BY) license (<http://creativecommons.org/licenses/by/4.0/>).

## 1. Introduction

Urbanisation and the replacement of permeable and vegetated surfaces to impermeable surfaces, such as asphalt and concrete, reduces lag times and increases peak flows in receiving watercourses, influencing the likelihood and severity of high-flow or flooding events across the UK (Ferguson and Fenner, 2020a; Ellis *et al.*, 2021). Coupled with this, the global climate is predicted to change in ways unseen in recorded history (Lowe *et al.*, 2019). In the UK, sea levels are expected to rise, the frequency of extreme weather events will increase, summers will become hotter and drier, and winters will become warmer and wetter (Lowe *et al.*, 2019; Murphy *et al.*, 2021). Consequently, authorities responsible for managing flood risk in the UK have increased investment in alternative, more sustainable methods of mitigating flooding, such as natural flood management (NFM) techniques (Metcalf *et al.*, 2018; Shuttleworth *et al.*, 2019; Ferguson and Fenner, 2020a).

The design and operation of any NFM feature is based primarily on emulating the natural hydrology of a catchment as it was prior to human interaction, with the intention of reducing fluvial flood risk (Forbes *et al.*, 2016; Ellis *et al.*, 2021). Common NFM methods can be categorised into those that (a) reduce hydrological or hydraulic connectivity; (b) create storage; or (c) increase infiltration (Ferguson and Fenner, 2020b). Examples of these methods include vegetation planting to increase infiltration and interception, changing animal grazing and farming routines to reduce compaction and increase lag time, and reconnecting or introducing offline marshlands and mudflat areas, to slow the flow of flooding water during a storm event (Forbes *et al.*, 2016; Dadson *et al.*, 2017; Ngai *et al.*, 2017; Burgess-Gamble *et al.*, 2018).

Whilst continuous academic investigations into the real-world applicability of NFM methods are ongoing, NFM implementation is slow, primarily due to the lack of long-term

evidence-based studies (Wells *et al.*, 2020; Ellis *et al.*, 2021). One method of NFM that is assumed valuable, although under-investigated, is woodland planting (Lacob *et al.*, 2014; Dittrich *et al.*, 2019; Murphy *et al.*, 2021). Tree roots break up the surrounding soil, increasing infiltration rate and water storage capacity, whilst simultaneously offering a higher opportunity for interception and evapotranspiration (Chandler *et al.*, 2018; Zhang *et al.*, 2019a). The value of woodland planting has been identified by the UK government, who have allocated GBP 4 million to various organizations to increase woodland planting for flood risk reduction, and the Environment Agency (England), who have been awarded GBP 1.4 million for the same purpose (GOV.UK, 2020). However, whilst some studies have attempted to investigate the link between woodland planting and soil infiltration characteristics (Chandler *et al.*, 2018; Murphy, 2021; Murphy *et al.*, 2021), evidence-based studies focusing solely on the impacts of changing infiltration as a result of woodland planting are sparse, posing a challenge to researchers in this discipline.

In light of the changing climate, and the predicted increases to flood frequency and severity, the policy shift towards NFM methods, and the lack of evidence-based studies investigating the feasibility of woodland planting as a method of NFM, this study aims to determine the extent to which woodland planting has influenced infiltration at a site in central England (Lowe *et al.*, 2019; Ferguson and Fenner, 2020a; Ellis *et al.*, 2021; Murphy *et al.*, 2021). Two hydrological models were built using HEC-HMS, calibrated and validated using the NSE method, and simulations were undertaken to predict the ability of woodland to increase infiltration and reduce peak runoff to the receiving watercourse.

## **2. Materials and Methods**

### *2.1. Infiltration Data Collection*

Infiltration data were collected once every two weeks from specific areas of a 2.2 km<sup>2</sup> site in Warwickshire, UK (52.1511° N, 1.5139° W). The HofE charity began planting woodland in 2006, continuing every year until 2012. Infiltration data were collected from the woodland in plots planted in 2006 (*Betula Pendula*), 2008 (*Populus Tremula*), 2010 (*Betula Pendula*), and 2012 (*Populus Tremula*). Additionally, infiltration data were collected from a plot planted in *ca.*1900 (*Quercus Petraea*), and a control site consisting of a grassland area that pre-exists the HofE forest. The grassland area was sampled for comparison with the woodland areas, and the *ca.*1900 area was sampled to provide information on the infiltration characteristics of mature woodland, and for comparison to more recently planted areas. Figure 1 shows the locations of the infiltration sample plots and sampling locations.

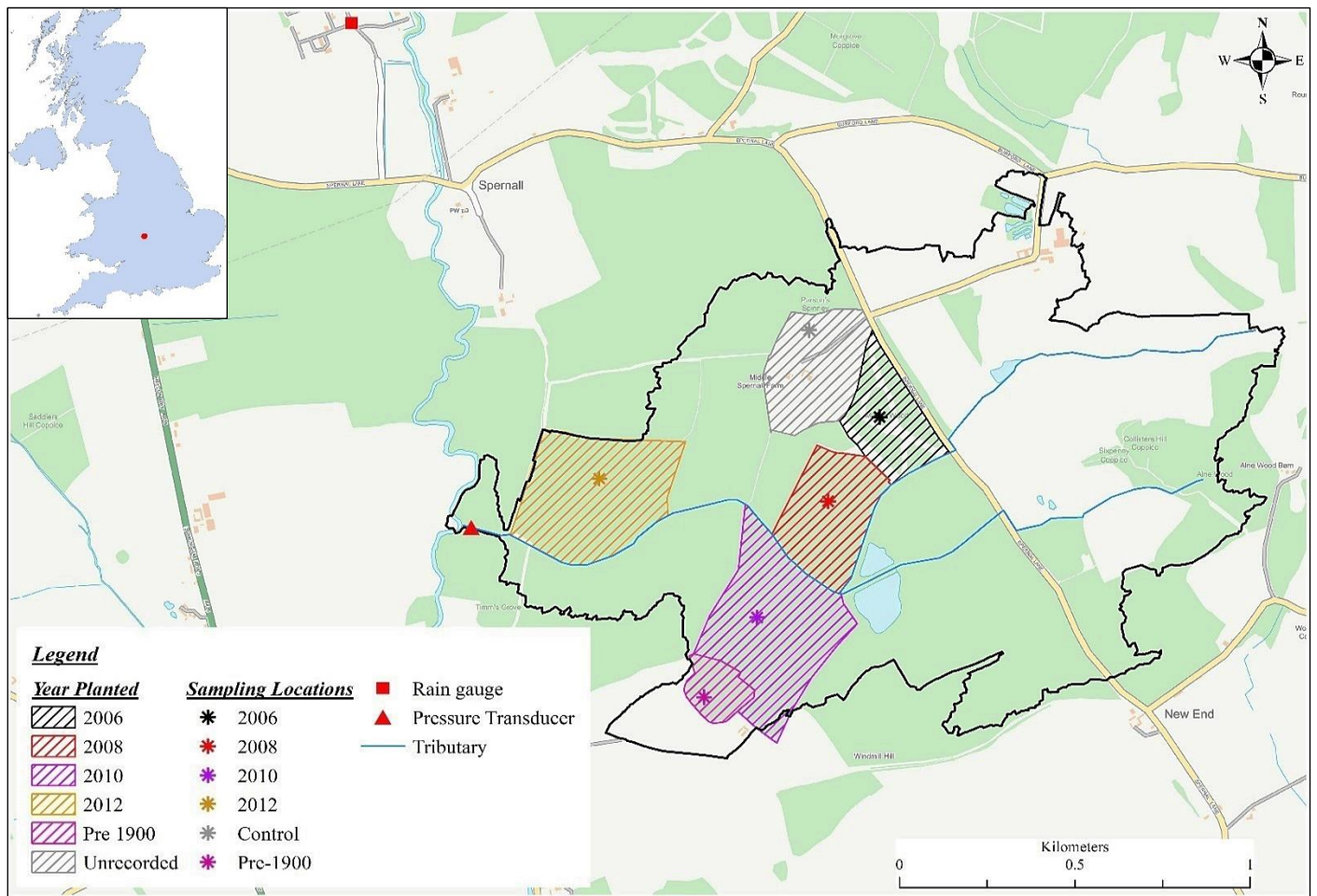


**Figure 1.** Sample sites, sampling locations, rain gauge, and telemetry locations (Ordnance Survey, 2021). Data is reproduced under the open government license.

Infiltration rates are influenced by soil texture (Rahman *et al.*, 2019; Bátková *et al.*, 2020; Ren *et al.*, 2020). Therefore, soil samples were extracted from the surface (~5 cm depth) of the soil surrounding the area of MDI measurement using a trowel. The soil texture of these samples was then determined using a LaMotte soil texture testing kit (LaMotte, 2020). The percentiles of sand, silt, and clay for each soil were compared against the UK soil texture triangle to determine the classification name of the sample soils. The percentiles and soil texture classifications of the sample area are shown in Table 1.

**Table 1.** Soil percentiles and texture classification of each sample site.

Sample Site	Sand %	Silt %	Clay %	UK Soil Classification	
Control	53	20	27	SaCL	Sandy clay loam
Pre-1900	47	40	13	SSL	Sandy silt loam
2006	20	20	60	C	Clay
2008	13	20	67	C	Clay
2010	53	33	14	SaL	Sandy loam
2012	33	13	54	C	Clay

Infiltration measurements were collected (10 and 200 cm away from the base of the sample trees) using a Mini Disk infiltrometer (MDI) (METER® Group Inc., 2020). The 10 cm proximity was chosen to represent the influence of the tree on infiltration directly adjacent to the trunk, and the 200 cm proximity was chosen to account for potential root spread due to tree growth (Perry, 1982; Mauer and Palátová, 2003; Hepner *et al.*, 2020). As the MDI required a watertight seal with the sample soil, vegetation was removed from the surface of the soil before infiltration measurement proceeded. See Figure 2a,b.



**Figure 2.** (a) MDI performing measurement at the study site; (b) 10 and 200 cm proximity MDI sample replication points outlined in orange.

Collecting infiltration data from two proximities allowed for the comparison and representation of both proximities in hydrological modelling. Infiltration measurements were carried out until three consecutive volumes were recorded (~10 min) and replicated three times at both proximities around the sample tree (Bagarello and Sgroi, 2004; Chandler *et al.*, 2018).

It is acknowledged that, in addition to infiltration, woodland can influence hydrology through interception and evapotranspiration, which is also accounted for in this study (and discussed in Section 2.5.3) (Forbes *et al.*, 2016; Dadson *et al.*, 2017; Burgess-Gamble *et al.*, 2018). These additional factors are important for justifying the use of woodland as a method of NFM, and are accounted for throughout the modelling and results of this study (this is discussed further in Section 2.5.3). A total of 1617 individual infiltration measurements were collected from October 2019 to August 2021; 888 from the 10 cm proximity (including a grassland control), and 729 from the 200 cm proximity. Infiltration data were not collected from March to July 2020 due to the UK national COVID-19 lockdown.

## 2.2. Hydrometric Data Collection and HEC-HMS Modelling

Rainfall data (in mm) were collected via a tipping bucket rain gauge (accuracy  $\pm 4\%$  between 0.2 and 50 mm) located at the NextGen (2020) waste water treatment plant, 1 km north of the HofE site (see Figure 1). Whilst not located directly on the HofE site, the rain gauge is the only one located within eyeshot of the study site and is representative of local rainfall (Roberts, 2008; Terink *et al.*, 2018; Maier *et al.*, 2020). The stage (in mm) of the study site tributary was recorded every 15 min via a pressure transducer (accuracy  $\pm 0.05\%$  FS) located at the downstream end of the site watercourse (Figure 1). Upon instillation, the transducer was calibrated to a flow meter, enabling the generation of a ratings curve to determine watercourse flow (in L/s) relative to measured water pressure (Malik and Pal, 2020; Rampinelli *et al.*, 2020).

The US Hydrologic Engineering Center Hydrological Modelling System (HEC-HMS) allows the application of various numerical methods to each stage of the rainfall–runoff process, meaning a model can be tailored to serve a very specific purpose dependent on the required output (Derdour *et al.*, 2018; Al-Mukhtar and Al-Yaseen, 2019; Joshi *et al.*, 2019; Rangari *et al.*, 2020). The software is also capable of modelling simple hydraulic elements, allowing watercourses to be inputted as either user-defined open channels, or specified-shape culvers/pipes.

For this study, ArcMap 10.6.1 was used in conjunction with a 1 m resolution digital terrain model (downloaded from the Department for Environment, Food and Rural Affairs) (Department for Environment Food & Rural Affairs, 2020), and the shapefile of the study site tributary to delineate the watershed and generate a flow accumulation file. The area defined by the watershed delineation was overlain with HofE field boundaries. Each field boundary was treated as a separate sub-catchment model input, and these were individually digitised to represent the 10 cm woodland proximity, the 200 cm proximity, and the grassland areas

individually. This was implemented so that the model would account for the collected infiltration data of both the 10 and 200 cm proximities and the grassland (taken from the control site) data separately.

The watercourse of the HofE site was added to the model in a series of reaches and junctions, the dimensions of which were validated from cross-section measurements taken on site. After the watercourse, sub-catchment nodes were added. Each node represented a different land cover type of each sub-catchment, meaning there were up-to three nodes for each catchment (10 cm proximity, 200 cm proximity, grassland, and impermeable). ArcGIS, the flow accumulation, and personal knowledge of the site (field visits, observations of flow paths during storm events, topography) were used to determine where the nodes representing the different plots should connect to the tributary. The HEC-HMS model is shown in Figure 3.

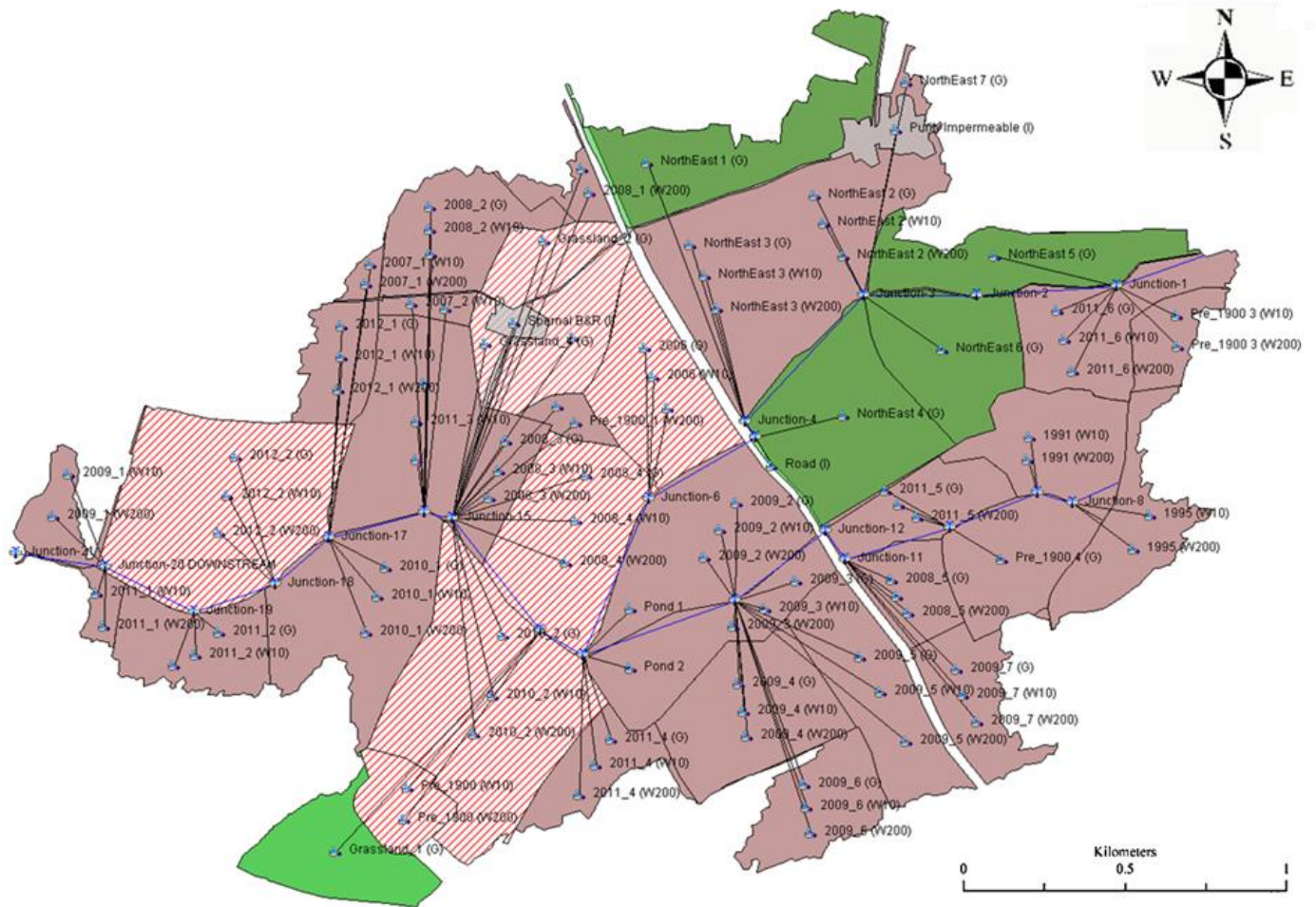


**Figure 3.** HEC-HMS hydrological model. Brown indicates forested plots, green indicates grassland only plots, grey indicates impermeable surfaces, and cross-hatching represents infiltration sample plots.

The Muskingum-Cunge routing method (Equations (1)–(6)) was used for modelling tributary flow (Kafle, 2019; Ramly *et al.*, 2020; Rangari *et al.*, 2020):

$$Q_{j+1}^{n+1} = C_0 Q_j^{n+1} + C_1 Q_j^n + C_2 Q_{j+1}^n \quad (1)$$

where  $Q$  is discharge,  $j$  is a spatial index,  $n$  is time index.  $C_0$ ,  $C_1$ , and  $C_2$  are calculated as follows (Cunge, 1969):

$$C_0 = \frac{\Delta t - 2KX}{2K(1-X) + \Delta t} \quad (2)$$

$$C_1 = \frac{\Delta t + 2KX}{2K(1-X) + \Delta t} \quad (3)$$

$$C_2 = \frac{2K(1-X) - \Delta t}{2K(1-X) + \Delta t} \quad (4)$$

$K$  and  $X$  are calculated as follows (Cunge, 1969):

$$K = \frac{\Delta x}{c} \quad (5)$$

$$X = \frac{1}{2} \left( 1 - \frac{q}{S_o c \Delta x} \right) \quad (6)$$

where  $\Delta x$  is reach length,  $c$  is flood wave celerity,  $q$  is unit width discharge, and  $S_o$  is channel bed slope (Cunge, 1969)

The initial and constant loss method (Equation (7)) was used to simulate the collected infiltration data (Section 2.1), the constant rate element is calculated as follows:

$$pe_t \begin{cases} 0 & \text{if } \sum p_i < I_a \\ p_1 - f_c & \text{if } \sum p_i > I_a \text{ and } p_t > f_c \\ 0 & \text{if } \sum p_i > I_a \text{ and } p_t < f_c \end{cases} \quad (7)$$

where  $pe_t$  is excess overland flow,  $p_1$  is precipitation depth,  $f_c$  is the maximum potential rate of precipitation, and  $I_a$  is initial loss. The initial and constant method (equation) was chosen for use in this study due to the nature of collected infiltration data; however, it is acknowledged that other authors have modified the Richards equation to account for root water uptake in soils (Kuhlmann *et al.*, 2012; Dong, 2016; Broadbridge *et al.*, 2017). Whilst these physics-based infiltration models can account for variations in soil texture, the wetting front and unsaturated hydraulic conductivity (Kuhlmann *et al.*, 2012; Blengino Albrieu *et al.*, 2015; Difonzo *et al.*, 2021); they can be prone to error and require in-depth data of the soil column for accurate execution compared with the initial and constant method used here.

The Snyder unit hydrograph transform (Equations (8) and (9)) was used to simulate the observed runoff and lag times of the catchment areas, Snyder's equation for lag time is (Fedorova *et al.*, 2018):

$$T_{lag} = C_t (LL_c)^{0.2} \quad (8)$$

where  $T_{lag}$  is the catchment lag time (hours),  $C_t$  is the catchment gradient coefficient,  $L$  is flow path length (km), and  $L_c$  is length of flow path from outlet to closest point of the catchment centroid (km).

For peak discharge, is (Fedorova *et al.*, 2018):

$$Q_p = \frac{2.78 \times C_p \times A}{T_{lag}} \quad (9)$$

where  $Q_p$  is peak discharge related to 1 cm of effective rainfall ( $\text{m}^3 \text{s}^{-1}$ ),  $A$  is catchment area ( $\text{km}^2$ ), and  $C_p$  is an empirical coefficient of peak intensity.

The constant monthly baseflow method was used to simulate antecedent baseflow of the site, which applied a user-defined constant flow to all models as required (see Section 2.5.4) (Koneti *et al.*, 2018; Zelelew and Melesse, 2018; Kaffle, 2019).

Two identical models, 'winter' and 'summer' were constructed and independently calibrated and validated (see Sections 2.3 and 2.4) to generate the results for this study. This approach was decided as a result of observed hydrological variations across the site from dry-to-wet seasons. The winter model is representative of hydrological data (infiltration, telemetry, rainfall) from October to March (2019/2020 and 2020/2021), and the summer model from April to September (2019/2020 and 2020/2021). These timeframes are based on UK average annual rainfall and temperature data, as defined by the Met Office (2021).

### 2.3. Model Calibration

Model calibration involved setting the initial baseflow to match that of the observed tributary value for the selected event, then gradually adjusting unobserved model parameters until the modelled output best simulated those of the observed values (Derdour *et al.*, 2018; Kumarasamy and Belmont, 2018; Al-Mukhtar and Al-Yaseen, 2019). Regarding the observed model parameters, infiltration was the key parameter for the hydrological model, it had been collected from October 2019 to August 2021 (with a break from March to July 2020 due to COVID-19), and this parameter could not be changed during the calibration process. The same applied to rainfall and baseflow, as these had been observed through use of the rain gauge and in-channel telemetry. This meant the only adjustable parameters were the lag times and peaking coefficients of the Snyder unit hydrograph transform (Equations (8) and (9)), so these parameters were adjusted through trial-and-error until one set of Snyder values (based on site observations and observed and simulated model output) could be used across all events and produce a similar outcome to the observed flow. This process was undertaken

for both the summer and winter models, using available data from the time periods specified in Section 2.2.

The Nash and Sutcliffe (1970) Efficiency (NSE) method was used to determine the closeness-of-fit between the simulated and observed values in calibration. The NSE equation is displayed as follows:

$$NSE = 1 - \left[ \frac{\sum_{i=1}^n (Y_i^{obs} - Y_i^{sim})^2}{\sum_{i=1}^n (Y_i^{obs} - Y^{mean})^2} \right] \quad (10)$$

where  $Y_i^{obs}$  is the observed discharge,  $Y_i^{sim}$  is the simulated discharge, and  $Y^{mean}$  is the mean of observed discharge. Table 2 shows the timeframes of the model calibration for winter and summer models, in addition to the individual and mean NSE values. The NSE method produces a value between 0 and 1, as an indication of how well the simulated dataset ( $Y_i^{sim}$ ) fits the observed dataset ( $Y_i^{obs}$ ) (Nash and Sutcliffe, 1970; Naik *et al.*, 2019). A value of 1 indicates a perfect fit between the two datasets, whereas a value of 0 (or a negative value) indicates a poor fit.

**Table 2.** Calibration events for winter and summer models. Note that the start and end time describes the time at which modelling began, not the start of the storm event.

Calibration Events						
Winter						
Duration (h)	Start Date	Start Time	End Date	End Time	Rainfall (mm)	NSE
24	16 January, 2021	04:00	17 January, 2021	04:00	1.8	0.41
72	17 January, 2021	16:00	20 January, 2021	16:00	10.60	0.30
96	30 November, 2019	04:00	04 December, 2019	04:00	0.80	0.92
120	08 October, 2020	07:00	13 October, 2020	07:00	6.70	0.98
Summer						
24	09 September, 2020	03:00	10 September, 2020	03:00	1.20	0.62
72	19 August, 2020	07:00	22 August, 2020	07:00	19.60	0.80
96	01 August, 2020	01:00	05 August, 2020	01:00	7.90	0.29
120	28 August, 2020	07:00	02 September, 2020	07:00	13.40	0.89

The mean NSE of both the winter and summer calibrations are 0.65. Seen from Table 2, the shorter duration events (24 and 72 h) showed a lower calibration NSE output compared with longer duration events (96 and 120 h). Across the summer calibration events, the lowest NSE value of 0.29 was produced by the 96-h duration, influencing the average NSE. Figures 4 and 5 show the observed and simulated discharge flow graphs for winter and summer model calibration events.

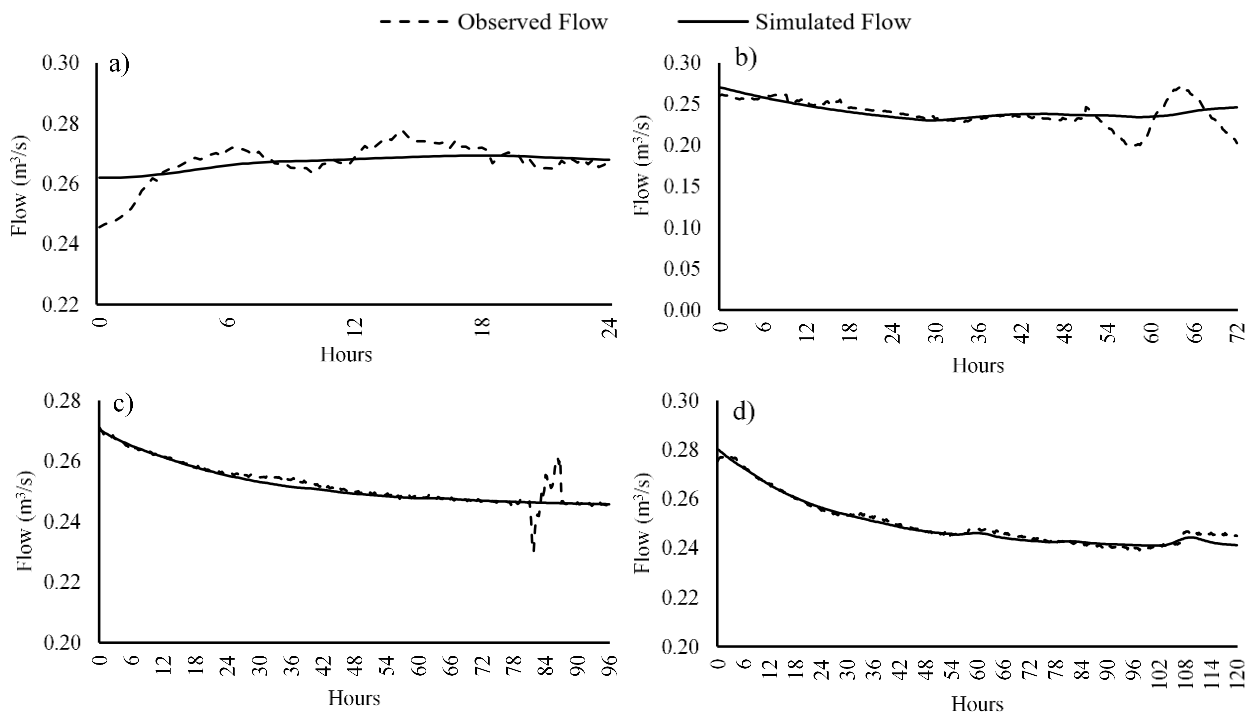


**Figure 4.** Observed and simulated discharge for winter model calibration events; (a) is the 24-h duration, (b) is the 72-h duration, (c) is the 96-h duration and (d) is the 120-h duration.

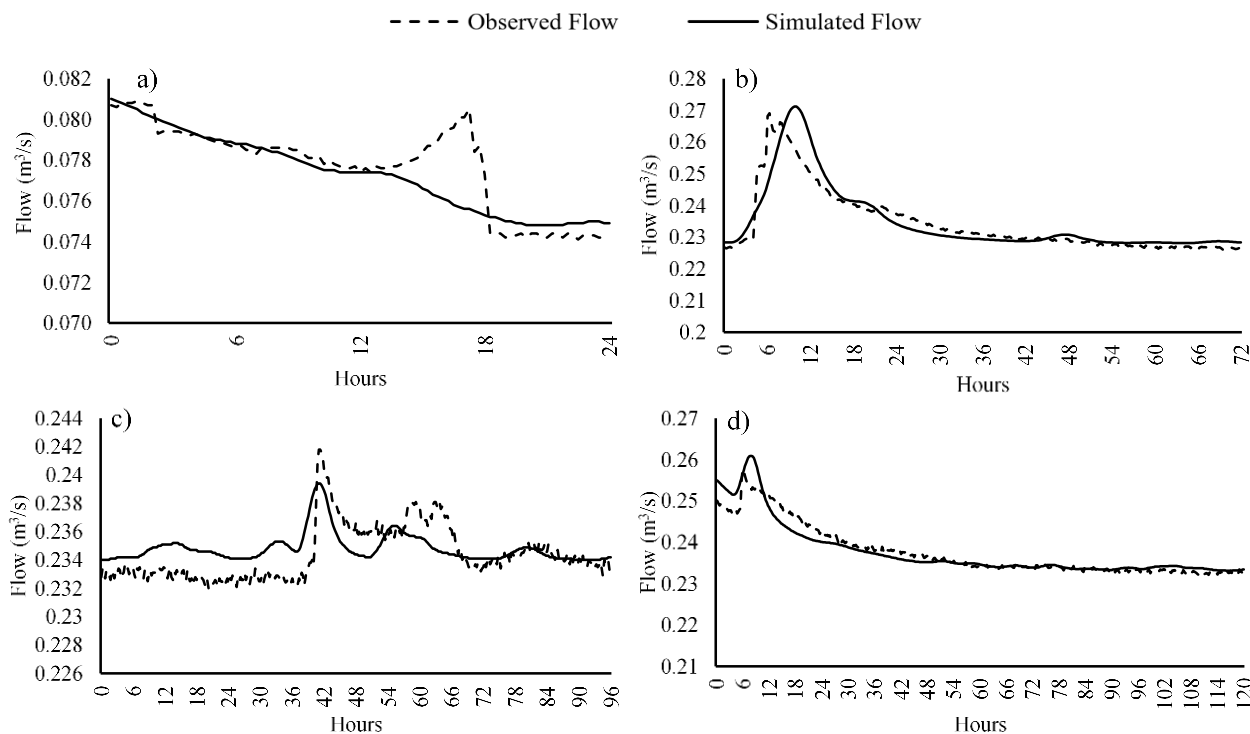


**Figure 5.** Observed and simulated discharge for summer model calibration events; (a) is the 24-h duration, (b) is the 72-h duration, (c) is the 96-h duration and (d) is the 120-h duration.

#### 2.4. Model Validation

The model was validated, again, using the NSE method for determination of relationship; however, different storm events were used to those used in calibration (using the same durations) (Table 3) (McMillan *et al.*, 2016; Al-Mukhtar and Al-Yaseen, 2019). Table 3 shows the timeframes of model validation for winter and summer models, in addition to the individual and mean NSE values.

**Table 3.** Validation events for winter and summer models. Note that the start and end time describes the time at which modelling began, not the start of the storm event.

Validation Events						
Winter						
Duration (h)	Start Date	Start Time	End Date	End Time	Rainfall (mm)	NSE
24	14 January, 2021	04:30	15 January, 2021	04:30	1.10	0.90
72	06 December, 2020	07:00	09 December, 2020	07:00	2.70	0.81
96	02 November, 2020	01:00	06 November, 2020	01:00	6.70	0.87
120	13 October, 2020	07:00	18 October, 2020	07:00	4.50	0.88
Summer						
24	04 September, 2020	02:00	05 September, 2020	02:00	0.70	0.35
72	09 September, 2020	22:00	12 September, 2020	22:00	1.00	0.23
96	04 September, 2020	22:00	08 September, 2020	22:00	4.20	0.74
120	30 August, 2020	02:00	04 September, 2020	02:00	8.00	0.42

The mean NSE of the winter validations is 0.87, and summer 0.44. The NSE average for validation events in the winter is high (0.87) indicating that the winter model is very effective at modelling the observed response from the site; whereas the summer validation NSE is 0.44, indicating that the output from the summer models is less accurate than the winter model. Figures 6 and 7 show the observed and simulated discharge flow graphs for winter and summer model validation events.

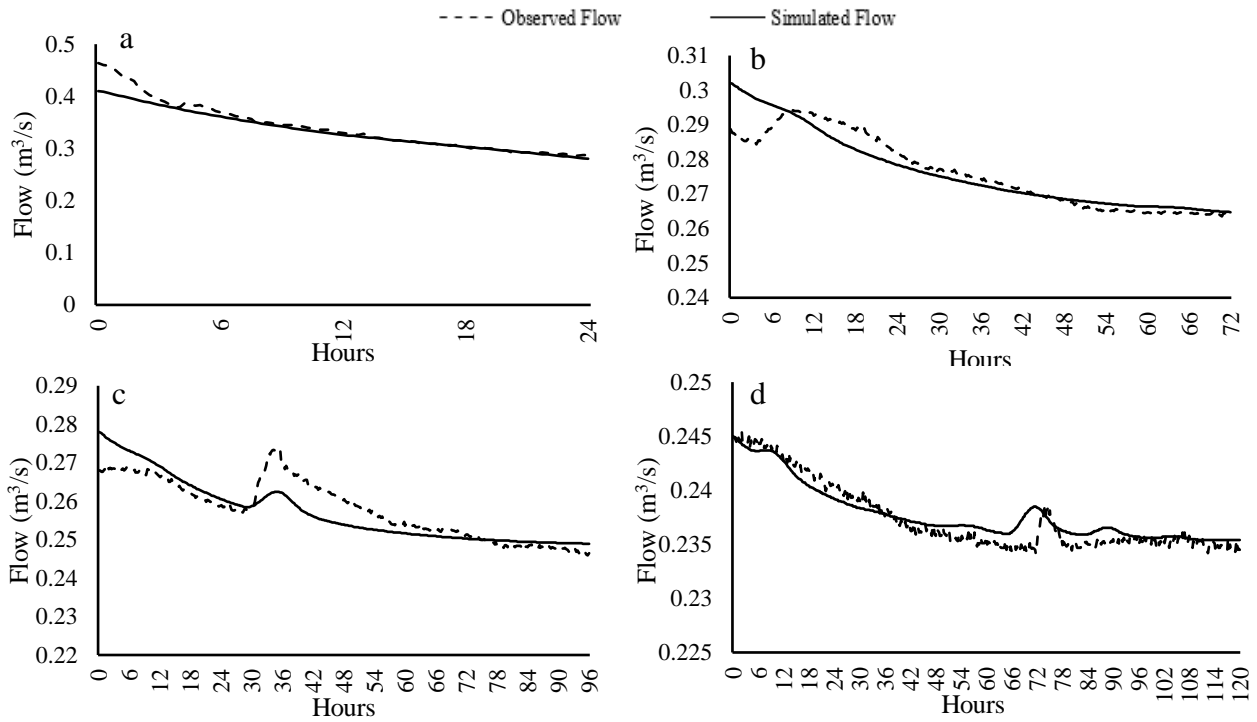


**Figure 6.** Observed and simulated discharge for winter model validation events; (a) is the 24-h duration, (b) is the 72-h duration, (c) is the 96-h duration and (d) is the 120-h duration.

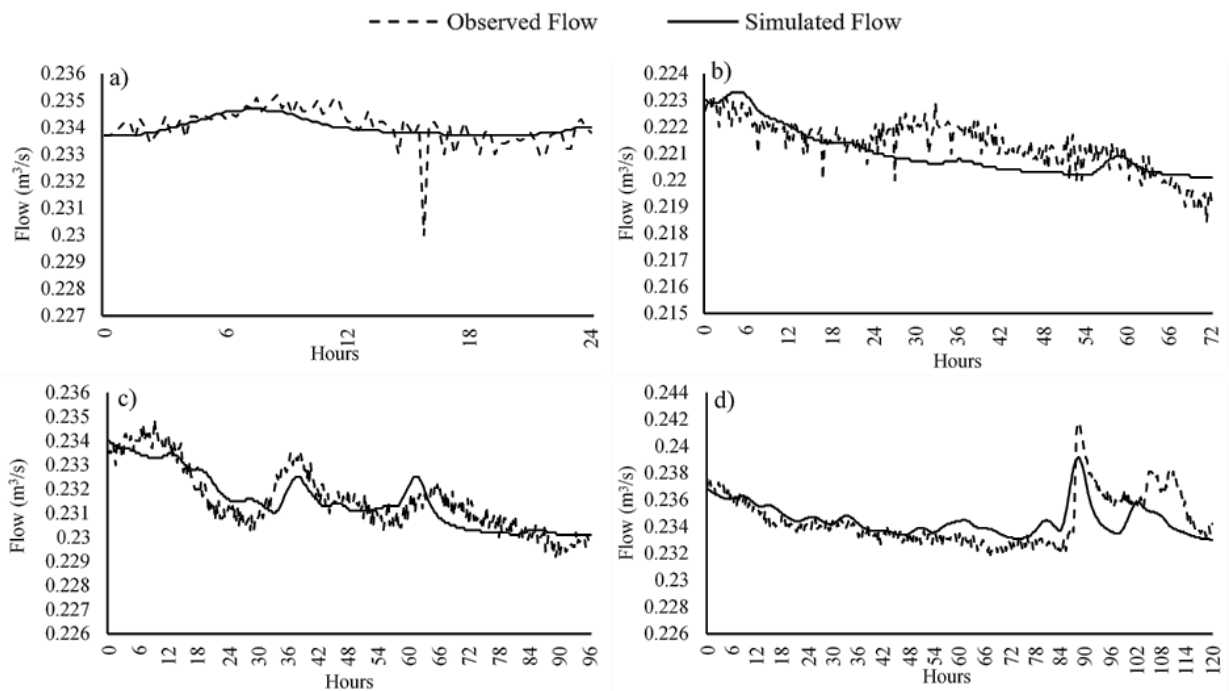


**Figure 7.** Observed and simulated discharge for summer model validation events; (a) is the 24-h duration, (b) is the 72-h duration, (c) is the 96-h duration and (d) is the 120-h duration.

The chosen calibration and validation datasets were selected primarily due to the scarcity of collected telemetry data from the study site and the timescales from which the data needed to be collected. Therefore, replication of calibration and validation events for the purposes of accuracy was not possible in this instance. Data scarcity for calibration and hydrological modelling is a common occurrence in the field of hydrological modelling. The methods presented throughout this section could be adopted by other researchers in the discipline aiming to simulate similar scenarios to those presented here.

## 2.5. Model Boundary Conditions

### 2.5.1. Precipitation and AEP Events

The Flood Estimation Handbook (FEH) was used to generate the design storms used in simulations (UK Centre for Ecology and Hydrology, 2021). Annual exceedance probabilities

(AEPs) representing 50% (1 in 2), 10% (1 in 10), 2% (1 in 50), and 1% (1 in 100) rainfall intensities were simulated over 6-, 24-, and 96-h durations (Wobus *et al.*, 2017; Darwish *et al.*, 2021; UK Centre for Ecology and Hydrology, 2021). The 24- and 96-h durations were chosen to test the short-to-medium scale impacts of woodland planting on infiltration. The 6 h duration was chosen due to the requirement of all UK sustainable drainage systems (SuDS) to be tested to this level (Defra, 2014; Local Authority SuDS Officer Organisation (LASOO), 2016). The rainfall intensities were chosen for similar reasons: the modelled results would enable further understanding regarding the true ability of woodland planting to mitigate runoff from low intensity (50% AEP) to very high intensity (1% AEP) storms, offering insight in to their use as a method of NFM.

#### 2.5.2. Infiltration Data

The collected infiltration data (Section 2.1) were interpreted and included as a primary focus of the modelling process. As this study focuses on the impacts of woodland planting on runoff, the mean infiltration rate (in mL) from every sample site at 10 and 200 cm proximities through both winter and summer (see Section 2.1) were compiled and averaged. The HofE forest planted new woodland every year from 2006 to 2012, but infiltration data were only collected every other year from 2006 (plus a control and the *ca.*1900 woodland area). To account for the infiltration values of woodland areas planted in the years between the sample plots (2007, 2009, 2011), which needed to be included in the model to fully represent the land cover of the study site, the median value of observed data in both years before and after was calculated. For example, the infiltration value for the unobserved 2007 areas were calculated using the median of the average 2006 and 2008 infiltration data (etc.). Given the lack of observed data and supporting literature in this area, this method is based on mathematical extrapolation and the observation of similar soil texture across the site (Table 1).

#### 2.5.3. Interception

As the sampled woodland is deciduous, interception needed to be considered as it would vary seasonally across the study site (Komatsu *et al.*, 2011; Klamerus-Iwan, 2014; Rahman and Ennos, 2016). Interception loss was not empirically monitored for this study; however, it was accounted for, considering the interception loss for grassland to be negligible (<10%) (Nisbet, 2005; Ngai *et al.*, 2017), and the interception from broadleaves to be between 10–34% (mean 24.25 %) (Calder, 2003; Lunka and Patil, 2016). FEH values were adjusted in the summer model to account for the rainfall loss due to interception, as simulating the site in both winter and summer with uniform rainfall would not account for any interception loss encountered. This method allows for the inclusion of interception loss in the model without the use of specialised equipment or continuous monitoring, and was an important process, as the influence of interception loss would vary seasonally across the site, both at present and in the future.

#### 2.5.4. Baseflow

Antecedent baseflow had to be calculated, as neglecting to consider this parameter could result in the total discharge from each simulated storm being inaccurate, and not represent true site conditions (Yusop *et al.*, 2007; Schütte and Schulze, 2017). To calculate the baseflow, telemetry data from both winter and summer periods (Section 2.2) were averaged, the average baseflow for winter models is  $0.284 \text{ m}^3 \text{ s}^{-1}$  and for summer models is  $0.239 \text{ m}^3 \text{ s}^{-1}$ .

#### 2.6. Hydrological Simulations

Three scenarios were simulated using both the winter and summer models with the intention of simulating the peak outflow of the site dependent on varying observed infiltration. Infiltration values for the first simulation scenario were derived from the collected infiltration data from the HofE site (Section 2.1); these data were simulated to reflect the “current HofE (woodland) land cover” as it is at present, and would allow a representation of current site peak discharge. Infiltration values for the second simulation scenarios were altered to represent sites discharge if it was impermeable land cover (developed). The rationale for this originates in Section 1, where it is acknowledged that urbanisation is a key influence of rising flood risk in the UK (Ferguson and Fenner, 2020a; Ellis *et al.*, 2021). Infiltration for scenario three were adjusted to represent infiltration collected from the grassland control site (Figure 1). This was to enable a comparison (Section 3) between peak flows from current woodland cover, impermeable land cover, and grassland land cover. It was decided to use the above scenarios as they could be based on collected infiltration data from the site, and provide an accurate representation of the hydrological variations of the sampled study site compared to using published values.

### 3. Results

Figure 8 shows the peak discharge of the 6-h summer and winter simulations, Table 4 shows the tabulated data with the discrepancy between land cover types shown in comparison to the current HofE site as a percentage.

●— 1 in 2 Peak Flow Winter    ●- - - 1 in 10 Peak Flow Winter    ●- - - 1 in 50 Peak Flow Winter    ●- - - 1 in 100 Peak Flow Winter  
 ▲— 1 in 2 Peak Flow Summer    ▲- - - 1 in 10 Peak Flow Summer    ▲- - - 1 in 50 Peak Flow Summer    ▲- - - 1 in 100 Peak Flow Summer

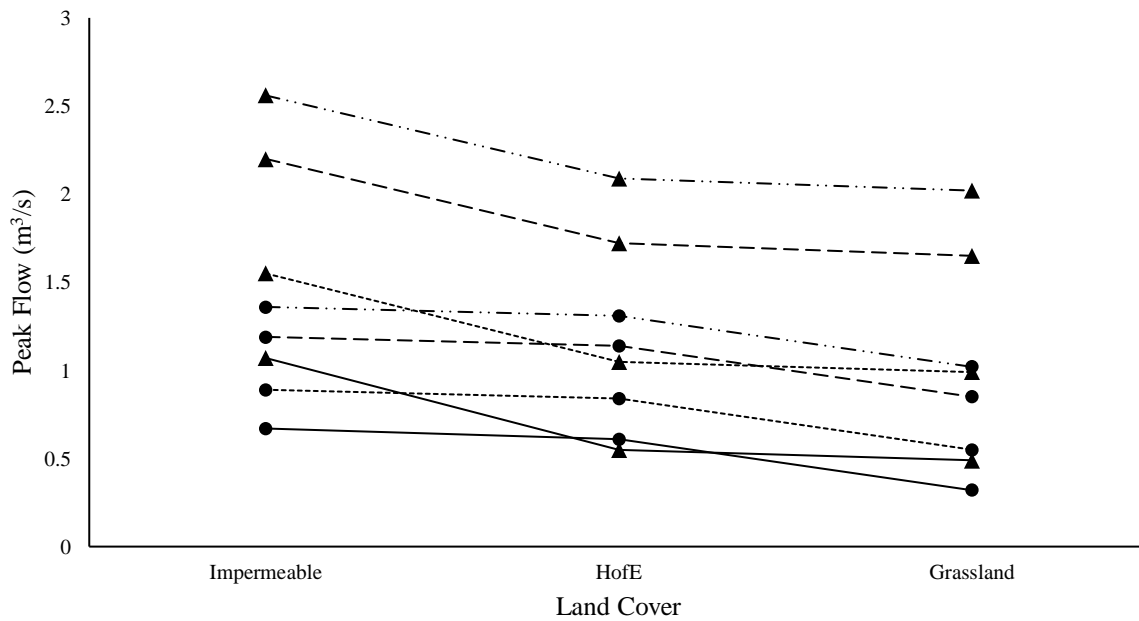


Figure 8. Output peak flows from all simulated land cover types.

Table 4. Peak discharge of all simulated land cover types over a 6-h duration rainfall event.

6-h	AEP %	HofE (Wooded Land Cover) (m³ s⁻¹)	Impermeable Land Cover (m³ s⁻¹)	Change from HofE (as %)	Grassland Land Cover (m³ s⁻¹)	Change from HofE (as %)
<b>Winter</b>						
Peak volume	50	0.61	0.67	9.84	0.32	-47.54
	10	0.84	0.89	5.95	0.55	-34.52
	2	1.14	1.19	4.39	0.85	-25.44
	1	1.31	1.36	3.82	1.02	-22.14
<b>Summer</b>						
Peak volume	50	0.55	1.07	94.55	0.49	-10.91
	10	1.05	1.55	47.62	0.99	-5.71
	2	1.72	2.2	27.91	1.65	-4.07
	1	2.09	2.56	22.49	2.02	-3.35

Figure 8 and Table 4 show that peak runoffs from the impermeable land cover simulations are higher than current and grassland simulations across all modelled storm events in both summer and winter; however, the discrepancy in the winter was slight. Peak flows from HofE land cover were 9.84%, 5.95%, 4.39%, and 3.82% lower than impermeable for a 50%, 10%, 2%, and 1% AEP events, respectively. However, in the summer this difference was higher, with peak flows being 94.55%, 47.62%, 27.91%, and 22.49% greater across 50%, 10%, 2%, and 1% AEP events for impermeable land cover compared to HofE. Grassland peak flows for winter and summer differ significantly, with summer peak flows being 84.71%, 41.67%, 23.52%, and 18.67% higher for 50%, 10%, 2%, and 1% AEP events, respectively. In the winter, grassland shows a 47.54%, 34.52%, 25.44%, and 22.14% reduction in peak flows compared to HofE land cover; this reduction is less in the summer, being 10.91%, 5.71%, 4.07%, and 3.35% for 50%, 10%, 2%, and 1% AEP storms.

Figure 8 and Table 5 show that impermeable cover produces the highest peak flows, compared to the HofE and grassland simulations, over both summer and winter. Current HofE site values are similar to impermeable values throughout the winter; however, this trend is not seen in the summer, where HofE site values are much lower. Grassland produces the lowest peak flows overall; however, grassland values are more similar to current HofE site values in the summer.

Figure 9 shows the peak discharge of the 24-h summer and winter simulations, Table 5 shows the tabulated data with the discrepancy between land cover types shown in comparison to the HofE site as a percentage.

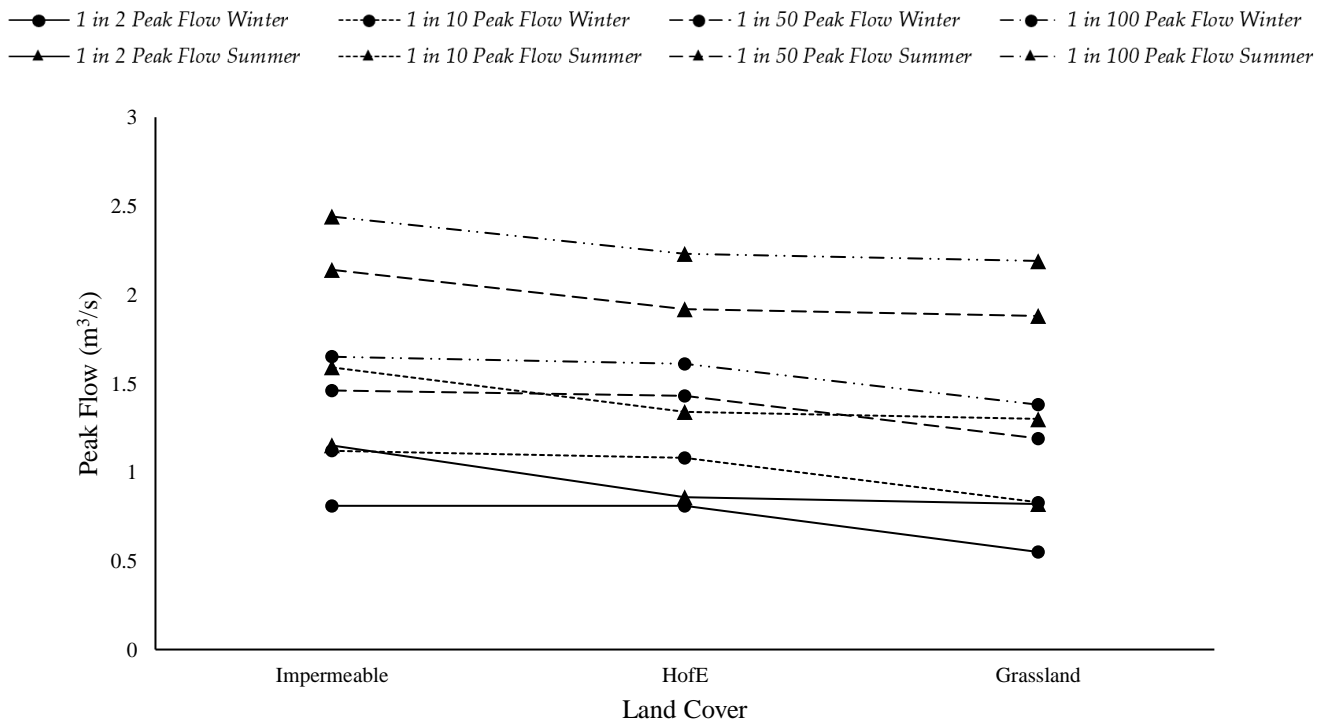


Figure 9. Output peak flows from all simulated land cover types.

Table 5. Peak discharge of all simulated land cover types over a 24-h duration rainfall event.

24-h	AEP %	HofE (Wooded Land Cover) (m <sup>3</sup> s <sup>-1</sup> )	Impermeable Land Cover (m <sup>3</sup> s <sup>-1</sup> )	Change from HofE (as %)	Grassland Land Cover (m <sup>3</sup> s <sup>-1</sup> )	Change from HofE (as %)
Winter						
Peak volume	50	0.61	0.67	9.84	0.32	-47.54
	10	0.84	0.89	5.95	0.55	-34.52
	2	1.14	1.19	4.39	0.85	-25.44
	1	1.31	1.36	3.82	1.02	-22.14
Summer						
Peak volume	50	0.55	1.07	94.55	0.49	-10.91
	10	1.05	1.55	47.62	0.99	-5.71
	2	1.72	2.2	27.91	1.65	-4.07
	1	2.09	2.56	22.49	2.02	-3.35

Figure 9 and Table 5 show the highest peak runoff of all simulated land cover types over both winter and summer to be generated by the impermeable land cover; being on average 2.07% higher than HofE land cover in the winter, and 18.31% higher in the summer over all AEPs. The impermeable cover, however, produces the same peak runoff as the HofE site for the 50% AEP in the winter, and peak flows for the impermeable land cover for 10%, 2%, and 1% AEPs in the winter are on average higher than that of the HofE site land cover by only 1.39%. A similar trend is seen in the summer, where peak flows from HofE land cover are only 0.24% lower than impermeable values for all AEPs. All 24-h events show less of a discrepancy between the HofE and impermeable land covers in the winter compared to the 6-h simulations, showing that, as storm duration increases, the flows from impermeable and HofE land cover become more similar in the winter months. Similar to the 6-h duration, grassland peak flows are lower than impermeable and HofE site land cover throughout the winter, however HofE site and grassland peak flows vary less in the summer. In the winter, grassland peak flow is 32.10%, 23.15%, 16.78%, and 14.29% lower than HofE land cover for 50%, 10%, 2%, and 1% AEPs; however, in the summer, grassland is only 4.65%, 2.99%, 2.08%, and 1.79% lower than the current site for all respective AEPs.

Results from the 24-h simulations are similar in trend to those of the 6-h simulations. Impermeable cover produces the highest peak flows over both summer and winter. These values are similar to HofE site discharge in the winter, but not the summer. Grassland produces the lowest peak flows; however, grassland values are more similar to HofE site values in the summer. Summer peak flows for all land cover types are higher than winter values.

Figure 10 shows the peak discharge of the 96-h summer and winter simulations; Table 6 shows the tabulated data with the discrepancy between land cover types shown in comparison to the HofE site as a percentage.

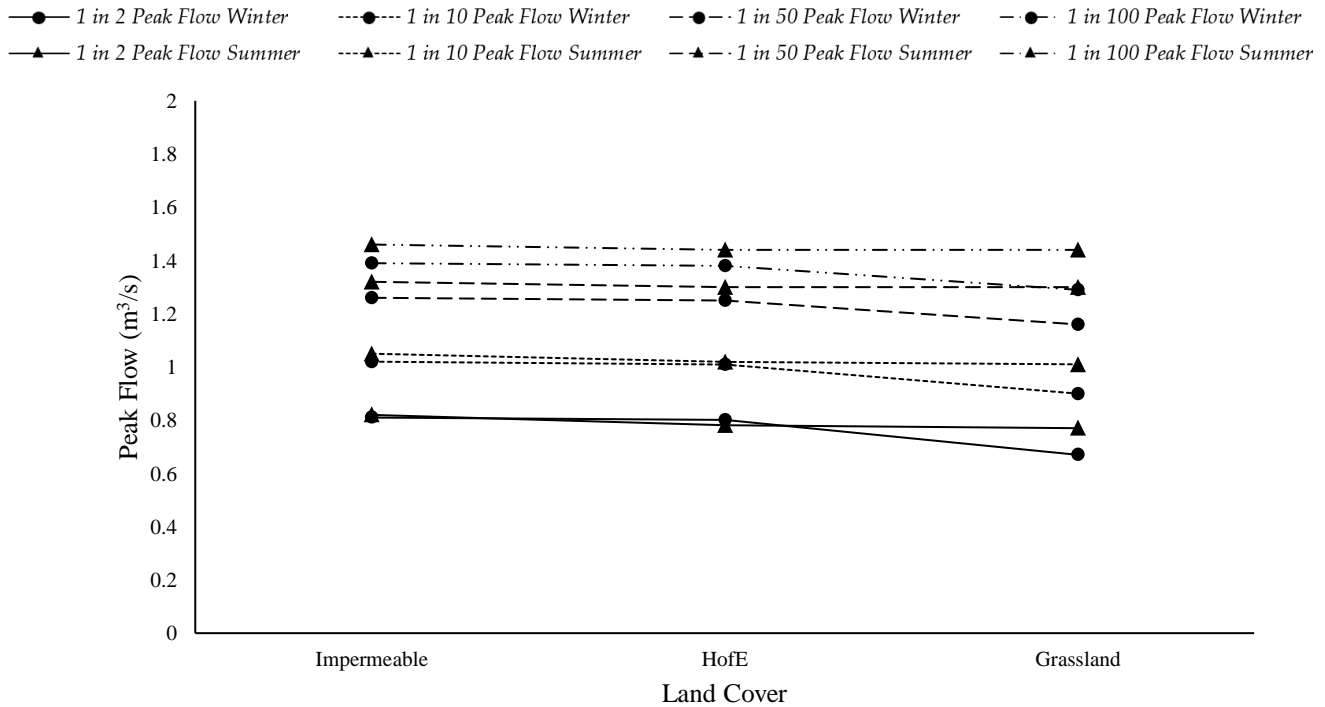


Figure 10. Output peak flows from all simulated land cover types.

**Table 6.** Peak discharge of all simulated land cover types over a 96-h duration rainfall event.

96-h	AEP %	HofE (Wooded land Cover) (m <sup>3</sup> s <sup>-1</sup> )	Impermeable Land Cover (m <sup>3</sup> s <sup>-1</sup> )	Change from HofE (as %)	Grassland Land Cover (m <sup>3</sup> s <sup>-1</sup> )	Change from HofE (as %)
Winter						
Peak volume	50	0.61	0.67	9.84	0.32	-47.54
	10	0.84	0.89	5.95	0.55	-34.52
	2	1.14	1.19	4.39	0.85	-25.44
	1	1.31	1.36	3.82	1.02	-22.14
Summer						
Peak volume	50	0.55	1.07	94.55	0.49	-10.91
	10	1.05	1.55	47.62	0.99	-5.71
	2	1.72	2.2	27.91	1.65	-4.07
	1	2.09	2.56	22.49	2.02	-3.35

As apparent from Figure 10 and Table 6, the results from the 96-h simulations show similar trends to 6- and 24-h simulations; however, the discrepancy in peak flow between land cover simulations are less notable, as are the seasonal variations in peak flows. Impermeable cover exhibits the highest peak flows compared to HofE and grassland cover; however, this difference is marginal. Impermeable peak flows are 1.25%, 0.99%, 0.80%, and 0.72% higher in the winter, and 5.13%, 2.94%, 1.54%, and 1.39% higher in the summer than HofE land cover for 50%, 10%, 2%, and 1% AEP events, respectively. There is more variation between HofE land cover and grassland in the winter than the summer. Peak flows from the grassland cover are 16.25%, 10.89%, 7.20%, and 6.52% higher than the HofE site in the winter for 50%, 10%, 2%, and 1% AEP events, respectively; however, only showing a difference of 1.28%, 0.98% for 50% and 10% AEP events, and 0 change for the 2%, and 1% AEPs in the summer. Peak flows show less variation between summer and winter for all land cover types, compared to the trends seen in the 6- and 24-h duration simulations.

The results displayed in Figure 10 and Table 6 show that the 96-h duration simulations show less variation in peak flows across all land cover types. There is very little variation in peak flows between land cover types; however, impermeable is slightly higher compared to both current HofE land cover and grassland cover over both summer and winter.

Overall, Figures 8–10 and Tables 4–6 show that, at present, impermeable cover produces the highest peak flows over all durations and storm intensities compared to other simulated land cover types. However, this is somewhat expected as it is known that the increase in impermeable surface cover is driving the push towards NFM (see Section 1) (Burgess-Gamble *et al.*, 2018; Ferguson and Fenner, 2020a; Ellis *et al.*, 2021). The current land cover of the site shows less of a peak flow compared to impermeable; however, the discrepancy is small and reduces with increased storm duration and intensity. The grassland simulations result in the lowest peak flows, regardless of season or storm scenario. The summer simulations show significantly higher peak flows compared to winter values across all land cover types in the lower duration storms (6 and 24 h); however, this is less significant in the higher duration simulations (96 h).

#### 4. Discussion

The results of the HEC-HMS models presented throughout Section 3 show that woodland planting across the HofE site has reduced peak runoff compared to if the entire site was impermeable, by an average of 6% for 6-h, 2% for 24-h, and 1% for 96-h duration events in the winter; and 48%, 18%, and 2.7% for 6-, 24-, and 96-h durations in the summer. This finding reinforces the benefit that woodland planting can have on increasing the surrounding soils infiltration potential, storage potential, resultantly reducing peak flow from the study area. Whereas the current HofE site does reduced peak flow compared to the impermeable scenario, an entirely grassland catchment shows the greatest reduction in peak flow, being 32%, 21%, and 10% lower than the current site in the winter, and 6%, 2%, and 0.5% lower than the HofE site in the summer for 6-, 24-, and 96-h duration storms, respectively.

It is worth considering that the reduction in peak flows exhibited by grassland compared to both the impermeable and current HofE site reduces as storm duration and intensity increases. This can be explained through considering both the age, and relative root spread of the woodland species sampled (Randrup, 2001; Birkinshaw *et al.*, 2014). As discussed in Section 2.1, aside from the *ca.*1900 (*Quercus Petraea*) woodland, the oldest trees sampled were

planted in 2006 (*Betula Pendula*) and the youngest in 2012 (*Populus Tremula*). Therefore, the 2006 trees have only been developing for 15 years, and the 2012 trees for 9. *Betula Pendula* reaches its ultimate height at around 60 years from planting, and can live for up to 100 years in total, meaning that the infiltration data collected and simulated in this study is only representative of the beginning of the likely effects that this tree will have, and infiltration will only improve as the tree (and its root system) develop, as the tree approaches maturity (Hynynen *et al.*, 2010; Kuparinen *et al.*, 2010; Lee *et al.*, 2015; Zeltiņš *et al.*, 2018). A similar rationale can be applied to the *Populus Tremula* (2012) tree; the growth of Aspen in the UK slows at around 30 years, and trees can live for 100–120 years (MacKenzie, 2010; CAB International, 2013; Savill, 2019). Thus, if this project was to be replicated in 20 years, tree roots would have developed, breaking up the surrounding soil, and infiltration would likely be greater due to the increased porosity (Chandler *et al.*, 2018; Zhang *et al.*, 2019a). Consequently, the modelled data show that, whilst some reduction in runoff is possible during the growth phase of trees, it will not be until they mature that the total potential reduction is demonstrated in comparison to grassland peak flow reduction.

#### 4.1. Woodland Planting Mentality

The findings of this project are significant when considering the way in which woodland areas are currently managed, regarding the growth and felling of trees and the removal of mature woodlands to make way for either newer areas of woodland or, more significantly, impermeable developments (Thomas and Nisbet, 2016; Chandler *et al.*, 2018; Murphy *et al.*, 2021). It is not uncommon for mature(ing) woodland to be removed to make way for impermeable developments, which significantly alters the local hydrology of an area, sealing-off once permeable areas and excluding them from participating in infiltration processes (Chandler *et al.*, 2018; Hankin *et al.*, 2018; Cooper *et al.*, 2021; Murphy *et al.*, 2021). Felled trees as a result of development are commonly ‘balanced out’ by planting saplings in alternate locations, however newly planted saplings will not have a comparable moderating impact on flood risk compared with the felled mature trees (Hynynen *et al.*, 2010; Archer *et al.*, 2013; Cooper *et al.*, 2021; Murphy, 2021). This project has demonstrated the above through presenting modelled results, showing that young trees, whilst they do reduce peak flows compared to impermeable land cover, have not yet developed the root systems, and influenced surrounding infiltration rates, to the extent they will with maturity.

#### 4.2. The Influence of Precipitation, Interception, and Model Calibration

Apparent throughout Section 3 is that summer peak flows over all simulated land cover types are higher than the corresponding winter values, this discrepancy reduces in the 96-h duration storm; however, it is more apparent in the 6- and 24-h duration storms. As discussed in Section 2.5.3, the hydrological effects of interception were accounted for in the summer through reducing the precipitation received. Therefore, it would be assumed that summer peak flows would be reduced; however, this is not the case. A reason for this output may be effect of surface pooling (as discussed above); however, another explanation may be due to the parameters used in calibration. The summer and winter models were calibrated individually (Section 2, Table 2), and a set of parameters used for each. The purpose of calibration is to align the observed and simulated outputs as closely as possible over varying events, leaving a final set of values that will produce a reliable output (Sharu, 2020; Hamdan *et al.*, 2021). In this case, the only variables that could be adjusted were the components of the Snyder transform method, and the summer model had a quicker lag and a higher peaking coefficient than the winter model. It is possible that this caused the variation seen between summer and winter; however, the calibration was comprehensive, resulting in a final calibration and validation NSE of 0.65 and 0.44 for summer.

#### 4.3. Antecedent Conditions and Results

Grassland continually showing the greatest reduction in peak flow may have been influenced by several external factors. The grassland control site comprises of a sandier soil texture than the pedology of the other sample sites (with the exception of 2010, see Table 1), making it more permeable (Folorunso and Aribisala, 2018). This means that when the grassland infiltration data are applied to the whole site to represent grassland coverage, it is not accounting for variations in soil texture across the site (Rabot *et al.*, 2018; Sun *et al.*, 2018; Silber, 2019). Additionally, Table 1 shows that the ca. 1900, 2008, and 2012 sites are comprised of a clay-heavy soil texture, meaning that they are naturally less permeable due to the smaller particle sizes of clay compared with sand (Folorunso and Aribisala, 2018). This may be an indication as to why the current HofE site peak flow is higher than that of grassland, particularly in the winter. The winter of 2020 was the fifth wettest on record (329.4

mm/143% higher than the 1981–2010 baseline), and February of 2020 was the wettest ever recorded, with 155 mm of precipitation (258% higher than the 1981–2010 baseline) (The Met Office, 2020; Davies *et al.*, 2021b). These dates are within the time periods that winter infiltration data were collected, and the excess rainfall received would have contributed to the study site saturation, influencing infiltration data collection. See Figure 11.



**Figure 11.** (a,b) saturation of the 2006 sample site during winter data collection, (c) cracking of the 2006, and (d) 2008 sample sites in the winter (locations can be identified using Figure 1).

As seen in Figure 11, the variation between antecedent rainfall and clay-saturation throughout winter, and cracking and drying-out throughout summer may have led to infiltration rates being significantly higher than the grassland for the current site simulations in the winter. These effects may also explain the higher peak flows observed throughout summer compared with winter; the increase in surface pooling of the sample sites in the winter (Figure 11a,b) held water in place across the study site. Infiltration would have been slowed due to the clay-geology and antecedent conditions of the site (Groenendyk *et al.*, 2015; Leung *et al.*, 2018), meaning runoff was slowed, creating more of a lag between precipitation and peak flow in the winter. Whereas in the summer, the cracking of the ground (Figure 11c,d) reduced infiltration, with the dry clay acting similarly to an impermeable surface. Due to this, rainfall was able to runoff into the watercourse, causing a quicker lag time and a higher peak.

#### 4.4. Study Applications

Whilst antecedent weather conditions and soil texture have influenced the trends seen between woodland and grassland land cover (see Section 3), the clay-heavy soil textures of the sample site are representations of the conditions of many sites around the UK. With the woodland sites being clay, and the ongoing comprehensive infiltration data collection, this project provides an assessment of the impact of NFM (woodland planting) over one of the most impermeable soil types throughout the UK.

Area calculations regarding the coverage of superficial alluvium, clay, peat, and fluvial deposits throughout the UK show that 15% (39,269.24 km<sup>2</sup>) of UK superficial geology is similar in infiltration to the geology of the HofE site (British Geological Survey, 2021). This demonstrates that the results of this study are significant, and are representative of 15% of UK geology, demonstrating that the results found throughout this study with regard to woodland planting and their runoff reduction capabilities can be extrapolated, furthering the usage of NFM across the UK. This therefore shows that woodland planting can be considered

as a method of NFM throughout other areas of the UK, and once could expect to find similar positive results to those found in this study.

## 5. Conclusions and Future Work

The results from the simulations undertaken in this study have shown that woodland can reduce peak flows when compared to impermeable cover; however, at present, grassland reduces peak flow most in both winter and summer. The values of the data collected throughout is that; if woodland can reduce peak flows at present over a predominantly clay (impermeable) geology, then the value of woodland planting on a site with slightly more permeable geology would show greater results than this study. This presents an opportunity for this research to be extrapolated and applied to other geologies and soil textures, to potentially aid in justifying the use of NFM (woodland planting), as a viable method of increasing infiltration and reducing ruff peaks to watercourses.

Woodland planting is gaining momentum as a method of NFM due to its ability to break up soil and increase infiltration and water storage. This study took infiltration measurements at 10 and 200 cm away from woodland planted at a 2.2 km<sup>2</sup> area in Warwickshire, England, from November 2019 until August 2021. Infiltration data were incorporated into two calibrated and validated HEC-HMS models, and the reductions in peak flow for woodland, grassland, and impermeable land cover were quantified. Results of this study show that, across a predominantly clay-site:

- Woodland planting across the HofE site shows less of a peak flow compared to impermeable land cover simulations; however, the discrepancy is small and reduces with increase storm duration and intensity.
- The grassland simulations result in the lowest peak flows, regardless of season or storm scenario.
- Impermeable land cover produces the highest peak flows throughout all durations and storm intensities compared to woodland and grassland; however, this is somewhat expected as it is known that the increase in impermeable surface cover is aiding the push towards NFM [1,2,10].
- The summer simulations show significantly higher peak flows compared to winter values across all land cover types in the lower duration storms (6 hour and 24 hour); however this is less significant in the higher duration simulations (96 hour).

The quantified results of this study show woodland to have a positive impact on peak flow reduction after only 15 years (since 2006), and indicate that the impacts will become more significant with root spread as the site matures (Zhang *et al.*, 2019a; Xie *et al.*, 2020). This study is also representative of a clay-textured site, the same soil texture as 15% of the UK, indicating that if woodland can show a reducing in peak flow across this study site, similar results will be seen in other similar sites. Further to this, the results will likely be more significant in areas inherent of a more permeable soil texture (Folorunso and Aribisala, 2018).

Additionally, this study has provided insight into how to collect and extrapolate infiltration data and model such information in HEC-HMS. Additionally, it has provided a methodology regarding the calibration and validation of HEC-HMS models where empirical data are sparse. This will enable other authors in the field of hydrology to use this project as a framework when contributing to the knowledge base regarding infiltration, NFM, woodland planting, and hydrology as a whole.

Future work will involve developing a method of projecting the collected infiltration data, with the intention of using the HEC-HMS model to project the ability of woodland planting to mitigate flow and overland runoff into the future, regarding precipitation and baseflow increases in light of climate change.

**Author Contributions:** Conceptualization, methodology, software, validation, formal analysis, investigation, resources, data curation, writing—original draft preparation N.R.; writing—review and editing, M.R., C.L., M.B.; visualization, N.R., C.L., M.B., M.R.; supervision, C.L., M.B., M.R. All authors have read and agreed to the published version of the manuscript.

**Funding:** This research received no external funding.

**Data Availability Statement:** To access the data collected and analysed in this study, please contact the corresponding author: Nathaniel Revell (revelln@uni.coventry.ac.uk).

**Acknowledgments:** Special thanks are extended to the HofE forest, in particular Stephen Coffey, for their support and assistance throughout the data collection phase of this project.

**Conflicts of Interest:** The authors declare no conflict of interest.

## References

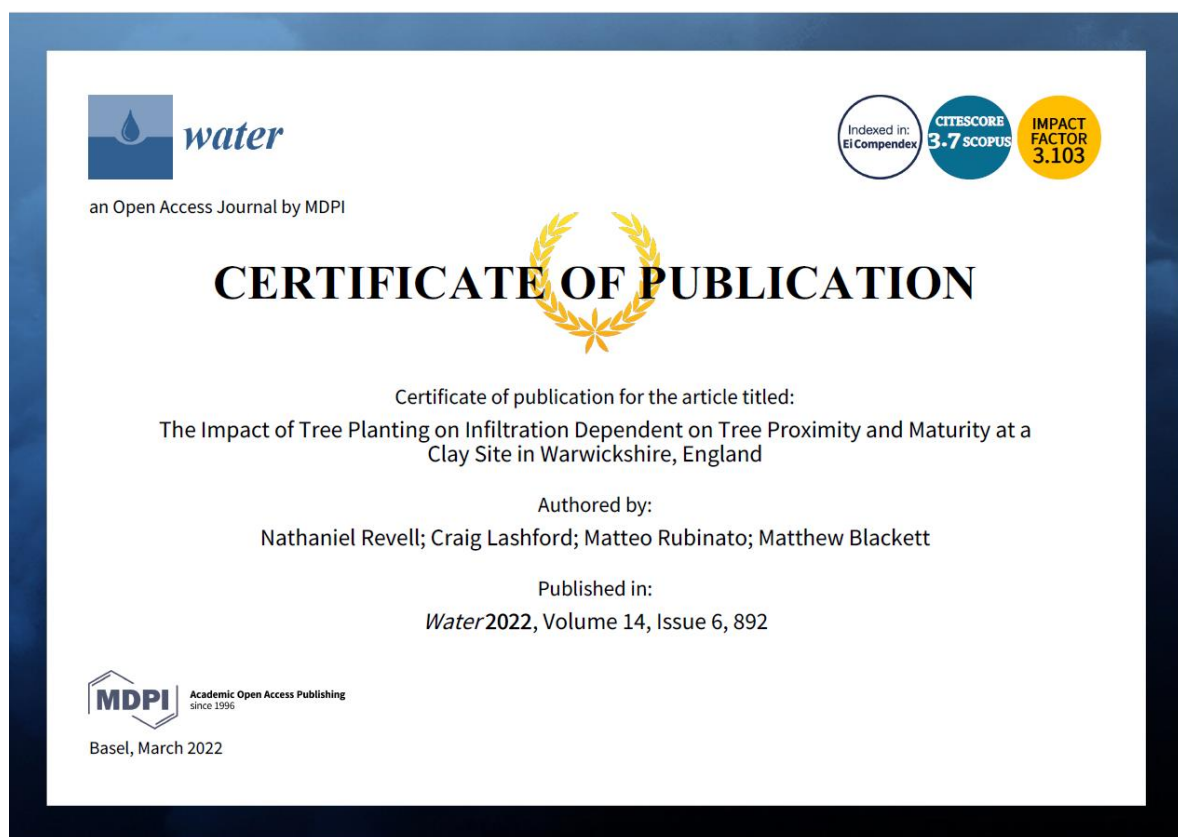
1. Ellis, N.; Anderson, K.; Brazier, R. Mainstreaming natural flood management: A proposed research framework derived from a critical evaluation of current knowledge. *Prog. Phys. Geogr. Earth Environ.* **2021**, 1–23, doi:10.1177/0309133321997299.
2. Ferguson, C.; Fenner, R. The impact of Natural Flood Management on the performance of surface drainage systems: A case study in the Calder Valley. *J. Hydrol.* **2020**, 590, 125354, doi:10.1016/j.jhydrol.2020.125354.
3. Lowe, J.A.; Bernie, D.; Bett, P.; Bricheno, L.; Brown, S.; Calvert, D.; Clark, R.; Edwards, T.; Fosser, G.; Fung, F.; et al. *UKCP18 Science Overview Report*; Met Office: Exeter, UK, 2019.
4. Murphy, T.R.; Hanley, M.E.; Ellis, J.S.; Lunt, P.H. Native woodland establishment improves soil hydrological functioning in UK upland pastoral catchments. *Land Degrad. Dev.* **2021**, 32, 1034–1045, doi:10.1002/ldr.3762.
5. Shuttleworth, E.L.; Evans, M.G.; Pilkington, M.; Spencer, T.; Walker, J.; Milledge, D.; Allott, T.E.H. Restoration of blanket peat moorland delays stormflow from hillslopes and reduces peak discharge. *J. Hydrol. X* **2019**, 2, 100006, doi:10.1016/j.hydroa.2018.100006.
6. Metcalfe, P.; Beven, K.; Hankin, B.; Lamb, R. A new method, with application, for analysis of the impacts on flood risk of widely distributed enhanced hillslope storage. *Hydrol. Earth Syst. Sci.* **2018**, 22, 2589–2605, doi:10.5194/hess-22-2589-2018.
7. Forbes, H.; Ball, K.; McLay, F. *Natural Flood Management Handbook*; Scottish Environment Protection Agency: Stirling, UK, 2016; ISBN 978-0-85759-024-4.
8. Ferguson, C.R.; Fenner, R.A. The potential for natural flood management to maintain free discharge at urban drainage outfalls. *J. Flood Risk Manag.* **2020**, 13, 1–15, doi:10.1111/jfr3.12617.
9. Dadson, S.J.; Hall, J.W.; Murgatroyd, A.; Acreman, M.; Bates, P.; Beven, K.; Heathwaite, L.; Holden, J.; Holman, I.P.; Lane, S.N.; et al. A restatement of the natural science evidence concerning catchment-based “natural” flood management in the UK. *Proc. R. Soc. A Math. Phys. Eng. Sci.* **2017**, 473, 20160706, doi:10.1098/rspa.2016.0706.
10. Burgess-Gamble, L.; Ngai, R.; Wilkinson, M.; Nisbet, T.; Pontee, N.; Harvey, R.; Kipling, K.; Addy, S.; Rose, S.; Maslen, S.; et al. *Working with Natural Processes – Evidence Directory*; Environment Agency: Bristol, UK, 2018.
11. Rachelle, N.; Wilkinson, M.; Nisbet, T.; Harvey, R.; Addy, S.; Burgess-Gamble, L.; Rose, S.; Maslen, S.; Nicholson, A.; Page, T.; et al. *Working with Natural Processes – Evidence Directory Appendix 2: Literature Review*; Environment Agency: Bristol, UK, 2017.
12. Wells, J.; Labadz, J.C.; Smith, A.; Islam, M.M. Barriers to the uptake and implementation of natural flood management: A social-ecological analysis. *J. Flood Risk Manag.* **2020**, 13, 1–12, doi:10.1111/jfr3.12561.
13. Lacob, O.; Rowan, J.S.; Brown, I.; Ellis, C. Evaluating wider benefits of natural flood management strategies: An ecosystem-based adaptation perspective. *Hydrol. Res.* **2014**, 45, 774–787, doi:10.2166/nh.2014.184.
14. Dittrich, R.; Ball, T.; Wreford, A.; Moran, D.; Spray, C.J. A cost-benefit analysis of afforestation as a climate change adaptation measure to reduce flood risk. *J. Flood Risk Manag.* **2019**, 12, 1–11, doi:10.1111/jfr3.12482.
15. Chandler, K.R.; Stevens, C.J.; Binley, A.; Keith, A.M. Influence of tree species and forest land use on soil hydraulic conductivity and implications for surface runoff generation. *Geoderma* **2018**, 310, 120–127, doi:10.1016/j.geoderma.2017.08.011.
16. Zhang, D.; Wang, Z.; Guo, Q.; Lian, J.; Chen, L. Increase and Spatial Variation in Soil Infiltration Rates Associated with Fibrous and Tap Tree Roots. *Water* **2019**, 11, 1700, doi:10.3390/w11081700.
17. GOV.UK. £3.9 Million to Drive Innovative Tree Planting. Available online: <https://www.gov.uk/government/news/39-million-to-drive-innovative-tree-planting> (accessed on 13 July 2021).
18. Murphy, T. *Optimising Oak Woodland Establishment into UK Upland Pastures in the Context of Climate Change; And the Role of Oak Woodland in Soil Hydrological Recovery for Natural Flood Management*; University of Plymouth: Plymouth, UK, 2021.
19. Ordnance Survey Ordnance Survey Open Data Download Available online: <https://www.ordnancesurvey.co.uk/opendatadownload/products.html> (accessed on 15 February 2019).
20. Ren, X.; Hong, N.; Li, L.; Kang, J.; Li, J. Effect of infiltration rate changes in urban soils on stormwater runoff process. *Geoderma* **2020**, 363, doi:10.1016/j.geoderma.2019.114158.
21. Bátková, K.; Miháliková, M.; Matula, S. Hydraulic properties of a cultivated soil in temperate continental climate determined by mini disk infiltrometer. *Water* **2020**, 12, 843, doi:10.3390/w12030843.
22. Rahman, M.A.; Moser, A.; Anderson, M.; Zhang, C.; Rötzer, T.; Pauleit, S. Comparing the infiltration potentials of soils beneath the canopies of two contrasting urban tree species. *Urban For. Urban Green.* **2019**, 38, 22–32, doi:10.1016/j.ufug.2018.11.002.
23. LaMotte Soil Texture Test Kit. Available online: <https://lamotte.com/products/soil/individual-soil-plant-tissue-test-kits/soil-texture-test-1067> (accessed on 15 October 2020).
24. METER® Group Inc. *Mini Disk Infiltrometer User’s Manual*; METER: Pullman, WA, USA, 2018.
25. Hepner, H.; Lutter, R.; Tullus, A.; Kanal, A.; Tullus, T.; Tullus, H. Effect of Early Thinning Treatments on Above-Ground Growth, Biomass Production, Leaf Area Index and Leaf Growth Efficiency in a Hybrid Aspen Coppice Stand. *Bioenergy Res.* **2020**, 13, 197–209, doi:10.1007/s12155-020-10111-0.
26. Mauer, O.; Palátová, E. The role of root system in silver birch (*Betula pendula* Roth) dieback in the air-polluted area of Krušné hory Mts. *J. For. Sci.* **2003**, 49, 191–199, doi:10.17221/4693-jfs.
27. Perry, T.O. Tree Roots: Facts and Fallacies. *J. Arboric.* **1982**, 8, 199–211.
28. Bagarello, V.; Sgroi, A. Using the single-ring infiltrometer method to detect temporal changes in surface soil field-saturated hydraulic conductivity. *Soil Tillage Res.* **2004**, 76, 13–24, doi:10.1016/j.still.2003.08.008.
29. NextGen NextGen Sternal, UK. Available online: <https://nextgenwater.eu/demonstration-cases/spernal/> (accessed on 16 March 2020).
30. Terink, W.; Leijnse, H.; van den Eertwegh, G.; Uijlenhoet, R. Spatial resolutions in areal rainfall estimation and their impact on hydrological simulations of a lowland catchment. *J. Hydrol.* **2018**, 563, 319–335, doi:10.1016/j.jhydrol.2018.05.045.
31. Roberts, N. Assessing the spatial and temporal variation in the skill of precipitation forecasts from an NWP model. *Meteorol. Appl.* **2008**, 15, 163–169, doi:10.1002/met.57.
32. Maier, R.; Krebs, G.; Pichler, M.; Muschalla, D.; Gruber, G. Spatial Rainfall Variability in Urban Environments—High-Density Precipitation Measurements on a City-Scale. *Water* **2020**, 12, 1157, doi:10.3390/w12041157.

33. Malik, S.; Pal, S.C. Application of 2D numerical simulation for rating curve development and inundation area mapping: A case study of monsoon dominated Dwarkeswar river. *Int. J. River Basin Manag.* **2020**, 1–11, doi:10.1080/15715124.2020.1738447.
34. Rampinelli, C.G.; Knack, I.; Smith, T. Flood mapping uncertainty from a restoration perspective: A practical case study. *Water* **2020**, *12*, 1948, doi:10.3390/w12071948.
35. Derdour, A.; Bouanani, A.; Babahamed, K. Modelling rainfall runoff relations using HEC-HMS in a semi-arid region: Case study in Ain Sefra watershed, Ksour Mountains (SW Algeria). *J. Water Land Dev.* **2018**, *36*, 45–55, doi:10.2478/jwld-2018-0005.
36. Joshi, N.; Bista, A.; Pokhrel, I.; Kalra, A.; Ahmad, S. Rainfall-Runoff Simulation in Cache River Basin, Illinois, Using HEC-HMS. In Proceedings of the World Environmental and Water Resources Congress 2019, Pittsburgh, PA, USA, 19–23 May 2019; American Society of Civil Engineers: Reston, VA, USA, 2019; pp. 348–360.
37. Al-Mukhtar, M.; Al-Yaseen, F. Modeling water quality parameters using data-driven models, a case study Abu-Ziriq marsh in south of Iraq. *Hydrology* **2019**, *6*, 21, doi:10.3390/hydrology6010021.
38. Rangari, V.A.; Sridhar, V.; Umamahesh, N.V.; Patel, A.K. Rainfall Runoff Modelling of Urban Area Using HEC-HMS: A Case Study of Hyderabad City. In *Advances in Water Resources Engineering and Management*; AlKhaddar, R., Singh, R.K., Dutta, S., Kumari, M., Eds.; Lecture Notes in Civil Engineering; Springer Singapore: Singapore, 2020; Volume 39, pp. 113–125, ISBN 978-981-13-8180-5.
39. Department for Environment Food & Rural Affairs LIDAR Composite DTM. Available online: <https://environment.data.gov.uk/dataset/668881ad-4f8f-42bd-b835-89acf0269496> (accessed on 16 July 2021).
40. Kafle, M.R. Rainfall-Runoff Modelling of Koshi River Basin Using HEC-HMS. *J. Hydrogeol. Hydrol. Eng.* **2019**, *8*, 1–9.
41. Ramly, S.; Tahir, W.; Abdullah, J.; Jani, J.; Ramli, S.; Asmat, A. Flood Estimation for SMART Control Operation Using Integrated Radar Rainfall Input with the HEC-HMS Model. *Water Resour. Manag.* **2020**, *34*, 3113–3127, doi:10.1007/s11269-020-02595-4.
42. Cunge, J.A. On the subject of a flood propagation computation method (Maskingum method). *J. Hydraul. Res.* **1969**, *7*, 205–230.
43. Dong, X. How to put plant root uptake into a soil water flow model. *F1000Research* **2016**, *5*, 1–9, doi:10.12688/f1000research.7686.1.
44. Broadbridge, P.; Daly, E.; Goard, J. Exact Solutions of the Richards Equation with Nonlinear Plant-Root Extraction. *Water Resour. Res.* **2017**, *53*, 9679–9691, doi:10.1002/2017WR021097.
45. Kuhlmann, A.; Neuweiler, I.; Van Der Zee, S.E.A.T.M.; Helmig, R. Influence of soil structure and root water uptake strategy on unsaturated flow in heterogeneous media. *Water Resour. Res.* **2012**, *48*, 1–16, doi:10.1029/2011WR010651.
46. Blengino Albrieu, J.L.; Reginato, J.C.; Tarzia, D.A. Modeling water uptake by a root system growing in a fixed soil volume. *Appl. Math. Model.* **2015**, *39*, 3434–3447, doi:10.1016/j.apm.2014.11.042.
47. Difonzo, F.V.; Masciopinto, C.; Vurro, M.; Berardi, M. Shooting the Numerical Solution of Moisture Flow Equation with Root Water Uptake Models: A Python Tool. *Water Resour. Manag.* **2021**, *35*, 2553–2567, doi:10.1007/s11269-021-02850-2.
48. Darya, F.; Pavel, K.; Jan, G.; Andrea, J.; Jana, N. The use of Snyder synthetic hydrograph for simulation of overland flow in small ungauged and gauged catchments. *Soil Water Res.* **2018**, *13*, 185–192, doi:10.17221/237/2017-SWR.
49. Zelelew, D.G.; Melesse, A.M. Applicability of a spatially semi-distributed hydrological model for watershed scale runoff estimation in Northwest Ethiopia. *Water* **2018**, *10*, 923, doi:10.3390/w10070923.
50. Koneti, S.; Sunkara, S.L.; Roy, P.S. Hydrological modeling with respect to impact of land-use and land-cover change on the runoff dynamics in Godavari river basin using the HEC-HMS model. *ISPRS Int. J. Geo-Inf.* **2018**, *7*, 206, doi:10.3390/ijgi7060206.
51. Met Office UK Climate Averages. Available online: <https://www.metoffice.gov.uk/research/climate/maps-and-data/uk-climate-averages/gcq89t680> (accessed on 23/09/2021).
52. Kumarasamy, K.; Belmont, P. Calibration parameter selection and watershed hydrology model evaluation in time and frequency domains. *Water* **2018**, *10*, 710, doi:10.3390/w10060710.
53. Nash, J.E.; Sutcliffe, J.V. River flow forecasting through conceptual models Part I-A discussion of principles. *J. Hydrol.* **1970**, *10*, 282–290, doi:10.3917/difa.012.0161.
54. Naik, A.P.; Ghosh, B.; Pekkat, S. Estimating soil hydraulic properties using mini disk infiltrometer. *ISH J. Hydraul. Eng.* **2019**, *25*, 62–70, doi:10.1080/09715010.2018.1471363.
55. McMillan, H.K.; Booker, D.J.; Cattoën, C. Validation of a national hydrological model. *J. Hydrol.* **2016**, *541*, 800–815, doi:10.1016/j.jhydrol.2016.07.043.
56. UK Centre for Ecology and Hydrology. *The Flood Estimation Handbook*, UK Centre for Ecology and Hydrology, Wallingford, UK. Available online: <https://www.ceh.ac.uk/services/flood-estimation-handbook> (accessed on 12/07/2021).
57. Darwish, M.M.; Tye, M.R.; Prein, A.F.; Fowler, H.J.; Blenkinsop, S.; Dale, M.; Faulkner, D. New hourly extreme precipitation regions and regional annual probability estimates for the UK. *Int. J. Climatol.* **2021**, *41*, 582–600, doi:10.1002/joc.6639.
58. Wobus, C.; Gutmann, E.; Jones, R.; Rissing, M.; Mizukami, N.; Lorie, M.; Mahoney, H.; Wood, A.; Mills, D.; Martinich, J. Modeled changes in 100 year Flood Risk and Asset Damages within Mapped Floodplains of the Contiguous United States. *Nat. Hazards Earth Syst. Sci. Discuss.* **2017**, 1–21, doi:10.5194/nhess-2017-152.
59. Local Authority SuDS Officer Organisation (LASOO). *Non-Statutory Technical Standards for Sustainable Drainage*; LASOO, London: UK, 2016.
60. Department for Environment, Food and Rural Affairs. *Draft National Standards and Specified Criteria for Sustainable Drainage*; Defra: London, UK, 2014.
61. Klamerus-Iwan, A. Different views on tree interception process and its determinants. *For. Res. Pap.* **2014**, *75*, 291–300, doi:10.2478/frp-2014-0028.
62. Rahman, M.; Ennos, R. *What We Know and Don't Know about the Surface Runoff Reduction Potential of Urban Trees*; Technical Report; Technical University of Munich: Munich, Germany, 2016; pp. 1–14.
63. Komatsu, H.; Kume, T.; Otsuki, K. Increasing annual runoff-broadleaf or coniferous forests? *Hydrol. Process.* **2011**, *25*, 302–318, doi:10.1002/hyp.7898.
64. Nisbet, T. *Water Use by Trees*; Information Note FCIN065; Forestry Commission: Edinburgh, UK, 2005; pp. 1–8.
65. Calder, I.R. Assessing the water use of short vegetation and forests: Development of the Hydrological Land Use Change (HYLUC) model. *Water Resour. Res.* **2003**, *39*, 1–8, doi:10.1029/2003WR002040.
66. Lunka, P.; Patil, S.D. Impact of tree planting configuration and grazing restriction on canopy interception and soil hydrological properties: Implications for flood mitigation in silvopastoral systems. *Hydrol. Process.* **2016**, *30*, 945–958, doi:10.1002/hyp.10630.

67. Schütte, S.; Schulze, R.E. Projected impacts of urbanisation on hydrological resource flows: A case study within the uMngeni Catchment, South Africa. *J. Environ. Manag.* **2017**, *196*, 527–543, doi:10.1016/j.jenvman.2017.03.028.
68. Yusop, Z.; Chan, C.H.; Katimon, A. Runoff characteristics and application of HEC-HMS for modelling stormflow hydrograph in an oil palm catchment. *Water Sci. Technol.* **2007**, *56*, 41–48, doi:10.2166/wst.2007.690.
69. Randrup, T.B. A review of tree root conflicts with sidewalks, curbs, and roads. *Urban Ecosyst.* **2001**, *5*, 209–225, doi:10.1023/A:1024046004731.
70. Birkinshaw, S.J.; Bathurst, J.C.; Robinson, M. 45 years of non-stationary hydrology over a forest plantation growth cycle, Coalburn catchment, Northern England. *J. Hydrol.* **2014**, *519*, 559–573, doi:10.1016/j.jhydrol.2014.07.050.
71. Lee, S.J.; Connolly, T.; Wilson, S.M.; Malcolm, D.C.; Fonweban, J.; Worrell, R.; Hubert, J.; Sykes, R.J. Early height growth of silver birch (*Betula pendula* Roth) provenances and implications for choice of planting stock in Britain. *Forestry* **2015**, *88*, 484–499, doi:10.1093/forestry/cpv018.
72. Kuparinen, A.; Savolainen, O.; Schurr, F.M. Increased mortality can promote evolutionary adaptation of forest trees to climate change. *For. Ecol. Manag.* **2010**, *259*, 1003–1008, doi:10.1016/j.foreco.2009.12.006.
73. Zeltiņš, P.; Gailis, A.; Jansons, J.; Katrevičs, J.; Jansons, Ā. Genetic Parameters of Growth Traits and Stem Quality of Silver Birch in a Low-Density Clonal Plantation. *Forests* **2018**, *9*, 52, doi:10.3390/f9020052.
74. Hynynen, J.; Niemisto, P.; Vihera-Aarnio, A.; Brunner, A.; Hein, S.; Velling, P. Silviculture of birch (*Betula pendula* Roth and *Betula pubescens* Ehrh.) in northern Europe. *Forestry* **2010**, *83*, 103–119, doi:10.1093/forestry/cpp035.
75. CAB International. *The CABI Encyclopedia of Forest Trees*; CABI Publishing: Wallingford, UK, 2013; ISBN 9781780642369.
76. Savill, P. *The Silviculture of Trees Used in British Forestry*; 3rd ed.; CABI Publishing: Wallingford, UK, 2019.
77. MacKenzie, N.A. *Ecology, Conservation and Management of Aspen: A Literature Review*; CABI Publishing: Wallingford, UK, 2010.
78. Thomas, H.; Nisbet, T.R. Slowing the Flow in Pickering: Quantifying the Effect of Catchment Woodland Planting on Flooding Using the Soil Conservation Service Curve Number Method. *Int. J. Saf. Secur. Eng.* **2016**, *6*, 2–20.
79. Hankin, B.; Chappell, N.; Page, T.; Kipling, K.; Whitling, M.; Burgess-Gamble, L. *Mapping the potential for Working with Natural Processes – Technical Report*; Environment Agency: Bristol, UK, 2018.
80. Cooper, M.M.D.; Patil, S.D.; Nisbet, T.R.; Thomas, H.; Smith, A.R.; McDonald, M.A. Role of forested land for natural flood management in the UK: A review. *Wiley Interdiscip. Rev. Water* **2021**, *8*, 1–16, doi:10.1002/wat2.1541.
81. Archer, N.A.L.; Bonell, M.; Coles, N.; MacDonald, A.M.; Auton, C.A.; Stevenson, R. Soil characteristics and landcover relationships on soil hydraulic conductivity at a hillslope scale: A view towards local flood management. *J. Hydrol.* **2013**, *497*, 208–222, doi:10.1016/j.jhydrol.2013.05.043.
82. Sharu, E.H. Development of HEC-HMS Model for Flow Simulation at Dungun River Basin Malaysia. *Adv. Agric. Food Res. J.* **2020**, *1*, 1–16, doi:10.36877/aaftrj.a0000169.
83. Hamdan, A.N.A.; Almuktar, S.; Scholz, M. Rainfall-Runoff Modeling Using the HEC-HMS Model for the Al-Adhaim River Catchment, Northern Iraq. *Hydrology* **2021**, *8*, 58, doi:10.3390/hydrology8020058.
84. Folorunso, O.; Aribisala, J. Effect of Soil Texture on Soil Infiltration Rate. *Arch. Curr. Res. Int.* **2018**, *14*, 1–8, doi:10.9734/ACRI/2018/41974.
85. Silber, A. Chemical Characteristics of Soilless Media. In *Soilless Culture*; Elsevier: Amsterdam, The Netherlands, 2019; pp. 113–148, ISBN 9780444636966.
86. Rabot, E.; Wiesmeier, M.; Schlüter, S.; Vogel, H.J. Soil structure as an indicator of soil functions: A review. *Geoderma* **2018**, *314*, 122–137, doi:10.1016/j.geoderma.2017.11.009.
87. Sun, D.; Yang, H.; Guan, D.; Yang, M.; Wu, J.; Yuan, F.; Jin, C.; Wang, A.; Zhang, Y. The effects of land use change on soil infiltration capacity in China: A meta-analysis. *Sci. Total Environ.* **2018**, *626*, 1394–1401, doi:10.1016/j.scitotenv.2018.01.104.
88. The Met Office Record Breaking Rainfall. Available online: <https://www.metoffice.gov.uk/about-us/press-office/news/weather-and-climate/2020/2020-winter-february-stats> (accessed on 11 June 2021).
89. Davies, P.A.; McCarthy, M.; Christidis, N.; Dunstone, N.; Fereday, D.; Kendon, M.; Knight, J.R.; Scaife, A.A.; Sexton, D. The wet and stormy UK winter of 2019/2020. *Weather* **2021**, wea.3955, doi:10.1002/wea.3955.
90. Groenendyk, D.G.; Ferré, T.P.A.; Thorp, K.R.; Rice, A.K. Hydrologic-process-based soil texture classifications for improved visualization of landscape function. *PLoS ONE* **2015**, *10*, 1–17, doi:10.1371/journal.pone.0131299.
91. Leung, A.K.; Boldrin, D.; Liang, T.; Wu, Z.Y.; Kamchoom, V.; Bengough, A.G. Plant age effects on soil infiltration rate during early plant establishment. *Geotechnique* **2018**, *68*, 646–652, doi:10.1680/jgeot.17.T.037.
92. British Geological Survey 1:625k Bedrock and Superficial UK Geology. Available online: <https://www.bgs.ac.uk/datasets/bgs-geology-625k-digmapgb/> (accessed on 15 June 2021).
93. Xie, C.; Cai, S.; Yu, B.; Yan, L.; Liang, A.; Che, S. The effects of tree root density on water infiltration in urban soil based on a Ground Penetrating Radar in Shanghai, China. *Urban For. Urban Green.* **2020**, *50*, 126648, doi:10.1016/j.ufug.2020.126648.

*D.2.2 The Impact of Tree Planting on Infiltration Dependent on Tree Proximity and Maturity at a Clay Site in Warwickshire, England*

First author of the below article, published in the Water MDPI special issue ‘Surface Water Management: Recent Advances and Challenges’. The paper presents the methods and results of the infiltration data collection and analysis (presented and discussed in sections 5.2, 7.1 and 8.1) undertaken to allow for further hydrological modelling (presented and discussed in sections 5.3, 7.2 and 8.2.1) of this thesis.



The publication is inserted below

# The Impact of Tree Planting on Infiltration Dependent on Tree Proximity and Maturity at a Clay Site in Warwickshire, England

Nathaniel Revell <sup>1,\*</sup>, Craig Lashford <sup>1,2</sup>, Matteo Rubinato <sup>1,2,3</sup> and Matthew Blackett <sup>1,2</sup>

<sup>1</sup> Centre for Agroecology, Water and Resilience, Coventry University, Wolston Lane, Coventry CV8 3LG, UK; ab0874@coventry.ac.uk (C.L.); ad2323@coventry.ac.uk (M.R.); aa8533@coventry.ac.uk (M.B.)

<sup>2</sup> Faculty of Engineering, Environment & Computing, School of Energy, Construction and Environment, Coventry University, Coventry CV1 5FB, UK

<sup>3</sup> IKT-Institute for Underground Infrastructure, Exterbruch 1, 45886 Gelsenkirchen, Germany

\* Correspondence: revelln@uni.coventry.ac.uk

**Abstract:** Urbanisation and the replacement of previously vegetated areas with impermeable surfaces reduces the lag times of overland flow and increases peak flows to receiving watercourses; the magnitude of this will increase as a result of climate change. Tree planting is gaining momentum as a potential method of natural flood management (NFM) due to its ability to break up soil and increase infiltration and water storage. In this study, a 2.2 km<sup>2</sup> clay-textured area in Warwickshire, England, planted with trees every year from 2006 to 2012 was sampled to investigate how infiltration varies dependent on season and tree proximity and maturity. Infiltration data was collected from 10 and 200 cm away from selected sample trees from November 2019 to August 2021 using a Mini Disk infiltrometer (MDI). The results show that mean infiltration is higher at the 10 cm proximity compared with the 200 cm proximity by 75.87% in winter and 25.19% in summer. Further to this, mean 10 cm infiltration is 192% higher in summer compared with winter, and mean 200 cm infiltration is 310% higher in summer compared with winter. There is little evidence to suggest a relationship between infiltration and tree maturity at the study site.

**Keywords:** tree planting; tree proximity; infiltration; flood risk management; natural flood management; NFM

**Citation:** Revell, N.; Lashford, C.; Rubinato, M.; Blackett, M. The Impact of Tree Planting on Infiltration Dependent on Tree Proximity and Maturity at a Clay Site in Warwickshire, England. *Water* **2022**, *14*, x. <https://doi.org/10.3390/xxxxx>

Academic Editor(s):

Received: 15 February 2022

Accepted: 11 March 2022

Published: date

**Publisher's Note:** MDPI stays neutral with regard to jurisdictional claims in published maps and institutional affiliations.



**Copyright:** © 2022 by the authors. Submitted for possible open access publication under the terms and conditions of the Creative Commons Attribution (CC BY) license (<https://creativecommons.org/licenses/by/4.0/>).

## 1. Introduction

The global climate is predicted to change in ways unseen in recorded history [1,2]. Climate predictions show that across the UK, the frequency and severity of extreme weather events will increase, sea levels will rise, summers will become warmer and drier, and winters will be warmer and wetter [1,3]. Urbanisation and the replacement of previously vegetated areas with impermeable surfaces, such as asphalt and concrete, reduces the lag times of overland flow and increases peak flows to receiving watercourses; the magnitude of this will increase as a result of climate change [4–8]. Conventional methods of flood management prioritise moving flood waters downstream as quickly as possible [5,9]; however, the recent increase in flood frequency has led to increased investigations into more sustainable methods of managing flood risk, namely, Natural Flood Management (NFM) methods [5,10,11].

NFM methods aim to replicate pre-development catchment hydrology and encourage infiltration, interception, and evapo(transpi)ration, with the aim of storing and slowing precipitation before reaching the receiving watercourse [4,12,13]. Common examples include vegetation planting to increase infiltration and interception (and subsequent evapotranspiration), reducing soil compaction by changing farming and animal grazing routines, and ‘roughening’ and obstructing watercourse channels and overland flow pathways to slow the flow of water downstream during high-rainfall events [14–17]. Tree planting is often considered a valuable method of NFM as tree roots can enhance soil macroporosity, connect flow pathways, reduce compaction, and improve soil structure, which increases infiltration and water storage capacity [18–23]. The value of tree planting has been acknowledged by the UK Government, who have allocated GBP 4 million to organizations aiming to increase UK woodland coverage; and GBP 1.4 million to the Environment Agency

(England) for the same purpose [24]. Additionally, Government grants have been introduced to encourage farmers to convert arable land to woodland via the 'Woodland for Water' scheme, run in coalition with the Environment Agency and the Forestry Commission [25]. Furthermore, the UK Government have pledged to plant 30,000 ha of trees per year until 2024 (the end of the current Government), which highlights their acknowledgement of the benefits of tree planting [26].

However, regardless of funding allocations and the increased investment in tree planting, few studies have assessed the impacts of tree planting on infiltration, and contextualised this with regard to flood risk mitigation and the use of tree planting as a method of NFM [3,27–31]. Therefore, the aim of this study is to investigate the impacts of tree planting on infiltration dependent on tree maturity and tree proximity.

This work is the precursor to another study previously conducted by the same authors [31], which focused on the hydrological modelling of the collected infiltration data (used for this work and listed in Section 3) and the analysis and variations in peak flow and total discharge from the study site as a result of changing land cover. Therefore, the same sample site and infiltration data collection methods (presented in Section 2) are used in both studies. However, this study focuses solely on the variations in infiltration data, and the influence of tree proximity and tree maturity on infiltration—in addition to undertaking statistical testing on such data. Developing an understanding of the influences of tree planting on infiltration, and contextualising these findings in the context of the wider implementation of NFM and existing policy, will aid in the justification and subsequent uptake of NFM methods [15,32]. This will allow for enhanced flood risk reduction both at present, and in the future, considering the predicted impacts of climate change and continued urbanisation [1,3–5].

## **2. Materials and Methods**

### *2.1. The Heart of England Forest*

The Heart of England (HofE) Forest charity have planted 1,883,928 trees across 2,832 hectares of Warwickshire and Worcestershire, England. The charity aim to eventually plant and maintain 12,140 hectares of forest across the English Midlands for the benefit CO<sub>2</sub> mitigation, public amenity, habitat creation, wildlife, and biodiversity [33]. The HofE forest began planting trees across the study site in 2006, and continued annually until 2012, when the trees were left to grow with very little human interference. The HofE forest plant saplings in line with National Vegetation Classification (NVC) guidelines [34,35] to ensure that newly forested areas correspond with exiting native species for the area, defined as 'mature lowland broadleaved woodland'.

### *2.2. Sample Area and Infiltration Data Collection*

The study site is a 2.2 km<sup>2</sup> area in Warwickshire, UK (52.1511° N, 1.5139° W), owned by the HofE forest, and was defined by generating a watershed boundary using a 1 m digital terrain model of the area [36] (Figure 1). Infiltration data were collected every other week from specific sample trees planted in 2006 (*Betula pendula*), 2008 (*Populus tremula*), 2010 (*Betula pendula*) and 2012 (*Populus tremula*). In addition, infiltration data were collected from a plot of pre-existing woodland planted in *ca.*1900 (*Quercus petraea*), and a grassland control site. The data collected from the grassland control were used in comparison with the wooded areas, and the samples taken from the *ca.*1900 area provided information regarding the infiltration characteristics of mature trees and were used for comparison. Figure 1 shows the locations of the infiltration sample plots and sampling locations.

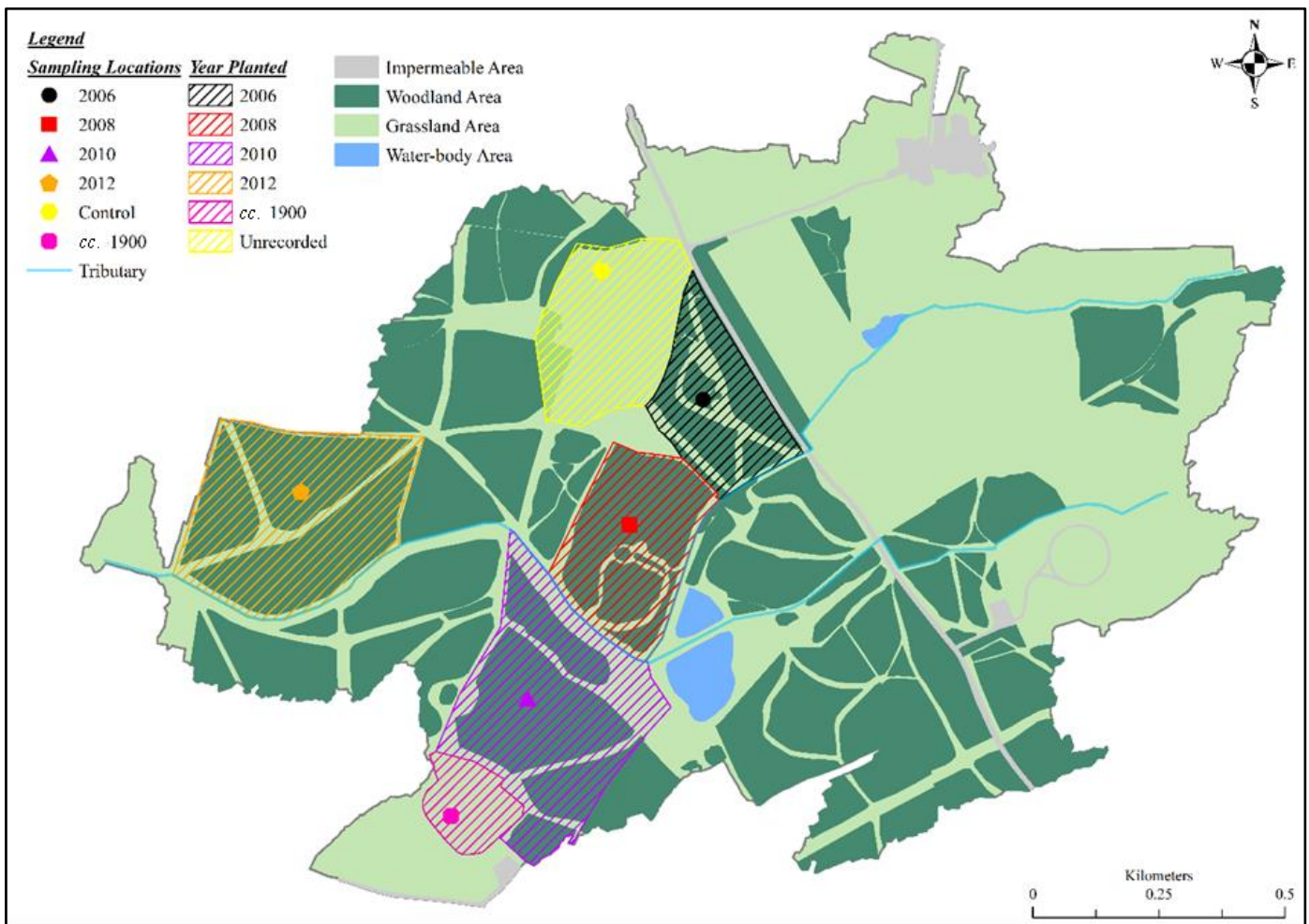


**Figure 1.** Sample sites and sampling locations with land cover highlighted [37]. Data is reproduced under the open government license.

As this study aims to determine the variation in infiltration dependent on proximity, infiltration measurements were taken from 10 cm and 200 cm away from the base of the sample trees. The 10 cm proximity was as close as any measurement instrument could get to the base of the tree without interference from the root system or growths around the base. The 200 cm proximity was defined using literature specific to the tree species sampled throughout the fieldwork [38–40], suggesting that the lateral root spread of all trees would surpass the 200 cm measuring distance by the time the tree matured. The 200 cm proximity would also act as a comparison for the 10 cm proximity, allowing for the influence of tree proximity on infiltration to be delineated.

The Mini Disk Infiltrometer (MDI) was chosen for infiltration data collection due to its portability, low water usage (in comparison to ring-infiltrometer methods), replicability, ease of individual operation, and durability [41–43]. Relevant literature indicates that the tension setting of the MDI is altered from study to study [41,44–46]; therefore, a tension setting of 2 cm was selected following the suggestion of the MDI user manual [47]. It is acknowledged that recent advancements in infiltration models are inclusive of plant-root water uptake such as the Feddes reduction function [48], the compensated non-linear uptake model [49], and methods involving Python [50]. However, this work utilised the infiltration-time model due to the study scope outlining the influence of tree roots on soil porosity and subsequent infiltration as the primary focus (see Section 1).

It is well regarded in the literature that field infiltration measurements inherit high spatial variability, and that replication is imperative for attaining accurate results [51–53]. Therefore, every MDI measurement was replicated twice (in addition to the first measurement) and all replicates were averaged to give a mean average total for that site. As the MDI required a watertight seal with the sample soil, vegetation was removed from the surface of the soil before infiltration measurement proceeded. Figures 2a and 2b show the method by which infiltration measurements were taken in proximity to the tree.

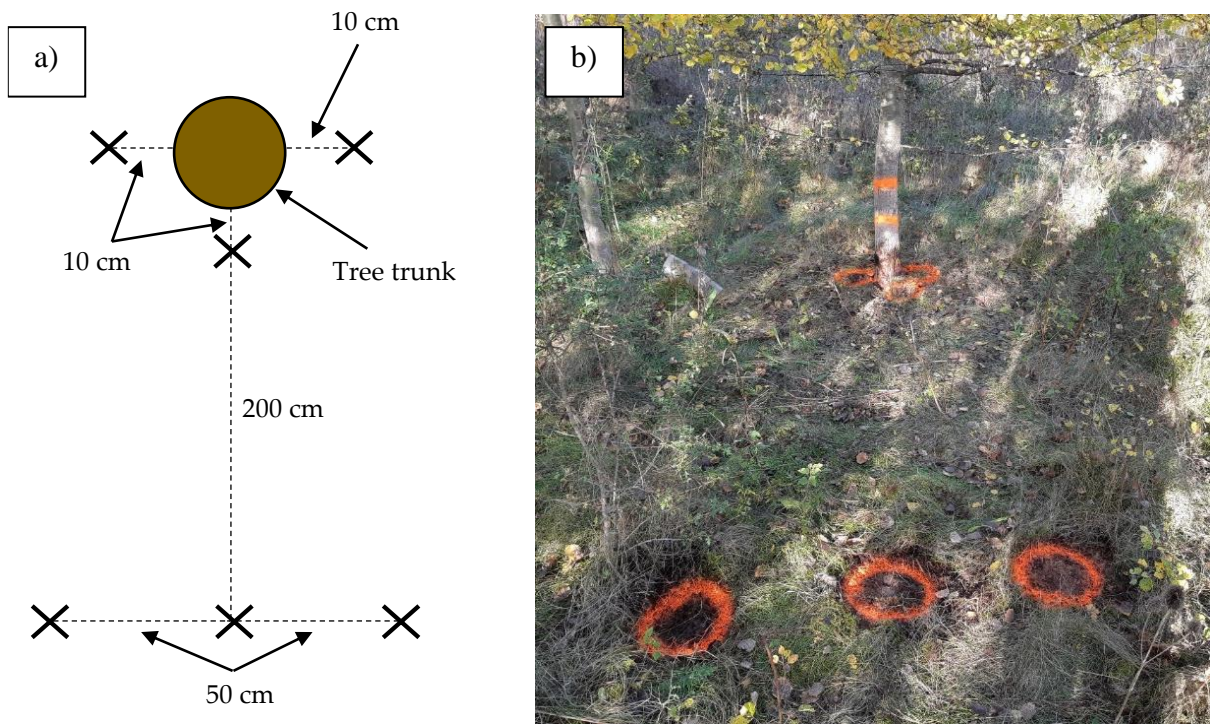


**Figure 2.** (a) Diagram of MDI measurement location in proximity to the sample tree. Black crosses (X) indicate MDI measurement location. (b) MDI measurement locations represented at the 2008 sample site.

The 10 cm datums were identified, and a line was measured from the base of the tree in the direction of least obstruction (i.e., no other trees, undergrowth, or shrubbery intruding the area) to mark the location of the 200 cm measurement locations; 50 cm was measured either side of the line to identify replica locations. Replication could not take place in the exact same location as the initial infiltration measurement, as any measurements would be skewed due to previous saturation of the soil; so, 50 cm was chosen to avoid lateral seepage (leading to the overestimation of infiltration values) [54–56]. The control site measurements were collected in a triangular pattern, with each replication being 50 cm from the last to avoid lateral seepage (Figures 3a and 3b).

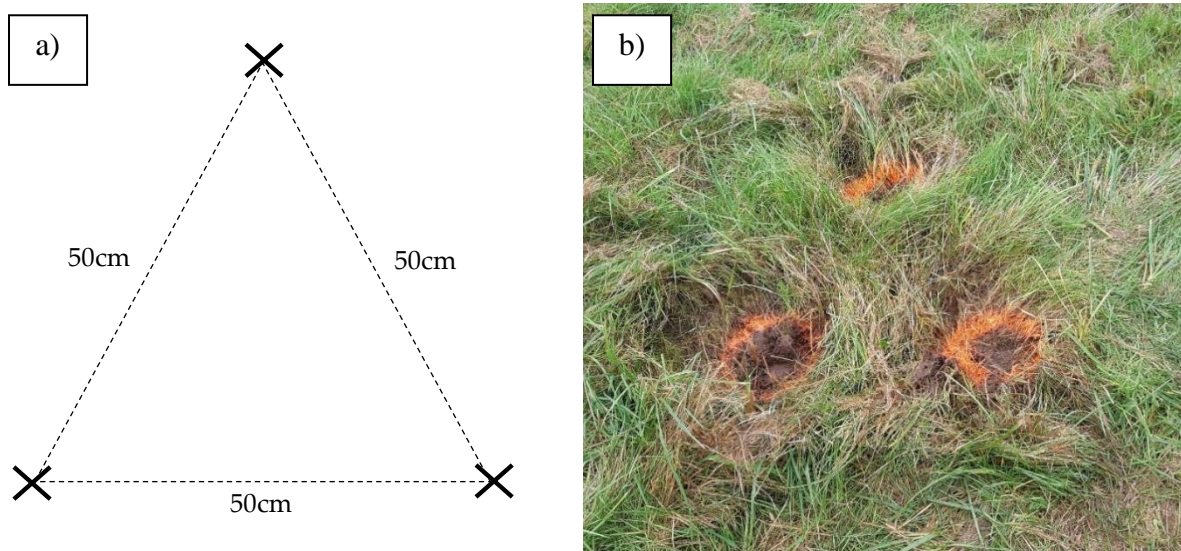


**Figure 3.** (a) Diagram of MDI measurement locations at the controls sample site. Black crosses (X) indicate MDI measurement location. (b) MDI measurement locations represented at the control sample site.

A total of 1287 individual infiltration measurements were collected from November 2019–August 2021; 702 from the 10 cm proximity (including the grassland control), and 585 from the 200 cm proximity. Infiltration data was not collected from March 2020 to July 2020 due to the UK national COVID-19 lockdown.

### 2.3. Soil Texture Analysis and Seasonal Variation

Soil texture influences infiltration characteristics (rate, capacity) [43,57,58]. To understand the influence that varying soil textures across the study site may have on the collected infiltration data, soil samples were extracted from the surface (~5 cm depth) of the soil surrounding the area of MDI measurement using a trowel. A LaMotte [59] soil texture test kit was used to determine the percentiles of sand, silt, and clay for each infiltration sample-area soil, and this information was compared against the UK soil texture triangle to determine the classification name of each sample soil. The percentiles and soil texture classifications of the sample area are shown in Table 1.

**Table 1.** Soil percentiles and texture classification of each sample site.

Sample Site	Sand %	Silt %	Clay %	UK Soil Classification	
Control	53	20	27	SaCL	Sandy clay loam
ca. 1900	47	40	13	SSL	Sandy silt loam
2006	20	20	60	C	Clay
2008	13	20	67	C	Clay
2010	53	33	14	SaL	Sandy Loam
2012	33	13	54	C	Clay

The 2006, 2008, and 2012 sites are comprised of a clay-heavy soil texture, meaning that they are naturally less permeable compared to other soil textures [55]. The grassland control, ca. 1900 and 2010 sites are comprised of a sandier soil texture, indicating that these areas are more permeable compared with other soil textures [55,60]. Due to the varying soil texture, the study site varied hydrologically between summer and winter—particularly across the clay-heavy soils. Throughout the summer, the clay-heavy soils began to crack, creating macropores; this is the opposite to winter, where the soil was bare and often completely saturated due to the inability of infiltration to take place (see Figure 4).



**Figure 4.** (a,b) saturation of the 2006 sample site throughout winter, (c,d) cracking of the 2006 and 2008 sample sites throughout summer.

These changes influenced the collected infiltration data and as such, it was decided that the collected infiltration data would be separated to represent soil conditions across the site in both wet and dry periods. This approach also allowed for the trends in infiltration change as a result of changing proximity to be compared through winter and summer, allowing an in-depth analysis of the influence of tree planting on infiltration seasonally across the site. Metrologically, December, January, and February are defined as winter, and June, July, and August are defined as summer by the UK met office [61,62]. However, as this collected data is the precursor to the development of a hydrological model (see Revell et al., (2021)); winter is defined as October to March, and summer is defined as April to September. These timeframes are based on UK average annual temperature and rainfall data, provided by the Met Office [63].

### **3. Results**

#### *3.1. Tree Proximity and Infiltration*

Table 2 shows the average infiltration values for each sample site throughout winter and summer 2019/20 and 2020/21.

**Table 2.** Average infiltration for 10 and 200 cm proximities throughout both winter and summer sample periods.

	Winter (ml)						Averages
	Control	ca. 1900	2006	2008	2010	2012	
2019/20 10 cm	3.4	9.96	0.67	7.04	4.85	3.07	5.42
2020/21 10 cm		5.64	2.17	1.98	2.80	2.31	2.80
10 cm average		7.80	1.42	4.51	3.83	2.69	4.11
2019/20 200 cm		4.22	0.37	2.56	4.70	2.30	3.16
2020/21 200 cm		3.78	0.83	1.36	1.50	1.69	1.51
200 cm average		4.00	0.60	1.96	3.10	2.00	2.34
Summer (ml)							
2019/20 10 cm	12.35	20.81	14.62	17.95	17.62	18.14	17.19
2020/21 10 cm		11.54	5.06	5.85	9.73	6.70	6.83
10 cm average		16.18	9.84	11.90	13.68	12.42	12.01
2019/20 200 cm		11.38	9.48	16.14	15.19	14.90	14.14
2020/21 200 cm		9.21	3.27	4.45	6.45	4.94	5.04
200 cm average		10.30	6.38	10.30	10.82	9.92	9.60

Mean 10 cm and 200 cm infiltration was 192% and 310% higher in summer compared with winter. In winter, the mean 10 cm infiltration was 75.87% higher than the mean 200 cm infiltration over both sample years; in summer, the mean 10 cm infiltration was 25.19% higher than 200 cm over both years. Throughout winter 2019/20, the mean 10 cm infiltration was 71.38% higher than the 200 cm proximity; in winter 2020/21, the infiltration at 10 cm was on average 85.26% higher than the infiltration at 200 cm across all sites. Summer 2019/20 showed the mean 10 cm infiltration to be 21.55% higher than the 200 cm infiltration, and the mean 10 cm infiltration data was 35.48% higher than the 200 cm proximity values throughout 2020/21. These results show that infiltration varies more between the 10 and 200 cm proximities in winter (71.38% and 85.26% for 2019/20 and 2020/20, respectively) compared with summer; however, the summer 10 cm infiltration was still higher than the 200 cm by 21.55% and 35.48% (in 2019/20 and 2020/21, respectively).

### 3.2. Tree Maturity and Infiltration

It would be expected that the discrepancy between infiltration at the 10 cm and 200 cm proximity would become greater as tree roots develop, break up the surrounding soil matrix, reduce compaction, and increase porosity [20,21,64,65]. Considering this, it would be expected that the most recently planted HofE trees would show a lower mean infiltration at both proximities compared with older trees across the site; however, this is not the case at the study site. Table 3 shows the two-year mean infiltration of each sample site in winter and summer at both measured proximities, sorted in ascending order.

**Table 3.** Sample sites in ascending order based on mean infiltration in winter and summer at both 10 and 200 cm proximity.

Winter 10 cm	ca. 1900	2008	2010	2012	2006
	7.8	4.51	3.83	2.69	1.42
Summer 10 cm	ca. 1900	2010	2012	2008	2006
	16.18	13.68	12.42	11.9	9.01
Winter 200 cm	ca. 1900	2010	2012	2008	2006
	4	3.1	2	1.96	0.6
Summer 200 cm	2010	ca. 1900	2008	2012	2006
	10.82	10.3	10.3	9.92	6.38

Table 3 shows that, aside from the 2006 site, which consistently showed the lowest mean infiltration regardless of season or proximity, the sorted mean infiltration data did not follow the expected chronological order. The ca. 1900 site showed the highest mean infiltration for winter (10 and 200 cm) and for summer at 10 cm; however, it was displaced by 2010 at the summer 200 cm proximity. There was no obvious trend between the highest and lowest infiltration values, with no consistent chronology, as would be expected based on the existing literature [20,21,64,65].

*Statistical Analysis: Mann–Whitney Testing*

To further test for trends and relationships across the collected infiltration data, statistical analysis was undertaken. Conducting a Kolmogorov–Smirnov test found the collected data to be non-parametric [66]; therefore, Mann–Whitney tests were undertaken [66–68]. The Mann–Whitney test is the non-parametric equivalent of the independent samples t-test, and is used to deliver a  $p$ -value indicating to what extent two sets of sample data are statistically significant. Both  $U_1$  and  $U_2$  (EQ's 1 and 2) can be interpreted as the number of observations in a sample that precede or follow observations in the other sample when all samples are ranked in ascending order [69]:

$$U_1 = n_1 n_2 + \frac{n_1(n_1 + 1)}{2} - R_1 \quad (1)$$

$$U_2 = n_1 n_2 + \frac{n_2(n_2 + 1)}{2} - R_2 \quad (2)$$

where  $n_1$  and  $n_2$  are the number of samples in group 1 and 2, respectively, and  $R_1$  and  $R_2$  are the sum of all ranks from the data in groups 1 and 2, respectively. To determine significance ( $p$ ), the normal approximation equation [70] can be used:

$$P = \frac{\left| U_{min} - \frac{n_1 n_2}{2} \right|}{\sqrt{\frac{n_1 n_2 (n_1 n_2 + 1)}{12}}} \quad (3)$$

where  $U_{min}$  is the smallest U value. The Mann–Whitney tests would indicate if there was a significant difference in infiltration between the 10 cm and 200 cm proximities—initially for all winter/summer data, then on a site-by-site basis. If  $p \leq 0.05$ , then there is a significant difference between the measured variables; if  $p > 0.05$ , then there is not a significant difference between the two measured variables. The results of the Mann–Whitney test are shown in Table 4.

**Table 4.** Test criteria, *p* values and significance levels of Mann–Whitney testing.

Test Criteria	<i>p</i> -Value
All 10 cm vs. 200 cm	<0.1
All winter 10 cm vs. 200 cm	<0.1
All summer 10 cm vs. 200 cm	0.02
<i>ca.</i> 1900 10 cm vs. 200 cm winter	0.03
2006 10 cm vs. 200 cm winter	0.02
2008 10 cm vs. 200 cm winter	0.15
2010 10 cm vs. 200 cm winter	0.23
2012 10 cm vs. 200 cm winter	0.07
<i>ca.</i> 1900 10 cm vs. 200 cm summer	0.26
2006 10 cm vs. 200 cm summer	0.07
2008 10 cm vs. 200 cm summer	0.08
2010 10 cm vs. 200 cm summer	0.17
2012 10 cm vs. 200 cm summer	0.17

Table 4 shows that overall, there was a significant difference between the mean infiltration data at the 10 cm tree proximity and the 200 cm tree proximity in both winter and summer. However, whilst the overall trends from the proximity infiltration data showed a significant difference between the 10 cm and 200 cm proximities, this trend was infrequently seen at each individual sample site. In winter, the only sites to show a *p*-value  $\leq 0.05$  were *ca.* 1900 and 2006; in summer, no sites showed a significant difference between the 10 cm and 200 cm infiltration data. Whilst only a few values were below the significance threshold (0.05), the *p*-values can still be used as an indication of how tree maturity may be influencing infiltration across the study site. As discussed, it would be expected that the more recently planted trees would show less discrepancy between infiltration at both proximities, and older planted trees would show more discrepancy. The difference between the sample site *p*-values (representative of the difference between 10 cm and 200 cm infiltration) are shown in Table 5.

**Table 5.** Sample sites sorted in ascending order of the relationship between infiltration difference between 10 cm and 200 cm for winter and summer.

Winter	<i>p</i> -Value	Summer	<i>p</i> -Value
2006	0.02	2006	0.07
<i>ca.</i> 1900	0.03	2008	0.08
2012	0.07	2010	0.17
2008	0.15	2012	0.17
2010	0.23	<i>ca.</i> 1900	0.26

The values in Table 5 do not follow the expected chronological increase of the 10 cm and 200 cm infiltration data, as would be expected based on existing literature; however, this trend may be due to varying soil textures, sample days, and antecedent soil saturation. Section 4 discusses and contextualises the presented results in further detail.

#### 4. Discussion

The results of the collected infiltration data show that mean infiltration was higher at the 10 cm proximity compared with the 200 cm proximity by 75.87% in winter and 25.19% in summer. Additionally, the mean 10 cm infiltration was 192% higher in summer compared with winter, and the mean 200 cm infiltration was 310% higher in summer compared with winter. There is no evidence to suggest a correlation between tree maturity and increase infiltration (Section 3.2). Infiltration was highest across both proximities at the *ca.* 1900 site, which supports literature indicating that maturity results in greater infiltration [3,18,71]; however, infiltration was lowest at the 2006 site (the oldest HofE trees), which would be expected to demonstrate the second-highest infiltration rate following chronology. When contextualizing the results of this study, it is important to consider tree maturity, current planting mentality, and antecedent conditions, which are discussed throughout this section.

##### 4.1. Infiltration and Tree Proximity

The results presented throughout Section 3 indicate that the presence of the tree, and particularly the developing root system, influences infiltration by increasing soil porosity,

allowing for soil-water storage and faster infiltration [18,20,58]. Mean infiltration was higher at the 10 cm proximity compared with the 200 cm proximity by 75.87% in winter and 25.19% in summer. It was discussed in Section 1 that tree roots connect flow pathways, reduce compaction, influence porosity, and change soil structure [18–23], and the results of this study support this. Further to this, Section 3.1 highlights the variance between winter and summer infiltration values, showing mean infiltration to be 235% higher in summer compared with winter, and summer 10 cm and 200 cm infiltration being 180% and 290% higher than winter values, respectively. This adds further evidence in support of tree planting, as results show that trees are capable of increasing infiltration at the 10 cm proximity throughout summer and winter, regardless of the naturally low permeability of the sample site soil (Table 1). These results contribute to the knowledge gap regarding both infiltration and proximity, as well as seasonal variations in infiltration, and indicate that tree planting is valuable as a method of NFM.

#### 4.2. Infiltration and Tree Maturity

Regarding the influence of tree maturity on infiltration, there is no evidence to suggest a correlation between tree maturity and increased infiltration at either proximity over time, which has been identified through use of the Mann–Whitney testing presented throughout Section 3. Whilst this finding does predominantly dispute what has been identified regarding tree maturity in the literature [3,71,72], it is important to consider these results in the context of the current ages of sampled trees. Aside from the *ca.*1900 site, the oldest trees sampled were planted in 2006 and the youngest in 2020. Thus, the 2006 woodland had only been in-situ for 15 years, and the 2012 woodland for 9 years (at the time of analysis). The maturity ages of the sampled tree species were discussed in Section 2.2, concluding that birch and aspen trees can live for 100–120 years, reaching their final heights (where infiltration will be at a maximum) at 60 and 30 years, respectively [38–40]. Considering this, the sample trees are still early in their development and the maturity-relationship presented throughout Section 3 are only representative of the beginning of the likely effects that the trees will have on infiltration. Whilst there are no obvious trends between infiltration and maturity, Tables 2 and 3 show that the *ca.*1900 sample site demonstrated the highest infiltration at the 200 cm proximity in the winter, and the 10 cm proximity in both winter and summer. This supports the existing literature regarding infiltration and maturity [18,28,73,74]. According to chronology, and based on the existing literature, it would be expected that the 2006 site would demonstrate the next highest infiltration (after *ca.* 1900); however, this was not the case. Table 3 shows the 2006 site to consistently show the lowest infiltration at both proximities, regardless of seasonality. Referring back to the age of trees planted at the site, particularly in comparison to their discussed maturity age and lifespan, this study has focused primarily on young trees (15 to 1 year old). The results of the infiltration data analysis have highlighted that very mature trees (*ca.*1900) promote high infiltration, which is an insight into what could potentially be expected from the HofE planted trees across the site.

#### 4.3. Antecedent Conditions

The results regarding tree proximity, maturity, and infiltration can be further contextualised when considering the influence of soil texture across the study site [23,60]. Seen in Table 1, the 2006, 2008, and 2012 sites are clay-textured, meaning they are less permeable compared with the control, *ca.*1900 and 2010 sites [75,76]. Antecedent moisture, compounded by the less permeable clay-texture, often resulted in surface water pooling during and after rainfall at the aforementioned sites. Infiltration data could not be collected (although it was always attempted) during surface pooling, and it is this phenomenon that may account for the recorded low permeability. Surface pooling was also exaggerated by the winter of 2020 being the fifth wettest on record (329.4 mm/143% higher than the 1981–2010 baseline), and the February of 2020 being the wettest ever recorded, with 155 mm of precipitation (258% higher than the 1981–2010 baseline) [77,78]. It is important to acknowledge the effect that soil texture and moisture may have had on the collected results. However, this study shows that tree planting still increased infiltration at the 10 cm proximity compared with the 200 cm proximity, which is a valuable contribution to the current knowledge regarding the impacts of tree planting on infiltration, and their potential use as a method of NFM.

#### 4.4. Trees and Construction

While this study has demonstrated that there is not a correlation between tree maturity and infiltration at both near and far proximities across the site, it is displayed in Tables 2 and

3 that the *ca.* 1900 sample site showed the highest infiltration at the 200 cm proximity in the winter, and the 10 cm proximity in both winter and summer. This finding is notable when considering the way in which woodland areas are currently managed regarding the felling and (less frequent) translocation of trees to make way for impermeable developments [3,18,79]. Urbanisation can often involve the removal of mature(ing) trees, and this study has shown that trees increase the nearby soil porosity and infiltration rate; so, the removal of established woodlands can alter the hydrology of an area [3,18,30,80]. Aside from the demonstrated improvements to soil porosity and infiltration (Section 3), trees are also proven to contribute to increased interception. Quantifying interception is difficult due to the need for specialised equipment or continuous monitoring [81–83]. However, it is suggested that broadleaf interception loss as a percentage of total precipitation is estimated to be between 10–34% (mean 24.25%) [84,85]. As a comparison, interception loss for grassland is negligible, being <1% [16,86]. In addition to the hydrological implications of mature woodland removal and translocation, it is widely acknowledged that woodlands capture and store significant volumes of CO<sub>2</sub> [72,87,88], and the value of woodland carbon sequestration has been identified by the UK Government as key to aiding in achieving net zero carbon emissions [26]. Furthermore, established woodlands are beneficial from the perspectives of habitat creation and protection [89] and public amenity [16]. Apparent from the benefits of established woodland areas, is that the removal and replacement of mature woodland is mostly detrimental to the surrounding area. Whilst the influences of woodland removal are sometimes ‘balanced out’ by planting saplings in alternate locations, the newly planted saplings will not have a comparable moderating impact on flood risk (and habitats and amenity) compared with the felled mature trees, as has been demonstrated throughout Section 3 [30,75,90].

#### 4.5. Study Applications

The results of this study have shown that trees (and subsequently woodland) are valuable as a method of NFM as they can increase infiltration at close proximities, and become more capable of doing so with increased maturity; this in addition to the associated benefits regarding carbon sequestration, biodiversity, habitat creation, and public amenity. Referred to in Section 2.3, the HofE site is predominantly clay-textured, which is known to demonstrate low permeability and infiltration [55,60]. This therefore indicates that the derived results are a low-end representation of what the impacts of tree planting could be over a more permeable geology. Area calculations of superficial alluvium, clay, peat, and fluvial deposits throughout the UK show 15% (36,374.25 km<sup>2</sup>) to be similar in geology to the HofE site [91]. Therefore, 15% of the UK is likely to demonstrate similar infiltration characteristics to the results of this study (Section 3) if trees were to be planted. However, this statistic can also be interpreted to show that 85% (206,120.75 km<sup>2</sup>) of the UK is non-clay textured; indicating that the low-end results derived throughout this study will likely be increased if applied to other areas of the UK [55,89]. Infiltration may be higher, and differing trends may be identified regarding seasonality and tree maturity [20,21]. This highlights the wider applicability of the collected data, emphasising the impact of the study results and proving the applicability of the methodology to other areas across the UK. This also presents an opportunity for this research to be extrapolated and applied to other geologies and soil textures, to potentially aid in justifying the use of tree planting as a method of NFM.

It was discussed throughout Section 4.4 that removing woodland does not only disrupt the ongoing processes of infiltration and interception, but that habitats and carbon sequestration are also influenced—something which the UK Government is trying to alleviate through woodland planting [26]. This is also applicable to planting new saplings to account for the removed established trees—new saplings take time to develop the root systems necessary to influence soil porosity (as has been shown throughout this study), and saplings cannot intercept precipitation to the same extent as an established tree with a larger canopy.

### 5. Conclusions and Future Work

This study used the MDI to collect 1287 infiltration measurements from 10 cm and 200 cm away from sample trees across a clay-texture site, owned by the HofE forest, in Warwickshire, UK. The results of the study show that mean infiltration was higher at the 10 cm proximity compared with the 200 cm proximity by 75.87% in winter and 25.19% in summer, and that mean infiltration was 180% and 290% higher in summer compared with winter at the 10 cm and 200 cm proximities, respectively. There is little evidence to show a relationship between tree maturity and infiltration; however, the sample trees were still early

in their development, and it is likely that infiltration will increase as the root systems of the trees develop [18–23].

The conclusions show that tree planting increases infiltration, even over less-permeable soil textures (see Section 2.3); therefore, is valuable as a method of NFM. The findings of this study also have connotations regarding the way in which woodlands are currently managed, with particular reference to development, construction, and forestry. Trees should be left in-situ wherever possible, and allowed to mature to achieve their maximum infiltration potential. Tree planting is not only beneficial to flood risk management, as Section 4.3 indicates that further benefits include carbon sequestration, public amenity, and habitat creation and preservation. It has been discussed in the literature [30] that published research and case studies reporting the results of long-term woodland infiltration studies are scarce. Shorter-term tree planting and infiltration studies have been undertaken [3,18,30,79]; however, this study has contributed to the wider understanding of the longer-term implications and relationships of tree planting and infiltration with regard to proximity and maturity.

Future work will involve developing a method for projecting the collected infiltration data, and simulating this using a hydrologic model to project the likely future hydrological response of the study site regarding precipitation and baseflow increases in light of climate change. Additionally, future studies could investigate likely variations to the study findings, with specific reference to the impact that climate change will have on woodland growth and rainfall patterns, and how this would influence the effectiveness of tree planting as a method of NFM. Furthermore, further considerations will be made regarding the incorporation of time domain reflectometry (TDR) measurements to compliment the derived infiltration data [92]; TDR instrumentation could be installed at both measurement proximities and the information interpreted to inform infiltration measurements. This would allow for a more robust interpretation of the influence of trees on infiltration characteristics dependent on maturity and proximity at greater depths [93–95].

**Author Contributions:** Conceptualization, methodology, software, validation, formal analysis, investigation, resources, data curation, writing—original draft preparation N.R.; writing—review and editing, C.L., M.R. and M.B.; visualization, N.R., M.R., C.L. and M.B.; supervision, C.L., M.R. and M.B. All authors have read and agreed to the published version of the manuscript.

**Funding:** This research received no external funding.

**Data Availability Statement:** To access the data collected and analysed in this study, please contact Nathaniel Revell (revelln@uni.coventry.ac.uk).

**Acknowledgments:** Special thanks are extended to the HofE forest, in particular Stephen Coffey, for their support and assistance throughout the data collection phase of this project.

**Conflicts of Interest:** The authors declare no conflict of interest.

## References

1. Lowe, J.A.; Bernie, D.; Bett, P.; Bricheno, L.; Brown, S.; Calvert, D.; Clark, R.; Edwards, T.; Fosser, G.; Fung, F.; et al. *UKCP18 Science Overview Report*; Met Office Hadley Centre: Exeter, UK, 2019.
2. Fowler, H.J.; Ali, H.; Allan, R.P.; Ban, N.; Barbero, R.; Berg, P.; Blenkinsop, S.; Cabi, N.S.; Chan, S.; Dale, M.; et al. Towards advancing scientific knowledge of climate change impacts on short-duration rainfall extremes. *Philos. Trans. R. Soc. A Math. Phys. Eng. Sci.* **2021**, *379*, 20190542. <https://doi.org/10.1098/rsta.2019.0542>.
3. Murphy, T.R.; Hanley, M.E.; Ellis, J.S.; Lunt, P.H. Native woodland establishment improves soil hydrological functioning in UK upland pastoral catchments. *L. Degrad. Dev.* **2021**, *32*, 1034–1045. <https://doi.org/10.1002/ldr.3762>.
4. Ellis, N.; Anderson, K.; Brazier, R. Mainstreaming natural flood management: A proposed research framework derived from a critical evaluation of current knowledge. *Prog. Phys. Geogr. Earth Environ.* **2021**, *45*, 819–841. <https://doi.org/10.1177/0309133321997299>.
5. Ferguson, C.; Fenner, R. The impact of Natural Flood Management on the performance of surface drainage systems: A case study in the Calder Valley. *J. Hydrol.* **2020**, *590*, 125354. <https://doi.org/10.1016/j.jhydrol.2020.125354>.
6. Kitsikoudis, V.; Erpicum, S.; Rubinato, M.; Shucksmith, J.D.; Archambeau, P.; Piroton, M.; Dewals, B. Exchange between drainage systems and surface flows during urban flooding: Quasi-steady and dynamic modelling in unsteady flow conditions. *J. Hydrol.* **2021**, *602*, 126628. <https://doi.org/10.1016/j.jhydrol.2021.126628>.
7. Rubinato, M.; Luo, M.; Zheng, X.; Pu, J.H.; Shao, S. *Advances in Modelling and Prediction on the Impact of Human Activities and Extreme Events on Environments*; MDPI: St. Alban-Anlage 66 4052 Basel, Switzerland, 2020; Volume 12, ISBN 9783039368020.
8. Rubinato, M.; Nichols, A.; Peng, Y.; Zhang, J.M.; Lashford, C.; Cai, Y.P.; Lin, P.Z.; Tait, S. Urban and river flooding: Comparison of flood risk management approaches in the UK and China and an assessment of future knowledge needs. *Water Sci. Eng.* **2019**, *12*, 274–283. <https://doi.org/10.1016/j.wse.2019.12.004>.

9. Palla, A.; Colli, M.; Candela, A.; Aronica, G.T.; Lanza, L.G. Pluvial flooding in urban areas: The role of surface drainage efficiency. *J. Flood Risk Manag.* **2018**, *11*, S663–S676. <https://doi.org/10.1111/jfr3.12246>.
10. Wells, J.; Labadz, J.C.; Smith, A.; Islam, M.M. Barriers to the uptake and implementation of natural flood management: A social-ecological analysis. *J. Flood Risk Manag.* **2020**, *13*, e12561. <https://doi.org/10.1111/jfr3.12561>.
11. Bosseler, B.; Salomon, M.; Schlüter, M.; Rubinato, M. Living with Urban Flooding: A Continuous Learning Process for Local Municipalities and Lessons Learnt from the 2021 Events in Germany. *Water* **2021**, *13*, 2769. <https://doi.org/10.3390/w13192769>.
12. Ferguson, C.R.; Fenner, R.A. The potential for natural flood management to maintain free discharge at urban drainage outfalls. *J. Flood Risk Manag.* **2020**, *13*, e12617. <https://doi.org/10.1111/jfr3.12617>.
13. Shuttleworth, E.L.; Evans, M.G.; Pilkington, M.; Spencer, T.; Walker, J.; Milledge, D.; Allott, T.E.H. Restoration of blanket peat moorland delays stormflow from hillslopes and reduces peak discharge. *J. Hydrol. X* **2019**, *2*, 100006. <https://doi.org/10.1016/j.hydroa.2018.100006>.
14. Dadson, S.J.; Hall, J.W.; Murgatroyd, A.; Acreman, M.; Bates, P.; Beven, K.; Heathwaite, L.; Holden, J.; Holman, I.P.; Lane, S.N.; et al. A restatement of the natural science evidence concerning catchment-based 'natural' flood management in the UK. *R. Soc. Publ.* **2017**, *473*, 20160706. <https://doi.org/10.1098/rspa.2016.0706>.
15. Burgess-Gamble, L.; Ngai, R.; Wilkinson, M.; Nisbet, T.; Pontee, N.; Harvey, R.; Kipling, K.; Addy, S.; Rose, S.; Maslen, S.; et al. *Working with Natural Processes – Evidence Directory*; Environment Agency, Horizon House, Deanery Road, Bristol, UK, 2018.
16. Ngai, R.; Wilkinson, M.; Nisbet, T.; Harvey, R.; Addy, S.; Burgess-Gamble, L.; Rose, S.; Maslen, S.; Nicholson, A.; Page, T.; et al. *Working with Natural Processes-Evidence Directory Appendix 2: Literature Review*; Environment Agency, Horizon House, Deanery Road, Bristol, UK, 2017.
17. Forbes, H.; Ball, K.; McLay, F. *Natural Flood Management Handbook*; Scottish Environment Protection Agency Strathallan House Castle Business Park Stirling, 2016; ISBN 978-0-85759-024-4.
18. Chandler, K.R.; Stevens, C.J.; Binley, A.; Keith, A.M. Influence of tree species and forest land use on soil hydraulic conductivity and implications for surface runoff generation. *Geoderma* **2018**, *310*, 120–127. <https://doi.org/10.1016/j.geoderma.2017.08.011>.
19. Malik, I.; Pawlik, Ł.; Ślęzak, A.; Wistuba, M. A study of the wood anatomy of *Picea abies* roots and their role in biomechanical weathering of rock cracks. *Catena* **2019**, *173*, 264–275. <https://doi.org/10.1016/j.catena.2018.10.018>.
20. Xie, C.; Cai, S.; Yu, B.; Yan, L.; Liang, A.; Che, S. The effects of tree root density on water infiltration in urban soil based on a Ground Penetrating Radar in Shanghai, China. *Urban For. Urban Green.* **2020**, *50*, 126648. <https://doi.org/10.1016/j.ufug.2020.126648>.
21. Zhang, D.; Wang, Z.; Guo, Q.; Lian, J.; Chen, L. Increase and Spatial Variation in Soil Infiltration Rates Associated with Fibrous and Tap Tree Roots. *Water* **2019**, *11*, 1700. <https://doi.org/10.3390/w11081700>.
22. Guo, F.X.; Wang, Y.P.; Hou, T.T.; Zhang, L.S.; Mu, Y.; Wu, F.Y. Variation of soil moisture and fine roots distribution adopts rainwater collection, infiltration promoting and soil anti-seepage system (RCIP-SA) in hilly apple orchard on the Loess Plateau of China. *Agric. Water Manag.* **2021**, *244*, 106573. <https://doi.org/10.1016/j.agwat.2020.106573>.
23. Leung, A.K.; Boldrin, D.; Liang, T.; Wu, Z.Y.; Kamchoom, V.; Bengough, A.G. Plant age effects on soil infiltration rate during early plant establishment. *Geotechnique* **2018**, *68*, 646–652. <https://doi.org/10.1680/jgeot.17.T.037>.
24. GOV.UK £3.9 Million to Drive Innovative Tree Planting. Available online: <https://www.gov.uk/government/news/39-million-to-drive-innovative-tree-planting> (accessed on 13 July 2021).
25. GOV.UK; Environment Agency. Forestry Commission Reduce Flood Risk with the Woodland for Water Scheme. Available online: <https://www.gov.uk/government/news/reduce-flood-risk-with-the-woodlands-for-water-scheme> (accessed on 27 October 2021).
26. UK Government. *The England Trees Action Plan 2021–2024*; APS Group: Defra, Seacole Building, 2 Marsham Street, London, UK, 2021.
27. Waylen, K.A.; Holstead, K.L.; Colley, K.; Hopkins, J. Challenges to enabling and implementing Natural Flood Management in Scotland. *J. Flood Risk Manag.* **2018**, *11*, S1078–S1089. <https://doi.org/10.1111/jfr3.12301>.
28. Xiao, L.; Robinson, M.; O'Connor, M. Woodland's role in natural flood management: Evidence from catchment studies in Britain and Ireland. *Sci. Total Environ.* **2021**, *813*, 151877. <https://doi.org/10.1016/j.scitotenv.2021.151877>.
29. Kay, A.L.; Old, G.H.; Bell, V.A.; Davies, H.N.; Trill, E.J. An assessment of the potential for natural flood management to offset climate change impacts. *Environ. Res. Lett.* **2019**, *14*, 044017. <https://doi.org/10.1088/1748-9326/aafdb>.
30. Cooper, M.M.D.; Patil, S.D.; Nisbet, T.R.; Thomas, H.; Smith, A.R.; McDonald, M.A. Role of forested land for natural flood management in the UK: A review. *Wiley Interdiscip. Rev. Water* **2021**, *8*, e1541. <https://doi.org/10.1002/wat2.1541>.
31. Revell, N.; Lashford, C.; Blackett, M.; Rubinato, M. Modelling the Hydrological Effects of Woodland Planting on Infiltration and Peak Discharge Using HEC-HMS. *Water* **2021**, *13*, 3039. <https://doi.org/10.3390/w13213039>.
32. McLean, L.; Beever, L.; Pender, G.; Haynes, H.; Wilkinson, M. Natural Flood Management in the UK: Developing a Conceptual Management Tool. In Proceedings of the 35th IAHR World Congress, Chengdu, China, 8–13 September 2013; p. 12. <https://doi.org/10.1039/a800340h>.
33. The Heart of England Forest Charity The Heart of England Forest. Available online: <https://www.heartofenglandforest.com/> (accessed on 13 March 2019).
34. JNCC. *National Vegetation Classification – Ten Years Experience Using the Woodland Section*; Goldberg, E., Ed.; JNCC: Monkstone House, City Road, Peterborough, 2003.
35. Rodwell, J.S. *National Vegetation Classification : Users Handbook*; JNCC: Monkstone House, City Road, Peterborough 2006.
36. Environment Agency LIDAR Composite 1 m DTM. Available online: <https://environment.data.gov.uk/DefraDataDownload/?Mode=survey> (accessed on 13 October 2018).
37. Ordnance Survey OS VectorMap District. Available online: <https://osdatahub.os.uk/downloads/open/VectorMapDistrict> (accessed on 14 December 2021).
38. Perry, T.O. Tree Roots : Facts and Fallacies. *J. Arboric.* **1982**, *8*, 197–211.
39. Mauer, O.; Palátová, E. The role of root system in silver birch (*Betula pendula* Roth) dieback in the air-polluted area of Krušné hory Mts. *J. For. Sci.* **2003**, *49*, 191–199. <https://doi.org/10.17221/4693-jfs>.

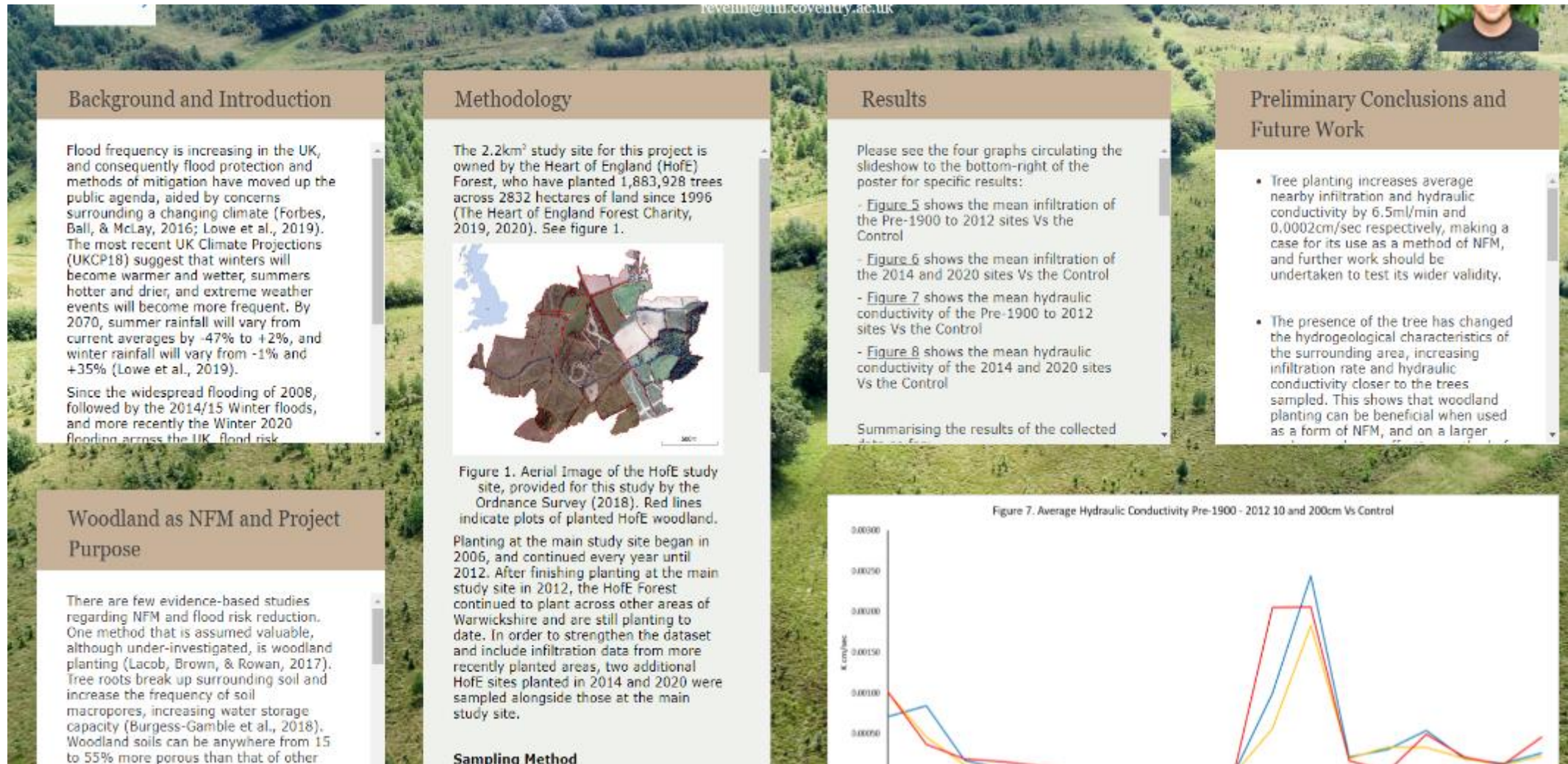
40. Hepner, H.; Lutter, R.; Tullus, A.; Kanal, A.; Tullus, T.; Tullus, H. Effect of Early Thinning Treatments on Above-Ground Growth, Biomass Production, Leaf Area Index and Leaf Growth Efficiency in a Hybrid Aspen Coppice Stand. *Bioenergy Res.* **2020**, *13*, 197–209. <https://doi.org/10.1007/s12155-020-10111-0>.
41. Robichaud, P.R.; Lewis, S.A.; Ashmun, L.E. New procedure for sampling infiltration to assess post-fire soil water repellency. *USDA For. Serv.-Res. Note RMRS-RN* **2008**, *14*, 33.
42. Naik, A.P.; Ghosh, B.; Pekkat, S. Estimating soil hydraulic properties using mini disk infiltrometer. *ISH J. Hydraul. Eng.* **2019**, *25*, 62–70. <https://doi.org/10.1080/09715010.2018.1471363>.
43. Bátková, K.; Miháliková, M.; Matula, S. Hydraulic properties of a cultivated soil in temperate continental climate determined by mini disk infiltrometer. *Water* **2020**, *12*, 843. <https://doi.org/10.3390/w12030843>.
44. Nestingen, R.; Asleson, B.C.; Gulliver, J.S.; Hozalski, R.M.; Nieber, J.L. Laboratory Comparison of Field Infiltrometers. *J. Sustain. Water Built Environ.* **2018**, *4*, 04018005. <https://doi.org/10.1061/JSWBAY.0000857>.
45. Fatehnia, M.; Tawfiq, K.; Ye, M. Estimation of saturated hydraulic conductivity from double-ring infiltrometer measurements. *Eur. J. Soil Sci.* **2016**, *67*, 135–147. <https://doi.org/10.1111/ejss.12322>.
46. Matula, S.; Miháliková, M.; Lufinková, J.; Bátková, K. The role of the initial soil water content in the determination of unsaturated soil hydraulic conductivity using a tension infiltrometer. *Plant Soil Environ.* **2015**, *62*, 515–521. <https://doi.org/10.17221/527/2015-PSE>.
47. METER Group Inc. *Mini Disk Infiltrometer User's Manual*; METER Group, Inc. USA: 2365 NE Hopkins Court, Pullman, 2020.
48. de Melo, M.L.A.; de Jong van Lier, Q. Revisiting the Feddes reduction function for modeling root water uptake and crop transpiration. *J. Hydrol.* **2021**, *603*, 126952. <https://doi.org/10.1016/j.jhydrol.2021.126952>.
49. Sonkar, I.; Sudesan, S.; Suryanarayana Rao Kotnoor, H.P. Compensated non-linear root water uptake model and identification of soil hydraulic and root water uptake parameters. *Irrig. Drain.* **2022**, *71*, 157–174. <https://doi.org/10.1002/ird.2636>.
50. Difonzo, F.V.; Masciopinto, C.; Vurro, M.; Berardi, M. Shooting the Numerical Solution of Moisture Flow Equation with Root Water Uptake Models: A Python Tool. *Water Resour. Manag.* **2021**, *35*, 2553–2567. <https://doi.org/10.1007/s11269-021-02850-2>.
51. Logsdon, S.D.; Jaynes, D.B. Spatial variability of hydraulic conductivity in a cultivated field at different times. *Soil Sci. Soc. Am. J.* **1996**, *60*, 703–709.
52. Prieksat, M.A.; Kaspar, T.C.; Ankeny, M.D. Positional and temporal changes in ponded infiltration in a corn field. *Soil Sci. Soc. Am. J.* **1994**, *58*, 181–184.
53. Khodaverdiloo, H.; Khani Cheraghbdal, H.; Bagarello, V.; Iovino, M.; Asgarzadeh, H.; Ghorbani Dashtaki, S. Ring diameter effects on determination of field-saturated hydraulic conductivity of different loam soils. *Geoderma* **2017**, *303*, 60–69. <https://doi.org/10.1016/j.geoderma.2017.04.031>.
54. Rönnqvist, H. Double-Ring Infiltrometer for In-Situ Permeability Determination of Dam Material. *Engineering* **2018**, *10*, 320–328. <https://doi.org/10.4236/eng.2018.106022>.
55. Folorunso, O.; Aribisala, J. Effect of Soil Texture on Soil Infiltration Rate. *Arch. Curr. Res. Int.* **2018**, *14*, 1–8. <https://doi.org/10.9734/ACRI/2018/41974>.
56. Muneer, A.S.; Sayl, K.N.; Kamal, A.H. A Comparative Study to Assess the Suitable Models for Predicting the Infiltration Rate in an Arid Region. *Iraqi J. Civ. Eng.* **2020**, *14*, 29–38.
57. Ren, X.; Hong, N.; Li, L.; Kang, J.; Li, J. Effect of infiltration rate changes in urban soils on stormwater runoff process. *Geoderma* **2020**, *363*, 114158. <https://doi.org/10.1016/j.geoderma.2019.114158>.
58. Rahman, M.A.; Moser, A.; Anderson, M.; Zhang, C.; Rötzer, T.; Pauleit, S. Comparing the infiltration potentials of soils beneath the canopies of two contrasting urban tree species. *Urban For. Urban Green.* **2019**, *38*, 22–32. <https://doi.org/10.1016/j.ufug.2018.11.002>.
59. LaMotte Soil Texture Test Kit. Available online: <https://lamotte.com/products/soil/individual-soil-plant-tissue-test-kits/soil-texture-test-1067> (accessed on 15 October 2020).
60. Groenendyk, D.G.; Ferré, T.P.A.; Thorp, K.R.; Rice, A.K. Hydrologic-process-based soil texture classifications for improved visualization of landscape function. *PLoS ONE* **2015**, *10*, e0131299. <https://doi.org/10.1371/journal.pone.0131299>.
61. The Met Office When Does Summer Start? Available online: <https://www.metoffice.gov.uk/weather/learn-about/weather/seasons/summer/when-does-summer-start> (accessed on 02/02/2022).
62. The Met Office When Does Winter Start? Available online: <https://www.metoffice.gov.uk/weather/learn-about/weather/seasons/winter/when-does-winter-start> (accessed on 12/12/2021).
63. Met Office UK Climate Averages. Available online: <https://www.metoffice.gov.uk/research/climate/maps-and-data/uk-climate-averages/gcq89t680> (accessed on 13/11/2021).
64. Martinez, P.; Buurman, P.; do Nascimento, D.L.; Almquist, V.; Vidal-Torrado, P. Substantial changes in podzol morphology after tree-roots modify soil porosity and hydrology in a tropical coastal rainforest. *Plant Soil* **2021**, *463*, 77–95. <https://doi.org/10.1007/s11104-021-04896-y>.
65. Mölder, A.; Sennhenn-Reulen, H.; Fischer, C.; Rumpf, H.; Schönfelder, E.; Stockmann, J.; Nagel, R.V. Success factors for high-quality oak forest (*Quercus robur*, *Q. petraea*) regeneration. *For. Ecosyst.* **2019**, *6*, 49. <https://doi.org/10.1186/s40663-019-0206-y>.
66. Mishra, P.; Pandey, C.; Singh, U.; Keshri, A.; Sabaretnam, M. Selection of appropriate statistical methods for data analysis. *Ann. Card. Anaesth.* **2019**, *22*, 297–301. [https://doi.org/10.4103/aca.ACA\\_248\\_18](https://doi.org/10.4103/aca.ACA_248_18).
67. Kamis, A.S.; Ahmad Fuad, A.F.; Ashaari, A.; Mohd Noor, C.W. Development of WOP mathematical model for efficient course alteration: LNG tanker manoeuvring analysis and Mann-Whitney U test. *Ocean Eng.* **2021**, *239*, 109768. <https://doi.org/10.1016/j.oceaneng.2021.109768>.
68. Fay, M.P.; Proschan, M.A. Wilcoxon-Mann-Whitney or t-test? On assumptions for hypothesis tests and multiple interpretations of decision rules. *Stat. Surv.* **2010**, *4*, 1–37. <https://doi.org/10.1214/09-SS051>.
69. Nachar, N. The Mann-Whitney U: A Test for Assessing Whether Two Independent Samples Come from the Same Distribution. *Tutor. Quant. Methods Psychol.* **2008**, *4*, 13–20. <https://doi.org/10.20982/tqmp.04.1.p013>.
70. Mann, H.B.; Whitney, D.R. On a Test of Whether one of Two Random Variables is Stochastically Larger than the Other. *Ann. Math. Stat.* **1947**, *18*, 50–60. <https://doi.org/10.1214/aoms/1177730491>.

71. Dittrich, R.; Ball, T.; Wreford, A.; Moran, D.; Spray, C.J. A cost-benefit analysis of afforestation as a climate change adaptation measure to reduce flood risk. *J. Flood Risk Manag.* **2019**, *12*, e12482. <https://doi.org/10.1111/jfr3.12482>.
72. Lacob, O.; Rowan, J.S.; Brown, I.; Ellis, C. Evaluating wider benefits of natural flood management strategies: An ecosystem-based adaptation perspective. *Hydrol. Res.* **2014**, *45*, 774–787. <https://doi.org/10.2166/nh.2014.184>.
73. Lacob, O.; Brown, I.; Rowan, J. Natural flood management, land use and climate change trade-offs: The case of Tarland catchment, Scotland. *Hydrol. Sci. J.* **2017**, *62*, 1931–1948. <https://doi.org/10.1080/02626667.2017.1366657>.
74. Birkinshaw, S.J.; Bathurst, J.C.; Robinson, M. 45 years of non-stationary hydrology over a forest plantation growth cycle, Coalburn catchment, Northern England. *J. Hydrol.* **2014**, *519*, 559–573. <https://doi.org/10.1016/j.jhydrol.2014.07.050>.
75. Archer, N.A.L.; Bonell, M.; Coles, N.; MacDonald, A.M.; Auton, C.A.; Stevenson, R. Soil characteristics and landcover relationships on soil hydraulic conductivity at a hillslope scale: A view towards local flood management. *J. Hydrol.* **2013**, *497*, 208–222. <https://doi.org/10.1016/j.jhydrol.2013.05.043>.
76. Rabot, E.; Wiesmeier, M.; Schlüter, S.; Vogel, H.J. Soil structure as an indicator of soil functions: A review. *Geoderma* **2018**, *314*, 122–137. <https://doi.org/10.1016/j.geoderma.2017.11.009>.
77. The Met Office Record Breaking Rainfall. Available online: <https://www.metoffice.gov.uk/about-us/press-office/news/weather-and-climate/2020/2020-winter-february-stats> (accessed on 11 June 2021).
78. Davies, P.A.; McCarthy, M.; Christidis, N.; Dunstone, N.; Fereday, D.; Kendon, M.; Knight, J.R.; Scaife, A.A.; Sexton, D. The wet and stormy UK winter of 2019/2020. *Weather* **2021**, *76*, 396–402. <https://doi.org/10.1002/wea.3955>.
79. Thomas, H.; Nisbet, T.R. Slowing the Flow In Pickering: Quantifying the Effect of Catchment Woodland Planting on Flooding Using the Soil Conservation Service Curve Number Method. In *International Journal of Safety and Security Engineering*; WIT Press: Ashurst, New Forest, England, 2016; Volume 6, pp. 12–20.
80. Hankin, B.; Chappell, N.; Page, T.; Whiting, M.; Burgess-gamble, L. *Mapping the potential for Working with Natural Processes: User Guide*; Environment Agency: Bristol, UK, 2017.
81. Klamerus-Iwan, A. Different views on tree interception process and its determinants. *For. Res. Pap.* **2014**, *75*, 291–300. <https://doi.org/10.2478/frp-2014-0028>.
82. Rahman, M.; Ennos, R. *What We Know and Don't Know about the Surface Runoff Reduction Potential of Urban Trees*; School of Biological, Biomedical and Environmental Sciences, University of Hull, Cottingham Road, Kingston-upon-Hull, UK, 2016.
83. Komatsu, H.; Kume, T.; Otsuki, K. Increasing annual runoff-broadleaf or coniferous forests? *Hydrol. Process.* **2011**, *25*, 302–318. <https://doi.org/10.1002/hyp.7898>.
84. Calder, I.R. Assessing the water use of short vegetation and forests: Development of the Hydrological Land Use Change (HYLUC) model. *Water Resour. Res.* **2003**, *39*, 1–8. <https://doi.org/10.1029/2003WR002040>.
85. Lunka, P.; Patil, S.D. Impact of tree planting configuration and grazing restriction on canopy interception and soil hydrological properties: Implications for flood mitigation in silvopastoral systems. *Hydrol. Process.* **2016**, *30*, 945–958. <https://doi.org/10.1002/hyp.10630>.
86. Nisbet, T. *Water Use by Trees—Forestry Commission Information Note FCIN065*; Forestry Commission, Corstorphine Road Edinburgh, 2005; pp. 1–8.
87. Forestry Commission. *Forestry Statistics 2018*; Forestry Commission: Aylesbury, UK, 2018.
88. Ellison, D.; Morris, C.E.; Locatelli, B.; Sheil, D.; Cohen, J.; Murdiyarso, D.; Gutierrez, V.; van Noordwijk, M.; Creed, I.F.; Pokorny, J.; et al. Trees, forests and water: Cool insights for a hot world. *Glob. Environ. Chang.* **2017**, *43*, 51–61. <https://doi.org/10.1016/j.gloenvcha.2017.01.002>.
89. Anderson, R.L.; Brye, K.R.; Wood, L.S. Landuse and soil property effects on infiltration into Alfisols in the Lower Mississippi River Valley, USA. *Geoderma Reg.* **2020**, *22*, e00297. <https://doi.org/10.1016/j.geodrs.2020.e00297>.
90. Hynynen, J.; Niemisto, P.; Vihera-Aarnio, A.; Brunner, A.; Hein, S.; Velling, P. Silviculture of birch (*Betula pendula* Roth and *Betula pubescens* Ehrh.) in northern Europe. *Forestry* **2010**, *83*, 103–119. <https://doi.org/10.1093/forestry/cpp035>.
91. British Geological Survey 1:625k Bedrock and Superficial UK Geology. Available online: <https://www.bgs.ac.uk/datasets/bgs-geology-625k-digmapgb/> (accessed on 15 June 2021).
92. He, H.; Aogu, K.; Li, M.; Xu, J.; Sheng, W.; Jones, S.B.; González-Teruel, J.D.; Robinson, D.A.; Horton, R.; Bristow, K.; et al. *A Review of Time Domain Reflectometry (TDR) Applications in Porous Media*, 1st ed.; Elsevier Inc.: Amsterdam, The Netherlands, 2021; Volume 168, ISBN 9780128245897.
93. Cataldo, A.; De Benedetto, E.; Masciullo, A.; Cannazza, G. A new measurement algorithm for TDR-based localization of large dielectric permittivity variations in long-distance cable systems. *Meas. J. Int. Meas. Confed.* **2021**, *174*, 109066. <https://doi.org/10.1016/j.measurement.2021.109066>.
94. Ahmed, F.; Borst, M. Monitoring infiltration rates with time domain reflectometers. *Water Environ. Res.* **2019**, *91*, 1638–1649. <https://doi.org/10.1002/wer.1165>.
95. Samimi, S.; Marshall, S.J.; Vandecrux, B.; MacFerrin, M. Time-Domain Reflectometry Measurements and Modeling of Firn Meltwater Infiltration at DYE-2, Greenland. *J. Geophys. Res. Earth Surf.* **2021**, *126*, e2021JF006295. <https://doi.org/10.1029/2021JF006295>.

### **D.3 Conferences, Presentations and Posters**

This section details conferences attended, presentations and posters created throughout the duration of study

Online oral poster presentation at the 2020 American Geophysical Union (AGU) conference in San Francisco. The presentation outlined and explained the methodology and preliminary results of infiltration data collection from the HofE site.



Background and Introduction

Flood frequency is increasing in the UK, and consequently flood protection and methods of mitigation have moved up the public agenda, aided by concerns surrounding a changing climate (Forbes, Ball, & McLay, 2016; Lowe et al., 2019). The most recent UK Climate Projections (UKCP18) suggest that winters will become warmer and wetter, summers hotter and drier, and extreme weather events will become more frequent. By 2070, summer rainfall will vary from current averages by -47% to +2%, and winter rainfall will vary from -1% and +35% (Lowe et al., 2019).

Since the widespread flooding of 2008, followed by the 2014/15 Winter floods, and more recently the Winter 2020 flooding across the UK, flood risk

Methodology

The 2.2km<sup>2</sup> study site for this project is owned by the Heart of England (HofE) Forest, who have planted 1,883,928 trees across 2832 hectares of land since 1996 (The Heart of England Forest Charity, 2019, 2020). See figure 1.



Figure 1. Aerial Image of the HofE study site, provided for this study by the Ordnance Survey (2018). Red lines indicate plots of planted HofE woodland.

Planting at the main study site began in 2006, and continued every year until 2012. After finishing planting at the main study site in 2012, the HofE Forest continued to plant across other areas of Warwickshire and are still planting to date. In order to strengthen the dataset and include infiltration data from more recently planted areas, two additional HofE sites planted in 2014 and 2020 were sampled alongside those at the main study site.

Sampling Method

Results

Please see the four graphs circulating the slideshow to the bottom-right of the poster for specific results:

- Figure 5 shows the mean infiltration of the Pre-1900 to 2012 sites Vs the Control
- Figure 6 shows the mean infiltration of the 2014 and 2020 sites Vs the Control
- Figure 7 shows the mean hydraulic conductivity of the Pre-1900 to 2012 sites Vs the Control
- Figure 8 shows the mean hydraulic conductivity of the 2014 and 2020 sites Vs the Control

Summarising the results of the collected

Preliminary Conclusions and Future Work

- Tree planting increases average nearby infiltration and hydraulic conductivity by 6.5ml/min and 0.0002cm/sec respectively, making a case for its use as a method of NFM, and further work should be undertaken to test its wider validity.
- The presence of the tree has changed the hydrogeological characteristics of the surrounding area, increasing infiltration rate and hydraulic conductivity closer to the trees sampled. This shows that woodland planting can be beneficial when used as a form of NFM, and on a larger

Woodland as NFM and Project Purpose

There are few evidence-based studies regarding NFM and flood risk reduction. One method that is assumed valuable, although under-investigated, is woodland planting (Lacob, Brown, & Rowan, 2017). Tree roots break up surrounding soil and increase the frequency of soil macropores, increasing water storage capacity (Burgess-Gamble et al., 2018). Woodland soils can be anywhere from 15 to 55% more porous than that of other

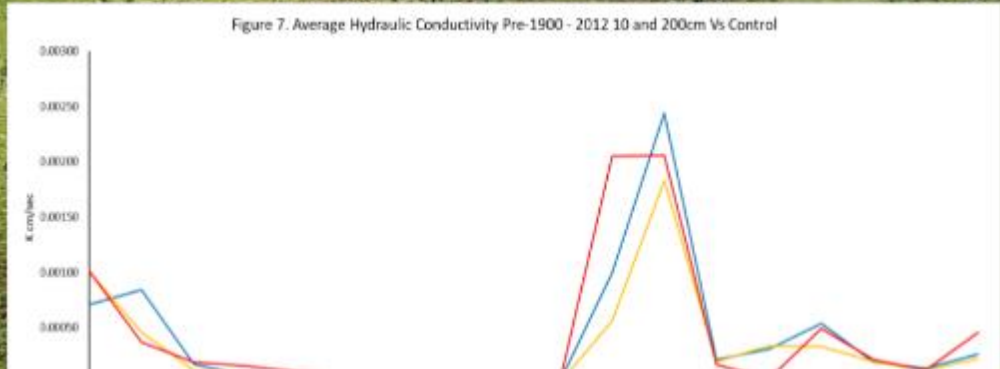


Figure 7. Average Hydraulic Conductivity Pre-1900 - 2012 10 and 200cm Vs Control

*D.3.2 ICUD Conference, Melbourne (Presentation)*

Online oral poster presentation at the 2021 International Conference on Urban Drainage (ICUD) in Melbourne. The presentation outlined and explained the methodology and results involved in the hydrological modelling of infiltration data.



*D.3.3 Coventry University Postgraduate Research Seminar (Oral Presentation)*

Oral presentation to university staff and research students of CAWR (Centre for Agroecology, Water and Resilience) focusing on the methods and results of infiltration data and hydrological modelling.

*D.3.4 Cov-Unovi (Oral Presentation)*

Oral presentation to university staff and other invited attendees of CAWR (Centre for Agroecology, Water and Resilience), and the students and staff of the university of Oviedo, Spain. I was the sole presenter, and the presentation revolved around the methods and results of infiltration data and hydrological modelling.

Poster presentation at the Coventry University trailblazer conference. The poster included information on the background, justification, methods, and results of the project.

# The Effects of Woodland Planting on Flooding Risk

## 1. WHY?

- Increasing urbanisation is reducing natural land cover, reducing the time it takes water to reach the watercourse, increasing flooding is development is
- These effects will only worsen with climate change
- The Environment Agency are investigating more sustainable methods of flood risk management, working with nature rather than against it
- One of these methods is through afforestation and the restoration of woodland areas

## 2. WHERE?

- The HofE forest have planted over 1.9 million trees across 7000 acres of Warwickshire and Worcestershire.
- Infiltration data was collected from the Heart of England Forest woodland plots planted in 2006, 2008, 2010 and 2012.
- Additionally, a plot planted in c.1900, and a control site consisting of a grassland were sampled for comparison against the newly planted trees.



## 3. HOW?

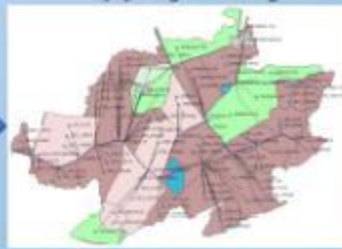
**A) Infiltration Sample Sites**



**B) Land Cover Identification**



**C) Hydrological Modelling**



## 4. CONCLUSIONS

- Woodland planting across the site can reduce flood risk compared to if the site was developed.
- However, grassland shows the greatest reduction in flood risk overall.
- River flows are more aggressive in summer compared with winter, however there is less rainfall.
- Flood risk in both winter and summer recues as storm duration increases.

## 5. IMPACTS AND BIGGER PICTURE

- Results show that woodland planting can reduce flood risk after only 15 years, so this is only likely to improve as woodland matures.
- This study is representative of a clay (non-permeable) geology site, therefore if the methods were applied elsewhere, it is likely that the impacts of woodland planting would demonstrate more significant results in comparison.
- This study can be used by other authors who wish to investigate changing infiltration trends, and model it using computer software.
- This project has shown that the governments idea of working with nature to reduce flood risk is a viable option.
- Future work will model the influences of climate change, and simulate the flood risk as a response to these changes.



#### **D.4 Additional Development and Engagement**

This section outlines all additional and miscellaneous development, both academic and professional, undertaken throughout the course of study.

##### *D.4.1 Development Activity Log*

Table D.1 lists all development activities and the hours accumulated in partial fulfilment of the requirements of this study.

*Table D.1. Extracurricular additional activities undertaken throughout the course of study*

<b>Date</b>	<b>Activity/Event</b>	<b>Hours</b>	<b>Total</b>
23/09/2018 - 24/09/2018	SuDSNet	20	20
25/10/2018	Lecture preparation	8	28
29/10/2018	Lecture delivery	4	32
29/10/2018	Tutoring in GIS	5	37
01/11/2018	Study site tour with tutors	5	42
05/11/2018 - 30/11/2018	External data management and GIS project	50	92
11/04/2019	Site walk around Staffordshire with Staffordshire Wildlife Trust and my DoS	8	100
15/04/2019	Meeting with Jacobs in Leeds to discuss my project and how they may be able to assist	10	110
24/06/2019	Day on site with Dr. Sim Reaney flying drone to survey study site	10	120
04/11/2019	Meeting with Jacobs in Peterborough regarding the modelling elements of my PhD	5	125
07/11/2019	CAWR Ethics Training	3	128
19/02/2020	SIGMA Stats Workshop: Intro to SPSS	3	131
20/02/2020	Tutoring in modelling and GIS	7	138
19/04/2020	Being tutored on the advanced features of Flood Modeller Pro by a modelling consultant	8	146
05/05/2020	SIGMA Stats Workshop: Descriptive Statistics	3	149
06/05/2020	SIGMA Stats Workshop: Statistical Inference	3	152
06/05/2020	SIGMA Stats Workshop: Non-Parametric Statistics	3	155
07/05/2020	SIGMA Stats Workshop: Analysis of Variance Workshop	3	158
07/05/2020	SIGMA Stats Workshop: Correlation and Regression	3	161
03/09/2020 - 08/09/2020	Presentation preparation for upcoming presentation to all CAWR staff and students	7	168
09/09/2020	Presentation to all CAWR staff and students	2	170
11/09/2020	Meeting with HofE head forester for a walk around the study site and general questions	5	175

20/11/2020 -	Preparation of poster presentation for the virtual AGU conference	20	195
09/12/2020	(2020)		
10/12/2020	Presentation of poster, and time spent taking questions	1	196
19/01/2021	Tutoring in GIS and HEC-HMS	10	206
20/05/2021 -	Preparation for the upcoming Cov-Unovi workshop presentation	10	216
25/04/2021			
25/05/2021	Cov-Unovi workshop presentation	2	218
31/10/2021	First Peer Reviewed Publication	60	278
27/10/2021	ICUD Conference	2	280
01/11/2021	Preparation of poster of upcoming trailblazer presentation	10	290
09/11/2021	Trailblazer Poster Presentation	2	292
10/11/2021	Meeting with Michigan Tech Professors about the MDI app	2	294
12/01/2022	Meeting with HofE head forester, biodiversity manager and Environment Agency	3	297
11/03/2022	Second peer Reviewed Publication	60	357
15/03/2022	Feedback session with the development team of the MDI app	2	359
		Total Hours	359

#### *D.4.2 Mini-Disk Infiltrometer App Development*

Working with Dr. Mary Miller and (Research Scientist) and Dr Robert Pastel (Computer Science Associate Professor) from Michigan Tech Research Institute (MTRI), to feedback, discuss and test a new app to assist in the use of the Mini Disk Infiltrometer.